United States
Environmental Protection
Agency

Atmospheric Sciences
Research Laboratory
Research Triangle Park NC 27711

Research and Development

December 1987

EPA

PROJECT REPORT

EPA COMPLEX TERRAIN MODEL DEVELOPMENT: FINAL REPORT

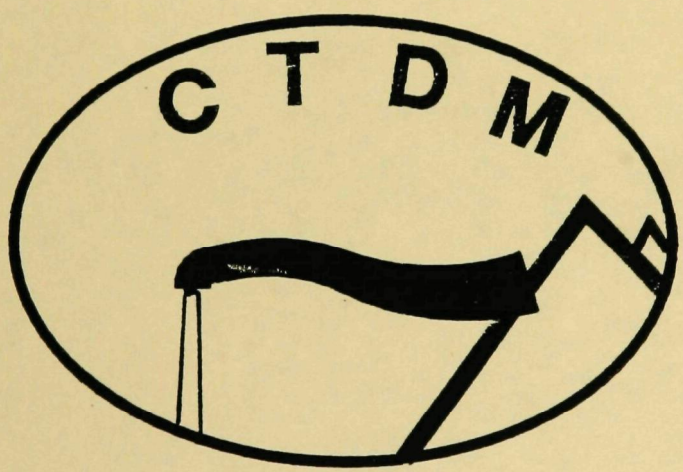

EPA COMPLEX TERRAIN MODEL DEVELOPMENT: FINAL REPORT

by

David G. Strimaitis[1]
Robert J. Paine[2]
Bruce A. Egan[2]
Robert J. Yamartino[1]

[1]Sigma Research Corp.
Lexington, MA 02173

[2]ERT, Inc.
Concord, MA 01742

Contract No. 68-02-3421

Project Officer

Peter L. Finkelstein
Meteorology Division
Atmospheric Sciences Research Laboratory
Research Triangle Park, NC 27711

ATMOSPHERIC SCIENCES RESEARCH LABORATORY
OFFICE OF RESEARCH AND DEVELOPMENT
U.S. ENVIRONMENTAL PROTECTION AGENCY
RESEARCH TRIANGLE PARK, NC 27711

NOTICE

The information in this document has been funded by the United States Environmental Protection Agency Under Contract No. 68-02-3421 to ERT, Inc. It has been subjected to the Agency's peer and administrative review, and it has been approved for publication as an EPA document. Mention of trade names or commercial products does not constitute endorsement or recommendation for use.

ABSTRACT

The Complex Terrain Model Development (CTMD) project has met its original objectives of producing an atmospheric dispersion model appropriate for regulatory agency application to elevated sources of air pollutants located in mountainous terrain settings. The model development effort has focused on predicting concentrations during stable atmospheric conditions.

The program, initiated in June 1980, has involved the performance of 4 major field experiments which produced a wealth of data for model development and verification purposes. The first experiment, held at Cinder Cone Butte (CCB) in Idaho, involved the extensive use of a mobile release system to provide a high capture rate of ground-level concentrations resulting from elevated plumes flowing toward the butte. The second experiment, at Hogback Ridge (HBR) near Farmington, New Mexico, featured a very long ridge that provided a site for testing the importance of terrain aspect ratio on the flow dynamics. The final field experiments were held at the Tracy Power Plant (TTP) near Reno, Nevada. This Full Scale Plume Study (FSPS) provided a large-scale test of the modeling concepts developed. Data were also obtained from a series of fluid modeling studies performed at EPA's Fluid Modeling Facility. These tests provided confirmation of some of the basic theoretical principles adopted in the modeling effort and provided information on plume behavior as a function of systematic changes in terrain shapes, release heights and distances to terrain objects.

The Complex Terrain Dispersion Model (CTDM), fully described in this report, is an advanced Gaussian model that uses a flow algorithm to provide terrain-induced plume trajectory and deformation information. CTDM is suitable for regulatory use, but it requires substantially more information on terrain and local meteorology than complex terrain screening models. With simpler data bases, it demonstrates degraded performance.

The model evaluation effort concentrated first on the use of field data collected within this program. Subsequent tests were made with two other data sets obtained from SO_2 monitoring networks near a large paper mill and a large power plant, both located in complex terrain. Statistical performance results of CTDM were compared with those of other complex terrain models of current regulatory interest or use. The model evaluation demonstrates that CTDM has superior performance in the majority of tests and has consistently good performance among all the sites. The statistical performance of CTDM in complex terrain settings is shown to be comparable to the performance of EPA's current refined flat terrain models in simple terrain settings.

CONTENTS

CONTENTS (Continued)

FIGURES

FIGURES (Continued)

FIGURES (Continued)

TABLES

TABLES (Continued)

LIST OF SYMBOLS AND ABBREVIATIONS

SYMBOL	
a	Major axis length of an ellipse, m (also denoted as L_a)
A_z	Term used in F_z formulation
b	Minor axis length of an ellipse, m (also denoted as L_b)
b_1, b_2, b_3	Factors involved in B_1, B_2 terms in WRAP calculation
B	Function of h/L used in computation of wind direction adjustment with height
B_o	Parameter used in analytical expression for convolution integral I
B_1, B_2	Factors involved in vertical term in WRAP concentration calculation
C	CTDM modeled concentration, $\mu g/m^3$
d	Stack top inner diameter, m; also crosswind distance from plume centerline, m
dQ	Source strength of a point source element at the impingement point on the hill, g/sec
$d\theta/dz$	Vertical potential temperature gradient, °K/m
f	Coriolis parameter = $1.458 \times 10^{-4} \cdot \sin(\text{latitude})$, sec^{-1}
F	Buoyancy flux, m^4/sec^3
F_z	Vertical distribution function in Gaussian plume equation
g	Acceleration due to gravity = 9.8 m/sec^2
G	Soil heat flux, watts/m^2; also, a constant used in determining vector wind speed from scalar wind speed and σ_θ; also denotes Green's function

h	Mixed layer height, m; also final plume height, m; also hill height function, m
h_r	Release height above reference base height, m
h_R	Height of receptor above reference base height, m
h'_R	Modified height of receptor (relative to plume height) due to terrain effects, m
h_s	Stack height, m
H	Height at the top of the hill, m; also the sensible heat flux, watts/m^2
H_c	Critical dividing streamline height, m
i_y	Horizontal component of the turbulence intensity
i_z	Vertical component of the turbulence intensity
I	Convolution integral of Green's function with the hill height function
k	von Karman constant
K_y	Eddy diffusivity, horizontal component (m^2/sec)
K_z	Eddy diffusivity, vertical component (m^2/sec)
ℓ	Mixing length, m; also crosswind distance from plume centerline to receptor, m
ℓ_n	Mixing length in neutral conditions, m
ℓ_s	Mixing length in stable conditions, m
L	Monin-Obukhov length, m
L_a	Major axis length of an ellipse, m (also denoted as "a")
L_b	Minor axis length of an ellipse, m (also denoted as "b")
L_n, L_z	Parameters used in analytical expression for convolution integral I
L_x	Length scale of hill in along-wind direction, m
L_y	Length scale of hill in cross-wind direction, m
m	Modified inverse length scale = $n(1+L_x^2/L_y^2)^{1/2}$

n	ratio of N/u, m^{-1}
N	Brunt-Vaisala frequency, sec^{-1}
N_m	Average value of N in a layer, sec^{-1}
N_o	Value of N at s_o (flat terrain value)
Q	Emission rate, g/sec
r	Ratio of ellipse major axis length to minor axis length, r=a/b
R	Displacement from a reference point ($R^2= x^2+y^2+z^2$),m
R_i	Richardson number
R_L	Parameter used in analytical expression for convolution integral I
s	Square of the Brunt-Vaisala frequency, sec^{-2}
s_o	Downwind distance at which the plume impinges upon or is deflected by terrain, m
S_T	Speed of the incident flow at the tower location, m/sec
S_∞	Speed of the incident flow approaching a hill, m/sec
t	Travel time, sec
T_a	Ambient air temperature, °K
T_h	Factor for streamline distortion in the vertical (height correction factor)
T_ℓ	Distortion factor due to terrain effects in the horizontal direction
T_L	Lagrangian time scale, sec.
T_{Lo}	Value of T_L at s_o (flat terrain value), sec.
T_s	Stack gas temperature, °K
T_u	Factor for wind speed distortion due to terrain influences
T_y	Terrain effect factor equal to ratio of $\sigma_y^*/\sigma_y^{*'}$
T_z	Terrain effect factor equal to ratio of $\sigma_z^*/\sigma_z^{*'}$

$T_{\sigma v}$	Terrain effect factor equal to ratio of σ_v/σ_{vo}
$T_{\sigma w}$	Terrain effect factor equal to ratio of σ_w/σ_{wo}
u	Scalar wind speed, along-flow component (m/sec)
u_*	Friction velocity, m/sec.
u_g	Geostrophic wind speed, m/sec
u_m	Average wind speed in a layer, m/sec
u_s	Stack-top wind speed, m/sec
u_v	Vector wind speed, m/sec
u',v',w'	Perturbation wind velocities (Boussinesq flow) in downwind, crosswind, and vertical directions, respectively (m/sec)
v	Cross-flow wind speed component, m/sec
w	Vertical component of the wind speed, m/sec
w_*	Convective velocity scale, m/sec
w_d	Mean downdraft velocity in unstable conditions, m/sec
w_s	Stack gas exit velocity, m/sec
x	Distance in downwind direction, m
x_o	Downwind distance at s_o, the impingement point of the approach flow on the hill, m
x_m	Length parameter used in analytical expression for convolution integral I
x_r,y_r,z_r	Position in space of the plume release
y	Distance in crosswind direction, m
y_R	Crosswind distance of receptor from plume centerline, m
y_R'	Modified crosswind distance of receptor from plume centerline due to terrain effects, m
z	Measurement height, m; also receptor height, m
z_o	Surface roughness length, m

z_m	Height of a streamline above the base of the hill far upwind, m
z'	Height above terrain surface, m
α	Wind speed shear (vertical component), sec^{-1}
α_1, α_2	Parameters used in analytical expression for conduction integral I
α_w	Direction of the incident flow approaching a hill, degrees
β	Strain function from theory of Hunt and Mulhearn (1973) used in computation of T_y, T_z, also, rotation angle between wind flow and stagnation streamline
δ_z	Vertical deflection experienced by a streamline due to terrain influences, m
$\Delta\alpha$	Wind direction change within the mixed layer, degrees
$\Delta h, \Delta H$	Plume rise, m
ϵ	Variable used to relate scalar and vector wind speeds, a function of σ_θ
$\Delta\theta$	Jump in potential temperature at the top of the mixed layer, °K
η	Height of a streamline above the surface of the hill
γ	Constant of proportionality between the mixing length in a stable atmosphere and σ_w/N; α=0.52
Γ	Constant of proportionality between the mixing length in a neutral atmosphere and z, Γ = 0.36
μ, ν	Elliptical coordinates
μ_o	Value of μ along the boundary of an ellipse
μ_s, ν_s	Elliptical coordinates of the point of the plume release
μ_T, ν_T	Elliptical coordinates of the point where wind speed and direction are measured (tower)
Φ_T	Wind direction measured at the tower location
Ψ	Orientation angle of Gaussian hill

Ψ_m	Stability correction for wind profile formulation in the surface layer
Ψ_s	Stream function through the source
ρ_o	Initial unperturbed fluid density in Boussinesq flow
σ	Generic representation of either σ_y or σ_z due to ambient turbulence, m
$\sigma_{\ell b}$	σ_y, σ_z due to buoyancy-enhanced dispersion, m
$\sigma_{\ell s}$	σ_y, σ_z due to source-induced turbulence, m
σ_θ	Standard deviation of wind direction, degrees
σ_v	Standard deviation of the crosswind component of the wind speed, m/sec.
σ_{vo}	Value of σ_v at s_o (flat terrain value)
σ_w	Standard deviation of vertical wind speed, m/sec.
σ_{wo}	Value of σ_w at s_o (flat terrain value)
σ_y	Crosswind distance from plume centerline in a Gaussian plume at which the concentration falls to $e^{-1/2}$ of the value at the plume centerline, m
σ_{yo}	Value of σ_y at s_o, m
σ_y^*	Growth in σ_y between s_o and the receptor position of interest for flat terrain, m
$\sigma_y^{*'}$	Growth in σ_y between s_o and the receptor position of interest with terrain influences considered, m
σ_{ya}	σ_y due to ambient turbulence, accounting for terrain-influenced changes in turbulence parameters, m
σ_{ye}	Effective σ_y, accounting for effect of strain in the flow over terrain on horizontal diffusion
σ_z	Vertical distance from plume centerline in a Guassian plume at which the concentration falls to $e^{-1/2}$ of the value at the plume centerline, m
σ_{zo}	Value of σ_z at s_o, m
σ_z^*	Growth in σ_z between s_o and the receptor position of interest for flat terrain
$\sigma_z^{*'}$	Growth in σ_z between s_o and the receptor position of interest with terrain influences considered, m

σ_{za}	σ_z due to ambient turbulence, accounting for terrain-influenced changes in turbulence parameters, m
σ_{ze}	Effective σ_z, accounting for effect of strain in the flow over terrain on vertical diffusion
θ_o	Surface potential temperature (at z=o), °K
θ_m	Mean potential temperature of the mixed layer, °K

ABBREVIATIONS

AGA	American Gas Association
ARLFRD	Air Resources Laboratory Field Research Division
CCB	Cinder Cone Butte
CTDM	Complex Terrain Dispersion Model
ERF	Error Function
EPA	Environmental Protection Agency
EPRI	Electric Power Research Institute
FMF	Fluid Modeling Facility
FSPS	Full Scale Plume Study, conducted at the Tracy Power Plant near Reno, NV
GLC	Ground-Level Concentration
HBR	Hogback Ridge
LHS	Left Hand Side of Equation
MSE	Mean Square Error
NMSE	Normalized Mean Square Error
RHS	Right Hand Side of Equation
RMSE	Root Mean Square Error
RTDM	Rough Terrain Diffusion Model
SHIS	Small Hill Impact Study (#1 was at Cincer Cone Butte, #2 was at the Hogback Ridge.
TPP	Tracy Power Plant
VPTG	Vertical Potential Temperature Gradient

ACKNOWLEDGEMENTS

This project has been over seven years in duration. The number of people who contributed significantly to the success of the program and to whom we are indebted is correspondingly large.

First we wish to thank those at EPA who have provided consistent and devoted support and encouragement.

- George Holzworth is a clear "father figure" for the project. His initial clear definition of EPA's needs was essential and helped to guide us throughout the project. We also appreciated George's experience at the first field experiments and his staying with the project even after his initial "retirement."

- Bill Snyder's insight and interest regarding the role that fluid modeling should play in this effort was very influential and benefited the program design. The experiments performed under his direction at the EPA Fluid Modeling Facility provided data on phenomena difficult to analyze in the field data as well as verification of basic flow concepts incorporated in the final dispersion models. His counsel on the photographic program and his goat-like ability to find ways to get himself to remote but significant locations for observations were major contributions to the field experiments.

- Frank Schiermeier enthusiastically supported our efforts and kept the project going and on target through the ups and downs of fiscal policy. We appreciate his confidence in us and his negotiative skills in assuring cooperation among all the different organizations who contributed to the effort.

- Peter Finkelstein, our EPA project manager during the final phases of our effort, has been another source of encouragement and also a great resource to us. His willingness to test and exercise early versions of the model provided us with otherwise unobtainable feedback. We appreciate his more general encouragement regarding the needs for good science and his patience with our (sometimes meandering) resolution of problems.

- Steve Perry, having worked through our computerized products has provided a number of suggestions for improvements. His diplomacy in identifying 'glitches' along the way didn't go unnoticed.

Our five progress reports acknowledge many of those external to ERT and EPA who contributed to our field programs. The groups form a substantial list.

- North American Weather Consultants was responsible for the field operations at Cinder Cone Butte. Tim Spangler and George Taylor showed ingenuity and patience in developing and executing the logistics of this complicated effort. Their efforts were essential to the success of these experiments.

- Wynn Eberhard and his colleagues from the National Oceanographic and Atmospheric Administration's Wave Propagation Laboratory (NOAA WPL) generated the ground- based lidar data for all the field experiments. Bill Neff provided the Doppler acoustic sounders and, later, sonic anemometers and other instruments to supplement our more conventional meteorological measurements. The unique information gained by these operations has contributed significantly to our understanding of the phenomena observed. We appreciate the dedication these groups showed in their efforts.

- Ray Dickson, Gene Start, and their associates at the NOAA ARLFRD were responsible for the tracer release, sampling, and analysis and many of the meteorological measurements at the Hogback Ridge and Tracy Power Plant experiments. These operations, which involved a large number of people and many items of equipment, required significant logistics, and we credit their leadership and experience for contributions to this program.

- Norm Ricks, first from ERT, then from Morrison/Knudsen, should receive the "most-devoted contributor" award through his dedication to obtaining good photographic and video tape data. Those cold hours atop our 150-m tower at HBR exemplified Norm's extraordinary efforts. His wizardry in keeping equipment going was also outstanding.

- The field crews from NOAA's ATDL who contributed and operated their tethersonde throughout the long nights deserve our appreciation.

- Julian Hunt and Rex Britter of Cambridge University consulted with us at various stages. They put fluid modeling results in perspective and explored theoretical aspects of the effort. We benefited from our several discussions with them.

- The Electric Power Research Institute, under the inspiring guidance of Glenn Hilst, provided direct support of the field experiments at Tracy. They co-sponsored the entire first effort and contributed the airborne lidar capability to the final experiment. EPRI's participation, via their subcontractors Rockwell International, SRI International, TRC Environmental Consultants, and the Research Triangle Institute, added greatly to the value of this program.

Finally, we want to acknowledge the efforts of the many ERT staff, past and present, who contributed beyond the call of duty in this program.

- Tom Lavery, project manager through the field experiment phases, provided leadership and follow-through to our staff and our subcontractors. His willingness to let others "do their thing" helped provide the research environment needed.

- Ben Greene, our quality assurance conscience, was also our most articulate phenomena reporter in the field experiments. His devotion to understanding what the data collected really meant was crucial to our subsequent interpretations of the field studies. His persistence in addressing problems needing resolution was needed and is appreciated.

- Akula Venkatram contributed many of the early theoretical concepts which have carried through to the end product of the CTDM. His intuition and suggestions for exploration provided the team with avenues to pursue when the path to progress became mired.

- Dan Godden manned our field headquarters and, with a sense of humor in the middle of the night, kept our spirits up and eyes open.

- Don DiCristofaro did much of the coding and testing of CTDM during the development stage of the program, and was instrumental in preparing The Modelers' Data Archives, which should be of use to other for years.

- Liz Insley prepared many of the meteorological and terrain data sets used in the final evaluation of CTDM, providing important feedback on decisions faced by users of the model.

- Michael Mills joined the team in time to develop the terrain preprocessor programs necessary to run the model. The computer graphics developed by Mike that are associated with the terrain preprocessor, receptor generator, and CTDM postprocessor will go a long way toward increasing user understanding and acceptance of the CTDM package. His quick understanding of all that had been done previously was a tremendous boost to the project.

- Michael Dennis became responsible for documenting and testing much of the CTDM and its pre- and post-processors. His ability to prevent and/or chase down problems is especially appreciated.

- Art Bass contributed significantly to our original proposal effort and to the model development work plan. We appreciate the long-lasting forethought he provided in these efforts.

- Steve Andersen, Chris Johnson, and others from ERT's Fort Collins office were responsible for the 150-meter tower, other tower and ground-based meteorological instrumentation, site preparation and restoration, and the care and feeding of 40-year old arc lamps. Their long hours, ingenuity, experience with instruments and data acquisition systems, and lack of vertigo were vital to the success of the field data collection.

There are others, too numerous to specifically call out, who helped us accomplish this program. We thank them all!

SECTION 1

INTRODUCTION

The Complex Terrain Model Development (CTMD) project, sponsored by the U.S. Environmental Protection Agency (EPA), was initiated in 1980. Its purpose is to develop, evaluate, and refine practical plume models for calculating ground-level air pollutant concentrations that result from elevated emission sources located in complex terrain (i.e., terrain which rises to heights well above expected plume levels). The primary objective of the project is to develop models to simulate 1-hour average concentrations during stable atmospheric conditions.

These models are to be used in a wide variety of applications, such as the siting of new energy development facilities and other sources of air pollution, regulatory decision making, and environmental planning. Therefore, the models should be easy to understand and use, with known accuracy and limitations.

The objectives of the program were described by Holzworth (1980) and generally follow the recommendations of the participants of the EPA-sponsored workshop to consider the issues and problems of simulating air pollutant dispersion in complex terrain (Hovind et al. 1979). The program was subsequently designed to include model development efforts based on physical modeling, field experiments, and theoretical work.

Four major CTMD field experiments have been completed during the last seven years to collect data for development and evaluation of various modeling approaches. The first field experiment, the Small Hill Impaction Study No. 1 (SHIS #1), was conducted during the fall of 1980 at Cinder Cone Butte (CCB), Idaho. CCB is a roughly axisymmetric, isolated and approximately 100-m tall hill located in the broad Snake River Basin near Boise, Idaho. The second field experiment, SHIS #2, was performed during October 1982 at the Hogback Ridge (HBR) near Farmington, New Mexico. HBR is a long, 90-m tall ridge located on the Colorado Plateau near the western slopes of the San Juan Mountains. Both small hill studies consisted of flow visualization and tracer experiments conducted during stable flow conditions with supporting meteorological, lidar, and photographic measurements. At these sites, the tracer gases were released from mobile cranes or a tower.

The third and fourth field experiments were conducted at the Tracy Power Plant (TPP) located in the Truckee River Valley east of the Reno, Nevada. The third experiment, performed in November 1983, was undertaken as a feasibility and design study for the Full Scale

Plume Study (FSPS). It was co-sponsored by the Electric Power Research Institute (EPRI). The November experiment not only demonstrated the feasibility of conducting the FSPS at the TPP, but with the expanded scope made possible by EPRI's participation, it also produced a data base that itself is useful for modeling purposes. The FSPS was subsequently performed at Tracy in August 1984.

The data bases compiled from the CCB, HBR, and the FSPS experiments are available from the EPA Project Officer. The data bases compiled from each of the experiments include the following components:

- Source information: emission rates, locations, and heights of SF_6, CF_3Br, and oil-fog releases.
- Meteorological data: measurements of the approach flow as well as information on flow and dispersion near the terrain.
- Tracer gas concentrations: data from more than 50,000 individual samples collected during the experiments from as many as 100 sampler locations in each experiment.
- Lidar data (archived at the Wave Propagation Laboratory): sections across the plume characterizing the trajectory and growth of the plume upwind of, interacting with, and sometimes in the lee of, key terrain features.
- Photographic data: still photographs taken from fixed locations, aerial photographs taken at CCB and Tracy from an aircraft flying overhead, and (occasional) 16-mm and 8-mm movies and videotapes.

During the course of the CTMD project, five Milestone Reports (Lavery et al. 1982, Strimaitis et al. 1983, Lavery et al. 1983, Strimaitis et al. 1985, and DiCristofaro, et al. 1986) have been published. These reports, which are available from EPA, describe the progress in developing and evaluating complex terrain models using the CCB, HBR, and TPP data bases. They also describe in detail the two small hill studies, the November 1983 Tracy study, the FSPS, and a series of towing tank and wind tunnel studies performed at the EPA Fluid Modeling Facility (FMF) in support of the modeling.

A preliminary partially validated model was delivered to the Project Officer in October 1985. A workshop was held in February 1986 to present to the scientific community results from the field experiments, model development activities, and related work done both within and outside the CTMD project and to obtain feedback from users working with the preliminary model.

This final report provides a brief overview of the program and discusses the major accomplishments with respect to the model development and validation efforts since the Fifth Milestone Report. A detailed description of the final version of CTDM is provided in

Section 3. CTDM now contains a flow model which computes the deflection experienced by a streamline passing through a given point over the hill. The model uses a "backwards-looking" solution of linearized equations of motion of a steady-state Boussinesq flow. The deflection calculation provides a more realistic and theoretically satisfying method for estimating the distance between plume centerlines and terrain surfaces and for estimating the distortion of plume shape associated with streamline spacing changes. Appendix A provides additional details of the algorithm.

The evaluation of CTDM with field data is described in Section 4. The development of CTDM was guided by the findings and observations from the field experiments conducted as part of this project at CCB, HBR and TPP (FSPS). These programs were designed specifically to gather the meteorological information, observations and ground level concentration data needed for the model development effort. CTDM and several other models of regulatory interest were tested with the same data sets. In addition, CTDM was tested against two other data sets from studies at the Westvaco paper mill at Luke, Maryland and at the Tennessee Valley Authority's Widow's Creek Steam Plant. The data sets from these monitoring programs provide an independent means of evaluating the models. Although the meteorological and ground-level concentration data were not as extensive as that collected at the field sites, full years of data are available. The results of these tests are also presented in Section 4.

CTDM was also subjected to a series of sensitivity tests which are reported on in Section 5. These tests largely emanated from recommendations received at the CTDM workshop held in February 1986. The analyses focus on the effect that variations in measured or predicted quantities would have on the terrain effect in CTDM. The terrain effect is defined as the ratio of the predicted peak ground-level concentration to the concentrations at the plume centerline for the same travel time. This measure of sensitivity is appropriate for the intended use of the model as it focuses attention to the magnitude of predicted concentrations rather than to changes in the location of the peak values.

Limitations to the use and applicability of CTDM are addressed in Section 6 of this report. The specific guidance emerges in part from the results of the evaluation and sensitivity test efforts and also from recognizing that testing of the model has not subjected it to all of the important terrain obstacle shapes and configurations which may be encountered. The limitations must be placed in the context of implicit or explicit limitations applicable to EPA's prior complex terrain modeling techniques.

Finally, a series of conclusions and recommendations which emerge from this model development effort are presented in Section 7. Appendices to the report include a paper on the flow model, statistical results from the model evaluation efforts and a document describing the contributions made to the CTMD program by EPA's Fluid Modeling Facility.

SECTION 2

OVERVIEW OF THE CTMD PROGRAM

2.1 Background and Overall Program Plan

The CTMD program was initiated by EPA in response to long-standing controversies in the technical and regulatory communities over the lack of reliable methods for predicting air quality concentrations in regions of mountainous or complex terrain. Of particular concern was the absence of a verified dispersion model for predicting ambient air concentrations during stable atmospheric conditions, the conditions expected to give rise to the highest short-term concentrations. EPA had employed "screening" models (most notably, the Valley model (Burt, 1977)) which were known to be strongly biased toward overprediction in high terrain areas, but EPA guidance did not recommend a "refined" model for use in such settings. It was recognized that a major data collection and model development effort would be required to develop such a capability.

EPA convened a workshop (Hovind et al., 1979) of specialists in field measurement programs, fluid modeling and mathematical modeling for purposes of helping to define the specific elements of such a program. The workshop report recommended that a two-phased field program be initiated with a first phase being performed at an isolated and relatively small terrain feature of simple geometric shape. This hill would be heavily instrumented and studied at relatively small cost and the tracer release and sampling program would be capable of being altered in response to different meteorological conditions. A second phase field program would involve a "full-scale" site and increased topographic complexity. An underlying concept was that the dynamics of an elevated plume's interaction with a terrain feature could be studied at smaller hills, whereas the effects of larger scale meteorological flows on transporting plumes toward high terrain would be better studied at large terrain shapes. In accordance with the above concept, the workshop report also suggested the complementary use of physical or fluid-modeling facilities to investigate the flow dynamics involved in a systematic way with scaled-down models of terrain features.

Mathematical model development was an essential, organizing component of the proposed program because the ultimate product was to be a model for regulatory use. The workshop recommended reliance upon Gaussian-based or "K-Theory" models because of their conceptual simplicity and ease of use. Holzworth (1980) stated the overall need succintly as "the production of a useful model (or models) with demonstrated reliability and prescribed applicability."

The program was to focus on understanding the impact during stable atmospheric conditions and for one-hour averaging periods. EPA developed a request for proposals for the effort and awarded the contract for the Complex Terrain Model Development program to ERT in June, 1980. A parallel and complementary fluid modeling effort was also expanded upon at the EPA Fluid Modeling Facility (FMF). Scale model experiments were to be performed on a variety of terrain shapes including that of the first field experiment site at Cinder Cone Butte in Idaho.

The components of the CTMD program and the progress made are well-detailed and documented in a number of reports. In particular, five Milestone Reports* were written during the course of the program which describe in detail the model development efforts, the field experiments, the data gathering and interpretation efforts, and the model evaluation efforts performed during the course of this program.

These reports also contain, as appendices, relevant contributions from EPA's Fluid Modeling Facility efforts. In addition, separate documents (Greene and Heisler, 1982; Greene, 1985; and Greene, 1986), describe the quality assurance aspects of various components of the program. Another document (Lavery et al., 1986) summarizes the results of a workshop held with users of an early version of the Complex Terrain Dispersion Model (CTDM). In addition, a number of other reports relating to this effort have been produced by members of EPA's FMF and will be referenced as appropriate.

The remaining portions of this section describe the program components and also identify specific documents containing more detailed information about these components.

2.2 Field Program

2.2.1 Goals and Design

A program to gather high quality and relevant data from field experiments was an essential element of the overall study. The measurements desired were driven by the needs of the model development effort. In accordance with EPA's conceptual plan, the first field experiment was held in the fall of 1980 at Cinder Cone Butte (CCB) near Boise, Idaho. This volcanic hill stands about 100 m high and has a nearly circular base about 1 kilometer in diameter. Set in a broad section of the Snake River valley, CCB is an isolated feature surrounded by relatively flat terrain for tens of kilometers. Meteorological data showed that stable drainage flows occurred on a relatively routine basis at night, but there was moderate variability in wind direction, probably associated with the broadness of the valley. The field program design had at its core several concepts:

*In the following discussion, these milestone reports will be referred to as the First, Second, etc. Milestone Reports; they are formally referenced in Section 1.

(1) two different tracer gases would be released from a mobile crane at a variety of heights relative to terrain and the critical dividing streamline heights. The crane would be capable of being moved to different positions upwind of the butte in accordance with predicted wind directions, (2) tracer gas concentrations would be obtained at approximately 90 locations on or around the butte (with sampling time periods of one hour or less), (3) dense smoke releases would allow photographic and lidar documentation of plume behavior, and (4) extensive measurement of meteorological variables of importance to the model development effort would be made with both fixed and remote sensing instrumentation.

Because of the emphasis on understanding the flow dynamics under stable atmospheric conditions, the field experiments were generally begun in the evening and continued until after daybreak. Weather forecasting and on-site monitoring of meteorological conditions were relied upon to set the initial locations of the cranes releasing the smoke and tracer gases. Participants at the experiments at CCB were: ERT (overall project management); Western Scientific Services, Inc. (fixed meteorological data collection); North American Weather Consultants (smoke and tracer releases, tracer data collection, photography and mobile meteorology); NOAA Wave Propagation Laboratory (lidar systems); and TRC, Inc. (independent data audits).

The First Milestone Report provides a detailed description of the first field experiment configurations at CCB including a discussion of the quality assurance program.

The second field experiment took place at Hogback Ridge (HBR) near Farmington, New Mexico in October 1982. This ridge was chosen because it represents a more-or-less two-dimensional terrain feature, having a height of about 85 meters, but extending several kilometers to either side of the experiment site. An important modeling issue which needed resolution was the importance of aspect ratio (of length to height) to plume trajectory behavior. Also needed was an understanding of how plumes would be transported under stable, "blocking" conditions upwind of nearly two-dimensional terrain features. The experimental setup at HBR was similar to that established at CCB, but included an additional capability for releasing tracer gases from different levels of a 150-m tower. Approximately 125 tracer gas samplers were set out for each experiment, concentrating the coverage in the upwind and downwind sides of the ridge nearest the tracer releases, but also providing samplers at considerable distances along the ridge axis.

The NOAA ARLFRD (Air Resources Laboratory Field Research Division) was responsible for the tracer gas releases, sampling and analyses, the smoke visualization and the telemetry and meteorological data archive and display systems for this experiment. Morrison-Knudsen was responsible for the photographic program. The NOAA WPL performed lidar measurements and contributed additional meteorological instrumentation to the program. The HBR field experiment design is described in the Third Milestone Report.

The final field experiments were conducted at the Tracy Power Plant (TPP) near Reno, Nevada. A feasibility study was conducted at the site in November 1983 and the Full Scale Plume Study (FSPS) took place in August 1984. The TPP is located in the Truckee River Valley and has a 91.4-meter stack. Nocturnal drainage winds were shown to routinely transport plumes toward the east. Mountain peaks rise to several times stack and expected plume heights in the down-valley wind direction. The site was chosen to test the concepts and preliminary models developed on the basis of findings from the two prior field experiment sites. The feasibility study conducted in 1983 was co-sponsored by EPA and the Electric Power Research Institute. ERT erected and instrumented the 150-m tower on site. Almost all of the planned tests for the FSPS were performed. The data collected showed that the TPP plume would interact with high terrain, especially near a bend in the valley, down-valley of the plant. The tracer gas release and measurement systems were shown to work well. An airborne lidar was added to the program and tested. Intermountain Film Productions conducted the photographic program under the direction of ERT. EMSI and TRC, Inc. provided the tracer gas sampling and on-site management, respectively, for the EPRI-sponsored efforts.

The FSPS conducted in August 1984 continued with the use of two tracer gases and extensive meteorological measurements. One-hour samples of ground-level tracer gas concentrations were collected at over 100 locations. Principal participants were ERT, NOAA/WPL, and NOAA ARLFRD. Meteorological Standards Institute provided external audits of instrumentation and Morrison-Knudsen collected the photographic data. SRI International, under sponsorship of the EPRI, made airborne lidar measurements. The design and results of the preliminary field study at TPP are described in ERT's Fourth Milestone Report. A full description of the final FSPS is provided in ERT's Fifth Milestone Report. A separate document (Eberhard, 1986) describes the NOAA Wave Propagation Laboratory's contributions to all of the CTMD field programs.

2.2.2 Field Program Results

The Modelers' Data Archives

Data collected at each of the field experiments were archived for use in the model development and evaluation phases of this program and for future use. Recognizing the difficulty others have had trying to utilize raw data from large field experiments, ERT also developed Modelers' Data Archives (MDA's) for each experiment. The MDA's are subsets of the complete data sets which are thought to be of most use to those involved in dispersion model development. The MDA's also contain the data in an organized format providing greatly increased ease-of-use. The MDA's for the CCB and HBR experiments are described in the Third and Fourth Milestone Reports, respectively. The MDA for the TPP experiment is described in a separate document (DiCristofaro, 1986). The MDA's have been made available to interested parties through EPA's Terrain Effects Branch.

The raw data have been collected in a series of computer files which are available on magnetic tape from the Terrain Effects Branch of EPA. Three reports documenting these files (Truppi and Holzworth,

1983; Truppi, 1985; and Truppi, 1986) have been prepared and are available. In addition, these data files have been transferred to a series of SAS™ data sets. They and a report describing them (Truppi, 1987) are also available from the Terrain Effects Branch.

Field Program Findings

The field programs provided basic data on ground-level concentrations as a function of source-hill geometries and meteorological conditions. In addition, the flow visualization through smoke releases and the photography program together with the lidar measurements and observer notes provided other information on the air flow dynamics encountered. Detailed descriptions of the findings are a main component of the Milestone Reports. The First and Second Milestone Reports discuss the findings of the CCB experiment. The Third and Fourth Milestone Reports discuss the results of the HBR experiment. The Fourth and Fifth Milestone Reports provide results from the FSPS.

A progression of understanding emerged from these experiments. Observations from CCB demonstrated the validity of the dividing streamline concept or critical height, H_c, in simulating the flow fields during stable atmospheric conditions. The critical height can be defined in terms of the meteorological measurements of the wind speed and temperature as a function of height. Tracers and smoke released directly upwind of the hill and above H_c were generally observed to flow up and over the hill, in accordance with theory. Plumes released below this height were generally observed to pass around to the side of the hill, also in accordance with theory. Maximum ground-level concentrations at CCB were most commonly associated with tracer gas releases near the calculated dividing-streamline height.

At HBR, the dividing streamline concept also was shown to be applicable, although the flow behavior below this height was different from that observed at CCB. In particular, at HBR, the lower portion of the flow was "blocked" behaving as a relatively stagnant flow with correspondingly low wind speeds. This occurs also in accordance with theoretical considerations as the two-dimensionality of the ridge shape offers only a very long path for the air to flow around to the side. The largest concentrations observed at HBR occurred for releases below H_c and the magnitude of the concentrations (normalized by release rate) were much larger than those observed at CCB, or subsequently at the FSPS. Smoke and tracers released above H_c were observed to flow over the ridge and resulted in peak concentrations near the top or on the lee side.

Observations from the FSPS at the Tracy site showed both kinds of behavior as well. There were portions of the flow which, when they encountered high terrain away from the river valley walls, became relatively stagnant as observed at HBR. Plumes embedded in down-valley flows and encountering terrain obstacles protruding from the valley side walls, on the other hand, exhibited an ability to lift

up and over the terrain or readily pass around the sides as seen at CCB. In each case, H_c for each hill proved to be a reliable parameter for differentiating between these two regimes. Peak concentrations at the FSPS were most often associated with releases near the calculated dividing streamline heights.

2.3 Fluid Modeling Program

An integral part of the CTMD program from the beginning was the efforts undertaken at EPA's Fluid Modeling Facility (FMF) at Research Triangle Park, NC. Theoretical aspects of the phenomena associated with interactions of stably-stratified atmospheric flow with terrain obstacles suggested that scaled-down, fluid modeling experiments could be used to investigate many of the fluid mechanical issues. The implications of the dividing streamline concept, in particular, were especially well-suited to the types of systematic investigations which could be undertaken with wind tunnels and with stratified towing tanks. Although the field experiments provide "real world," "ground truth" data on the relationship of ground-level concentrations to emission rates, the results are specific to the field study configuration and to the meteorological conditions encountered. Through fluid modeling, one can investigate in a systematic and reproducible manner, the effects of many geometric configuration or flow parameter changes which would be virtually impossible and prohibitively expensive through field experiments. A key justification for reliance upon the fluid modeling results is a demonstration that there is a correspondence between field measurements and a physical model simulation of the field measurements.

Experiments at the FMF included simulations with models of CCB and HBR and for conditions corresponding to some of the interesting field experiments. Verification of the dividing streamline concept was a central focus for experiments that included testing of the effects of changes in release height and terrain shape. Another series of experiments addressed the effects on maximum surface concentrations of sources of different heights being placed upwind and downwind of simply-shaped terrain obstacles. W. Snyder produced an independent report summarizing the above and other contributions of the FMF to the CTMD program. This report is self-standing and is included in its entirety as Appendix H to this document.

2.4 Model Design for Regulatory Use

The CTMD program has an ultimate goal of providing a dispersion model for routine use by the air pollution modeling community. CTDM is to fill the need for a refined model for complex terrain settings where terrain heights exceed the heights of the sources under review. This goal provided specific guidance to the form of the model development effort. First of all, the model had to be based upon experimental data relevant to the kinds of meteorological and topographical conditions of historic and expected future concern to EPA. It was anticipated that many of the future regulatory permitting requests would emerge from the Western USA. Past efforts had clearly

shown that conditions under nighttime stable meteorological conditions were the most constraining for compliance with the short-term (1-hour, 3-hour, or 24-hour) National Ambient Air Quality Standards (NAAQS) or Prevention of Significant Deterioration (PSD) increments. Demonstrations of compliance with NAAQS and PSD increments require that the very highest values expected from hour-by-hour sequential modeling up to five years of meteorological data be used. Practicality calls for the need for relatively cost-effective computer code for such demonstrations. In effect, this constrained the program from pursuing advanced numerical simulation techniques as a modeling method and supported the concept of advancing Gaussian plume modeling types of methods to meet the program's needs. There was also a concern that more advanced techniques might not display improved performance given the realities constraining meteorological measurement programs and inherent uncertainties associated with atmospheric turbulent flows. Another concept influencing the design of the dispersion model was that the model should be readily understood and explainable to others who are affected by the results of the model, but may have little background in theoretical fluid mechanics. From this perspective, an approach based more on analytical equations rather than on turbulence simulation methods was preferred.

More specifics on the model development plan are presented in the First and Second Milestone Reports. Subsequent Milestone Reports describe improvements made to the model in the course of its development. Section 3 describes the technical basis of the final version of the CTDM in detail. Separate user's manuals have been provided for those concerned with operating the model or the model preprocessors.

2.5 Model Evaluation Program

The model development program called for use of findings from the field experiments and the fluid modeling efforts in assisting with the theoretical development of equations for the CTDM. In essence, this took place in several stages. Initially, the confirmation of the dividing streamline concept from the results from CCB contributed to the development of separate models for addressing flows above and below H_c. A series of tests were made with these models and with models being used at the time by EPA in its regulatory practice. Results of these early comparisons are presented in the First Milestone Report. Subsequent model evaluation efforts focused also on case-study analyses of model predictions with observations for a large number of the hours at each of the field sites. Results of these analyses are presented in each of the subsequent Milestone Reports. A preliminary version of the model was completed in October 1985 and was provided to a number of interested groups for independent evaluation. Representatives of these groups convened at a workshop in February 1986 to share the results of experiences with the model. The results, especially those from some further fluid modeling tests, suggested that additional modifications be made to CTDM which would incorporate the growth of an internal boundary layer as the approach flow above H_c was influenced by the terrain.

Upon completion of a "final" model, the model evaluation effort focused on several existing data bases from SO_2 measurement programs near large point sources in complex terrain settings. This effort is described in Section 4 of this report and represents a "hands-off" evaluation of the CTDM along with several other dispersion models of regulatory interest. The results show CTDM to be superior to the other models in its ability to produce concentration estimates that are in better agreement with observations. In a broad sense, the model evaluation effort also included tests quantifying the sensitivity of the model predictions to changes in input parameters or conditions. Model performance is shown to decline when degraded meteorological data are used, as might be expected. The results of the sensitivity tests are presented in Sections 4 and 5 of this document.

SECTION 3

DESCRIPTION OF THE COMPLEX TERRAIN DISPERSION MODEL (CTDM)

This section provides a detailed description of CTDM, including its mathematical derivation. As an introduction to the model, sub-section 3.1 explains in qualitative terms how the Gaussian plume framework is modified to include the effects of terrain, and how the modifications differ from adjustments made for terrain in models presently used in regulatory applications. Sub-section 3.2 describes the meteorological and terrain variables needed by the model, and how these are obtained from the data provided by the meteorological and terrain preprocessors. Finally, sub-section 3.3 contains the derivation of the dispersion model formulations. Operational aspects of CTDM and its preprocessors are discussed by Mills et al. (1987), Paine (1987), and Paine et al. (1987).

3.1 Qualitative Overview

CTDM is a point-source Gaussian plume dispersion model designed to estimate hourly-averaged concentrations of plume material at receptors near an isolated hill or near a well-defined segment of an array of hills. The Gaussian plume model for simulating the dispersion of pollutants from a continuous point-source describes a plume by its average properties as a function of distance along the flow downwind of the point of release. The concentration of material in the plume is described by a Gaussian distribution in a plane perpendicular to the flow. The vertical distribution in this plane has a length scale denoted as sigma-z, and the lateral distribution has a scale denoted as sigma-y. Complete reflection of the plume at the ground assures that no plume material disappears from the atmosphere. The concentration of plume material at any point downwind of the source is determined by the size of the plume (sigma-y and sigma-z), the wind speed, the strength of the source, and the distance of the sampling point from the axis of the plume. For example, if the plume is narrow in the vertical (sigma-z is substantially less than the height of the axis of the plume), the peak concentration is found at the center of the plume. Sampling points away from the center would record smaller concentrations. Over level ground, peak ground-level concentrations are found when sigma-z is of the same order as the height of the plume.

When a hill is present, the changed flow alters the way in which plume material can reach the surface. Obviously, the path of the plume can change as the flow spreads over or around the hill so that there is a shift in the relative position of a receptor and the center of the plume. There are also mechanisms for changing the rate at which the material diffuses toward the surface, as well as allowing the center of the plume to impinge on the surface of the hill. These mechanisms are generally responsible for increasing peak

concentrations expected on terrain beyond those concentrations that would have been expected for the same meteorological conditions on level terrain.

In the absence of stratification, all streamlines in the flow pass over a hill. The centerline of a plume in this flow follows the streamline that passes through the source of that plume. As the plume grows in the vertical and horizontal directions (in the plane perpendicular to the flow), plume material diffuses across adjacent streamlines, eventually reaching the set of streamlines that marks the surface of the terrain. Distortions in the flow which are induced by the hill change the position and relative spacing of the streamlines from their initial distribution over level terrain, and therefore change the shape of the plume as it passes over the hill. Ground-level concentrations (GLC's) of plume material also change, and this happens in two ways. The first and most obvious change in the GLC's is the shift in the distribution on the surface of the hill, arising from the change in the shape of the plume. Typically, the plume stretches in the horizontal as it passes over the crest of a simple three-dimensional hill and this stretching produces a wider footprint over the hill. The second change in the GLC's is the change in magnitude, arising from the effect of the distortion on the rate of diffusion of plume material across streamlines. Typically, spacing between streamlines is reduced in the vertical and expanded in the horizontal, while the speed of the flow increases over the crest. These changes tend to increase the diffusion in the vertical and reduce it somewhat in the horizontal, thereby altering the magnitude of the GLC's on the hill. If the diffusion were not altered by the distortion in the flow, the peak GLC would not change from that obtained on level terrain.

The nature of the flow changes dramatically when the flow is very stably stratified. A two-layer structure develops in which the flow in the lower layer primarily deflects around the hill, while the flow in the upper layer travels over the top of the hill. A critical height H_c defines the boundary of these two layers in CTDM. This concept was suggested by theoretical arguments of Drazin (1961) and Sheppard (1956) and was demonstrated through laboratory experiments by Riley et al. (1976), Brighton (1978), Hunt and Snyder (1980), Snyder et al. (1980), and Snyder and Hunt (1984). In the layer above H_c, the approach flow has sufficient kinetic energy to transport a fluid parcel up and over the hill against the density gradient of the ambient stratification. In the layer below H_c, the approach flow has insufficient kinetic energy to push the parcel over the hill, so that the flow below H_c is restricted to lie in a nearly horizontal plane, allowing little motion in the vertical. Consequently, plume material below H_c travels along and around the terrain rather than over it.

Above H_c, the flow is similar to that just described above although the degree of distortion depends on the stratification. Below H_c, the flow is approximated as an ideal, steady, two-dimensional flow. Within this flow, only one streamline at each elevation touches and follows the surface of a hill, and is referred to as the stagnation streamline. Plume material reaches the surface of the hill only if it reaches the stagnation streamline. If the

plume centerline lies along the stagnation streamline and if it also lies below H_c, the center of the plume impinges on the hill. But if it lies to one side of the stagnation streamline, the centerline will pass to one side of the hill.

The position of H_c and the stagnation streamline relative to the centerline of the plume dominates the degree to which a hill in stratified flow is able to alter the peak ground-level concentration obtained in the absence of the hill. Figure 1 illustrates this. In the model, the H_c surface slices the plume into two pieces as the hill is encountered. Plume material now residing below H_c is sliced once again by the stagnation streamline. Concentrations on the surface of the hill above H_c are determined by the cut made by the H_c surface because this now coincides with the bottom of the plume, which is in contact with the surface of the hill. Concentrations on the surface of the hill below H_c are determined by the cut made by the plane of the stagnation streamlines because this cut coincides with the sides of the plume segments that are in contact with the surface of the hill. As illustrated, receptors on the hill record concentrations that are much nearer the center of the plume than do receptors in the absence of the hill. Figures 2 and 3 provide further insight into how the plume is modeled in CTDM.

Figure 2 addresses plume material above H_c. The upper portion illustrates what the plume may actually look like in vertical cross-section as it travels along the surface. Material below H_c is removed at s_o, and the remaining material is distorted in the flow and reflected from the surface of the hill. The size of the plume in the vertical at s depends on the amount of distortion in the shape of the plume as well as the amount of additional growth of the plume caused by changes to the rate of diffusion. The lower portion of Figure 2 illustrates how the model actually treats the plume. Reflection of plume material from the surface z=0 is allowed from the source to s_o, and reflection of plume material above H_c is allowed from the surface $z=H_c$ beyond s_o. Furthermore, the distortion in the flow (and the plume) beyond s_o is scaled out, leaving only the effect of the distortion on the diffusivity in what is termed the effective sigma-z (σ_{ze}). As illustrated, σ_{ze} exceeds σ_z, the plume size in the absence of the hill, because the diffusion in the vertical across streamlines is increased by the contraction in the vertical spacing of the streamlines.

Figure 3 addresses plume material below H_c. The diagram on the left illustrates the plume in horizontal cross- section as it splits and flows around a hill. In this case, plume material has crossed the stagnation streamline before the hill is encountered, so plume material is found on both sides of the hill. Once the plume wraps around the leading edge of the hill, the stagnation streamline (which forms the boundary of the hill) becomes a reflecting surface in addition to the plane z=0, and material cannot diffuse from the segment of the plume on one side of the hill to the segment on the other side of the hill. The diagram on the right side of Figure 3 illustrates how the model treats this flow. The actual surface of the hill is replaced by a line in the plume which corresponds to the

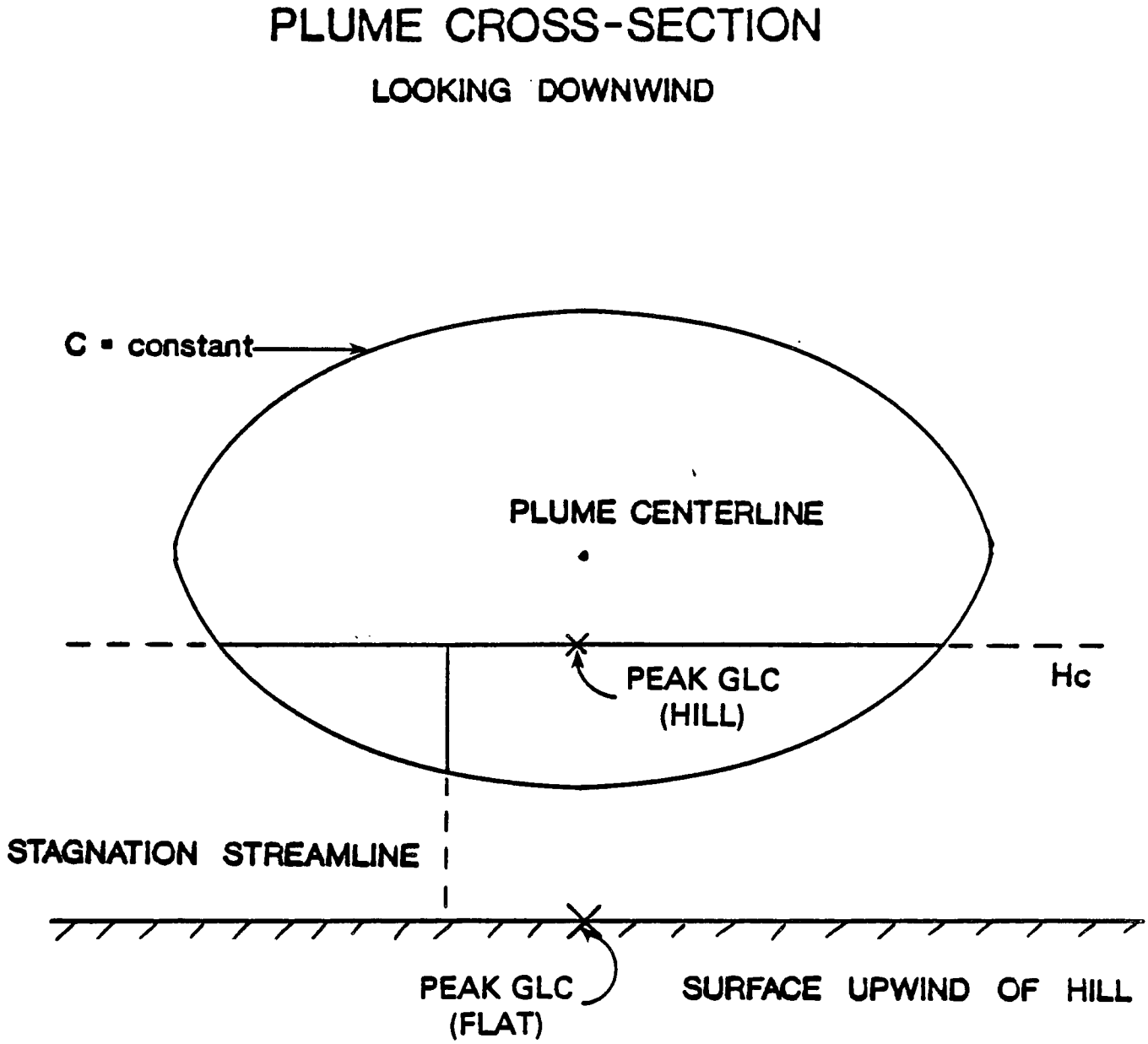

Figure 1. Idealized picture of how the dividing-streamline (H_c) plane and the plane of stagnation streamlines "cut" into a plume, allowing material nearer the center of a plume to contact the surface of a hill.

8708098

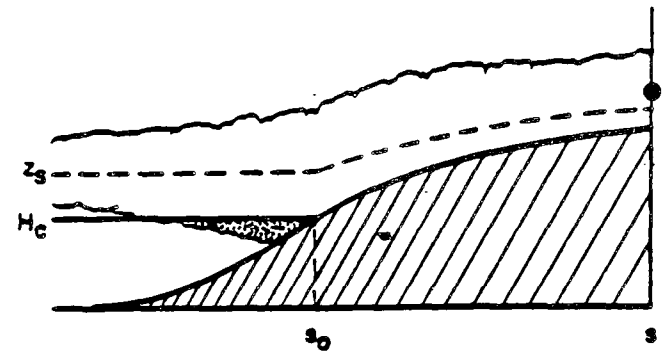

PHYSICAL PICTURE: material above H_c rides up and over hill in a distorted flow. Material below H_c passes round the side.

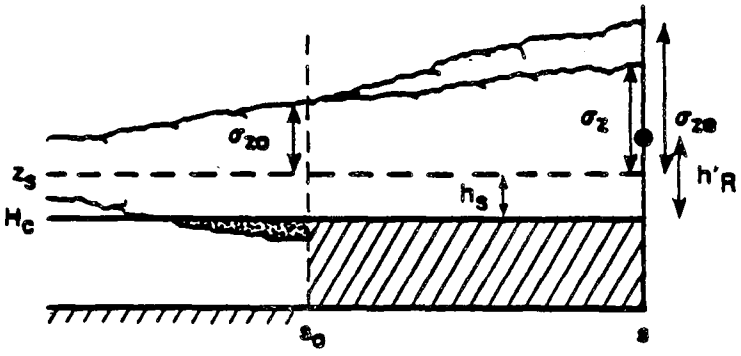

LIFT CALCULATION: net effect of flow distortion is to increase the effective rate of plume growth (σ_{ze}) over that in the absence of the hill (σ_z)

Figure 2. Illustration of terrain effect on the vertical distribution of plume material above H_c as modeled in LIFT.

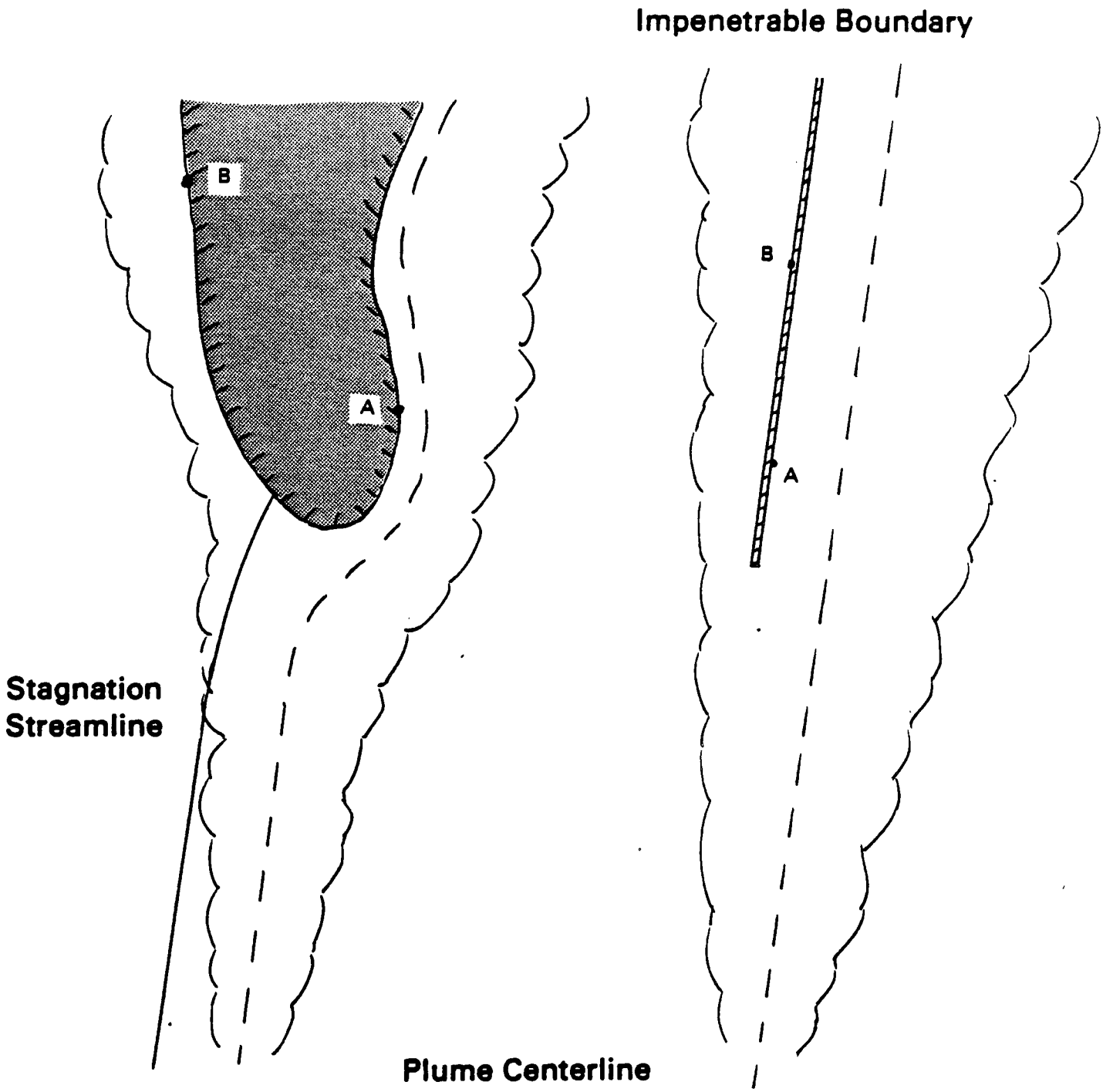

Figure 3. Depiction of plume behavior in CTDM as it is deflected around a hill as seen from above: the stagnation streamline in the left figure separates flow going around the right and left sides of the hill. In CTDM, the hill is treated as being collapsed into an impenetrable wall that separates the flow and plume material going on either side of the hill, with an effective crosswind distance and σ_y.

8708101

stagnation streamline cut in Figure 1. All distortion is scaled out as was done for the flow above H_c, but the effect of the distortion on lateral diffusion is ignored as a second order effect. The lateral position of all receptors below H_c essentially collapses onto the stagnation streamline, as depicted by the points labeled A and B, so that each is the same distance from the plume centerline. However, concentrations along one side of the line differ from those on the other side because diffusion through the line is not allowed.

Adjusting receptor positions while keeping the trajectory of the plume a straight line simplifies the mathematics of CTDM a great deal. Rather than keeping track of the actual boundary of a hill and the deformed trajectory of each of the segments of the plume as in the left portion of Figure 3, concentrations are computed at receptor points A and B for a plume geometry like that of the right portion of Figure 3, which is only slightly more complicated than that for flat terrain. A similar adjustment of receptor positions is employed for receptors above H_c, as illustrated in Figure 4. The upper portion of the figure shows how a plume in the flow above H_c distorts over a hill as viewed from above. Three streamlines are marked, the centerline of the plume, and streamlines passing through receptors A and B. When the deflection of each streamline is removed, and the distortion in the plume is scaled out, an equivalent plume-receptor geometry is obtained, as illustrated in the lower portion of the figure.

Many of the concepts contained in CTDM are not present in complex terrain screening models currently in use for regulatory assessments. Partitioning of plume material about H_c in the vertical and about the stagnation streamline in the horizontal is unique to CTDM. This partitioning is fundamental to describing the transport of plume material in the flow field around hills. Furthermore, the treatment of the effect of the hill on the dispersion process for material above H_c avoids the use of the plume height correction factor found in other models. This factor is typically applied as a function of stability and receptor height only, and it leads to an inconsistent treatment of reflection of plume material from the lower boundary. Essentially, the height of the plume above the ground is constant all of the way from the source to a receptor, but this height varies from receptor to receptor. Hence, adjacent receptors at unequal terrain elevations are modeled with two very different plumes. If an impingement computation is invoked, this treatment produces a concentration equal to twice that at the center of the plume in the absence of terrain. In CTDM, the impingement concentration is equal to that at the center of the plume.

The method used to specify the rate of plume growth also differs from the other models. Both σ_y and σ_z functions depend on the turbulence intensity, rather than stability class. In the case of σ_z, the function describing the rate of growth with time also depends on the scale of the mixing processes, which depends on the elevation of the plume above the surface, and on the stratification and turbulence near this elevation. In contrast, the other models incorporate a fixed rate-of-growth function for each stability class, and do not contain the influence of processes at plume height.

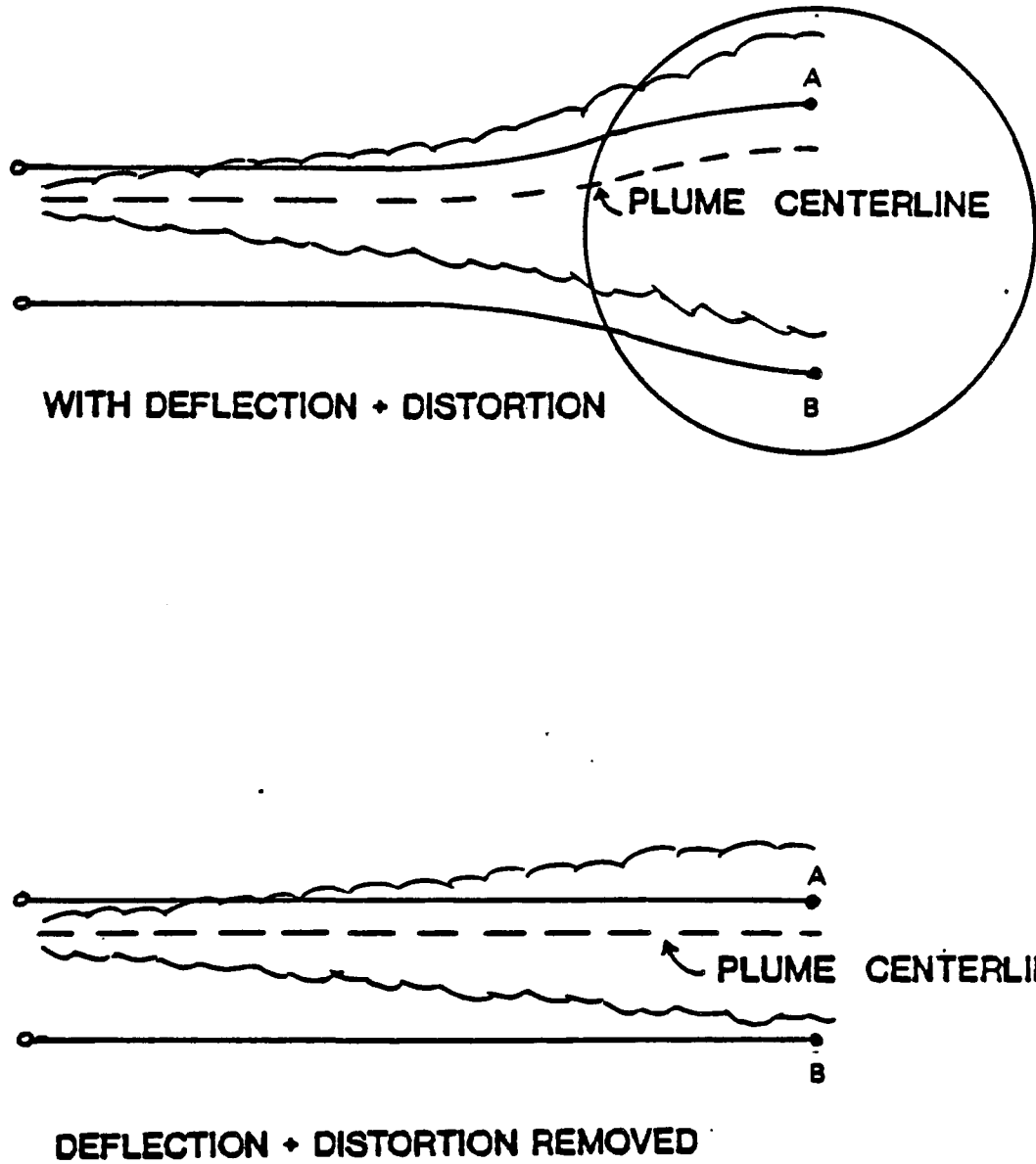

Figure 4. Depiction of plume behavior in CTDM as it passes over a hill as seen from above: upper figure shows actual deflection and distortion of the plume, bottom figure shows treatment within CTDM with source-receptor spacing equal to spacing between streamlines upwind of hill and appropriate adjustment of effective σ_y.

8706103

3.2 Use of Meteorological and Terrain Information

The preprocessors for meteorological data and terrain data provide CTDM with the information needed to compute concentrations, but several assumptions are made within the model to convert this information into specific variables used in the computations. This subsection describes those assumptions.

3.2.1 Meteorological Data

The meteorological preprocessor provides CTDM with meteorological data at several heights above the ground (corresponding to measurement heights), and it also provides CTDM with surface boundary layer parameters which allow the model to compute profiles of wind, temperature, and turbulence within the surface layer, when needed. Whenever CTDM needs meteorological data at a certain elevation, linear interpolation between measurement levels is employed. If the elevation exceeds the uppermost measurement level, the measurements at the uppermost level are used if this height is above the mixing height; otherwise the value at the uppermost height is scaled upward.

The most extensive use of the profile data is made in the course of computing the dividing streamline height H_c and the Froude number for the flow above H_c. H_c is computed for each hill by locating the lowest height at which the kinetic energy of the approach flow just balances the potential energy attained in elevating a fluid parcel from this height to the top of the hill. The statement that defines this balance is:

$$\frac{1}{2} u^2(H_c) = \int_{H_c}^{H} N^2(z)(H-z)\, dz \qquad (1)$$

where $u(H_c)$ is the wind speed at $z = H_c$, H is the elevation of the top of the hill, and $N(z)$ is the Brunt-Vaisala frequency at height z. In practice, the value of H_c is obtained by rewriting the integral on the right-hand side (RHS) of Equation 1 as a series of sums over layers of constant N. For each layer, say the i^{th} layer,

$$RHS_i = \int_{z_{i-1}}^{z_i} N_i^2 (H-z)dz = N_i^2 (H-z_{mi}) (z_i - z_{i-1}). \qquad (2)$$

where z_{mi} denotes the mean height of the layer, $0.5 (z_i + z_{i-1})$. The layer that contains H_c is found by comparing the LHS of Equation 1 at each measurement height with the accumulated RHS_i for all of the layers between that measurement height and the top of the hill. If the LHS exceeds the accumulated RHS_i, then H_c must lie below that measurement level, and so the process is repeated until the lowest level is found for which the LHS becomes less than the RHS. This then identifies the layer that contains H_c.

H_c is computed within this layer by assuming that the wind speed follows a linear profile. Denote this as layer j, where the elevations at the top and bottom of the layer are z_j and z_{j-1}, respectively. Denote u(z) in the layer as

$$u(z) = a_j + b_j z$$

then equation 1 becomes

$$\frac{1}{2}(a_j + b_j H_c)^2 = N_j^2 (H - 1/2[z_j + H_c])(z_j - H_c) + \Sigma RHS_i \qquad (3)$$

where the last term, ΣRHS_i, denotes a sum of the RHS_i of all layers between z_j and the top of the hill. Equation 3 is quadratic in H_c, and is readily solved for H_c.

Once H_c is computed for a hill, the Froude number above H_c is computed as

$$Fr = \frac{u_m / N_m}{H - H_c} \qquad (4)$$

where u_m and N_m are average values over a layer of depth 1.5 $(H-H_c)$, above H_c. This Froude number characterizes the degree of stratification of the flow above H_c. Note that N_m is computed from the temperature difference across the layer.

The wind speed shear in the flow above H_c is computed between the plume height and H_c. However, if the plume height less H_c is less than one tenth of the hill height, the shear is computed between the top of the hill and H_c. This wind speed shear is used in computing the flow over the hill (see Section 3.3.6).

3.2.2 Terrain Data

The terrain preprocessor provides CTDM with the location, size, shape, and orientation of each hill or segment of a hill identified by the user. This information is tabulated as a series of ellipses which make up a family of horizontal cross-sections of the hill, and a series of variables describing inverse polynomial (bell-shaped) profiles which approximate the portion of the hill above each of the ellipses.

For non-zero H_c, CTDM uses an ellipse to characterize the shape of the hill below H_c. The ellipse used for plume material below H_c is found at the minimum of H_c and the height of the plume. The center of this ellipse, its orientation, and the axis lengths are obtained by linear interpolation between the ellipses provided by the preprocessor at elevations above and below the target elevation.

Above H_c, CTDM uses the orientation, height, and length scales of the inverse polynomial shape used to approximate the portion of the hill that lies above the elevation of H_c. However, the current version of CTDM assumes a Gaussian shape in the formulation of the flow algorithm rather than the inverse polynomial function. To convert from the inverse polynomial description to the Gaussian description, the length scale used in the former shape is divided by $\sqrt{.75}$ to convert it to the length scale of the Gaussian shape.

This factor had actually been derived to convert from an inverse polynomial shape to an equivalent elliptical shape used in an earlier version of the model. The length scale in the inverse polynomial description is the half-length of the hill at one-half of the height of the hill. By demanding that the equivalent ellipse shape coincide with this profile at the top of the hill and at the point at half of the height (See Figure 5), the length of the axis of the ellipse is found to be equal to the length scale at half of the height divided by $\sqrt{.75}$. For the Gaussian profile, the length scale is half the length of the hill at an elevation of 1/e of the height of the hill. This length scale is approximately 4% less than the axis length of the ellipse (conversion factor = $\sqrt{.693}$), so the earlier conversion factor was retained.

3.3 Derivation of Concentration Equations

3.3.1 Plume Rise Calculations

Momentum Rise

Momentum rise is used only if the plume rise due to buoyancy flux is zero (stack temperature not greater than ambient). The following formulas are used (Briggs, 1975) for momentum rise:

$$\text{neutral/unstable } \Delta h = 3\, d w_s / u_s \tag{5}$$

$$\text{stable} \quad \Delta h = 1.5 \left(\frac{w_s^2\, d^2\, T_a}{4 T_s\, u_s} \right)^{1/3} s^{-1/6} \tag{6}$$

where d = stack diameter
w_s = stack gas exit velocity
u_s = stack top wind speed
T_a = ambient temperature
T_s = stack gas temperature
$s = N^2 = (g/T_a)\ (d\theta/dz)$.

If $L > 0$ (stable), the minimum plume rise from equation (5) and (6) is used.

An iterative technique is used for calculating buoyancy rise, since the plume rise is assumed to be a function of the wind speed and temperature gradient at a height halfway between the stack top and

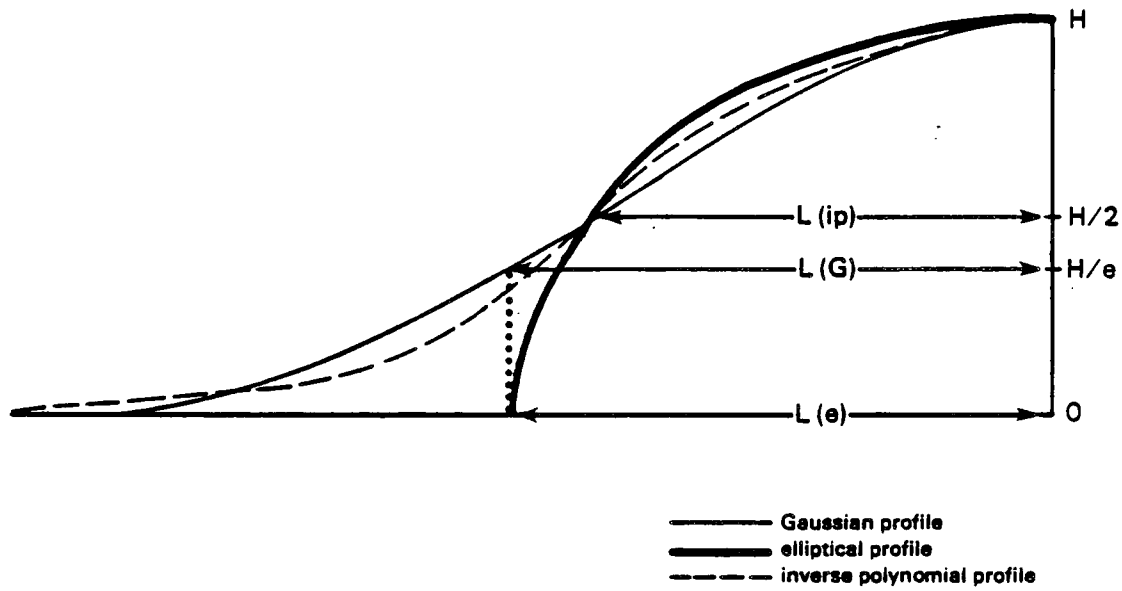

Figure 5. Relationship among length scales used to specify inverse polynomial (ip), Gaussian (G), and elliptical (e) profiles Note that the equivalence of L(G) and L(e) is approximate.

8710007

final plume height. For some plume rise formulas, this method does not converge for certain profiles of wind speed and/or $d\theta/dz$. Therefore iteration is stopped after five tries at convergence (defined by less than 1% change between successive iterations). After each iteration (and the fifth one, if no convergence), the plume rise guess for the next iteration (or the final rise, if no convergence) is the average of the plume rise estimate for the previous two iterations.

Neutral/Unstable Buoyant Final Rise

These formulas from Briggs (1975) apply for plumes within the mixed layer:

Final transitional rise: $\Delta h = 1.6\ (F x_f^2)^{1/3}/u$ (7a)

where $x_f = 119\ F^{2/5}$ for $F > 55 m^4\ s^{-3}$ and (7b)

$x_f = 49\ F^{5/8}$ for $F \leq 55 m^4\ s^{-3}$ (7c)

Unstable breakup rise: $\Delta h = 4.3\ (F/u)^{3/5} H^{-2/5}$ (8)

Touchdown plume rise: $$\Delta h = 1.0 \frac{F}{u w_d^2} \left(1 + \frac{2h_s}{\Delta h}\right)^2 \quad (9)$$

Neutral breakup rise: $$\Delta h = 1.3 \frac{F}{u u_*^2} \left(1 + \frac{h_s}{\Delta h}\right)^2 \quad (10)$$

where u = wind speed at height $h_s + \Delta h/2$,
F = buoyancy flux, $0.25\ w_s d^2 g\ (T_s - T_a)/T_s$,
$H = -u_*^3/(0.4L)$ is the surface heat flux,
$w_d = 0.4\ w_*$.

The final neutral/unstable plume rise is the minimum of Equations 7 through 10.

Neutral/Stable Buoyant Final Rise

There are several final plume rise formulas available for stable conditions, depending on whether winds are nearly calm or not, and depending on whether conditions are close to neutrality. The final neutral/stable rise that is used in CTDM is the minimum of those calculated by means of Equations 7, 10, and the following equations (11 and 12):

Neutral high wind rise:

$$Wh = 1.54\ [F/(u u_*^2)]^{2/3} h_s^{1/3} \quad (11)$$

Bent-over stable: $\Delta h = 2.6\ (F/(us))^{1/3})$ (12a)

Calm stable: $$\Delta h = 4\ F^{1/4}\ s^{-3/8} \qquad (12b)$$

In stable conditions, the distance to final rise, x_f, is given by

$$x_f = 2.07\ u\ s^{-1/2}. \qquad (12c)$$

3.3.2 Dispersion Parameters

Derivation of σ_z

The formulation for σ_z is described in Venkatram et al. (1984). It is based on the form of Taylor's (1921) theorem of diffusion for very short and very long times of travel:

$$\sigma_z = \sigma_w t \qquad ; t<<T_L \qquad (13a)$$

$$\sigma_z = (2K_z t)^{1/2} \qquad ; t>>T_L \qquad (13b)$$

where σ_w is the standard deviation of the vertical velocity fluctuations, t is the travel-time, T_L is the Lagrangian time-scale, and K_z is the eddy diffusivity. Using mixing-length arguments, K_z is defined as

$$K_z = \sigma_w\ \ell \qquad ; \ell = \sigma_w T_L \qquad (14)$$

so that in the limit $t>>T_L$, Equation 13b becomes

$$\sigma_z = \sigma_w\ (2t\ T_L)^{1/2}. \qquad (15)$$

An interpolation formula used by other authors (Deardorff and Willis, 1975) is employed to span the gap between small and large times of travel:

$$\sigma_z = \sigma_w\ t/(1 + t/2T_L)^{1/2}. \qquad (16)$$

In Equation 16, σ_w is measured directly, but T_L must be related to other measurements before σ_z can be calculated in the model. This is accomplished by using the empirical flux-profile relationships of surface similarity theory (Businger, 1973) to estimate the mixing length, ℓ. The derivation relies on the appropriateness of surface similarity theory and on the assumption that σ_w is proportional to the friction velocity, u_*. If σ_w is due mainly to turbulent fluctuations, then the formulation is appropriate.

Assume that passive material diffuses in the same way as heat in a turbulent flow so that $K_z = K_H$, and

$$K_z = \frac{u_* kz}{\varphi_h} \simeq \frac{\sigma_w kz}{a\varphi_h} \tag{17}$$

where k is the von Karman constant, φ_h is the non-dimensional potential temperature gradient, and a is the constant of proportionality between σ_w and u_* applicable to the stable boundary layer:

$$\sigma_w \simeq a\, u_* . \tag{18}$$

From Equation 14, the length scale, ℓ, can be written as

$$\ell = \frac{K_z}{\sigma_w} = \frac{kz}{a\varphi_h} = \frac{kz}{a(\alpha+\beta z/L)} \tag{19}$$

where α and β are parameters in the surface similarity profiles, and L is the Monin-Obukhov length. The quotient z/L is related to the gradient Richardson number (Ri), and hence to N/σ_w, where N is the Brunt-Vaisala frequency. By assuming once again that $\sigma_w = au_*$,

$$\frac{z}{L} = \frac{\varphi_m^2}{\varphi_h} Ri = \left(\frac{Nkaz}{\sigma_w}\right)^2 / \varphi_h \tag{20}$$

and noting that $\varphi_h = (\alpha + \beta z/L)$, Equation 20 can be solved for z/L:

$$\frac{z}{L} = \frac{1}{2}\frac{\alpha}{\beta}\left[1 + \beta(2Nkaz/\alpha\sigma_w)^2\right]^{1/2} - 1 . \tag{21}$$

By introducing two new constants γ and Γ whose role will become clear shortly, the length scale, ℓ, in Equation 19 can be expressed as

$$\frac{1}{\ell} = \frac{1}{2\Gamma z} + \left[\left(\frac{1}{2\Gamma z}\right)^2 + \left(\frac{N}{\gamma^2 \sigma_w}\right)^2\right]^{1/2} \tag{22}$$

where

$$\gamma^2 = 1/(a^2\sqrt{\beta})$$
$$\Gamma = k/(a\alpha). \tag{23}$$

Equation 22 has two distinct limiting forms. When z is very large, for non-zero N, stratification dominates the scale of the mixing process and

$$\ell = \gamma^2 \sigma_w / N = \ell_s. \tag{24}$$

When N is nearly zero and z is finite, the length scale for the mixing process is proportional to height above the surface

$$\ell = \Gamma z = \ell_n. \tag{25}$$

The quantities ℓ_s and ℓ_n are introduced to distinguish the mixing lengths for the stable and neutral limits.

Equation 24 states that the length scale for turbulent mixing in the stable limit is proportional to σ_w/N, where γ^2 is the constant of proportionality. This is consistent with the notion that a fluid element in this limit must overcome a stable potential temperature gradient in order to be displaced vertically. Given that the velocity scale for vertical dispersion is σ_w, the length scale that naturally follows is proportional to σ_w/N. In the neutral limit, the size of the turbulent eddies is restricted by the height above the surface, so that the mixing length should be proportional to z, where Γ is the constant of proportionality. Note that

$$\begin{aligned} \gamma &= .52 \\ \Gamma &= .36 \end{aligned} \tag{26}$$

for the choices $\beta = 4.7$, $a = 1.3$, and $k = .35$.

Equation 22 may be viewed as in weighting function for ℓ between the limits ℓ_s and ℓ_n. A simpler weighting function is actually used in CTDM:

$$\frac{1}{\ell} = \frac{1}{\ell_n} + \frac{1}{\ell_s}. \tag{27}$$

It produces values of ℓ which are within 20% of those produced by Equation 22. With this expression for ℓ, T_L is computed as ℓ/σ_w (Equation 14). and σ_z is computed from Equation 16 as a function of the time-of-travel, including source effects.

Derivation of σ_y

An equation similar to that used for σ_z is used to compute σ_y as a function of the time of travel and the turbulence velocity scale for lateral fluctuations, σ_v:

$$\sigma_y = \sigma_v t/(1 + t/2T_L')^{1/2}. \tag{28}$$

The departure of this expression from that for σ_z arises in specifying the functional form of T_L', which is the Lagrangian time-scale of the transverse correlogram. In this case, T_L' cannot be derived from measurements of the mean flow and its statistics.

Attempts were made to relate T_L' to the difference among the statistics of lateral fluctuations over periods of five minutes and those for periods of one hour, but these types of data are typically not available for routine applications of CTDM. Because no clear improvement in the performance of the model could be associated with the use of these data in a formulation of T_L', that formulation was not incorporated in CTDM.

Instead, T_L' is set equal to the time-of-travel required to cover a distance of 10 km. This choice reduces σ_y by about 18% from the value that would be obtained using a linear growth law at a distance of 10 km. All of the CTMD field experiments included sampler locations within 10 km of the source, so that the growth in σ_y beyond 10 km was not documented. Nearly linear growth in σ_y over the first 5 km was typical of many of the experiments, and the recommendation of the workshop participants was to use a linear growth law. The use of the 10 km length scale is meant to underscore the uncertainty of using linear growth beyond 10 km, while allowing nearly linear growth within 5 km of the source. Note that the scale used by Briggs (1973) for dispersion in open country corresponds to 5 km, which would reduce σ_y at 10 km by about 29%.

In summary, the following equations are used to calculate the plume spread parameters σ_z and σ_y:

$$\sigma_z = \frac{\sigma_w t}{[1 + \sigma_w t(\frac{1}{.72\ z}) + \frac{N}{.54\ \sigma_w}]^{1/2}} \tag{29a}$$

$$\sigma_y = \frac{\sigma_v t}{[1 + ut/20{,}000]^{1/2}}. \tag{29b}$$

Allowance for Source-Induced Effects

A virtual time of travel is introduced to account for increases in σ_y and σ_z caused by how the plume is released into the atmosphere. For buoyant releases, the initial growth during plume rise is characteristically much greater than the growth caused by ambient turbulence alone. Therefore, once the plume reaches its equilibrium height and ambient turbulence becomes dominant, the plume evolves as if it had experienced a greater time of travel.

Write the general form for σ_z or σ_y as:

$$\sigma_\ell = \sigma t/(1 + t/2T_L)^{1/2} \tag{30}$$

and solve for t:

$$t = \frac{1 + \left[1 + 4\left(\frac{2T_L\,\sigma}{\sigma_\ell}\right)^2\right]^{1/2}}{T_L\left(\frac{2\sigma}{\sigma_\ell}\right)^2} \quad . \tag{31}$$

The virtual time of travel (t_v) is found by setting σ_ℓ equal to the plume size caused by source-induced effects ($\sigma_{\ell s}$) and setting t equal to $t_s + t_v$, where t_s is the time-of-travel to the point where ambient turbulence dominates source-induced turbulence:

$$t_v = -t_s + \frac{1 + \left[1 + 4\left(\frac{2T_L\sigma}{\sigma_{\ell s}}\right)^2\right]^{1/2}}{T_L\left(\frac{2\sigma}{\sigma_{\ell s}}\right)^2} \quad . \tag{32}$$

As implemented, $\sigma_{\ell s}$ is just the size of the plume resulting from buoyant rise (buoyancy-enhanced dispersion):

$$\sigma_{\ell s} = \sigma_{\ell b} = \Delta h/3.5 \tag{33}$$

where Δh is the plume rise. Similarly, t_s is the time-of-travel to final rise (see Section 3.3.1). Ambient turbulence is assumed to dominate source-induced turbulence quickly during neutral and unstable conditions, so that t_s is set to zero for these conditions. Depending on the relative values of σ (ambient turbulence) and $\sigma_{\ell s}$ for the time t_s, t_v can become negative in Equation 32. Physically, this indicates that the growth of the plume due to ambient turbulence exceeds that due to source effects. In the case of σ_y, this frequently happens when meandering is great. Consequently, t_v is never allowed to be less than zero, so that buoyancy enhancement is active only when it exceeds the growth rate due to the ambient turbulence. In fact, t_v is always greater than zero, as it is given a minimum that corresponds to the time it takes the plume to grow to the radius of the stack. Once t_v is calculated for both the lateral and vertical scale of the plume, it is added to the actual time of travel in Equations 16 and 28.

3.3.3 The LIFT Component

The flow above H_c is considered to be weakly stratified. That is, the stratification is strong enough to influence the flow pattern (e.g., lee waves), but not strong enough to inhibit significant vertical motion. To simplify the modeling task, H_c is assumed to be a level surface, and the flow above H_c is only affected by that portion of the hill that lies above H_c.

The plume is allowed to develop as if the terrain were perfectly flat until it reaches the point where its trajectory crosses the height contour equal to H_c in elevation (say, at a distance s_o

from the source, see Figure 2). If H_c is zero, then this zone extends from the source to the base of the hill, although it conceptually could extend to any point where the hill is thought to exert a significant influence on the flow. Beyond s_o, the plume material below H_c is disregarded by the LIFT component, and the evolution of the remaining material is modeled as if the terrain were flat, and the lower boundary were H_c (with full reflection). However, the rate of plume spread and the position of the plume centerline relative to the receptor are modified to reflect the net alternation of these properties between s_o and s (where s is the distance from the source to the receptor) induced by the presence of the hill. The simplicity of the Gaussian plume solution is retained in this way, while the full dilution of the plume from the source to the hill (s_o) as well as the effects of the hill on both flow and dispersion beyond s_o are explicitly incorporated.

The terrain effect as modeled in LIFT includes re-initializing the flow at a distance s_o downwind of the release. This re-initialization can be illustrated first for flat terrain and uniform flow. The concentration at a receptor downwind of s_o is composed of contributions from the entire concentration distribution at s_o. Conceptually, the flux of plume material through the plane $x = x_s + s_o$ (note that the x-axis lies along the flow direction, and the plume is released at x_s, y_s, z_s) can be thought of as a distribution of point sources. If we track the plume material in terms of the distance downwind of the source, $s = x - x_s$, then the source strength of one of these point source elements located at the point (s_o, y, z) is given by:

$$dQ(s_o, y, z) = C(s_o, y, z)\, u\, dy\, dz. \tag{34}$$

Because the flow beyond s_o is considered to be uniform, the influence of each of these sources follows the Gaussian plume solution to the advective diffusion equation so that the contribution of the source element at the point (s_o, y, z) to the concentration at the point (s, ℓ, h) is:

$$dC(s,\ell,h;s_o) = \frac{dQ(s_o,y,z)}{2\pi\sigma_y^*\sigma_z^* u}\, e^{-0.5\left(\frac{y-\ell}{\sigma_y^*}\right)^2} \left[e^{-0.5\left(\frac{z-h}{\sigma_z^*}\right)^2} + e^{-0.5\left(\frac{z+h}{\sigma_z^*}\right)^2}\right] \tag{35}$$

where σ_y^*, σ_z^* denote the plume spread statistics for each point source element over the interval $s - s_o$ (see Figure 6). The total concentration at (s,ℓ,h) is found by integrating Equation 35 over all point source elements, so that

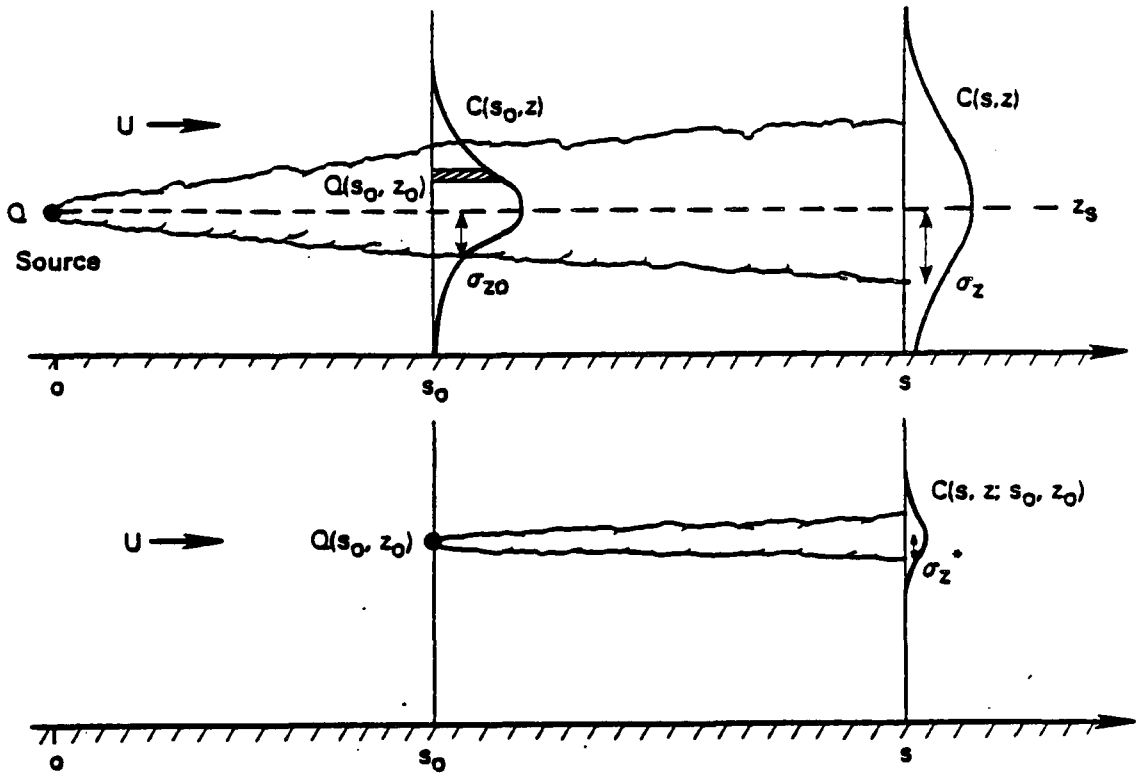

$$C(s, z) = \int_0^\infty C(s, z; s_o, z_o) dz_o$$

where $\sigma_z^{*2} = \sigma_z^2 - \sigma_{zo}^2$

Figure 6. Illustration of the relationship between the crosswind-average concentration profiles at s_o and s, and the plume from one of many point-source elements representing the flux of material across the plane at s_o. The total concentration at a particular point C(s,z) is constructed by summing the contribution $C(s,z; s_o,z_o)$ from each point-source element $Q(s_o,z_o)$.

$$C(s,\ell,h;s_o) = \int_0^{\infty} \int_{-\infty}^{+\infty} \frac{C(s_o,y,z)}{2\pi\sigma_y^*\sigma_z^*} e^{-0.5(\frac{y-\ell}{\sigma_y^*})^2} [e^{-0.5\ (\frac{z-h}{\sigma_z^*})^2} +$$

$$e^{-0.5(\frac{z+h}{\sigma_z^*})^2}] \, dy \, dz. \qquad (36)$$

The plume spread statistics σ_y^* and σ_z^* for the interval $s-s_o$ are specified by the requirement that Equation 36 for flat terrain reduces to the expression obtained for the original point source located at $s = 0$ (i.e., Equation 35 with $s_o = 0$ and $\sigma^* = \sigma(s)$). Equating these two expressions for C, with $h = 0$, we obtain

$$\sigma_z^{*2} = \sigma_z^2(s) - \sigma_z^2(s_o) \equiv \sigma_z^2 - \sigma_{zo}^2 \qquad (37a)$$

$$\sigma_y^{*2} = \sigma_y^2(s) - \sigma_y^2(\sigma_o) \equiv \sigma_y^2 - \sigma_{yo}^2. \qquad (37b)$$

Equations 36 and 37 illustrate the re-initialization technique for the limiting case of flat terrain and uniform flow. Overcamp (1983) has developed a similar technique for replacing a simple image source in a general treatment of the lower boundary condition for the case of non-Fickian diffusion.

Terrain influences are incorporated by altering the rate of diffusion within the interval $s-s_o$, and by changing the position of the receptor relative to the centerline of the deflected plume. Furthermore, because no plume material below H_c travels over the hill and because H_c defines the lower boundary over the hill beyond s_o (see Figure 3), the integration in the vertical in Equation 36 is performed over the domain $z=H_c$ to $z=\infty$ and material from each point source element is reflected from the boundary $z=H_c$ rather than $z=0$.

Denote the receptor height above ground relative to the terrain-altered plume as h_R' (see the lower part of Figure 2) and its lateral position relative to the terrain-altered plume centerline as y_R'. Further denote the height of a point source element above the ground at s_o as $h_s + H_c$, and the altered growth rates of the plume as $\sigma_z^{*'}$ and $\sigma_y^{*'}$. Then the contribution of the element at the point (s_o, y, h_s) to the concentration at the point (s, y_R', h_R') is:

$$dC(s,y_R',h_R') = \frac{dQ(s_o,y,h_s)}{2\pi\sigma_y^{*'}\sigma_z^{*'}u} e^{-0.5(\frac{y-y_R'}{\sigma_y^{*'}})^2} [e^{-0.5(\frac{h_s-h_R'}{\sigma_z^{*'}})^2} +$$

$$e^{-0.5(\frac{h_s+h_R'}{\sigma_z^{*'}})^2}]. \qquad (38)$$

The total concentration at the receptor (s, y_R', h_R') is found by integrating Equation 38 over all point source elements above H_c (at s_o), so that:

$$C(s,y_R',h_R';\ s_o)= \int_{H_c}^{\infty}\int_{-\infty}^{+\infty} \frac{C(s_o,y,h_s)}{2\pi\sigma_y^{*'}\sigma_z^{*'}} e^{-0.5(\frac{y-y_R'}{\sigma_y^{*'}})^2}\left[e^{-0.5(\frac{h_s-h_R'}{\sigma_z^{*'}})^2} + e^{-0.5(\frac{h_s+h_R'}{\sigma_z^{*'}})^2}\right] dy\ dh_s \qquad (39)$$

where the concentration profile at s_o is expressed in terms of h_s:

$$C(s_o,y,h_s)= \frac{Q}{2\pi u\sigma_{yo}\sigma_{zo}} e^{-0.5(\frac{y_s-y}{\sigma_{yo}})^2}\left[e^{-0.5(\frac{z_s-h_s-H_c}{\sigma_{zo}})^2} + e^{-0.5(\frac{z_s+h_s+H_c}{\sigma_{zo}})^2}\right] \qquad (40)$$

for a plume released at $(0,y_s,z_s)$.

The result of doing the integrals in Equation 39 is simplified by defining the effective plume spread parameters σ_{ze} and σ_{ye}. First, define terrain-effect factors T_z and T_y so that

$$\sigma_z^{*'} = \sigma_z^{*}/T_z$$

$$\sigma_y^{*'} = \sigma_y^{*}/T_y. \qquad (41)$$

Then the effective plume spread, accounting for the effect of strain in the flow on the rate at which material diffuses across streamlines, is defined as

$$\sigma_{ze}^{\ 2} = \sigma_{zo}^{\ 2} + (\sigma_z^{*}/T_z)^2$$

$$\sigma_{ye}^{\ 2} = \sigma_{yo}^{\ 2} + (\sigma_y^{*}/T_y)^2. \qquad (42)$$

Equation 40 can be substituted into Equation 39, and after isolating terms containing y and h_s, we find that the exponential functions containing either y or h_s can be combined and isolated. By completing the squares in the argument of these functions, and using the definitions of Equation 42, the concentration at the receptor can be written as:

$$C(s,y_R',h_R';s_o) = \frac{Qe^{-0.5\left(\frac{y_R'-y_s}{\sigma_{ye}}\right)^2}}{4\pi u\sigma_{ye}\sigma_{ze}} F_z \qquad (43a)$$

where

$$F_z = e^{-0.5\left(\frac{h_R'-z_s+H_c}{\sigma_{ze}}\right)^2}\{1+ERF\ A_z[(z_s-H_c)(\sigma_z^*/T_z)^2+h_R'\sigma_{zo}^2]\}$$

$$+ e^{-0.5\left(\frac{h_R'+z_s-H_c}{\sigma_{ze}}\right)^2}\{1+ERF\ A_z[(z_s-H_c)(\sigma_z^*/T_z)^2-h_R'\sigma_{zo}^2]\}$$

$$+ e^{-0.5\left(\frac{h_R'+z_s+H_c}{\sigma_{ze}}\right)^2}\{1-ERF\ A_z[(z_s+H_c)(\sigma_z^*/T_z)^2-h_R'\sigma_{zo}^2]\}$$

$$+ e^{-0.5\left(\frac{h_R'-z_s-H_c}{\sigma_{ze}}\right)^2}\{1-ERF\ A_z[(z_s+H_c)(\sigma_z^*/T_z)^2+h_R'\sigma_{zo}^2]\} \qquad (43b)$$

and

$$A_z = (\sqrt{2}\ \sigma_{zo}\sigma_{ze}\sigma_z^*/T_z)^{-1}. \qquad (43c)$$

Equation 43 provides the framework for estimating concentrations due to plume material that travels up and over a hill. It shows how the influence of the terrain affects the magnitude and the distribution of GLC's. The most complicated part of Equation 43 is the expression for F_z, the vertical distribution factor. It contains four terms because it applies to an elevated receptor, so the image source contribution is not equal to the contribution from the primary source (hence two terms are needed rather than one). And it also applies to a plume segment above H_c rather than an entire plume profile, so that an image source contribution at s_o must be explicitly maintained (hence, two more terms). The error functions also arise from treating only the portion of plume material that lies above H_c at s_o. If H_c is zero, then Equation 43 becomes:

$$C(s,y_R',h_R';s_o) = \frac{Qe^{-0.5\left(\frac{y_R'-y_s}{\sigma_{ye}}\right)^2}}{2\pi u\sigma_{ye}\sigma_{ze}}\left[e^{-0.5\left(\frac{h_R'-z_s}{\sigma_{ze}}\right)^2} + \right.$$

$$e^{-0.5\left(\frac{h_R'+z_s}{\sigma_{ze}}\right)^2}] \qquad (44)$$

which, with the exception of alterations in the plume size and in the distance between the plume centerline and the receptor, is the familiar Gaussian plume equation for the concentration at an elevated receptor.

The receptor position in Equation 43 is denoted as (h_R', y_R'), where the primes indicate that the distance of the receptor from the centerline of the plume has been altered by the presence of the hill. Upwind of the hill, streamlines are straight and parallel. Over the hill, the spacing is variable and the streamlines are subject to deflections. Because concentrations are computed for a parallel flow in which the influence of terrain is manifested in the H_c-partition of plume material, in the altered rates of diffusion, and in the altered streamline that passes through the receptor, the chief task in computing (h_R',y_R') is in identifying the streamline that passes through the source, and the streamline that passes through the receptor. The position of these two streamlines in the undisturbed flow upwind of the hill defines the effective receptor location relative to the centerline of the plume. These streamlines are obtained from the flow model described in subsection 3.3.6.

The design of the flow model is particularly well-suited to obtaining h_R' and y_R' because it is formulated as a "backwards-looking" solution. It is designed to compute the deflection experienced by a streamline that passes through a given point over the hill. If the given point is a receptor, then the model will compute the deflection experienced by the streamline that passes through that receptor. Knowing the actual position of the receptor, the deflections allow h_R' and y_R' to be computed.

The LIFT equation for concentration, Equation 43, is applied to all receptors on a hill that lie above H_c, and are downwind of the point of impingement or the upwind base of the hill (for $H_c = 0$). Given the way the model must deal with a highly idealized description of the terrain, there are times when a receptor may lie above H_c, but may be positioned upwind of the point of impingement. For example, the receptor may be on a mast which places it above H_c, or the terrain on which a ground-level receptor is placed may exceed H_c. Concentrations at both of these receptors would be estimated with Equation 44 with two changes:

1) no terrain-effects would be included in computing σ_{ye}, σ_{ze}, and the lateral position of the receptor;

2) If the surface of the terrain were less than H_c, the vertical position of the receptor would be its actual elevation, relative to z_s, as if it were placed on a pole. If the surface actually exceeded the elevation of H_c, the difference in elevation would be subtracted from

the height of the "pole". In this way, the flow above H_c rides up and over any portion of the hill that lies above H_c.

3.3.4 Terrain Factors for LIFT: T_z and T_y

For axi-symmetric strain, the theory of Hunt and Mulhearn (1973) shows that

$$\sigma^2(t) = \frac{2}{\beta^2(t)} \int_o^t \beta^2(t')K(t')dt' \qquad (45)$$

where σ denotes either σ_y or σ_z, β is the strain function for the corresponding component, and K is the diffusivity for that component. In the case of σ_z,

$$\sigma_z^2(t) = \frac{2}{\beta_z^2(t)} \int_o^t \beta_z^2(t')K(t_z')dt' \quad . \qquad (46)$$

The strain function β_z is given by

$$\beta_z(t) = e^{-\int_o^t \frac{\partial w}{\partial z}(t')dt'} = e^{-\frac{\partial}{\partial z}\int_o^t w(t')dt'} \qquad (47)$$

where w is the vertical component of the flow. For small deflections, the strain function is approximately

$$\beta_z(t) = e^{-\frac{\partial}{\partial z}(\delta_z(t))} \qquad (48)$$

where $\delta_z(t)$ is the vertical deflection experienced by a streamline at time t.

The derivation of Equation 45 depends on a local analysis of the flow field near the centerline of the plume. The strain function is treated as a constant about the centerline, varying only with distance (time) along the flow. In using this result, we assume that the strain function can be assigned a representative value for the layer that contains the bulk of plume material.

Let $T_h(z_m, t)$, the factor for distortion of streamlines in the vertical, be the ratio of the spacing of streamlines in the vertical in the strained flow to that in the incident flow, evaluated at time t along a streamline whose height far from the hill is z_m. The streamline of height z_m is chosen to represent the layer in which the plume resides. Then the distortion factor for the layer at time t is defined as (Figure 7):

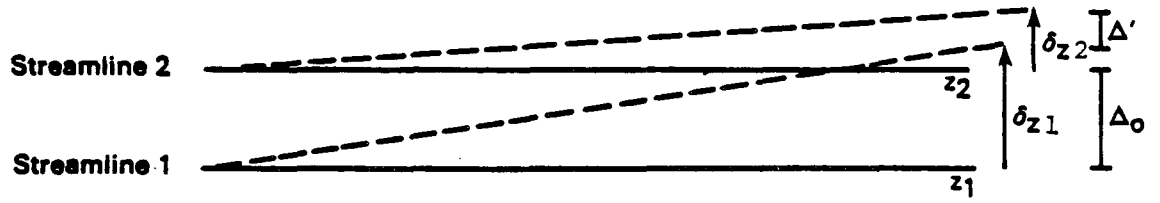

$$T_h = \frac{\Delta'}{\Delta_o} = \frac{(z_2 + \delta_{z2}) - (z_1 + \delta_{z1})}{z_2 - z_1} = \frac{\Delta z + \Delta \delta_z}{\Delta z} = 1 + \frac{\Delta \delta_z}{\Delta z}$$

Figure 7. Derivation of the factor T_h in finite-difference form. The dashed lines represent the path of two adjacent streamlines, as they are deflected by the presence of terrain.

8711036

$$T_h(z_m,t) = 1 + \frac{\partial}{\partial z}\,[\delta_z(z,t)]\,|_{z=z_m}. \tag{49}$$

With this mean distortion, the height $\eta(z,t)$ of a streamline above the surface of the hill at time t is approximately

$$\eta(z,t) = zT_h(z_m,t) \tag{50}$$

where z is the height of streamline well upwind of the hill. Because of the form of Equation 50, T_h is equivalent to a "height-correction factor" for a plume.

To evaluate T_z, consider the argument of the exponential function in the vertical distribution factor of Equation 44 when the elevation of the receptor above the surface is zero. The primary quantity in this argument is the ratio z_s/σ_{ze}, where σ_{ze} is given in Equation 42. The corresponding ratio in the approach of Hunt and Mulhearn is $\eta(z_s,t)/\sigma_z(t)$ where $\eta(z_s,t)$ is given by Equation 50, and $\sigma_z(t)$ is given by Equation 46. T_z can be evaluated by equating these two quotients. First, rewrite Equation 45 as the sum of two terms:

$$\sigma_z^2(t) = \frac{2}{\beta_z^2(t)}\left[\int_o^{t_o} \beta_z^2(t')K_z(t')dt' + \int_{t_o}^{t} \beta_z^2(t')K_z(t')dt'\right]. \tag{51}$$

where t_o is the time-of-travel from the source to the upwind base of the cut-off hill.

Because the strain is very weak away from the hill, $\beta_z(t')$ is virtually unity in the range $t<t_o$, so that the first term is approximately equal to $\sigma_{zo}^2/\beta_z^2(t)$, the size of the plume just upwind of the hill divided by the strain function at the receptor (travel-time t). Therefore,

$$\frac{\eta^2(z_s,t)}{\sigma_z^2(t)} = \frac{\beta_z^2(t)z_s^2T_h^2(z_m,t)}{\sigma_{zo}^2 + \int_{t_o}^{t} \beta_z^2(t')2K_z(t')dt'}. \tag{52}$$

Equating η/σ_z with z_s/σ_{ze} and solving for T_z:

$$\frac{1}{T_z^2} = \frac{\sigma_{zo}^2(1-\beta_z^2(t)T_h^2(z_m,t)) + \int_{t_o}^{t} \beta_z^2(t')2K_z(t')dt'}{\beta_z^2(t)T_h^2(z_m,t)(\sigma_z^2 - \sigma_{zo}^2)} \tag{53}$$

Using Equations 48 and 49, the strain function can be rewritten in terms of T_h as:

$$\beta_z(t) = e^{-(T_h-1)} . \tag{54}$$

For weak strain, T_h is of order 1, so that $\beta_z(t) = 1/T_h(z_m,t)$. Adopting the weak-strain form of the product $\beta_z T_h$, the expression for T_z becomes:

$$\frac{1}{T_z^2} = \frac{\int_{t_o}^{t} 2K_z(t')\, e^{-2(T_h(z_m,t')-1)}\, dt'}{\sigma_z^2 - \sigma_{zo}^2} . \tag{55}$$

Note that the denominator is the difference of the squares of the plume size across the interval $t-t_o$ in the absence of any effects of terrain.

This expression is implemented in CTDM by breaking the integral into 25 subintervals along the streamline trajectory over the hill. Within each subinterval, the strain function is assumed to be constant, equal to its value at the midpoint of the subinterval. This allows the integral for one of the subintervals to be written as:

$$\int_{t_1}^{t_2} 2K_z(t')\beta_z^2(t')dt' = \beta_z^2(t_m)(\sigma_{za}^2(t_2) - \sigma_{za}^2(t_1)) \tag{56}$$

where β_z is obtained from Equation 54. The altered value of σ_z (σ_{za}) is given by Equation 16, except σ_w and T_L have been altered by the changes in the flow over the hill.

The Lagrangian time-scale in the absence of any strain in the flow is given by the relation

$$\frac{1}{T_{Lo}} = \frac{N_o}{\gamma^2} + \frac{\sigma_{wo}}{\Gamma z_r} \tag{57}$$

where the subscripts 'o' denote flat-terrain quantities. The strain in the flow alters the stratification (temperature gradient), the turbulence velocity, and the length scale of the dominant eddies, so that

$$\frac{1}{T_L} = \frac{N_o/\gamma^2}{\sqrt{T_h(z_m,t)}} + \frac{\sigma_{wo}}{\Gamma z_s} \quad \frac{T_{\sigma w}}{T_h(z_m,t)} \tag{58}$$

where $T_{\sigma w}$ is the ratio σ_w/σ_{wo}.

Close to the surface of a hill, the turn-over time of a characteristic eddy is much shorter than the tranport time over the hill, so that the turbulence has time to adjust to changes in the surface shear stress. Under these conditions the results of inner-layer theory apply (see Britter et al., 1981) and $T_{\sigma w} = T_u$, the speedup factor for the flow. Because the turbulence intensity (i_z) is σ_w/u, this is equivalent to saying that the turbulence intensity is not altered. Far from the hill, the changes to the flow field and turbulence are small, so the turbulence intensity remains virtually the same. Between these two limits, when stratification is not important, rapid distortion theory (RTD) may apply, and Britter et al. report that the turbulence intensity i_z decreases (σ_w increases, but at a rate slower than the rate of increase in the wind speed). This applies to eddies whose turn-over time is less than the time scale for changes in the flow. For stratified flow, the eddy turn-over time scale may remain small, and RDT may not apply. Therefore, we have chosen to use the inner-layer result for all plumes in the model.

A parallel development for T_y leads to a similar result. The distortion factor in the horizontal direction is denoted by $T_\ell(z_m,t)$ so that

$$\frac{1}{T_y^2} = \frac{\int_{t_o}^{t} 2K_y(t')\, e^{-2(T_\ell(z_m,t')-1)}\, dt'}{\sigma_y^2 - \sigma_{yo}^2}. \qquad (59)$$

This integral is also broken into subintervals, as in Equation 56. In this case though, $\sigma_{ya}(t)$ is given by the linear growth form:

$$\sigma_{ya}(t) = T_{\sigma v}\, \sigma_{vo} t \qquad (60)$$

because this form holds for distances of travel of nearly 10 km. $T_{\sigma v}$ is set to unity, rather than T_u, as was done for $T_{\sigma w}$. This choice was made in recognition of the distinction between large-scale fluctuations in wind direction (meandering) and small-scale turbulence.

The deformation factors T_h and T_ℓ, and the speed-up factor T_u are obtained from the flow model. These are computed along the path of the streamline chosen to be representative of the layer containing the plume material. Far from the hill, this streamline is taken to be half of the way between H_c and the elevation of the center of mass of plume material above H_c.

Because a particular streamline must be followed along the flow (a "forward-looking" process), its position at any time t must be found from the "backwards-looking" flow model by an iterative

process. Each "guess" at where the streamline may be at time t produces a computed position of that streamline in the incident flow. New guesses are dependent on the difference between the last computed position, and the position of the targeted streamline.

3.3.5 Internal Mixing Layer for LIFT

A central assumption involved in the use of the LIFT equations is that the turbulence field is homogeneous. While this assumption is violated in nearly all applications of the Gaussian plume model, there is one situation in modeling the dispersion of plume material over a hill where such a violation is severe.

An elevated plume in a very stably-stratified flow may reside in a region of nearly laminar flow, with very little turbulence. The turbulent boundary layer beneath this region can be very shallow. When H_c is greater than the depth of the turbulent flow, the entire laminar region may flow over the terrain, and an internal boundary layer must form at the bottom of this layer. If this internal boundary layer were ignored, then the diffusivity of plume material would remain virtually zero, and the effect of the terrain would only be seen in the H_c-partition of plume material.

To provide a more realistic treatment of the very stable limit, a simple mixing layer is included. Within the mixing layer, the vertical distribution of plume material is uniform, and the concentration is obtained by sampling the vertical distribution in the absence of the mixing layer, and taking the average value over the depth of the layer.

The depth of the mixing layer is estimated by focusing on the initial stages in the development of such a layer, when turbulent mixing is very strong. Assume that the turbulence in the layer produces a layer of constant potential temperature (see Figure 8). As a result of the rapid mixing in the layer, assume that buoyancy effects are negligible in the layer, so that the wind speed takes on a logarithmic structure in the vertical. Wind speed is continuous at the top of the layer, but its gradient is not.

Csanady (1974) discusses a theory for estimating the evolution of the depth of such a surface layer. He uses the result of laboratory simulations by Kato and Phillips (1969) in which a layer is thickening into a fluid with constant Brunt-Vaisala frequency N, as a result of a constant stress applied at the bottom of the layer:

$$\frac{1}{u_*}\ \frac{dh}{dt} = \frac{2.5\ u_*^{\,2}\ \theta_m}{g\ \Delta\theta\ h}\ . \qquad (61)$$

Here, h is the thickness of the layer, u_* is the surface friction velocity, g is the acceleration due to gravity, θ_m is the potential temperature of the mixed layer, and $\Delta\theta$ is the jump in

potential temperature at the top of the layer. This result is consistent with the notion that the rate of thickening of the layer is a function of a buoyancy parameter,

$$b = g\Delta\theta/\theta_m, \tag{62}$$

the surface stress (expressed as u_*), and the thickness of the layer so that the entrainment velocity, when scaled by the friction velocity, is a function of the dimensionless group bh/u_*^2:

$$\frac{u_e}{u_*} = F(bh/u_*^2). \tag{63}$$

In essence, the entrainment depends on the turbulence generated at the surface of the layer, and not on any assumptions about shear-generated turbulence at the interface.

Referring to Figure 8,

$$\theta_m = \theta_o + \Delta\theta = \theta_o + \frac{d\theta}{dz}\ \frac{h}{2} \tag{64}$$

so that

$$\frac{dh}{dt} = \frac{2.5u_*^3}{gh}\left(\frac{2\theta_o}{hd\theta/dz} + 1\right). \tag{65}$$

If we assume that the layer depths will generally be small enough that $\theta_o >> h\ d\theta/dz$, or that $\theta_m \simeq \theta_o$, then the subsequent evaluation of the integral is greatly simplified.

The friction velocity in Equation 65 is given by

$$u_* = \frac{ku}{\ln(h/z_o)} \tag{66}$$

where u is the mean wind speed outside of the layer, k is von Karman's constant, and z_o is the roughness length for the surface of the hill. Rewriting Equation 65 with $\theta_o = \theta_m$, we find

$$\frac{dh}{dx} = \frac{5\theta_o}{g\ d\theta/dz}\ \frac{k^3u^2}{h^2[\ln(h/z_o)]^3}. \tag{67}$$

Noting that $15\ k^3 \simeq 1$, an implicit equation for h is obtained:

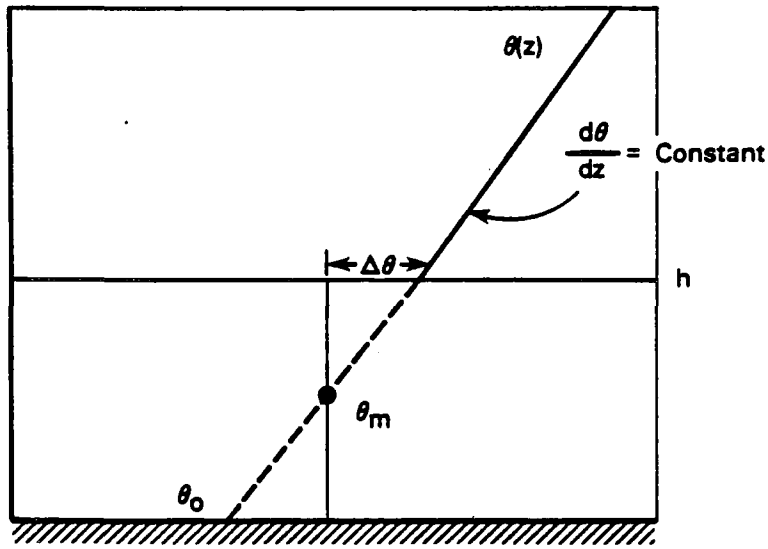

Potential Temperature Profile

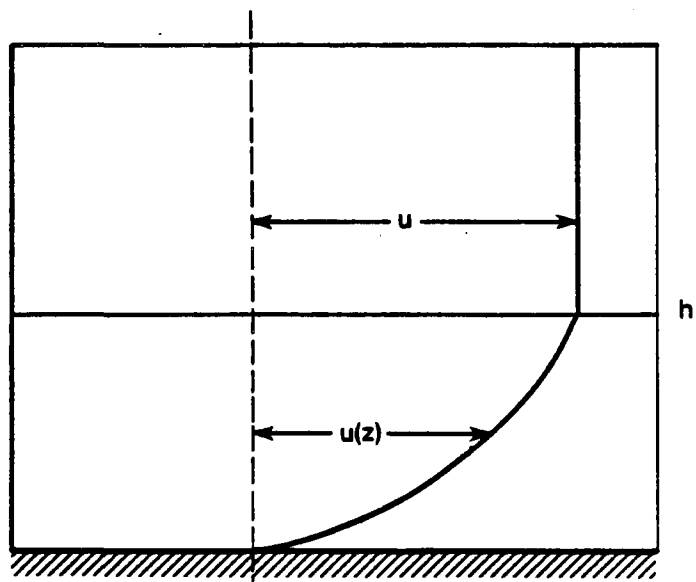

Wind Speed Profile

Figure 8. Illustration of the structure assumed for the developing internal mixing layer over the hill above H_c.

8708104

$$\left(\frac{h}{u/N}\right)^3 \left\{ \left(\ln\frac{h}{z_o}\right)^3 - \left(\ln\frac{h}{z_o}\right)^2 + \left(\frac{2}{3}\ln\frac{h}{z_o}\right) - \frac{2}{9}\left(1 - \left(\frac{z_o}{h}\right)^3\right)\right\}$$

$$= \frac{x - x_o}{u/N}. \qquad (68)$$

This implicit equation has two undesirable traits. The growth of the mixing layer is extremely rapid for very small times-of-travel (downwind distance) from the point where the flow first encounters the hill above H_c, and the estimates of mixing depths "blow up" for weak stratification. The first of these traits is removed by demanding that the rate-of-growth not exceed unity (slope of the interface equals 45°). The second trait is removed by limiting how large u/N can be in Equation 68.

For convenience, u/N is set equal to the minimum of u/N and H_c. This is done because we wish to turn on the mixing layer primarily for those cases in which turbulence at plume height is decoupled from the surface. As H_c becomes less than half the hill height, there is a strong likelihood that the turbulent boundary layer in the approach flow encompasses most of the depth of the flow over the hill. Hence, in using the minimum of u/N and H_c, the stability is artificially increased for H_c less than H/2 so that the depth of the mixing layer will decrease. As H_c goes to zero, the mixing layer is completely absent, as desired.

3.3.6 Flow Model for LIFT

Model Development

CTDM simplifies the treatment of stratified flow over a hill by separating the flow into two regimes: a lower portion, below H_c, which is either blocked (in the case of a long ridge) or flows around the hill, and an upper portion, above H_c, which has sufficient kinetic energy to flow up and over the hill. This simplification means that for a flow of constant speed, u, which lifts up and over the hill, one always has the property that $(H-H_c)N/u \leq 1$; or equivalently, that the Froude number for this portion of the flow exceeds unity and the flow is not "strongly" stratified. This fact, coupled with the assumption that the hill is not too steep (i.e., less than about 15°) enables one to use the linearized equations of motion for steady-state Boussinesq flow (Smith, 1980):

$$\rho_o u \frac{\partial u'}{\partial x} = -\frac{\partial p'}{\partial x} \qquad (69a)$$

$$\rho_o u \frac{\partial v'}{\partial x} = -\frac{\partial p'}{\partial y} \qquad (69b)$$

$$\rho_o u \frac{\partial w'}{\partial x} = -\frac{\partial p'}{\partial z} - \rho' g \qquad (69c)$$

$$\frac{\partial u'}{\partial x} + \frac{\partial v'}{\partial y} + \frac{\partial w'}{\partial z} = 0 \qquad (69d)$$

and

$$\rho' = - \left(\frac{\partial \rho_o}{\partial z}\right) \eta \qquad (69e)$$

These equations, in which x, y, and z indicate downstream, cross-stream, and vertical coordinates respectively, relate the perturbation velocities u', v' and w' to the perturbation density, ρ', pressure p', and vertical fluid displacement, $\eta = \eta(x,y,z)$, and to the unperturbed initial velocity u and density ρ_o. It should be noted that $\eta(x, y, z)$ is the vertical displacement that a parcel of air at the point (x, y, z) <u>has</u> experienced. Adding the kinematic condition for steady flow in a shear-free approach flow gives

$$w' = u \frac{\partial \eta}{\partial x} . \qquad (70)$$

Equation 69 can be reduced to the single partial differential equation;

$$\frac{\partial^2}{\partial x^2} (\nabla^2 \eta) + n^2 \nabla_H^2 \eta = 0, \qquad (71a)$$

where

$$\nabla_H^2 \equiv \frac{\partial^2}{\partial x^2} + \frac{\partial^2}{\partial y^2} ,$$

$$n = N/u, \text{ and } N^2 = -(g/\rho_o) \frac{d\rho_o}{dz} . \qquad (71b)$$

Yamartino (1987; See Appendix A) discusses exact solutions to Equation 71, but steep terrain or strong stratification tend to invalidate these solutions because higher-order terms in Equation 69 (e.g., quadratic in a perturbation quantity) can no longer be neglected. Thus, the great complexity associated with the exact solution is abandoned in favor of a more easily integrated, approximate solution. The easiest way to reach the approximate solution is to integrate Equation 71 twice with respect to x,

$$\nabla^2 \eta + n^2 \left(\eta + \int_{-\infty}^{x} \int_{-\infty}^{x'} \frac{\partial^2 \eta}{\partial y^2} \, dx'' \, dx'\right) = 0 \qquad (72a)$$

and approximate the troublesome last term via length scale or predominant wavenumber arguments, as

$$\int_{-\infty}^{x} \int_{-\infty}^{x'} \frac{\partial^2 h}{\partial y^2} \, dx'' \, dx' \simeq \eta \cdot (L_x^2/L_y^2), \qquad (72b)$$

where L_x, L_y are the length scales of the hill in the along-, cross-wind directions, respectively. This approximation, which is shown in Appendix A to be exact for an infinite field of cosine hills, leads to the Helmholtz equation,

$$\nabla^2 \eta + m^2 \eta = 0 \qquad (73a)$$

where

$$m = n\,(1 + L_x^2/L_y^2)^{1/2}. \tag{73b}$$

It has the simple particular solution

$$\eta = -\frac{\partial G}{\partial z} \tag{74}$$

with $G = \cos(mR)/R$ and $R^2 = x^2 + y^2 + z^2$.

This is the Green's function solution for a delta function hill (i.e., a mathematically narrow but high hill of unit volume). It is extended to a general hill shape h(x,y) via a two-dimensional integration combining the hill shape function and the Green's funtion (i.e, the convolution theorem) and the lower boundary condition that the flow at the surface follow the hill shape. Thus, for an arbitrary hill

$$I = \int\int dx'dy'\ h(x-x',\ y-y')\ G(x',y',z') \tag{75}$$

and

$$\eta = -\frac{\partial I}{\partial z'} \tag{76a}$$

where use of the height above terrain, z', instead of absolute z reflects the fact that the lower boundary condition has been linearized; that is, the transformation to terrain-following coordinates assumes very shallow terrain.

The other quantities needed for a complete description of the flow are obtained by using Equation 76a and going back to the basic equations of motion, yielding:

$$u'/u = -\left[\frac{\partial^2}{\partial x^2}\,(I) + n^2 I\right] = p'/(\rho_o u^2) \tag{76b}$$

$$v'/u = -\left[\frac{\partial}{\partial x}\frac{\partial}{\partial y}\,(I) + n^2 \int_{-\infty}^{x} \frac{\partial I}{\partial y}\,dx'\right] \tag{76c}$$

and

$$w'/u = -\frac{\partial^2 I}{\partial x^2}. \tag{76d}$$

It should be noted that lateral perturbation velocity, v', and the subsequent definition of lateral deflection, δ, as

$$\delta = \int_{-\infty}^{x} dx'\ (v'/u) = -\left[\frac{\partial I}{\partial y} + n^2 \int_{-\infty}^{x}\int_{-\infty}^{x'} \frac{\partial I}{\partial y}\,dx''\,dx'\right] \tag{76e}$$

make the additional assumption that streamline deflections are small enough that integrating along the x-axis at y, z' from $x = -\infty$ to x is equivalent to integrating along the streamline from $x = -\infty$.

Equation 76e also provides another example of how higher-order terms are neglected, because a geometrical picture of lateral deflection would indicate that the denominator factor u should actually be the true x-component of velocity, or approximately u + u'. Note that the deflections η and δ are those experienced by a streamline that passes through the point (x,y,z'). They tell us where that streamline originates in the incident flow.

The local strain factors T_ℓ and T_h used in CTDM can also be related to I through these quantities:

$$T_h = \left(1 - \frac{\partial \eta}{\partial z}\right)^{-1} = \left(1 + \frac{\partial^2 I}{\partial z^2}\right)^{-1} \qquad (76f)$$

$$T_\ell = \left(1 - \frac{\partial \delta}{\partial y}\right)^{-1} = \left(1 + \frac{\partial^2 I}{\partial y^2} + n^2 \int_{-\infty}^{x} \int_{-\infty}^{x'} \frac{\partial^2 I}{\partial y^2}\, dx''dx'\right)^{-1}. \qquad (76g)$$

T_h and T_ℓ are factors that relate the spacing between adjacent streamlines in the deformed flow to the spacing in the incident flow. The gradient of the deflection (either $\partial\eta/\partial z$ or $\partial\delta/\partial y$) measures the difference in the deflection experienced by adjacent streamlines and hence, the degree to which the streamlines converge or diverge. In this backwards-looking formulation, the deflection is a function of the streamline position (coordinates) after deformation (see Figure 9). As detailed in the figure, the finite-difference form of Equation 76f (and 76g) is readily obtained from the definitions of streamline positions before and after the deformation. Note that $\partial\eta/\partial z = 1$ is a singular point. This condition would result if streamlines that pass through z_1, and z_2, were to originate at the same height in the incident flow. Also note that Equation 76f differs from Equation 49 because the deflection in Equation 49 is that for a forward-looking formulation.

Before evaluating Equations 75 and 76 for a realistic hill shape, it is worthwhile to look back to the solution, G = cos(mR)/R, given by Equation 74, as properties of the delta function hill solution will show up for finite hills as well. One positive aspect is that as stratification disappears (i.e., N, n, m go to zero and cos(mR) equals one), the exact neutral result G = 1/R is recovered. This exact neutral result of 1/R is the well-known solution of Laplace's equation, $\nabla^2 G = 0$ (i.e., except at x=y=0), that is incorporated into neutral flow solvers such as that of Hess and Smith (1962). Thus, the approximation expressed by Equation 72b will not affect neutral flow but only the modifications to the neutral flow solution created by stratification. That these stratification influences might not be too severe can be anticipated by noting that expansion of the cosine term, as $\cos(mR) \approx 1 - 1/2\ m^2R^2$, indicates that changes to the flow are second-order in m (i.e., m^2) rather than first-order. However, a disturbing aspect of this cos(mR) dependence

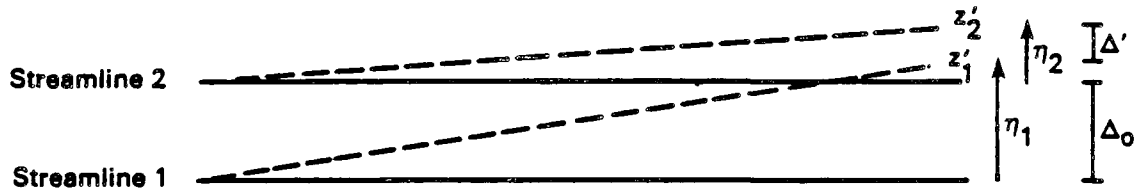

$$T_h = \frac{\Delta'}{\Delta_o} = \frac{z_2' - z_1'}{(z_2' - \eta_2) - (z_1' - \eta_1)} = \frac{\Delta z'}{\Delta z' - \Delta \eta} = \frac{1}{1 - \frac{\Delta \eta}{\Delta z'}}$$

Figure 9. Derivation of the factor T_h in finite-difference form for the "backwards-looking" formulation. The dashed lines represent the path of two adjacent streamlines, as they are deflected by the presence of terrain.

8710066

is its isotropic nature; that is, z has no special significance in the equation, despite the fact that the density stratification and thus the atmosphere's "springiness" is a z-oriented phenomenon. Exact solutions to Equation 71 do not display this isotropic behavior. Thus, one physically significant ramification of the approximation in Equation 72b becomes apparent. Such isotropic and thus lateral springiness does, however, occur in the aforementioned infinite field of cosine hills problem but steps must be taken to suppress this effect in the single isolated hill problem.

Finally, the connection to the neutral limit solution, G = 1/R, suggests a way to inject wind speed shear (with height) back into this shear-free solution. Crapper (1959) points out that the corresponding vertical deflection in a neutral, shear flow is just

$$\eta = \left[\frac{u(0)}{u(z')}\right] \cdot z'/R^3 \tag{77a}$$

whereas our current neutral form, G = 1/R, yields

$$\eta = z'/R^3 \tag{77b}$$

in the shear-free case. Unfortunately, even this simple factor is awkward to superpose back onto G exactly. The approximation chosen for this model yields a final Green's function of

$$G = [u(0)/u(z')]^{1/2} \cos(mR)/R. \tag{78}$$

Use of the shear exponent of 1/2 represents a compromise between including shear effects and avoiding negative impacts on the flow prediction generated by the inexact nature of the approximate solution given by Equation 78. Any remaining unwanted residual consequences of this approximation are suppressed by enforcing the constraint that the deflection of the streamline at the ground equal the rise of the surface of the hill: $-I_{z'} = \eta = h(x,y)$ at $z' = 0$. This ensures that no stremalines pass beneath the surface of the hill.

Algorithm Development

Referring back to Equation 76, one notes that all quantities of interest depend on integrals and derivatives of the basic quantity I, given by Equation 75 and with the use of the approximate shear solution G expressed by Equation 78. Evaluation of I requires that the shape of the hill be chosen carefully. Selection of an appropriate hill shape was governed by

i) the desire to treat as general a shape and orientation as possible, and
ii) the necessity for performing the integrations in Equation 75 analytically.

A Gaussian-shaped hill is used because it contains the overall orientation and scales of the "cut-off" hill, and because it has a tractable mathematical form. The most general Gaussian shape that is considered involves a hill of height h, having elliptical contours with major axis L_a, and a minor axis L_b, oriented at an angle ψ which is counter-clockwise with respect to the flow direction. For a coordinate system with the x-axis aligned with the direction of flow, the hill is prescribed by

$$h(x,y) = h \exp\{-[x^2/L_x^2 + y^2/L_y^2 + 2\gamma xy]\} \qquad (79)$$

where

$$\frac{1}{L_x^2} = \left[\frac{\cos^2\psi}{L_b^2} + \frac{\sin^2\psi}{L_a^2}\right] \quad , \quad \frac{1}{L_y^2} = \left[\frac{\cos^2\psi}{L_a^2} + \frac{\sin^2\psi}{L_b^2}\right] \quad ,$$

and

$$\gamma = \left[\frac{1}{L_b^2} - \frac{1}{L_a^2}\right] \cos\psi \sin\psi \quad .$$

These equations are generated by first writing the hill shape function, $h(x'', y'') = h \exp\{-[x''^2/L_b^2 + y''^2/L_a^2]\}$, in the hill's natural coordinate system (x'', y''), where x'' and y'' are distances along the minor and major axes, respectively, from the hill center, and then inserting the rotational relationships, $x'' = x \cos\psi + y \sin\psi$ and $y'' = y \cos\psi - x \sin\psi$, to eliminate the appearance of the coordinates (x'', y'').

For the symmetric hill with $L_a = L_b = L$, the expression simplifies greatly, as $L_x = L_y = L$ and $\gamma = 0$. In fact, once the convoluted form of the hill function (i.e., $h(x,y)$ is rewritten as $h(x-x',y-y')$) and is substituted into the integral for I, one finds that the exact analytic integration can be accomplished for a receptor position (x,y,z') at the crest (and just off the crest) of such a symmetric Gaussian hill. However, this analytic result, expressed in terms of the real and imaginary parts of the complex error function, can be greatly simplified without substantial loss of accuracy via the approximation

$$\exp(Z^2)\ \mathrm{erfc}(Z) \simeq 1/(1 + 2Z/\sqrt{\pi}),$$

where Z is a complex number having a positive real part. The expression finally arrived at is

$$I = \frac{h(x,y)\ L_n}{(1+b_o^2)(1+z'/L_n)^2} \cdot \left[\frac{u(0)}{u(z')}\right]^{1/2}\{(1+z'/L_n) \cdot \cos(mz')$$

$$- \alpha_1 \cdot \sin(mz')/m - \alpha_2 \cdot (x_m/L_x)[m \cdot \cos(mz') + (\frac{2}{L_n} + \frac{1}{2}\frac{\alpha}{u(0)}) \cdot \sin(mz')]\} \qquad (80)$$

where $b_o = B_o m L_z / \pi$, $L_z = R_L[\frac{1}{2}(\frac{1}{L_x^2} + \frac{1}{L_y^2})]^{1/2}$,

$L_n = \frac{1}{2}\pi L_z$,

α is from the shear equation $u(z') = u(0) + \alpha z'$, and

$\alpha_1 = b_o^2/L_n - \frac{1}{2}\frac{\alpha}{u(0)}$,

$\alpha_2 = \frac{2}{\pi^{3/2}} \cdot L_z \cdot (1 + L_z^2/L_y^2)^{1/2}$,

and $x_m = x + \gamma L_x^2 y$

all represent convenient clustering or redefinition of terms. The two parameters, B_o and R_L, arose because there was some conflict between small and large argument, low-order expansions of the complex error function and an ambiguity in the definition of L_z, respectively. The parameter B_o was set to $(\pi/2)^{1/2}$, the geometric mean of the small and large argument limit values, whereas R_L was tuned to $\ln(2) \approx 0.693$ based on optimization studies using the tow tank data described by Snyder et al. (1986).

The expression for I given above is best described as an admixture of analytic results for the symmetric hill and empirical extensions for the asymmetric hill subject to the constraints that the surface boundary condition be obeyed and that known results be recovered for the 2-d ridge limit of $L_y \to \infty$ and $\psi=0$. Higher-order terms (e.g., $(y/L_y)^2$ or other such terms arising far from the crest) are neglected. In addition, we took the liberty of switching-off the (x_m/L_x) term upwind of the hill (i.e., $x_m < 0$), as it seemed to create excessive early streamline rise as the hill was approached and because appropriate damping terms in x_m^2 had already been neglected in the denominator.

Evaluation of the flow variables in Equation 76 involve straightforward integrations and differentiations of the basic quantity I, given by Equation 80. Two exceptions to this involve:

(i) Replacement of $\{1 + ERF(x_m/L_x)\}$ with $\{1 - ERF|x_m/L_x|\}$. This appears in terms involving integrations and double integrations of I with respect to x, and has the major effect of allowing streamlines to return laterally to their initial upwind positions more rapidly after passing by the hill. This relaxation adjustment can be rationalized on the basis that Equation 80 is most valid near the crest of the hill.

(ii) A "fully-implicit" style computation of the lateral deflection. That is, instead of assuming that the streamline spent most of its time at its current lateral displacement y, we conjecture that most of its time was spent at its undeflected position, y_∞, evaluated back at $x = -\infty$. This enables one to write down the Taylor series relation $\delta^* = \delta + (d\delta/dy)(y_\infty - y)$ between the δ from Equation 76e and the new corrected lateral deflection, δ^*. Recognizing that $y-y_\infty$ is just the corrected deflection, δ^*, one may rearrange terms and solve for δ^* as $\delta^* = \delta/[1 + (d\delta/dy)]$. Such an approach is called "implicit" because y_∞ is never explicitly computed and "fully" implicit because the streamline is assumed to spend "all" of its time at lateral position y_∞ before rapidly moving out to its deflected position y. This compensates for the fact that lateral deflections can be large and therefore badly violate the "small deflection" assumption invoked for Equation 76e. The resulting lateral deflections are unfortunately smaller than before the correction, but streamline crossover situations (which create a severe problem for an iterative streamline solver) for large lateral aspect ratio hills are greatly suppressed. This suppression did not quite achieve the required elimination of crossovers. The above described procedure had to be carried to second order, i.e., $\delta^* = \delta - (d\delta/dy)\ \delta^* + 1/2\ (d^2\delta/dy^2)\ \delta^{*2}$ and solved, and the absolute value of $(d\delta/dy)$ taken (to account for a somewhat spurious sign flip far from the center of the hill), before streamline crossover could be completely blocked for high lateral aspect-ratio hills (e.g., $L_a = 10\ L_b$).

These adjustments to the model, as well as the adjustment of some of the parameters discussed in association with Equation 80, represent empirical tuning of the flow algorithm to improve model performance while avoiding pathologies (e.g., streamline crossover) which create havoc for an iterative algorithm. It should be noted that these, sometimes conflicting, considerations led us to consider several other forms for the Green's function, G, other than the basic $G = \cos(mR)/R$, later augmented for shear via Equation 78. Some of these trial Green's functions represented solutions to the governing Equation 73a; whereas others, such as $G = [1-\sin(mR)]/R$, were designed to inject a first-order dependence on stratification (i.e., m rather than the leading m^2 dependence from the cosine) into the solution. In general, Green's functions incorporating a first-order dependence on m

were much more successful in reproducing the tow tank data for 3-d hills (to be discussed in the following section), but were also more difficult to tame in terms of pathologies, especially those developing far from the hill. Damping of these Green's functions at large R provided some relief from these problems, but the need for an operational algorithm totally free of pathologies ultimately dictated that the more conservative cos(mR)/R form, with its relatively gentle leading m^2 stratification dependence, be adopted. Thus, there remains opportunity for improvement in this field.

Algorithm Evaluation

The behavior of streamlines produced by the flow model is qualitatively illustrated in the following 7 figures.

Figure 10 shows the paths followed by five streamlines (initially released at 20, 40, 60, 80, and 100 m above the surface well upwind of the hill) as they pass over the crest of a symmetric 100 m tall Gaussian hill of aspect ratio 1. The aspect ratio is defined to be the ratio of the half-length of the hill at one-half the height of the hill, to the height of the hill. Therefore, a Gaussian hill of aspect ratio 1, and height equal to 100 m, has a length scale L=120 m. The streamline patterns in the figure span hill Froude numbers of 1, 2, 4 and infinity. Qualitative features apparent in these patterns include:

- compression of streamlines near the crest, with the degree of compression increasing at greater stratifications (lower Froude number); and

- greater upwind/downwind asymmetry of the streamlines with increasing stratification such that the point of closest approach of the streamline to the surface of the hill shifts from the crest to the downwind side of the hill.

The same information is repeated in Figures 11 and 12 for a symmetric Gaussian hill of aspect ratio 2 (L = 240 m), and an asymmetric hill with an alongwind aspect ratio of 2 (L = 240m) and a crosswind aspect ratio of 10 (L = 1200 m). The flow over the latter hill is taken to represent nearly two-dimensional flow in the vicinity of the plane y=0, which is the plane that contains the streamlines illustrated in the figure. The compression of streamlines over the crest of the hill of aspect ratio 2 is weaker than that over the crest of the hill of aspect ratio 1, but the upwind/downwind asymmetry is stronger. Approaching the limit of the two-dimensional ridge, with an alongwind aspect ratio of 2, the compression over the crest becomes somewhat weaker while the upwind/downwind asymmetry is similar to that for the symmetric hill of aspect ratio 2. These results are in qualitative agreement with laboratory studies.

Figures 13 and 14 illustrate the lateral deflections produced by the algorithm for a matrix of streamlines. All streamlines lie originally at the same elevations used in the previous figures, but they are arranged in a series of eight bands across the flow. The

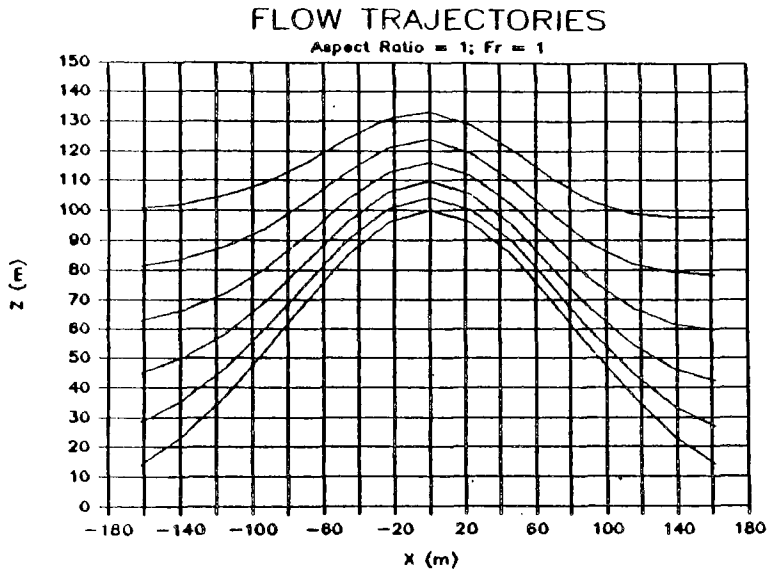

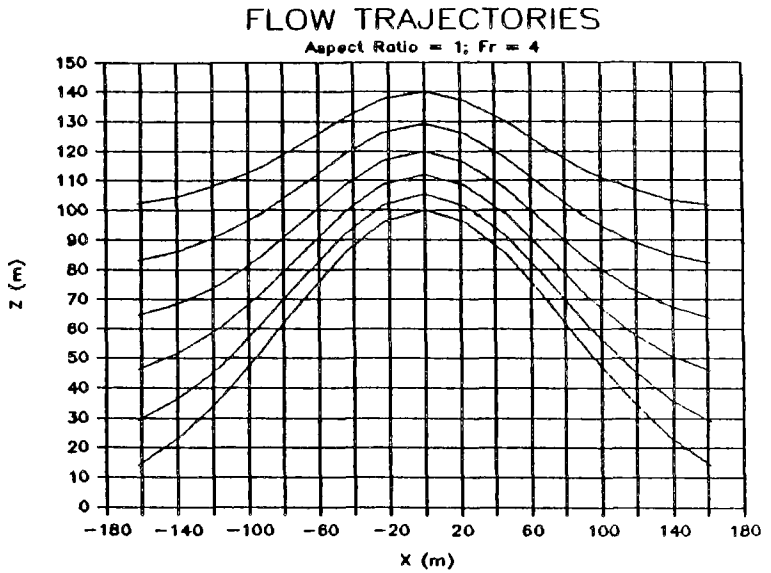

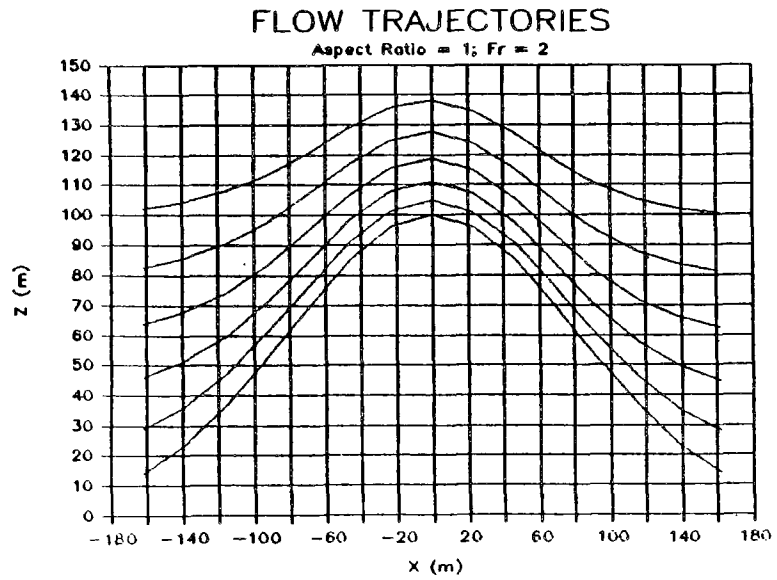

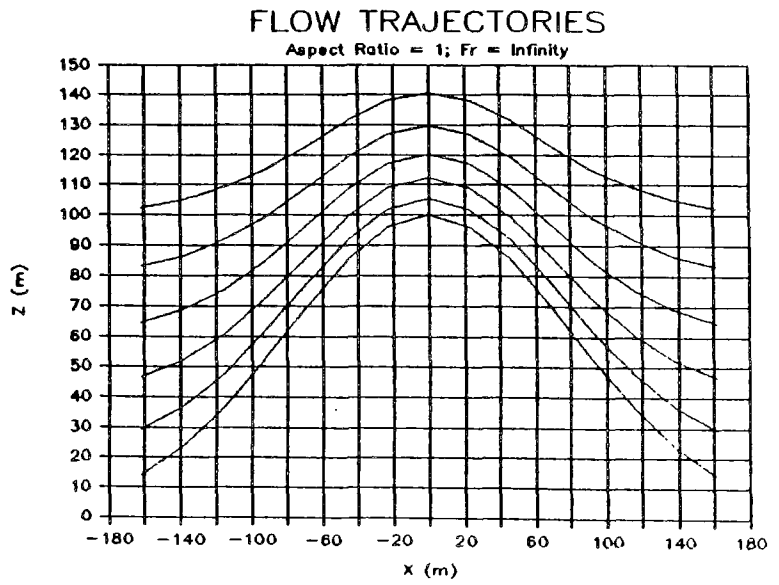

Figure 10. Side view of computed streamlines of flow passing from left to right over a symmetric Gaussian hill of aspect ratio 1.

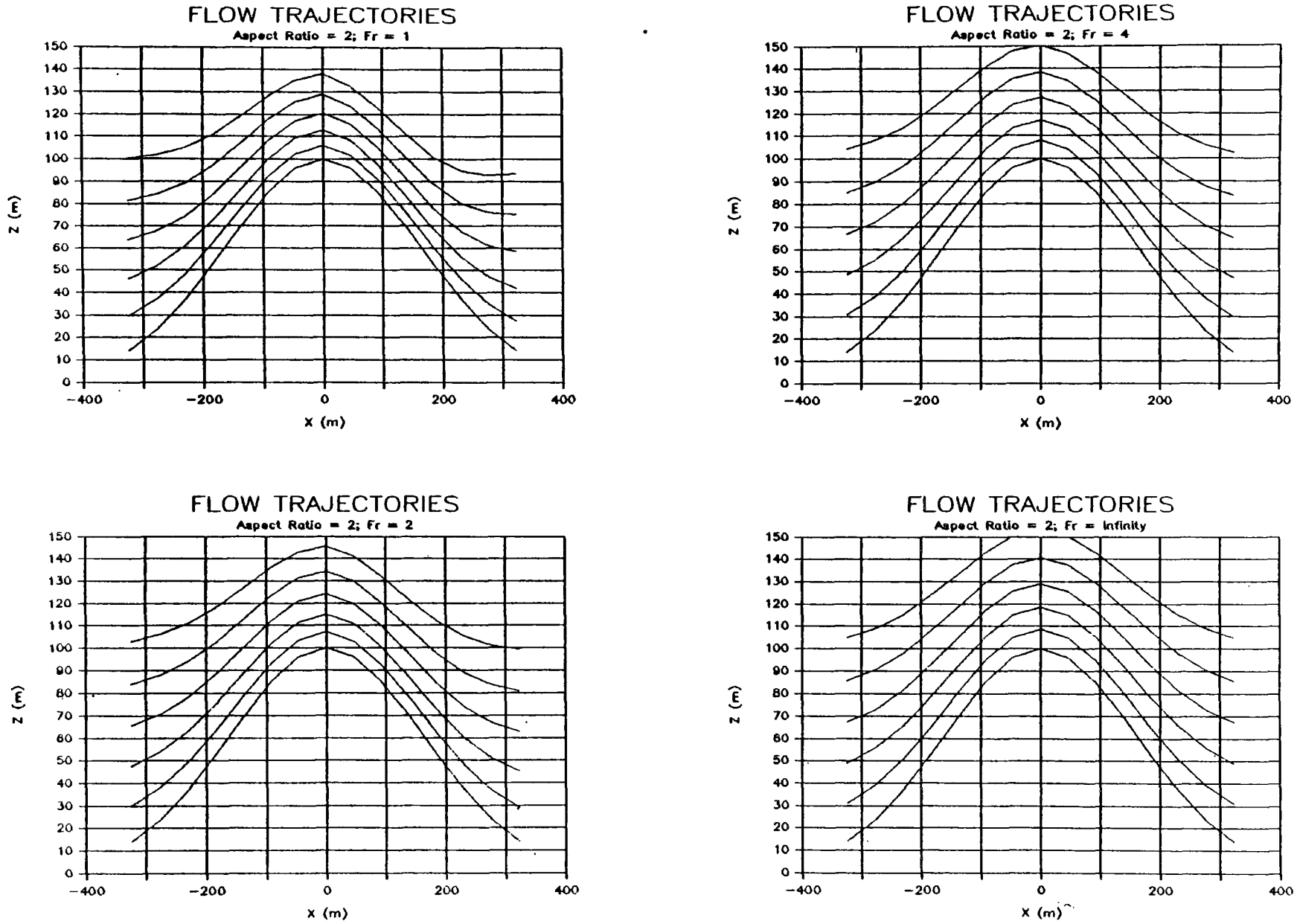

Figure 11. Side view of computed streamlines of flow passing from left to right over a symmetric Gaussian hill of aspect ratio 2.

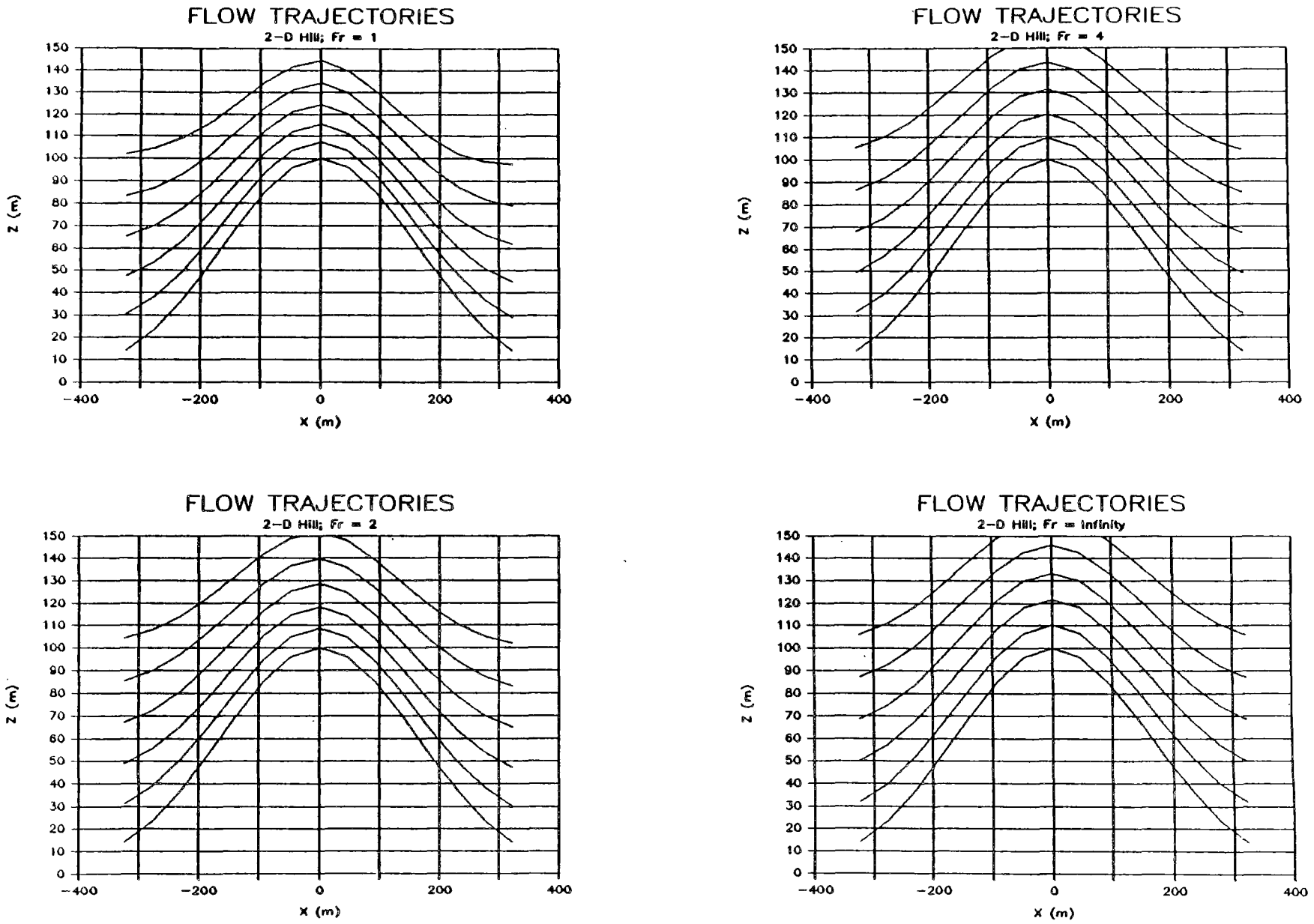

Figure 12. Side view of computed streamlines of flow passing from left to right over an asymmetric Gaussian hill of aspect ratio 2 along the flow, and to across the flow.

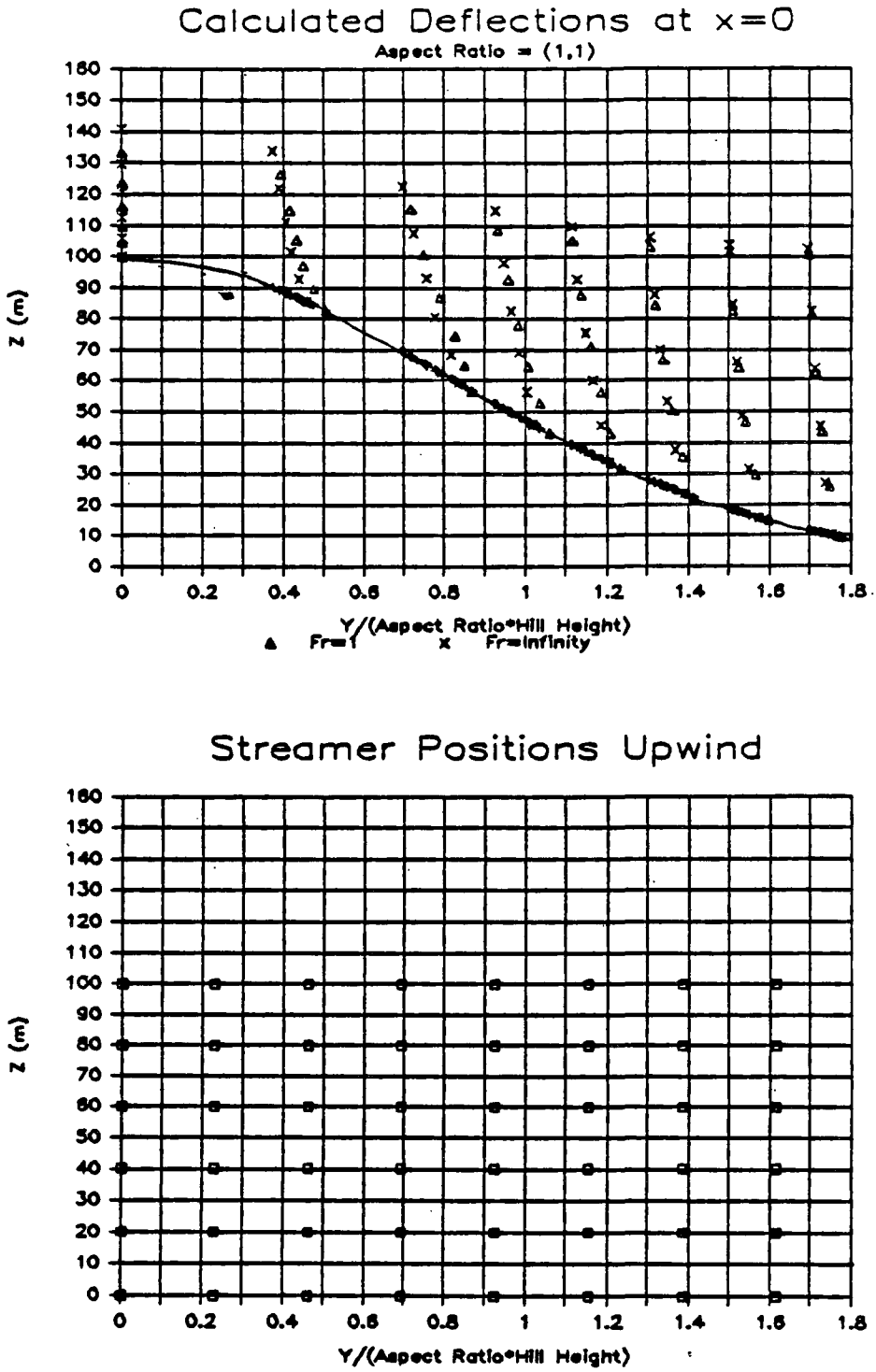

Figure 13. End-on view of streamlines at x=0 over a symmetric Gaussian hill of aspect ratio 1, and at $x=-\infty$ (i.e., far upwind of the hill).

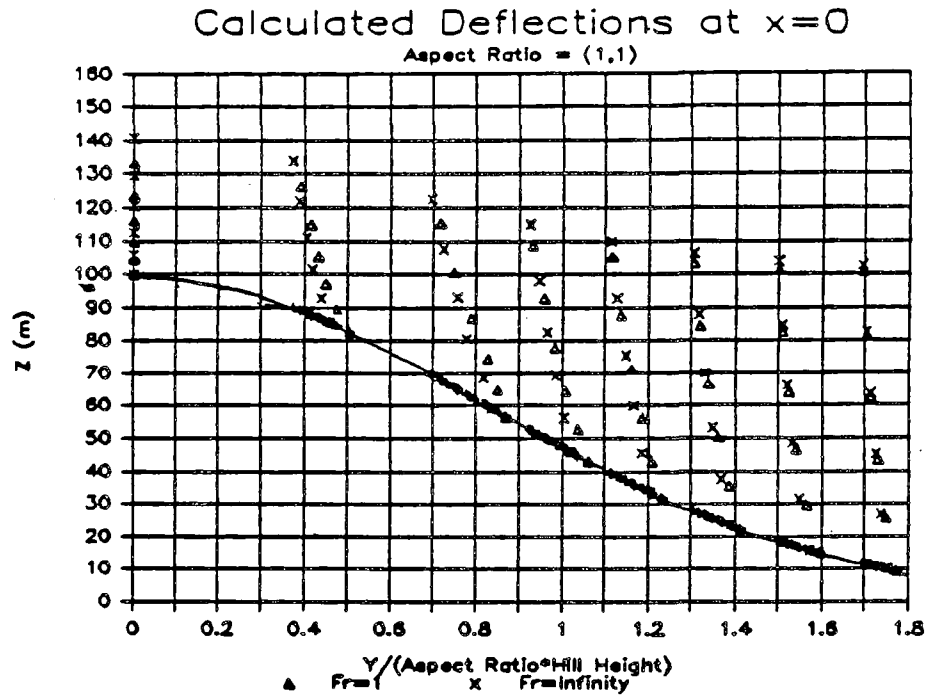

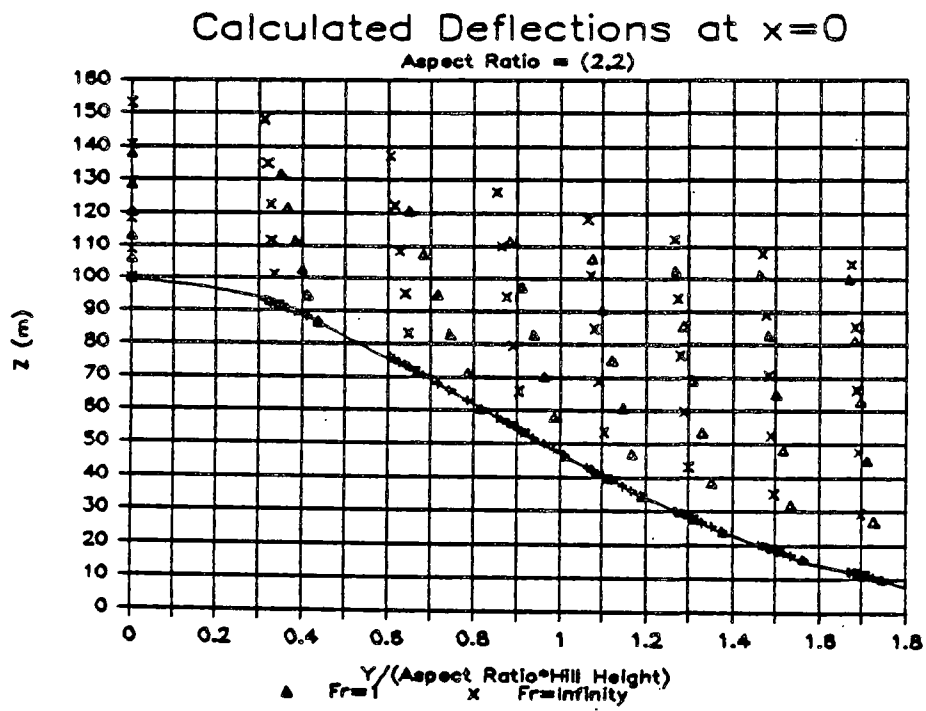

Figure 14. Comparison of lateral positions of streamlines in the plane x=0 over symmetric Gaussian hills of aspect ratio 1 and 2.

position of each streamline well upwind of the hill is shown in the lower portion of Figure 13, and the position of each over the hill is also marked in the plane x=0, where the x-axis lies along the flow and the origin lies at the center of the hill. Froude numbers of 1 and infinity are simulated for symmetric Gaussian hills of aspect ratio 1 and 2. The compression of streamlines in the vertical is most evident for the streamlines that pass nearest the crest. The greatest lateral spread in streamlines in seen in the first two streamer bands beyond the band that travels directly over the crest. As expected, the deformation in the flow is greatest near the top of the hill. In the region of greatest lateral deformation, the scaled deformation decreases with an increase in the aspect ratio of the hill. This is especially pronounced for neutral flow (Froude number very large), but not for highly stratified flow (Froude number equals one).

Results for hills that are axi-symmetric are shown in Figure 15. In the upper panel, the cross-wind aspect ratio is 1, and the along-wind aspect ratio is 2, so that the flow is along the longer axis. In the lower panel, the hill is rotated 90 degrees so that the flow is along the shorter axis. The streamline positions over the crest lie approximately midway between those for axi-symmetric hills of aspect ratio 1 and 2. Away from the crest, lateral deflections are larger when the flow is along the shorter side of the hill, and the effect of stratification on the streamlines is also greater.

Predictions of streamline position in the plane x=0 are compared with streamline positions observed in laboratory simulations in Figure 16. The laboratory simulations (Snyder et al. 1986) were performed with an axi-symmetric hill, described by a fourth order inverse polynomial function, immersed in a towing tank. Streamline positions were measured optically for a number of release positions upwind of the hill, and for various degrees of fluid stratification. The results displayed in Figure 16 include no stratification (neutral), Froude number equal to 2, and Froude number equal to 1.

The shape of the hill used in CTDM is restricted to Gaussian shapes, so that the hill used in the laboratory simulations is not represented exactly in the model. The Gaussian shape chosen to represent the inverse polynomial shape matches at the crest, and at the height contour approximately one-half the height of the crest. In the figure, the Gaussian shape is a heavy solid line, while the polynomial shape is a heavy dashed line. As illustrated, the polynomial hill exhibits a flatter top, and steeper sides. This difference must be recognized when one compares the modeled streamline positions with those observed, especially with regard to the height of a streamline above the surface of the hill.

The upper panel in Figure 16 illustrates the correspondence between the laboratory simulation and modeled results for streamlines in the limit of neutral flow. Over the crest, there is a bias towards underestimating streamline height above the surface. Away from the crest, the streamline heights above the surface (not the absolute heights) are in generally good agreement. The agreement in the

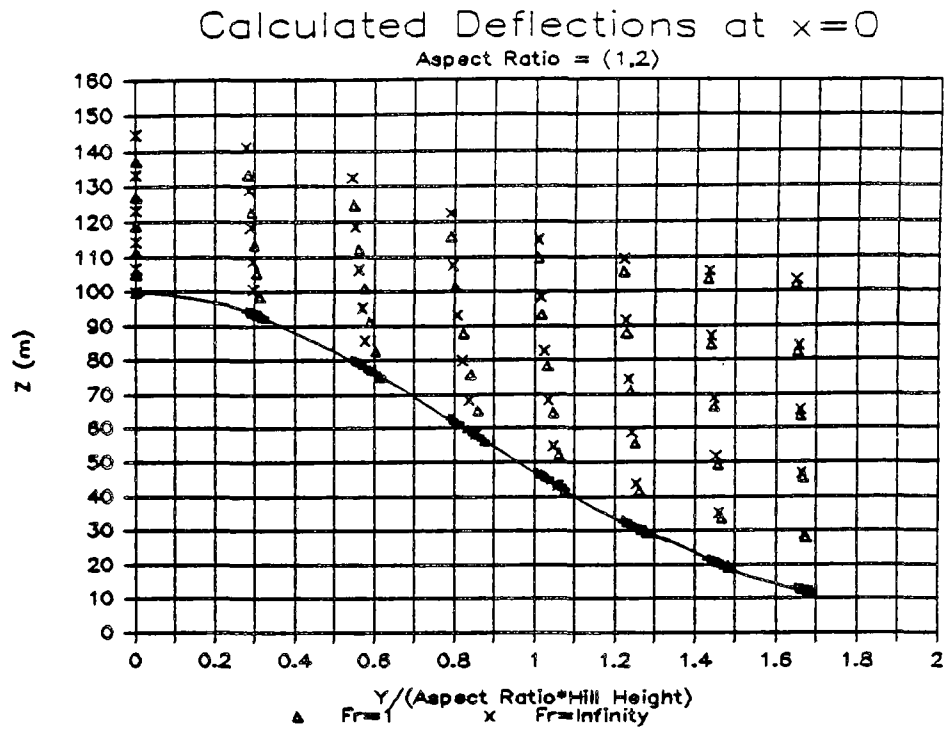

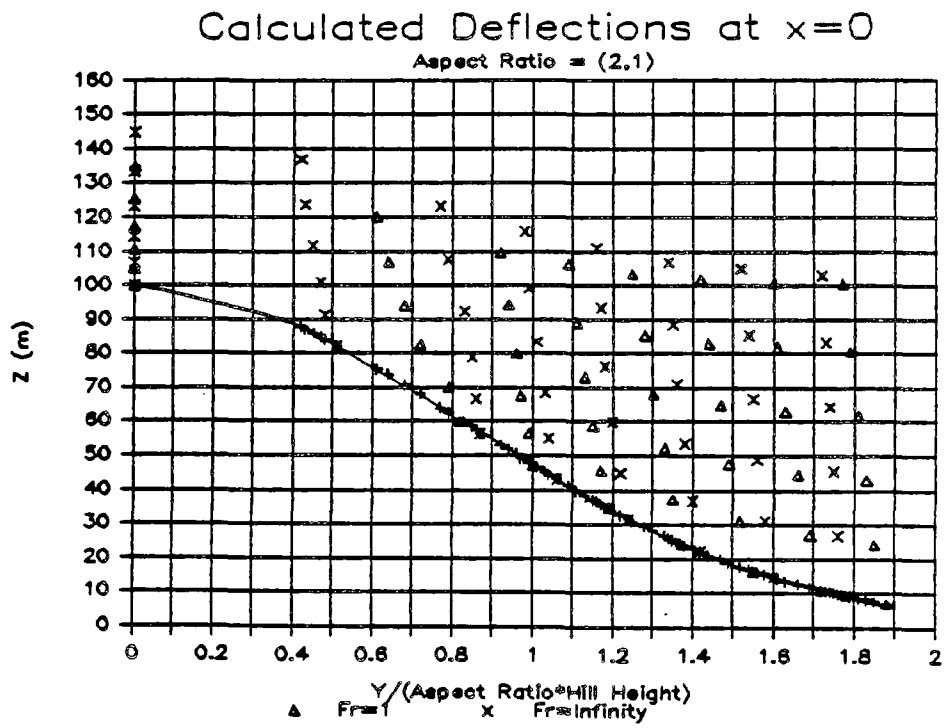

Figure 15. Illustration of streamline positions in the plane x=0 for an asymmetric hill of aspect ratio 1 and 2. The notation (1,2) indicates that the longer side (2) is aligned with the flow.

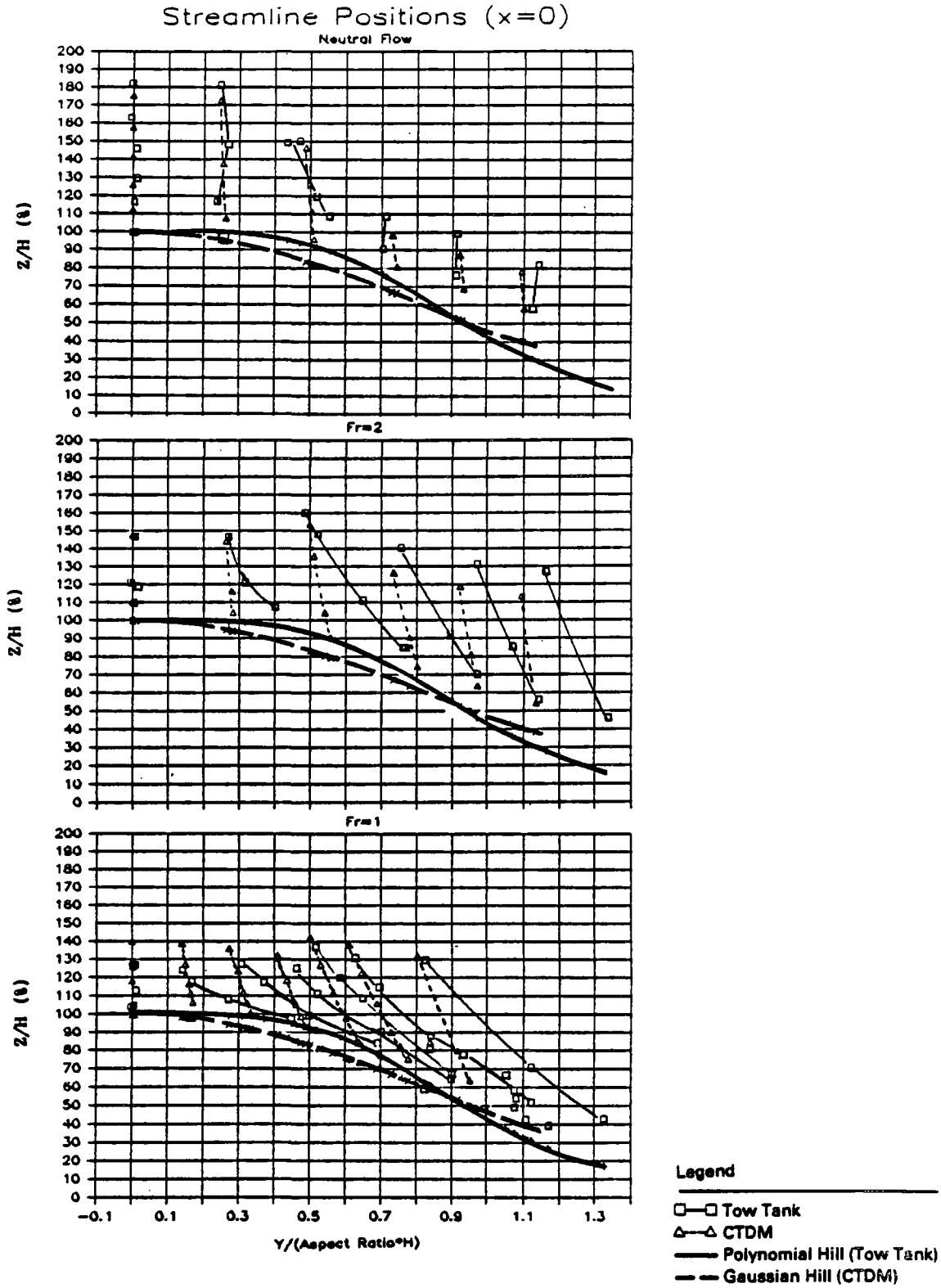

Figure 16 Comparison of streamline positions in the plane x=0 observed in tow-tank simulations by Snyder et al. (1985), with those obtained from CTDM. Positions of streamlines measured in the tow-tank are marked by squares, while those modeled by CTDM are marked as triangles. Streamlines that originated at the same lateral position are joined by either a thin line (tow-tank) or a thin dashed line (CTDM). Note that the polynomial hill used in the tow-tank (heavy solid line) differs from the Ganssian hill used by CTDM (heavy dashed line).

lateral position of the streamline is quite good. Perhaps the bias towards greater compression of streamlines in the vertical over the crest is caused by the difference in the degree of "flatness" between the two hills. Near the crest, the polynomial hill used in laboratory simulations, is broader than the Gaussian hill. A broader hill should, on the basis of the aspect ratios studied above, promote a smaller degree of compression over the crest.

The center panel in Figure 16 illustrates the results for moderately stratified flow with a Froude number of 2. Deformation of streamlines in the vertical over the crest is modeled very well. However, away from the crest, the streamlines are observed to deflect more laterally than is predicted by the model. This is especially the case for streamlines released well below the top of the hill. In spite of the bias toward underestimating the lateral deflections, the streamline heights above the surface are modeled fairly well.

The lack of good agreement in modeling the lateral deflections is consistent with the use of the linearized theory in the limit of small Froude number. Snyder et al. (1986) report results of computations that make use of the Fast Fourier Transform (FFT) technique in solving the linearized equations of Smith (1980).

The use of the FFT, although much more computer-intensive, allows the actual hill shape to be incorporated, and it precludes the need for many of the approximations adopted in developing the CTDM algorithm. A comparison of the modeled lateral positions of the lowest streamline in Figure 16 (center) is presented in Table 1. The deflections obtained by Synder et al. are virtually matched by those obtained from CTDM for streamlines that originate within about one-half the lateral length scale of the hill (from the plane y=0). Beyond this, out to streamlines that originate near y = (aspect ratio) •H, the deflection obtained by CTDM becomes smaller than that obtained by Snyder et al. This would appear to arise from approximations contained in the CTDM algorithm for sampling points away from the center of the hill.

The lower panel in Figure 16 illustrates the results for strongly stratified flow with a Froude number of 1. The observed lateral deflections near the surface of the hill become much larger than those obtained from CTDM, and the compression of streamlines in the vertical over the crest is stronger. Essentially, the linear theory substantially underestimates the effects of strong stratification. This is true of the FFT results also. In fact, because the FFT solution was formulated as a forward-looking algorithm, streamlines modeled by Snyder et al. actually pass through the surface of the hill in the lee, even for streamlines whose initial height upwind of the hill is equal to the height of the hill. The CTDM algorithm contains no such pathologies, and can therefore be utilized for Froude numbers as small as unity. The results of CTDM calculations for a Froude number equal to 1.0 should therefore be viewed as representative of significantly stratified flow, but not strongly stratified flow.

TABLE 1

COMPARISON OF THE LATERAL POSITION* OF STREAMLINES MODELED BY SNYDER ET AL. (1985) USING FFT'S AND THE CTDM ALGORITHM FOR A FROUDE NUMBER OF 2

Lateral Position (y/[aspect ratio * H])			
Initial Position (x= $-\infty$)	Observed (x=0)	FFT (x=0)	CTDM (x=0)
0	0	0	0
.192	.40	.30	.28
.385	.77	.56	.56
.577	.97	.82	.80
.769	1.14	1.06	.97
.962	1.34	1.27	1.14

*The streamlines are sampled in the plane x=0, which corresponds to a plane perpendicular to the flow and passes through the center of the hill. All streamlines were initially at an elevation equal to one-quarter the hight of the hill. The aspect ratio of the hill is 2.6. Note that the product of H * (aspect ratio) is just the length scale of the hill at one-half the hill height.

3.3.7 The WRAP Component

A particle in a steady two-dimensional flow around an obstacle will experience both accelerations and decelerations as it passes by. The magnitude of these changes in speed depends upon how close the particle is to the stagnation streamline of the flow. Maximum changes occur for particles on the stagnation streamline. Furthermore, the spacing between adjacent streamlines varies in inverse proportion to these changes in the speed along streamlines. Figure 17 is a representation of a typical streamline pattern for flow around an ellipse when the incident flow is at an angle to the axes of the ellipse.

A plume in this steady flow (with some small-scale turbulence) will follow the streamline patterns, spreading slowly across adjacent streamlines. However, as streamlines spread apart (or contract) the plume size in the horizontal will expand (or shrink) to the same extent. In the absence of diffusion, these kinematic changes in the horizontal size of the plume will not alter the concentration of material within the plume. Changes to the horizontal scale of the plume are balanced by changes in the flow speed so that the flux of material is unchanged. With the addition of small-scale diffusion, the rate of plume growth in the horizontal can be altered by changes in streamline spacing (Hunt and Mulhearn, 1973). However, based on the observations at CCB and Tracy we choose to ignore the effects of small-scale diffusion on concentrations in the WRAP component of CTDM. The observations suggest that low frequency turbulence--meanders--control crosswind plume growth over hourly averaging times.

To simulate ground-level concentrations due to dispersion of releases below H_c in complex terrain settings, CTDM must approximate the key features of steady two-dimensional flow around an ellipse that were described above. Two key approximations in the WRAP component are (1) lateral diffusion is insensitive to accelerations in the flow (i.e., the kinematic deformation of the plume has no effect on the diffusion rate), and (2) the mean flow for the averaging period (one hour) is considered steady, while all of the variability in the flow over the period, including that due to meandering, is considered "turbulence."

A primary difference between WRAP and LIFT formulations arises from the location of solid boundaries and the relationship between the position of these boundaries and the wind direction fluctuations. The terrain effect is modeled in WRAP by re-initializing the flow at the distance s_o downwind of the source (see Figure 3). The concentration at a receptor downwind of s_o is composed of concentrations from that part of the concentration distribution at s_o that lies below H_c, and that also lies on the same side of the stagnation streamline as the receptor (see Figure 18). Reflection of plume material in the vertical is allowed from the plane $z = 0$ over the entire distance s, and reflection in the horizontal is also allowed from the hillside beyond s_o. Note that the stagnation streamline forms the boundary of the hill surface in horizontal cross section.

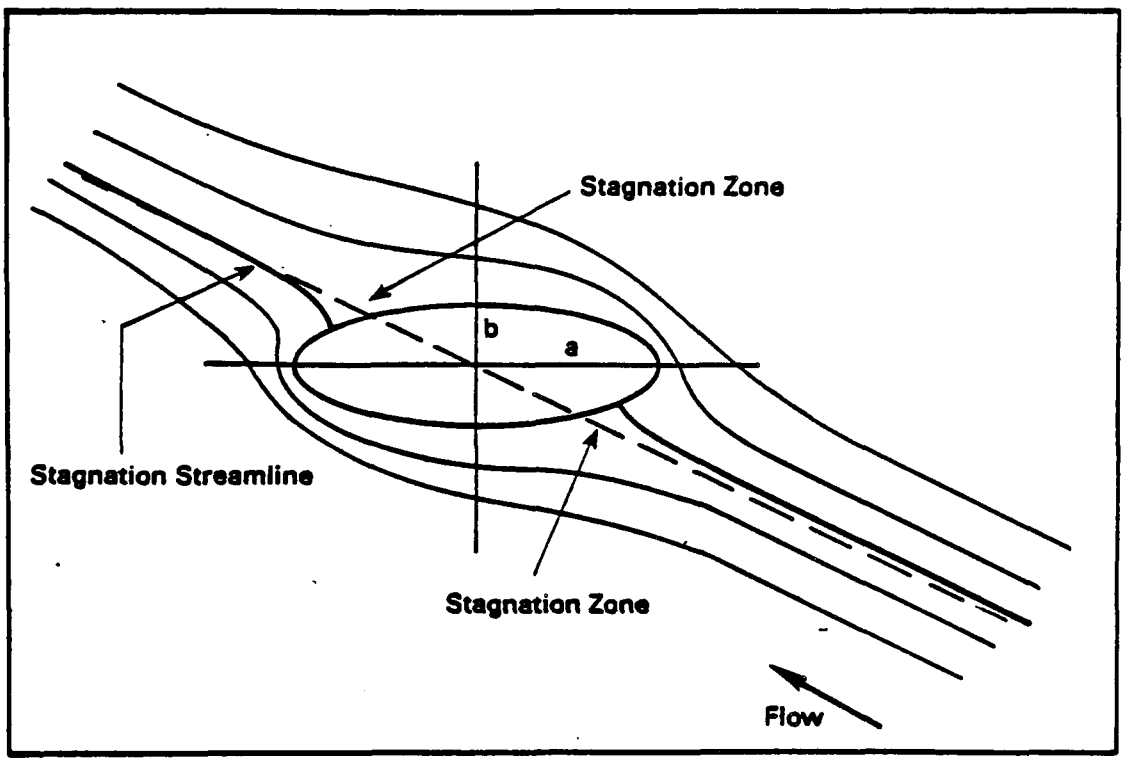

Figure 17. Typical streamline patterns in two-dimensional flow around an elliptical cylinder.

For a receptor located on the hillside at a distance s (see Figure 18) and a height z_R above the plane z = 0, the concentration due to one elemental point source located at (s_o,y,z) in the plume is given by

$$dC(s,0,z_R;s_o) = \frac{dQ(s_o,y,z)}{2\pi u\sigma_y^*\sigma_z^*}\, 2e^{-0.5(\frac{y}{\sigma_y^*})^2}$$

$$\cdot \left[e^{-0.5(\frac{z-z_R}{\sigma_z^*})^2} + e^{-0.5(\frac{z+z_R}{\sigma_z^*})^2}\right] \qquad (81)$$

Equation 81 assumes that the x-axis of the coordinate system points along the stagnation streamline, and that the source is located at (x_s,y_s,z_s). The total concentration at the receptor contains contributions from those elements below H_c and on the same side of the stagnation streamline as y_s:

$$C(s,0,z_R;s_o) = \int_o^{H_c} \int_{(o)}^{(\infty)} \frac{C(s_o,y,z)}{2\pi\sigma_y^*\sigma_z^*}\, 2e^{-0.5(\frac{y}{\sigma_y^*})^2}$$

$$\cdot \left[e^{-0.5(\frac{z-z_R}{\sigma_z^*})^2} + e^{-0.5(\frac{z+z_R}{\sigma_z^*})^2}\right] dydz \qquad (82)$$

where

$$C(s_o,y,z) = \frac{Q}{2\pi u\sigma_{yo}\sigma_{zo}}\, e^{-0.5(\frac{y-y_s}{\sigma_{yo}})^2} \left[e^{-0.5(\frac{z-z_s}{\sigma_{zo}})^2}\right.$$

$$\left. + e^{-0.5(\frac{z+z_s}{\sigma_{zo}})^2}\right]. \qquad (83)$$

These expressions are analogous to Equations 38 through 40 of the LIFT component. The integral for dy has the limits (0) and (∞). This is meant to denote integrating from 0 to +∞ if the receptor lies on the "positive" side of the stagnation streamline, and integrate from −∞ to 0 if the receptor lies on the "negative" side. Note that material is allowed to diffuse upwards through H_c so that receptors which lie above H_c, and which are downwind of s_o, can receive a contribution from the elemental point-sources below H_c at s_o. The total concentration at such receptors is the sum of both the LIFT and WRAP contributions.

8406068

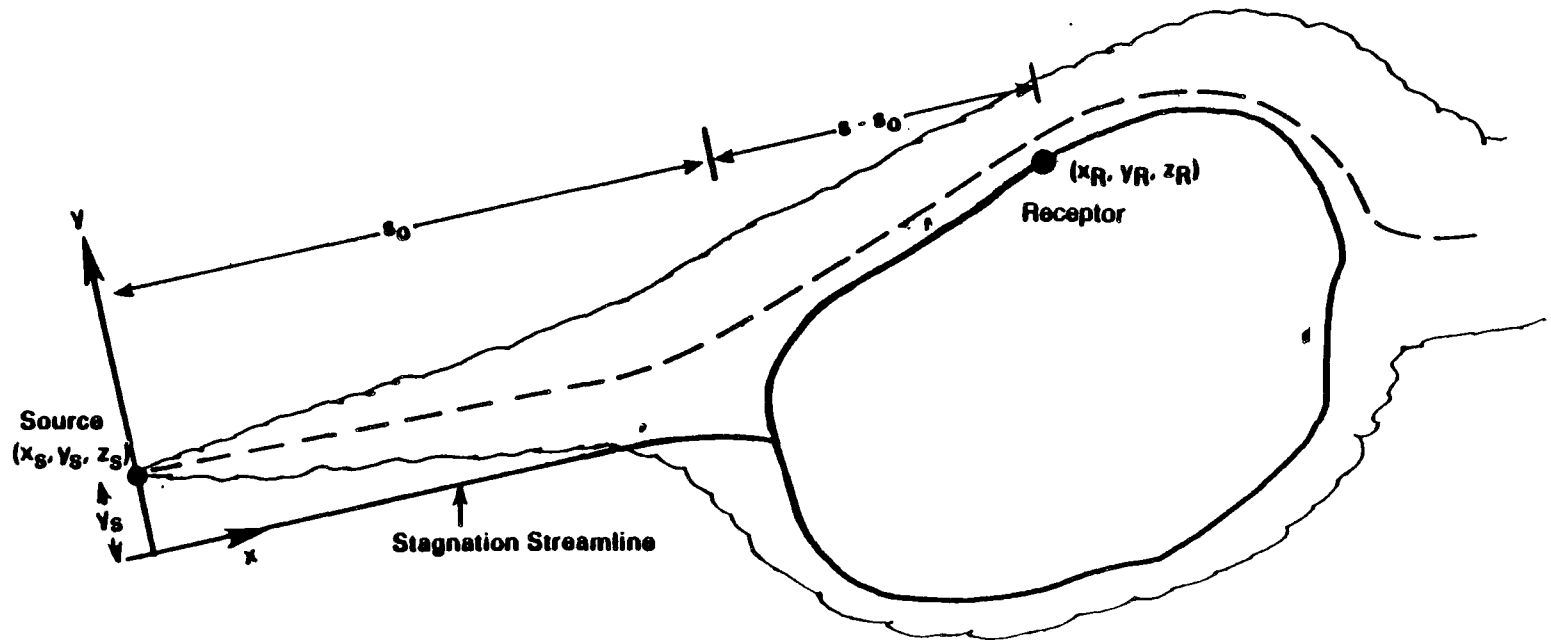

Figure 18. Top view of a plume in two-dimensional flow around a hill. The shape of the hill in crossection at the receptor height is assumed to be invariant with height so that the deformation of the entire plume around the hill is a function of the receptor location.

The integrals in Equation 82 are evaluated (using the same methods as those employed in the LIFT section) to obtain:

$$C(s,0,z_R;s_o) = \frac{Q}{4\pi u \sigma_y \sigma_z} e^{-0.5(\frac{d}{\sigma_y})^2} (1 + \text{sign}(y_R)\ \text{ERF}\ (\frac{d\sigma_y^*}{\sqrt{2}\sigma_{yo}\sigma_y}))$$

$$\cdot [B_1 e^{-0.5(\frac{z_s - z_R}{\sigma_z})^2} + B_2 e^{-0.5(\frac{z_s + z_R}{\sigma_z})^2}] \qquad (84)$$

Most of the notation here has already been encountered in Section 3.3.3. The factor sign(y_R) denotes the sign of the receptor position in the coordinate system with x-axis aligned with the flow, and it results from the choice of integrating over the "positive" or "negative" portion of the flow in Equation 82. The factors B_1 and B_2 are given by

$$B_1 = \text{ERF}\ (\frac{b_1 - b_2 - b_3}{b_o}) + \text{ERF}\ (\frac{b_1 + b_2 + b_3}{b_o})$$

$$B_2 = \text{ERF}\ (\frac{b_1 - b_2 + b_3}{b_o}) + \text{ERF}\ (\frac{b_1 + b_2 - b_3}{b_o}) \qquad (85)$$

where

$$b_0 = \sqrt{2}\ \sigma_z\ \sigma_{zo}\ \sigma_z^*$$

$$b_1 = H_c\ \sigma_z^2$$

$$b_2 = z_R\ \sigma_{zo}^2$$

$$b_3 = z_s\ \sigma_z^{*2}\ .$$

The subscript R denotes the receptor location, and the subscript s denotes the source location (see Figure 19). The distance from the stagnation streamline associated with the mean wind direction to the centerline of the plume is denoted as d, the total sigma-y (for horizontal spread of the mean plume) as σ_y, and the total sigma-z (for the vertical spread) as σ_z. The amount of plume spread experienced over the distance to the stagnation point is denoted as σ_{zo} and σ_{yo}, and the rate of plume growth beyond the stagnation point to the receptor is denoted as σ_z^* and σ_y^*, where

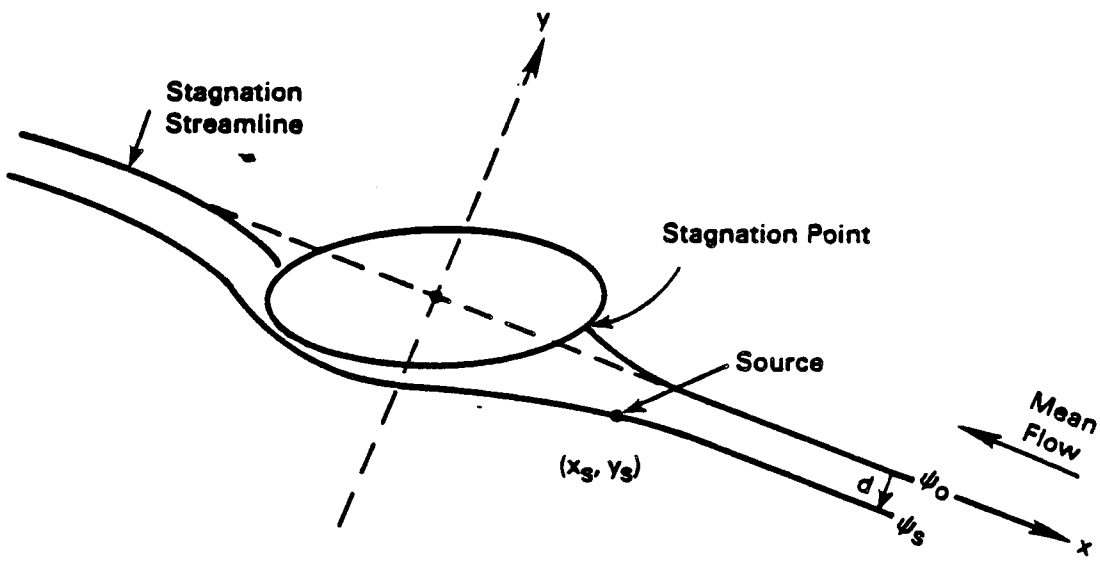

Figure 19. Sketch of the flow around an ideal cylinder of elliptical cross-section. The section shown is taken either at the elevation of the centerline of the plume (z_s), or at H_c, depending on which is smaller, and it indicates the relationship between the streamline through the source (Ψ_s), the stagnation streamline (Ψ_o=0), and the coordinate system with x-axis aligned with the mean wind direction.

8508124

$$\sigma_z^{*2} = \sigma_z^2 - \sigma_{zo}^2$$

$$\sigma_y^{*2} = \sigma_y^2 - \sigma_{yo}^2. \qquad (86)$$

The ellipse that is used to estimate the flow below H_c is taken from the horizontal cross-section of the hill at the minimum of the following two elevations: either the elevation of the centerline of the plume, or the elevation of H_c. In this way the shape of the hill selected is associated with the peak concentration of plume material found within the layer of fluid below H_c.

Concentrations at receptors located below H_c just upwind of the stagnation point are estimated as if the receptor sits on a pole of height equal to the receptor elevation above the base of the stack. Furthermore, the lateral distance between the plume centerline and the receptor is set equal to d, so that concentrations at all of these receptors are controlled by the amount of material on the stagnation streamline (see Equation 102 for d). In this way plume material below H_c follows streamlines around the hill, and only material which diffuses onto the stagnation streamline impinges on the hill. The equation for estimating these concentrations is:

$$C = \frac{Q}{2\pi u \sigma_y \sigma_z} \exp(-0.5(d/\sigma_y)^2) \left[\exp(-0.5 \left(\frac{z_R - z_s}{\sigma_z}\right)^2 \right.$$

$$\left. + \exp(-0.5 \left(\frac{z_R + z_s}{\sigma_z}\right)^2)\right]. \qquad (87)$$

Equations 87 and 84 provide estimates of ground-level concentrations of plume material before and after plume material above H_c is "removed," respectively. That is, the upper and lower portions of the flow do not become distinct in CTDM until the impingement or stagnation point is reached.

3.3.8 Model for Streamlines

The central features of WRAP are the distance between the stagnation streamline and the streamline that passes through the source and the relative locations of the source, the receptor, and the point of impingement. These require a flow model to obtain streamlines. Because the flow is two-dimensional in this strongly stratified limit, potential flow solutions are used to obtain the streamlines.

The hill below H_c is represented as a cylinder of elliptical cross-section, set on end. This shape is chosen because it contains the overall scale and orientation of the hill, and it is simple enough that streamline patterns can be expressed analytically. As already

stated, the ellipse used for the entire flow below H_c is the result of fitting an ellipse to the height-contour that corresponds to the minimum of H_c and the plume height. The potential flow solution is expressed in elliptical coordinates following the notation of Batchelor (1970).

Let the x-axis be aligned with the major axis of ellipse, let a be the length of the semi-major axis, and b be the length of the semi-minor axis. Then the elliptical coordinates (μ,ν) are related to the cartesian coordinates by the relations

$$x^2 = (a^2-b^2)\cosh^2(\mu+\mu_o)\cos^2(\nu)$$

$$y^2 = (a^2-b^2)\sinh^2(\mu+\mu_o)\sin^2(\nu). \qquad (88)$$

Note that $\mu = \mu'-\mu_o$, where μ_o is the value of μ' along the boundary of the ellipse (μ is constant along ellipses in the family of confocal ellipses of which the boundary of the hill is a member). Using the elliptical coordinates, a streamline in the flow is given by

$$\psi = - S_\infty (a+b)\sinh(\mu)\sin(\nu+\alpha_w) \qquad (89)$$

where S_∞ is the speed of the incident flow, and α_w is its direction. Note that α_w is zero when the flow is directed along the -x direction, and it increases in the clockwise direction, as noted in Figure 20.

The wind speed and direction measured at a tower near a hill may be influenced by the presence of the hill, so that a mean speed and direction must be estimated at infinity to define the incident flow. This is calculated from the theory of two-dimensional potential flow around an ellipse. Let (μ_T,ν_T) be the coordinates of the point (e.g., a tower) at which the speed and direction (S_T, ϕ_T) are measured, where ϕ_T is the direction counter-clockwise from the major axis of the ellipse. Then the wind direction is parallel to the tangent to the streamline defined by $\psi=\psi_T$ at the point (μ_T,ν_T).

From Equation 89,

$$\psi_T = - S_\infty (a+b)\sinh(\mu_T)\sin(\nu_T+\alpha_w). \qquad (90)$$

The rate of change of μ with ν along ψ_T at the tower position is found by differentiating Equation 90 with respect to ν, and evaluating it at the point (μ_T, ν_T):

$$\left.\frac{d\mu}{d\nu}\right|_T = - \frac{\tanh \mu_T}{\tan(\nu_T+\alpha_w)} . \qquad (91)$$

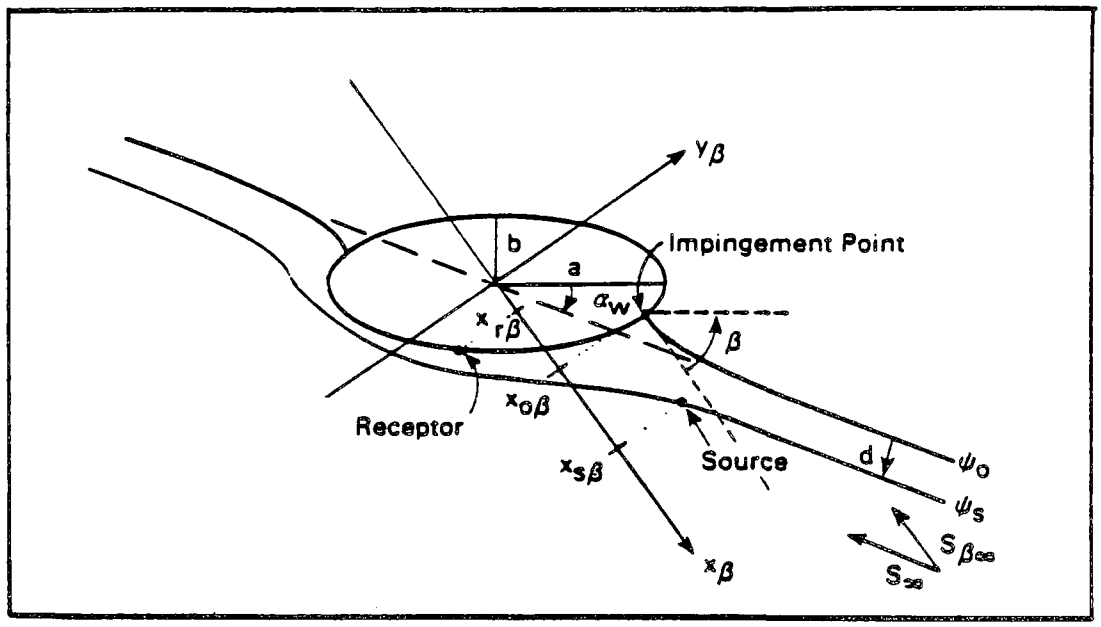

Figure 20. Definition of modeling variables, illustrating in particular the coordinate system in which the x_β-axis is aligned with the tangent to the stagnation streamline at the impingement point (the ß-coordinate system). The coordinates along the x_β-axis of the source are denoted by $x_{s\beta}$, $x_{o\beta}$, and $x_{r\beta}$, respectively.

Similarly, the slope of the tangent to the streamline is expressed in terms of the x-y coordinate system by forming the quantity dy/dx by differentiating Equation 88, and evaluating this at the position of the tower:

$$\frac{dy}{dx}\Big|_T = \frac{(b\tanh(\mu_T) + a)\tan(\nu_T)\,(d\mu/d\nu)|_T + (b + a\tanh(\mu_T))}{(a\tanh(\mu_T) + b)\,(d\mu/d\nu)|_T - (a + b\tanh(\mu_T))\tan(\nu_T)} \tag{92}$$

Noting that $\tan(\phi_T) = (dy/dx)|T$ and setting $a/b = r$, Equation 92 can now be solved for $\tan(\alpha_w)$, so that

$$-\tan(\alpha_w) =$$

$$\frac{[\tan(\nu_T)/\cosh^2(\mu_T)+\tan(\phi_T)\tanh(\mu_T)/\cos^2(\nu_T)]+r\,\tan(\phi_T)[\tan^2(\nu_T)+\tanh^2(\mu_T)]}{(\tan^2(\nu_T)\tanh^2(\mu_T)+1)+r[\tanh(\mu_T)/\cos^2(\nu_T)+\tan(\phi_T)\tan(\nu_T)/\cosh^2(\mu_T)]} \tag{93}$$

The wind speed at (μ_T, ν_T) is given by (Batchelor, 1970):

$$S_T^2 = S_\infty^2 \left(\frac{a+b}{a-b}\right) \frac{\sinh^2(\mu_T)+\sin^2(\nu_T + \alpha_w)}{\sinh^2(\mu_T+\mu_o) + \sin^2(\nu_T)}. \tag{94}$$

Upon expanding the $\sinh^2(\mu_T+\mu_o)$ term and noting that

$$\cosh(\mu_o) = a/(a^2-b^2)^{1/2}$$

$$\sinh(\mu_o) = b/(a^2-b^2)^{1/2} \tag{95}$$

and also using $r = a/b$, the speed at infinity (far away from the influence of the hill) is given by

$$S_\infty = \frac{S_T}{r+1} \left(\frac{[(r^2-1)\sin^2(\nu_T)+1]/\sinh^2\mu_T+r^2+1+2r/\tanh(\mu_T)}{1+\sin^2(\nu_T+\alpha_w)/\sinh^2(\mu_T)} \right)^{1/2} \tag{96}$$

Once the angle of the incident flow, relative to the major axis of the ellipse, and the speed S_∞ are known, the stream function through the source (ψ_s) can be calculated from

$$\psi_s = -S_\infty(a+b)\sinh(\mu_s)\sin(\nu_s+\alpha_w) \quad . \tag{97}$$

The stagnation point can also be calculated. Along the stagnation streamline, ψ_o=0, so that Equation 94 becomes

$$0 = -S_\infty(a+b)\ \sinh(\mu)\ \sin(\nu+\alpha_w) \quad . \tag{98}$$

Because this must be satisfied for all μ, ν must be equal to $-\alpha_w$ along the stagnation streamline. Therefore, the stagnation point is at $(0, -\alpha_w)$, because μ equals zero on the boundary of the ellipse.

Distance is tracked along the x_β-axis, which is parallel to the stagnation streamline at the stagnation point. This coordinate system is needed to provide a convenient Cartesian coordinate system that allows the streamline through the source to be a single-valued function of x for all α_w. At the stagnation point, the stagnation streamline meets the boundary of the ellipse at an angle of 90°. The tangent to an ellipse is given by

$$\tan(\gamma) = \frac{dy}{dx}\Big|_{\text{ellipse}} = -\left(\frac{b}{a}\right)^2 x/y. \tag{99}$$

The coordinates of the impingement point, (x_i, y_i) are given by Equation 93 with $(\mu,\nu) = (0, -\alpha_w)$, so that

$$\begin{aligned} x_i &= a\cos(\alpha_w) \\ y_i &= b\sin(\alpha_w). \end{aligned} \tag{100}$$

Because the stagnation streamline is perpendicular to the tangent to the ellipse at (x_i, y_i), the tangent of the rotation angle, β, must be $-1/\tan(\gamma)$.

$$\tan(\beta) = -\frac{a}{b}\tan(\alpha_w) \quad . \tag{101}$$

The distance between the streamline through the source (ψ_s) and the stagnation streamline (ψ_o=0) far from the hill is related to the value of ψ_s and the wind speed at infinity, S_∞. Because the speed of the flow equals the gradient of the stream function far from the hill, $S_\infty = (\psi_s - \psi_o)/d$, or

$$d = \psi_s/S_\infty. \tag{102}$$

However, because σ_y may be measured closer to the hill, the speed at the source is substituted for S_∞ to estimate d near the source.

3.3.9 Receptors not Influenced by Hills

In theory, the main subroutines of CTDM give results which are identical to flat-terrain results in the limit that the hill height goes to zero. However, the code in the model is not designed to check

for hill height of zero before executing statements that may require division by the hill height; and if it were, many extensive calculations would be needlessly executed, with the model returning no terrain-effects. Furthermore, the structure of the model requires that receptors be associated with specific hills wherein each hill requires extensive information. A flat terrain algorithm is included in the model to avoid such numerical problems and extra input requirements.

The flat terrain algorithm simply performs a Gaussian plume computation which assumes that there is no mixing lid, that all receptors lie on a single ground-plane, and that plumes travel in straight lines. All plume rise and growth algorithms match those used in the other sections of the model. For a plume at height z_s above the surface, released from $y = y_s$, the concentration of plume material at a receptor placed at a height h_R above the surface, and set at $y = y_R$, is given for a time of travel t from the virtual source (including a virtual time) by

$$C(t,y_R,h_R) = \frac{Q\, e^{-0.5\,(\frac{y_R-y_s}{\sigma_y})^2}}{2\pi u \sigma_y \sigma_z} \left[e^{-0.5(\frac{h_R-z_s}{\sigma_z})^2} + e^{-0.5(\frac{h_R+z_s}{\sigma_z})^2} \right]. \quad (103)$$

Note that the time of travel appears in the expressions for σ_y and σ_z (Equation 29).

SECTION 4

CTDM EVALUATION ANALYSIS

An assessment of the performance of CTDM is described in this section. CTDM and two other complex terrain models used for rural applications, COMPLEX I and RTDM (Paine and Egan, 1987), were evaluated at five sites. These sites included the three CTMD sites (CCB, HBR, FSPS) as well as two other sites with conventional SO_2 data obtained over a one-year period (the Westvaco Lake paper mill and the Widows Creek steam generating station). The models that were evaluated and the data bases used are discussed further in Sections 4.1 and 4.2, respectively.

A large part of the CTMD data base (CCB, HBR, FSPS) was used in the development of CTDM, so the overall results for CTDM at these three sites do not represent an unbiased test of CTDM versus COMPLEX I and RTDM. The CCB data base for both SF_6 and CF_3Br was used extensively in the development of CTDM. Model development use of the HBR data base concentrated on only a subset of the CF_3Br data (35 hours; see Strimaitis et al., 1985) and none of the SF_6 data (for which lidar-derived plume heights were not obtained until the evaluation task). The use of the Tracy Power Plant data for model development was focused upon hours involving plume travel toward Beacon Hill and Target Mountain; hours involving impacts on samplers on other hills were not used. In addition, the model development used meteorological data from the 150-m tower only, while the model evaluation data base also included tethersonde and doppler sodar data. Withheld data that are available for future model evaluations include 20 hours from HBR (see Lavery et al., 1983, page 184) and all of the data from the preliminary Tracy experiment in the fall of 1983.

A series of statistical tests (described in Section 4.3) were run on the models for data sets both paired or unpaired in time and/or space. These tests examined the models' overprediction or underprediction bias as well as the root-mean-square (RMS) error, and the percentage of predictions within a factor of two of observations. Results are described in Section 4.4.

Another aspect of the evaluation analysis involved an examination of the spatial distribution and magnitude of CTDM concentrations for each hour at the three CTDM tracer sites. CTDM performance in the LIFT and WRAP components was assessed by examining the behavior of hourly patterns of predicted and observed concentrations. Results are given in Section 4.5.

4.1 Models Evaluated

At the CTMD tracer sites, CTDM was evaluated using the plume height set to the tracer release height for near-neutrally buoyant releases. In some cases with buoyant tracer plumes (for SF_6 at HBR and FSPS), CTDM was run using a final plume height based upon lidar observations of the plume. At FSPS, CTDM runs for SF_6 releases were done for both observed and calculated plume heights. The "observed" plume height at the Tracy Power Plant was obtained by examining the lidar observations. The first two lidar cross-sections through the plume were both used independently to define two final observed plume height. The first cross-section occurred at a downwind distance of roughly 500 meters, while the second typically occurred at a distance between 1000 and 1500 meters. The resulting two alternative observed plume heights were tested using CTDM (results are shown in Section 4.4). The calculated plume heights at FSPS were derived from conventional stack gas exit parameters (temperature, velocity, stack diameter). For the conventional SO_2 data bases, plume heights were calculated for each hour.

Other rural complex terrain models that were evaluated included COMPLEX I and RTDM, which was run in both "default" and "on-site" modes. RTDM in default mode does not employ vertical and horizontal turbulence intensity information nor vertical temperature gradient data. The on-site mode does use these meteorological variables, and in so doing, is similar to CTDM in taking advantage of these available measurements. COMPLEX I and RTDM were run using observed plume heights where applicable, except that only calculated plume heights were evaluated at FSPS.

Tables 2, 3, and 4 list several important features of these models, including plume transport, plume dispersion and stability determination, plume rise and terrain impingement, and limits to vertical mixing. Of the three models, COMPLEX I is the least refined because it requires no terrain profile or shape information and does not consider a critical dividing streamline height. The number of meteorological input variables available to COMPLEX I and to RTDM in default mode is limited; no hourly temperature gradient or σ_θ and σ_w data can be accommodated. In on-site mode, RTDM can use these additional variables. RTDM requires the input of terrain profiles and hill-top heights for 36 directions in 10° increments about a common source location. This information is used for partial reflection and critical dividing streamline height calculations.

CTDM requires more terrain information; a complete three-dimensional description of each separate hill involved in the modeling is supplied by a terrain preprocessor. Up-to-date techniques for computing the mixed layer height and boundary layer parameters such as Monin-Obukhov length, L, and the friction velocity, u_* are provided by a meteorological preprocessor. CTDM, unlike COMPLEX I and RTDM, accounts for the horizontal deflection of streamlines in the vicinity of terrain. The model also can read meteorological input data from many levels and interpolate or scale wind, temperature, and turbulence variables to plume height.

TABLE 2

FEATURES OF COMPLEX TERRAIN MODELS

USED IN THE EVALUATION: CTDM

Plume Transport And Dilution

- Wind speed and direction interpolated from multiple levels of input data or scaled from the highest available level to final plume height.
- Plume deflection around (or over) terrain obstacles accounted for.
- Plume height wind speed used in Gaussian equation.

Plume Dispersion/Stability

- Meteorological preprocessor provides Monin-Obukhov length, a continuous stability parameter.
- Plume σ_y, σ_z determined from measured σ_θ (or σ_v), σ_w data and estimated Lagrangian time scales.
- Off-centerline (rather than sector averaging) used in concentration calculations.
- Buoyancy-enhanced vertical and horizontal dispersion.
- Model does not calculate concentrations for unstable conditions.

Plume Rise/Terrain Impaction

- Plume lifting (terrain adjustment) over terrain varies hourly as a function of distance to hill, hill shape, and critical dividing streamline height.
- No minimum terrain approach; direct plume impingement is possible.
- Briggs final plume rise used; meteorology for plume rise calculations obtained halfway between stack top and final plume height.

TABLE 2 (Continued)

- Measured values of $d\theta/dz$ used for stable rise.

Limits to Vertical Mixing

- Full reflection at the ground, unlimited growth above
- Local internal boundary layer used in vicinity of hills.
- No mixing lid restriction used in stable conditions, but mixing height governs profiles of wind and turbulence within the surface layer.
- Nocturnal lid determined from diagnostic boundary layer depth formula.

Terrain Depiction

- Digitized terrain contours as read by terrain preprocessor.
- Mathematical description of each hill is used by CTDM.

TABLE 3

FEATURES OF COMPLEX TERRAIN MODELS

USED IN THE EVALUATION: RTDM

Plume Transport and Dilution

- Wind speed scaled to stack-top height for plume rise, to final plume height for use in Gaussian equation.
- Wind direction as input, not scaled with height.
- No plume deflection around hills (in the horizontal).

Plume Dispersion/Stability

- Discrete Pasquill-Gifford stability categories (A-F).
- In default mode, plume σ_z growth determined from Briggs (1973) rural dispersion coefficients.
- In on-site mode, plume σ_z growth determined by observed σ_θ, σ_w data (if available).
- 22.5° horizontal sector averaging for all stability classes in default mode; off-centerline Gaussian concentration calculations in on-site mode.
- Buoyancy-enhanced vertical and horizontal dispersion.

Plume Rise/Terrain Impaction

- Terrain adjustments = 0.5 for all stability classes; changed to 0 for stable classes if the plume is below the critical dividing streamline height.
- No minimum terrain approach; direct plume impingement is possible.
- Briggs final rise used as calculated from stack-top meteorology.
- Stability-dependent values of $d\theta/dz$ used for stable rise in default mode; measured values used in on-site mode.

TABLE 3 (Continued)

Limits to Vertical Mixing

- Full reflection at ground and mixing lid, but unlimited mixing height for stable conditions.

Terrain Depiction

- Terrain profiles (elevation versus distance from source) specified in 10° angular intervals; appropriate profile is chosen each hour based upon wind direction.

TABLE 4

FEATURES OF COMPLEX TERRAIN MODELS

USED IN THE EVALUATION: COMPLEX I

Plume Transport and Dilution

- Wind speed scaled to stack-top height for plume rise.
- Wind direction as input, not scaled with height.
- No plume deflection around hills (in the horizontal).
- Stack-top height wind speed used in Gaussian equation.

Plume Dispersion/Stability

- Discrete Pasquill-Gifford (P-G) stability categories (A-F).
- Plume σ_y, σ_z growth using P-G dispersion coefficients (rural).
- 22.5° horizontal sector averaging for all stability classes.
- Buoyancy-enhanced vertical and horizontal dispersion.

Plume Rise/Terrain Impaction

- Terrain adjustments = .5 for stabilities A-D, 0 for E and F.
- Closest plume centerline approach to terrain = 10 meters.
- Briggs final rise used, calculated from stack-top meteorology.
- Stability-dependent values of $d\theta/dz$ used for stable rise.
- Critical dividing streamline height is not accounted for.

TABLE 4 (Continued)

Limits to Vertical Mixing

- Full or partial reflection at ground and mixing lid, but unlimited mixing height for stable conditions.

Terrain Depiction

- Receptor heights given only; no hill shape or terrain profile information used.

4.2 Data Sets Used for Evaluation

CTDM, COMPLEX I, and RTDM were evaluated with data from the three CTMD sites: Cinder Cone Butte (CCB), the Hogback Ridge (HBR), and the Tracy Power Plant (FSPS). For these model runs, the emissions, meteorological and receptor data were reformatted to be compatible with the operational version of CTDM. A special provision was made to allow these models to read observed plume height data, which varied hourly at the Hogback Ridge and at Tracy.

To supplement the CTMD sites, two other data bases were selected for the model evaluation: the Westvaco pulp and paper mill in Luke, Maryland (Wackter and Londergan, 1984) and the Widows Creek Steam Plant (TVA) in northeastern Alabama (Egan et al., 1985).

At Cinder Cone Butte, an isolated hill, SF_6 and CF_3Br releases were modeled. There were 107 hours of SF_6 releases and 51 hours of CF_3Br releases modeled at 93 receptors (See Figure 21). The tracers were released from cranes, which were repositioned several times during the experiment. Each new release position and/or height was considered as a separate source. Therefore, there were 55 SF_6 sources and 22 CF_3Br sources modeled in this evaluation.

The Hogback Ridge (Figure 22) was viewed as one long hill for the CTDM evaluation. A total of 99 hours were modeled at 106 receptors from 36 release heights/locations for SF_6 and CF_3Br.

At the Tracy Power Plant, the terrain was divided into 18 individual hills (Figure 23) for the CTDM evaluations. SF_6 was released from the Tracy stack and CF_3Br was released from 3 levels of the 150-m tower during the experiment. A total of 128 hours were modeled at 110 receptors. Each receptor was identified as being on one of the 18 hills.

Three sets of meteorological inputs were prepared for each site: a preferred data set using all available data and two versions of degraded meteorological data. The degraded meteorological data consisted of either only one or two levels of wind, temperature, and turbulence data. At CCB, 8 levels of data were used in the profile (2, 10, 40, 60, 80, 100, 150 m), plus a level obtained from the Modelers Data Archives (MDA's) for the meteorological data at plume height for each hour. The first degraded data set at CCB consisted of 10-m and 80-m tower data and the second degradation contained only 10-m tower data.

The preferred meteorological data set at HBR consisted of 10 levels from the 150-m tower (2, 5, 10, 30, 40, 60, 80, 100, 150 m). The first degraded data set had only the 10-m and 100-m levels. The second degradation used only the 10-m tower data.

At FSPS, 16 levels of meteorological data were contained in the preferred data set. The composite profile was obtained from the 150-m tower, the sodar and the tethersonde. Wind data was extended above the top of the 150-m tower in 25-m increments up to about 400 m with

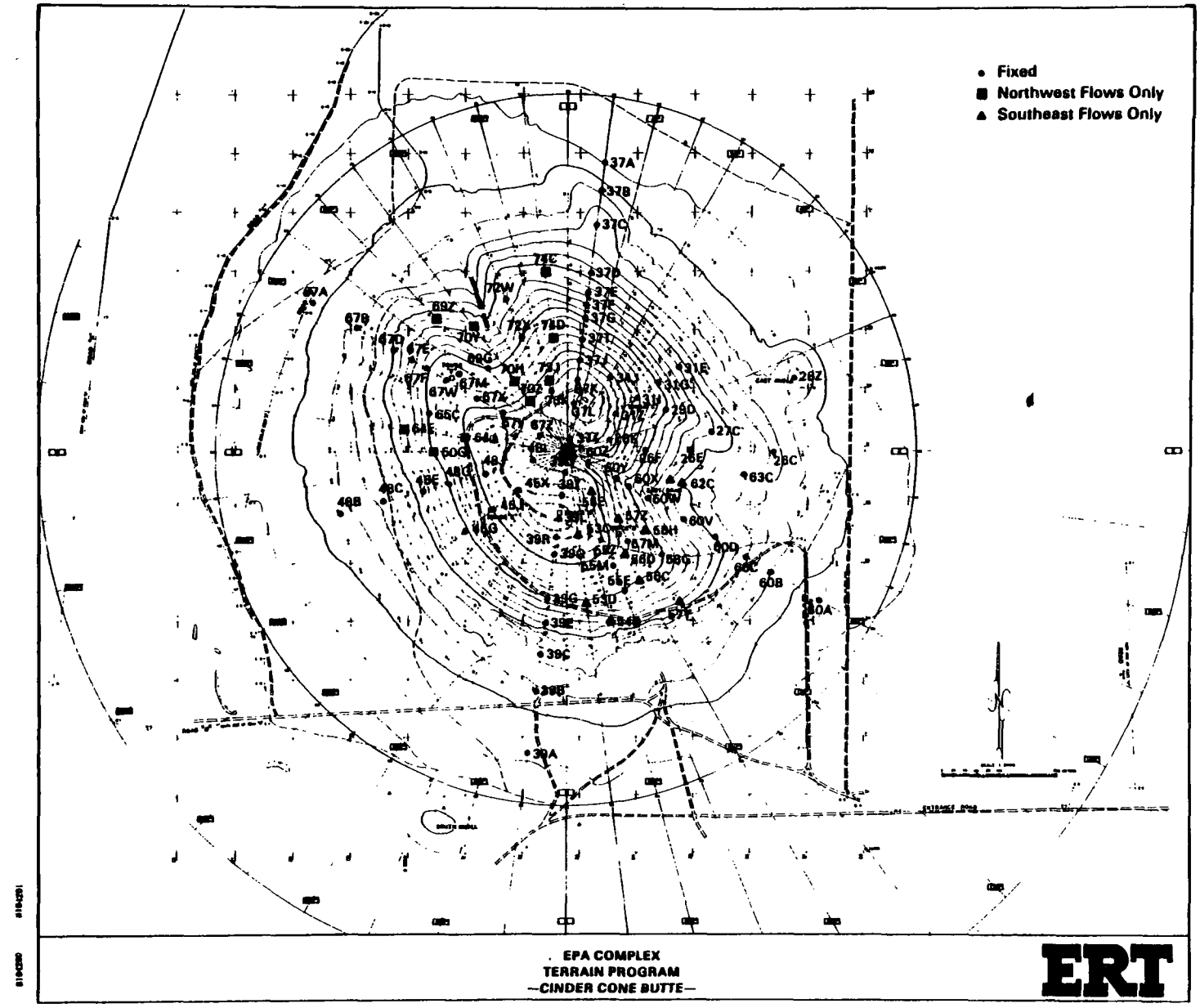

Figure 21. Tracer gas sampler locations on Cinder Cone Butte.

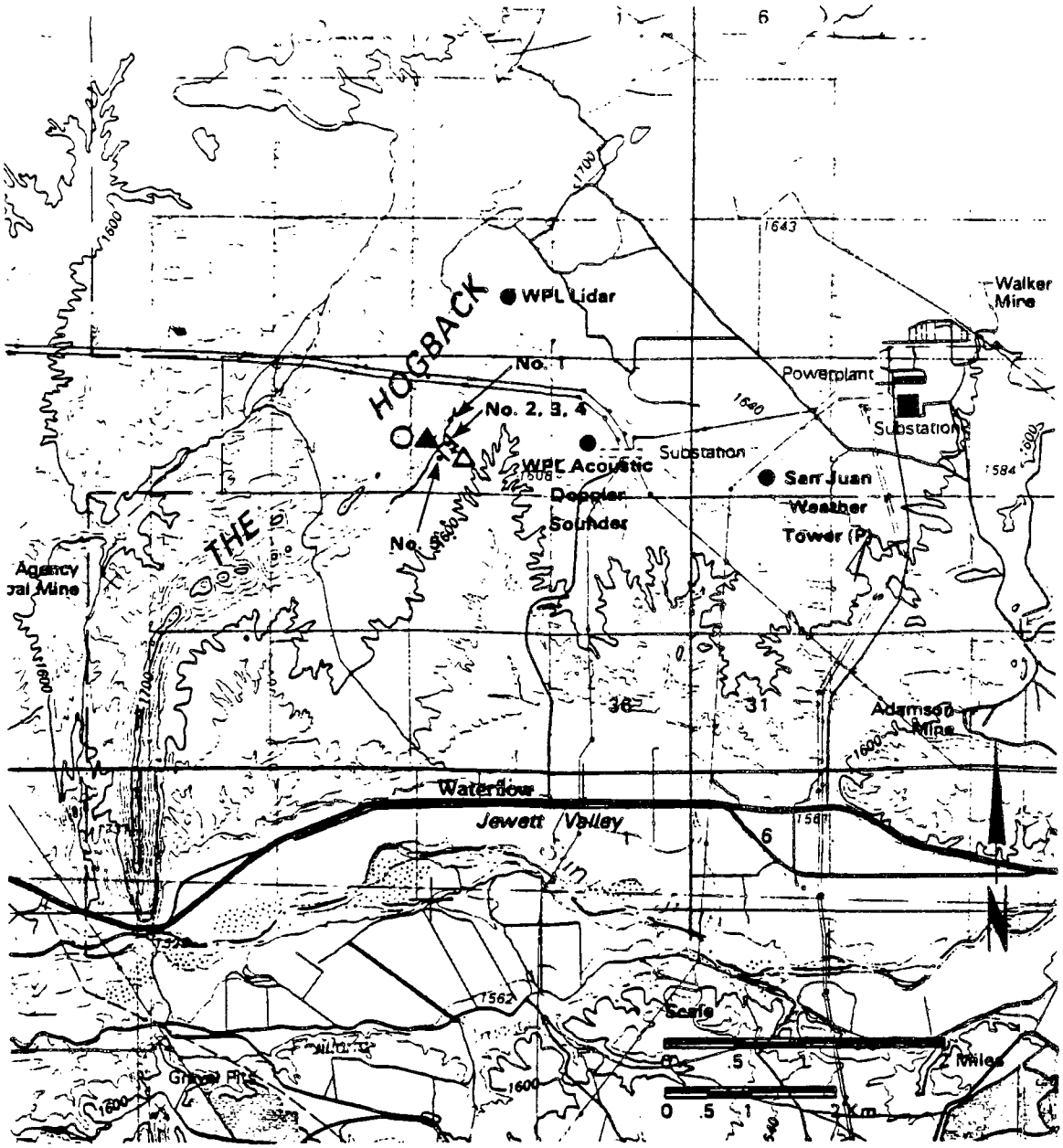

Figure 22. Field experiment layout in the vicinity of the Hogback Ridge.

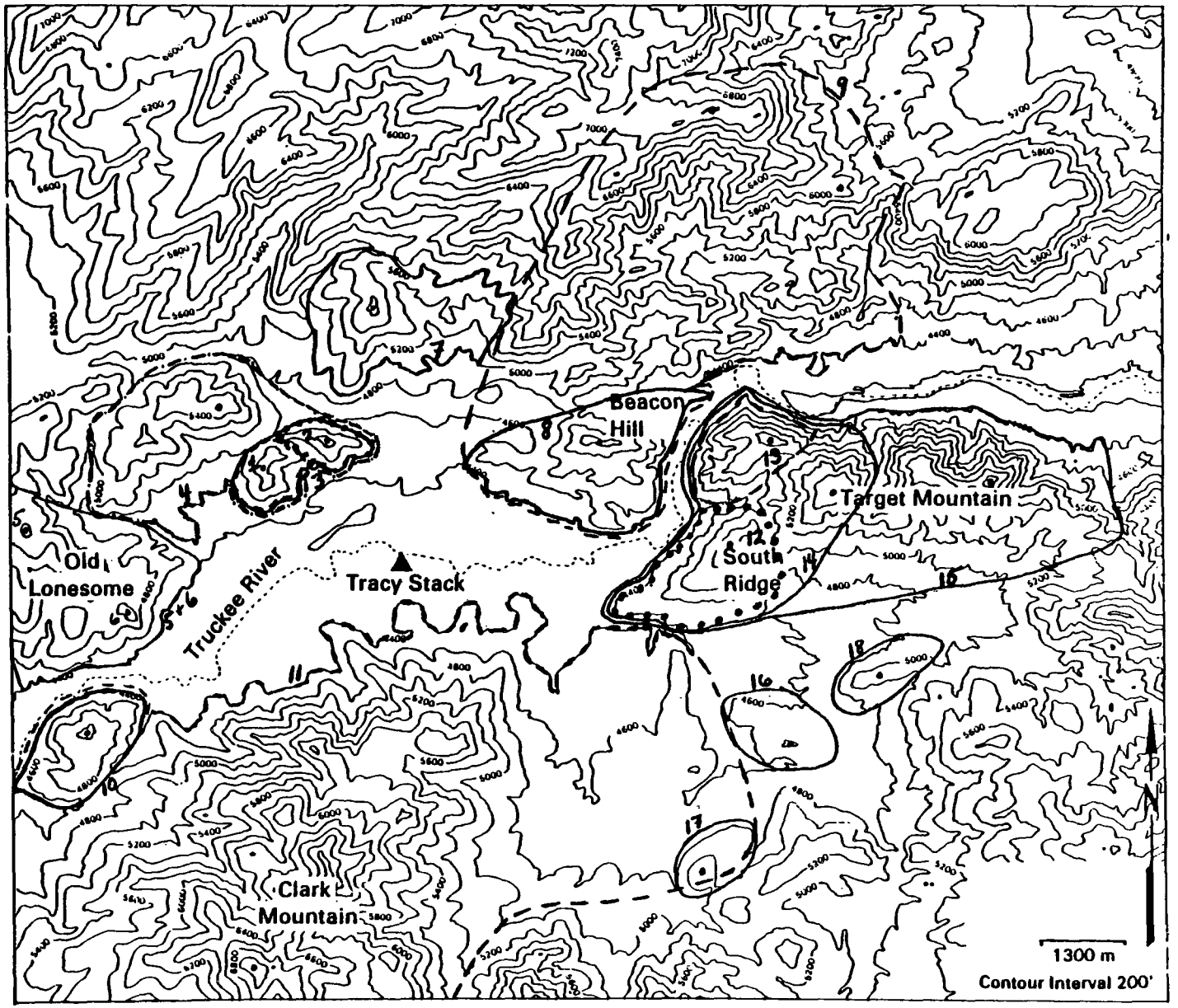

Figure 23. Terrain features surrounding the Tracy Power Plant as modeled by CTDM.

the use of sodar data. Inconsistencies between the tower and sodar data at 150 m were smoothed out between the levels of 100 and 200 meters. The difference for any hour was handled by linearly interpolating between the tower level at 100 m and the sodar level at 200 m. Temperatures were extended above 150 m through the use of the tethersonde temperature gradient above 150 m. In the input data degradation tests, only the tower data was used. The bottom (10-m) and top (150-m) levels were used in the first degraded data set and the second degradation consisted only of the bottom level.

Four hills were identified for modeling with CTDM in the vicinity of Westvaco's Luke Mill (Figure 24). A single stack was modeled for 11 receptors for a one-year period (December 1980-November 1981). CTDM was run sequentially for the entire year, but did not calculate concentrations when the plume was in an unstable layer (Monin-Obukhov length is negative and the plume is within the mixed layer).

The meteorological profile was obtained from the 30-m Luke Tower (near site #2, north of the stack) and also from the 100-m meteorological tower on the hill to the southeast (at site #1). The use of a temperature gradient obtained between the tops of these two towers was expected to result in better CTDM performance than the use of a single tower with the lower temperature measurement from 10 meters. (A similar result had previously been obtained independently for RTDM at Widows Creek, where balloon soundings verified this finding (Egan et al. 1985)). The "full" profile of meteorological data involved 5 levels: 190, 210, 326, 366, and 416 meters above the base of the 190-m stack. The first degrade involved only the 190- and 210-m levels (Luke Tower 10- and 30-m levels) and the second degrade used only the 190-m level.

A total of five hills were used in the CTDM modeling of the Widow Creek Steam Plant (Figure 25). Three stacks were modeled for 14 receptors for calendar year 1980. The meteorological data profile was assembled from two 61-m towers, one in the Tennessee River valley and one on the top of Sand Mountain (near Station 3). The full meteorological profile included data at 10, 61, and 312 meters above stack base (all of the valley tower and the top of the mountain tower). One data degrade employed only the valley tower (10- and 61-m levels) while a second degrade used the 10-m level of the mountain tower (261 m above stack base).

For both the Westvaco Lake and Widows Creek data base, the background concentration was determined for each hour as the lowest monitored concentration in the network. The hourly background concentrations were subtracted from the total monitored concentrations to obtain a residual concentration attributable to the source in question. The use of the lowest monitored observation always resulted in a non-negative concentration from the source in question.

4.3 Statistical Tests and Case-Study Analyses

Hourly concentration predictions were obtained for each of the models described in Section 4.1. Although RTDM and COMPLEX I

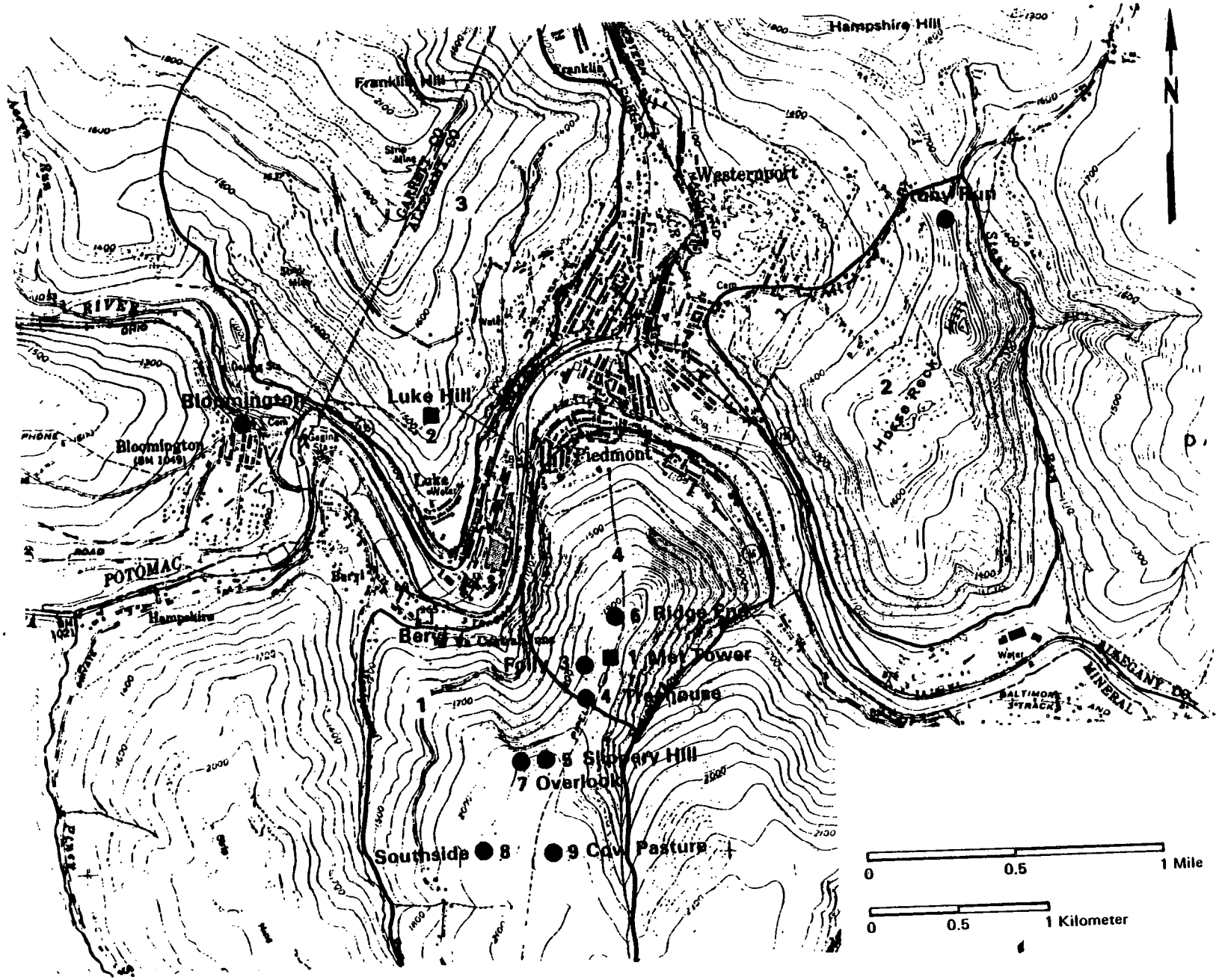

Figure 24. Terrain features and monitors in the vicinity of the Westvaco Luke Mill.

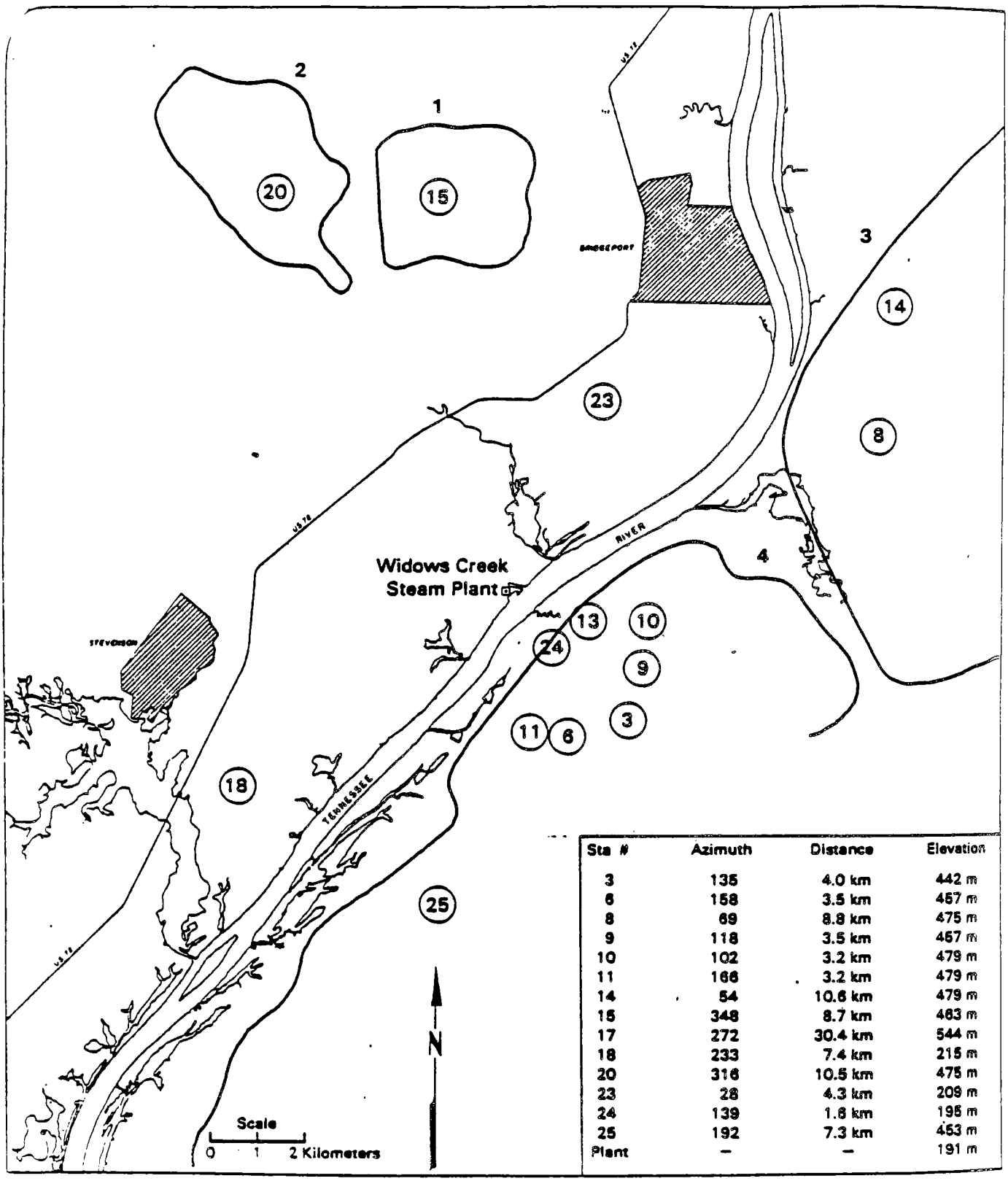

Sta #	Azimuth	Distance	Elevation
3	135	4.0 km	442 m
6	158	3.5 km	457 m
8	69	8.8 km	475 m
9	118	3.5 km	457 m
10	102	3.2 km	479 m
11	166	3.2 km	479 m
14	54	10.6 km	479 m
15	348	8.7 km	463 m
17	272	30.4 km	544 m
18	233	7.4 km	215 m
20	316	10.5 km	475 m
23	28	4.3 km	209 m
24	139	1.8 km	195 m
25	192	7.3 km	453 m
Plant	–	–	191 m

Figure 25. 1980 Widows Creek monitoring network with outlines of terrain features used in CTDM.

calculate concentrations for every hour, CTDM does not give predictions for unstable hours if the plume is within the surface layer. Therefore, it was necessary to restrict the evaluation results to only those hours for which CTDM results were available. In addition, comparisons had to be restricted to only those sampler sites that were operational for any given hour. Analyses were performed for 1-hour averages for the tracer experiments (CCB, HBR, FSPS) and for 1-hour and 3-hour averages for the conventional SO_2 data bases (Westvaco Luke and Widows Creek).

Specific statistical tests and data subsets to which they were applied are listed in Table 5. For tracer data such as the CTMD sites, primary tests involve data sets paired in time or paired in time and space. The excellent spatial resolution in these tracer experiments maximizes the likelihood that the peak observed and predicted concentrations will be found somewhere in the network. The occasional movement of the sources and the monitoring network, especially for CCB and HBR, causes a paired-in-space test to be less important for some of the tracer data. The data set unpaired in time and space is similarly difficult to interpret and sometimes misleading for these tracer data bases because the sources and network are not fixed in location. For these reasons, results for the test unpaired in time and space are not presented for the CCB or HBR data sets.

For the conventional data bases, tests that are unpaired in time are important because of the long time record but relatively poor spatial resolution. The number of SO_2 monitors is, however, large enough to allow testing with data sets paired in time and paired in time and space.

The model bias test involves the difference of the averages of the hourly peak model predictions and observations. For each of the five data sets analyzed, the highest concentration only was used to compile this statistic. An additional data base employed at the tracer sites consisted of the average of the highest 5 predictions and observations each hour. This data base produced results less dependent upon extreme concentrations and was feasible because of the high spatial resolution of the tracer samplers. The computed model bias is the average observation minus the average prediction, so a negative bias denotes a model overprediction.

The root-mean-square (RMS) error and normalized mean square error (NMSE) statistics show a measure of model scatter and also incorporate the model bias. The mean square error is represented as $(C_o - C_p)^2$, where C_o is an observed concentration, C_p is a predicted concentration and an overbar denotes an average over all samples. While the RMS error is simply the square root of the mean square error, the NMSE error is represented here in two forms:

$$NMSE_1 \text{ (or M1)} = \overline{(C_o - C_p)^2}/\overline{C_o}^2$$

$$NMSE_2 \text{ (or M2)} = \overline{(C_o - C_p)^2}/[\overline{C_o}\,\overline{C_p}]$$

TABLE 5

DATA SUBSETS AND EVALUATION TESTS FOR TRACER (CTMD) AND CONVENTIONAL DATA BASES

1) Unpaired in Time and Space
   (Model bias only for measures listed below)
   a) Highest concentration
   b) Second-highest
   c) Highest Second-Highest
   d) Average of Top N values*

2) Paired in Time, Not in Space (peak hourly values)
   a) Model bias
   b) Root-mean-square (RMS) error
   c) Normalized mean square error (NMSE)
   d) % of predicted peaks within
      a factor of 2 of observations

3) Paired in Space (peak values and Top 10 values at each monitor)
   a) Model bias
   b) RMS error
   c) NMS error
   d) % within factor of 2

4) Paired in Time and Space (each site, each hour)
   a) Model bias
   b) RMS error
   c) NMS error
   d) % within factor of 2

* N = 5 for tracer experiments, 10 for conventional data bases.

The first of these formulations is desirable because of its simplicity (no use of the average predicted concentration), while the second one results in equal treatment for under- and overpredicting models.

The percentage of cases with predictions within a factor of 2 of observations is listed to summarize the results of a scatter plot of predictions versus observations. This statistic is also a rule-of-thumb indicator as to how accurate the model being evaluated is on a case-by-case basis.

The bias, RMS error, NMSE, and % within a factor of 2 statistics were also prepared for concentrations paired in time for several classes of meteorological conditions. These conditions included stability classes D, E, and F (based upon near-surface conditions) and 3 categories of release-height wind speeds: 0-1, 1-3, and >3 meters per second.

In addition to the tabulated results described above, scatter plots of predicted versus observed 1-hour and 3-hour average concentrations were prepared for peak concentrations paired in time. The results of the statistical tables and scatter plots for the five evaluation sites are discussed in Section 4.4.

Case-study analyses involving plots of predicted (CTDM only) and observed concentrations were also performed at the tracer sites. The concentrations were plotted on pairs of maps for each hour: one for predicted and one for observed concentrations (See Figure 26a and 26b). The plots include a listing of plume height, H_c and Froude number values as well as the location of the source and the positions of the highest predicted and observed concentrations. Results of the analyses of these maps are discussed in Section 4.5.

4.4 Results of Statistical Evaluation (All Models)

Excerpts of the results of the statistical evaluation of CTDM, COMPLEX I, and RTDM are presented in this section, including results for data sets unpaired in time and space, and paired in time but not in space. Additional results are listed elsewhere:

- complete statistics for observed and predicted concentrations paired in time, but not in space - Appendix B;
- statistics for concentrations paired in space, not in time (conventional data bases only) - Appendix C;
- statistics for concentrations paired in time and space - Appendix D;
- statistics based upon meteorological category for concentrations paired in time, not in space - Appendix E.
- scatter plots of peak hourly predictions and observations and residual plots predicted/observed ratios versus distance (Appendix F).

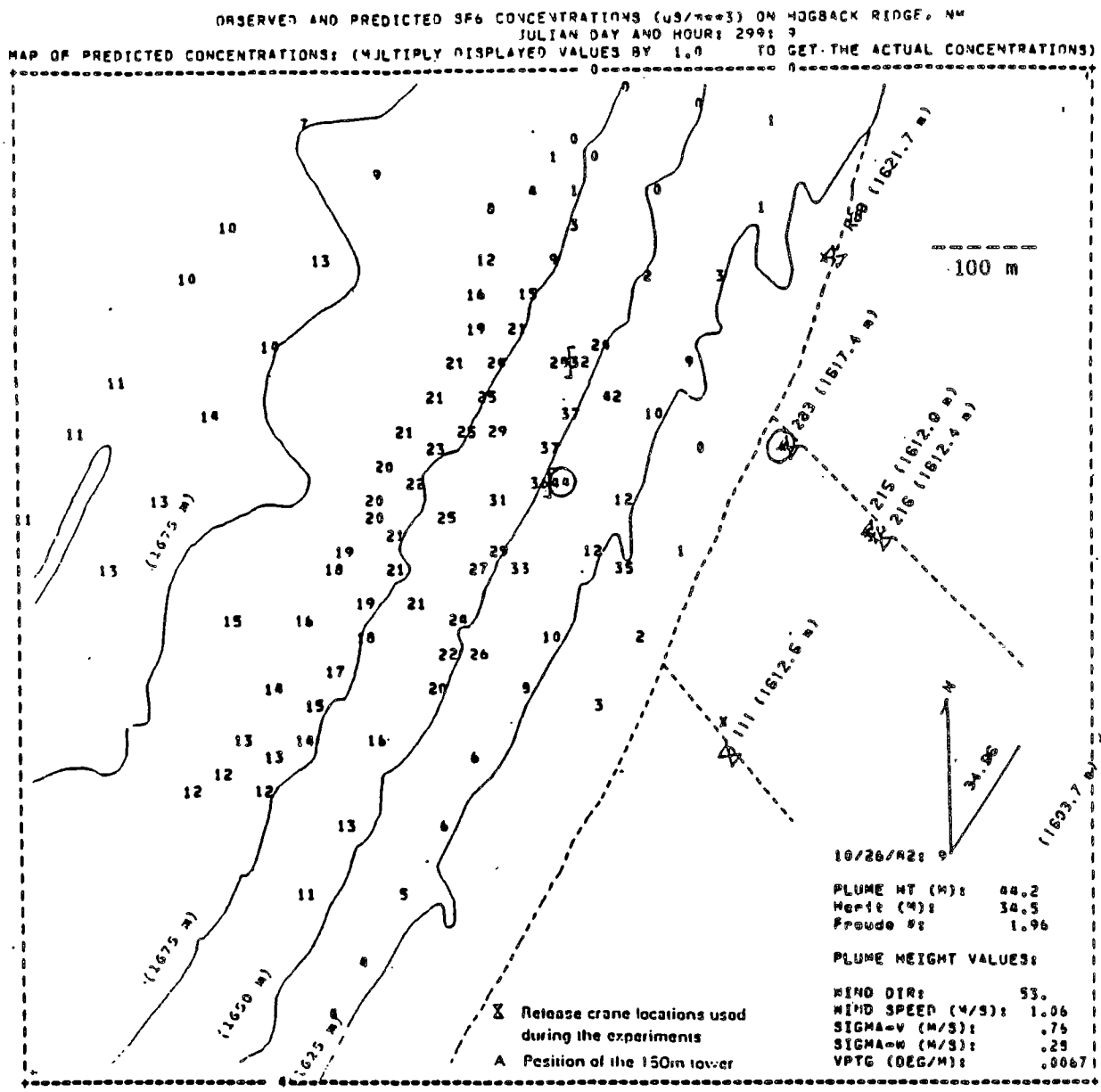

Figure 26a. Sample map showing the distribution of CTDM predictions at tracer sample locations for one of the Hogback Ridge experiments; plume height variables are listed in an inset on the map.

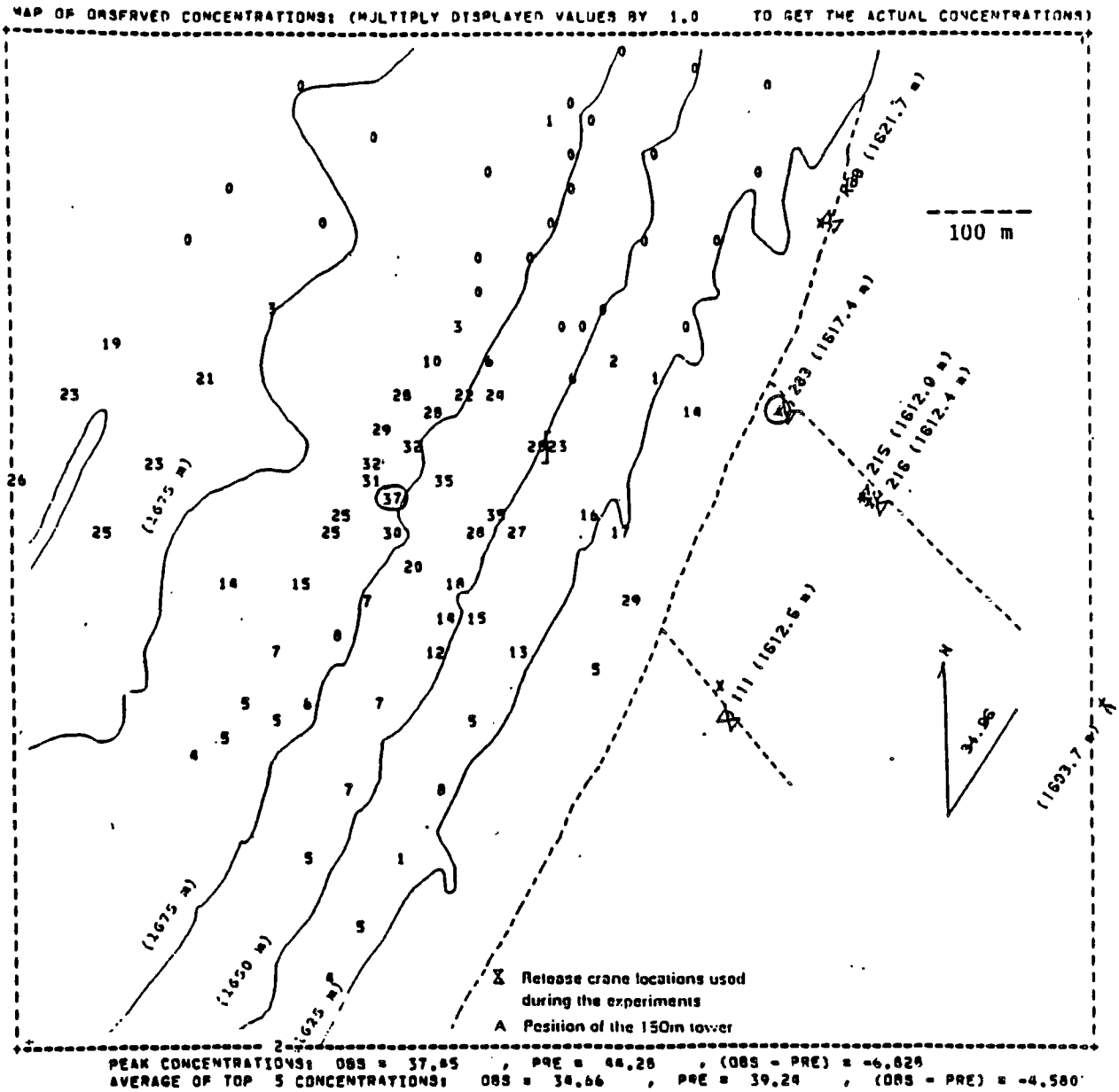

Figure 26b. Sample map showing observed tracer concentrations corresponding to the CTDM predictions in Figure 26a; summary case statistics are also included.

Tables 6 through 13 contain the following results:

	Unpaired in Time and Space	Paired in Time Only
CCB (SF_6)		Table 9a
CCB (CF_3Br)		Table 9b
HBR (SF_6)		Table 10a
HBR (CF_3Br)		Table 10b
FSPS (SF_6)	Table 6a	Table 11a
FSPS (CF_3Br)	Table 6b	Table 11b
Westvaco (SO_2)	Table 7a,b	Table 12a,b
Widows Creek (SO_2)	Table 8a,b	Table 13a,b

For each evaluation site, CTDM results for all available tower levels (see Section 4.2), just two levels, and a single level of meteorological input data are listed. COMPLEX I and RTDM were run with a single level of meteorology close to stack top (See Section 4.2).

At the Tracy Power Plant, CTDM with all tower levels showed an underprediction tendency in the unpaired extreme value tests (Table 6, a and b), while use of fewer levels resulted in higher concentrations. COMPLEX I overpredicted for both tracers and RTDM (on-site mode) underpredicted for both tracers. RTDM in default mode exhibited a modest overprediction tendency.

Table 7 (a and b) shows 1-hour and 3-hour average evaluation results for the unpaired data sets at Westvaco. CTDM shows an overprediction tendency for the three combinations of meteorological input data. Use of two tower levels gives poor results - the $d\theta/dz$ values are probably too large because one temperature level is too close to the ground. COMPLEX I shows severe overprediction problems, while RTDM exhibits a moderate overprediction tendency. The on-site run of RTDM gives better results than the default mode run.

As shown in Table 8 (a and b), all models overpredict at Widows Creek. Once again, the CTDM run with two tower levels shows higher concentrations than the other CTDM runs, again probably due to the high $d\theta/dz$ values. COMPLEX I shows the highest overpredictions, while RTDM (default) moderately overpredicts and RTDM (on-site) slightly overpredicts.

The CCB evaluation results for the paired in time, unpaired in space data set (Table 9, a and b) show a significant decline in CTDM performance toward underprediction for both SF_6 and CF_3Br as the meteorological input is degraded. CTDM results for the full meteorological data set are quite good, however. COMPLEX I overpredicts for both tracers, but by less than a factor of 2. RTDM in on-site mode shows a modest underprediction tendency, while in default mode it overpredicts for SF_6 and underpredicts for CF_3Br.

TABLE 6a

SUMMARY STATISTICS FOR DATA UNPAIRED IN TIME AND SPACE

SITE: TRACY POWER PLANT TRACER: SF6 UNITS: uS/m**3

1-HOUR AVERAGES, 111 HOURS

DATA SUBSET	HIGHEST	SECOND-HIGHEST	HIGHEST SECOND-HIGHEST	AVG OF TOP 5
OBSERVED	10.227	8.241	6.452	8.092
CTDM, SEVERAL TOWER LEVELS	7.551	6.314	5.356	6.100
CTDM, SEVERAL TOWER LEVELS (ALT. PLUME HT 1)*	6.581	6.314	5.356	5.648
CTDM, SEVERAL TOWER LEVELS (ALT. PLUME HT 2)*	6.725	6.661	5.356	5.677
CTDM, TWO TOWER LEVELS	8.067	6.617	3.970	6.374
CTDM, ONE TOWER LEVEL	11.755	11.679	11.194	10.014
COMPLEX I	22.605	22.587	22.587	21.686
RTDM, DEFAULT MODE	12.944	11.407	11.407	11.097
RTDM, FULL ONSITE MODE	6.180	3.966	2.832	3.877

* Alternative plume height #1 was obtained from lidar measurements at the first cross section downwind from the source. Plume height #2 was obtained from the second lidar cross section.

TABLE 6b

SUMMARY STATISTICS FOR DATA UNPAIRED IN TIME AND SPACE

SITE: TRACY POWER PLANT TRACER: CF3Br UNITS: uS/m**3

1-HOUR AVERAGES, 111 HOURS

DATA SUBSET	HIGHEST	SECOND-HIGHEST	HIGHEST SECOND-HIGHEST	AVG OF TOP 5
OBSERVED	19.463	13.351	7.482	12.900
CTDM, SEVERAL TOWER LEVELS	8.875	8.433	8.433	7.960
CTDM, TWO TOWER LEVELS	31.598	16.630	9.530	15.889
CTDM, ONE TOWER LEVEL	36.402	23.554	11.641	17.320
COMPLEX I	31.715	30.304	27.107	27.312
RTDM, DEFAULT MODE	21.994	20.943	20.943	19.339
RTDM, FULL ONSITE MODE	7.917	6.502	5.560	5.834

TABLE 7a

SUMMARY STATISTICS FOR DATA UNPAIRED IN TIME AND SPACE

SITE: WESTVACO LUKE TRACER: SO2 UNITS: uS/m**3

1-HOUR AVERAGES

DATA SUBSET	HIGHEST	SECOND-HIGHEST	HIGHEST SECOND-HIGHEST	AVG OF TOP 10
OBSERVED	7.227	6.911	5.755	5.725
CTDM, SEVERAL TOWER LEVELS	13.593	11.076	11.076	9.356
CTDM, TWO TOWER LEVELS	24.838	24.308	23.214	22.325
CTDM, ONE TOWER LEVEL	9.641	9.556	8.353	8.515
COMPLEX I	50.647	49.478	49.382	47.503
RTDM, DEFAULT MODE	15.369	14.250	13.953	13.619
RTDM, FULL ONSITE MODE	15.460	8.843	8.519	7.879

TABLE 7b

SUMMARY STATISTICS FOR DATA UNPAIRED IN TIME AND SPACE

SITE: WESTVACO LUKE TRACER: SO2 UNITS: uS/m**3

3-HOUR AVERAGES

DATA SUBSET	HIGHEST	SECOND-HIGHEST	HIGHEST SECOND-HIGHEST	AVG OF TOP 10
OBSERVED	5.036	4.405	4.405	3.434
CTDM, SEVERAL TOWER LEVELS	7.011	5.728	5.728	4.951
CTDM, TWO TOWER LEVELS	19.556	18.621	17.036	15.754
CTDM, ONE TOWER LEVEL	7.003	6.905	6.461	6.053
COMPLEX I	42.780	36.749	36.749	32.384
RTDM, DEFAULT MODE	11.745	10.274	10.274	9.175
RTDM, FULL ONSITE MODE	7.945	6.839	3.769	3.864

TABLE 8a

SUMMARY STATISTICS FOR DATA UNPAIRED IN TIME AND SPACE

SITE: WIDOWS CREEK TRACER: SO2 UNITS: ug/m**3

1-HOUR AVERAGES

DATA SUBSET	HIGHEST	SECOND-HIGHEST	HIGHEST SECOND-HIGHEST	AVG OF TOP 10
OBSERVED	4609	3850	2776	2627
CTDM, SEVERAL TOWER LEVELS	6857	6220	5283	5435
CTDM, TWO TOWER LEVELS	8866	8634	7097	6892
CTDM, ONE TOWER LEVEL	6704	6464	6335	5303
COMPLEX I	12453	11474	11255	10857
RTDM, DEFAULT MODE	4773	4517	4517	4420
RTDM, FULL ONSITE MODE	9555	7739	4435	5373

TABLE 8b

SUMMARY STATISTICS FOR DATA UNPAIRED IN TIME AND SPACE

SITE: WIDOWS CREEK TRACER: SO2 UNITS: ug/m**3

3-HOUR AVERAGES

DATA SUBSET	HIGHEST	SECOND-HIGHEST	HIGHEST SECOND-HIGHEST	AVG OF TOP 10
OBSERVED	2374	1955	1082	1049
CTDM, SEVERAL TOWER LEVELS	2670	2286	1798	1868
CTDM, TWO TOWER LEVELS	3042	2588	2588	2326
CTDM, ONE TOWER LEVEL	3915	2992	2805	2782
COMPLEX I	6871	6412	5440	5446
RTDM, DEFAULT MODE	3470	3403	3403	2757
RTDM, FULL ONSITE MODE	3293	2349	1478	1603

TABLE 9a

SUMMARY STATISTICS FOR DATA PAIRED IN TIME, NOT IN SPACE

SITE: CINDER CONE BUTTE TRACER: SF6 UNITS: uS/m**3 THRESHOLD: 0.00

(HIGHEST VALUE FROM EACH HOUR USED), 100 HOURS

DATA SUBSET	AVERAGE HOURLY PEAK VALUE	RATIO OF PRE/OBS	RMS ERROR	% CASES: 0.5 < PRE/OBS < 2.0
OBSERVED	27.96	---	---	---
CTDM, SEVERAL TOWER LEVELS	26.16	0.94	28.66	37
CTDM, TWO TOWER LEVELS	12.19	0.44	36.92	21
CTDM, ONE TOWER LEVEL	6.58	0.24	37.54	17
COMPLEX I	42.18	1.51	45.55	38
RTDM, DEFAULT MODE	36.35	1.30	58.33	27
RTDM, FULL ONSITE MODE	21.50	0.77	26.10	38

TABLE 9b

SUMMARY STATISTICS FOR DATA PAIRED IN TIME, NOT IN SPACE

SITE: CINDER CONE BUTTE TRACER: CF3Br UNITS: uS/m**3 THRESHOLD: 0.0

(HIGHEST VALUE FROM EACH HOUR USED), 44 HOURS

DATA SUBSET	AVERAGE HOURLY PEAK VALUE	RATIO OF PRE/OBS	RMS ERROR	% CASES: 0.5 < PRE/OBS < 2.0
OBSERVED	15.01	---	---	---
CTDM, SEVERAL TOWER LEVELS	20.95	1.40	29.21	23
CTDM, TWO TOWER LEVELS	7.51	0.50	19.92	14
CTDM, ONE TOWER LEVEL	4.57	0.30	20.94	34
COMPLEX I	24.45	1.62	28.68	46
RTDM, DEFAULT MODE	11.04	0.74	24.29	50
RTDM, FULL ONSITE MODE	13.68	0.91	19.25	32

The HBR results (Table 10, a and b) show CTDM overpredictions for SF_6 (except for the run with one tower level), but underpredictions for CF_3Br. COMPLEX I shows a large overprediction for SF_6 (released usually above H_c) and a moderate overprediction for CF_3Br (usually released below H_c). These differences reveal a critical weakness in COMPLEX I: the inability to distinguish between flow regimes passing over rather than around a terrain obstacle. RTDM results for the on-site mode are very good for both tracers, showing a modest overprediction tendency. The default mode exhibits a large overprediction tendency, a result that is not unexpected due to the large default values of $d\theta/dz$ that are used. Note that CTDM's relatively good performance with the HBR SF_6 data set (not used in the model development) is consistent with its performance at other CTMD sites. This result suggests that CTDM's relatively good evaluation results at the CTMD sites are due to theoretically sound design rather than from "tuning" and calibration.

Table 11, a and b (FSPS), shows very good results for CTDM, which has predicted-to-observed ratios close to 1.0 and a high number of cases with predictions within a factor of 2 of observations. COMPLEX I shows large overpredictions while RTDM (default) overpredictions are more modest. For this site, RTDM (on-site mode) shows a moderate underprediction tendency. Results for the models are consistent between the two tracers.

For the Westvaco conventional data base, results are shown for 1-hour averages (Table 12a) and for 3-hour averages (Table 12b). Results from Table 12 show good performance for both CTDM (all tower levels) and RTDM (on-site mode). With fewer tower levels, CTDM overpredicts significantly, probably due to the use of unrepresentative or default $d\theta/dz$ values that are too high. Overpredictions are quite apparent for RTDM default ($d\theta/dz$ too high) and especially COMPLEX I ($d\theta/dz$ too high and no plume lifting over terrain in stable conditions).

Table 13 (a and b) gives results for Widow Creek for 1- and 3-hour averages, respectively. As is the case for Westvaco, the CTDM results show more overpredictions as the meteorological data input is degraded. The best results are attained by CTDM (all tower levels) and RTDM (on-site onsite), while RTDM (default) and COMPLEX I overpredict for the same reasons as stated above for Westvaco.

Statistics for observed and predicted concentrations paired in space but unpaired in time are presented in Appendix C. The results for this test are consistent in general with those for the data set paired in time only.

In Appendix D, results are given for concentrations paired in time and space for the five sites. For this test, results are presented both for all data points as well as predicted-observed concentration pairs that are both above a nominal value of 0.01 microseconds per cubic meter at tracer sites or 1 microgram per cubic meter at conventional sites. There are no results that are markedly

TABLE 10a

SUMMARY STATISTICS FOR DATA PAIRED IN TIME, NOT IN SPACE

SITE: HOGBACK RIDGE TRACER: SF6 UNITS: uS/M**3 THRESHOLD: 0.0

(HIGHEST VALUE FROM EACH HOUR USED), 59 HOURS

DATA SUBSET	AVERAGE HOURLY PEAK VALUE	RATIO OF PRE/OBS	RMS ERROR	% CASES: 0.5 < PRE/OBS < 2.0
OBSERVED	23.48	---	---	---
CTDM, SEVERAL TOWER LEVELS	47.84	2.04	58.29	37
CTDM, TWO TOWER LEVELS	30.09	1.28	44.25	29
CTDM, ONE TOWER LEVEL	10.82	0.46	29.42	17
COMPLEX I	117.50	5.00	125.10	2
RTDM, DEFAULT MODE	74.66	3.18	159.86	14
RTDM, FULL ONSITE MODE	32.60	1.39	69.33	54

TABLE 10b

SUMMARY STATISTICS FOR DATA PAIRED IN TIME, NOT IN SPACE

SITE: HOGBACK RIDGE TRACER: CF3Br UNITS: uS/m**3 THRESHOLD: 0.01

(HIGHEST VALUE FROM EACH HOUR USED), 61 HOURS

DATA SUBSET	AVERAGE HOURLY PEAK VALUE	RATIO OF PRE/OBS	RMS ERROR	% CASES: 0.5 < PRE/OBS < 2.0
OBSERVED	104.32	---	---	---
CTDM, SEVERAL TOWER LEVELS	49.12	0.47	93.05	57
CTDM, TWO TOWER LEVELS	47.33	0.45	144.72	38
CTDM, ONE TOWER LEVEL	58.53	0.56	101.89	38
COMPLEX I	173.67	1.66	125.62	40
RTDM, DEFAULT MODE	444.08	4.26	678.30	13
RTDM, FULL ONSITE MODE	142.24	1.36	572.34	25

TABLE 11a

SUMMARY STATISTICS FOR DATA PAIRED IN TIME, NOT IN SPACE

SITE: TRACY POWER PLANT TRACER: SF6 UNITS: uS/m**3 THRESHOLD: 0.00

(HIGHEST VALUE FROM EACH HOUR USED), 111 HOURS

DATA SUBSET	AVERAGE HOURLY PEAK VALUE	RATIO OF PRE/OBS	RMS ERROR	% CASES: 0.5 < PRE/OBS < 2.0
OBSERVED	1.96	---	---	---
CTDM, SEVERAL TOWER LEVELS	1.94	0.99	2.11	61
CTDM, SEVERAL TOWER LEVELS (ALT. PLUME HT 1)*	1.92	0.98	1.84	68
CTDM, SEVERAL TOWER LEVELS (ALT. PLUME HT 2)*	1.77	0.90	1.88	69
CTDM, TWO TOWER LEVELS	2.07	1.07	2.24	49
CTDM, ONE TOWER LEVEL	2.41	1.24	3.08	38
COMPLEX I	6.14	3.13	7.27	19
RTDM, DEFAULT MODE	3.05	1.56	3.38	48
RTDM, FULL ONSITE MODE	1.18	0.60	2.22	34

* Alternative plume height #1 was obtained from lidar measurements at the first cross section downwind from the source. Plume height #2 was obtained from the second lidar cross section.

TABLE 11b

SUMMARY STATISTICS FOR DATA PAIRED IN TIME, NOT IN SPACE

SITE: TRACY POWER PLANT TRACER: CF3Br UNITS: uS/m**3 THRESHOLD: 0.00

(HIGHEST VALUE FROM EACH HOUR USED), 111 HOURS

DATA SUBSET	AVERAGE HOURLY PEAK VALUE	RATIO OF PRE/OBS	RMS ERROR	% CASES: 0.5 < PRE/OBS < 2.0
OBSERVED	2.84	---	---	---
CTDM, SEVERAL TOWER LEVELS	2.46	0.87	2.94	60
CTDM, TWO TOWER LEVELS	3.02	1.06	4.01	53
CTDM, ONE TOWER LEVEL	3.04	1.07	4.99	31
COMPLEX I	8.54	3.01	9.14	23
RTDM, DEFAULT MODE	3.76	1.32	4.79	39
RTDM, FULL ONSITE MODE	1.95	0.69	3.17	52

TABLE 12a

SUMMARY STATISTICS FOR DATA PAIRED IN TIME, NOT IN SPACE

SITE: WESTVACO LUKE TRACER: SO2 UNITS: uS/M**3 1-HOUR AVGS

(HIGHEST VALUE FROM EACH HOUR USED)

DATA SUBSET	AVERAGE HOURLY PEAK VALUE	RATIO OF PRE/OBS	RMS ERROR	% CASES: 0.5 < PRE/OBS < 2.0
OBSERVED	0.33	---	---	---
CTDM, SEVERAL TOWER LEVELS	0.29	0.88	0.83	14
CTDM, TWO TOWER LEVELS	1.60	4.85	3.30	19
CTDM, ONE TOWER LEVEL	1.70	5.15	2.00	15
COMPLEX I	4.12	12.48	9.44	14
RTDM, DEFAULT MODE	0.98	2.97	2.46	16
RTDM, FULL ONSITE MODE	0.21	0.64	0.82	15

* All hours used with stable conditions

TABLE 12b

SUMMARY STATISTICS FOR DATA PAIRED IN TIME, NOT IN SPACE

SITE: WESTVACO LUKE TRACER: SO2 UNITS: uS/m**3 3-HOUR AVGS

(HIGHEST VALUE FROM EACH HOUR USED)

DATA SUBSET	AVERAGE 3-HOURLY PEAK VALUE	RATIO OF PRE/OBS	RMS ERROR	% CASES: 0.5 < PRE/OBS < 2.0
OBSERVED	0.30	---	---	---
CTDM, SEVERAL TOWER LEVELS	0.27	.90	0.62	17
CTDM, TWO TOWER LEVELS	1.57	5.23	2.89	18
CTDM, ONE TOWER LEVEL	1.65	5.16	1.82	12
COMPLEX I	3.98	13.27	7.96	9
RTDM, DEFAULT MODE	0.95	3.17	2.03	11
RTDM, FULL ONSITE MODE	0.21	0.70	0.64	18

* All stable hours used for which both the highest predicted and highest observed concentration was at least 0.01 uS/m**3

TABLE 13a

SUMMARY STATISTICS FOR DATA PAIRED IN TIME, NOT IN SPACE

SITE: WIDOWS CREEK TRACER: SO2 UNITS: ug/m**3 1-HOUR AVGS

(HIGHEST VALUE FROM EACH HOUR USED)

DATA SUBSET	AVERAGE HOURLY PEAK VALUE	RATIO OF PRE/OBS	RMS ERROR	% CASES: 0.5 < PRE/OBS < 2.0
OBSERVED	71.87	---	---	---
CTDM, SEVERAL TOWER LEVELS	141.78	1.97	403.58	23
CTDM, TWO TOWER LEVELS	151.91	2.11	575.81	12
CTDM, ONE TOWER LEVEL	390.43	5.43	766.83	16
COMPLEX I	412.78	5.74	1239.13	13
RTDM, DEFAULT MODE	322.34	4.49	764.58	7
RTDM, FULL ONSITE MODE	47.56	0.66	298.58	15

* All hours used with stable conditions

TABLE 13b

SUMMARY STATISTICS FOR DATA PAIRED IN TIME, NOT IN SPACE

SITE: WIDOWS CREEK TRACER: SO2 UNITS: ug/m**3 3-HOUR AVGS

(HIGHEST VALUE FROM EACH HOUR USED)

DATA SUBSET	AVERAGE 3-HOURLY PEAK VALUE	RATIO OF PRE/OBS	RMS ERROR	% CASES: 0.5 < PRE/OBS < 2.0
OBSERVED	66.4	---	---	---
CTDM, SEVERAL TOWER LEVELS	112.0	1.69	230.3	31
CTDM, TWO TOWER LEVELS	127.0	1.91	323.1	17
CTDM, ONE TOWER LEVEL	342.4	5.15	579.2	20
COMPLEX I	349.0	5.26	827.8	15
RTDM, DEFAULT MODE	278.6	4.20	521.4	9
RTDM, FULL ONSITE MODE	41.2	0.62	169.2	20

* All stable hours used for which both the highest predicted and highest observed concentration was at least 1.00 ug/m**3

different from those presented for the data set paired in time, unpaired in space. However, the inclusion of many zero versus zero comparisons for all data pairs causes some sharp differences between results with and without a minimum concentration threshold.

Test results involving the data set paired in time but unpaired in space with results given as a function of wind speed and stability class are shown in Appendix E. CTDM results (for all tower levels) are discussed here.

At CCB, an overall slight underprediction for SF_6 was comprised of underpredictions for neutral, windy conditions and overpredictions for stable, light wind hours. For CF_3Br, slight underpredictions for stability D and E conditions were offset by overpredictions for stability F.

Hogback Ridge experiments were dominated by stability F conditions, so no model performance differences among stability classes can be determined for that site. CTDM peak hourly predictions were, on average, quite good at the Tracy Power Plant. Model performance was consistently good over stability classes D, E, and F.

For the Westvaco data base, CTDM's predicted average peak hourly value was close to the observed average value. This good agreement was not consistent over all meteorological conditions. CTDM showed a significant underprediction tendency for neutral, windy conditions and underpredicted somewhat for near-calm, stability F conditions. These underpredictions were offset by slight to moderate overpredictions for low-wind stability D and E conditions.

CTDM showed an overall overprediction bias (by about a factor of 2) for the peak hourly SO_2 concentrations at Widows Creek. Among the meteorological categories examined, none showed underpredictions at Widows Creek. The very slight overprediction for neutral windy conditions is in contrast to the underprediction tendency at Westvaco. However, this difference may be due to the fact that at Westvaco, about 25% of the hours have wind speeds greater than 8 m/sec (at the top of the tower at site #1), while only about 3% of the hours at Widows Creek are as windy (at the top of the mountain tower). The highest overprediction biases for CTDM occurred for low speeds (less than 3 m/sec at release height) for all stability classes.

In an attempt to assess the overall skill of CTDM relative to COMPLEX I and RTDM, we have assigned arbitrary skill scores to selected model results. This scoring scheme was not established in advance and does not reflect a conclusive means of rating the models' comparative performances. However, this exercise does serve to condense the large array of statistical results to a more manageable level for evaluation purposes.

For model bias, an ideal value for the ratio of predicted to observed concentrations is 1.0. A scoring scale from 1 to 5 has been established for this exercise, with maximum skill assigned a score of 1 and minimum skill assigned a score of 5. We have devised the

following scoring scheme for ratios of predicted to observed concentrations:

Score = 1 if ratio is between 0.8 and 1.25 (geometrically centered at 1.0).
= 2 if ratio is outside bounds listed above, but between 0.67 and 1.50,
= 3 if ratio is outside bounds listed above, but between 0.50 and 2.00,
= 4 if ratio is outside bounds listed above, but between 0.33 and 3.00,
= 5 if ratio is outside bounds listed above.

Measures of model scatter include normalized mean square error, or "M" values, such as

$$M1 = MSE/\bar{C}_o^2 \text{ or } M2 = MSE/(\bar{C}_o \cdot \bar{C}_p)$$

where

MSE is the mean square error of model predictions about the observations,
$\bar{C}_o$ is the mean observed value, and
$\bar{C}_p$ is the mean predicted value.

The use of C_p instead of C_o in M2 is meant to provide the same skill scores for models that overpredict and underpredict by the same ratio. A perfect model would have a mean square error of zero, but the best available models have M values of order 1. Models with poor skill have high M values.

The arbitrary scoring method to assess measures of model prediction scatter about observations involves computing both M1 and M2. For each data set, the lowest M value among all models evaluated is first identified. Then a skill score ranging from 1 (most skill) to 5 (least skill) is assigned as follows, based upon a model's M value divided by the minimum M value over all models:

If ratio is less than 1.2, skill score = 1;
If ratio is between 1.2 and 1.5, skill score = 2;
If ratio is between 1.5 and 2.0, skill score = 3;
If ratio is between 2.0 and 5.0, skill score = 4;
If ratio exceeds 5.0, skill score = 5.

The results of our attempt to assess skill levels of the complex terrain models are listed in Tables 14 through 18. Note that the lowest scores are associated with the model with the best performance. In each table, a skill score is given for each data base and each model. For data unpaired in time and space, the highest concentration (Table 14) and the average of the top 5 or 10 values, depending upon the site (Table 15), are analyzed. For data paired in time, the average peak hourly values are examined: ratio of mean predicted to mean observed (Table 16), model scatter measure M1 (Table 17), and model scatter measure M2 (Table 18).

TABLE 14

SUMMARY OF MODEL EVALUATION RESULTS (SKILL SCORES*)

DATA SUBSET:HIGHEST VALUE UNPAIRED IN TIME AND SPACE

	<------- CTDM ------->				<---- RTDM ---->	
DATA BASE	SEVERAL TOWER LEVELS	TWO TOWER LEVELS	ONE TOWER LEVEL	COMPLEX I	DEFAULT MODE	FULL ONSITE MODE
TRACY:						
SF6	2	2	1	4	2	3
CF3BR	4	3	3	3	1	4
WESTVACO						
SO2	3	5	2	5	4	4
WIDOWS CREEK						
SO2	4	4	3	4	1	4
TOTAL SKILL SCORE	13	14	9	16	8	15

* FOR RATIO OF PREDICTED/OBSERVED, THE FOLLOWING ARBITRARY SKILL SCORES ARE ASSIGNED:

PRE/OBS RATIO	SCORE
0.80 - 1.25	1
0.67 - 1.50	2
0.50 - 2.00	3
0.33 - 3.00	4
< 0.33 - > 3.	5

THIS SCHEME ASSIGNS THE LOWEST SCORE TO THE BEST PERFORMANCE.

TABLE 15

SUMMARY OF MODEL EVALUATION RESULTS (SKILL SCORES*)

DATA SUBSET:AVERAGE OF TOP N VALUES UNPAIRED IN TIME AND SPACE
(N=5 FOR CCB, HBR, TRACY; N=10 FOR WESTVACO AND WIDOWS CREEK)

	<------- CTDM ------->				<---- RTDM ---->	
DATA BASE	SEVERAL TOWER LEVELS	TWO TOWER LEVELS	ONE TOWER LEVEL	COMPLEX I	DEFAULT MODE	FULL ONSITE MODE
TRACY:						
SF6	2	2	1	4	2	4
CF3BR	3	1	2	4	2	4
WESTVACO						
SO2	3	5	2	5	4	2
WIDOWS CREEK						
SO2	4	5	4	5	3	4
TOTAL SKILL SCORE	12	13	9	18	11	14

* FOR RATIO OF PREDICTED/OBSERVED, THE FOLLOWING ARBITRARY SKILL SCORES ARE ASSIGNED:

PRE/OBS RATIO	SCORE
0.80 - 1.25	1
0.67 - 1.50	2
0.50 - 2.00	3
0.33 - 3.00	4
< 0.33 - > 3.	5

THIS SCHEME ASSIGNS THE LOWEST SCORE TO THE BEST PERFORMANCE.

TABLE 16

SUMMARY OF MODEL EVALUATION RESULTS (SKILL SCORES*)

DATA SUBSET:AVERAGE PEAK HOURLY VALUE, PAIRED IN TIME, UNPAIRED IN SPACE

	<------- CTDM ------->				<---- RTDM ---->	
DATA BASE	SEVERAL TOWER LEVELS	TWO TOWER LEVELS	ONE TOWER LEVEL	COMPLEX I	DEFAULT MODE	FULL ONSITE MODE
CCB:						
SF6	1	4	5	3	2	2
CF3BR	3	4	4	3	2	1
HBR:						
SF6	3	1	5	5	5	2
CF3BR	4	4	3	3	5	2
TRACY:						
SF6	1	1	1	5	3	3
CF3BR	1	1	1	5	2	2
WESTVACO						
SO2	1	5	5	5	4	3
WIDOWS CREEK						
SO2	4	4	5	5	5	3
TOTAL SKILL SCORE	18	24	29	34	28	18

* FOR RATIO OF PREDICTED/OBSERVED, THE FOLLOWING ARBITRARY SKILL SCORES ARE ASSIGNED:

PRE/OBS RATIO	SCORE
0.80 - 1.25	1
0.67 - 1.50	2
0.50 - 2.00	3
0.33 - 3.00	4
< 0.33 - > 3.	5

THIS SCHEME ASSIGNS THE LOWEST SCORE TO THE BEST PERFORMANCE.

TABLE 17

SUMMARY OF MODEL EVALUATION RESULTS (SKILL SCORES*)

DATA SUBSET:AVERAGE PEAK HOURLY VALUE, PAIRED IN TIME, UNPAIRED IN SPACE, (RMS/OBS)**2

	<------- CTDM ------->				<---- RTDM ---->	
DATA BASE	SEVERAL TOWER LEVELS	TWO TOWER LEVELS	ONE TOWER LEVEL	COMPLEX I	DEFAULT MODE	FULL ONSITE MODE
CCB:						
SF6	2	3	4	4	4	1
CF3BR	4	1	1	4	3	1
HBR:						
SF6	4	4	1	5	5	5
CF3BR	1	2	2	2	5	5
TRACY:						
SF6	1	1	4	5	4	1
CF3BR	1	3	4	5	4	1
WESTVACO						
SO2	1	5	5	5	5	1
WIDOWS CREEK						
SO2	3	4	5	5	5	1
TOTAL SKILL SCORE	17	23	26	35	35	16

* FOR MODEL PERFORMANCE MEASURES INVOLVING VARIANCE, THE FOLLOWING ARBITRARY SKILL SCORES ARE ASSIGNED FOR M = (RMS/OBS)**2

(MODEL M)/(LOWEST MODEL M)	SCORE
1.00 - 1.20	1
1.20 - 1.50	2
1.50 - 2.00	3
2.00 - 5.00	4
> 5.00	5

THIS SCHEME ASSIGNS THE LOWEST SCORE TO THE BEST PERFORMANCE.

TABLE 18

SUMMARY OF MODEL EVALUATION RESULTS (SKILL SCORES*)

DATA SUBSET:AVERAGE PEAK HOURLY VALUE, PAIRED IN TIME, UNPAIRED IN SPACE, (RMS*RMS)/(OBS*PRE)

	<------- CTDM ------->				<---- RTDM ---->	
DATA BASE	SEVERAL TOWER LEVELS	TWO TOWER LEVELS	ONE TOWER LEVEL	COMPLEX I	DEFAULT MODE	FULL ONSITE MODE
CCB:						
SF6	1	4	5	3	4	1
CF3BR	3	3	4	2	3	1
HBR:						
SF6	1	1	2	4	5	4
CF3BR	4	4	4	1	5	5
TRACY:						
SF6	1	1	3	4	3	3
CF3BR	1	3	4	4	3	2
WESTVACO						
SO2	1	4	1	5	4	2
WIDOWS CREEK						
SO2	1	3	2	4	3	3
TOTAL SKILL SCORE	13	23	25	27	30	21

* FOR MODEL PERFORMANCE MEASURES INVOLVING VARIANCE, THE FOLLOWING ARBITRARY SKILL SCORES ARE ASSIGNED FOR M = (RMS*RMS)/(OBS*PRE)

(MODEL M)/(LOWEST MODEL M)	SCORE
1.00 - 1.20	1
1.20 - 1.50	2
1.50 - 2.00	3
2.00 - 5.00	4
> 5.00	5

THIS SCHEME ASSIGNS THE LOWEST SCORE TO THE BEST PERFORMANCE.

Results in Table 14 for the highest concentrations are based upon three sites. For the limited period represented by Tracy Power Plant data base (111 hours), CTDM moderately underpredicted except for the run using only one tower level. Similarly, RTDM in on-site mode underpredicted, while RTDM (default) slightly overpredicted. For the Westvaco data base, CTDM overpredicted for each set of meteorological data used, but showed the closest agreement (on an unpaired basis) for the run using the single tower level. RTDM (on-site) overpredicted less at Westvaco than did RTDM (default), but the reverse was true for the Widows Creek data base. CTDM run with all available tower levels showed results similar to that of CTDM run with one tower level at Widows Creek. In summary, the single-tower-level runs of CTDM and RTDM (default) showed somewhat better results for this unpaired statistic over the three data sets examined than the model runs that used all available meteorological data. Table 15, which is based upon a larger sample size, shows similar results. This outcome, showing a favorable result with the use of minimal on-site data for the comparisons unpaired in time and space, may be fortuitous in light of the results for tests paired in time to be discussed below. However, the unexpected favorable results for unpaired data occurs for both CTDM and RTDM, and imply that the default choices for vertical potential temperature gradient and wind profiles for these models give acceptable results for the highest concentrations unpaired in time and space.

Table 16 is of critical importance, for it evaluates model skill on an event-by-event basis. The skill levels of the models are clearly distinguishable here, with CTDM using several tower levels (CTDM-S) and RTDM in on-site mode (RTDM-O) clearly superior to the others. The models currently designated or proposed for screening purposes in complex terrain, COMPLEX I and RTDM in default mode (RTDM-D), show considerably less skill.

Tables 17 and 18 show results for the measures of model scatter. Once again, CTDM-S and RTDM-O show more skill than the other models. The use of M2, a measure preferred to M1 by statisticians (although not as simple as M1), gives a distinct advantage to CTDM-S. (Note, however, that RTDM-O is mostly penalized by poor performance at HBR.)

CTDM-S and RTDM-O show more skill than the other models evaluated, for reasons that include the following model features:

- plume growth is determined directly from turbulence measurements;
- hourly values of $d\theta/dz$ are used;
- superior estimates of the critical dividing streamline height are used.

The results clearly show that the use of meteorological data with good resolution in the vertical is necessary to assure good model performance by CTDM on an event-by-event basis.

Although CTDM-S and RTDM-O show comparable skill, CTDM is preferable to RTDM for the following reasons:

- RTDM performed quite poorly at HBR, with large overpredictions, which are associated with centerline impacts at short distances from plumes modeled below H_c with low dilution wind speeds and small σ_y and σ_z values. CTDM avoids these very large overpredictions because it considers deflection of streamlines by the ridge and so avoids a direct impingement of plumes on the ridge at short distances. A major component incorporated into CTDM that RTDM lacks is the modeling of streamline flow around a hill; RTDM does not allow deflections in the horizontal plane.

- RTDM-O underpredicts concentrations more than CTDM at the Tracy Power Plant site, which features a relatively long travel distance to terrain features of interest (at least 3 km). The RTDM values of σ_y and σ_z for very stable conditions are evidently too large at these distances, causing an overestimate in the plume cross-sectional area and therefore an underestimate of the centerline concentration. CTDM, on the other hand, calculates σ_z growth based upon the wind speed and the Brunt-Vaisala frequency, not just the stability class. This refined treatment results in more accurate predictions of plume size, especially σ_z, at large distances.

- CTDM is better able to use meteorological data at plume height because multiple levels of data can be input to the model. RTDM, on the other hand, can accept only one level of data, and therefore cannot readily compute plume height values of wind and turbulence. Only wind speed profiles are considered in RTDM; all other meteorological parameters are assumed to be constant with height, a less sophisticated treatment.

The tests unpaired in time and space generally show that CTDM does not underpredict the peak concentrations that would be important for regulatory application. Exceptions are CF_3Br at Hogback Ridge and SF_6 at Tracy. Of course, the application of the unpaired test at tracer sites with intermittently operating monitors results in an incomplete test. Therefore, the minor underprediction at Tracy of the highest second-highest 1-hour concentration (5.36 $\mu s/m^3$ predicted, 6.45 $\mu s/m^3$ observed) is not cause for concern, especially since tests paired in time show good results (Table 11, a and b).

A more serious underprediction at HBR (129.5 $\mu s/m^3$ predicted, 390.0 $\mu s/m^3$ observed) is likely caused by many hours for which the plume was blown toward the ridge, but for which the wind direction input to the model indicated otherwise. The 42 case hours involving CTDM predictions of CF_3Br at the Hogback Ridge were segregated into two groups: one involving hours with releases at Tower A, where the meteorological data were taken, and the other groups involving

releases much closer to the ridge. These releases sites are shown in Figure 26(a,b). Over all these cases, the predicted/observed ratio for the average of the top 5 concentrations from each hour was 0.67, a significant underprediction. However, the 19 cases involving releases from tower A showed a slight overprediction ratio of 1.04; other remaining cases had a more serious underprediction ratio of 0.36. This case classification shows that the modeling of release very close to the ridge using meteorological data a considerable distance away (in terms of the ridge width length scale) resulted in poor CTDM performance. This result may not have occurred so dramatically for other terrain shapes for which small changes in wind direction cause smaller shifts in plume displacement.

4.5 Results of Case Study Evaluation (CTDM Only)

An in-depth study of the behavior of CTDM predictions relative to observations was conducted for the three tracer sites. For the three sites, a total of 255 hourly patterns and 191 CF_3B_r hourly patterns were analyzed, with an observed and predicted pair of maps for each.

For each hour, several characteristics of the observed and predicted concentration fields were noted:

- the location of the plume height relative to H_c (above, below, or close);
- plume height wind speed category (0-1, 1-3, 3-6, >6 m/sec);
- the average of the top five predictions and observations and the ratio of these averages;
- a categorization of the ratio discussed above (<0.2, 0.2-0.5, 0.5-1.0, 1.0-2.0, 2.0-5.0, > 5.0);
- the locations of the peak predicted and the peak observed concentrations relative to H_c;
- the comments about the general comparison of predicted and observed concentrations patterns.

The detailed tabulation of these characteristics for each hour is included in Appendix G. A summary of CTDM performance for categories of wind speed and plume height relative to H_c is also included in Appendix G. These results are discussed below.

A summary of the findings from the case studies is given in Table 19. This table lists the distribution of case hours by ratio of peak predictions to peak observations as a function of plume height relative to H_c. Each site and tracers are listed individually, and are discussed separately below.

For Cinder Cone Butte SF_6 release hours, the overall outcome shows an unbiased model because nearly equal numbers of cases have predicted-to-observed ratios both above and below 1.0. Cases with plumes below H_c exhibit a slight overprediction while those with plumes above H_c show an overall underprediction bias. Windy conditions are associated with the underpredictions in the latter

TABLE 19

SUMMARY OF CTDM CASE STUDIES:

PREDICTION BIAS AS A FUNCTION OF PLUME LOCATION

RELATIVE TO H_c

Site	Plume Height Relative to Hc**	Distribution of Hours by Ratio Category* of top 5 C_p/C_o <<	<	<=	>=	>	>>	Total Hours
CCB,SF_6	Below	4	4	5	10	6	4	33
	Near	0	2	7	1	4	5	19
	Above	8	8	9	9	3	5	42
	Total	12	14	21	20	13	14	94
CCB,CF_3Br	Below	0	0	1	0	0	1	2
	Near	1	0	2	0	3	4	10
	Above	2	5	4	4	3	9	27
	Total	3	5	7	4	6	14	39
HBR,SF_6	Below	0	1	2	5	13	2	23
	Near	0	0	0	0	7	3	10
	Above	0	1	0	6	6	5	18
	Total	0	2	2	11	26	10	51
HBR,CF_3Br	Below	1	12	8	9	3	3	36
	Near	0	0	4	0	0	1	5
	Above	0	0	0	0	1	0	1
	Total	1	12	12	9	4	4	42
FSPS,SF_6	Below	0	8	12	11	10	2	43
	Near	0	2	2	6	1	0	11
	Above	2	9	7	24	14	0	56
	Total	2	19	21	41	25	2	110
FSPS,CF_3Br	Below	4	12	24	11	8	1	60
	Near	0	1	1	2	3	0	7
	Above	0	0	14	21	8	0	43
	Total	4	13	39	34	19	1	110
Grand Total		22	65	102	119	93	45	446

* Ratio categories: <0.2 is "<<", 0.2-0.5 is "<", 0.5-1.0 is "<=", 1.0-2.0 is ">=", 2.0-5.0 is ">", >5.0 is ">>"

** "Near H_c" was within 5 meters at CCB and HBR, and within 10 meters at FSPS.

category, an outcome consistent with that found at Westvaco. In many of these cases, the observed maximum is on the near side of the hill and the predicted maximum is on the far side of the hill.

The CCB CF_3Br hours show an overall overprediction bias, contributed to in large part by the LIFT component of the model. The hours where overpredictions occur often feature a predicted maximum on the near side of the hill and an observed maximum farther up the hill or on the far side of the hill. There are also fewer windy hours associated with the CF_3Br LIFT cases than with the SF_6 LIFT cases, which may partly explain the difference in the overall outcome between the SF_6 and CF_3Br LIFT cases at CCB.

At Hogback Ridge, a sharp distinction is evident between the SF_6 results (overprediction bias) and the CF_3BR results (underprediction bias). The SF_6 plumes were released higher than the CF_3Br plumes were. The SF_6 predicted maxima were often located on the near side of the ridge closer to the source than the observed peak were located. The predicted CF_3Br peaks were almost always on the near side of the ridge, but displaced laterally from the observed peaks for hours in which CTDM underpredicted. The hours of poor CTDM predictions of CF_3Br, while being associated with releases very close to the ridge, also featured large wind direction variability, causing a poorly defined mean wind direction and a large effective hourly plume σ_y.

CTDM predictions at FSPS show an overall modest overprediction tendency for SF_6 and a nearly unbiased overall prediction for CF_3Br. Results for LIFT predictions in windy conditions show little overall bias.

SECTION 5

SENSITIVITY TESTS

This section describes a sensitivity study that was performed to illustrate how the magnitude of the terrain effect in CTDM varies with meteorology, and with the slope and orientation of the hill. Because CTDM is a modified Gaussian plume model, many of the characteristics are already familiar, such as its sensitivity to wind direction. However, many of the modifications introduce new and complex responses to variations in meteorology, and these also change depending on the scale and shape of the terrain that is being modeled. It is the illustration of these responses that is the subject of this study.

Specific recommendations for analysis of sensitivity had been made at the CTMD Workshop held in February, 1986. These are discussed in Section 5.1. The rationale adopted in the sensitivity study, and a description of how the matrix of model-runs was constructed is contained in Section 5.2. The results of the study are discussed in Section 5.3.

Also described is an operational test of the sensitivity of CTDM to the manner in which the shape of a hill is specified. In this test, model performance at the Widows Creek site was evaluated for two alternatives in defining the shape parameters of one of the hills. This test is discussed in Section 5.4.

5.1 Workshop Recommendations for Sensitivity Analyses

The CTDM Workshop held in February, 1986 made several recommendations for testing the sensitivity of CTDM. These are:

1. Sensitivity to wind direction, noting whether the effects of errors are to move the location of the peak only, or to change its value as well;
2. Sensitivity to vertical dispersion, both as specified by the sigma-w input, and the formulation of the model itself;
3. Sensitivity to the definition of the hill shape and orientation;
4. Sensitivity to plume height relative to the dividing streamline height;
5. Sensitivity to the potential temperature gradient through its effect on plume rise, dividing streamline height, sigma-z, and Froude number; and
6. Sensitivity to horizontal diffusion over a range of travel times.

Many of these are addressed through the matrix of input data discussed in Section 5.2, but several are better addressed analytically here.

The spread of the plume in the vertical direction is the subject of recommendation 2 as well as part of recommendation 5. As described in Section 3.3.2, sigma-z in the absence of any hill effects is given by

$$\sigma_z = \sigma_w t/[1 + t/2T_L]^{1/2} \quad (104)$$

so that the initial growth of sigma-z is linearly proportional to sigma-w. When the time of travel (this includes a virtual time which incorporates spread due to source-effects) is large compared to the Lagrangian time-scale, sigma-z grows as the square root of the time,

$$\sigma_z = \sigma_w [2tT_L]^{1/2} \quad (105)$$

and is proportional to $\sigma_w\sqrt{T_L}$. The Lagrangian time-scale is given by

$$T_L = 1/[\sigma_w (2.8/z + 3.7 N/\sigma_w)] \quad (106)$$

where N is the Brunt-Vaisala frequency, proportional to the square root of the potential temperature gradient, and z is the elevation of the plume. For larger sources which may have plume heights on the order of 100 m, T_L is approximately equal to .27/N whenever a non-zero value of N is measured, so that

$$\sigma_z = \sigma_w [.54t/N]^{1/2}. \quad (107)$$

When stratification is absent, T_L equals $.36z/\sigma_w$ and

$$\sigma_z = [.72zt\sigma_w]^{1/2}. \quad (108)$$

This analysis indicates that, in the absence of significant source-effects, sigma-z is generally most sensitive to the turbulence. The potential temperature gradient and plume height are most important in changing the dependence of plume growth on time from a linear to a square root trend. Once the square root trend is established, sigma-z is only weakly dependent on changes in these because the gradient enters as a one-fourth power, and the plume height enters as a square root. But note that the jump between the z/σ_w-scaling and a 1/N-scaling can be abrupt for high plumes because of the limit in the ability of temperature observations to resolve very weak temperature gradients.

Source-effects can dominate sigma-z when the virtual travel-time is large compared to T_L because additional growth occurs at a rate $(\partial\sigma_z/\partial t)$ that is inversely proportional to the square root of the travel-time. As the virtual time exceeds T_L several-fold (due to source-effects), the rate of additional growth diminishes so that sigma-z can remain nearly equal to its initial value. This is particularly evident when the stratification is strong and the turbulence is weak.

The spread of the plume in the lateral direction is the subject of recommendation 6. Unlike sigma-z, the Lagrangian time-scale for sigma-y is not computed within the model. It is set to the time it

takes the plume to travel 10 km. This scale is chosen because there appears to be no method available for estimating it, and evidence suggests that a linear growth is generally seen over distances up to 10 km. Consequently, sigma-y is solely determined in the model by the wind speed and the turbulence, and is linearly proportional to changes in sigma-v.

Recommendation 5 was addressed in part in the discussion of sigma-z, and the sensitivity of CTDM to the difference between plume height and H_c (recommendation 4) will be discussed in Section 5.3. Beyond these issues, the intent of recommendation 5 is to assess the overall sensitivity of the model to the resolution of the temperature profile measurements. This has been done to some extent at the five sites discussed in the evaluation results in Section 4. In general, such a sensitivity study is possible to do only in a very site-specific way. H_c is a function of the hill height and the wind speed profile as well as the temperature profile. The height of the plume depends on the wind speed and temperature profiles between the top of the stack and plume height, and also on the stack height and buoyancy flux. Furthermore, the Froude number (above H_c) depends on the bulk speed and stratification between H_c and the top of the hill. It seems that estimates of a matrix of plume heights, Froude numbers, and H_c values could be obtained for a range of temperature gradients and wind speed profiles for a specific source and hill. The sensitivity of the hill effect in CTDM for each cell in the matrix might then be obtained from the information in Section 5.3, and an assessment could be made of the ability of a monitoring system to resolve that range of gradients for which the model is most sensitive.

5.2 Test Design

The intent of this study is to illustrate how the magnitude of the terrain effect in CTDM varies with meteorology for various hill-shapes and orientations, so that the sensitivity of the model to these aspects of the input data can be discussed. The measure of the terrain effect used here was obtained by taking the peak concentration for a simulation, and dividing by the concentration that is predicted in the center of the plume for the same travel time, but in the absence of the hill. This "flat/centerline" concentration contains all of the same dispersion formulations that are contained in CTDM, it includes complete reflection of plume material from the surface on which the hill "sits", and it applies to the same downwind distance or time of travel. Being a centerline concentration, it also represents what may be thought of as a peak impingement concentration for that travel time. What it does not include are any of the terrain-specific features of CTDM, such as changes to the rate of diffusion (above H_c), steering of the plume away from the hill (below H_c), or trapping of plume material against the hill (reflection from H_c for that portion of the hill above H_c, or reflection from the stagnation streamline for that portion of the hill below H_c). As a result, the terrain effect is a measure of how close (or far) the sampling "cuts" through the plume (see Figure 1) along H_c and the stagnation streamline push the receptor toward (or away from) the center of the plume, combined with how much the alterations in the diffusion and reflection processes have altered concentrations within the plume.

Focusing on the predicted terrain effect rather than predicted concentrations is deliberate. CTDM remains a Gaussian plume model, as discussed in Section 3, and shares many properties with other widely used plume models. Instead of demonstrating all of the features common to this type of model such as sensitivity to wind direction and source height (relative to the plume spread), we have chosen to illustrate how the unique features of this model respond to various input conditions. Also, in exploring various shapes and orientations of hills, and various wind directions, we have found that resolving peak concentrations becomes dependent on having a very dense array of receptors all over the hill, regardless of how large the hill may become. The terrain effect measure reduces the need for such a dense array of receptors and it is a concise indicator of how the terrain is either fostering impingement or avoidance behavior.

The matrix of data used as input in this study was based in large part on the scale of the setting at the Tracy power plant, the site of the FSPS. A hill that is 300 m tall was placed 4 km from the source. Several aspect ratios and source positions were specified. The aspect ratio of a hill was defined for each of its axes as the length of the axis at one half of the hill height, divided by the height of the hill. The longer of the axes was oriented north-south (0°), and the source was placed at several azimuths between 0° and 90° relative to the center of the hill:

Aspect Ratios (Major Minor)	Source Positions (degrees)
2-2	90
3-2	90 80 70 45 20 10 0
5-2	90 80 70 45 20 10 0
10-2	90 80 70

Note that the hill with aspect ratios of 2-2 is a symmetric hill so that only one source position was required. The longest hill, 10-2, was modeled only for azimuths of 90°, 80°, and 70° to keep the source upwind of the hill -- recall that the source is 4 km from the center of the hill and a hill of aspect ratio 10 and height 300 m has a length of 3 km at half its height.

Receptors were placed on each of the hills along azimuths at intervals of 30°, starting at 0°. Along each azimuth, the receptors were placed every 30 m in elevation between 30 m and 270 m. One receptor was also placed at the top of the hill at 300 m elevation. Figure 27 illustrates the relative positions of the hill, the source locations, and the receptor azimuths for the hill of aspect ratios 3-2.

Meteorological data were chosen to be consistent with the range of conditions observed during the experiments. The data obtained at the elevation of the Freon release from the 150-m meteorological tower indicate that wind speed and σ_w are strongly correlated (the turbulence intensity is fairly steady), but σ_v is only weakly correlated with the wind speed. In spite of the weak correlation exhibited by σ_v and wind speed, we have chosen to represent σ_v

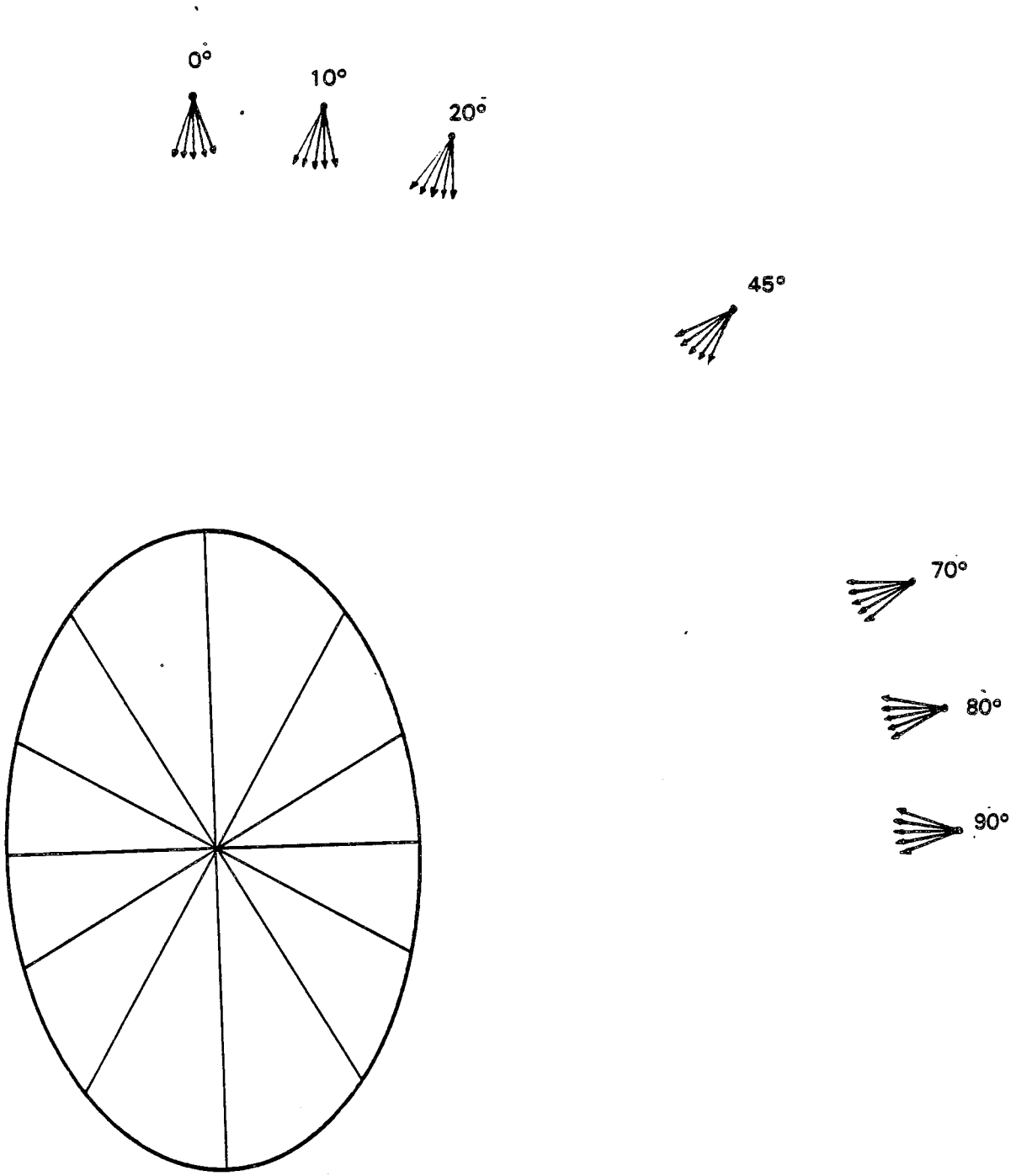

Figure 27. Illustration of receptor radials, source locations, and wind directions used in the sensitivity analysis of hill 3-2.

as a quarter of the wind speed. This choice removes the contributions to the scatter in Figure 28 that are apparently due to meandering at low wind speed. The stratification (Brunt-Vaisala frequency, N) is largely independent of the other variables. Figure 28 presents scatterplots of σ_w, σ_v, and N versus the wind speed for these data. On the basis of this observed behavior, the following matrix of meteorological data was used in the sensitivity modeling:

Met. Variable	Values Chosen
wind speed (m/s)	1.0, 1.5, 2.5, 4.0, 7.0
N (1/s)	.01, .02, .03
sigma-w (m/s)	0.1 · wind speed
sigma-v (m/s)	0.25 · wind speed
direction (deg)	0, +/-10, +/-20

The direction indicated above is not simply the wind direction. It is the difference between the wind direction and the direction from the center of the hill to the source. For a direction of 0°, the flow direction is from the source, wherever it may be located, to the center of the hill.

All other parameters needed in the model were computed from these values and the assumption that wind speed and stratification are constant with height. Values computed for H_c were 0, 50, 67, 100, 150, 167, 175, 200, 217, 225, 250, and 267 m. Given this range, the plume height was fixed at 225 m to supply an adequate number of cases in which the plume is marginally above H_c. In practice, the height of the plume will vary with the meteorology as well, but it was kept constant in these runs to simplify the assessment of model sensitivity, recognizing that sources typically operate at variable loads which also alters plume height.

This combination of values for wind speed, direction, and stratification combine to give 75 simulations for each source position, for each hill. The peak concentration obtained for each simulation was saved as was the terrain-effect parameter. The results allow us to see how much the terrain-effect changes with the shape of the hill, with the orientation of the hill to the flow, with small changes in wind direction (+/-20°), and with changes in wind speed and stratification.

5.3 Test Results

5.3.1 Sensitivity to H_c and Hill Shape

Figure 29 displays the trend in the terrain effect as a function of H_c for the case of a source located at 90° and a wind direction deviation of 0° (the source is directly upwind of the center of the hill). All of the hills used in the analysis are shown on this plot, as indicated by the legend. Note that the aspect ratios that identify each hill place the aspect ratio of the axis that is oriented along 0°

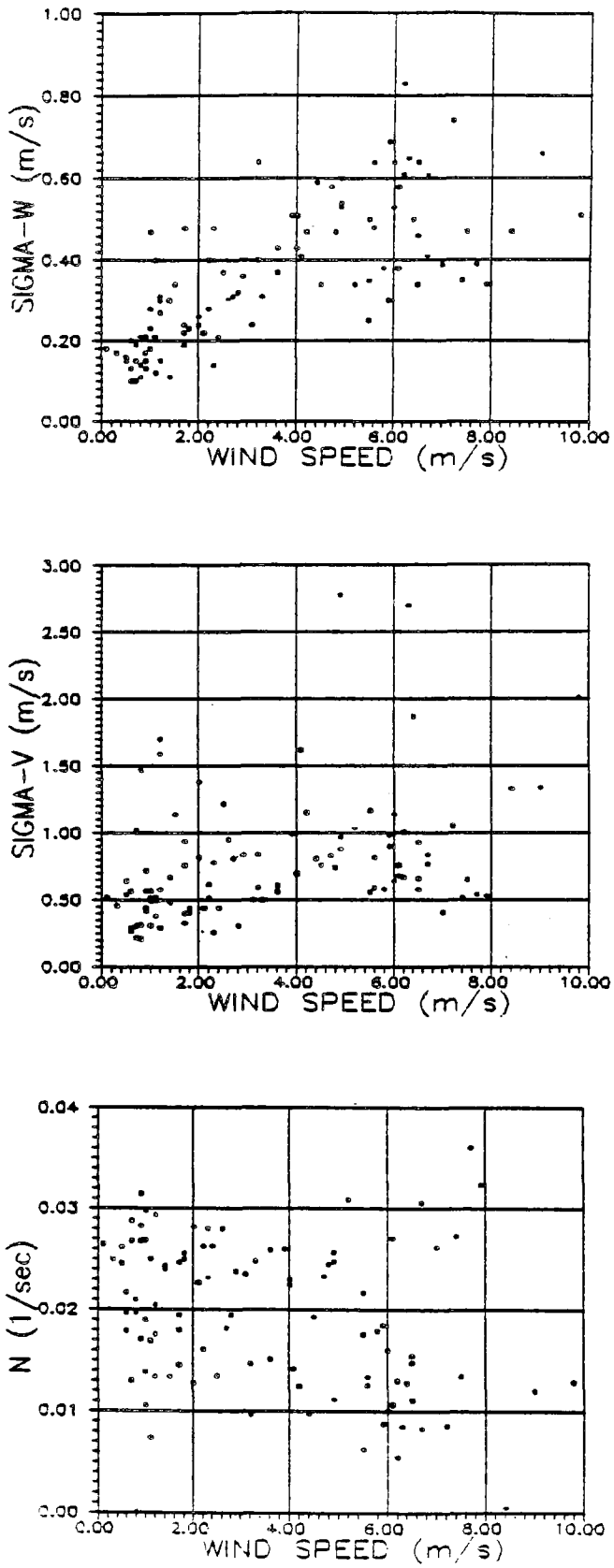

Figure 28. Scatter plots of sigma-w, sigma-v, and Brunt-Vaisala frequency (n) versus wind speed. Data are taken from the MDA for Freon releases at FSPS.

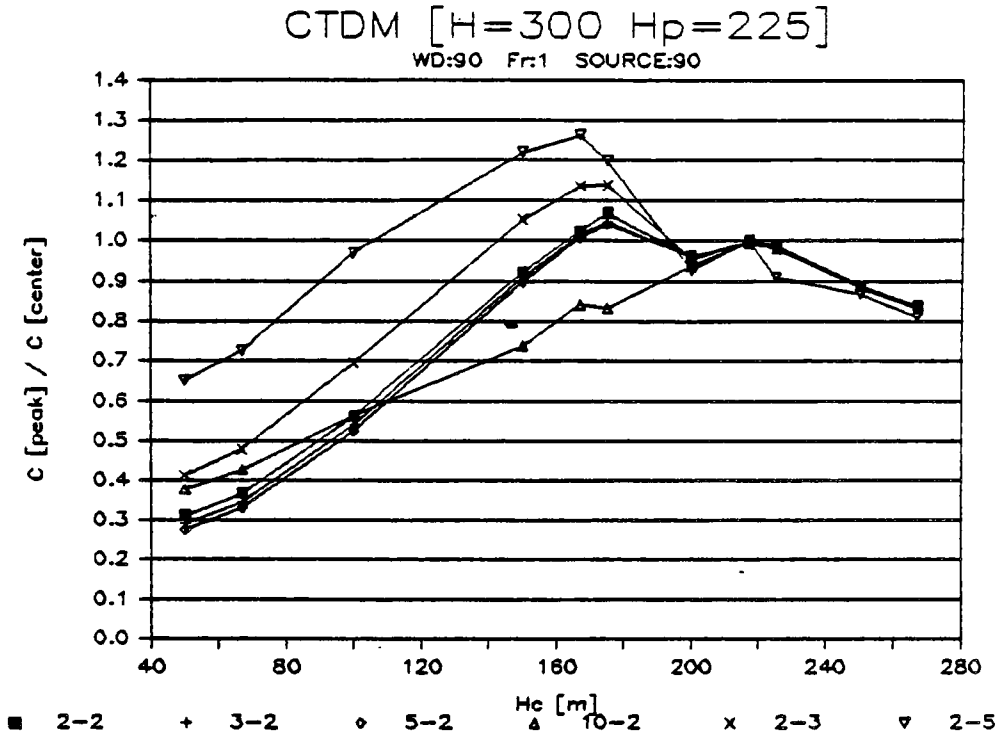

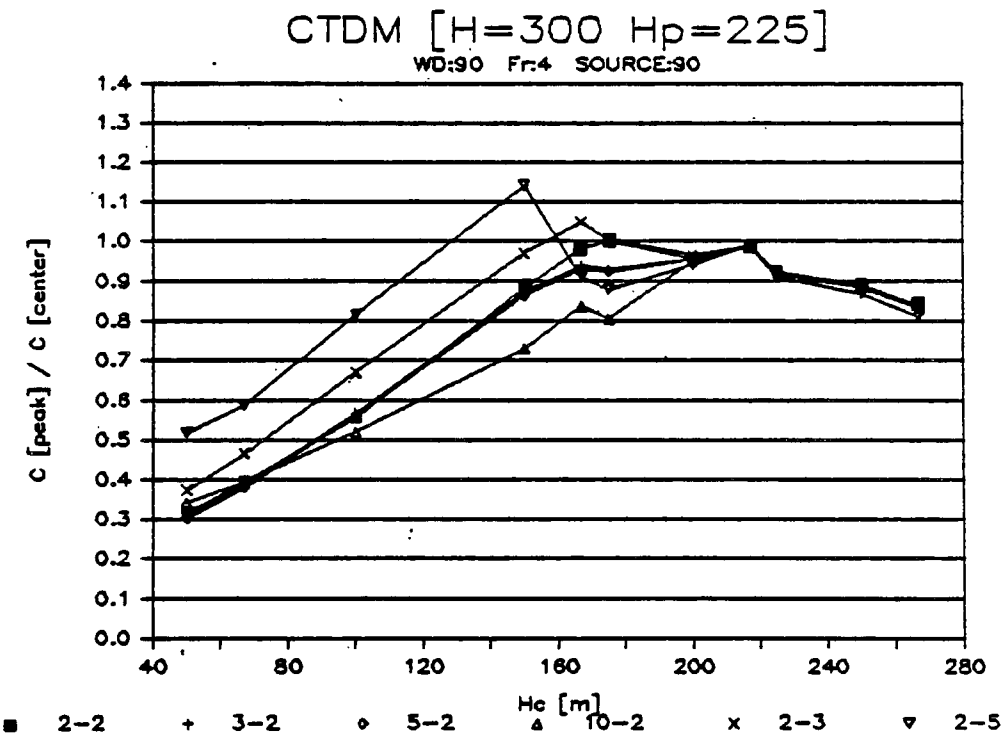

Figure 29. Terrain-effect factor versus H_c for wind and source aligned perpendicular to the center of the hill. Symbols denote hill shape by aspect ratios perpendicular to and parallel to the wind.

first so that the hill designated 3-2 is modeled for a plume that passes over its shorter side, while the hill designated 2-3 is modeled for a plume that passes over its longer side. (Results for hill 2-3 with a source at 90° are equivalent to the results for hill 3-2 with a source at 0° so long as the wind takes the plume directly over the hill in each case.) The results in the upper portion of this figure are for a Froude number equal to 1.0 above H_c, which is consistent with the assumption that the wind speed and the stratification are constant with height. The Froude number above H_c is set equal to 4.0 in the lower portion to simulate more weakly stratified conditions above H_c.

H_c Greater Than or Equal to Plume Height (225 m)

This class contains peak concentrations which are primarily associated with impingement conditions. The terrain effect factor lies between .8 and 1.0 and the results are nearly identical for all hill-shapes. Although a factor of 1.0 may have been anticipated for this class, lower values result because peak concentrations are found at receptors upwind of the point at which the centerline of the plume meets the hill, due to smaller values of σ_z and σ_y at these distances. The single difference between the upper and lower portions of the figure in this class occurs for H_c equal to plume height. In this case, plume growth rates differ and the peak concentration is actually found at a receptor above H_c at 240 m for all hills except 2-5 for a Froude number of 1.0. When the Froude number is 4.0, the peak concentration occurs at a receptor below H_c at 210 m. Note that the results for all hills with the same along-wind aspect ratio and for the same Froude number are identical.

H_c Less Than Plume Height (225 m)

Three features dominate the behavior of the terrain-effect factor in this class. (1) For H_c just below the height of the plume (H_c equals 217 m and the plume is at 225 m for these simulations), the factor equals approximately 0.99 for all of the hill-shapes. Peak concentrations are found as the plume material above H_c just begins to move up the hill, and the scale or shape of the hill has little influence on the magnitude of the terrain-effect. This is nearly an impingement situation even though the center of the plume lies above H_c. (2) For smaller values of H_c, as small as 140 m, the factor may increase or decrease depending on the Froude number and the shape of the hill. In this region, the effects of strain in the flow and reflection from the surface of the hill determine the magnitude of the hill-effect, which may exceed unity. (3) Beyond this range, at ever smaller values of H_c, the terrain-effect diminishes for all of the hills because the bulk of the plume lies far above the hill and receptors remain far from the centerline of the plume. Over the latter two regimes, the magnitude of the terrain-effect increases with the degree of strain and the length of time that the plume experiences the strain. The terrain-effect is generally weakest for flow across a ridge, and strongest for flow along an elongated hill.

5.3.2 Sensitivity to Source Position and Wind Direction: Symmetric Hill and 2D Hill

Figure 30 illustrates the sensitivity of the model to wind direction and the azimuthal position of a source for the extremes of a three-dimensional hill and a nearly two-dimensional ridge. As indicated by the legend, the various curves on each of the plots correspond to differences in wind direction of 0°, +/-10°, and +/-20° from the direction that aligns the center of the hill and the source. Note that the Froude number above H_c is equal to 1.0 in all of the remaining figures in this section.

H_c Greater Than Plume Height (225 m)

The sensitivity of the model to wind direction is extreme for this class. When the source is located at 90°, the terrain-effect drops from .85 or .9 to .6 for a shift in wind direction of 10°, and it drops to a factor as small as .2 for an additional change of 10°. This behavior is the result of steering the plume away from the hill when it is well within the stable layer below H_c. The primary difference between hill 2-2 and hill 10-2 occurs for a shift of 20° with H_c equal to 250 m in which case the peak concentration at hill 10-2 occurs above H_c on the north side of the hill, while that at hill 2-2 remains below H_c. When the source moves more to the north (azimuths 80° and 70°) the symmetry for differences of +/-10° and 20° disappears, as expected, and the range in the terrain-effect factors extends to smaller values.

H_c Less Than or Equal to Plume Height (225 m)

The sensitivity of the model to wind direction remains substantial for hill 2-2, but not for hill 10-2. This results from the length of hill 10-2 in the cross-wind direction compared to hill 2-2. The plumes in this analysis always pass over a substantial portion of hill 10-2, but pass more to the side of hill 2-2 with increasing shifts in the wind direction. Differences among the three plots for hill 10-2 occur primarily for H_c between 160 m and 200 m. Over this range, changes in the wind direction and the orientation of the source produce changes in both the strain in the flow and in the length of the path over the hill, and this fosters relatively minor changes in the terrain effect. Some of the variability is also associated with the spacing between receptors in that the centerline of the plumes may pass nearer a receptor for one of the combinations of source location and wind direction.

5.3.3 Sensitivity to Source Position and Wind Direction: Asymmetric Hills

Figure 31 illustrates the sensitivity of the model to wind direction and the azimuthal position of the source for hills intermediate in scale between the extremes of a symmetric hill and a ridge. The extreme sensitivity to wind direction when the plume is well below H_c remains evident in each of the plots. At smaller

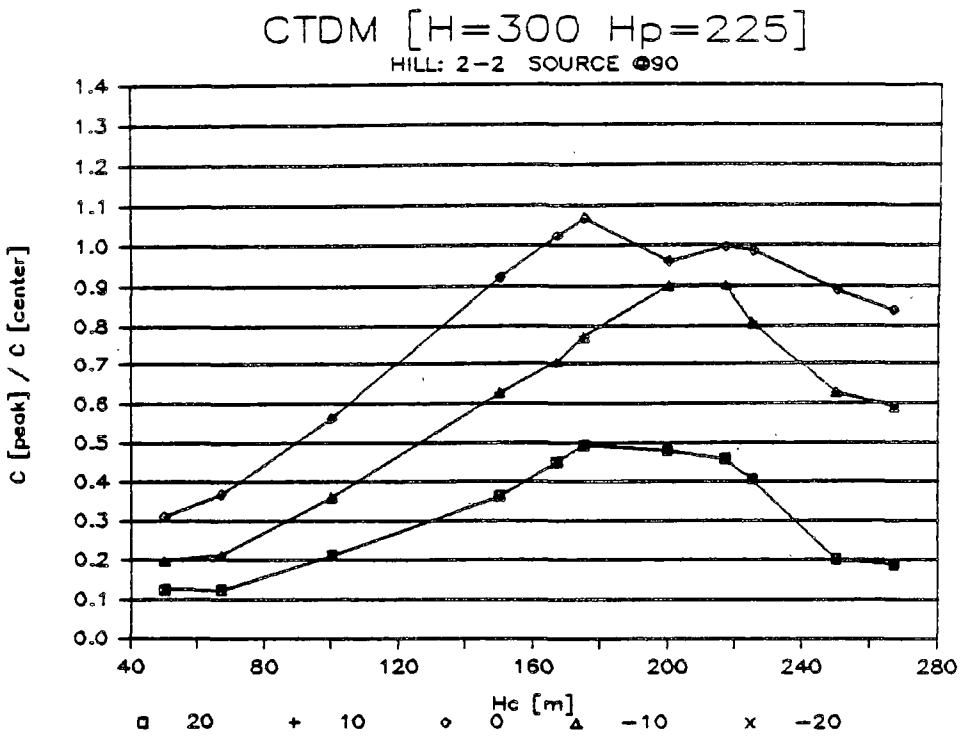

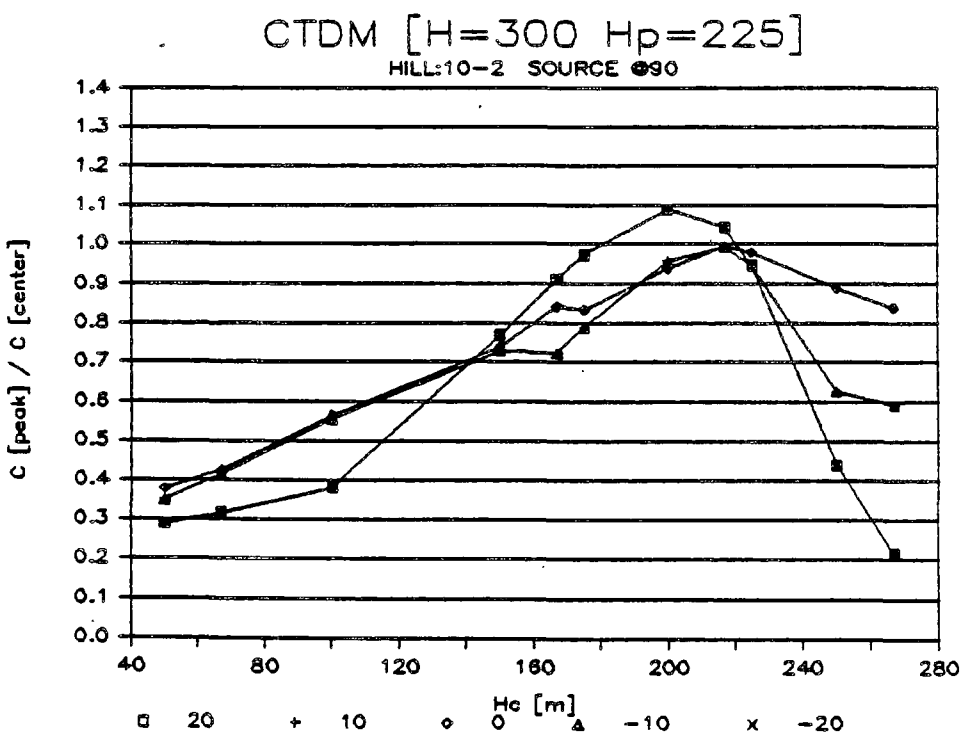

Figure 30. Terrain-effect factor versus H_c for symmetric 3-D hill and a long ridge. Symbols denote deviation of wind direction from that which places the source upwind of the center of the hill.

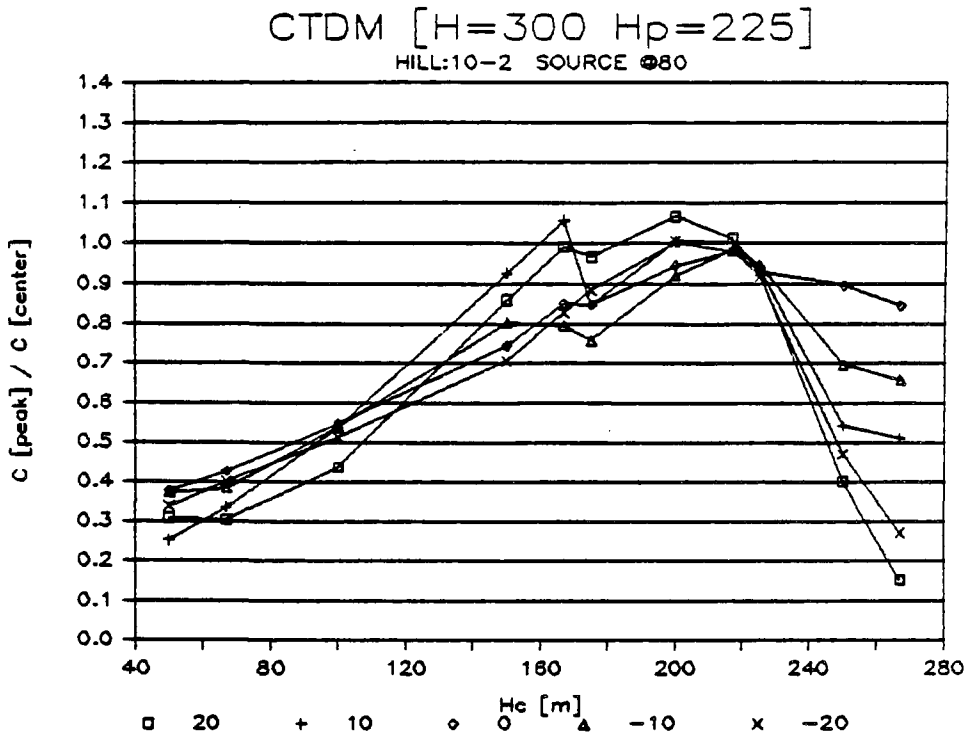

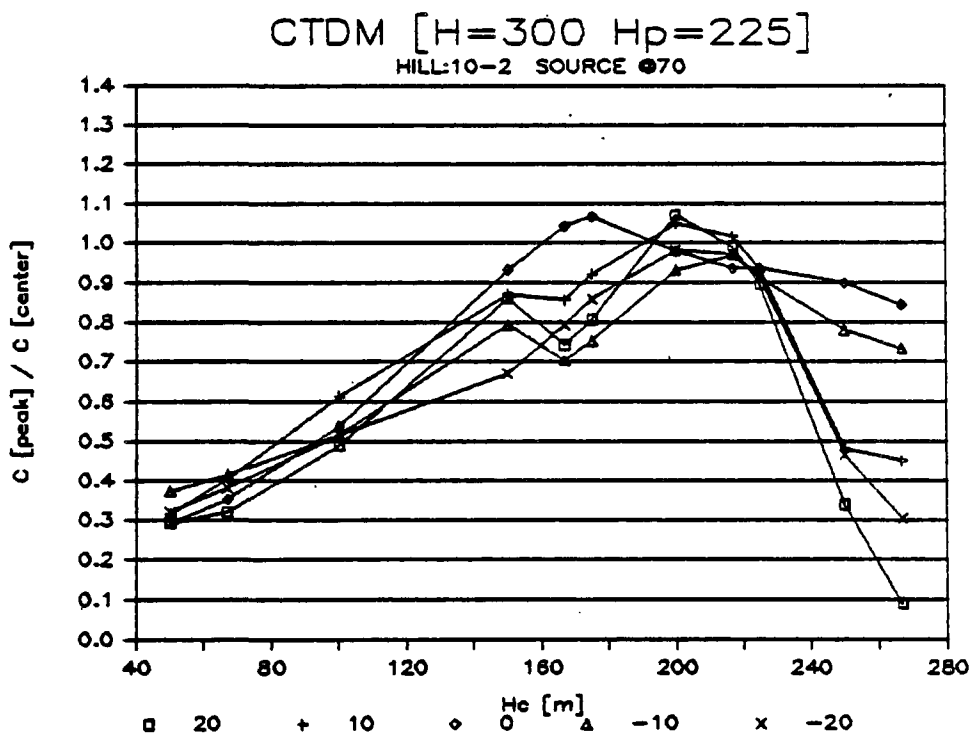

Figure 30. (Continued).

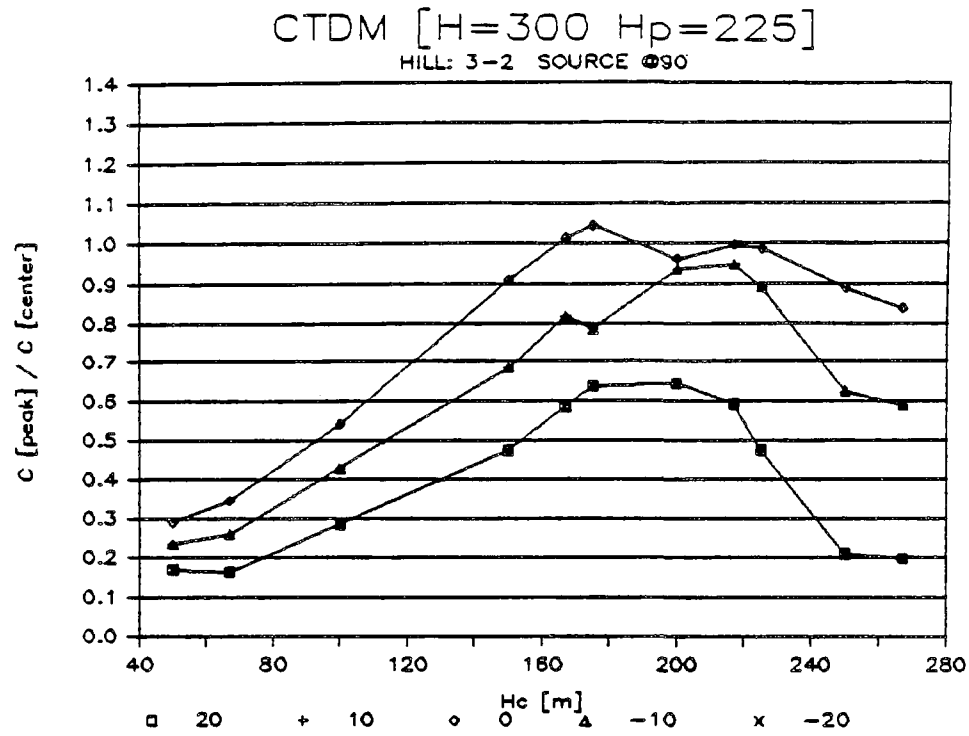

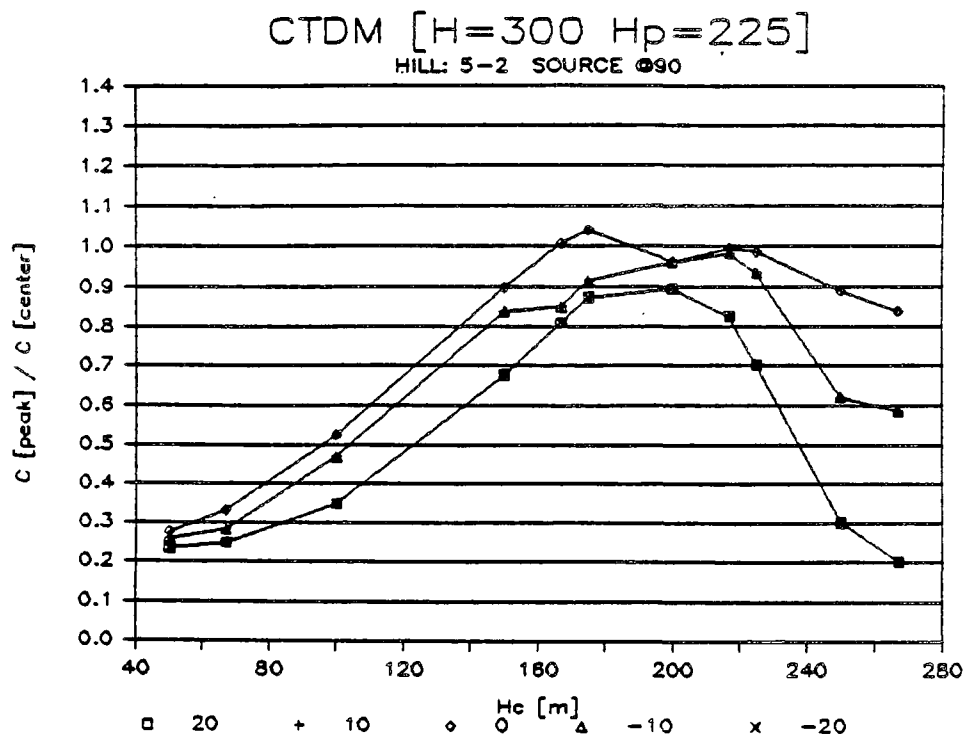

Figure 31. Terrain-effect factor versus H_c for hills of aspect ratios 3-2 and 5-2. Source positions are aligned with both the major and minor axes, and 45° in between.

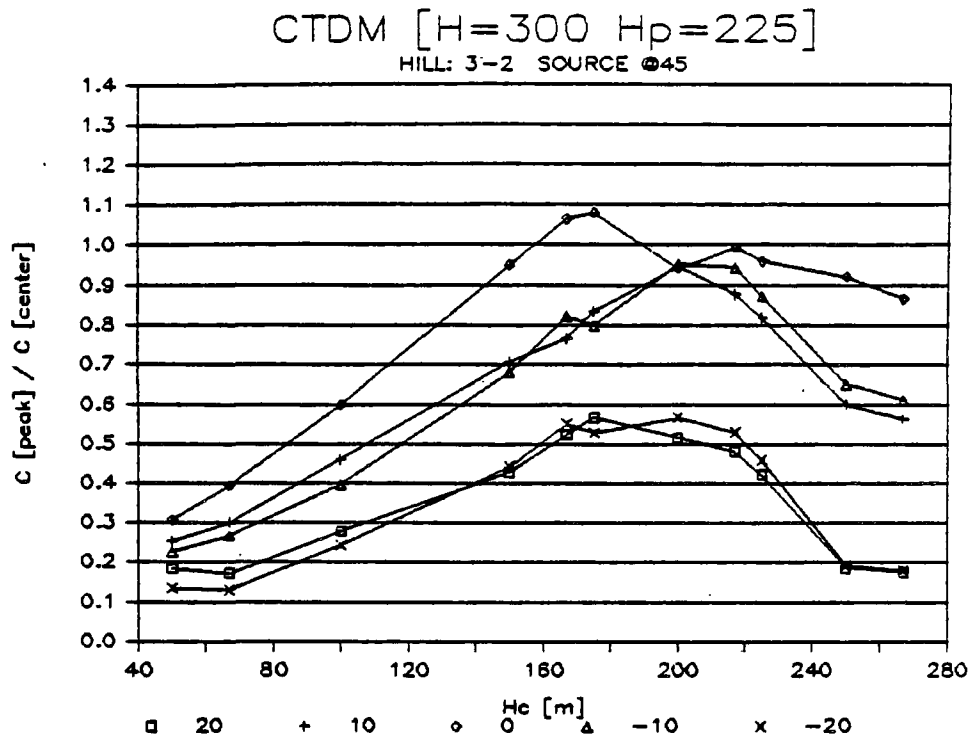

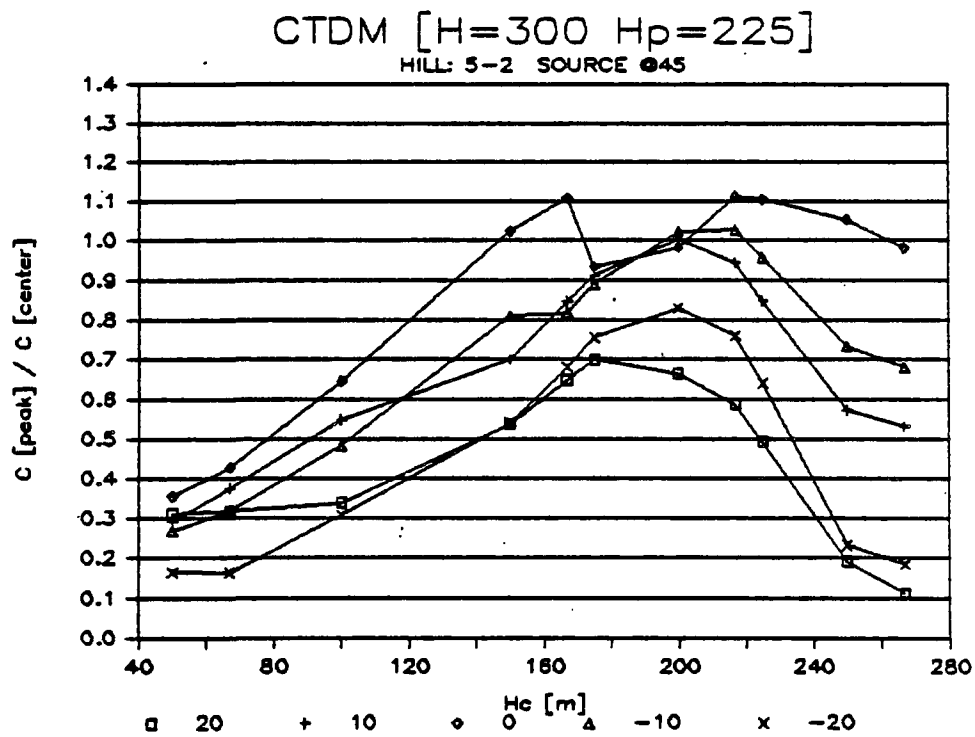

Figure 31. (Continued).

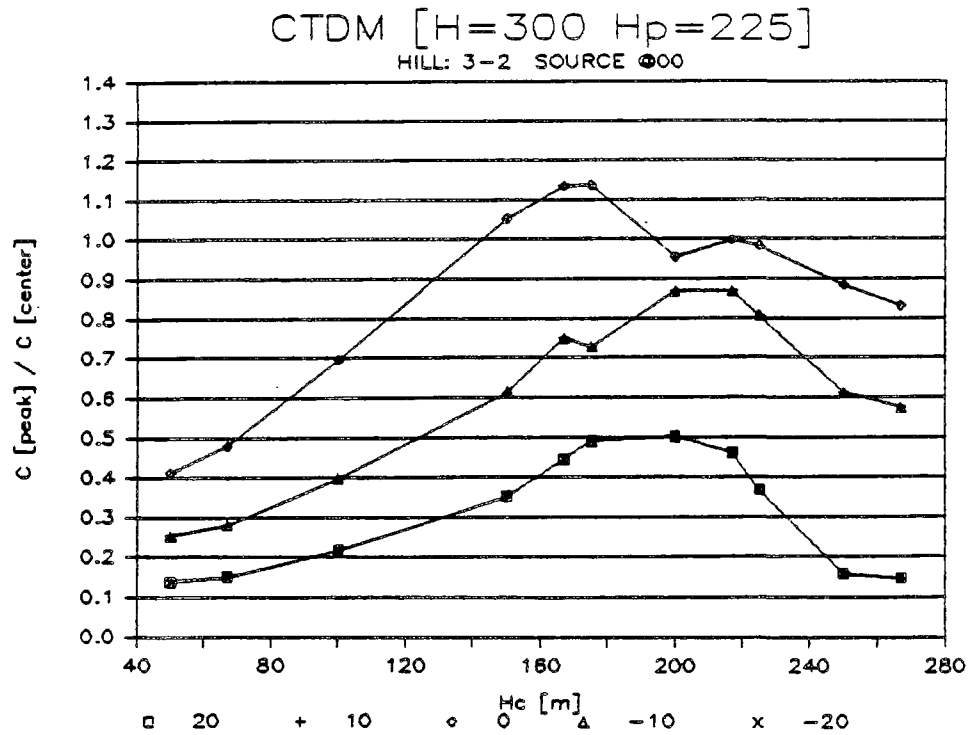

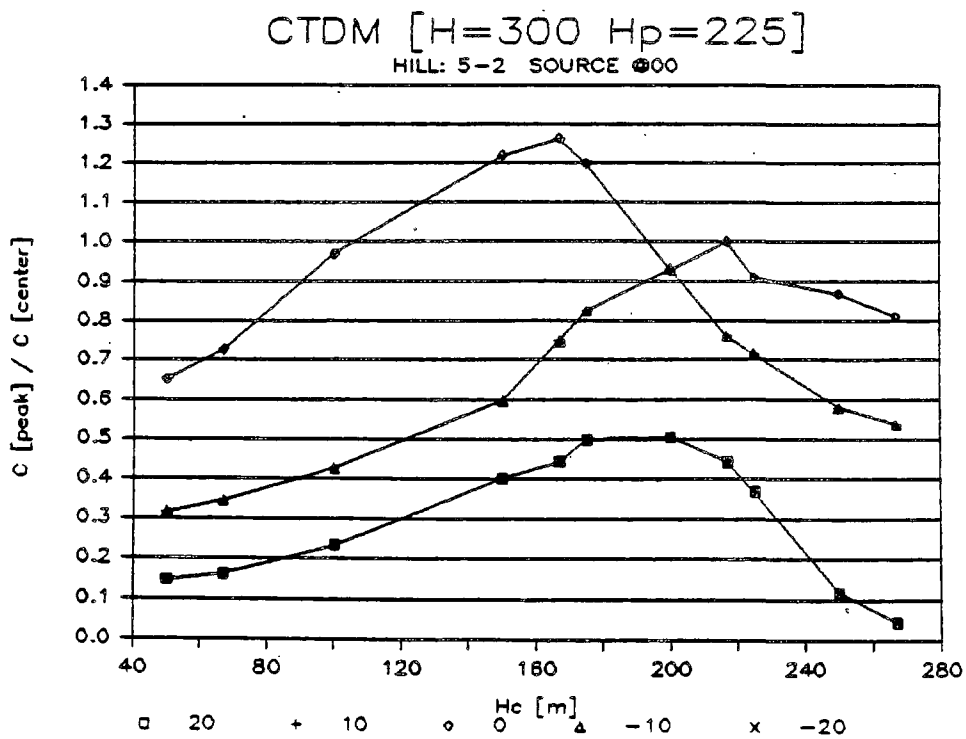

Figure 31. (Continued).

values of H_c, sensitivity to wind direction is smallest for plumes crossing an elongated hill over its shorter side, and greatest for plumes crossing the same hill along its longer side. Intermediate results are obtained for sources midway, at 45°. This behavior is consistent with the results already discussed.

All of these results indicate the importance of H_c and the stagnation streamline in allowing the center of the plume to either impact a receptor on a hill, or avoid it. Regardless of the overall shape of the hill, the stagnation streamline is directly related to the wind direction and the direction from the center of the hill to the source. Peak concentrations are obtained for plumes well below H_c only when the source lies on the stagnation streamline, and concentrations drop rapidly as the wind direction deviates from this condition. The terrain-effect factor for plumes above H_c may exceed that of direct impingement, depending on the shape and orientation of the hill, but peak concentrations are generally less than those resulting from impingement, because the increase in travel time leads to an increase plume dilution.

5.4 Operational test on Hill Shape Sensitivity

Terrain features in the vicinity of the Widows Creek Steam Plant presented an opportunity to test the sensitivity of CTDM to uncertainties in specifying the shape of the hill. Sand Mountain, which lies to the southeast of the power plant, is actually a broad plateau with a sharp rise from the Tennessee River valley to the plateau level. Because this hill is not an isolated feature, it is unclear how to digitize it for the terrain preprocessor and how to specify the center. For this exercise, two hill centers were chosen after a sufficient amount of the hill was digitized (See Figure 32). One center was positioned to create a rather narrow hill (Figure 33), while a second choice caused a wider hill to be created for input to CTDM (Figure 34). CTDM was then run for a full year of meteorological data, using all available tower levels, to test the sensitivity of the model to these alternative choices.

Peak concentrations at the 7 monitors on the hill (positioned as shown in Figure 32) are listed in Table 20. The location of the peak concentrations change, but their magnitude is nearly the same in this case. The orientations of the two fitted hills differ by about 10°, resulting in a different deflection of the plume being modeled. In this case, it is likely that if adequate receptor coverage is given, the peak concentrations will not be very sensitive to changes in the terrain input.

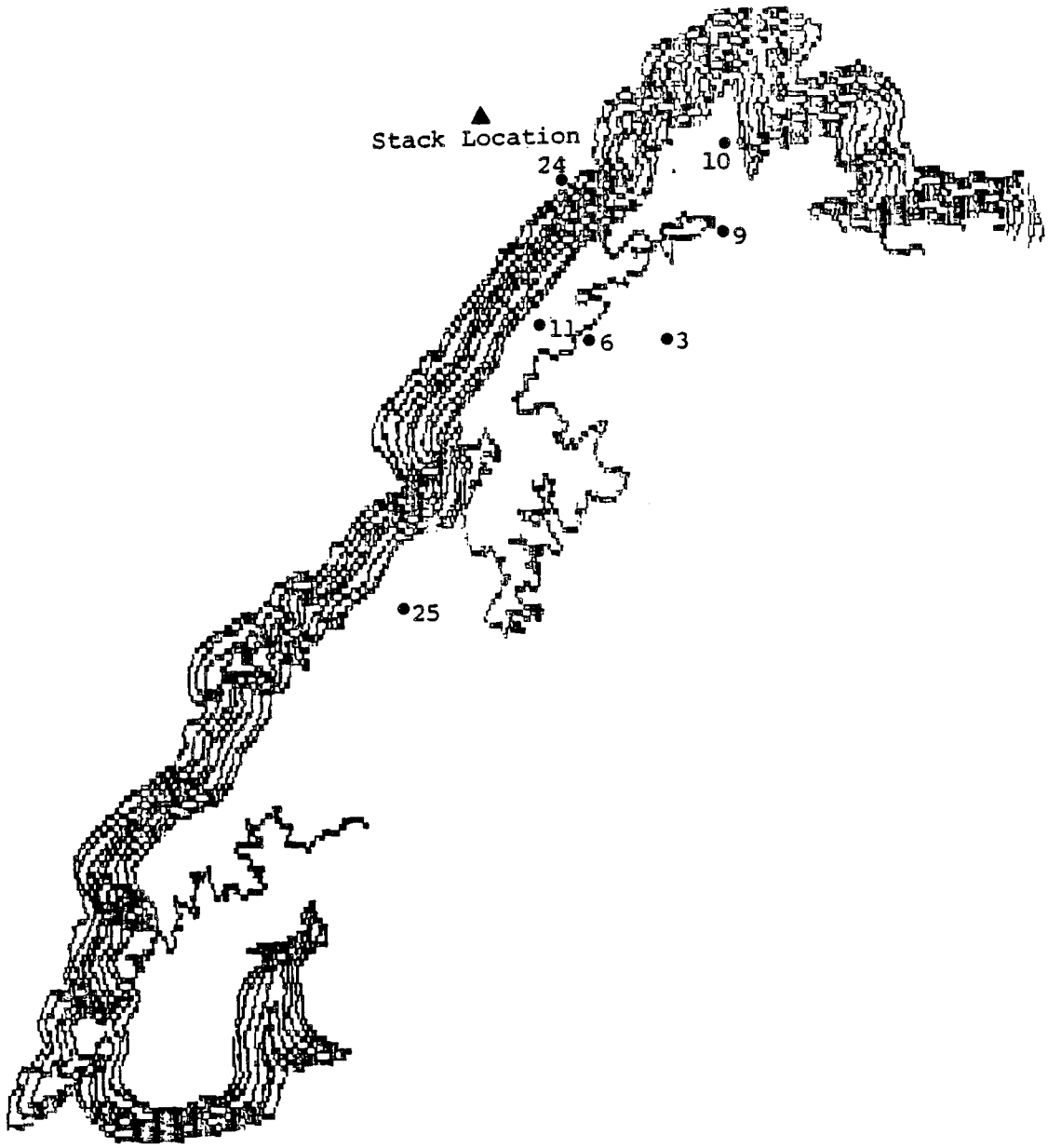

Figure 32. Digitized contours of Sand Mountain, located southeast of the Widow's Creek steam station (see triangle), with positions of SO_2 monitors indicated by site number.

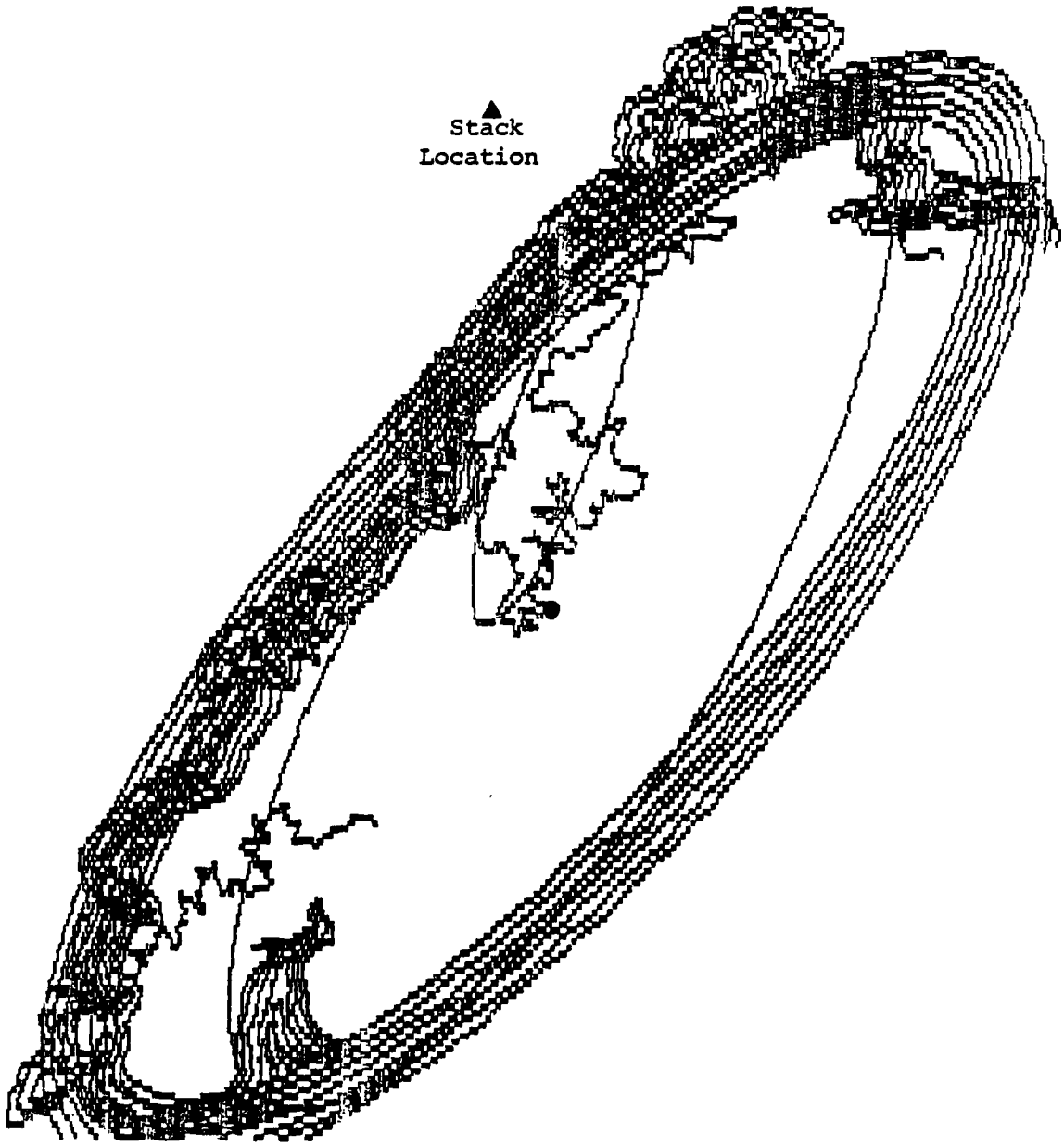

Figure 33. Elliptical fits to contours with hill "center" (see heavy circle) positioned relatively close to the edge of the plateau (narrow hill).

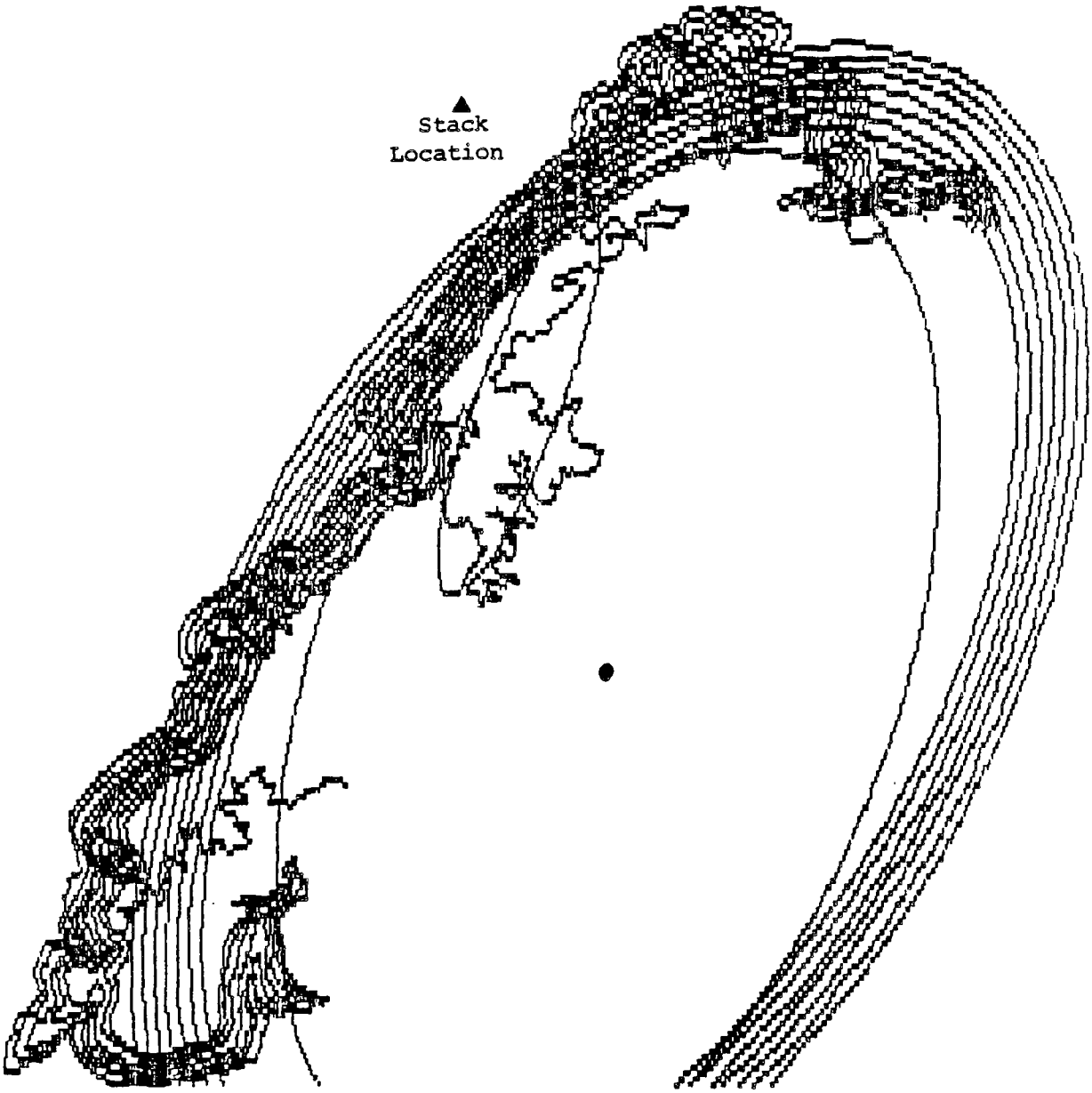

Figure 34. Elliptical fits to contours with hill "center" (see heavy circle) located far from the edge of the plateau (wide hill)

TABLE 20

PEAK 1-HOUR SO_2 CONCENTRATIONS ($\mu g/m^3$)

PREDICTED BY CTDM FOR SAND MOUNTAIN MONITORS USING

TWO DIFFERENT HILL CONFIGURATIONS

(WIDOWS CREEK 1980 DATA)

	Narrow Hill				Wide Hill			
	Highest		Second Highest		Highest		Second Highest	
Rank	Site #	Concentration	Site #	Concentration	Site #	Concentration	Site #	Concentration
1	6	6857	6	5283	25	6847	25	4942
2	25	6219	3	5034	6	6303	6	4896
3	10	5437	9	4725	9	5957	3	4828
4	3	5394	10	4579	3	5491	10	4816
5	11	5330	25	4531	10	5328	9	4794
6	9	4882	11	2374	11	3111	11	2421
7	24	1607	24	1345	24	2008	24	718

SECTION 6

MODEL APPLICABILITY AND LIMITATIONS

The question of applicability requires a discussion of the theoretical limitations inherent in the algorithms of CTDM as well as a discussion of how well the model performed for the various sites and meteorological data sets reported in Section 5. Theoretical limitations are addressed first.

The focus of much of the model development activity that has culminated in CTDM is the stable plume impingement problem. A plume is emitted into a stably-stratified flow which carries it toward elevated terrain. The growth rate of the plume in the vertical is small compared to that typically found in non-stably-stratified flows. As the plume encounters the terrain, concentrations of plume material on the hill are much greater than those that would have occurred if the plume had diffused to the surface in the absence of the terrain. This focus places primary emphasis on the interaction of a plume with one terrain feature, in a flow that is documented by measurements of wind, turbulence, and temperature stratification at many levels in the vertical near the source. During impingement, peak concentrations are expected along the windward face of the terrain, or in the case of near-impingement, near the crest of the hill.

As a result, CTDM is most applicable for periods of stable stratification at sites in which nearby terrain exceeds plume height and at which the terrain elements can be isolated. Meteorological data should provide adequate definition of the vertical structure of the approach flow to the terrain, and generally should be obtained near the source. The degree of stratification that can be accommodated in CTDM includes near-neutral conditions as well as strongly stratified conditions.

Implicit in this statement of applicability are several restrictions and assumptions that were adopted in the overall design of the model:

1. CTDM contains no wake algorithms for simulating the mixing and recirculation found in cavity zones in the lee of a hill. Therefore, sources within the lee of terrain features are not treated in the model and estimates of concentrations at receptors in the lee may not be reliable when such zones are present.

2. CTDM contains no global flow calculation that accounts for the presence of many hills. The path taken by a plume through an array of hills cannot be simulated by the model. It relies on measurements of the flow taken in the neighborhood of the source to define the incident flow field

for each of the hills or terrain segments independently. If there is a strong channeling of the flow due to large-scale terrain features (e.g. a valley setting), then this will be reflected in the modeling only insofar as it is contained in the measurements.

3. All hills that are explicitly modeled are done so in isolation; any changes to the plume size caused by one hill are not carried forward to subsequent simulations downwind.

4. CTDM assumes that the meteorological data are representative of the entire 1-hour averaging period, and apply to the entire spatial domain. Spatial and temporal variability that may be resolved by an array of meteorological towers cannot be used directly in the model.

5. As an outgrowth of 4 in combination with the Gaussian plume formulation, unsteady conditions which foster recirculation of plume material are not treated in CTDM.

Other limitations arise from assumptions adopted in formulating algorithms for phenomena included in the model. The flow-field solutions used both above and below H_c demand simple models for the shape of the hill. Below H_c, the model is a cylinder of elliptical cross-section. Above H_c, the model is a hill of Gaussian profile in the vertical and elliptical cross-section in the horizontal. The choice of length scales for these shapes becomes less apparent as the complexity of the terrain increases. Typical problems encountered in selecting terrain attributes are discussed in the terrain preprocessor user manual (Mills et al., 1987). But beyond the problem of representing the terrain is the question of whether a terrain feature can be modeled at all by CTDM. Above H_c, the flow model is formulated for hills of low-to-moderate slope. Steep-walled buttes and mesas violate the low-slope assumption, and the LIFT computation is clearly inappropriate. However, the formulation for the flow below H_c is quite appropriate for such steep-walled features, provided that a suitable ellipse can be used. Hence, CTDM may be considered for use in modeling such features in the limit of very stable stratification.

Lest these restrictions on the application of CTDM appear too severe, we point out that CTDM is an extension to the level-terrain Gaussian plume model. It is designed for use in the near-field of a source where the steady-state formulation is most appropriate. It simulates the effect of actual terrain on flow and dispersion by using simplified terrain elements as a surrogate for the actual terrain features. The surrogate features reflect the overall scale and orientation of the actual terrain. Within this context, the lack of a global treatment of transport and diffusion among an array of terrain features is not a crippling deficiency.

A potential limitation of CTDM involves its neglect of drainage flows. Certainly, large-scale drainage flows would be resolved by on-site meteorological measurements, and a drainage flow would in some circumstances be the transport flow for the plume calculation. But in a complex array of tributary valleys, the combined effect of these

large-scale flows on the elevation and transport of a plume would not be modeled. Local drainage flows are another matter. Although these too are neglected, it is not clear that this represents a limitation. Shallow, local drainage flows were observed during the field experiments conducted during the course of this program, but they never had an observable effect on the location or magnitude of the peak concentrations. The effect of the local flows appears to have been limited to the transport of diluted plume material into the lower basins.

The limits on the vertical growth of a plume trapped in an elevated layer are qualitatively understood, but could not be easily incorporated into the operational version of CTDM. The depth of such a layer involves detailed sodar observations which are often difficult to interpret. Underpredictions can occur, therefore, when the modeled σ_z growth exceeds the thickness of the elevated layer occupied by the plume.

Application of CTDM in the model evaluation tasks raises several additional issues regarding limitations to the model. At the Westvaco site, CTDM shows a tendency toward underpredicting peak concentrations under high wind speed (neutral) conditions. For these conditions for SF_6 predictions at CCB, the peak observed concentrations are typically found on the windward face of the hill, while the model typically places them on the leeward side. This suggests that the rate of plume growth in the vertical in the presence of the hill is underestimated for this condition. This may be attributable to the formulation of sigma-z in the neutral limit for high plumes. The evaluations at Westvaco and Widows Creek also underscore the need for temperature gradient measurements that properly resolve the stratification of the flow. When a single delta-T is measured, the elevation of the lower measurement must not be too close to the surface. If it is too close, the degree of stratification is overestimated and the performance of CTDM suffers. In fact, all of the tests of the model that involved the use of less than the full set of on-site measurements showed a degradation in model performance. This trend should not be viewed as a limitation of the model, but rather as a guide to what can be expected from it in certain applications with poor resolution in the vertical structure of the flow.

A special note of caution in applying CTDM to sources very close to a ridge may be read into its performance at the Hogback Ridge site. When all of the cases in which the plume is below H_c are grouped together, CTDM shows a strong bias toward underestimating peak concentrations. But in many of these cases, the plume was released at the foot of the ridge, while the meteorology was measured further away. Upon removing these cases, the bias is largely removed. Most of the cases remaining in this data set involved the release of the plume from the main meteorological tower. Hence, it appears that one should strive to capture the properties of the flow as close to the source as is practical, especially for sources in the vicinity of large, two-dimensional hills that have a substantial impact on the flow near the source.

SECTION 7

CONCLUSIONS AND RECOMMENDATIONS

The Complex Terrain Model Development program objectives have been met. The Complex Terrain Dispersion Model, CTDM, is the primary product of the effort. This model displays considerable improvement over the models that EPA has been using in regulatory practice, especially on an event-by-event basis. It also shows improved performance over RTDM, a model EPA is adopting as a third-level screening model and which benefited from the early findings of the CTMD program on the importance of the dividing streamline concept to understanding stable flows.

Before describing more specific conclusions about CTDM, it is appropriate to identify some of the other products and contributions which have resulted from this effort.

The four field programs have produced a wealth of data for others to use. Although the CTMD field programs were designed to focus on specific model development needs, the data bases contain information which should be of interest to future researchers in a number of areas. Examples include information for further development of dispersion models for unstable conditions and lee side effects. The density of the sampling arrays provides sufficient coverage for statistical analyses of monitoring plan efficiencies. The meteorological data is extensive. The multiple towers and supplementary remote sensing and sounding data provide detailed information on time and spatial variations in wind and temperature fields of special interest to micrometeorologists and, as well, to those interested in measurement technology issues.

One of the key technical concepts in the CTMD program was the complementary use of field experiment data together with fluid modeling experiment data in the development and testing of mathematical modeling concepts. This program represents, to our knowledge, the largest endeavor in the area of dispersion modeling to effectively utilize this approach. The fluid modeling efforts assisted in the design of the field experiments, in the verification of some of the field experiment findings, and in exploring technical areas of uncertainty in the late stages of the mathematical model development. The success of our use of these complementary approaches will, hopefully, encourage others to consider similar use in future model development efforts.

CTDM Attributes and Limitations

CTDM is an improved and versatile refined air quality model for use with elevated point sources in high terrain settings during stable conditions. Its improvements over the screening models currently used in complex terrain applications can be attributed to several factors:

- its ability to use observed vertical profiles of meteorological data (rather than just one level) to obtain plume height estimates of these variables;

- computation of plume dispersion parameters, σ_y and σ_z, directly from turbulence measurements rather than indirectly from discrete stability classes.

Despite these advances, CTDM still contains several limitations:

- Its framework is a steady-state Gaussian model. It is not designed for extreme light-wind conditions with highly variable wind directions.

- The mathematical depiction of terrain shapes is simplified from actual shapes.

- Flow interactions among different terrain features are not explicitly accounted for.

- Meteorological data can be input to the model for only one location.

- Flow deformation in the LIFT module is treated with linearized equations of motion for steady-state Boussinesq flow, with higher order terms neglected. These assumptions are not valid for applications involving steep terrain (greater than about 15^{o}) or strongly stable flow (Froude number of order 1).

CTDM can be used for regulatory applications involving a long series (e.g., a full year) of model simulations. Several of its limitations are related to the desire to keep the computer execution time reasonable.

An operational limitation of the current version of CTDM is that it provides concentration estimates only for stable hours. For averages of concentrations over several hours, including nonstable conditions, a second model must be run to augment the CTDM predictions. CTDM also presents operational challenges to the user. Detailed terrain and meteorological data must be provided. "Isolated" terrain elements need to be defined, and this task can be complicated by superimposed and/or interconnected features. The considerable demands for meteorological input, while necessary, represent a significant increase over those for current models that use a single level of data.

The CTDM user must be careful in obtaining the proper meteorological data for the model. As has been stated in Section 5, CTDM can be very sensitive to errors in wind direction, for example. Plume σ_y and σ_z calculations are critically dependent upon on-site turbulence measurements at plume height. The evaluation results have shown that use of near-surface data or data with poor

resolution in the vertical will degrade the performance of CTDM (on an event-by-event basis, at least). The use of tall towers or doppler acoustic sounders will be necessary to obtain representative wind and turbulence data. The capability for accurate remote temperature sensing is still being developed, but representative ΔT measurements are essential for obtaining accurate concentration estimates. Such measurements can be obtained from two levels on a tall tower or from two separate (but electronically linked) shorter towers (one on a hill) if instruments are placed well away from the ground (e.g., 50 meters or higher) on each tower.

Performance Assessment

The accuracy of CTDM has been assessed in the model evaluation analysis described in Section 4. Various statistical measures used in the evaluation include model bias, model "scatter," and the percentage of model predictions within a factor of 2 of the observations. A particularly relevant statistic for model evaluation (Hanna and Heinold, 1985) is the normalized mean square error (version 2 as used in Section 4):

$$M \text{ value} = MSE/(\overline{C_o} \cdot \overline{C_p}).$$

This parameter is chosen because it contains no arbitrary weighting and accounts for both model bias and random variances in the model predictions. To simplify comparisons among data sets, the mean square error is made dimensionless by dividing it by the product of the mean observed and predicted concentrations. Low values of M are associated with good models. High concentrations are strongly weighted in this scheme because the difference, C_p-C_o, is likely to be large for high concentrations. In general, a very good model has an M value of the order 1 or less, while models with little skill have on M value of about 5 or more (see Hanna and Heinold, 1985).

The M values from the evaluation results reported in Section 4 are summarized in Table 21. For the tracer experiments, with high spatial resolution, results are shown for the data sets paired in time, not space. For the conventional SO_2 networks with low spatial resolution but a long monitoring record, results are reported for the data subset paired in space, not time. The CTDM results for all tower levels are quite good, with most M values between 1 and 2. A deterioration in performance is evident for CTDM using the degraded data. RTDM (on-site) shows good performance except for HBR; reasons for its problems at HBR have been discussed in Section 4. The benefit of on-site meteorological data is evident for both CTDM (all tower levels) and RTDM (on-site).

It is useful to compare CTDM's M values with those of EPA refined models as listed in Appendix A of the Guideline on Air Quality Models (Revised), 1986. CRSTER has been tested at tracer sites in Illinois (flat site) and Tennessee (moderately hilly site; see Hanna et al, 1986). These experiments, sponsored by the Electric Power Research

TABLE 21

SUMMARY OF M VALUES FROM THE COMPLEX TERRAIN EVALUATION DATA BASES*

	CTDM, All Tower Levels	CTDM, 2 Tower Levels	CTDM, 1 Tower Level	Complex I	RTDM, Default	RTDM, On-Site
CCB, SF_6	1.12	4.00	7.66	1.76	3.35	1.13
CCB, CF_3Br	2.71	3.52	6.39	2.22	3.56	1.80
HBR, SF_6	3.03	2.77	3.41	5.59	14.58	6.28
HBR, CF_3Br	1.92	3.75	1.94	0.82	9.37	22.52
FSPS, SF_6	1.17	1.25	2.03	4.41	1.92	2.13
FSPS, CF_3Br	1.24	1.88	2.88	3.44	2.15	1.82
Westvaco, SO_2	0.27	1.58	0.16	5.58	0.64	0.36
Widows Creek, SO_2	1.27	1.82	1.30	3.02	0.98	2.22

*Data subset paired in time, not space was used for the tracer experiments (CCB, HBR, FSPS); data subset paired in space not time was used for the SO_2 sites, 1-hour averages (Westvaco, Widows Creek).

Institute, featured several weeks of data collection at a network of 150-200 tracer samples. ISC was tested by Hanna and Schulman (1985) with tracer data bases collected by the American Gas Association (AGA) at two natural gas compressor stations. These tests featured movable arrays of some 40 tracer samples that were located in the wake zone of a building; the aerodynamic building downwash algorithm in ISC was tested.

The M values from these evaluation results are summarized in Table 22. It is evident that CTDM's performance at the CTMD tracer sites is comparable to those of EPA-designated refined models in similar test environments.

CTDM, while showing good performance at the evaluation sites, also exhibits an overprediction tendency for most of the data bases; this is important for regulators who are interested in protecting air quality through the use of analytical modeling techniques. The most serious underprediction result, at Hogback Ridge (CF_3Br), is associated with mobile crane tracer releases close to the ridge, while using meteorological data from the main tower farther from the ridge. This supports the concept that the location as well as the vertical resolution of the meteorological data must be designed with care for CTDM use.

Recommendations

The additional number of meteorological and terrain input variables requires more care on the part of the user. The terrain must be specified for each receptor; the best model performance is realized when the terrain feature most local to each receptor is specified (see terrain preprocessor user guide, Mills et al., 1987). Receptor coverage on each terrain feature should be extensive to assure the identification of the highest concentrations. Meteorological measurements made close to the release point's horizontal and vertical positions are essential for good model results. Some testing on the sensitivity of CTDM to less ideal input to the model has been discussed in Sections 4 and 5. We recommend more testing of CTDM by the user community in real-world applications to provide additional information on model sensitivity. The terrain input requirements are new to complex terrain modelers and feedback on actual experience will be valuable. Requirements for meteorological data are quite demanding. Situations to avoid due to poor resulting model performance need to be further defined, such as the HBR CF_3Br releases very close to the ridge that were accompanied by, perhaps, misrepresentative meteorological input. Special attention should be given to model performance for two-dimensional ridge or mountain valley situations. In addition, cases involving plume transport for several kilometers before terrain is encountered (such as buttes or mesas in the western U.S.) need to be tested.

CTDM does not predict concentrations for hours when the modeled plumes are in a convective boundary layer. We see the need for further model development to close this gap and provide a "complete"

TABLE 22

SUMMARY OF M VALUES FROM TRACER EXPERIMENTS*
FOR CTDM AND OTHER REFINED AIR QUALITY MODELS

Data Base	Model	M Value
CCB, SF_6	CTDM	1.12
CCB, CF_3Br	CTDM	2.71
HBR, SF_6	CTDM	3.03
HBR, CF_3Br	CTDM	1.92
FSPS, SF_6	CTDM	1.17
FSPS, CF_3Br	CTDM	1.24
Kincaid, SF_6**	CRSTER	1.26
Bull Run, SF_6**	CRSTER	7.04
AGA***	ISC	4.32

* All data base subsets are paired in time, not space

** M value reported is the average from developmental and evaluation portions of the data (Hanna et al., 1986). Kincaid is a flat site and Bull Run is a moderately hilly site.

*** Test of ISC's building wake dispersion algorithm (Schulman and Hanna, 1985)

model for regulatory applications requiring sequential use of meteorological data. Some of the CTMD experiments did cover the period of inversion breakup and subsequent convective activity. These data could be used as part of the recommended further development.

Future work on complex terrain models should also seek to improve the estimates of meteorological data at release height for cases where observations are not ideally designed. A model preprocessor that takes into account terrain interactions and thermal stratification as well as multiple sources for meteorological data could be used to refine the input data to CTDM.

The CTMD program was designed to focus upon plume impingement cases on nearby terrain features. This project has resulted in a model that has been applied to a larger variety of plume interactions with terrain. For example, concentration estimates at receptors on the lee side of the hills have been attempted for the CTMD sites, even though CTDM was not specifically designed and developed for that application. Synder, 1987 (Appendix H) reports upon the ratio of maximum ground-level concentrations measured in the Fluid Modeling Facility tow tank in the presence of hills versus those with the hill removed. This ratio, called the terrain amplification factor, can be highest on the lee side of the hill in some cases. Therefore, we recommend more investigation into the phenomena of lee-side effects as well as plume behavior on terrain features beyond those adjacent to a source.

The data analyses performed during this program effort support the concept that there are inherent limits to our ability to predict measured or observed air quality concentrations. Improvements to models, such as those accomplished in this effort, establish confidence that a model is properly accounting for the physical phenomena involved, and is therefore "fair" in its application to different situations. It is especially noteworthy in this regard that CTDM consistently performed well with all of the data sets used, in contrast to the other models tested. Nevertheless, the effort has not resulted in a "breakthrough" in reducing statistical uncertainty associated with individual predictions versus observations. The use of a high resolution profile of meteorology measurements with height resulted in improvements to CTDM's performance. It is apparent from our case-study analyses that further model performance improvements would emerge from an increase in the information on horizontal as well as vertical variations in meteorological data (i.e., better local, geographic coverage).

REFERENCES

Batchelor, G.K. 1970. An Introduction to Fluid Dynamics. Cambridge University Press, London NW1, England.

Briggs, G.A. 1973. Diffusion Estimation for Small Emissions. ATDL Contribution File No. 79, Atmospheric Turbulence and Diffusion Laboratory.

Briggs, G.A. 1975. Plume Rise Predictions. Lectures on Air Pollution and Environmental Impact Analyses. AMS, Boston.

Brighton, P.W.M. 1978. Strongly Stratified Flow Past Three-Dimensional Obstacles. Quarterly Journal of the Royal Meteorological Society, 104: 289-307.

Britter, R.E., J.C.R. Hunt and K.J. Richards 1981. Airflow Over a Two-Dimensional Hill: Studies of Velocity Speed-Up, Roughness Effects and Turbulence. Quart. J.R. Met. Soc., 107: 91-110.

Burt, E.W. 1977. Valley Model User's Guide. EPA-450/2-77-018. U.S. EPA, Office of Air Quality Planning and Standards, Research Triangle Park, NC.

Businger, J.A. 1973. Turbulent Transfer in the Atmospheric Surface Layer. Chapter 2 in Workshop on Micrometeorology. D.A. Haugen (ed.). American Meteorological Society, Boston, MA.

Carson, D.J. 1973. The Development of a Dry Inversion - Capped Convectively Unstable Boundary Layer. Quart. J.R. Meteorol. Soc., 99: 450-467.

Crapper, G.D., 1959. A Three-Dimensional Solution for Waves in the Lee of Mountains, J. Fluid Mech., 6: 51-76.

Csanady, G.T. 1974. Equilibrium Theory of the Planetary Boundary Layer with an Inversion Lid. Boundary Layer Meteor., 6: 63-79.

Deardorff, J.W. and G.E. Willis 1975. A Parameterization of Diffusion into the Mixed Layer. J. Appl. Met., 14: 1451-1458.

DiCristofaro, D.C. 1986. EPA Complex Terrain Model Development FSPS Modelers' Data Archive - 1986. U.S. EPA, Atmospheric Sciences Research Laboratory, Research Triangle Park, NC.

DiCristofaro, D.C., D.G. Strimaitis, B.R. Greene, R.J. Yamartino, A. Venkatram, D.A. Godden, T.F. Lavery, and B.A. Egan 1986. EPA Complex Terrain Model Development Program: Fifth Milestone Report - 1985. EPA/600/3-85/069, U.S. Environmental Protection Agency, Research Triangle Park, NC.

Drazin, P.G. 1961. On The Steady Flow of a Fluid of Variable Density Past an Obstacle. Tellus, 13: 239-251.

Eberhard, W.L. 1986. Contributions by Wave Propagation Laboratory to EPA's Complex Terrain Model Development Project. NOAA Technical Memorandum ERL WPL-143. Wave Propagation Laboratory, Boulder, CO.

Egan, B.A., R.J. Paine, P.E. Flaherty and J.E. Pleim 1985. Evaluation of COMPLEX I and RTDM Using 1979-1980 Data from the TVA Widows Creek Monitoring Network. ERT Document PD523-400. Available from Hunton & Williams (UARG), Washington, D.C.

Greene, B.R. 1985. Complex Terrain Model Development Quality Assurance Project for Small Hill Impaction Study No. 2. ERT Document P-B876-350. Prepared for U.S. EPA, Research Triangle Park, NC.

Greene, B.R. 1986. Complex Terrain Model Development: Quality Assurance Project Report for Full-Scale Plume Study. ERT Document P-B876-725. Prepared for U.S. EPA, Research Triangle Park, NC.

Greene, B.R. and S. Heisler 1982. EPA CTMD Quality Assurance Project Report for SHIS #1. ERT Document P-B348-350. Prepared for U.S. EPA, Research Triangle Park, NC.

Guldberg, P.H., J.P. Myers, K.W. Wiltsee, and P. Morgenstern, 1977. Handbook for the Single Source (CRSTER) Model. EPA-450/2-77-013. EPA Office of Research and Development, Research Triangle Park, NC.

Hanna, S.R., 1983. Lateral Turbulence Intensity and Plume Meandering During Stable Conditions. J. Clim. and Appl. Meteor., 22: 1424-1430.

Hanna, S.R. and D.W. Heinold 1985. Simple Methods for Comparative Evaluation of Air Quality Models. in Proceedings of the 15th International Technical Meeting on Air Pollution Modeling and Its Applications, NATO/CCMS.

Hanna, S.R., J.C. Weil, and R.J. Paine, 1986. Plume Model Development and Evaluation - Hybrid Approach EPRI Contract No. RP-1616-27. Prepared for Electric Power Research Institute, Palo Alto, CA.

Hess, J.L. and A.M.D. Smith, 1962. Calculation of Non-Lifting Potential Flow About Arbitrary Three-Dimensional Bodies. McDonnell-Douglas Report E.S. 40622.

Holzworth, G.C. 1980. The EPA Program for Dispersion Model Development for Sources in Complex Terrain. Second Joint Conference on Applications of Air Pollution Meteorology, New Orleans, LA. AMS, Boston.

Hovind, E.L., M.W. Edelstein, and V.C. Sutherland, 1979. Workshop on Atmospheric Dispersion Models in Complex Terrain. EPA-600/9-79-041. U.S. EPA. Research Triangle Park, N.C.

Hunt, J.C.R., and R.J. Mulhearn 1973. Turbulent Dispersion from Sources Near Two-Dimensional Obstacles. J. Fluid Mech., 61: 245-274.

Hunt, J.C.R. and W.H. Snyder 1980. Experiments on Stably and Neutrally Stratified Flow Over a Model Three-Dimensional Hill. J. Fluid Mech., 96: 671-704.

Kato H., O.M. Phillips 1969. On the Penetration of a Turbulent Layer Into Stratified Fluid, J. Fluid Mech., 37: 643-655.

Lavery, T.F., A. Bass, D.G. Strimaitis, A. Venkatram, B.R. Greene, P.J. Drivas, and B.A. Egan, 1982. EPA Complex Terrain Model Development Program: First Milestone Report - 1981. EPA-600/3-82/036, U.S. Environmental Protection Agency, Research Triangle Park, NC.

Lavery, T.F., D.G. Strimaitis, A. Venkatram, B.R. Greene, D.C. DiCristofaro, and B.A. Egan, 1983. EPA Complex Terrain Model Development Program: Third Milestone Report - 1983. EPA-600/3-83/101, U.S. Environmental Protection Agency, Research Triangle Park, NC.

Lavery, T.F., D.G. Strimaitis, and B.A. Egan 1986. A Workshop Report on the Complex Terrain Model Development Project (February 4-6, 1986). Prepared for U.S. EPA, Atmospheric Sciences Research Laboratory, Research Triangle Park, NC.

Mills, M.T., R.J. Paine, E.M. Insley, and B.A. Egan 1987. The Complex Terrain Dispersion Model (CTDM) Terrain Preprocessor System - User Guide and Program Descriptions. Prepared for U.S. EPA, Atmospheric Sciences Research Laboratory, Research Triangle Park, NC.

Overcamp, T.J. 1983. A Surface-Corrected Gaussian Model for Elevated Sources. J. Clim. and Appl. Met., 22: 111-1115.

Paine, R.J. 1987. User's Guide to the CTDM Meteorological Preprocessor (METPRO) Program. Prepared for U.S. EPA, Atmospheric Sciences Research Laboratory, Research Triangle Park, NC.

Paine, R.J. and B.A. Egan 1987. User's Guide to the Rough Terrain Diffusion Model (RTDM) - Revision 3.20. ERT Document PD-535-585. ERT, Inc., 696 Virginia Road, Concord, MA 01742.

Paine, R.J., D.G. Strimaitis, M.G. Dennis, R.J. Yamartino, M.T. Mills, and E.M. Insley 1987. User's Guide to the Complex Terrain Dispersion Model. Prepared for U.S. EPA, Atmospheric Sciences Research Laboratory, Research Triangle Park, NC.

Riley, J.J., Liu, H.T. and Geller, E.W. 1976. A Numerical and Experimental Study of Stably Stratified Flow Around Complex Terrain, EPA Report No. EPA-600/4-76-021, Res. Tri. Pk., NC, 41p.

Schulman, L.L. and S.R. Hanna 1985. Evaluation of Downwash Modifications to the Industrial Source Complex Model. JAPCA, 36: 258-264.

Sheppard, P.A. 1956. Airflow Over Mountains. Quart. J. R. Meteor. Soc., 82: 528-529.

Smith, R.B., 1980. Linear Theory of Stratified Hydrostatic Flow Past an Isolated Mountain, Tellus, 32: 348-64.

Snyder W.H. 1987. Contributions of the Fluid Modeling Facility to EPA's Complex Terrain Model Development Program. May 1987 EPA Report. Atmospheric Sciences Research Laboratory. Research Triangle Park, NC.

Snyder, W.H., R.E. Britter and J.C.R. Hunt 1980. A Fluid Modeling Study of the Flow Structure and Plume Impingement on a Three-Dimensional Hill in Stably Stratified Flow. Proc. Fifth Int. Conf. on Wind Engr. (J.E. Cermak, ed.). 1: 319-329, Pergamon Press, NY,NY.

Snyder, W.H. and J.C.R. Hunt 1984. Turbulent Diffusion from a Point Source in Stratified and Neutral Flows Around a Three-Dimensional Hill; Part II - Laboratory Measurement of Surface Concentrations. Atmos. Envir., 18: 1969-2002.

Snyder, W.H., R.S. Thompson, M.S. Shipman 1986. Streamline Trajectories in Neutral and Stratified Flow Over a Three-Dimensional Hill. Appendix to EPA Complex Terrain Model Development: Fifth Milestone Report - 1985, EPA/600/3-85/069, January, 1986.

Strimaitis, D.G., A. Venkatram, B.R. Greene, S. Hanna, S. Heisler, T.F. Lavery, A. Bass, and B.A. Egan, 1983. EPA Complex Terrain Model Development Program: Second Milestone Report - 1982. EPA-600/3-83/015, U.S. Environmental Protection Agency. Research Triangle Park, NC.

Strimaitis, D.G., T.F. Lavery, A. Venkatam, D.C. Dicristofaro, B.R. Greene, and B.A. Egan, 1984. EPA Complex Terrain Model Development Program: Fourth Milestone Report - 1984. EPA-600/3-84/110, U.S. Environmental Protection Agency, Research Triangle Park, NC.

Taylor, G.I. 1921. Diffusion by Continuous Movements. Proc. London Math. Soc. Ser. 2., 20: 196.

Truppi, L.E. and G.C. Holzworth. 1983. EPA Complex Terrain Model Development: Description of a Computer Data Base from Small Hill Impaction Study #1, Cinder Cone Butte, Idaho. EPA/600/3-84/008. U.S. Environmental Protection Agency, Research Triangle Park, NC. 98 pp.

Truppi, L.E. 1985. EPA Complex Terrain Model Development: Description of a Computer Data Base from Small Hill Impaction Study #2, Hogback Ridge, New Mexico. EPA/600/3-84-038. U.S. Environmental Protection Agency, Research Triangle Park, NC. 87 pp.

Truppi, L.E. 1986. EPA Complex Terrain Model Development: Description of a Computer Data Base from the Full Scale Plume Study, Tracy Power Plant, Nevada. EPA/600/3-86/068. U.S. Environmental Protection Agency, Research Triangle Park, NC. 105 pp.

Truppi, L.E. 1987. EPA Complex Terrain Terrain Model Development: Description of a Computer Data base of SAS™ System Data Sets from Tracer Field Studies at CCB, Idaho, Hogback Ridge, New Mexico, and the Tracy Power Plant, Nevada. U.S. Environmental Protection Agency, Research Triangle Park, NC (in press).

U.S. Environmental Protection Agency 1986. Guidelines on Air Quality Models (Revised). EPA-450/2-78/027R. July 1986. Office of Air Quality Planning and Standards. Research Triangle Park, NC

Venkatram, A., D. Strimaitis, and D. DiCristofaro 1984. A Semiempirical Model to Estimate Vertical Dispersion of Elevated Releases in the Stable Boundary Layer. Atmos. Environ., 18: 923-928.

Wackter, D.J. and R.J. Londergan 1984. Evaluation of Complex Terrain Air Quality Simulation Models. EPA-450/4-84-017, Office of Air Quality Planning and Standards, EPA, Research Triangle Park, NC. 243 pp.

Yamartino, R.J. 1987. Exact Solutions to the Linearized Equation for Stratified Flow Over Terrain in Multi-Dimensional Space. To be published. (see Appendix A)

APPENDIX A
EXACT SOLUTIONS TO THE LINEARIZED EQUATION FOR STRATIFIED FLOW OVER TERRAIN IN MULTIDIMENSIONAL SPACE

Exact Solutions to the Linearized Equation for Stratified Flow Over Terrain in Multidimensional Space

Robert J. Yamartino
Sigma Research Corporation

1. Introduction

In an attempt to improve the theoretical basis of the U.S. EPA's Complex Terrain Dispersion Model (CTDM) and enhance its predictive power under a range of stratification (and shear) conditions, a basic investigation of the linearized, partial differential governing equations was undertaken. A number of researchers have examined various aspects of the problem of stratified flow over two- and three-dimensional obstacles. Queney (1947) considered hydrostatic (i.e., highly stratified) flow past a 2-d ridge and Smith (1980) extended this to 3-d symmetric hills. The hydrostatic assumption makes it difficult, however, to connect these solutions to those appropriate for neutral flows. Hunt, Leibovich, and Lumley (1981) and Hunt and Richards (1984) suggest interpolative methods for connecting these regimes. Other researchers have focused on the nature of the lee waves far downwind of the hill. Wurtele (1957) and Crapper (1959) examined the vertical velocity field of these far field waves, whereas Janowitz (1984) provides a complete description of all flow quantities in the far field of a dipole (i.e., Dirac delta function) obstacle. Berkshire (1985) and Bois (1984) provide detailed analyses of far field lee waves in two dimensions.

As the EPA is concerned with estimating pollutant concentrations in hilly terrain, it becomes necessary to predict the path followed by pollutant plumes in the near vicinity of such terrain. Thus, far field solutions are of limited usefulness and efforts must be focused on the near field (or complete) solutions. In addition, the moderately stratified conditions that often exist in nature, correspond to hill Froude numbers of order unity: a regime that satisfies neither the near neutral assumption of $F_r >> 1$ nor the hydrostatic assumption of $F_r << 1$. Hence , effort must be directed to eliminating approximations in several areas. Finally, the results must be easy to use and inexpensive to compute; thus, eliminating integral formulations (e.g.,

Trubnikov, 1959) or numerical methods requiring repeated application of Fast Fourier Transform (FFT) techniques. In this paper we report on the pure theoretical developments associated with this effort.

Section 2 describes the basis for the partial differential equation governing the three-dimensional (3-d) problem and the integral formulation of this problem. Section 3 presents the exact solution for the 3-d problem, whereas solutions in fewer dimensional space and their interrelations are discussed in Section 4. Finally, Section 5 summarizes the results of this paper.

2. The Mathematical Model

We begin with the linearized equation of motion for steady-state flow of a Boussinesq fluid (Smith, 1980):

$$\rho_o \, U u'_x = -P'_x \tag{1a}$$

$$\rho_o \, U v'_x = -P'_y \tag{1b}$$

$$\rho_o \, U w'_x = -P'_z - \rho' g \tag{1c}$$

$$u'_x + v'_y + w'_z = 0 \tag{1d}$$

and $$\rho' = -\left[\frac{d\rho_o}{dz}\right]\eta \tag{1e}$$

These equations, in which subscripts x, y, and z indicate derivatives with respect to downstream, cross-stream, and vertical coordinates respectively, relate the perturbation velocities, u', v', and w', to the perturbation density, ρ', and vertical fluid displacement, $\eta = \eta(x,y,z)$, and to the unperturbed initial velocity U and density ρ_o. Adding the kinematic condition for steady flow in a shear-free flow,

$$w' = U\eta_x \tag{2}$$

Eqs. (1) can be reduced to the single partial differential equation (PDE) for η,

$$(\nabla^2\eta)_{xx} + n^2\nabla_H^2\,\eta = 0 \qquad (3)$$

where $\nabla_H^2 \equiv \dfrac{\partial^2}{\partial x^2} + \dfrac{\partial^2}{\partial y^2}$,

$n = N/U$, and the Brunt Vaisala frequency, N, is defined as

$$N^2 = -(g/\rho_o)\,\frac{d\rho_o}{dz} \quad .$$

Representing $\eta(x,y,z)$ as the 2-d Fourier transform

$$\eta \equiv \int_{-\infty}^{\infty}\!\!\int dk\, dl\hat{\eta}\, \exp\{i(kx + \ell y)\} \qquad (4)$$

reduces Eq.(3) to the equation

$$\hat{\eta}_{zz} + m^2\hat{\eta} = 0 \qquad (5)$$

where $m^2 = n^2\,(k^2 + \ell^2)/k^2 - (k^2 + \ell^2)$, (6)

and the outgoing wave, or radiation, condition dictates that the exp(+imz) solution choice be made. Smith (1980) chose to work with the solution of Eq.(5), that is, $\hat{\eta}(k,\ell,z) = \hat{\eta}(k,\ell,0)\,\exp(imz)$; however, this is cumbersome as m involves a branch cut. Instead, we utilize the relation

$$\exp(imz) \equiv \frac{-\partial}{\partial z}\left\{\frac{1}{\pi}\int_{-\infty}^{\infty}\frac{dq\,\exp(iqz)}{q^2 - m^2}\right\} \qquad (7)$$

to convert the singularity to a simple pole and re-express the problem, including the linearized terrain boundary condition that flow at the ground follow the ground or $\eta(x,y,z' = 0) = h(x,y)$, (where h(x,y) is the terrain height function and z′ represents height above terrain), in terms of the convolution

$$\eta = -I_z \quad , \qquad (8a)$$

where $I = \mathrm{Re}\,\frac{1}{2\pi}\iint_{}^{\infty} dx'dy'h(x-x',\ y-y')\ G(x',y',z')$, (8b)

$-\infty$

Re denotes the real part, and G is the Green's function

$$G(x',y',z') = \frac{1}{2\pi^2} \iiint_{-\infty}^{\infty} dk\, d\ell\, dq\, \exp(i(k\,x'+\ell\,y'+q\,z'))/(q^2-m^2) \qquad (9)$$

For the Dirac delta function hill, normalized such that $\iint dx'dy'\ h(x',y') = 1$, we see that $I(x,y,z') = G(x,y,z')/(2\pi)$, as one expects from the definition of a Green's function solution.

In Appendix A, one solution of Eq.(9) is determined to be

$$G(x',y',z') = \sin(nRz'/d)/R \qquad , \qquad (10a)$$

where $R^2 \equiv x'^2 + y'^2 + z'^2$ and $d^2 \equiv y'^2 + z'^2$; however, this solution does not obey the surface boundary condition that the vertical deflection, $\eta = -I_{z'} = -G_{z'}/(2\pi)$, vanish at the surface away from the origin ($x'=y'=0$). Yamartino and Pavelle (1987) show by direct substitution, using the algebraic processor MACSYMA, that both Eq.(10a) and

$$G(x',y',z') = \cos(nRz'/d)/R \qquad (10b)$$

are solutions to the equation

$$(\nabla^2 I)_{xx} + n^2 \nabla_H^2 I = 0 \qquad (11)$$

for the delta function hill and therefore are solutions to the basic PDE given by Eq.(3).

The solution given by Eq.(10b) obeys the aforementioned surface boundary condition and also has the desirable property that G goes to the well known solution $G = 1/R$ in the neutral ($n = 0$) limit. However, Eqs.(10a) and (10b) are not the only solutions. Any linear combination of these solutions and any spatial derivative of these solutions is also a solution. Hence, after struggling to obtain one solution, we now have the ambiguity of an infinity of solutions, that can only be resolved by obtaining the correct particular solution via proper evaluation of the integral in Eq.(9). Thus, there is no guarantee that Eq.(10b) is the correct choice; nevertheless, it is one of the

simplest.

In Appendix AB, the Eq.(10b) solution is applied to the problem of the infinite field of cosine hills and is found to yield a solution that differs from the correct solution by a factor of $(n^2/k_H^2 - 1)^{1/2}$, where k_H is the x-wavenumber of the hills. This implies that Eq.(10b) is not the correct full form of the Green's function and that other combinations should be checked (e.g., derivatives and/or linear combinations); however, very few of the possible candidates can even be checked via the direct integration approach of Appendix AB, as the integrals are not presently doable. This, of course, raises the practical consideration of the value of expending substantial effort to find the correct particular Green's function solution if integrals convolving it (e.g., I, I^x, I^{xx}) together with practical hill functions can not be easily evaluated. Nevertheless, it would be of considerable theoretical interest to have the correct form of the solution.

Janowitz (1984) has isolated the leading term of the far-field portion (i.e., nR >> 1) of the problem and his solution has the same argument of the trigonometric functions as in Eq.(10), but does not appear computable as simple derivatives of either Eq.(10a) or (10b). This is not surprising, as the stationary phase technique he employed projects out the leading dependence and not necessarily a complete or exact solution. Nevertheless, Janowitz's solution represents an important theoretical milestone.

The closest we can presently come to matching his far field expression involves taking $\frac{\partial}{\partial x'}$ of the expression presented in Eq.(10b). Thus, (ignoring the primes on x and y) $\eta = -G_{xz'}/2\pi$ and the longest lived, or wave, part (i.e., decays slowest in R) of this expression is just

$$\eta_w \simeq \frac{n^2}{2\pi} \cdot \frac{z'}{d^3} \cdot \frac{x}{R^2} \cdot \left[d^4 + x^2y^2\right]^{1/2} \cdot \left\{ \frac{\left[d^4 + x^2y^2\right]^{1/2}}{Rd} \right\} \cos(nRz'/d).$$

In the limit x >> y >> z', one finds that { } → 1 and, with the exception of a factor n/2, Janowitz's result is obtained. Hence, Eq.(10b) cannot be too far from the desired result.

The correct particular solution could also possibly involve an

integration $\left[\text{e.g., } \int_{-\infty}^{x} dx \cos(nRz'/d)/R\right]$ however, this would lead us into the realm of the generalized cosine-integral functions, about which little seems to have been done analytically since the studies of Aiken (1949).

Several other issues also emerge when the exact particular solution is sought. The first of these involves the related differential equation governing the conjugate[1], potential function variable. If the formal solution for η as $\eta = -I_z$ is substituted back through the Eq.(1) system of governing equations, one obtains

$$u'/U = - [I_{xx} + n^2 I] = P'/(\rho_o U^2) \qquad (12a)$$

$$v'/U = - [I_{xy} + n^2 I_y^x] \qquad (12b)$$

and $$w'/U = -I_{xz} \quad , \qquad (12c)$$

as a complete description of the flow. If one now integrates Eq.(11) twice with respect to x and assumes that no f(x) quantities appear on the right hand side, one has

$$\nabla^2 I + n^2 \left[I + I_{yy}^{xx}\right] = 0 \quad , \qquad (13)$$

which for $n \to 0$ is identical to the $\nabla^2\phi = 0$ PDE for the potential function ϕ. Hence, if I_x is reset to ϕ, such that Eq.(12a) becomes

$$u'/U = - \left[\phi_x + n^2 \phi^x\right] \quad ,$$

for example, then the divergence-free relation (1d) leads immediately to

---

[1]Janowitz (1984) shows that the delta function hill problem is without swirl and therefore describable in terms of a potential.

$$\nabla^2\phi + n^2\left[\phi + \phi^{xx}_{yy}\right] = 0 \qquad (14)$$

Thus, the identical nature of the PDE's for ϕ and I as given by Eqs.(13) and (14) could suggest that the solutions given by Eq.(10) might be more correctly called ϕ solutions, with I being subsequently computed as $I = \phi^x$.

Finally, the richness of the solution possibilities offered by a fourth-order PDE should not be underestimated. One approach to evaluating the integral, Eq.(9), for the simplified case of $x' = y' = 0$ leads to the particular solution.

$$G(0,0,z') = \frac{1}{R}\left\{1 - aJ_o(a) - \frac{\pi a}{2}\left[J_1(a)H_o(a) - J_o(a)\,H_1(a)\right]\right., \qquad (15)$$

where $a = nz'$ and whe J and H indicate Bessel and Struve functions respectively. While quite cumbersome to work with, Eq.(15) has the interesting feature that it has a lowest-order n (rather than n^2) dependence. Such a stronger dependence on the stratification variable n appeared desirable during efforts to reproduce laboratory studies.

3. A Related 3-d Problem

The twice integrated PDE given by Eq.(13) seen in a Fourier transform sense converts the rightmost term into $(\ell^2/k^2)\hat{I}$. In the case of the infinite field of cosine hills problem (Appendix B), only the wave numbers (k_H, ℓ_H) associated with the hill shape survive. In the language of hill length scales (L_x, L_y) this term becomes $(L_x^2/L_y^2)I$ and Eq.(13) can be rewritten as the Helmholtz equation

$$\nabla^2 I + n'^2 I = 0 \qquad (16a)$$

where $n' = n\,(1 + L_x^2/L_y^2)^{1/2}$, (16b)

which has the known Green's function solution

$$G = \cos(n'R)/R \qquad (17)$$

(plus other solutions) in three dimensions. As anticipated from the foregoing discussion, Eq.(17) correctly solves the field of cosine hills problem and the necessary integrals are discussed in Appendix B. This solution is quite useful because it is easier to deal with in subsequent integrations and because it provides a valuable bridge between the three- and two-dimensional problems. However, a clear shortcoming is that its simple R dependence suggests isotropy; that is, z has no special significance in the equation, despite the fact that the density stratification and thus the atmosphere's "springiness" is a z-oriented phenomenon. Such isotropic "springiness" is, however, expected for a repetitive field of cosine hills.

It should be noted that for use in Eq.(8b), the Green's function given by Eq.(17) represents only the real part. For completeness, and to satisfy the outgoing wave energy constraint, the full complex Green's function,

$$G = \exp(i\, n'\, R)/R\ , \qquad (17a)$$

should be used in Eq.(8b). The real part is then taken after the convolution process is complete. The same argument holds in the fewer dimension problems that follow.

4. Solutions in Fewer Dimensions

As our 3-d hill starts to spread in the crosswind (i.e., $\pm$ y) direction, variability in the y direction drops (i.e., $\frac{\partial}{\partial y}$ terms get smaller, except near the hill's y boundaries) until the situation of the infinite crosswind ridge is achieved. In this case all $\frac{\partial}{\partial y}$ and $\frac{\partial^2}{\partial y^2}$ terms vanish and the PDE for shear-free flow given by Eq.(13) becomes

$$\nabla_2^2 I + n^2 I = 0\ , \qquad (18)$$

where $\nabla_2^2 = \frac{\partial^2}{\partial x^2} + \frac{\partial^2}{\partial z^2}$.

Thus, the most troublesome I^{xx}_{yy} term has disappeared and, along with it, any differences between the Eq.(17) solution, with $n' = n$ (as $L_y \to \infty$), and whatever the correct particular solution of Eq.(3) or (13) should be. Eq.(18) is known to have zeroth-order Bessel function solutions, $J_o(nr)$ and $Y_o(nr)$ where $r^2 = x^2 + z^2$, but it should be possible to obtain the correct 2-d Green's function, G_2, by integrating the 3-d Green's function, G_3, over y. It is here where the "dimensional bridge" solution provided by Eq.(17) proves particularly useful. Using it, one finds

$$G_2 = \int_{-\infty}^{\infty} dy\, G_3 = \int_{-\infty}^{\infty} dy\, \cos(nR)/R$$

$$= 2 \int_0^{\infty} \frac{dp}{\sqrt{p^2 - 1}} \cos(nrp) = -\pi\, Y_o(nr) \qquad (19)$$

via the aid of the transformation $p = R/r$ and an integral representation of Y_ν found in Abramowitz and Stegun (1972) (pg. 360, Eq. 9.1.24). Writing G_2 in its full complex form as

$$G_2 = i\, \pi\, H_o^{(1)}(nr) \qquad (20)$$

where $H_o^{(1)}(x) = J_o(x) + i\, Y_o(x)$ is the Hankel function, then enables one to proceed easily to the 1-d problem. Integrating over x from $-\infty$ to $+\infty$, one obtains the one-dimensional Green's function

$$G_1 = 2\pi \frac{e^{inz'}}{im} \quad , \qquad (21)$$

which corresponds to upward travelling waves resulting from a displacement of the entire x-y plane.

5. Discussion

Several solutions to the fourth-order PDE for linearized fluid flow over a 3-d obstacle, as expressed by Eqs.(3) and (11), are found. These solutions are given by Eq.(10) and have been verified to be exact solutions by the algebraic processor MACSYMA. Two steps that aided in determining these

Green's function solutions involved,

- working with the integrated quantity I, such that $\eta = - I_{z'}$, and
- converting the branch cut to a contour integral over a pole.

The first of these steps actually goes a long way toward restructuring the integral into a form more closely related to known tabulated integrals.

The candidate solution, Eq.(10b), is used in connection with the problem of an infinite 2-d field of cosine hills and found not to be the exact particular solution. However, comparison with the far-field, wave solution of Janowitz (1984) suggests that Eq.(10b) (or actually its derivative with respect to x) may be appropriate. Unfortunately, the needed integrals to test this hypothesis are not presently tractable.

A related Helmholtz PDE, Eq.(16), is developed along dimensional arguments and its solution, Eq.(17), is also found to yield the correct solution to the above-mentioned, field of cosine hills problem. In addition, this solution, Eq.(17), provides a convenient bridge to the Green's function solutions to the stratified flow problem in fewer (i.e., 2- and 1-d) dimensions.

Acknowledgment

This work was supported as part of U.S. EPA Contract 68-02-3421 to Environmental Research and Technology, Inc. The author wishes to acknowledge the project officer, Peter Finkelstein, for his encouragement to pursue this topic.

References

Abramowitz, M. and I.A. Stegun, 1972. Handbook of Mathematical Functions, National Bureau of Standards, Applied Mathematics Series 55, Washington, DC, Tenth printing with corrections.

Aiken, H.H. (editor), 1949. Tables of Generalized Sine- and Cosine-Integral Functions: Part I. Harvard University Press.

Berkshire, F.H., 1985. Two-dimensional linear lee wave modes for models including a stratosphere, Quart. J.R. Met. Soc., 101, 259-266.

Bois, P.A., 1984. Asymptotic theory of lee waves in an unbounded atmosphere. Geophys. Astropys. Fluid Dynamics, 29, 267-303.

Crapper, G.D., 1959. A three-dimensional solution for waves in the lee of mountains. J. Fluid Mech., 6, 51-76.

Gradshteyn, I.S. and I.M. Ryzhik, 1965. Tables of Integrals, Series, and Products, Fourth Edition. Academic Press, New York.

Hunt, J.C.R., S. Leibovich, and J.L. Lumley, 1981. Prediction Methods for the Dispersal of Atmospheric Pollutants in Complex Terrain. Flow Analysis Associates. Report P85-81-04, Ithaca, NY 14850.

Hunt, J.C.R. and K.J. Richards, 1984. Stratified airflow over one or two hills. Boundary-Layer Met., 30, 223-259.

Janowitz, G.S., 1984. Lee waves in three-dimensional stratified flow. J. Fluid Mech., 148, 97-108.

Queney, P., 1947. Theory of Perturbations in Stratified Currents with Applications to Airflow Over Mountain Barriers. Dept. of Met., Univ. of Chicago Report No. 23, Univ. of Chicago Press. Also described in Dynamic Meteorology, P. Morel (ed.), D. Reidel Publishing Co., Boston, MA 622 pp., 1970.

Smith, R.B., 1980. Linear theory of stratified hydrostatic flow past an isolated mountain. Tellus, 32, 348-364.

Trubnikov, B.N., 1959. The three-dimensional problem of the flow over a barrier of an air current unbounded at the top. Dokl. of the Acad. of the U.S.S.R, 129, 4, 781-3 (English translation pgs. 1136-1138).

Wurtele, M., 1957. The three-dimensional lee wave. Beitr. Phys. frei Atmos., 29, 242-252.

Yamartino, R.J. and R. Pavelle, 1987. An application of MACSYMA to the fourth-order partial differential equation for linearized, stratified fluid flow in three-dimensions. Submitted to J. Symbolic Computation.

Appendix AA: The 3-d Green's Function Integral

Eq.(9) can be put in a more compact form by first defining the vectors $\vec{Q} = (k,\ell,q)$ and $\vec{R} = (x',y',z')$ and noting that $kx'+\ell y'+qz' = \vec{Q}\cdot\vec{R} = QR\cos\theta'$. In spherical coordinates, Eq.(9) then becomes

$$G(x',y',z') = \frac{1}{2\pi^2}\int_0^\infty dQ\, Q^2 \int_0^{2\pi} d\phi \int_{-1}^{1} d(\cos\theta)\, \frac{e^{iQR\cos\theta'}}{Q^2 - n^2/\cos^2\phi} \qquad (A\text{-}1)$$

where $k = Q\sin\theta\cos\phi$, $\ell = Q\sin\theta\sin\phi$, $q = Q\cos\theta$; $x' = R\sin\theta_R\cos\phi_R$, $y' = R\sin\theta_R\sin\phi_R$, $z' = R\cos\theta_R$,

$$\cos\theta' = \cos\theta\cdot\cos\theta_R + \sin\theta\cdot\sin\theta_R\left\{\cos\phi\cdot\cos\phi_R + \sin\phi\cdot\sin\phi_R\right\},$$
$$= \cos\theta\cdot\cos\theta_R + \sin\theta\cdot\sin\theta_R\cdot\cos\left[\phi-\phi_R\right]$$

and $q^2 - m^2 = q^2 + k^2 + \ell^2 - n^2(k^2+\ell^2)/k^2$

$$= Q^2 - n^2/\cos^2\phi$$

The presence of the $\cos^2\phi$ term prevents one from beneficially rotating the system so that θ becomes θ' (i.e., this simplicity is offset by the resulting complexity in the rotated $\cos\phi$ term).

Next, we non-dimensionalize the Q integration by defining $\alpha \equiv QR$ and $a \equiv nr$, and then alter the usual spherical integration limits to yield

$$G = G'/R \qquad (A\text{-}2a)$$

$$\text{with } G' = \frac{1}{2\pi^2}\cdot\frac{1}{2}\int_{-\infty}^{\infty} d\alpha\cdot\alpha^2 \int_0^{2\pi} d\theta\sin\theta\cdot\int_{-\pi/2}^{+\pi/2} d\phi\, \frac{e^{i\alpha\cos\theta'}}{\alpha^2 - a^2/\cos^2\phi} \qquad (A\text{-}2b)$$

Doing the α integration first, by picking up the pole at $\alpha = a/\cos\phi$ and closing the contour in the upper-half-plane (UHP), we obtain

$$G' = \frac{ia}{4\pi} \int_{-\pi/2}^{+\pi/2} \frac{d\phi}{\cos\phi} \int_{o}^{2\pi} d\theta \, \sin\theta \, e^{ia\cos\theta'/\cos\phi} \qquad \text{(A-3)}$$

The θ integration is made possible by substituting the complex form for $\sin\theta$ and extending a result given in Groebner and Hofreiter (1973, pg. 337, 9b) via the analytic continuation $I_1(ix)=iJ_1(x)$, where I_1, and J_1 are Bessel functions of order 1. The result is

$$G' = -\frac{a}{2} \cos\theta_R \int_{-\pi/2}^{\pi/2} \frac{d\phi}{\cos\phi} \cdot \frac{J_1\left[\frac{a}{\cos\phi}\sqrt{\quad}\right]}{\sqrt{\quad}} \qquad \text{(A-4)}$$

where $\sqrt{\quad} \equiv \left\{\cos^2\theta_R + \sin^2\theta_R \cdot \cos^2(\phi-\phi_R)\right\}^{1/2}$.
However, because a number of square roots, and thus sign ambiguities, are involved in the intermediate calculation leading up to Eq.(A-4), it is not clear that (A-4) represents the only solution for G'.

The ϕ integration could not be accomplished analytically, but was instead evaluated to a high degree of accuracy[2] for hundreds of different values of $a = nR$, θ_r, and ϕ_R. In all cases the computations were consistent with the result

$$G' = -\sin(nRz'/d) \qquad \text{(A-5)}$$

with $d^2 \equiv y'^2 + z'^2$, so that

$$G = -\sin(nRz'/d)/R \qquad \text{(A-6)}$$

becomes the needed result.

---

[2] The integrand was sampled at 50,000 points, judiciously avoiding the end points at $\phi=\pm\pi/2$, and the results appeared to be accurate to within a few percent.

Appendix AB: Solution for a Field of Cosine Hills

Consider the case of the infinitely repetitive grouping of cosine hills, given by the hill function

$$h(x,y) = h\cos(k_H x)\cdot\cos(\ell_H y), \tag{B-1}$$

where $k_H = 2\pi/\lambda_H$ and $\ell_H = 2\pi/\lambda_y$

relate the hill's x,y wavelengths λ_x, λ_y, respectively, to equivalent wave numbers.

The fact that the actual peak-to-trough height of the hills is 2h is not of particular concern; however, the relationship between the Fourier transform and the Dirac delta function proves particularly useful. That is,

$$\frac{1}{2\pi}\int_{-\infty}^{\infty} dx\,\cos(k_H x)e^{-ikx} = \frac{1}{2\pi}\int_{-\infty}^{\infty} dx\cdot\frac{1}{2}\left[e^{ix(k_H-k)} + e^{-ix(k_H+k)}\right]$$

$$= \frac{1}{2}\left\{\delta(k_H-k) + \delta(-k_H-k)\right\}$$

$$= \delta(k_H-k), \tag{B-2}$$

where the last line in Eq.(B-2) reflects the fact that there are no differences between plus and minus k_H properties of the hill function. Thus, the Fourier transform of the hill shape function is simply

$$\hat{h}(k,\ell) = h\,\delta(k_H-k)\cdot\delta(\ell_H-\ell) \tag{B-3}$$

In the sections which follow, the vertical deflection, η, will be computed from both the wavenumber space (i.e., Eq.(B-3)) and coordinate space (i.e., Eq.(B-1)) representations of the hill.

Wavenumber Space Approach

The fundamental defintion of the Dirac delta function as

$$\int_{-\infty}^{\infty} dk\ f(k)\delta(k_H - k) \equiv f(k_H), \tag{B-4}$$

coupled with the outgoing wave solution of Eq.(5) as

$$\hat{\eta}(k,\ell,z) = \hat{h}(k,\ell,0)\ \exp(+imz), \tag{B-5}$$

and the Fourier transform of the linearized (i.e., $z \rightarrow z'$ = height above terrain) surface boundary condition

$$\hat{\eta}(k,\ell,0) = \hat{h}(k,\ell), \tag{B-6}$$

enables one to solve directly for η. Guided by Eq.(4), one may then write

$$\eta(x,y,z) = \int_{-\infty}^{\infty}\int dk \cdot d\ell \cdot \hat{h}(k,\ell)\ \exp\left[im(k,\ell)z'\right]\ \exp\left\{i(kx + \ell y)\right\} \tag{B-7a}$$

$$= h\ \exp\left\{im(k_H,\ell_H)z'\right\} \cdot \exp\left\{i(k_H x + \ell_H y)\right\} \tag{B-7b}$$

where $m(k_H,\ell_H) = \left\{n^2(k_H^2 + \ell_H^2)/k_H^2 - (k_H^2 + \ell_H^2)\right\}^{1/2}$ from Eq.(6).

After taking the appropriate real parts, one obtains

$$\eta(x,y,z') = \begin{cases} h\ \cos\left\{m(k_H,\ell_H)z' + k_H x\right\} \cdot \cos(\ell_H y) & \text{for } n \geq k_H \\ k\ \exp\left\{-\left|m(k_H,\ell_H)z'\right|\right\} \cdot \cos(k_H x) \cdot \cos(\ell_H y) & \text{for } 0 \leq n \leq k_H \end{cases} \tag{B-7c}$$

The two solutions given by (B-7c) are equivalent for $n=k_H$ and correspond to reasonant driving of the entire fluid in a z-independent (i.e., as m=0) mode.

Coordinate Space Approach

The simplicity of Eq.(8) seems to suggest that this may be the simpler

route, but that does not turn out to be the case. First, it is necessary to consider the hill shape function in the convolution form

$$h(x-x',\ y-y') = h\cos\left\{k_H(x-x')\right\}\cdot\cos\left\{\ell_H(y-y')\right\}; \qquad \text{(B-8)}$$

however, noting that

$$\cos\left\{k_H(x-x')\right\} = \cos(k_H x)\cdot\cos(k_H x') + \sin(k_H x)\cdot\sin(k_H x'),$$

and that integration from $x' = -\infty$ to $+\infty$ will kill off terms odd in x' (assuming that the Green's function is purely even in x'), one obtains

$$\eta(x,y,z) = -I_z \qquad \text{(B-9a)}$$

with

$$I = \mathrm{Re}\cdot\frac{h}{2\pi}\cdot\cos(k_H x)\cdot\cos(\ell_H y)\cdot \qquad \text{(B-9b)}$$

$$2\int_0^\infty dy'\cos(\ell_H y')\cdot 2\int_0^\infty dx'\cos(k_H x')\ G(x',y',z')$$

Before proceeding further, a candidate Green's function is required. Using the exact solution expressed by Eq.(10b) and noting that (e.g. see Gradshteyn and Ryzhik, 1965, pg. 472)

$$\int_0^\infty dx\cos(k_H x')\frac{\cos\left[p\sqrt{x'^2+d^2}\right]}{\sqrt{x'+d^2}} = -\frac{\pi}{2}\ Y_o\left[d\sqrt{p^2-k_H^2}\ \right]$$

$$\text{for } 0 < k_H < p,$$

where $p = nz'/d$ and $d^2 = y'^2 + z'^2$,
one obtains,

$$I = -\mathrm{Re}\ h(x,y)\int_0^\infty dy'\cos(\ell_H y')\ Y_o\left[\sqrt{n^2z'^2-k_H^2d^2}\ \right]. \qquad \text{(B-10a)}$$

Rewriting the argument of the Y_o Bessel function as $k_H\sqrt{z'^2(n^2-k_H^2)/k_H^2 - y'^2}$ and referring to the above cited reference (pg. 737, involving the Hankel function $H_o^{(1)}$), one finally obtains

$$I = -\mathrm{Re}\ h(x,y) \cdot \sin\left\{z'\left[n^2-k_H^2\right]^{1/2}\left[k_H^2+\ell_H^2\right]^{1/2}/k_H\right\}\left[k_H^2+\ell_H^2\right]^{1/2} \quad \text{(B-10b)}$$

Inspection of the argument of the sin() shows that it is just $m(k_H,\ell_H)z'$ as expected from comparison with Eq.(B-7c), but computation of $\eta = -I_z$ yields

$$\eta(x,y,z) = h(x,y) \cdot \cos\left\{m\left[k_H,\ell_H\right]z'\right\} \cdot m\left[k_H,\ell_H\right]/\left[k_H^2+\ell_H^2\right]^{1/2} . \quad \text{(B-11)}$$

Eq.(B-11) exhibits two departures from Eq.(B-7c):

- the $k_H x$ term is separated from the $m(k_H,\ell_H)z'$ term, and
- the presence of a multiplicative term

$$m\left[k_H,\ell_H\right]/\left[k_H^2+\ell_H^2\right]^{1/2} = \left[\frac{n^2}{k_H^2}-1\right]^{1/2} .$$

The first of these problems is minor and could be justifiably corrected by keeping the x-portion of the hill shape function in complex form and taking the real part at the end. The second problem is fatal, however, and tells us that the solution given by Eq.(10b) cannot be the particular solution that is needed.

Repeating the above steps for the trial Green's function

$$G(x',y',z') = \cos(n'R)/R \quad \text{(B-12)}$$

with $n' \equiv n\left[1+\ell_H^2/k_H^2\right]^{1/2}$

does lead to the desired result given by Eq.(B-7c); however, it is not legitimate that the Green's function contain characteristics of the hill function (i.e., a factor such as $\left[1+\ell_H^2/k_H^2\right]^{1/2}$). In addition, Eq.(B-12) is not a solution of the basic PDE given by Eq.(3); nevertheless, it is a solution of Eq.(16a), does provide the solution for the infinite field of cosine hills, and has other uses as one reduces the number of dimensions under consideration.

APPENDIX B
EVALUATION RESULTS FOR CONCENTRATIONS PAIRED IN TIME, UNPAIRED IN SPACE

APPENDIX B

EVALUATION RESULTS FOR CONCENTRATIONS PAIRED IN TIME, UNPAIRED IN SPACE

Evaluation statistics for data subsets paired in time, not in space, are presented in tabular form in this appendix. A guide to the tables is given below. The statistical tests and their results are discussed further in Section 4.

Table #	Description
B-1	Evaluation results for SF_6 at CCB
B-2	Evaluation results for CF_3Br at CCB
B-3	Evaluation results for SF_6 at HBR
B-4	Evaluation results for CF_3Br at HBR
B-5	Evaluation results for SF_6 at FSPS
B-6	Evaluation results for CF_3Br at FSPS
B-7	Evaluation results for SO_2 at Westvaco, 1-hour averages
B-8	Evaluation results for SO_2 at Westvaco, 3-hour averages
B-9	Evaluation results for SO_2 at Widows Creek, 1-hour averages
B-10	Evaluation results for SO_2 at Widows Creek, 3-hour averages

For the CTMD (tracer) sites, the average of the top 5 concentrations is considered as well as the peak hourly value to provide a larger sample size. In nearly all cases, all of the top 5 values represent significant plume impacts.

TABLE B-1

EVALUATION STATISTICS FOR DATA SUBSET PAIRED IN TIME

1-HOUR AVERAGES TRACER: SF6 SITE: CINDER CONE BUTTE

(Concentrations* given in units of microseconds per cubic meter.)

	# HOURS	$\overline{OBS}$	$\overline{PRE}$	$\overline{PRE}/\overline{OBS}$	RMS	$V/\bar{C}o2$	$V/(\bar{C}o\bar{C}p)$	% CASES: 0.5 < PRE/OBS < 2.0
HIGHEST 1-HOUR VALUES:								
CTDM, SEVERAL TOWER LEVELS	100	28.0	26.2	0.94	28.7	1.05	1.12	37
TWO TOWER LEVELS	100	28.0	12.2	0.44	36.9	1.74	4.00	21
ONE TOWER LEVEL	100	28.0	6.6	0.24	37.5	1.80	7.66	17
COMPLEX I	100	28.0	42.2	1.51	45.6	2.65	1.76	38
RTDM (DEFAULT)	100	28.0	36.4	1.30	58.3	4.35	3.35	27
RTDM (ONSITE)	100	28.0	21.5	0.77	26.1	0.87	1.13	38
AVERAGE OF THE TOP 5 VALUES FROM EACH HOUR:								
CTDM, SEVERAL TOWER LEVELS	100	18.4	19.5	1.06	21.4	1.36	1.28	38
TWO TOWER LEVELS	100	18.4	8.5	0.46	24.9	1.83	3.96	19
ONE TOWER LEVEL	100	18.4	5.2	0.28	25.0	1.84	6.49	16
COMPLEX I	100	18.4	33.3	1.81	38.0	4.27	2.36	39
RTDM (DEFAULT)	100	18.4	25.1	1.37	34.1	3.45	2.53	28
RTDM (ONSITE)	100	18.4	15.8	0.86	17.6	0.92	1.07	36

* Threshold for both observed and predicted concentrations = .00 uS/M**3

TABLE B-2

EVALUATION STATISTICS FOR DATA SUBSET PAIRED IN TIME

1-HOUR AVERAGES TRACER: CF3BR SITE: CINDER CONE BUTTE

(Concentrations* given in units of microseconds per cubic meter.)

	# HOURS	$\overline{OBS}$	$\overline{PRE}$	$\overline{PRE}/\overline{OBS}$	RMS	$V/\bar{C}o2$	$V/(\bar{C}o\bar{C}p)$	% CASES: 0.5 < PRE/OBS < 2.0
HIGHEST 1-HOUR VALUES:								
CTDM, SEVERAL TOWER LEVELS	44	15.0	21.0	1.40	29.2	3.79	2.71	23
TWO TOWER LEVELS	44	15.0	7.5	0.50	19.9	1.76	3.52	14
ONE TOWER LEVEL	44	15.0	4.6	0.30	20.9	1.95	6.39	34
COMPLEX I	50	15.1	24.5	1.62	28.7	3.59	2.22	46
RTDM (DEFAULT)	44	15.0	11.0	0.74	24.3	2.62	3.56	50
RTDM (ONSITE)	44	15.0	13.7	0.91	19.3	1.65	1.80	32
AVERAGE OF THE TOP 5 VALUES FROM EACH HOUR:								
CTDM, SEVERAL TOWER LEVELS	44	8.0	13.8	1.72	20.0	6.19	3.60	16
TWO TOWER LEVELS	44	8.0	4.9	0.62	12.8	2.54	4.12	14
ONE TOWER LEVEL	44	8.0	2.7	0.34	12.6	2.46	7.20	30
COMPLEX I	50	8.4	19.5	2.32	23.4	7.84	3.38	28
RTDM (DEFAULT)	44	8.0	8.7	1.09	17.6	4.79	4.42	45
RTDM (ONSITE)	44	8.0	9.0	1.12	11.9	2.20	1.97	36

* Threshold for both observed and predicted concentrations = .00 uS/M**3

TABLE B-3

EVALUATION STATISTICS FOR DATA SUBSET PAIRED IN TIME

1-HOUR AVERAGES TRACER: SF6 SITE: HOGBACK RIDGE

(Concentrations* given in units of microseconds per cubic meter.)

	# HOURS	$\overline{OBS}$	$\overline{PRE}$	$\overline{PRE}/\overline{OBS}$	RMS	$V/\bar{C}o2$	$V/(\bar{C}o\bar{C}p)$	% CASES: 0.5 < PRE/OBS < 2.0
HIGHEST 1-HOUR VALUES:								
CTDM, SEVERAL TOWER LEVELS	59	23.5	47.8	2.04	58.3	6.16	3.03	37
TWO TOWER LEVELS	59	23.5	30.1	1.28	44.3	3.55	2.77	29
ONE TOWER LEVEL	59	23.5	10.8	0.46	29.4	1.57	3.41	17
COMPLEX I	60	23.8	117.5	4.94	125.1	27.61	5.59	2
RTDM (DEFAULT)	59	23.5	74.7	3.18	159.9	46.35	14.58	14
RTDM (ONSITE)	59	23.5	32.6	1.39	69.3	8.72	6.28	54
AVERAGE OF THE TOP 5 VALUES FROM EACH HOUR:								
CTDM, SEVERAL TOWER LEVELS	59	18.3	36.4	1.99	37.6	4.22	2.12	25
TWO TOWER LEVELS	59	18.3	22.6	1.23	29.6	2.60	2.11	27
ONE TOWER LEVEL	59	18.3	9.0	0.49	23.7	1.67	3.40	14
COMPLEX I	60	18.6	101.6	5.47	109.5	34.68	6.34	2
RTDM (DEFAULT)	59	18.3	46.6	2.54	77.0	17.66	6.94	15
RTDM (ONSITE)	59	18.3	22.3	1.22	31.7	3.00	2.46	54

* Threshold for both observed and predicted concentrations = .00 uS/M**3

TABLE B-4

EVALUATION STATISTICS FOR DATA SUBSET PAIRED IN TIME

1-HOUR AVERAGES TRACER: CF3BR SITE: HOGBACK RIDGE

(Concentrations* given in units of microseconds per cubic meter.)

	# HOURS	$\overline{OBS}$	$\overline{PRE}$	$\overline{PRE}/\overline{OBS}$	RMS	V/$\overline{Co}$2	V/($\overline{Co}\overline{Cp}$)	% CASES: 0.5 < PRE/OBS < 2.0
HIGHEST 1-HOUR VALUES:								
CTDM, SEVERAL TOWER LEVELS	42	92.0	49.1	0.53	93.1	1.02	1.92	57
TWO TOWER LEVELS	24	118.2	47.3	0.40	144.7	1.50	3.75	38
ONE TOWER LEVEL	13	91.6	58.5	0.64	101.9	1.24	1.94	38
COMPLEX I	40	111.3	173.7	1.56	125.6	1.27	0.82	40
RTDM (DEFAULT)	38	110.6	444.1	4.02	678.3	37.63	9.37	13
RTDM (ONSITE)	61	102.3	142.2	1.39	572.3	31.33	22.52	25
AVERAGE OF THE TOP 5 VALUES FROM EACH HOUR:								
CTDM, SEVERAL TOWER LEVELS	42	59.9	40.2	0.67	48.5	0.65	0.98	50
TWO TOWER LEVELS	24	75.1	39.8	0.53	77.4	1.06	2.01	38
ONE TOWER LEVEL	13	58.0	51.7	0.89	52.2	0.81	0.91	62
COMPLEX I	40	73.0	151.0	2.07	112.3	2.37	1.14	40
RTDM (DEFAULT)	37	67.7	179.7	2.65	218.9	10.45	3.94	3
RTDM (ONSITE)	61	63.7	52.9	0.83	145.1	5.18	6.24	20

* Threshold for both observed and predicted concentrations = .01 uS/M**3

TABLE B-5

EVALUATION STATISTICS FOR DATA SUBSET PAIRED IN TIME

1-HOUR AVERAGES TRACER: SF6 SITE: TRACY POWER PLANT

(Concentrations* given in units of microseconds per cubic meter.)

	# HOURS	$\overline{OBS}$	$\overline{PRE}$	$\overline{PRE}/\overline{OBS}$	RMS	$V/\bar{C}o2$	$V/(\bar{C}o\bar{C}p)$	% CASES: 0.5 < PRE/OBS < 2.0
HIGHEST 1-HOUR VALUES:								
CTDM, SEVERAL TOWER LEVELS	110	1.96	1.94	0.99	2.11	1.16	1.17	61
(ALT. PLUME HT 1)**	110	1.96	1.92	0.98	1.84	0.88	0.90	68
(ALT. PLUME HT 2)**	110	1.96	1.77	0.90	1.88	0.92	1.02	69
TWO TOWER LEVELS	109	1.94	2.07	1.07	2.24	1.33	1.25	49
ONE TOWER LEVEL	105	1.94	2.41	1.24	3.08	2.52	2.03	38
COMPLEX I	111	1.95	6.14	3.15	7.27	13.90	4.41	19
RTDM (DEFAULT)	111	1.95	3.05	1.56	3.38	3.00	1.92	48
RTDM (ONSITE)	110	1.96	1.18	0.60	2.22	1.28	2.13	34
AVERAGE OF THE TOP 5 VALUES FROM EACH HOUR:								
CTDM, SEVERAL TOWER LEVELS	110	1.29	1.36	1.05	1.15	0.80	0.75	55
TWO TOWER LEVELS	109	1.28	1.36	1.06	1.33	1.08	1.02	49
ONE TOWER LEVEL	105	1.27	1.36	1.07	1.95	2.36	2.20	37
COMPLEX I	111	1.28	4.14	3.23	4.83	14.24	4.40	16
RTDM (DEFAULT)	111	1.28	1.87	1.46	1.86	2.11	1.45	44
RTDM (ONSITE)	110	1.29	0.76	0.59	1.33	1.06	1.80	37

* Threshold for both observed and predicted concentrations = .00 uS/M**3

** Alternative plume height #1 was obtained from lidar measurements at the first cross section downwind from the source. Plume height #2 was obtained from the second lidar cross section.

TABLE B-6

EVALUATION STATISTICS FOR DATA SUBSET PAIRED IN TIME

1-HOUR AVERAGES TRACER: CF3BR SITE: TRACY POWER PLANT

(Concentrations* given in units of microseconds per cubic meter.)

	# HOURS	$\overline{OBS}$	$\overline{PRE}$	$\overline{PRE}/\overline{OBS}$	RMS	$V/\overline{Co}2$	$V/(\overline{Co}\overline{Cp})$	% CASES: 0.5 < PRE/OBS < 2.0
HIGHEST 1-HOUR VALUES:								
CTDM, SEVERAL TOWER LEVELS	110	2.84	2.46	0.87	2.94	1.07	1.24	60
TWO TOWER LEVELS	109	2.84	3.02	1.06	4.01	1.99	1.88	53
ONE TOWER LEVEL	105	2.84	3.04	1.07	4.99	3.09	2.88	31
COMPLEX I	111	2.84	8.54	3.01	9.14	10.36	3.44	23
RTDM (DEFAULT)	111	2.84	3.76	1.32	4.79	2.85	2.15	43
RTDM (ONSITE)	110	2.84	1.95	0.69	3.17	1.25	1.82	52
AVERAGE OF THE TOP 5 VALUES FROM EACH HOUR:								
CTDM, SEVERAL TOWER LEVELS	110	1.74	1.30	0.75	1.45	0.69	0.93	66
TWO TOWER LEVELS	109	1.73	1.24	0.72	1.54	0.79	1.11	57
ONE TOWER LEVEL	105	1.73	1.02	0.59	2.04	1.39	2.36	32
COMPLEX I	111	1.73	5.27	3.05	5.55	10.29	3.38	30
RTDM (DEFAULT)	111	1.73	1.74	1.01	1.83	1.12	1.11	46
RTDM (ONSITE)	110	1.74	1.15	0.66	1.55	0.79	1.20	57

Threshold for both observed and predicted concentrations = .00 uS/M**3

TABLE B-7

EVALUATION STATISTICS FOR DATA SUBSET PAIRED IN TIME

1-HOUR AVERAGES TRACER: SO2 SITE: WESTVACO LUKE

(Concentrations* given in units of microseconds per cubic meter.)

	# HOURS	$\overline{OBS}$	$\overline{PRE}$	$\overline{PRE}/\overline{OBS}$	RMS	$V/\bar{C}o2$	$V/(\bar{C}o\bar{C}p)$	% CASES: 0.5 < PRE/OBS < 2.0
HIGHEST 1-HOUR VALUES:								
CTDM, SEVERAL TOWER LEVELS	4687	0.33	0.29	0.88	0.83	6.3	7.2	14
TWO TOWER LEVELS	4702	0.33	1.60	4.85	3.30	100.0	20.6	19
ONE TOWER LEVEL	4022	0.34	1.70	5.00	2.00	34.6	6.9	15
COMPLEX I	4687	0.33	4.12	12.48	9.44	818.3	65.5	14
RTDM (DEFAULT)	4687	0.33	0.98	2.97	2.46	55.6	18.7	16
RTDM (ONSITE)	4687	0.33	0.21	0.64	0.82	6.2	9.7	15

* Threshold for both observed and predicted concentrations = .00 uS/M**3

TABLE B-8

EVALUATION STATISTICS FOR DATA SUBSET PAIRED IN TIME

3-HOUR AVERAGES TRACER: SO2 SITE: WESTVACO LUKE

(Concentrations* given in units of microseconds per cubic meter.)

	# HOURS	$\overline{OBS}$	$\overline{PRE}$	$\overline{PRE}/\overline{OBS}$	RMS	$V/\bar{C}o2$	$V/(\bar{C}o\bar{C}p)$	% CASES: 0.5 < PRE/OBS < 2.0
HIGHEST 3-HOUR VALUES:								
CTDM, SEVERAL TOWER LEVELS	1318	0.30	0.27	0.90	0.62	4.3	4.7	17
TWO TOWER LEVELS	1322	0.30	1.57	5.23	2.89	92.8	17.7	18
ONE TOWER LEVEL	1136	0.32	1.65	5.16	1.82	32.3	6.3	12
COMPLEX I	1318	0.30	3.98	13.27	7.96	704.0	53.1	9
RTDM (DEFAULT)	1318	0.30	0.95	3.17	2.03	45.8	14.5	11
RTDM (ONSITE)	1318	0.30	0.21	0.70	0.64	4.6	6.5	18

---

* Threshold for both observed and predicted concentrations = .00 uS/M**3

TABLE B-9

EVALUATION STATISTICS FOR DATA SUBSET PAIRED IN TIME

1-HOUR AVERAGES, 1980 TRACER: SO2 SITE: WIDOWS CREEK

(Concentrations* given in units of micrograms per cubic meter.)

	# HOURS	$\overline{OBS}$	$\overline{PRE}$	$\overline{PRE}/\overline{OBS}$	RMS	$V/\overline{Co}2$	$V/(\overline{Co}\overline{Cp})$	% CASES: 0.5 < PRE/OBS < 2.0
HIGHEST 1-HOUR VALUES:								
CTDM, SEVERAL TOWER LEVELS	4942	71.9	142	1.97	404	31.5	16.0	23
TWO TOWER LEVELS	4809	70.8	152	2.15	576	66.1	30.8	12
ONE TOWER LEVEL	4131	70.3	390	5.55	767	118.9	21.4	16
COMPLEX I	5065	71.1	413	5.80	1239	303.4	52.3	13
RTDM (DEFAULT)	5065	71.1	322	4.53	765	115.5	25.5	7
RTDM (ONSITE)	5065	71.1	48	0.67	299	17.6	26.3	15

---

* Threshold for both observed and predicted concentrations = .00 uG/M**3

TABLE B-10

EVALUATION STATISTICS FOR DATA SUBSET PAIRED IN TIME

3-HOUR AVERAGES, 1980 TRACER: SO2 SITE: WIDOWS CREEK

(Concentrations* given in units of micrograms per cubic meter.)

	# HOURS	$\overline{OBS}$	$\overline{PRE}$	$\overline{PRE}/\overline{OBS}$	RMS	$V/\bar{C}o2$	$V/(\bar{C}o\bar{C}p)$	% CASES: 0.5 < PRE/OBS < 2.0
HIGHEST 3-HOUR VALUES:								
CTDM, SEVERAL TOWER LEVELS	1370	66.4	112.	1.69	230.	12.0	7.1	31
TWO TOWER LEVELS	1321	65.4	127.	1.94	323.	24.4	12.6	17
ONE TOWER LEVEL	1089	64.3	342.	5.33	579.	81.2	15.2	20
COMPLEX I	1423	65.4	349.	5.34	828.	160.3	30.0	15
RTDM (DEFAULT)	1423	65.4	279.	4.26	521.	63.6	14.9	9
RTDM (ONSITE)	1423	65.4	41.	0.63	169.	6.7	10.6	20

* Threshold for both observed and predicted concentrations = .00 uS/M**3

APPENDIX C
EVALUATION RESULTS FOR CONCENTRATIONS PAIRED IN SPACE, UNPAIRED IN TIME

APPENDIX C

EVALUATION RESULTS FOR CONCENTRATIONS PAIRED IN SPACE, UNPAIRED IN TIME

Statistics for the evaluation data subset paired in space, not in time are presented here. These tests and their results are discussed in more detail in Section 4. A guide to the tables in this appendix is given below.

Table #	Description
C-1	Evaluation results for SF_6 at CCB
C-2	Evaluation results for CF_3Br at CCB
C-3	Evaluation results for SF_6 at HBR
C-4	Evaluation results for CF_3Br at HBR
C-5	Evaluation results for SF_6 at FSPS
C-6	Evaluation results for CF_3Br at FSPS
C-7	Evaluation results for SO_2 at Westvaco, 1-hour averages
C-8	Evaluation results for SO_2 at Westvaco, 3-hour averages
C-9	Evaluation results for SO_2 at Widows Creek, 1-hour averages
C-10	Evaluation results for SO_2 at Widows Creek, 3-hour averages

The number of monitoring sites in the evaluation sample are listed in each table. The average over the top 5 events for the tracer sites and the top 10 events at the SO_2 sites were computed to provide a larger evaluation sample then just the highest concentration event at each receptor.

TABLE C-1

EVALUATION STATISTICS FOR DATA SUBSET PAIRED IN SPACE

1-HOUR AVERAGES TRACER: SF6 SITE: CINDER CONE BUTTE

(Concentrations* given in units of microseconds per cubic meter.)

	# SITES	$\overline{OBS}$	$\overline{PRE}$	$\overline{PRE}/\overline{OBS}$	RMS	$V/\bar{C}o2$	$V/(\bar{C}o\bar{C}p)$	% CASES: 0.5 < PRE/OBS < 2.0
AVERAGE OF HIGHEST VALUES FOR EACH MONITOR:								
CTDM, SEVERAL TOWER LEVELS	93	46.37	51.08	1.10	37.11	0.64	0.58	67
TWO TOWER LEVELS	93	46.37	30.47	0.66	29.92	0.42	0.63	65
ONE TOWER LEVEL	93	46.37	19.03	0.41	39.18	0.71	1.74	33
COMPLEX I	93	46.37	84.34	1.82	51.80	1.25	0.69	51
RTDM (DEFAULT)	93	46.37	77.37	1.67	56.03	1.46	0.88	56
RTDM (ONSITE)	93	46.37	36.87	0.80	27.54	0.35	0.44	72
AVERAGE OF THE TOP 5 VALUES OBTAINED FOR EACH MONITOR:								
CTDM, SEVERAL TOWER LEVELS	93	27.26	28.52	1.05	17.68	0.42	0.40	71
TWO TOWER LEVELS	93	27.26	14.42	0.53	18.65	0.47	0.89	57
ONE TOWER LEVEL	93	27.26	9.58	0.35	23.39	0.74	2.10	23
COMPLEX I	93	27.26	55.36	2.03	35.59	1.71	0.84	39
RTDM (DEFAULT)	93	27.26	43.23	1.59	31.22	1.31	0.83	67
RTDM (ONSITE)	93	27.26	21.20	0.78	13.38	0.24	0.31	76

Threshold for both observed and predicted concentrations = .00 uS/M**3

TABLE C-2

EVALUATION STATISTICS FOR DATA SUBSET PAIRED IN SPACE

1-HOUR AVERAGES TRACER: CF3BR SITE: CINDER CONE BUTTE

(Concentrations* given in units of microseconds per cubic meter.)

	# SITES	$\overline{OBS}$	$\overline{PRE}$	$\overline{PRE}/\overline{OBS}$	RMS	$V/\bar{C}o2$	$V/(\bar{C}o\bar{C}p)$	% CASES: 0.5 < PRE/OBS < 2.0
AVERAGE OF HIGHEST VALUES FOR EACH MONITOR:								
CTDM, SEVERAL TOWER LEVELS	80	15.18	27.03	1.78	29.50	3.78	2.12	25
TWO TOWER LEVELS	80	15.18	11.65	0.77	17.89	1.39	1.81	33
ONE TOWER LEVEL	80	15.18	7.13	0.47	18.31	1.46	3.10	24
COMPLEX I	81	15.59	35.02	2.25	36.24	5.40	2.41	32
RTDM (DEFAULT)	80	15.18	18.69	1.23	27.86	3.37	2.74	34
RTDM (ONSITE)	80	15.18	14.74	0.97	19.37	1.63	1.68	36
AVERAGE OF THE TOP 5 VALUES OBTAINED FOR EACH MONITOR:								
CTDM, SEVERAL TOWER LEVELS	93	4.53	8.50	1.88	10.43	5.30	2.83	34
TWO TOWER LEVELS	93	4.53	3.31	0.73	5.68	1.57	2.15	45
ONE TOWER LEVEL	93	4.53	1.78	0.39	6.05	1.78	4.54	34
COMPLEX I	93	5.18	13.12	2.53	13.04	6.34	2.50	34
RTDM (DEFAULT)	93	4.53	5.41	1.19	7.36	2.64	2.21	46
RTDM (ONSITE)	93	4.53	5.09	1.12	6.35	1.97	1.75	47

* Threshold for both observed and predicted concentrations = .00 uS/M**3

TABLE C-3

EVALUATION STATISTICS FOR DATA SUBSET PAIRED IN SPACE

1-HOUR AVERAGES TRACER: SF6 SITE: HOGBACK RIDGE

(Concentrations* given in units of microseconds per cubic meter.)

	# SITES	$\overline{OBS}$	$\overline{PRE}$	$\overline{PRE}/\overline{OBS}$	RMS	$V/\bar{C}o2$	$V/(\bar{C}o\bar{C}p)$	% CASES: 0.5 < PRE/OBS < 2.0
AVERAGE OF HIGHEST VALUES FOR EACH MONITOR:								
CTDM, SEVERAL TOWER LEVELS	106	35.86	61.65	1.72	62.77	3.06	1.78	58
TWO TOWER LEVELS	106	35.86	49.84	1.39	41.19	1.32	0.95	67
ONE TOWER LEVEL	106	35.86	32.17	0.90	25.52	0.51	0.57	61
COMPLEX I	106	36.04	127.85	3.55	132.13	13.44	3.79	14
RTDM (DEFAULT)	106	35.86	111.08	3.10	157.67	19.33	6.24	32
RTDM (ONSITE)	106	35.86	36.13	1.01	57.68	2.59	2.57	43
AVERAGE OF THE TOP 5 VALUES OBTAINED FOR EACH MONITOR:								
CTDM, SEVERAL TOWER LEVELS	106	22.17	36.22	1.63	28.64	1.67	1.02	61
TWO TOWER LEVELS	106	22.17	29.10	1.31	21.83	0.97	0.74	59
ONE TOWER LEVEL	106	22.17	15.75	0.71	16.34	0.54	0.77	53
COMPLEX I	106	22.44	79.19	3.53	82.59	13.55	3.84	9
RTDM (DEFAULT)	106	22.17	40.01	1.81	46.29	4.36	2.42	36
RTDM (ONSITE)	106	22.17	19.09	0.86	17.26	0.61	0.70	53

Threshold for both observed and predicted concentrations = .00 uS/M**3

TABLE C-4

EVALUATION STATISTICS FOR DATA SUBSET PAIRED IN SPACE

1-HOUR AVERAGES TRACER: CF3BR SITE: HOGBACK RIDGE

(Concentrations* given in units of microseconds per cubic meter.)

	# SITES	$\overline{OBS}$	$\overline{PRE}$	$\overline{PRE}/\overline{OBS}$	RMS	$V/\overline{Co}2$	$V/(\overline{Co}\overline{Cp})$	% CASES: 0.5 < PRE/OBS < 2.0
AVERAGE OF HIGHEST VALUES FOR EACH MONITOR:								
CTDM, SEVERAL TOWER LEVELS	106	122.9	43.4	0.35	104.6	0.72	2.05	14
TWO TOWER LEVELS	106	122.9	39.0	0.32	111.2	0.82	2.58	22
ONE TOWER LEVEL	105	121.4	28.8	0.24	114.0	0.88	3.72	15
COMPLEX I	106	122.9	190.6	1.55	118.1	0.92	0.60	41
RTDM (DEFAULT)	104	123.9	271.1	2.19	381.4	9.48	4.33	32
RTDM (ONSITE)	106	122.9	120.8	0.98	400.7	10.63	10.82	19
AVERAGE OF THE TOP 5 VALUES OBTAINED FOR EACH MONITOR:								
CTDM, SEVERAL TOWER LEVELS	106	73.2	27.7	0.38	55.82	0.58	1.54	19
TWO TOWER LEVELS	106	73.2	21.9	0.30	62.79	0.74	2.46	12
ONE TOWER LEVEL	105	72.8	14.9	0.21	68.22	0.88	4.28	11
COMPLEX I	106	73.2	123.3	1.68	85.32	1.36	0.81	38
RTDM (DEFAULT)	102	74.6	91.4	1.23	114.05	2.34	1.91	49
RTDM (ONSITE)	106	73.2	38.6	0.53	98.73	1.82	3.45	25

---

* Threshold for both observed and predicted concentrations = .01 uS/M**3

TABLE C-5

EVALUATION STATISTICS FOR DATA SUBSET PAIRED IN SPACE

1-HOUR AVERAGES TRACER: SF6 SITE: TRACY POWER PLANT

(Concentrations* given in units of microseconds per cubic meter.)

	# SITES	$\overline{OBS}$	$\overline{PRE}$	$\overline{PRE}/\overline{OBS}$	RMS	$V/\bar{C}o2$	$V/(\bar{C}o\bar{C}p)$	% CASES: 0.5 < PRE/OBS < 2.0
AVERAGE OF HIGHEST VALUES FOR EACH MONITOR:								
CTDM, SEVERAL TOWER LEVELS	106	2.19	1.80	0.82	2.25	1.06	1.28	40
(ALT. PLUME HT 1)*	106	2.19	1.67	0.76	2.02	1.46	1.12	42
(ALT. PLUME HT 2)*	106	2.19	1.68	0.77	2.09	1.55	1.19	43
TWO TOWER LEVELS	106	2.18	1.72	0.79	2.36	1.17	1.49	37
ONE TOWER LEVEL	106	2.15	2.08	0.97	3.57	2.76	2.85	25
COMPLEX I	106	2.19	5.95	2.72	7.10	10.51	3.87	23
RTDM (DEFAULT)	106	2.19	2.80	1.28	3.50	2.55	2.00	30
RTDM (ONSITE)	106	2.19	1.25	0.57	2.17	0.98	1.72	43
AVERAGE OF THE TOP 5 VALUES OBTAINED FOR EACH MONITOR:								
CTDM, SEVERAL TOWER LEVELS	106	1.32	1.05	0.80	1.04	0.62	0.78	41
TWO TOWER LEVELS	106	1.30	1.03	0.79	1.20	0.85	1.08	36
ONE TOWER LEVEL	106	1.27	1.11	0.87	1.97	2.41	2.75	21
COMPLEX I	106	1.32	4.02	3.05	4.83	13.39	4.40	13
RTDM (DEFAULT)	106	1.32	1.66	1.26	1.89	2.05	1.63	31
RTDM (ONSITE)	106	1.32	0.76	0.58	1.09	0.68	1.18	47

Threshold for both observed and predicted concentrations = .00 uS/M**3

* Alternative plume height #1 was obtained from lidar measurements at the first cross section downwind from the source. Plume height #2 was obtained from the second lidar cross section.

TABLE C-6

EVALUATION STATISTICS FOR DATA SUBSET PAIRED IN SPACE

1-HOUR AVERAGES TRACER: CF3BR SITE: TRACY POWER PLANT

(Concentrations* given in units of microseconds per cubic meter.)

	# SITES	$\overline{OBS}$	$\overline{PRE}$	$\overline{PRE}/\overline{OBS}$	RMS	V/$\overline{Co}$2	V/($\overline{Co}\overline{Cp}$)	% CASES: 0.5 < PRE/OBS < 2.0
AVERAGE OF HIGHEST VALUES FOR EACH MONITOR:								
CTDM, SEVERAL TOWER LEVELS	106	2.70	1.49	0.55	2.93	1.18	2.13	41
TWO TOWER LEVELS	106	2.70	1.64	0.61	4.21	2.43	4.00	32
ONE TOWER LEVEL	106	2.69	1.66	0.62	4.99	3.44	5.58	20
COMPLEX I	106	2.70	6.89	2.55	7.50	7.72	3.02	13
RTDM (DEFAULT)	106	2.70	2.40	0.89	3.47	1.65	1.86	37
RTDM (ONSITE)	106	2.70	1.58	0.59	2.86	1.12	1.92	53
AVERAGE OF THE TOP 5 VALUES OBTAINED FOR EACH MONITOR:								
CTDM, SEVERAL TOWER LEVELS	106	1.57	0.93	0.59	1.34	0.73	1.23	37
TWO TOWER LEVELS	106	1.57	0.89	0.57	1.83	1.36	2.40	25
ONE TOWER LEVEL	106	1.55	0.78	0.50	2.15	1.92	3.82	15
COMPLEX I	106	1.58	4.62	2.92	5.52	12.21	4.17	11
RTDM (DEFAULT)	106	1.58	1.36	0.86	1.99	1.59	1.84	35
RTDM (ONSITE)	106	1.57	1.01	0.64	1.22	0.60	0.94	58

* Threshold for both observed and predicted concentrations = .00 uS/M**3

TABLE C-7

EVALUATION STATISTICS FOR DATA SUBSET PAIRED IN SPACE

1-HOUR AVERAGES TRACER: SO2 SITE: WESTVACO LUKE

(Concentrations* given in units of microseconds per cubic meter.)

	# SITES	$\overline{OBS}$	$\overline{PRE}$	$\overline{PRE}/\overline{OBS}$	RMS	$V/\bar{C}o2$	$V/(\bar{C}o\bar{C}p)$	% CASES: 0.5 < PRE/OBS < 2.0
AVERAGE OF HIGHEST VALUES FOR EACH MONITOR:								
CTDM, SEVERAL TOWER LEVELS	11	4.77	6.48	1.36	2.86	0.36	0.27	64
TWO TOWER LEVELS	11	4.77	10.09	2.12	8.71	3.33	1.58	45
ONE TOWER LEVEL	11	4.61	5.71	1.24	2.03	0.19	0.16	82
COMPLEX I	11	4.77	23.97	5.03	25.26	28.04	5.58	9
RTDM (DEFAULT)	11	4.77	7.44	1.56	4.78	1.00	0.64	45
RTDM (ONSITE)	11	4.77	5.80	1.22	3.16	0.44	0.36	73
AVERAGE OF THE TOP 10 VALUES OBTAINED FOR EACH MONITOR:								
CTDM, SEVERAL TOWER LEVELS	11	3.05	3.97	1.30	1.56	0.26	0.20	73
TWO TOWER LEVELS	11	3.05	7.20	2.36	7.63	6.26	2.65	45
ONE TOWER LEVEL	11	2.95	4.15	1.41	1.97	0.45	0.32	73
COMPLEX I	11	3.05	20.13	6.60	22.51	54.47	8.25	9
RTDM (DEFAULT)	11	3.05	6.04	1.98	4.67	2.34	1.18	55
RTDM (ONSITE)	11	3.05	3.10	1.02	1.17	0.15	0.15	91

* Threshold for both observed and predicted concentrations = .00 uS/M**3

TABLE C-8

EVALUATION STATISTICS FOR DATA SUBSET PAIRED IN SPACE

3-HOUR AVERAGES TRACER: SO2 SITE: WESTVACO LUKE

(Concentrations* given in units of microseconds per cubic meter.)

	# SITES	$\overline{OBS}$	$\overline{PRE}$	$\overline{PRE}/\overline{OBS}$	RMS	$V/\bar{C}o2$	$V/(\bar{C}o\bar{C}p)$	% CASES: 0.5 < PRE/OBS < 2.0
AVERAGE OF HIGHEST VALUES FOR EACH MONITOR:								
CTDM, SEVERAL TOWER LEVELS	11	2.76	3.27	1.19	1.41	0.26	0.22	64
TWO TOWER LEVELS	11	2.76	6.03	2.19	7.19	6.79	3.11	55
ONE TOWER LEVEL	11	2.76	3.34	1.21	1.61	0.34	0.28	73
COMPLEX I	11	2.76	17.38	6.30	19.34	49.10	7.80	0
RTDM (DEFAULT)	11	2.76	5.07	1.84	3.84	1.94	1.05	45
RTDM (ONSITE)	11	2.76	3.09	1.12	1.79	0.42	0.38	73
AVERAGE OF THE TOP 10 VALUES OBTAINED FOR EACH MONITOR:								
CTDM, SEVERAL TOWER LEVELS	11	1.63	1.69	1.04	0.69	0.18	0.17	73
TWO TOWER LEVELS	11	1.63	4.07	2.50	5.18	10.10	4.05	55
ONE TOWER LEVEL	11	1.62	2.57	1.59	1.57	0.94	0.59	65
COMPLEX I	11	1.63	12.17	7.47	14.59	80.12	10.73	0
RTDM (DEFAULT)	11	1.63	3.63	2.23	3.30	4.10	1.84	45
RTDM (ONSITE)	11	1.63	1.48	0.91	0.67	0.17	0.19	82

---

* Threshold for both observed and predicted concentrations = .00 uS/M**3

TABLE C-9

EVALUATION STATISTICS FOR DATA SUBSET PAIRED IN SPACE

1-HOUR AVERAGES, 1980 TRACER: SO2 SITE: WIDOWS CREEK

(Concentrations* given in units of micrograms per cubic meter.)

	# SITES	$\overline{OBS}$	$\overline{PRE}$	$\overline{PRE}/\overline{OBS}$	RMS	$V/\bar{C}o2$	$V/(\bar{C}o\bar{C}p)$	% CASES: 0.5 < PRE/OBS < 2.0
AVERAGE OF HIGHEST VALUES FOR EACH MONITOR:								
CTDM, SEVERAL TOWER LEVELS	14	1695	3720	2.20	2830	2.79	1.27	43
TWO TOWER LEVELS	14	1695	4142	2.44	3577	4.46	1.82	43
ONE TOWER LEVEL	14	1609	2822	1.75	2433	2.29	1.30	43
COMPLEX I	14	1695	4953	2.92	5033	8.82	3.02	36
RTDM (DEFAULT)	14	1695	2189	1.29	1911	1.27	0.98	36
RTDM (ONSITE)	14	1695	3700	2.18	3727	4.84	2.22	43
AVERAGE OF THE TOP 10 VALUES OBTAINED FOR EACH MONITOR:								
CTDM, SEVERAL TOWER LEVELS	14	740	1886	2.55	1548	4.38	1.72	50
TWO TOWER LEVELS	14	724	2456	3.39	2304	10.14	2.99	14
ONE TOWER LEVEL	14	645	2079	3.22	1940	9.04	2.80	14
COMPLEX I	14	740	3919	5.30	4582	38.36	7.24	14
RTDM (DEFAULT)	14	740	1914	2.59	1762	5.67	2.19	36
RTDM (ONSITE)	14	740	994	1.34	748	1.02	0.76	50

* Threshold for both observed and predicted concentrations = .00 uG/M**3

TABLE C-10

EVALUATION STATISTICS FOR DATA SUBSET PAIRED IN SPACE

3-HOUR AVERAGES, 1980 TRACER: SO2 SITE: WIDOWS CREEK

(Concentrations* given in units of micrograms per cubic meter.)

	# SITES	$\overline{OBS}$	$\overline{PRE}$	$\overline{PRE}/\overline{OBS}$	RMS	V/$\overline{Co}$2	V/($\overline{Co}\overline{Cp}$)	% CASES: 0.5 < PRE/OBS < 2.0
AVERAGE OF HIGHEST VALUES FOR EACH MONITOR:								
CTDM, SEVERAL TOWER LEVELS	14	840	1454	1.73	1058	1.59	0.92	50
TWO TOWER LEVELS	14	840	1288	1.53	843	1.01	0.66	43
ONE TOWER LEVEL	14	725	1629	2.25	1409	3.77	1.68	29
COMPLEX I	14	840	2859	3.40	3113	13.74	4.04	36
RTDM (DEFAULT)	14	840	1476	1.76	1296	2.38	1.36	50
RTDM (ONSITE)	14	840	1137	1.35	1239	2.18	1.61	43
AVERAGE OF THE TOP 10 VALUES OBTAINED FOR EACH MONITOR:								
CTDM, SEVERAL TOWER LEVELS	14	324	719	2.22	559	2.98	1.34	57
TWO TOWER LEVELS	14	319	752	2.36	637	3.98	1.69	36
ONE TOWER LEVEL	14	279	1139	4.09	1130	16.48	4.03	7
COMPLEX I	14	325	1755	5.40	2089	41.38	7.66	14
RTDM (DEFAULT)	14	325	1001	3.08	992	9.34	3.03	36
RTDM (ONSITE)	14	325	341	1.05	294	.82	.78	43

* Threshold for both observed and predicted concentrations = .00 uG/M**3

APPENDIX D
EVALUATION RESULTS FOR CONCENTRATIONS PAIRED IN TIME AND SPACE

APPENDIX D

EVALUATION RESULTS FOR CONCENTRATIONS PAIRED IN TIME AND SPACE

Evaluation statistics for data for all hours and monitoring sites - paired in time and space - are given in this appendix. Further discussions can be found in Section 4. A guide to the table showing the results is listed below.

Table #	Description
D-1	Evaluation results for SF_6 at CCB
D-2	Evaluation results for CF_3Br at CCB
D-3	Evaluation results for SF_6 at HBR
D-4	Evaluation results for CF_3Br at HBR
D-5	Evaluation results for SF_6 at FSPS
D-6	Evaluation results for CF_3Br at FSPS
D-7	Evaluation results for SO_2 at Westvaco, 1-hour averages
D-8	Evaluation results for SO_2 at Westvaco, 3-hour averages
D-9	Evaluation results for SO_2 at Widows Creek, 1-hour averages
D-10	Evaluation results for SO_2 at Widows Creek, 3-hour averages

These tables contain results for two concentration thresholds. The zero threshold retains all cases, while the nonzero threshold must be exceeded by both the prediction and the observation to be included in the statistics. The nonzero threshold effectively deletes the uninteresting zero versus zero matchup.

TABLE D-1

EVALUATION STATISTICS FOR DATA SUBSET PAIRED IN TIME AND SPACE

1-HOUR AVERAGES TRACER: SF6 SITE: CINDER CONE BUTTE

(Concentrations given in units of microseconds per cubic meter.)

	# SITE-HOURS	$\overline{OBS}$	$\overline{PRE}$	$\overline{PRE}/\overline{OBS}$	RMS	$V/\bar{C}o2$	$V/(\bar{C}o\bar{C}p)$	% CASES: 0.5 < PRE/OBS < 2.0
DATA FROM ALL PERIODS AND MONITORS:								
1) THRESHOLD = 0.0 uS/M**3								
CTDM, SEVERAL TOWER LEVELS	3683	5.87	5.74	0.98	14.2	5.83	5.96	20
TWO TOWER LEVELS	3683	5.87	2.52	0.45	14.1	5.73	12.74	14
ONE TOWER LEVEL	3683	5.87	1.62	0.28	13.2	5.07	18.38	15
COMPLEX I	3683	5.87	11.96	2.04	23.7	16.26	7.98	25
RTDM (DEFAULT)	3683	5.87	8.60	1.47	21.7	13.65	9.32	25
RTDM (ONSITE)	3683	5.87	4.95	0.84	12.2	4.33	5.13	25
2) THRESHOLD = 0.01 uS/M**3								
CTDM, SEVERAL TOWER LEVELS	2079	9.34	8.99	0.96	17.2	3.38	3.51	30
TWO TOWER LEVELS	1584	9.44	4.89	0.52	16.3	2.99	5.77	19
ONE TOWER LEVEL	1214	9.71	4.19	0.43	15.3	2.49	5.76	19
COMPLEX I	1351	10.83	27.57	2.55	33.5	9.59	3.77	29
RTDM (DEFAULT)	1329	10.42	20.35	1.95	31.1	8.91	4.56	28
RTDM (ONSITE)	2203	8.82	7.05	0.80	14.2	2.59	3.24	29

TABLE D-2

EVALUATION STATISTICS FOR DATA SUBSET PAIRED IN TIME AND SPACE

1-HOUR AVERAGES TRACER: CF3BR SITE: CINDER CONE BUTTE

(Concentrations given in units of microseconds per cubic meter.)

	# SITE-HOURS	$\overline{OBS}$	$\overline{PRE}$	$\overline{PRE}/\overline{OBS}$	RMS	$V/\bar{C}o2$	$V/(\bar{C}o\bar{C}p)$	% CASES: 0.5 < PRE/OBS < 2.0
DATA FROM ALL PERIODS AND MONITORS:								
1) THRESHOLD = 0.0 uS/M**3								
CTDM, SEVERAL TOWER LEVELS	566	3.90	7.39	1.90	16.3	17.49	9.23	9
TWO TOWER LEVELS	566	3.90	2.77	0.71	10.5	7.29	10.26	13
ONE TOWER LEVEL	566	3.90	1.48	0.38	10.0	6.55	17.26	29
COMPLEX I	565	3.90	11.30	2.90	18.9	23.49	8.10	40
RTDM (DEFAULT)	566	3.90	4.87	1.25	13.4	11.84	9.48	42
RTDM (ONSITE)	566	3.90	4.69	1.20	11.2	8.25	6.86	22
2) THRESHOLD = 0.01 uS/M**3								
CTDM, SEVERAL TOWER LEVELS	208	8.79	12.16	1.38	22.1	6.30	4.56	21
TWO TOWER LEVELS	164	9.69	5.36	0.55	15.9	2.71	4.89	18
ONE TOWER LEVEL	123	9.90	3.63	0.37	16.3	2.70	7.37	28
COMPLEX I	221	8.55	18.08	2.12	21.7	6.41	3.03	32
RTDM (DEFAULT)	182	8.51	8.65	1.02	18.9	4.91	4.83	41
RTDM (ONSITE)	225	8.41	6.37	0.76	13.8	2.70	3.56	26

TABLE D-3

EVALUATION STATISTICS FOR DATA SUBSET PAIRED IN TIME AND SPACE

1-HOUR AVERAGES TRACER: SF6 SITE: HOGBACK RIDGE

(Concentrations given in units of microseconds per cubic meter.)

	# SITE-HOURS	$\overline{OBS}$	$\overline{PRE}$	$\overline{PRE}/\overline{OBS}$	RMS	$V/\bar{C}o2$	$V/(\bar{C}o\bar{C}p)$	% CASES: 0.5 < PRE/OBS < 2.0
DATA FROM ALL PERIODS AND MONITORS:								
1) THRESHOLD = 0.0 uS/M**3								
CTDM, SEVERAL TOWER LEVELS	4714	5.19	8.45	1.63	17.9	11.86	7.28	19
TWO TOWER LEVELS	4714	5.19	4.60	0.89	14.8	8.18	9.22	9
ONE TOWER LEVEL	4714	5.19	1.94	0.37	11.8	5.20	13.90	4
COMPLEX I	4792	5.25	12.83	2.44	37.5	50.94	20.84	2
RTDM (DEFAULT)	4714	5.19	4.75	0.92	29.0	31.29	34.19	4
RTDM (ONSITE)	4714	5.19	4.30	0.83	13.2	6.47	7.81	20
2) THRESHOLD = 0.01 uS/M**3								
CTDM, SEVERAL TOWER LEVELS	3271	5.66	12.17	2.15	20.7	13.31	6.19	26
TWO TOWER LEVELS	1823	7.14	11.87	1.66	21.6	9.18	5.52	20
ONE TOWER LEVEL	957	4.62	9.54	2.07	16.4	12.63	6.12	17
COMPLEX I	903	7.64	68.08	8.91	84.3	121.61	13.65	6
RTDM (DEFAULT)	743	7.91	30.13	3.81	70.1	78.56	20.63	18
RTDM (ONSITE)	3162	5.98	6.39	1.07	14.8	6.14	5.75	29

TABLE D-4

EVALUATION STATISTICS FOR DATA SUBSET PAIRED IN TIME AND SPACE

1-HOUR AVERAGES TRACER: CF3BR SITE: HOGBACK RIDGE

(Concentrations given in units of microseconds per cubic meter.)

	# SITE-HOURS	$\overline{OBS}$	$\overline{PRE}$	$\overline{PRE}/\overline{OBS}$	RMS	V/$\bar{C}o2$	V/($\bar{C}o\bar{C}p$)	% CASES: 0.5 < PRE/OBS < 2.0
DATA FROM ALL PERIODS AND MONITORS:								
1) THRESHOLD = 0.0 uS/M**3								
CTDM, SEVERAL TOWER LEVELS	5026	15.31	6.55	0.43	32.1	4.39	10.27	22
TWO TOWER LEVELS	5026	15.31	3.22	0.21	33.0	4.64	22.05	15
ONE TOWER LEVEL	5026	15.31	1.86	0.12	34.7	5.15	42.38	13
COMPLEX I	5175	14.96	14.68	0.98	53.9	13.00	13.25	12
RTDM (DEFAULT)	5175	14.96	9.16	0.61	80.3	28.78	47.00	12
RTDM (ONSITE)	5026	15.31	5.61	0.37	72.7	22.55	61.54	21
2) THRESHOLD = 0.01 uS/M**3								
CTDM, SEVERAL TOWER LEVELS	2729	16.84	11.51	0.68	26.6	2.50	3.66	32
TWO TOWER LEVELS	1366	21.02	11.53	0.55	38.9	3.42	6.24	26
ONE TOWER LEVEL	613	15.96	14.64	0.92	32.2	4.08	4.44	21
COMPLEX I	557	19.29	134.60	6.98	129.8	45.26	6.49	6
RTDM (DEFAULT)	367	17.83	128.44	7.20	274.1	236.36	32.81	12
RTDM (ONSITE)	2333	16.56	11.80	0.71	99.4	36.05	50.59	29

TABLE D-5

EVALUATION STATISTICS FOR DATA SUBSET PAIRED IN TIME AND SPACE

1-HOUR AVERAGES TRACER: SF6 SITE:TRACY POWER PLANT

(Concentrations given in units of microseconds per cubic meter.)

	# SITE-HOURS	$\overline{OBS}$	$\overline{PRE}$	$\overline{PRE}/\overline{OBS}$	RMS	$V/\bar{C}o2$	$V/(\bar{C}o\bar{C}p)$	% CASES: 0.5 < PRE/OBS < 2.0
DATA FROM ALL PERIODS AND MONITORS:								
1) THRESHOLD = 0.0 uS/M**3								
CTDM, SEVERAL TOWER LEVELS	9713	0.19	0.13	0.68	0.59	9.64	14.09	7
(ALT. PLUME HT 1)*	9713	0.19	0.13	0.68	0.58	9.32	13.62	7
(ALT. PLUME HT 2)*	9713	0.19	0.12	0.63	0.58	9.32	14.75	7
TWO TOWER LEVELS	9633	0.19	0.12	0.63	0.61	10.31	16.32	5
ONE TOWER LEVEL	9291	0.19	0.09	0.47	0.75	15.58	32.90	2
COMPLEX I	9806	0.19	0.36	1.89	1.61	71.80	37.90	2
RTDM (DEFAULT)	9806	0.19	0.15	0.79	0.82	18.63	23.59	3
RTDM (ONSITE)	9713	0.19	0.08	0.42	0.53	7.78	18.48	6
2) THRESHOLD = 0.01 uS/M**3								
CTDM, SEVERAL TOWER LEVELS	2366	0.40	0.54	1.35	0.98	6.00	4.45	27
TWO TOWER LEVELS	2010	0.35	0.56	1.60	1.03	8.66	5.41	25
ONE TOWER LEVEL	918	0.33	0.94	2.85	1.89	32.80	11.52	19
COMPLEX I	1309	0.33	2.66	8.06	4.21	162.76	20.19	18
RTDM (DEFAULT)	1126	0.34	1.30	3.82	2.00	34.60	9.05	25
RTDM (ONSITE)	2329	0.37	0.34	0.92	0.76	4.22	4.59	25

* Alternative plume height #1 was obtained from lidar measurements at the first cross section downwind from the source. Plume height #2 was obtained from the second lidar cross section.

TABLE D-6

EVALUATION STATISTICS FOR DATA SUBSET PAIRED IN TIME AND SPACE

1-HOUR AVERAGES TRACER: CF3BR SITE:TRACY POWER PLANT

(Concentrations given in units of microseconds per cubic meter.)

	# SITE-HOURS	$\overline{OBS}$	$\overline{PRE}$	$\overline{PRE}/\overline{OBS}$	RMS	$V/\bar{C}o2$	$V/(\bar{C}o\bar{C}p)$	% CASES: 0.5 < PRE/OBS < 2.0
DATA FROM ALL PERIODS AND MONITORS:								
1) THRESHOLD = 0.0 uS/M**3								
CTDM, SEVERAL TOWER LEVELS	9713	0.28	0.11	0.39	0.72	6.61	16.83	6
TWO TOWER LEVELS	9633	0.27	0.09	0.33	0.82	9.22	27.67	5
ONE TOWER LEVEL	9291	0.27	0.06	0.22	0.89	10.87	48.90	1
COMPLEX I	9806	0.28	0.42	1.50	1.93	47.51	31.67	2
RTDM (DEFAULT)	9806	0.28	0.12	0.43	0.94	11.27	26.30	2
RTDM (ONSITE)	9713	0.28	0.11	0.39	0.70	6.25	15.91	6
2) THRESHOLD = 0.01 uS/M**3								
CTDM, SEVERAL TOWER LEVELS	2067	0.59	0.52	0.88	1.27	4.63	5.26	30
TWO TOWER LEVELS	1524	0.42	0.57	1.36	1.47	12.25	9.03	29
ONE TOWER LEVEL	556	0.48	1.02	2.13	2.62	29.79	14.02	20
COMPLEX I	1256	0.53	3.27	6.17	5.15	94.42	15.30	18
RTDM (DEFAULT)	1036	0.55	1.17	2.13	2.22	I6.29	7.66	23
RTDM (ONSITE)	2269	0.53	0.48	0.91	1.15	4.71	5.20	26

TABLE D-7

EVALUATION STATISTICS FOR DATA SUBSET PAIRED IN TIME AND SPACE

1-HOUR AVERAGES TRACER: SO2 SITE: WESTVACO LUKE

(Concentrations given in units of microseconds per cubic meter.)

	# SITE-HOURS	$\overline{OBS}$	$\overline{PRE}$	$\overline{PRE}/\overline{OBS}$	RMS	$V/\bar{C}o2$	$V/(\bar{C}o\bar{C}p)$	% CASES: 0.5 < PRE/OBS < 2.0
DATA FROM ALL PERIODS AND MONITORS:								
1) THRESHOLD = 0.0 uS/M**3								
CTDM, SEVERAL TOWER LEVELS	46092	0.09	0.05	0.56	0.38	17.8	32.1	40
TWO TOWER LEVELS	46283	0.09	0.24	0.67	1.20	177.8	66.7	38
ONE TOWER LEVEL	39838	0.10	0.32	3.20	0.86	74.0	23.1	32
COMPLEX I	46092	0.09	0.52	5.78	3.34	1377.2	238.4	55
RTDM (DEFAULT)	46092	0.09	0.13	1.44	0.92	104.5	72.3	55
RTDM (ONSITE)	46092	0.09	0.04	0.44	0.36	16.0	36.0	45
2) THRESHOLD = 0.01 uS/M**3								
CTDM, SEVERAL TOWER LEVELS	2865	0.53	0.60	1.13	1.18	5.0	4.4	26
TWO TOWER LEVELS	5119	0.35	1.39	3.97	2.93	70.1	17.6	23
ONE TOWER LEVEL	6796	0.28	1.10	3.93	1.44	26.4	6.7	21
COMPLEX I	1006	0.34	16.94	49.82	18.90	3090.1	62.0	1
RTDM (DEFAULT)	1668	0.36	2.49	6.92	3.86	115.0	16.6	7
RTDM (ONSITE)	3477	0.34	0.35	1.03	0.83	6.0	5.8	26

TABLE D-8

EVALUATION STATISTICS FOR DATA SUBSET PAIRED IN TIME AND SPACE

3-HOUR AVERAGES TRACER: SO2 SITE: WESTVACO LUKE

(Concentrations given in units of microseconds per cubic meter.)

	# SITE-HOURS	$\overline{OBS}$	$\overline{PRE}$	$\overline{PRE}/\overline{OBS}$	RMS	$V/\bar{C}o2$	$V/(\bar{C}o\bar{C}p)$	% CASES: 0.5 < PRE/OBS < 2.0
DATA FROM ALL PERIODS AND MONITORS:								
1) THRESHOLD = 0.0 uS/M**3								
CTDM, SEVERAL TOWER LEVELS	12969	0.09	0.05	0.56	0.28	9.7	17.4	32
TWO TOWER LEVELS	13020	0.09	0.26	2.89	1.05	136.1	47.1	30
ONE TOWER LEVEL	11252	0.10	0.33	3.30	0.78	60.8	18.4	25
COMPLEX I	12969	0.09	0.55	6.11	2.81	974.8	159.5	43
RTDM (DEFAULT)	12969	0.09	0.14	1.56	0.76	71.3	45.8	44
RTDM (ONSITE)	12969	0.09	0.04	0.44	0.30	11.1	25.0	35
2) THRESHOLD = 0.01 uS/M**3								
CTDM, SEVERAL TOWER LEVELS	1344	0.39	0.40	1.03	0.69	3.1	3.1	32
TWO TOWER LEVELS	2231	0.26	1.14	4.39	2.27	76.2	17.4	25
ONE TOWER LEVEL	2753	0.22	0.95	4.32	1.25	32.3	7.5	20
COMPLEX I	597	0.27	10.24	37.93	12.18	2035.0	53.7	2
RTDM (DEFAULT)	765	0.29	1.98	6.83	2.79	92.6	13.6	9
RTDM (ONSITE)	1542	0.27	0.27	1.00	0.59	4.8	4.8	29

TABLE D-9

EVALUATION STATISTICS FOR DATA SUBSET PAIRED IN TIME AND SPACE

1-HOUR AVERAGES, 1980 TRACER: SO2 SITE: WIDOWS CREEK

(Concentrations given in units of micrograms per cubic meter.)

	# SITE-HOURS	$\overline{OBS}$	$\overline{PRE}$	$\overline{PRE}/\overline{OBS}$	RMS	$V/\bar{C}o2$	$V/(\bar{C}o\bar{C}p)$	% CASES: 0.5 < PRE/OBS < 2.0
DATA FROM ALL PERIODS AND MONITORS:								
1) THRESHOLD = 0.0 uS/M**3								
CTDM, SEVERAL TOWER LEVELS	69762	14.76	13.28	0.90	132.8	81.0	90.0	47
TWO TOWER LEVELS	67900	14.71	16.95	1.15	186.8	161.3	140.0	47
ONE TOWER LEVEL	57876	14.97	56.91	3.80	278.0	344.9	90.7	44
COMPLEX I	71736	14.59	35.04	2.40	366.5	631.0	262.8	56
RTDM (DEFAULT)	71736	14.59	26.73	1.83	227.5	243.2	132.7	56
RTDM (ONSITE)	71736	14.59	5.24	0.36	96.5	43.8	121.9	49
2) THRESHOLD = 1.00 uG/M**3								
CTDM, SEVERAL TOWER LEVELS	3682	65.8	142	2.15	358	29.7	13.8	31
TWO TOER LEVELS	2184	50.3	265	5.27	744	219.2	41.6	22
ONE TOWER LEVEL	4144	57.1	414	7.25	753	174.0	24.0	20
COMPLEX I	1886	81.5	786	9.64	1756	463.9	48.1	21
RTDM (DEFAULT)	1330	66.9	742	11.10	1160	300.7	27.1	8
RTDM (ONSITE)	3133	67.5	66	0.97	318	22.1	22.8	25

TABLE D-10

EVALUATION STATISTICS FOR DATA SUBSET PAIRED IN TIME AND SPACE

3-HOUR AVERAGES, 1980 TRACER: SO2 SITE: WIDOWS CREEK

(Concentrations given in units of micrograms per cubic meter.)

	# SITE-HOURS	$\overline{OBS}$	$\overline{PRE}$	$\overline{PRE}/\overline{OBS}$	RMS	$V/\bar{C}o2$	$V/(\bar{C}o\bar{C}p)$	% CASES: 0.5 < PRE/OBS < 2.0
DATA FROM ALL PERIODS AND MONITORS:								
1) THRESHOLD = 0.0 uS/M**3								
CTDM, SEVERAL TOWER LEVELS	18021	15.93	13.51	0.85	93.2	34.2	40.3	37
TWO TOWER LEVELS	17377	15.88	16.15	1.02	112.0	49.8	48.9	34
ONE TOWER LEVEL	14449	15.85	55.52	3.50	218.9	190.8	54.5	33
COMPLEX I	18695	15.71	36.58	2.33	266.4	287.6	123.5	46
RTDM (DEFAULT)	18695	15.71	29.98	1.91	170.7	118.1	61.9	45
RTDM (ONSITE)	18695	15.71	5.42	0.35	67.5	18.4	53.5	38
2) THRESHOLD = 1.00 uG/M**3								
CTDM, SEVERAL TOWER LEVELS	1824	47.9	97	2.02	213	19.8	9.8	30
TWO TOER LEVELS	1370	38.5	136	3.53	305	62.8	17.8	24
ONE TOWER LEVEL	1926	42.3	295	6.97	516	149.1	21.4	20
COMPLEX I	1129	57.5	449	7.82	932	263.0	33.6	19
RTDM (DEFAULT)	927	53.0	402	7.59	619	136.2	18.0	13
RTDM (ONSITE)	1704	51.7	42	0.80	181	12.3	15.3	27

APPENDIX E
EVALUATION RESULTS BY METEOROLOGICAL CATEGORY FOR CONCENTRATIONS PAIRED IN TIME, UNPAIRED IN SPACE

APPENDIX E

EVALUATION RESULTS BY METEOROLOGICAL CATEGORY FOR CONCENTRATIONS PAIRED IN TIME, UNPAIRED IN SPACE

In this appendix, the results presented in Appendix B for concentrations paired in time, not space, are extended to meteorological categories. These categories include three stability classes (D,E,F) and three wind speed categories (0-1, 1-3 and >3 m/sec at release height). More discussion can be found in Section 4. A guide to these tables is listed below. Note that the six model runs (CTDM for several, two and one tower level(s), COMPLEX I, and RTDM (default and on-site) are grouped together for each site and tracer.

Table #	Description
E-1 through E-6	Evaluation results for SF_6 at CCB
E-7 through E-12	Evaluation results for CF_3Br at CCB
E-13 through E-18	Evaluation results for SF_6 at HBR
E-19 thorugh E-24	Evaluation results for CF_3Br at HBR
E-25 through E-30	Evaluation results for SF_6 at FSPS
E-31 through E-36	Evaluation results for CF_3Br at FSPS
E-37 through E-42	Evaluation results for SO_2 at Westvaco, 1-hour averages
E-43 through E-48	Evaluation results for SO_2 at Widows Creek, 1-hour averages

TABLE E-1

EVALUATION STATISTICS FOR DATA SUBSET PAIRED IN TIME
(SUBDIVIDED INTO STABILITY AND WIND SPEED CLASSES)

1-HOUR AVERAGES TRACER: SF6 SITE: CINDER CONE BUTTE

MODEL: CTDM THRESHOLD: .00 uS/M**3

(Concentrations given in units of microseconds per cubic meter.)

HIGHEST 1-HOUR VALUES, UNPAIRED IN SPACE:

	STABILITY D			STABILITY E			STABILITY F		
WIND SPEED(M/S)	0-1	1-3	GT 3	0-1	1-3	GT 3	0-1	1-3	GT 3
# OF DATA PAIRS	0	1	27	3	9	16	2	30	12
MEAN FOR OBS	---	---	21.73	---	13.31	30.31	---	33.58	36.35
MEAN FOR PRE	---	---	11.25	---	14.69	24.17	---	39.72	37.71
BIAS (PRE/OBS)	---	---	.52	---	1.10	.80	---	1.18	1.04
RMS ERROR	---	---	17.51	---	14.93	19.54	---	36.10	39.58
V/Co2	---	---	.65	---	1.26	.42	---	1.16	1.19
V/(CoCp)	---	---	1.26	---	1.14	.52	---	.98	1.14
% WITHIN FACTOR 2	---	---	26.	---	22.	50.	---	47.	42.

AVERAGE OF THE TOP 5 VALUES FROM EACH 1-HOUR PERIOD:

	STABILITY D			STABILITY E			STABILITY F		
WIND SPEED(M/S)	0-1	1-3	GT 3	0-1	1-3	GT 3	0-1	1-3	GT 3
# OF DATA PAIRS	---	---	27	---	9	16	---	30	12
MEAN FOR OBS	---	---	15.05	---	8.18	21.91	---	21.83	23.76
MEAN FOR PRE	---	---	8.02	---	9.48	16.88	---	30.83	28.44
BIAS (PRE/OBS)	---	---	.53	---	1.16	.77	---	1.41	1.20
RMS ERROR	---	---	11.18	---	11.45	14.59	---	28.41	31.00
V/Co2	---	---	.55	---	1.96	.44	---	1.69	1.70
V/(CoCp)	---	---	1.04	---	1.69	.58	---	1.20	1.42
% WITHIN FACTOR 2	---	---	33.	---	11.	50.	---	43.	50.

* Statistics are not presented for cases with less than 6 data pairs

TABLE E-2

EVALUATION STATISTICS FOR DATA SUBSET PAIRED IN TIME
(SUBDIVIDED INTO STABILITY AND WIND SPEED CLASSES)

1-HOUR AVERAGES TRACER: SF6 SITE: CINDER CONE BUTTE

MODEL: CTDM (DEGR1) THRESHOLD: .00 uS/M**3

(Concentrations given in units of microseconds per cubic meter.)

HIGHEST 1-HOUR VALUES, UNPAIRED IN SPACE:

	STABILITY D			STABILITY E			STABILITY F		
WIND SPEED(M/S)	0-1	1-3	GT 3	0-1	1-3	GT 3	0-1	1-3	GT 3
# OF DATA PAIRS	0	1	27	3	9	16	2	30	12
MEAN FOR OBS	---	---	21.73	---	13.31	30.31	---	33.58	36.35
MEAN FOR PRE	---	---	11.43	---	22.78	8.74	---	9.83	19.15
BIAS (PRE/OBS)	---	---	.53	---	1.71	.29	---	.29	.53
RMS ERROR	---	---	17.15	---	38.26	32.48	---	49.83	33.83
V/Co2	---	---	.62	---	8.27	1.15	---	2.20	.87
V/(CoCp)	---	---	1.18	---	4.83	3.98	---	7.52	1.64
% WITHIN FACTOR 2	---	---	33.	---	22.	19.	---	10.	33.

AVERAGE OF THE TOP 5 VALUES FROM EACH 1-HOUR PERIOD:

	STABILITY D			STABILITY E			STABILITY F		
WIND SPEED(M/S)	0-1	1-3	GT 3	0-1	1-3	GT 3	0-1	1-3	GT 3
# OF DATA PAIRS	0	1	27	3	9	16	2	30	12
MEAN FOR OBS	---	---	15.05	---	8.18	21.91	---	21.83	23.76
MEAN FOR PRE	---	---	8.78	---	12.28	5.56	---	7.00	14.50
BIAS (PRE/OBS)	---	---	.58	---	1.50	.25	---	.32	.61
RMS ERROR	---	---	11.21	---	22.87	25.42	---	34.71	22.25
V/Co2	---	---	.55	---	7.83	1.35	---	2.53	.88
V/(CoCp)	---	---	.95	---	5.21	5.30	---	7.89	1.44
% WITHIN FACTOR 2	---	---	30.	---	22.	19.	---	10.	25.

* Statistics are not presented for cases with less than 6 data pairs.

TABLE E-3

EVALUATION STATISTICS FOR DATA SUBSET PAIRED IN TIME
(SUBDIVIDED INTO STABILITY AND WIND SPEED CLASSES)

1-HOUR AVERAGES TRACER: SF6 SITE: CINDER CONE BUTTE

MODEL: CTDM (DEGR2) THRESHOLD: .00 uS/M**3

(Concentrations given in units of microseconds per cubic meter.)

HIGHEST 1-HOUR VALUES, UNPAIRED IN SPACE:

	STABILITY D			STABILITY E			STABILITY F		
WIND SPEED(M/S)	0-1	1-3	GT 3	0-1	1-3	GT 3	0-1	1-3	GT 3
# OF DATA PAIRS	0	1	27	3	9	16	2	30	12
MEAN FOR OBS	---	---	21.73	---	13.31	30.31	---	33.58	36.35
MEAN FOR PRE	---	---	7.09	---	3.16	8.46	---	4.35	10.70
BIAS (PRE/OBS)	---	---	.33	---	.24	.28	---	.13	.29
RMS ERROR	---	---	20.53	---	18.37	35.07	---	51.08	39.00
V/Co2	---	---	.89	---	1.90	1.34	---	2.31	1.15
V/(CoCp)	---	---	2.73	---	8.03	4.79	---	17.87	3.91
% WITHIN FACTOR 2	---	---	33.	---	0.	19.	---	10.	17.

AVERAGE OF THE TOP 5 VALUES FROM EACH 1-HOUR PERIOD:

	STABILITY D			STABILITY E			STABILITY F		
WIND SPEED(M/S)	0-1	1-3	GT 3	0-1	1-3	GT 3	0-1	1-3	GT 3
# OF DATA PAIRS	0	1	27	3	9	16	2	30	12
MEAN FOR OBS	---	---	15.05	---	8.18	21.91	---	21.83	23.76
MEAN FOR PRE	---	---	.40	---	.28	.32	---	.14	.37
BIAS (PRE/OBS)	---	---	.40	---	.28	.32	---	.14	.37
RMS ERROR	---	---	14.29	---	13.10	26.03	---	34.16	26.05
V/Co2	---	---	.90	---	2.57	1.41	---	2.45	1.20
V/(CoCp)	---	---	2.28	---	9.18	4.44	---	17.01	3.21
% WITHIN FACTOR 2	---	---	26.	---	0.	25.	---	10.	17.

* Statistics are not presented for cases with less than 6 data pairs.

TABLE E-4

EVALUATION STATISTICS FOR DATA SUBSET PAIRED IN TIME
(SUBDIVIDED INTO STABILITY AND WIND SPEED CLASSES)

1-HOUR AVERAGES TRACER: SF6 SITE: CINDER CONE BUTTE

MODEL: COMPLEX I THRESHOLD: .00 uS/M**3

(Concentrations given in units of microseconds per cubic meter.)

HIGHEST 1-HOUR VALUES, UNPAIRED IN SPACE:

	STABILITY D			STABILITY E			STABILITY F		
WIND SPEED(M/S)	0-1	1-3	GT 3	0-1	1-3	GT 3	0-1	1-3	GT 3
# OF DATA PAIRS	0	1	27	3	9	16	2	30	12
MEAN FOR OBS	---	---	21.73	---	13.31	30.31	---	33.58	36.35
MEAN FOR PRE	---	---	10.45	---	42.11	25.50	---	68.63	48.31
BIAS (PRE/OBS)	---	---	.48	---	3.16	.84	---	2.04	1.33
RMS ERROR	---	---	19.54	---	51.38	23.61	---	58.68	28.73
V/Co2	---	---	.81	---	14.91	.61	---	3.05	.62
V/(CoCp)	---	---	1.68	---	4.71	.72	---	1.49	.47
% WITHIN FACTOR 2	---	---	52.	---	11.	56.	---	20.	58.

AVERAGE OF THE TOP 5 VALUES FROM EACH 1-HOUR PERIOD:

	STABILITY D			STABILITY E			STABILITY F		
WIND SPEED(M/S)	0-1	1-3	GT 3	0-1	1-3	GT 3	0-1	1-3	GT 3
# OF DATA PAIRS	0	1	27	3	9	16	2	30	12
MEAN FOR OBS	---	---	15.05	---	8.18	21.91	---	21.83	23.76
MEAN FOR PRE	---	---	9.15	---	31.15	20.76	---	52.96	41.23
BIAS (PRE/OBS)	---	---	.61	---	3.81	.95	---	2.43	1.74
RMS ERROR	---	---	13.30	---	41.33	20.34	---	47.46	26.97
V/Co2	---	---	.78	---	25.56	.86	---	4.73	1.29
V/(CoCp)	---	---	1.28	---	6.71	.91	---	1.95	.74
% WITHIN FACTOR 2	---	---	59.	---	11.	56.	---	23.	50.

* Statistics are not presented for cases with less than 6 data pairs

TABLE E-5

EVALUATION STATISTICS FOR DATA SUBSET PAIRED IN TIME
(SUBDIVIDED INTO STABILITY AND WIND SPEED CLASSES)

1-HOUR AVERAGES TRACER: SF6 SITE: CINDER CONE BUTTE

MODEL: RTDM (DEFAULT) THRESHOLD: .00 uS/M**3

(Concentrations given in units of microseconds per cubic meter.)

HIGHEST 1-HOUR VALUES, UNPAIRED IN SPACE:

	STABILITY D			STABILITY E			STABILITY F		
WIND SPEED(M/S)	0-1	1-3	GT 3	0-1	1-3	GT 3	0-1	1-3	GT 3
# OF DATA PAIRS	0	1	27	3	9	16	2	30	12
MEAN FOR OBS	---	---	21.73	---	13.31	30.31	---	33.58	36.35
MEAN FOR PRE	---	---	8.15	---	27.23	13.67	---	75.15	23.24
BIAS (PRE/OBS)	---	---	.38	---	2.05	.45	---	2.24	.64
RMS ERROR	---	---	20.61	---	32.32	27.10	---	94.98	28.41
V/Co2	---	---	.90	---	5.90	.80	---	8.00	.61
V/(CoCp)	---	---	2.40	---	2.88	1.77	---	3.58	.96
% WITHIN FACTOR 2	---	---	26.	---	22.	44.	---	13.	50.

AVERAGE OF THE TOP 5 VALUES FROM EACH 1-HOUR PERIOD:

	STABILITY D			STABILITY E			STABILITY F		
WIND SPEED(M/S)	0-1	1-3	GT 3	0-1	1-3	GT 3	0-1	1-3	GT 3
# OF DATA PAIRS	0	1	27	3	9	16	2	30	12
MEAN FOR OBS	---	---	15.05	---	8.18	21.91	---	21.83	23.76
MEAN FOR PRE	---	---	6.72	---	20.57	11.91	---	46.75	21.95
BIAS (PRE/OBS)	---	---	.45	---	2.52	.54	---	2.14	.92
RMS ERROR	---	---	14.03	---	27.61	20.78	---	50.12	16.15
V/Co2	---	---	.87	---	11.41	.90	---	5.27	.46
V/(CoCp)	---	---	1.95	---	4.53	1.65	---	2.46	.50
% WITHIN FACTOR 2	---	---	30.	---	22.	44.	---	17.	50.

* Statistics are not presented for cases with less than 6 data pairs

TABLE E-6

EVALUATION STATISTICS FOR DATA SUBSET PAIRED IN TIME
(SUBDIVIDED INTO STABILITY AND WIND SPEED CLASSES)

1-HOUR AVERAGES TRACER: SF6 SITE: CINDER CONE BUTTE

MODEL: RTDM (ONSITE) THRESHOLD: .00 uS/M**3

(Concentrations given in units of microseconds per cubic meter.)

HIGHEST 1-HOUR VALUES, UNPAIRED IN SPACE:

	STABILITY D			STABILITY E			STABILITY F		
WIND SPEED(M/S)	0-1	1-3	GT 3	0-1	1-3	GT 3	0-1	1-3	GT 3
# OF DATA PAIRS	0	1	27	3	9	16	2	30	12
MEAN FOR OBS	---	---	21.73	---	13.31	30.31	---	33.58	36.35
MEAN FOR PRE	---	---	14.46	---	20.09	23.72	---	26.15	25.68
BIAS (PRE/OBS)	---	---	.67	---	1.51	.78	---	.78	.71
RMS ERROR	---	---	18.97	---	22.46	18.25	---	33.21	30.65
V/Co2	---	---	0.76	---	2.85	0.36	---	0.98	.71
V/(CoCp)	---	---	1.15	---	1.89	0.46	---	1.26	1.01
% WITHIN FACTOR 2	0.	100.	48.	0.	22.	44.	50.	33.	33.

AVERAGE OF THE TOP 5 VALUES FROM EACH 1-HOUR PERIOD:

	STABILITY D			STABILITY E			STABILITY F		
WIND SPEED(M/S)	0-1	1-3	GT 3	0-1	1-3	GT 3	0-1	1-3	GT 3
# OF DATA PAIRS	0	1	27	3	9	16	2	30	12
MEAN FOR OBS	---	---	15.05	---	8.18	21.91	---	21.83	23.76
MEAN FOR PRE	---	---	11.46	---	14.48	18.27	---	17.63	20.37
BIAS (PRE/OBS)	---	---	.76	---	1.77	.83	---	.81	.86
RMS ERROR	---	---	13.64	---	16.24	14.08	---	20.78	23.45
V/Co2	---	---	0.82	---	3.94	0.41	---	0.91	0.97
V/(CoCp)	---	---	1.08	---	2.23	0.50	---	1.12	1.14
% WITHIN FACTOR 2	---	---	48.	---	11.	56.	---	27.	25.

* Statistics are not presented for cases with less than 6 data pairs

TABLE E-7

EVALUATION STATISTICS FOR DATA SUBSET PAIRED IN TIME
(SUBDIVIDED INTO STABILITY AND WIND SPEED CLASSES)

1-HOUR AVERAGES TRACER: CF3BR SITE: CINDER CONE BUTTE

MODEL: CTDM THRESHOLD: .00 uS/M**3

(Concentrations given in units of microseconds per cubic meter.)

HIGHEST 1-HOUR VALUES, UNPAIRED IN SPACE:

	STABILITY D			STABILITY E			STABILITY F		
WIND SPEED(M/S)	0-1	1-3	GT 3	0-1	1-3	GT 3	0-1	1-3	GT 3
# OF DATA PAIRS	0	0	11	0	2	11	0	4	16
MEAN FOR OBS	---	---	17.04	---	---	23.43	---	---	9.53
MEAN FOR PRE	---	---	15.95	---	---	17.86	---	---	18.49
BIAS (PRE/OBS)	---	---	.94	---	---	.76	---	---	1.94
RMS ERROR	---	---	30.37	---	---	27.81	---	---	24.58
V/Co2	---	---	3.18	---	---	1.41	---	---	6.65
V/(CoCp)	---	---	3.40	---	---	1.85	---	---	3.43
% WITHIN FACTOR 2	---	---	9.	---	---	27.	---	---	31.

AVERAGE OF THE TOP 5 VALUES FROM EACH 1-HOUR PERIOD:

	STABILITY D			STABILITY E			STABILITY F		
WIND SPEED(M/S)	0-1	1-3	GT 3	0-1	1-3	GT 3	0-1	1-3	GT 3
# OF DATA PAIRS	0	0	11	0	2	11	0	4	16
MEAN FOR OBS	---	---	10.51	---	---	12.32	---	---	4.95
MEAN FOR PRE	---	---	10.15	---	---	12.51	---	---	12.91
BIAS (PRE/OBS)	---	---	.97	---	---	1.02	---	---	2.61
RMS ERROR	---	---	20.11	---	---	18.96	---	---	17.47
V/Co2	---	---	3.66	---	---	2.37	---	---	12.47
V/(CoCp)	---	---	3.79	---	---	2.33	---	---	4.78
% WITHIN FACTOR 2	---	---	9.	---	---	9.	---	---	25.

* Statistics are not presented for cases with less than 6 data pairs

TABLE E-8

EVALUATION STATISTICS FOR DATA SUBSET PAIRED IN TIME
(SUBDIVIDED INTO STABILITY AND WIND SPEED CLASSES)

1-HOUR AVERAGES TRACER: CF3BR SITE: CINDER CONE BUTTE

MODEL: CTDM (DEGR1) THRESHOLD: .00 uS/M**3

(Concentrations given in units of microseconds per cubic meter.)

HIGHEST 1-HOUR VALUES, UNPAIRED IN SPACE:

	STABILITY D			STABILITY E			STABILITY F		
WIND SPEED(M/S)	0-1	1-3	GT 3	0-1	1-3	GT 3	0-1	1-3	GT 3
# OF DATA PAIRS	0	0	11	0	2	11	0	4	16
MEAN FOR OBS	---	---	17.04	---	---	23.43	---	---	9.53
MEAN FOR PRE	---	---	6.39	---	---	11.61	---	---	7.16
BIAS (PRE/OBS)	---	---	.38	---	---	.50	---	---	.75
RMS ERROR	---	---	25.08	---	---	23.19	---	---	13.64
V/Co2	---	---	2.17	---	---	.98	---	---	2.05
V/(CoCp)	---	---	5.78	---	---	1.98	---	---	2.73
% WITHIN FACTOR 2	---	---	18.	---	---	9.	---	---	6.

AVERAGE OF THE TOP 5 VALUES FROM EACH 1-HOUR PERIOD:

	STABILITY D			STABILITY E			STABILITY F		
WIND SPEED(M/S)	0-1	1-3	GT 3	0-1	1-3	GT 3	0-1	1-3	GT 3
# OF DATA PAIRS	0	0	11	0	2	11	0	4	16
MEAN FOR OBS	---	---	10.51	---	---	12.32	---	---	4.95
MEAN FOR PRE	---	---	4.47	---	---	5.88	---	---	5.92
BIAS (PRE/OBS)	---	---	.43	---	---	.48	---	---	1.20
RMS ERROR	---	---	16.79	---	---	14.39	---	---	9.95
V/Co2	---	---	2.55	---	---	1.37	---	---	4.05
V/(CoCp)	---	---	5.99	---	---	2.86	---	---	3.38
% WITHIN FACTOR 2	---	---	9.	---	---	9.	---	---	13.

* Statistics are not presented for cases with less than 6 data pairs

TABLE E-9

EVALUATION STATISTICS FOR DATA SUBSET PAIRED IN TIME
(SUBDIVIDED INTO STABILITY AND WIND SPEED CLASSES)

1-HOUR AVERAGES TRACER: CF3BR SITE: CINDER CONE BUTTE

MODEL: CTDM (DEGR2) THRESHOLD: .00 uS/M**3

(Concentrations given in units of microseconds per cubic meter.)

HIGHEST 1-HOUR VALUES, UNPAIRED IN SPACE:

	STABILITY D			STABILITY E			STABILITY F		
WIND SPEED(M/S)	0-1	1-3	GT 3	0-1	1-3	GT 3	0-1	1-3	GT 3
# OF DATA PAIRS	0	0	11	0	2	11	0	4	16
MEAN FOR OBS	---	---	17.04	---	---	23.43	---	---	9.53
MEAN FOR PRE	---	---	6.83	---	---	6.11	---	---	3.49
BIAS (PRE/OBS)	---	---	.40	---	---	.26	---	---	.37
RMS ERROR	---	---	27.22	---	---	25.66	---	---	11.79
V/Co2	---	---	2.55	---	---	1.20	---	---	1.53
V/(CoCp)	---	---	6.37	---	---	4.60	---	---	4.18
% WITHIN FACTOR 2	---	---	45.	---	---	36.	---	---	25.

AVERAGE OF THE TOP 5 VALUES FROM EACH 1-HOUR PERIOD:

	STABILITY D			STABILITY E			STABILITY F		
WIND SPEED(M/S)	0-1	1-3	GT 3	0-1	1-3	GT 3	0-1	1-3	GT 3
# OF DATA PAIRS	0	0	11	0	2	11	0	4	16
MEAN FOR OBS	---	---	10.51	---	---	12.32	---	---	4.95
MEAN FOR PRE	---	---	5.07	---	---	2.80	---	---	2.05
BIAS (PRE/OBS)	---	---	.48	---	---	.23	---	---	.41
RMS ERROR	---	---	18.50	---	---	14.47	---	---	6.60
V/Co2	---	---	3.10	---	---	1.38	---	---	1.78
V/(CoCp)	---	---	6.42	---	---	6.07	---	---	4.29
% WITHIN FACTOR 2	---	---	45.	---	---	27.	---	---	19.

* Statistics are not presented for cases with less than 6 data pairs

TABLE E-10

EVALUATION STATISTICS FOR DATA SUBSET PAIRED IN TIME
(SUBDIVIDED INTO STABILITY AND WIND SPEED CLASSES)

1-HOUR AVERAGES TRACER: CF3BR SITE: CINDER CONE BUTTE

MODEL: COMPLEX I THRESHOLD: .00 uS/M**3

(Concentrations given in units of microseconds per cubic meter.)

HIGHEST 1-HOUR VALUES, UNPAIRED IN SPACE:

	STABILITY D			STABILITY E			STABILITY F		
WIND SPEED(M/S)	0-1	1-3	GT 3	0-1	1-3	GT 3	0-1	1-3	GT 3
# OF DATA PAIRS	0	0	14	0	2	13	0	4	16
MEAN FOR OBS	---	---	16.21	---	---	22.37	---	---	9.53
MEAN FOR PRE	---	---	12.01	---	---	20.90	---	---	25.60
BIAS (PRE/OBS)	---	---	.74	---	---	.93	---	---	2.68
RMS ERROR	---	---	19.86	---	---	22.82	---	---	22.21
V/Co2	---	---	1.50	---	---	1.04	---	---	5.43
V/(CoCp)	---	---	2.03	---	---	1.11	---	---	2.02
% WITHIN FACTOR 2	---	---	64.	---	---	54.	---	---	25.

AVERAGE OF THE TOP 5 VALUES FROM EACH 1-HOUR PERIOD:

	STABILITY D			STABILITY E			STABILITY F		
WIND SPEED(M/S)	0-1	1-3	GT 3	0-1	1-3	GT 3	0-1	1-3	GT 3
# OF DATA PAIRS	0	0	14	0	2	13	0	4	16
MEAN FOR OBS	---	---	10.41	---	---	12.10	---	---	4.95
MEAN FOR PRE	---	---	10.27	---	---	14.54	---	---	20.94
BIAS (PRE/OBS)	---	---	.99	---	---	1.20	---	---	4.23
RMS ERROR	---	---	12.37	---	---	13.36	---	---	19.53
V/Co2	---	---	1.41	---	---	1.22	---	---	15.59
V/(CoCp)	---	---	1.43	---	---	1.01	---	---	3.68
% WITHIN FACTOR 2	---	---	29.	---	---	54.	---	---	13.

* Statistics are not presented for cases with less than 6 data pairs

TABLE E-11

EVALUATION STATISTICS FOR DATA SUBSET PAIRED IN TIME
(SUBDIVIDED INTO STABILITY AND WIND SPEED CLASSES)

1-HOUR AVERAGES - TRACER: CF3BR SITE: CINDER CONE BUTTE

MODEL: RTDM (DEFAULT) THRESHOLD: .00 uS/M**3

(Concentrations given in units of microseconds per cubic meter.)

HIGHEST 1-HOUR VALUES, UNPAIRED IN SPACE:

	STABILITIES A-D			STABILITY E			STABILITY F		
WIND SPEED(M/S)	0-1	1-3	GT 3	0-1	1-3	GT 3	0-1	1-3	GT 3
#. OF DATA PAIRS	0	0	11	0	2	11	0	4	16
MEAN FOR OBS	---	---	17.04	---	---	23.43	---	---	9.53
MEAN FOR PRE	---	---	8.33	---	---	12.39	---	---	4.25
BIAS (PRE/OBS)	---	---	.49	---	---	.53	---	---	.45
RMS ERROR	---	---	22.40	---	---	20.00	---	---	10.84
V/Co2	---	---	1.73	---	---	.73	---	---	1.29
V/(CoCp)	---	---	3.53	---	---	1.38	---	---	2.90
% WITHIN FACTOR 2	---	---	64.	---	---	64.	---	---	38.

AVERAGE OF THE TOP 5 VALUES FROM EACH 1-HOUR PERIOD:

	STABILITY D			STABILITY E			STABILITY F		
WIND SPEED(M/S)	0-1	1-3	GT 3	0-1	1-3	GT 3	0-1	1-3	GT 3
# OF DATA PAIRS	0	0	11	0	2	11	0	4	16
MEAN FOR OBS	---	---	10.51	---	---	12.32	---	---	4.95
MEAN FOR PRE	---	---	6.50	---	---	8.61	---	---	3.65
BIAS (PRE/OBS)	---	---	.62	---	---	.70	---	---	.74
RMS ERROR	---	---	14.63	---	---	11.00	---	---	7.06
V/Co2	---	---	1.94	---	---	.80	---	---	2.04
V/(CoCp)	---	---	3.13	---	---	1.14	---	---	2.76
% WITHIN FACTOR 2	---	---	55.	---	---	64.	---	---	31.

* Statistics are not presented for cases with less than 6 data pairs

TABLE E-12

EVALUATION STATISTICS FOR DATA SUBSET PAIRED IN TIME
(SUBDIVIDED INTO STABILITY AND WIND SPEED CLASSES)

1-HOUR AVERAGES TRACER: CF3BR SITE: CINDER CONE BUTTE

MODEL: RTDM (ONSITE) THRESHOLD: .00 uS/M**3

(Concentrations given in units of microseconds per cubic meter.)

HIGHEST 1-HOUR VALUES, UNPAIRED IN SPACE:

	STABILITY D			STABILITY E			STABILITY F		
WIND SPEED(M/S)	0-1	1-3	GT 3	0-1	1-3	GT 3	0-1	1-3	GT 3
# OF DATA PAIRS	0	0	11	0	2	11	0	4	16
MEAN FOR OBS	---	---	17.04	---	---	23.43	---	---	9.53
MEAN FOR PRE	---	---	17.50	---	---	10.00	---	---	11.49
BIAS (PRE/OBS)	---	---	1.03	---	---	.43	---	---	1.20
RMS ERROR	---	---	22.01	---	---	25.01	---	---	12.24
V/Co2	---	---	1.67	---	---	1.14	---	---	1.65
V/(CoCp)	---	---	1.63	---	---	2.67	---	---	1.37
% WITHIN FACTOR 2	---	---	27.	---	---	45.	---	---	31.

AVERAGE OF THE TOP 5 VALUES FROM EACH 1-HOUR PERIOD:

	STABILITY D			STABILITY E			STABILITY F		
WIND SPEED(M/S)	0-1	1-3	GT 3	0-1	1-3	GT 3	0-1	1-3	GT 3
# OF DATA PAIRS	0	0	11	0	2	11	0	4	16
MEAN FOR OBS	---	---	10.51	---	---	12.32	---	---	4.95
MEAN FOR PRE	---	---	11.29	---	---	7.07	---	---	7.11
BIAS (PRE/OBS)	---	---	1.07	---	---	.57	---	---	1.44
RMS ERROR	---	---	14.72	---	---	13.88	---	---	7.04
V/Co2	---	---	1.96	---	---	1.27	---	---	2.03
V/(CoCp)	---	---	1.83	---	---	2.21	---	---	1.41
% WITHIN FACTOR 2	---	---	45.	---	---	45.	---	---	31.

* Statistics are not presented for cases with less than 6 data pairs

TABLE E-13

EVALUATION STATISTICS FOR DATA SUBSET PAIRED IN TIME
(SUBDIVIDED INTO STABILITY AND WIND SPEED CLASSES)

1-HOUR AVERAGES TRACER: SF6 SITE: HOGBACK RIDGE

MODEL: CTDM THRESHOLD: .00 uS/M**3

(Concentrations given in units of microseconds per cubic meter.)

HIGHEST 1-HOUR VALUES, UNPAIRED IN SPACE:

	STABILITY D			STABILITY E			STABILITY F		
WIND SPEED(M/S)	0-1	1-3	GT 3	0-1	1-3	GT 3	0-1	1-3	GT 3
# OF DATA PAIRS	0	1	1	0	0	1	2	43	11
MEAN FOR OBS	---	---	---	---	---	---	---	26.69	11.92
MEAN FOR PRE	---	---	---	---	---	---	---	52.44	22.94
BIAS (PRE/OBS)	---	---	---	---	---	---	---	1.96	1.93
RMS ERROR	---	---	---	---	---	---	---	63.96	12.25
V/Co2	---	---	---	---	---	---	---	5.74	1.06
V/(CoCp)	---	---	---	---	---	---	---	2.92	0.55
% WITHIN FACTOR 2	---	---	---	---	---	---	---	35.	55.

AVERAGE OF THE TOP 5 VALUES FROM EACH 1-HOUR PERIOD:

	STABILITY D			STABILITY E			STABILITY F		
WIND SPEED(M/S)	0-1	1-3	GT 3	0-1	1-3	GT 3	0-1	1-3	GT 3
# OF DATA PAIRS	0	1	1	0	0	1	2	43	11
MEAN FOR OBS	---	---	---	---	---	---	---	20.62	9.93
MEAN FOR PRE	---	---	---	---	---	---	---	39.36	21.50
BIAS (PRE/OBS)	---	---	---	---	---	---	---	1.91	2.17
RMS ERROR	---	---	---	---	---	---	---	41.03	12.40
V/Co2	---	---	---	---	---	---	---	3.96	1.56
V/(CoCp)	---	---	---	---	---	---	---	2.07	0.72
% WITHIN FACTOR 2	---	---	---	---	---	---	---	23.	36.

* Statistics are not presented for cases with less than 6 data pairs.

TABLE E-14

EVALUATION STATISTICS FOR DATA SUBSET PAIRED IN TIME
(SUBDIVIDED INTO STABILITY AND WIND SPEED CLASSES)

1-HOUR AVERAGES TRACER: SF6 SITE: HOGBACK RIDGE

MODEL: CTDM (DEGR1) THRESHOLD: .00 uS/M**3

(Concentrations given in units of microseconds per cubic meter.)

HIGHEST 1-HOUR VALUES, UNPAIRED IN SPACE:

	STABILITY D			STABILITY E			STABILITY F		
WIND SPEED(M/S)	0-1	1-3	GT 3	0-1	1-3	GT 3	0-1	1-3	GT 3
# OF DATA PAIRS	0	1	1	0	0	1	2	43	11
MEAN FOR OBS	---	---	---	---	---	---	---	26.69	11.92
MEAN FOR PRE	---	---	---	---	---	---	---	30.80	14.58
BIAS (PRE/OBS)	---	---	---	---	---	---	---	1.15	1.22
RMS ERROR	---	---	---	---	---	---	---	35.96	17.54
V/Co2	---	---	---	---	---	---	---	1.81	2.17
V/(CoCp)	---	---	---	---	---	---	---	1.57	1.77
% WITHIN FACTOR 2	---	---	---	---	---	---	---	30.	36.

AVERAGE OF THE TOP 5 VALUES FROM EACH 1-HOUR PERIOD:

	STABILITY D			STABILITY E			STABILITY F		
WIND SPEED(M/S)	0-1	1-3	GT 3	0-1	1-3	GT 3	0-1	1-3	GT 3
# OF DATA PAIRS	0	1	1	0	0	1	2	43	11
MEAN FOR OBS	---	---	---	---	---	---	---	20.62	9.93
MEAN FOR PRE	---	---	---	---	---	---	---	24.15	11.15
BIAS (PRE/OBS)	---	---	---	---	---	---	---	1.17	1.12
RMS ERROR	---	---	---	---	---	---	---	26.31	11.23
V/Co2	---	---	---	---	---	---	---	1.63	1.28
V/(CoCp)	---	---	---	---	---	---	---	1.39	1.14
% WITHIN FACTOR 2	---	---	---	---	---	---	---	30.	27.

* Statistics are not presented for cases with less than 6 data pairs

TABLE E-15

EVALUATION STATISTICS FOR DATA SUBSET PAIRED IN TIME
(SUBDIVIDED INTO STABILITY AND WIND SPEED CLASSES)

1-HOUR AVERAGES TRACER: SF6 SITE: HOGBACK RIDGE

MODEL: CTDM (DEGR2) THRESHOLD: .00 uS/M**3

(Concentrations given in units of microseconds per cubic meter.)

HIGHEST 1-HOUR VALUES, UNPAIRED IN SPACE:

	STABILITY D			STABILITY E			STABILITY F		
WIND SPEED(M/S)	0-1	1-3	GT 3	0-1	1-3	GT 3	0-1	1-3	GT 3
# OF DATA PAIRS	0	1	1	0	0	1	2	43	11
MEAN FOR OBS	---	---	---	---	---	---	---	26.69	11.92
MEAN FOR PRE	---	---	---	---	---	---	---	12.38	9.62
BIAS (PRE/OBS)	---	---	---	---	---	---	---	.46	.81
RMS ERROR	---	---	---	---	---	---	---	31.78	11.12
V/Co2	---	---	---	---	---	---	---	1.42	.87
V/(CoCp)	---	---	---	---	---	---	---	3.06	1.08
% WITHIN FACTOR 2	---	---	---	---	---	---	---	14.	36.

AVERAGE OF THE TOP 5 VALUES FROM EACH 1-HOUR PERIOD:

	STABILITY D			STABILITY E			STABILITY F		
WIND SPEED(M/S)	0-1	1-3	GT 3	0-1	1-3	GT 3	0-1	1-3	GT 3
# OF DATA PAIRS	0	1	1	0	0	1	2	43	11
MEAN FOR OBS	---	---	---	---	---	---	---	20.62	9.93
MEAN FOR PRE	---	---	---	---	---	---	---	10.31	8.05
BIAS (PRE/OBS)	---	---	---	---	---	---	---	.50	.81
RMS ERROR	---	---	---	---	---	---	---	25.49	9.69
V/Co2	---	---	---	---	---	---	---	1.53	.95
V/(CoCp)	---	---	---	---	---	---	---	3.06	1.17
% WITHIN FACTOR 2	---	---	---	---	---	---	---	9.	36.

* Statistics are not presented for cases with less than 6 data pairs

TABLE E-16

EVALUATION STATISTICS FOR DATA SUBSET PAIRED IN TIME
(SUBDIVIDED INTO STABILITY AND WIND SPEED CLASSES)

1-HOUR AVERAGES TRACER: SF6 SITE: HOGBACK RIDGE

MODEL: COMPLEX I THRESHOLD: .00 uS/M**3

(Concentrations given in units of microseconds per cubic meter.)

HIGHEST 1-HOUR VALUES, UNPAIRED IN SPACE:

	STABILITY D			STABILITY E			STABILITY F		
WIND SPEED(M/S)	0-1	1-3	GT 3	0-1	1-3	GT 3	0-1	1-3	GT 3
# OF DATA PAIRS	0	1	1	0	0	1	2	44	11
MEAN FOR OBS	---	---	---	---	---	---	---	27.05	11.92
MEAN FOR PRE	---	---	---	---	---	---	---	136.31	56.10
BIAS (PRE/OBS)	---	---	---	---	---	---	---	5.04	4.71
RMS ERROR	---	---	---	---	---	---	---	132.88	47.08
V/Co2	---	---	---	---	---	---	---	24.14	15.61
V/(CoCp)	---	---	---	---	---	---	---	4.79	3.32
% WITHIN FACTOR 2	---	---	---	---	---	---	---	2.	0.

AVERAGE OF THE TOP 5 VALUES FROM EACH 1-HOUR PERIOD:

	STABILITY D			STABILITY E			STABILITY F		
WIND SPEED(M/S)	0-1	1-3	GT 3	0-1	1-3	GT 3	0-1	1-3	GT 3
# OF DATA PAIRS	0	1	1	0	0	1	2	44	11
MEAN FOR OBS	---	---	---	---	---	---	---	20.93	9.93
MEAN FOR PRE	---	---	---	---	---	---	---	116.97	52.47
BIAS (PRE/OBS)	---	---	---	---	---	---	---	5.59	5.29
RMS ERROR	---	---	---	---	---	---	---	115.86	44.72
V/Co2	---	---	---	---	---	---	---	30.63	20.28
V/(CoCp)	---	---	---	---	---	---	---	5.48	3.84
% WITHIN FACTOR 2	---	---	---	---	---	---	---	2.	0.

* Statistics are not presented for cases with less than 6 data pairs

TABLE E-17

EVALUATION STATISTICS FOR DATA SUBSET PAIRED IN TIME
(SUBDIVIDED INTO STABILITY AND WIND SPEED CLASSES)

1-HOUR AVERAGES TRACER: SF6 SITE: HOGBACK RIDGE

MODEL: RTDM (DEFAULT) THRESHOLD: .00 uS/M**3

(Concentrations given in units of microseconds per cubic meter.)

HIGHEST 1-HOUR VALUES, UNPAIRED IN SPACE:

	STABILITY D			STABILITY E			STABILITY F		
WIND SPEED(M/S)	0-1	1-3	GT 3	0-1	1-3	GT 3	0-1	1-3	GT 3
# OF DATA PAIRS	0	1	1	0	0	1	2	44	11
MEAN FOR OBS	---	---	---	---	---	---	---	27.05	11.92
MEAN FOR PRE	---	---	---	---	---	---	---	78.77	1.74
BIAS (PRE/OBS)	---	---	---	---	---	---	---	2.91	.15
RMS ERROR	---	---	---	---	---	---	---	121.17	11.70
V/Co2	---	---	---	---	---	---	---	20.07	.96
V/(CoCp)	---	---	---	---	---	---	---	6.89	6.58
% WITHIN FACTOR 2	---	---	---	---	---	---	---	20.	0.

AVERAGE OF THE TOP 5 VALUES FROM EACH 1-HOUR PERIOD:

	STABILITY D			STABILITY E			STABILITY F		
WIND SPEED(M/S)	0-1	1-3	GT 3	0-1	1-3	GT 3	0-1	1-3	GT 3
# OF DATA PAIRS	0	1	1	0	0	1	2	44	11
MEAN FOR OBS	---	---	---	---	---	---	---	20.93	9.93
MEAN FOR PRE	---	---	---	---	---	---	---	58.75	1.52
BIAS (PRE/OBS)	---	---	---	---	---	---	---	2.81	.15
RMS ERROR	---	---	---	---	---	---	---	84.86	9.85
V/Co2	---	---	---	---	---	---	---	16.43	.98
V/(CoCp)	---	---	---	---	---	---	---	5.85	6.41
% WITHIN FACTOR 2	---	---	---	---	---	---	---	23.	0.

* Statistics are not presented for cases with less than 6 data pairs

TABLE E-18

EVALUATION STATISTICS FOR DATA SUBSET PAIRED IN TIME
(SUBDIVIDED INTO STABILITY AND WIND SPEED CLASSES)

1-HOUR AVERAGES TRACER: SF6 SITE: HOGBACK RIDGE

MODEL: RTDM (ONSITE) THRESHOLD: .00 uS/M**3

(Concentrations given in units of microseconds per cubic meter.)

HIGHEST 1-HOUR VALUES, UNPAIRED IN SPACE:

	STABILITY D			STABILITY E			STABILITY F		
WIND SPEED(M/S)	0-1	1-3	GT 3	0-1	1-3	GT 3	0-1	1-3	GT 3
# OF DATA PAIRS	0	1	1	0	0	1	2	43	11
MEAN FOR OBS	---	---	---	---	---	---	---	26.69	11.92
MEAN FOR PRE	---	---	---	---	---	---	---	38.70	13.65
BIAS (PRE/OBS)	---	---	---	---	---	---	---	1.45	1.14
RMS ERROR	---	---	---	---	---	---	---	80.10	4.53
V/Co2	---	---	---	---	---	---	---	9.00	.14
V/(CoCp)	---	---	---	---	---	---	---	6.21	.13
% WITHIN FACTOR 2	---	---	---	---	---	---	---	53.	82.

AVERAGE OF THE TOP 5 VALUES FROM EACH 1-HOUR PERIOD:

	STABILITY D			STABILITY E			STABILITY F		
WIND SPEED(M/S)	0-1	1-3	GT 3	0-1	1-3	GT 3	0-1	1-3	GT 3
# OF DATA PAIRS	0	1	1	0	0	1	2	43	11
MEAN FOR OBS	---	---	---	---	---	---	---	20.62	9.93
MEAN FOR PRE	---	---	---	---	---	---	---	25.88	11.75
BIAS (PRE/OBS)	---	---	---	---	---	---	---	1.25	1.18
RMS ERROR	---	---	---	---	---	---	---	35.70	4.33
V/Co2	---	---	---	---	---	---	---	3.00	.19
V/(CoCp)	---	---	---	---	---	---	---	2.39	.16
% WITHIN FACTOR 2	---	---	---	---	---	---	---	56.	73.

* Statistics are not presented for cases with less than 6 data pairs

TABLE E-19

EVALUATION STATISTICS FOR DATA SUBSET PAIRED IN TIME
(SUBDIVIDED INTO STABILITY AND WIND SPEED CLASSES)

1-HOUR AVERAGES TRACER: CF3BR SITE: HOGBACK RIDGE

MODEL: CTDM THRESHOLD: .01 uS/M**3

(Concentrations given in units of microseconds per cubic meter.)

HIGHEST 1-HOUR VALUES, UNPAIRED IN SPACE:

	STABILITY D			STABILITY E			STABILITY F		
WIND SPEED(M/S)	0-1	1-3	GT 3	0-1	1-3	GT 3	0-1	1-3	GT 3
# OF DATA PAIRS	0	1	0	0	1	0	14	26	0
MEAN FOR OBS	---	---	---	---	---	---	101.11	93.86	---
MEAN FOR PRE	---	---	---	---	---	---	60.69	45.29	---
BIAS (PRE/OBS)	---	---	---	---	---	---	.60	.48	---
RMS ERROR	---	---	---	---	---	---	87.34	99.25	---
V/Co2	---	---	---	---	---	---	.75	1.12	---
V/(CoCp)	---	---	---	---	---	---	1.24	2.32	---
% WITHIN FACTOR 2	---	---	---	---	---	---	64.	54.	---

AVERAGE OF THE TOP 5 VALUES FROM EACH 1-HOUR PERIOD:

	STABILITY D			STABILITY E			STABILITY F		
WIND SPEED(M/S)	0-1	1-3	GT 3	0-1	1-3	GT 3	0-1	1-3	GT 3
# OF DATA PAIRS	0	1	0	0	1	0	14	26	0
MEAN FOR OBS	---	---	---	---	---	---	59.17	64.72	---
MEAN FOR PRE	---	---	---	---	---	---	48.90	37.52	---
BIAS (PRE/OBS)	---	---	---	---	---	---	.83	.58	---
RMS ERROR	---	---	---	---	---	---	32.34	56.61	---
V/Co2	---	---	---	---	---	---	.30	.76	---
V/(CoCp)	---	---	---	---	---	---	.36	1.32	---
% WITHIN FACTOR 2	---	---	---	---	---	---	57.	46.	---

* Statistics are not presented for cases with less than 6 data pairs

TABLE E-20

EVALUATION STATISTICS FOR DATA SUBSET PAIRED IN TIME
(SUBDIVIDED INTO STABILITY AND WIND SPEED CLASSES)

1-HOUR AVERAGES TRACER: CF3BR SITE: HOGBACK RIDGE

MODEL: CTDM (DEGR1) THRESHOLD: .01 uS/M**3

(Concentrations given in units of microseconds per cubic meter.)

HIGHEST 1-HOUR VALUES, UNPAIRED IN SPACE:

	STABILITY D			STABILITY E			STABILITY F		
WIND SPEED(M/S)	0-1	1-3	GT 3	0-1	1-3	GT 3	0-1	1-3	GT 3
# OF DATA PAIRS	0	0	0	0	0	0	10	14	0
MEAN FOR OBS	---	---	---	---	---	---	113.28	121.63	---
MEAN FOR PRE	---	---	---	---	---	---	41.28	51.66	---
BIAS (PRE/OBS)	---	---	---	---	---	---	.36	.42	---
RMS ERROR	---	---	---	---	---	---	141.69	146.85	---
V/Co2	---	---	---	---	---	---	1.56	1.46	---
V/(CoCp)	---	---	---	---	---	---	4.29	3.43	---
% WITHIN FACTOR 2	---	---	---	---	---	---	30.	43.	---

AVERAGE OF THE TOP 5 VALUES FROM EACH 1-HOUR PERIOD:

	STABILITY D			STABILITY E			STABILITY F		
WIND SPEED(M/S)	0-1	1-3	GT 3	0-1	1-3	GT 3	0-1	1-3	GT 3
# OF DATA PAIRS	0	0	0	0	0	0	10	14	0
MEAN FOR OBS	---	---	---	---	---	---	63.96	82.98	---
MEAN FOR PRE	---	---	---	---	---	---	36.06	42.43	---
BIAS (PRE/OBS)	---	---	---	---	---	---	.56	.51	---
RMS ERROR	---	---	---	---	---	---	65.44	84.86	---
V/Co2	---	---	---	---	---	---	1.05	1.05	---
V/(CoCp)	---	---	---	---	---	---	1.86	2.05	---
% WITHIN FACTOR 2	---	---	---	---	---	---	30.	43.	---

* Statistics are not presented for cases with less than 6 data pairs

TABLE E-21

EVALUATION STATISTICS FOR DATA SUBSET PAIRED IN TIME
(SUBDIVIDED INTO STABILITY AND WIND SPEED CLASSES)

1-HOUR AVERAGES TRACER: CF3BR SITE: HOGBACK RIDGE

MODEL: CTDM (DEGR2) THRESHOLD: .01 uS/M**3

(Concentrations given in units of microseconds per cubic meter.)

HIGHEST 1-HOUR VALUES, UNPAIRED IN SPACE:

	STABILITY D			STABILITY E			STABILITY F		
WIND SPEED(M/S)	0-1	1-3	GT 3	0-1	1-3	GT 3	0-1	1-3	GT 3
# OF DATA PAIRS	0	0	0	0	1	0	6	7	0
MEAN FOR OBS	---	---	---	---	---	---	114.67	71.74	---
MEAN FOR PRE	---	---	---	---	---	---	70.64	48.14	---
BIAS (PRE/OBS)	---	---	---	---	---	---	.62	.67	---
RMS ERROR	---	---	---	---	---	---	146.08	31.43	---
V/Co2	---	---	---	---	---	---	1.62	.19	---
V/(CoCp)	---	---	---	---	---	---	2.63	.29	---
% WITHIN FACTOR 2	---	---	---	---	---	---	17.	57.	---

AVERAGE OF THE TOP 5 VALUES FROM EACH 1-HOUR PERIOD:

	STABILITY D			STABILITY E			STABILITY F		
WIND SPEED(M/S)	0-1	1-3	GT 3	0-1	1-3	GT 3	0-1	1-3	GT 3
# OF DATA PAIRS	0	0	0	0	1	0	6	7	0
MEAN FOR OBS	---	---	---	---	---	---	60.97	55.45	---
MEAN FOR PRE	---	---	---	---	---	---	61.80	43.05	---
BIAS (PRE/OBS)	---	---	---	---	---	---	1.01	.78	---
RMS ERROR	---	---	---	---	---	---	71.95	25.03	---
V/Co2	---	---	---	---	---	---	1.39	.20	---
V/(CoCp)	---	---	---	---	---	---	1.37	.26	---
% WITHIN FACTOR 2	---	---	---	---	---	---	33.	86.	---

* Statistics are not presented for cases with less than 6 data pairs

TABLE E-22

EVALUATION STATISTICS FOR DATA SUBSET PAIRED IN TIME
(SUBDIVIDED INTO STABILITY AND WIND SPEED CLASSES)

1-HOUR AVERAGES TRACER: CF3BR SITE: HOGBACK RIDGE

MODEL: COMPLEX I THRESHOLD: .01 uS/M**3

(Concentrations given in units of microseconds per cubic meter.)

HIGHEST 1-HOUR VALUES, UNPAIRED IN SPACE:

	STABILITY D			STABILITY E			STABILITY F		
WIND SPEED(M/S)	0-1	1-3	GT 3	0-1	1-3	GT 3	0-1	1-3	GT 3
# OF DATA PAIRS	0	0	1	0	1	0	12	26	0
MEAN FOR OBS	---	---	---	---	---	---	129.13	111.31	---
MEAN FOR PRE	---	---	---	---	---	---	215.96	163.69	---
BIAS (PRE/OBS)	---	---	---	---	---	---	1.67	1.47	---
RMS ERROR	---	---	---	---	---	---	142.59	121.39	---
V/Co2	---	---	---	---	---	---	1.22	1.19	---
V/(CoCp)	---	---	---	---	---	---	.73	.81	---
% WITHIN FACTOR 2	---	---	---	---	---	---	42.	42.	---

AVERAGE OF THE TOP 5 VALUES FROM EACH 1-HOUR PERIOD:

	STABILITY D			STABILITY E			STABILITY F		
WIND SPEED(M/S)	0-1	1-3	GT 3	0-1	1-3	GT 3	0-1	1-3	GT 3
# OF DATA PAIRS	0	0	1	0	1	0	12	26	0
MEAN FOR OBS	---	---	---	---	---	---	74.80	77.51	---
MEAN FOR PRE	---	---	---	---	---	---	192.12	141.72	---
BIAS (PRE/OBS)	---	---	---	---	---	---	2.57	1.83	---
RMS ERROR	---	---	---	---	---	---	135.55	104.26	---
V/Co2	---	---	---	---	---	---	3.28	1.81	---
V/(CoCp)	---	---	---	---	---	---	1.28	.99	---
% WITHIN FACTOR 2	---	---	---	---	---	---	33.	46.	---

* Statistics are not presented for cases with less than 6 data pairs

TABLE E-23

EVALUATION STATISTICS FOR DATA SUBSET PAIRED IN TIME
(SUBDIVIDED INTO STABILITY AND WIND SPEED CLASSES)

1-HOUR AVERAGES TRACER: CF3BR SITE: HOGBACK RIDGE

MODEL: RTDM (DEFAULT) THRESHOLD: .01 uS/M**3

(Concentrations given in units of microseconds per cubic meter.)

HIGHEST 1-HOUR VALUES, UNPAIRED IN SPACE:

	STABILITY D			STABILITY E			STABILITY F		
WIND SPEED(M/S)	0-1	1-3	GT 3	0-1	1-3	GT 3	0-1	1-3	GT 3
# OF DATA PAIRS	0	0	1	0	1	0	12	24	0
MEAN FOR OBS	---	---	---	---	---	---	129.13	110.15	---
MEAN FOR PRE	---	---	---	---	---	---	528.66	434.83	---
BIAS (PRE/OBS)	---	---	---	---	---	---	4.09	3.95	---
RMS ERROR	---	---	---	---	---	---	729.26	680.00	---
V/Co2	---	---	---	---	---	---	31.90	38.11	---
V/(CoCp)	---	---	---	---	---	---	7.79	9.65	---
% WITHIN FACTOR 2	---	---	---	---	---	---	17.	13.	---

AVERAGE OF THE TOP 5 VALUES FROM EACH 1-HOUR PERIOD:

	STABILITY D			STABILITY E			STABILITY F		
WIND SPEED(M/S)	0-1	1-3	GT 3	0-1	1-3	GT 3	0-1	1-3	GT 3
# OF DATA PAIRS	0	0	1	0	1	0	12	23	0
MEAN FOR OBS	---	---	---	---	---	---	74.80	69.67	---
MEAN FOR PRE	---	---	---	---	---	---	198.39	183.54	---
BIAS (PRE/OBS)	---	---	---	---	---	---	2.65	2.63	---
RMS ERROR	---	---	---	---	---	---	242.62	215.28	---
V/Co2	---	---	---	---	---	---	10.52	9.55	---
V/(CoCp)	---	---	---	---	---	---	3.97	3.62	---
% WITHIN FACTOR 2	---	---	---	---	---	---	0.	4.	---

* Statistics are not presented for cases with less than 6 data pairs

TABLE E-24

EVALUATION STATISTICS FOR DATA SUBSET PAIRED IN TIME
(SUBDIVIDED INTO STABILITY AND WIND SPEED CLASSES)

1-HOUR AVERAGES TRACER: CF3BR SITE: HOGBACK RIDGE

MODEL: RTDM (ONSITE) THRESHOLD: .01 uS/M**3

(Concentrations given in units of microseconds per cubic meter.)

HIGHEST 1-HOUR VALUES, UNPAIRED IN SPACE:

	STABILITY D			STABILITY E			STABILITY F		
WIND SPEED(M/S)	0-1	1-3	GT 3	0-1	1-3	GT 3	0-1	1-3	GT 3
# OF DATA PAIRS	0	0	1	0	1	0	16	34	0
MEAN FOR OBS	---	---	---	---	---	---	126.66	92.76	---
MEAN FOR PRE	---	---	---	---	---	---	127.40	58.63	---
BIAS (PRE/OBS)	---	---	---	---	---	---	1.01	.63	---
RMS ERROR	---	---	---	---	---	---	274.65	146.70	---
V/Co2	---	---	---	---	---	---	4.70	2.50	---
V/(CoCp)	---	---	---	---	---	---	4.68	3.96	---
% WITHIN FACTOR 2	---	---	---	---	---	---	25.	18.	---

AVERAGE OF THE TOP 5 VALUES FROM EACH 1-HOUR PERIOD:

	STABILITY D			STABILITY E			STABILITY F		
WIND SPEED(M/S)	0-1	1-3	GT 3	0-1	1-3	GT 3	0-1	1-3	GT 3
# OF DATA PAIRS	0	0	1	0	1	0	16	34	0
MEAN FOR OBS	---	---	---	---	---	---	72.31	63.50	---
MEAN FOR PRE	---	---	---	---	---	---	58.44	42.37	---
BIAS (PRE/OBS)	---	---	---	---	---	---	.81	.67	---
RMS ERROR	---	---	---	---	---	---	79.22	104.00	---
V/Co2	---	---	---	---	---	---	1.20	2.68	---
V/(CoCp)	---	---	---	---	---	---	1.49	4.02	---
% WITHIN FACTOR 2	---	---	---	---	---	---	25.	24.	---

* Statistics are not presented for cases with less than 6 data pairs

TABLE E-25

EVALUATION STATISTICS FOR DATA SUBSET PAIRED IN TIME
(SUBDIVIDED INTO STABILITY AND WIND SPEED CLASSES)

1-HOUR AVERAGES TRACER: SF6 SITE: TRACY POWER PLANT

MODEL: CTDM (MODEL) THRESHOLD: .00 uS/M**3

(Concentrations given in units of microseconds per cubic meter.)

HIGHEST 1-HOUR VALUES, UNPAIRED IN SPACE:

	STABILITY D			STABILITY E			STABILITY F		
WIND SPEED(M/S)	0-1	1-3	GT 3	0-1	1-3	GT 3	0-1	1-3	GT 3
# OF DATA PAIRS	0	1	23	2	2	13	10	42	17
MEAN FOR OBS	---	---	1.03	---	---	1.02	3.24	2.33	1.84
MEAN FOR PRE	---	---	.96	---	---	1.45	2.82	2.24	1.93
BIAS (PRE/OBS)	---	---	.92	---	---	1.42	.87	.96	1.05
RMS ERROR	---	---	.79	---	---	1.42	2.14	2.34	2.84
V/Co2	---	---	.58	---	---	1.94	.44	1.00	2.38
V/(CoCp)	---	---	.63	---	---	1.37	.50	1.04	2.27
% WITHIN FACTOR 2	---	---	61.	---	---	69.	80.	60.	53.

AVERAGE OF THE TOP 5 VALUES FROM EACH 1-HOUR PERIOD:

	STABILITY D			STABILITY E			STABILITY F		
WIND SPEED(M/S)	0-1	1-3	GT 3	0-1	1-3	GT 3	0-1	1-3	GT 3
# OF DATA PAIRS	0	1	23	2	2	13	10	42	17
MEAN FOR OBS	---	---	.71	---	---	.67	2.27	1.53	1.06
MEAN FOR PRE	---	---	.71	---	---	.90	1.77	1.57	1.36
BIAS (PRE/OBS)	---	---	1.01	---	---	1.35	.78	1.03	1.29
RMS ERROR	---	---	.51	---	---	.65	1.19	1.38	1.09
V/Co2	---	---	.52	---	---	.93	.27	.82	1.06
V/(CoCp)	---	---	.52	---	---	.69	.35	.80	.82
% WITHIN FACTOR 2	---	---	52.	---	---	54.	80.	55.	53.

* Statistics are not presented for cases with less than 6 data pairs

TABLE E-26

EVALUATION STATISTICS FOR DATA SUBSET PAIRED IN TIME
(SUBDIVIDED INTO STABILITY AND WIND SPEED CLASSES)

1-HOUR AVERAGES TRACER: SF6 SITE: TRACY POWER PLANT

MODEL: CTDM (DEGR1) THRESHOLD: .00 uS/M**3

(Concentrations given in units of microseconds per cubic meter.)

HIGHEST 1-HOUR VALUES, UNPAIRED IN SPACE:

	STABILITY D			STABILITY E			STABILITY F		
WIND SPEED(M/S)	0-1	1-3	GT 3	0-1	1-3	GT 3	0-1	1-3	GT 3
# OF DATA PAIRS	0	1	23	1	2	13	10	42	17
MEAN FOR OBS	---	---	1.03	---	---	1.02	3.24	2.33	1.84
MEAN FOR PRE	---	---	1.11	---	---	1.18	3.02	2.38	2.45
BIAS (PRE/OBS)	---	---	1.07	---	---	1.16	.93	1.02	1.33
RMS ERROR	---	---	.94	---	---	.88	3.18	2.20	3.33
V/Co2	---	---	.83	---	---	.75	.97	.89	3.27
V/(CoCp)	---	---	.78	---	---	.65	1.04	.87	2.46
% WITHIN FACTOR 2	---	---	61.	---	---	69.	20.	43.	47.

AVERAGE OF THE TOP 5 VALUES FROM EACH 1-HOUR PERIOD:

	STABILITY D			STABILITY E			STABILITY F		
WIND SPEED(M/S)	0-1	1-3	GT 3	0-1	1-3	GT 3	0-1	1-3	GT 3
# OF DATA PAIRS	0	1	23	1	2	13	10	42	17
MEAN FOR OBS	---	---	.71	---	---	.67	2.27	1.53	1.06
MEAN FOR PRE	---	---	.76	---	---	.78	1.99	1.55	1.58
BIAS (PRE/OBS)	---	---	1.07	---	---	1.17	.88	1.02	1.50
RMS ERROR	---	---	.62	---	---	.68	2.04	1.49	1.29
V/Co2	---	---	.77	---	---	1.03	.81	.96	1.50
V/(CoCp)	---	---	.72	---	---	.88	.92	.94	1.00
% WITHIN FACTOR 2	---	---	61.	---	---	54.	40.	48.	35.

* Statistics are not presented for cases with less than 6 data pairs

TABLE E-27

EVALUATION STATISTICS FOR DATA SUBSET PAIRED IN TIME
(SUBDIVIDED INTO STABILITY AND WIND SPEED CLASSES)

1-HOUR AVERAGES TRACER: SF6 SITE: TRACY POWER PLANT

MODEL: CTDM (DEGR2) THRESHOLD: .00 uS/M**3

(Concentrations given in units of microseconds per cubic meter.)

HIGHEST 1-HOUR VALUES, UNPAIRED IN SPACE:

	STABILITY D			STABILITY E			STABILITY F		
WIND SPEED(M/S)	0-1	1-3	GT 3	0-1	1-3	GT 3	0-1	1-3	GT 3
# OF DATA PAIRS	0	1	23	1	2	13	10	39	16
MEAN FOR OBS	---	---	1.03	---	---	1.02	3.24	2.36	1.84
MEAN FOR PRE	---	---	1.35	---	---	1.84	2.30	3.55	1.85
BIAS (PRE/OBS)	---	---	1.30	---	---	1.81	.71	1.50	1.01
RMS ERROR	---	---	1.13	---	---	2.33	3.09	3.99	2.76
V/Co2	---	---	1.20	---	---	5.23	.91	2.85	2.26
V/(CoCp)	---	---	.92	---	---	2.90	1.28	1.89	2.24
% WITHIN FACTOR 2	---	---	48.	---	---	38.	40.	36.	38.

AVERAGE OF THE TOP 5 VALUES FROM EACH 1-HOUR PERIOD:

	STABILITY D			STABILITY E			STABILITY F		
WIND SPEED(M/S)	0-1	1-3	GT 3	0-1	1-3	GT 3	0-1	1-3	GT 3
# OF DATA PAIRS	0	1	23	1	2	13	10	39	16
MEAN FOR OBS	---	---	.71	---	---	.67	2.27	1.54	1.02
MEAN FOR PRE	---	---	.73	---	---	.81	1.62	2.06	.93
BIAS (PRE/OBS)	---	---	1.04	---	---	1.21	.71	1.33	.91
RMS ERROR	---	---	.56	---	---	1.19	2.37	2.68	.74
V/Co2	---	---	.63	---	---	3.15	1.09	3.01	.53
V/(CoCp)	---	---	.61	---	---	2.61	1.53	2.26	.59
% WITHIN FACTOR 2	---	---	48.	---	---	54.	20.	26.	56.

* Statistics are not presented for cases with less than 6 data pairs

TABLE E-28

EVALUATION STATISTICS FOR DATA SUBSET PAIRED IN TIME
(SUBDIVIDED INTO STABILITY AND WIND SPEED CLASSES)

1-HOUR AVERAGES TRACER: SF6 SITE: TRACY POWER PLANT

MODEL: COMPLEX I THRESHOLD: .00 uS/M**3

(Concentrations given in units of microseconds per cubic meter.)

HIGHEST 1-HOUR VALUES, UNPAIRED IN SPACE:

	STABILITY D			STABILITY E			STABILITY F		
WIND SPEED(M/S)	0-1	1-3	GT 3	0-1	1-3	GT 3	0-1	1-3	GT 3
# OF DATA PAIRS	0	1	23	2	2	14	10	42	17
MEAN FOR OBS	---	---	1.03	---	---	.98	3.24	2.33	1.84
MEAN FOR PRE	---	---	.45	---	---	2.43	10.32	10.47	4.06
BIAS (PRE/OBS)	---	---	.44	---	---	2.48	3.18	4.48	2.21
RMS ERROR	---	---	1.09	---	---	1.72	10.89	10.12	3.77
V/Co2	---	---	1.10	---	---	3.06	11.31	18.79	4.20
V/(CoCp)	---	---	2.51	---	---	1.23	3.55	4.19	1.90
% WITHIN FACTOR 2	---	---	35.	---	---	29.	0.	12.	12.

AVERAGE OF THE TOP 5 VALUES FROM EACH 1-HOUR PERIOD:

	STABILITY D			STABILITY E			STABILITY F		
WIND SPEED(M/S)	0-1	1-3	GT 3	0-1	1-3	GT 3	0-1	1-3	GT 3
# OF DATA PAIRS	0	1	23	2	2	14	10	42	17
MEAN FOR OBS	---	---	.71	---	---	.65	2.27	1.53	1.06
MEAN FOR PRE	---	---	.37	---	---	1.76	6.91	6.82	2.97
BIAS (PRE/OBS)	---	---	.53	---	---	2.72	3.04	4.46	2.81
RMS ERROR	---	---	.70	---	---	1.26	8.03	6.49	2.30
V/Co2	---	---	.98	---	---	3.79	12.50	18.04	4.73
V/(CoCp)	---	---	1.84	---	---	1.39	4.11	4.04	1.68
% WITHIN FACTOR 2	---	---	39.	---	---	14.	10.	7.	6.

* Statistics are not presented for cases with less than 6 data pairs

TABLE E-29

EVALUATION STATISTICS FOR DATA SUBSET PAIRED IN TIME
(SUBDIVIDED INTO STABILITY AND WIND SPEED CLASSES)

1-HOUR AVERAGES TRACER: SF6 SITE: TRACY POWER PLANT

MODEL: RTDM (DEFAULT) THRESHOLD: .00 uS/M**3

(Concentrations given in units of microseconds per cubic meter.)

HIGHEST 1-HOUR VALUES, UNPAIRED IN SPACE:

	STABILITY D			STABILITY E			STABILITY F		
WIND SPEED(M/S)	0-1	1-3	GT 3	0-1	1-3	GT 3	0-1	1-3	GT 3
# OF DATA PAIRS	0	1	23	2	2	14	10	42	17
MEAN FOR OBS	---	---	1.03	---	---	.98	3.28	2.33	1.84
MEAN FOR PRE	---	---	.59	---	---	1.21	5.44	5.11	1.49
BIAS (PRE/OBS)	---	---	.57	---	---	1.23	1.68	2.19	.81
RMS ERROR	---	---	1.05	---	---	.94	5.99	4.18	2.49
V/Co2	---	---	1.03	---	---	.92	3.42	3.21	1.83
V/(CoCp)	---	---	1.79	---	---	.74	2.04	1.47	2.27
% WITHIN FACTOR 2	---	---	43.	---	---	43.	20.	45.	82.

AVERAGE OF THE TOP 5 VALUES FROM EACH 1-HOUR PERIOD:

	STABILITY D			STABILITY E			STABILITY F		
WIND SPEED(M/S)	0-1	1-3	GT 3	0-1	1-3	GT 3	0-1	1-3	GT 3
# OF DATA PAIRS	0	1	23	2	2	14	10	42	17
MEAN FOR OBS	---	---	.71	---	---	.65	2.27	1.53	1.06
MEAN FOR PRE	---	---	.49	---	---	.89	3.43	2.87	1.07
BIAS (PRE/OBS)	---	---	.69	---	---	1.38	1.51	1.88	1.01
RMS ERROR	---	---	.70	---	---	.55	3.70	2.20	.82
V/Co2	---	---	.99	---	---	.72	2.65	2.08	.60
V/(CoCp)	---	---	1.44	---	---	.52	1.75	1.11	.59
% WITHIN FACTOR 2	---	---	39.	---	---	57.	10.	40.	65.

* Statistics are not presented for cases with less than 6 data pairs

TABLE E-30

EVALUATION STATISTICS FOR DATA SUBSET PAIRED IN TIME
(SUBDIVIDED INTO STABILITY AND WIND SPEED CLASSES)

1-HOUR AVERAGES TRACER: SF6 SITE: TRACY POWER PLANT

MODEL: RTDM (ONSITE) THRESHOLD: .00 uS/M**3

(Concentrations given in units of microseconds per cubic meter.)

HIGHEST 1-HOUR VALUES, UNPAIRED IN SPACE:

	STABILITY D			STABILITY E			STABILITY F		
WIND SPEED(M/S)	0-1	1-3	GT 3	0-1	1-3	GT 3	0-1	1-3	GT 3
# OF DATA PAIRS	0	1	23	2	2	13	10	42	17
MEAN FOR OBS	---	---	1.03	---	---	1.02	3.24	2.33	1.84
MEAN FOR PRE	---	---	1.14	---	---	1.40	.97	1.07	1.32
BIAS (PRE/OBS)	---	---	1.10	---	---	1.37	.30	.46	.72
RMS ERROR	---	---	1.59	---	---	1.30	2.86	2.40	2.64
V/Co2	---	---	2.38	---	---	1.62	.78	1.05	2.06
V/(CoCp)	---	---	2.15	---	---	1.18	2.60	2.31	2.86
% WITHIN FACTOR 2	---	---	22.	---	---	46.	10.	33.	47.

AVERAGE OF THE TOP 5 VALUES FROM EACH 1-HOUR PERIOD:

	STABILITY D			STABILITY E			STABILITY F		
WIND SPEED(M/S)	0-1	1-3	GT 3	0-1	1-3	GT 3	0-1	1-3	GT 3
# OF DATA PAIRS	0	1	23	2	2	13	10	42	17
MEAN FOR OBS	---	---	.71	---	---	.67	2.27	1.53	1.06
MEAN FOR PRE	---	---	.75	---	---	.81	.61	.72	.83
BIAS (PRE/OBS)	---	---	1.06	---	---	1.22	.27	.47	.78
RMS ERROR	---	---	.94	---	---	.69	2.08	1.50	.90
V/Co2	---	---	1.77	---	---	1.07	.84	.96	.72
V/(CoCp)	---	---	1.67	---	---	.88	3.14	2.05	.92
% WITHIN FACTOR 2	---	---	17.	---	---	62.	30.	33.	53.

* Statistics are not presented for cases with less than 6 data pairs

TABLE E-31

EVALUATION STATISTICS FOR DATA SUBSET PAIRED IN TIME
(SUBDIVIDED INTO STABILITY AND WIND SPEED CLASSES)

1-HOUR AVERAGES TRACER: CF3BR SITE: TRACY POWER PLANT

MODEL: CTDM THRESHOLD: .00 uS/M**3

(Concentrations given in units of microseconds per cubic meter.)

HIGHEST 1-HOUR VALUES, UNPAIRED IN SPACE:

	STABILITY D			STABILITY E			STABILITY F		
WIND SPEED(M/S)	0-1	1-3	GT 3	0-1	1-3	GT 3	0-1	1-3	GT 3
# OF DATA PAIRS	0	1	23	2	3	12	11	41	17
MEAN FOR OBS	---	---	1.11	---	---	2.02	4.85	3.21	3.56
MEAN FOR PRE	---	---	1.49	---	---	2.04	2.87	2.81	2.42
BIAS (PRE/OBS)	---	---	1.34	---	---	1.01	.59	.88	.68
RMS ERROR	---	---	.98	---	---	2.44	5.03	2.86	3.59
V/Co2	---	---	.78	---	---	1.45	1.08	.79	1.01
V/(CoCp)	---	---	.58	---	---	1.44	1.82	.91	1.49
% WITHIN FACTOR 2	---	---	83.	---	---	50.	64.	51.	53.

AVERAGE OF THE TOP 5 VALUES FROM EACH 1-HOUR PERIOD:

	STABILITY D			STABILITY E			STABILITY F		
WIND SPEED(M/S)	0-1	1-3	GT 3	0-1	1-3	GT 3	0-1	1-3	GT 3
# OF DATA PAIRS	0	1	23	2	3	12	11	41	17
MEAN FOR OBS	---	---	.72	---	---	1.21	2.78	2.08	1.89
MEAN FOR PRE	---	---	.84	---	---	1.06	1.61	1.37	1.42
BIAS (PRE/OBS)	---	---	1.16	---	---	.88	.58	.66	.75
RMS ERROR	---	---	.42	---	---	1.56	2.26	1.63	1.18
V/Co2	---	---	.35	---	---	1.67	.66	.62	.39
V/(CoCp)	---	---	.30	---	---	1.91	1.14	.94	.52
% WITHIN FACTOR 2	---	---	74.	---	---	75.	55.	61.	65.

* Statistics are not presented for cases with less than 6 data pairs

TABLE E-32

EVALUATION STATISTICS FOR DATA SUBSET PAIRED IN TIME
(SUBDIVIDED INTO STABILITY AND WIND SPEED CLASSES)

1-HOUR AVERAGES TRACER: CF3BR SITE: TRACY POWER PLANT

MODEL: CTDM(DEGR1) THRESHOLD: .00 uS/M**3

(Concentrations given in units of microseconds per cubic meter.)

HIGHEST 1-HOUR VALUES, UNPAIRED IN SPACE:

	STABILITY D			STABILITY E			STABILITY F		
WIND SPEED(M/S)	0-1	1-3	GT 3	0-1	1-3	GT 3	0-1	1-3	GT 3
# OF DATA PAIRS	0	1	23	1	3	12	11	41	17
MEAN FOR OBS	---	---	1.11	---	---	2.02	4.85	3.21	3.56
MEAN FOR PRE	---	---	1.30	---	---	1.44	3.13	3.84	3.96
BIAS (PRE/OBS)	---	---	1.17	---	---	.71	.64	1.19	1.11
RMS ERROR	---	---	1.06	---	---	2.90	2.64	3.15	8.07
V/Co2	---	---	.91	---	---	2.06	.30	.96	5.14
V/(CoCp)	---	---	.78	---	---	2.89	.46	.81	4.62
% WITHIN FACTOR 2	---	---	57.	---	---	33.	45.	59.	41.

AVERAGE OF THE TOP 5 VALUES FROM EACH 1-HOUR PERIOD:

	STABILITY D			STABILITY E			STABILITY F		
WIND SPEED(M/S)	0-1	1-3	GT 3	0-1	1-3	GT 3	0-1	1-3	GT 3
# OF DATA PAIRS	0	1	23	1	3	12	11	41	17
MEAN FOR OBS	---	---	.72	---	---	1.21	2.78	2.08	1.89
MEAN FOR PRE	---	---	.84	---	---	.80	1.43	1.42	1.49
BIAS (PRE/OBS)	---	---	1.17	---	---	.66	.51	.68	.79
RMS ERROR	---	---	.51	---	---	1.84	1.82	1.62	1.97
V/Co2	---	---	.51	---	---	2.32	.43	.61	1.09
V/(CoCp)	---	---	.43	---	---	3.49	.84	.89	1.38
% WITHIN FACTOR 2	---	---	70.	---	---	67.	45.	51.	47.

* Statistics are not presented for cases with less than 6 data pairs

TABLE E-33

EVALUATION STATISTICS FOR DATA SUBSET PAIRED IN TIME
(SUBDIVIDED INTO STABILITY AND WIND SPEED CLASSES)

1-HOUR AVERAGES TRACER: CF3BR SITE: TRACY POWER PLANT

MODEL: CTDM(DEGR2) THRESHOLD: .00 uS/M**3

(Concentrations given in units of microseconds per cubic meter.)

HIGHEST 1-HOUR VALUES, UNPAIRED IN SPACE:

	STABILITY D			STABILITY E			STABILITY F		
WIND SPEED(M/S)	0-1	1-3	GT 3	0-1	1-3	GT 3	0-1	1-3	GT 3
# OF DATA PAIRS	0	1	23	1	3	12	11	38	16
MEAN FOR OBS	---	---	1.11	---	---	2.02	4.85	3.30	3.49
MEAN FOR PRE	---	---	1.85	---	---	2.13	4.16	3.27	4.09
BIAS (PRE/OBS)	---	---	1.67	---	---	1.05	.86	.99	1.17
RMS ERROR	---	---	1.66	---	---	1.25	3.72	7.04	5.31
V/Co2	---	---	2.24	---	---	.38	.59	4.55	2.32
V/(CoCp)	---	---	1.34	---	---	.36	.69	4.60	1.98
% WITHIN FACTOR 2	---	---	57.	---	---	50.	18.	16.	25.

AVERAGE OF THE TOP 5 VALUES FROM EACH 1-HOUR PERIOD:

	STABILITY D			STABILITY E			STABILITY F		
WIND SPEED(M/S)	0-1	1-3	GT 3	0-1	1-3	GT 3	0-1	1-3	GT 3
# OF DATA PAIRS	0	1	23	1	3	12	11	38	16
MEAN FOR OBS	---	---	.72	---	---	1.21	2.78	2.13	1.82
MEAN FOR PRE	---	---	.82	---	---	.56	1.36	1.01	1.41
BIAS (PRE/OBS)	---	---	1.14	---	---	.47	.49	.47	.78
RMS ERROR	---	---	.63	---	---	1.22	1.89	2.88	1.61
V/Co2	---	---	.77	---	---	1.02	.46	1.82	.78
V/(CoCp)	---	---	.67	---	---	2.19	.94	3.83	1.01
% WITHIN FACTOR 2	---	---	57.	---	---	42.	36.	13.	38.

* Statistics are not presented for cases with less than 6 data pairs

TABLE E-34

EVALUATION STATISTICS FOR DATA SUBSET PAIRED IN TIME
(SUBDIVIDED INTO STABILITY AND WIND SPEED CLASSES)

1-HOUR AVERAGES TRACER: CF3BR SITE: TRACY POWER PLANT

MODEL: COMPLEX I THRESHOLD: .00 uS/M**3

(Concentrations given in units of microseconds per cubic meter.)

HIGHEST 1-HOUR VALUES, UNPAIRED IN SPACE:

	STABILITY D			STABILITY E			STABILITY F		
WIND SPEED(M/S)	0-1	1-3	GT 3	0-1	1-3	GT 3	0-1	1-3	GT 3
# OF DATA PAIRS	0	1	23	2	3	13	11	41	17
MEAN FOR OBS	---	---	1.11	---	---	2.05	4.85	3.21	3.56
MEAN FOR PRE	---	---	.97	---	---	3.20	15.82	13.78	5.60
BIAS (PRE/OBS)	---	---	.88	---	---	1.56	3.26	4.29	1.57
RMS ERROR	---	---	1.01	---	---	1.71	15.23	12.01	4.39
V/Co2	---	---	.83	---	---	.70	9.87	13.99	1.52
V/(CoCp)	---	---	.95	---	---	.45	3.02	3.26	.97
% WITHIN FACTOR 2	---	---	30.	---	---	54.	18.	10.	29.

AVERAGE OF THE TOP 5 VALUES FROM EACH 1-HOUR PERIOD:

	STABILITY D			STABILITY E			STABILITY F		
WIND SPEED(M/S)	0-1	1-3	GT 3	0-1	1-3	GT 3	0-1	1-3	GT 3
# OF DATA PAIRS	0	1	23	2	3	13	11	41	17
MEAN FOR OBS	---	---	.72	---	---	1.18	2.78	2.08	1.89
MEAN FOR PRE	---	---	.67	---	---	2.14	9.41	8.34	3.77
BIAS (PRE/OBS)	---	---	.93	---	---	1.81	3.38	4.01	2.00
RMS ERROR	---	---	.63	---	---	1.22	8.72	7.55	2.32
V/Co2	---	---	.76	---	---	1.06	9.86	13.20	1.51
V/(CoCp)	---	---	.81	---	---	.59	2.91	3.29	.75
% WITHIN FACTOR 2	---	---	39.	---	---	46.	18.	20.	47.

* Statistics are not presented for cases with less than 6 data pairs

TABLE E-35

EVALUATION STATISTICS FOR DATA SUBSET PAIRED IN TIME
(SUBDIVIDED INTO STABILITY AND WIND SPEED CLASSES)

1-HOUR AVERAGES TRACER: CF3BR SITE: TRACY POWER PLANT

MODEL: RTDM (DEFAULT) THRESHOLD: .00 uS/M**3

(Concentrations given in units of microseconds per cubic meter.)

HIGHEST 1-HOUR VALUES, UNPAIRED IN SPACE:

	STABILITY D			STABILITY E			STABILITY F		
WIND SPEED(M/S)	0-1	1-3	GT 3	0-1	1-3	GT 3	0-1	1-3	GT 3
# OF DATA PAIRS.	0	1	23	2	3	13	11	41	17
MEAN FOR OBS	---	---	1.11	---	---	2.05	4.85	3.21	3.56
MEAN FOR PRE	---	---	1.17	---	---	1.53	8.66	4.92	2.82
BIAS (PRE/OBS)	---	---	1.05	---	---	.74	1.79	1.53	.79
RMS ERROR	---	---	1.19	---	---	1.90	10.35	4.77	4.08
V/Co2	---	---	1.16	---	---	.85	4.56	2.21	1.31
V/(CoCp)	---	---	1.10	---	---	1.15	2.55	1.44	1.65
% WITHIN FACTOR 2	---	---	39.	---	---	54.	18.	37.	47.

AVERAGE OF THE TOP 5 VALUES FROM EACH 1-HOUR PERIOD:

	STABILITY D			STABILITY E			STABILITY F		
WIND SPEED(M/S)	0-1	1-3	GT 3	0-1	1-3	GT 3	0-1	1-3	GT 3
# OF DATA PAIRS	0	1	23	2	3	13	11	41	17
MEAN FOR OBS	---	---	.72	---	---	1.18	2.78	2.08	1.89
MEAN FOR PRE	---	---	.79	---	---	1.09	2.87	2.08	1.63
BIAS (PRE/OBS)	---	---	1.10	---	---	.92	1.03	1.00	.86
RMS ERROR	---	---	.84	---	---	1.19	3.33	1.96	1.59
V/Co2	---	---	1.36	---	---	1.02	1.44	.88	.71
V/(CoCp)	---	---	1.23	---	---	1.10	1.39	.88	.82
% WITHIN FACTOR 2	---	---	48.	---	---	54.	36.	41.	53.

* Statistics are not presented for cases with less than 6 data pairs

TABLE E-36

EVALUATION STATISTICS FOR DATA SUBSET PAIRED IN TIME
(SUBDIVIDED INTO STABILITY AND WIND SPEED CLASSES)

1-HOUR AVERAGES TRACER: CF3BR SITE: TRACY POWER PLANT

MODEL: RTDM (ONSITE) THRESHOLD: .00 uS/M**3

(Concentrations given in units of microseconds per cubic meter.)

HIGHEST 1-HOUR VALUES, UNPAIRED IN SPACE:

	STABILITY D			STABILITY E			STABILITY F		
WIND SPEED(M/S)	0-1	1-3	GT 3	0-1	1-3	GT 3	0-1	1-3	GT 3
# OF DATA PAIRS	0	1	23	2	3	12	11	41	17
MEAN FOR OBS	---	---	1.11	---	---	2.02	4.85	3.21	3.56
MEAN FOR PRE	---	---	1.78	---	---	2.19	1.35	1.87	2.65
BIAS (PRE/OBS)	---	---	1.61	---	---	1.08	.28	.58	.74
RMS ERROR	---	---	1.88	---	---	2.55	5.90	2.88	3.41
V/Co2	---	---	2.88	---	---	1.59	1.48	.80	.92
V/(CoCp)	---	---	1.79	---	---	1.46	5.33	1.38	1.24
% WITHIN FACTOR 2	---	---	35.	---	---	42.	36.	63.	59.

AVERAGE OF THE TOP 5 VALUES FROM EACH 1-HOUR PERIOD:

	STABILITY D			STABILITY E			STABILITY F		
WIND SPEED(M/S)	0-1	1-3	GT 3	0-1	1-3	GT 3	0-1	1-3	GT 3
# OF DATA PAIRS	0	1	23	2	3	12	11	41	17
MEAN FOR OBS	---	---	.72	---	---	1.21	2.78	2.08	1.89
MEAN FOR PRE	---	---	1.02	---	---	1.20	1.03	1.17	1.35
BIAS (PRE/OBS)	---	---	1.42	---	---	.99	.37	.56	.72
RMS ERROR	---	---	1.07	---	---	1.42	2.52	1.64	1.12
V/Co2	---	---	2.22	---	---	1.38	.82	.62	.35
V/(CoCp)	---	---	1.56	---	---	1.40	2.22	1.10	.49
% WITHIN FACTOR 2	---	---	43.	---	---	58.	36.	61.	82.

* Statistics are not presented for cases with less than 6 data pairs

TABLE E-37

EVALUATION STATISTICS FOR DATA SUBSET PAIRED IN TIME
(SUBDIVIDED INTO STABILITY AND WIND SPEED CLASSES)

1-HOUR AVERAGES TRACER: SO2 SITE: WESTVACO LUKE

MODEL: CTDM THRESHOLD: .00 uS/m**3

(Concentrations given in units of microseconds per cubic meter.)

HIGHEST 1-HOUR VALUES, UNPAIRED IN SPACE:

	STABILITY D			STABILITY E			STABILITY F		
WIND SPEED(M/S)	0-1	1-3	GT 3	0-1	1-3	GT 3	0-1	1-3	GT 3
# OF DATA PAIRS	98	704	1180	33	271	639	75	497	845
MEAN FOR OBS	.36	.31	.30	.19	.48	.30	.18	.39	.37
MEAN FOR PRE	.48	.40	.06	.19	.57	.27	.09	.42	.40
BIAS (PRE/OBS)	1.33	1.29	.19	1.02	1.20	.88	.50	1.07	1.07
RMS ERROR	.80	.96	.44	.58	1.06	.87	.43	1.00	.97
V/Co2	4.89	9.39	2.12	9.70	4.93	8.22	5.93	6.41	6.85
V/(CoCp)	3.68	7.30	11.04	9.48	4.10	9.38	11.76	6.00	6.43
% WITHIN FACTOR 2	27.	21.	8.	30.	24.	8.	17.	19.	10.

AVERAGE OF THE TOP 10 VALUES FROM EACH 1-HOUR PERIOD:

	STABILITY D			STABILITY E			STABILITY F		
WIND SPEED(M/S)	0-1	1-3	GT 3	0-1	1-3	GT 3	0-1	1-3	GT 3
# OF DATA PAIRS	98	704	1180	33	271	639	75	497	845
MEAN FOR OBS	.11	.10	.07	.07	.15	.08	.07	.12	.11
MEAN FOR PRE	.11	.08	.01	.03	.12	.03	.02	.08	.05
BIAS (PRE/OBS)	.95	.79	.10	.51	.80	.40	.27	.67	.49
RMS ERROR	.22	.24	.10	.16	.28	.14	.19	.25	.23
V/Co2	3.76	5.82	1.73	5.89	3.73	3.22	7.37	3.95	4.14
V/(CoCp)	3.94	7.33	17.59	11.59	4.64	7.96	27.75	5.91	8.51
% WITHIN FACTOR 2	30.	21.	5.	24.	21.	6.	15.	18.	12.

TABLE E-38

EVALUATION STATISTICS FOR DATA SUBSET PAIRED IN TIME
(SUBDIVIDED INTO STABILITY AND WIND SPEED CLASSES)

1-HOUR AVERAGES TRACER: SO2 SITE: WESTVACO LUKE

MODEL: CTDM (DEGR1) THRESHOLD: .00 uS/m**3

(Concentrations given in units of microseconds per cubic meter.)

HIGHEST 1-HOUR VALUES, UNPAIRED IN SPACE:

	STABILITY D			STABILITY E			STABILITY F		
WIND SPEED(M/S)	0-1	1-3	GT 3	0-1	1-3	GT 3	0-1	1-3	GT 3
# OF DATA PAIRS	100	732	1167	34	270	640	71	497	846
MEAN FOR OBS	.36	.31	.30	.18	.47	.30	.18	.40	.37
MEAN FOR PRE	1.88	1.46	.34	2.15	3.14	1.60	1.45	3.09	2.10
BIAS (PRE/OBS)	5.28	4.78	1.13	11.65	6.62	5.27	8.12	7.82	5.66
RMS ERROR	2.55	2.88	1.23	4.08	4.97	3.35	2.64	4.99	3.79
V/Co2	51.11	88.38	16.20	487.96	109.67	121.80	218.91	159.48	104.00
V/(CoCp)	9.69	18.50	14.39	41.90	16.57	23.11	26.97	20.39	18.38
% WITHIN FACTOR 2	10.	22.	17.	15.	19.	19.	7.	19.	19.

AVERAGE OF THE TOP 10 VALUES FROM EACH 1-HOUR PERIOD:

	STABILITY D			STABILITY E			STABILITY F		
WIND SPEED(M/S)	0-1	1-3	GT 3	0-1	1-3	GT 3	0-1	1-3	GT 3
# OF DATA PAIRS	100	732	1167	34	270	640	71	497	846
MEAN FOR OBS	.11	.10	.07	.07	.15	.08	.07	.12	.11
MEAN FOR PRE	.63	.27	.05	.62	.49	.21	.36	.47	.27
BIAS (PRE/OBS)	5.72	2.74	.62	9.41	3.34	2.77	5.20	3.80	2.44
RMS ERROR	.94	.55	.17	1.09	.76	.42	.68	.74	.49
V/Co2	73.43	31.49	5.42	278.26	27.10	29.77	93.96	35.81	19.83
V/(CoCp)	12.83	11.51	8.73	29.57	8.12	10.76	18.06	9.42	8.12
% WITHIN FACTOR 2	11.	22.	12.	12.	23.	19.	8.	21.	18.

TABLE E-39

EVALUATION STATISTICS FOR DATA SUBSET PAIRED IN TIME
(SUBDIVIDED INTO STABILITY AND WIND SPEED CLASSES)

1-HOUR AVERAGES TRACER: SO2 SITE: WESTVACO LUKE

MODEL: CTDM (DEGR2) THRESHOLD: .00 uS/m**3

(Concentrations given in units of microseconds per cubic meter.)

HIGHEST 1-HOUR VALUES, UNPAIRED IN SPACE:

	STABILITY D			STABILITY E			STABILITY F		
WIND SPEED(M/S)	0-1	1-3	GT 3	0-1	1-3	GT 3	0-1	1-3	GT 3
# OF DATA PAIRS	87	678	1075	28	214	539	57	388	717
MEAN FOR OBS	.39	.31	.30	.19	.52	.31	.22	.45	.40
MEAN FOR PRE	2.23	2.03	1.20	2.18	2.17	1.40	2.03	2.35	1.59
BIAS (PRE/OBS)	5.69	6.55	3.97	11.22	4.20	4.46	9.35	5.26	4.00
RMS ERROR	2.35	2.58	1.31	2.50	2.43	1.65	2.32	2.52	1.71
V/Co2	35.83	69.27	18.72	165.95	22.12	27.65	114.76	31.91	18.60
V/(CoCp)	6.30	10.57	4.72	14.79	5.27	6.20	12.28	6.07	4.65
% WITHIN FACTOR 2	10.	9.	22.	4.	14.	17.	11.	11.	15.

AVERAGE OF THE TOP 10 VALUES FROM EACH 1-HOUR PERIOD:

	STABILITY D			STABILITY E			STABILITY F		
WIND SPEED(M/S)	0-1	1-3	GT 3	0-1	1-3	GT 3	0-1	1-3	GT 3
# OF DATA PAIRS	87	678	1075	28	214	539	57	388	717
MEAN FOR OBS	.12	.10	.07	.07	.16	.08	.09	.14	.12
MEAN FOR PRE	.77	.45	.22	.64	.42	.25	.59	.44	.26
BIAS (PRE/OBS)	6.40	4.63	2.97	8.97	2.60	3.13	6.88	3.11	2.17
RMS ERROR	.89	.60	.25	.80	.53	.31	.76	.50	.36
V/Co2	54.75	37.94	12.10	124.42	10.44	15.18	78.09	12.51	9.05
V/(CoCp)	8.56	8.20	4.08	13.86	4.01	4.84	11.35	4.02	4.17
% WITHIN FACTOR 2	13.	10.	30.	7.	16.	24.	9.	17.	23.

TABLE E-40

EVALUATION STATISTICS FOR DATA SUBSET PAIRED IN TIME
(SUBDIVIDED INTO STABILITY AND WIND SPEED CLASSES)

1-HOUR AVERAGES TRACER: SO2 SITE: WESTVACO LUKE

MODEL: COMPLEX I THRESHOLD: .00 uS/m**3

(Concentrations given in units of microseconds per cubic meter.)

HIGHEST 1-HOUR VALUES, UNPAIRED IN SPACE:

	STABILITY D			STABILITY E			STABILITY F		
WIND SPEED(M/S)	0-1	1-3	GT 3	0-1	1-3	GT 3	0-1	1-3	GT 3
# OF DATA PAIRS	98	704	1180	33	271	639	75	497	845
MEAN FOR OBS	.36	.31	.30	.19	.48	.30	.18	.39	.37
MEAN FOR PRE	.00	.00	.00	2.08	5.63	6.68	.83	7.74	7.73
BIAS (PRE/OBS)	.00	.01	.00	11.12	11.81	22.01	4.71	19.62	20.80
RMS ERROR	.69	.71	.42	8.18	11.11	9.84	5.23	14.82	12.12
V/Co2	3.63	5.03	1.96	1914.6	542.4	1051.9	881.3	1410.3	1063.9
V/(CoCp)	1104.7	895.7	630.4	172.3	45.9	47.8	187.0	71.9	51.1
% WITHIN FACTOR 2	13.	16.	11.	30.	18.	12.	27.	17.	12.

AVERAGE OF THE TOP 10 VALUES FROM EACH 1-HOUR PERIOD:

	STABILITY D			STABILITY E			STABILITY F		
WIND SPEED(M/S)	0-1	1-3	GT 3	0-1	1-3	GT 3	0-1	1-3	GT 3
# OF DATA PAIRS	98	704	1180	33	271	639	75	497	845
MEAN FOR OBS	.11	.10	.07	.07	.15	.08	.07	.12	.11
MEAN FOR PRE	.00	.00	.00	.21	.78	.82	.11	1.06	.94
BIAS (PRE/OBS)	.00	.00	.00	3.11	5.31	10.68	1.65	8.59	8.47
RMS ERROR	.20	.23	.10	.81	1.59	1.25	.77	2.07	1.54
V/Co2	3.32	5.41	1.88	145.44	116.94	263.10	126.20	280.09	192.48
V/(CoCp)	2149.0	2389.5	1310.7	46.72	22.01	24.64	76.61	32.60	22.73
% WITHIN FACTOR 2	13.	16.	11.	27.	20.	14.	24.	18.	13.

TABLE E-41

EVALUATION STATISTICS FOR DATA SUBSET PAIRED IN TIME
(SUBDIVIDED INTO STABILITY AND WIND SPEED CLASSES)

1-HOUR AVERAGES TRACER: SO2 SITE: WESTVACO LUKE

MODEL: RTDM(DEFAULT) THRESHOLD: .00 uS/M**3

(Concentrations given in units of microseconds per cubic meter.)

HIGHEST 1-HOUR VALUES, UNPAIRED IN SPACE:

	STABILITY D			STABILITY E			STABILITY F		
WIND SPEED(M/S)	0-1	1-3	GT 3	0-1	1-3	GT 3	0-1	1-3	GT 3
# OF DATA PAIRS	98	704	1180	33	271	639	75	497	845
MEAN FOR OBS	.36	.31	.30	.19	.48	.30	.18	.39	.37
MEAN FOR PRE	.01	.01	.01	.84	1.52	.86	.35	2.22	1.91
BIAS (PRE/OBS)	.02	.02	.04	4.50	3.20	2.83	1.96	5.63	5.13
RMS ERROR	.68	.70	.41	3.29	3.00	1.52	2.06	4.11	3.15
V/Co2	3.60	5.00	1.85	309.10	39.61	25.12	136.16	108.73	72.03
V/(CoCp)	180.11	214.57	46.08	68.67	12.39	8.89	69.50	19.33	14.04
% WITHIN FACTOR 2	15.	17.	11.	30.	21.	20.	27.	19.	14.

AVERAGE OF THE TOP 10 VALUES FROM EACH 1-HOUR PERIOD:

	STABILITY D			STABILITY E			STABILITY F		
WIND SPEED(M/S)	0-1	1-3	GT 3	0-1	1-3	GT 3	0-1	1-3	GT 3
# OF DATA PAIRS	98	704	1180	33	271	639	75	497	845
MEAN FOR OBS	.11	.10	.07	.07	.15	.08	.07	.12	.11
MEAN FOR PRE	.00	.00	.00	.08	.21	.11	.05	.31	.24
BIAS (PRE/OBS)	.01	.01	.02	1.26	1.43	1.42	.75	2.47	2.13
RMS ERROR	.20	.23	.10	.33	.48	.22	.37	.59	.45
V/Co2	3.31	5.39	1.83	24.16	10.85	8.06	28.95	22.45	16.61
V/(CoCp)	331.97	576.49	97.32	19.16	7.56	5.66	38.69	9.09	7.81
% WITHIN FACTOR 2	15.	17.	11.	27.	19.	22.	25.	19.	15.

TABLE E-42

EVALUATION STATISTICS FOR DATA SUBSET PAIRED IN TIME
(SUBDIVIDED INTO STABILITY AND WIND SPEED CLASSES)

1-HOUR AVERAGES TRACER: SO2 SITE: WESTVACO LUKE

MODEL: RTDM(ONSITE) THRESHOLD: .00 uS/m**3

(Concentrations given in units of microseconds per cubic meter.)

HIGHEST 1-HOUR VALUES, UNPAIRED IN SPACE:

	STABILITY D			STABILITY E			STABILITY F		
WIND SPEED(M/S)	0-1	1-3	GT 3	0-1	1-3	GT 3	0-1	1-3	GT 3
# OF DATA PAIRS	98	704	1180	33	271	639	75	497	845
MEAN FOR OBS	.36	.31	.30	.19	.48	.30	.18	.39	.37
MEAN FOR PRE	.30	.19	.11	.02	.25	.26	.05	.22	.41
BIAS (PRE/OBS)	.83	.61	.36	.10	.52	.84	.30	.56	1.09
RMS ERROR	1.01	1.02	.39	.30	1.00	.75	.35	.80	1.15
V/Co2	7.89	10.47	1.66	2.61	4.36	6.09	3.87	4.15	9.58
V/(CoCp)	9.53	17.28	4.62	26.75	8.32	7.21	12.74	7.44	8.75
% WITHIN FACTOR 2	12.	13.	16.	6.	13.	16.	16.	14.	19.

AVERAGE OF THE TOP 10 VALUES FROM EACH 1-HOUR PERIOD:

	STABILITY D			STABILITY E			STABILITY F		
WIND SPEED(M/S)	0-1	1-3	GT 3	0-1	1-3	GT 3	0-1	1-3	GT 3
# OF DATA PAIRS	98	704	1180	33	271	639	75	497	845
MEAN FOR OBS	.11	.10	.07	.07	.15	.08	.07	.12	.11
MEAN FOR PRE	.06	.04	.02	.00	.05	.04	.01	.05	.07
BIAS (PRE/OBS)	.53	.39	.23	.05	.35	.55	.16	.39	.64
RMS ERROR	.20	.26	.09	.12	.30	.16	.17	.24	.30
V/Co2	3.10	6.70	1.60	3.11	4.09	4.09	6.03	3.74	7.15
V/(CoCp)	5.80	17.16	7.02	64.43	11.76	7.41	37.17	9.58	11.19
% WITHIN FACTOR 2	17.	11.	11.	3.	11.	13.	13.	13.	13.

TABLE E-43

EVALUATION STATISTICS FOR DATA SUBSET PAIRED IN TIME
(SUBDIVIDED INTO STABILITY AND WIND SPEED CLASSES)

1-HOUR AVERAGES TRACER: SO2 SITE: WIDOWS CREEK

MODEL: CTDM THRESHOLD: .00 ug/m**3

(Concentrations given in units of micrograms per cubic meter.)

HIGHEST 1-HOUR VALUES, UNPAIRED IN SPACE:

	STABILITY D			STABILITY E			STABILITY F		
WIND SPEED(M/S)	0-1	1-3	GT 3	0-1	1-3	GT 3	0-1	1-3	GT 3
# OF DATA PAIRS	28	333	2051	25	372	1396	50	367	320
MEAN FOR OBS	165.5	71.0	57.8	407.5	93.3	64.9	161.8	84.6	105.6
MEAN FOR PRE	601.4	186.9	63.7	917.1	290.9	96.4	459.8	407.5	165.0
BIAS (PRE/OBS)	3.6	2.6	1.1	2.3	3.1	1.5	2.8	4.8	1.6
RMS ERROR	897.9	457.6	149.8	1273.9	628.0	312.3	832.1	842.6	387.2
V/Co2	29.4	41.5	6.7	9.8	45.3	23.2	26.4	99.1	13.5
V/(CoCp)	8.1	15.8	6.1	4.3	14.5	15.6	9.3	20.6	8.6
% WITHIN FACTOR 2	14.	23.	27.	28.	20.	20.	12.	16.	22.

AVERAGE OF THE TOP 10 VALUES FROM EACH 1-HOUR PERIOD:

	STABILITY D			STABILITY E			STABILITY F		
WIND SPEED(M/S)	0-1	1-3	GT 3	0-1	1-3	GT 3	0-1	1-3	GT 3
# OF DATA PAIRS	28	333	2051	25	372	1396	50	367	320
MEAN FOR OBS	33.58	22.26	17.97	74.58	26.76	19.40	33.10		2
MEAN FOR PRE	69.39	23.98	8.44	134.51	37.65	11.81	68.61		5
BIAS (PRE/OBS)	2.07	1.08	.47	1.80	1.41	.61	2.07		
RMS ERROR	79.90	72.82	25.27	236.26	89.00	39.11	138.92		11
V/Co2	5.66	10.70	1.98	10.03	11.06	4.06	17.61		2
V/(CoCp)	2.74	9.93	4.21	5.56	7.86	6.68	8.50		1
% WITHIN FACTOR 2	21.	28.	20.	32.	24.	17.	18.		

TABLE E-44

EVALUATION STATISTICS FOR DATA SUBSET PAIRED IN TIME
(SUBDIVIDED INTO STABILITY AND WIND SPEED CLASSES)

1-HOUR AVERAGES TRACER: SO2 SITE: WIDOWS CREEK

MODEL: CTDM (DEGR1) THRESHOLD: .00 ug/m**3

(Concentrations given in units of micrograms per cubic meter.)

HIGHEST 1-HOUR VALUES, UNPAIRED IN SPACE:

	STABILITY D			STABILITY E			STABILITY F		
WIND SPEED(M/S)	0-1	1-3	GT 3	0-1	1-3	GT 3	0-1	1-3	GT 3
# OF DATA PAIRS	27	321	2012	25	360	1364	48	353	299
MEAN FOR OBS	157.1	72.1	57.9	407.5	92.7	65.1	166.9	85.9	86.3
MEAN FOR PRE	276.3	199.5	135.3	120.9	202.1	132.7	214.1	191.4	174.4
BIAS (PRE/OBS)	1.8	2.8	2.	.3	2.2	2.0	1.3	2.2	2.0
RMS ERROR	887.2	579.9	532.6	1212.4	636.6	537.1	834.1	631.4	694.8
V/Co2	31.9	64.7	84.5	8.9	47.2	68.0	25.0	54.0	64.9
V/(CoCp)	18.1	23.4	36.2	29.9	21.6	33.4	19.5	24.2	32.1
% WITHIN FACTOR 2	15.	13.	13.	28.	11.	9.	13.	7.	14.

AVERAGE OF THE TOP 10 VALUES FROM EACH 1-HOUR PERIOD:

	STABILITY D			STABILITY E			STABILITY F		
WIND SPEED(M/S)	0-1	1-3	GT 3	0-1	1-3	GT 3	0-1	1-3	GT 3
# OF DATA PAIRS	27	321	2012	25	360	1364	48	353	299
MEAN FOR OBS	32.5	22.6	17.9	74.6	27.0	19.5	33.8	20.7	20.3
MEAN FOR PRE	29.8	28.7	20.5	17.0	27.3	21.0	30.4	31.4	29.3
BIAS (PRE/OBS)	.92	1.27	1.15	.23	1.01	1.08	.90	1.52	1.45
RMS ERROR	126.4	108.7	88.9	198.7	101.2	128.3	115.8	126.3	176.5
V/Co2	15.1	23.2	24.6	7.1	14.1	43.4	11.7	37.2	76.0
V/(CoCp)	16.5	18.3	21.5	31.2	13.9	40.4	13.0	24.6	52.5
% WITHIN FACTOR 2	15.	17.	11.	20.	13.	9.	15.	10.	16.

TABLE E-45

EVALUATION STATISTICS FOR DATA SUBSET PAIRED IN TIME
(SUBDIVIDED INTO STABILITY AND WIND SPEED CLASSES)

1-HOUR AVERAGES TRACER: SO2 SITE: WIDOWS CREEK

MODEL: CTDM (DEGR2) THRESHOLD: .00 ug/m**3

(Concentrations given in units of micrograms per cubic meter.)

HIGHEST 1-HOUR VALUES, UNPAIRED IN SPACE:

	STABILITY D			STABILITY E			STABILITY F		
WIND SPEED(M/S)	0-1	1-3	GT 3	0-1	1-3	GT 3	0-1	1-3	GT 3
# OF DATA PAIRS	9	267	1906	19	319	1302	7	143	159
MEAN FOR OBS	84.4	79.0	58.2	519.6	89.8	66.0	160.9	77.7	132.4
MEAN FOR PRE	494.2	430.1	369.3	334.3	460.0	404.4	254.9	334.2	381.3
BIAS (PRE/OBS)	5.89	5.45	6.34	.64	5.12	6.13	1.58	4.30	2.88
RMS ERROR	898.9	775.0	705.9	1589.5	875.7	812.0	445.8	813.5	637.2
V/Co2	113.5	96.4	147.0	9.4	95.1	151.4	7.7	109.8	23.2
V/(CoCp)	19.4	17.7	23.2	14.6	18.6	24.7	4.9	25.5	8.0
% WITHIN FACTOR 2	0.	10.	22.	5.	7.	13.	14.	11.	16.

AVERAGE OF THE TOP 10 VALUES FROM EACH 1-HOUR PERIOD:

	STABILITY D			STABILITY E			STABILITY F		
WIND SPEED(M/S)	0-1	1-3	GT 3	0-1	1-3	GT 3	0-1	1-3	GT 3
# OF DATA PAIRS	9	267	1906	19	319	1302	7	143	159
MEAN FOR OBS	19.5	24.5	17.9	90.3	26.7	19.6	54.6	21.9	25.9
MEAN FOR PRE	121.6	99.0	63.9	81.9	115.8	77.5	73.2	111.8	76.6
BIAS (PRE/OBS)	6.24	4.05	3.57	.91	4.34	3.95	1.34	5.12	2.96
RMS ERROR	268.0	212.8	136.7	346.6	276.7	182.3	140.1	325.3	151.9
V/Co2	189.0	75.7	58.3	14.7	107.7	86.3	6.6	221.7	34.4
V/(CoCp)	30.3	18.7	16.3	16.2	24.8	21.8	4.9	43.3	11.6
% WITHIN FACTOR 2	22.	16.	23.	5.	12.	16.	14.	8.	17.

TABLE E-46

EVALUATION STATISTICS FOR DATA SUBSET PAIRED IN TIME
(SUBDIVIDED INTO STABILITY AND WIND SPEED CLASSES)

1-HOUR AVERAGES TRACER: SO2 SITE: WIDOWS CREEK

MODEL: COMPLEX I THRESHOLD: .00 ug/m**3

(Concentrations given in units of micrograms per cubic meter.)

HIGHEST 1-HOUR VALUES, UNPAIRED IN SPACE:

	STABILITY D			STABILITY E			STABILITY F		
WIND SPEED(M/S)	0-1	1-3	GT 3	0-1	1-3	GT 3	0-1	1-3	GT 3
# OF DATA PAIRS	31	341	2118	26	385	1422	50	369	323
MEAN FOR OBS	158.8	70.2	57.1	392.8	92.9	64.4	161.8	84.4	105.
MEAN FOR PRE	.38	3.30	18.6	1729.8	1108.3	470.3	1637.8	1735.6	581.
BIAS (PRE/OBS)	.00	.05	.33	4.4	11.9	7.3	10.1	20.6	5.5
RMS ERROR	516.3	184.9	84.6	2014.5	1944.2	1090.2	2959.5	3146.0	1113.
V/Co2	10.6	6.9	2.2	26.3	438.5	286.9	334.4	1390.1	112.6
V/(CoCp)	4391.0	147.7	6.8	6.0	36.7	39.3	33.0	67.6	20.4
% WITHIN FACTOR 2	16.	6.	19.	15.	6.	10.	14.	3.	11.

AVERAGE OF THE TOP 10 VALUES FROM EACH 1-HOUR PERIOD:

	STABILITY D			STABILITY E			STABILITY F		
WIND SPEED(M/S)	0-1	1-3	GT 3	0-1	1-3	GT 3	0-1	1-3	GT 3
# OF DATA PAIRS	31	341	2118	26	385	1422	50	369	323
MEAN FOR OBS	32.57	22.19	17.71	71.81	26.72	19.30	33.10	20.48	21.93
MEAN FOR PRE	.04	.37	2.09	201.81	125.92	54.67	176.47	203.58	70.85
BIAS (PRE/OBS)	.00	.02	.12	2.81	4.71	2.83	5.33	9.94	3.23
RMS ERROR	100.9	55.4	22.6	262.6	223.8	131.0	328.7	392.0	143.4
V/Co2	9.60	6.24	1.63	13.37	70.14	46.07	98.63	366.3	42.74
V/(CoCp)	8176	376.6	13.82	4.76	14.89	16.27	18.50	36.85	13.23
% WITHIN FACTOR 2	16.	2.	12.	8.	11.	14.	10.	5.	15.

TABLE E-47

EVALUATION STATISTICS FOR DATA SUBSET PAIRED IN TIME
(SUBDIVIDED INTO STABILITY AND WIND SPEED CLASSES)

1-HOUR AVERAGES TRACER: SO2 SITE: WIDOW CREEK

MODEL: RTDM (DEFAULT) THRESHOLD: .00 ug/m**3

(Concentrations given in units of microseconds per cubic meter.)

HIGHEST 1-HOUR VALUES, UNPAIRED IN SPACE:

	STABILITY D			STABILITY E			STABILITY F		
WIND SPEED(M/S)	0-1	1-3	GT 3	0-1	1-3	GT 3	0-1	1-3	GT 3
# OF DATA PAIRS	31	341	2118	26	385	1422	50	369	323
MEAN FOR OBS	158.8	70.2	57.1	392.8	92.9	64.4	161.8	84.4	105.0
MEAN FOR PRE	191.1	315.2	229.2	602.6	502.2	297.9	421.5	634.2	452.5
BIAS (PRE/OBS)	1.20	4.49	4.02	1.53	5.41	4.63	2.60	7.52	4.31
RMS ERROR	896.9	799.4	622.6	1721.0	950.9	731.1	1006.2	1121.0	782.4
V/Co2	31.89	129.7	119.0	19.20	104.9	129.0	38.7	176.5	55.5
V/(CoCp)	26.50	28.9	29.7	12.51	19.4	27.9	14.8	23.5	12.9
% WITHIN FACTOR 2	16.	3.	8.	4.	4.	6.	12.	2.	10.

AVERAGE OF THE TOP 10 VALUES FROM EACH 1-HOUR PERIOD:

	STABILITY D			STABILITY E			STABILITY F		
WIND SPEED(M/S)	0-1	1-3	GT 3	0-1	1-3	GT 3	0-1	1-3	GT 3
# OF DATA PAIRS	31	341	2118	26	385	1422	50	369	323
MEAN FOR OBS	32.57	22.19	17.71	71.81	26.72	19.30	33.10	20.48	21.93
MEAN FOR PRE	19.11	34.75	25.56	60.26	57.84	33.83	47.64	74.29	51.71
BIAS (PRE/OBS)	.59	1.57	1.44	.84	2.16	1.75	1.44	3.63	2.36
RMS ERROR	123.2	94.3	72.4	223.5	115.9	87.4	127.8	134.6	94.5
V/Co2	14.31	18.05	16.69	9.69	18.79	20.50	14.91	43.20	18.56
V/(CoCp)	24.39	11.53	11.57	11.54	8.68	11.69	10.36	11.91	7.87
% WITHIN FACTOR 2	19.	7.	9.	8.	9.	12.	14.	9.	17.

TABLE E-48

EVALUATION STATISTICS FOR DATA SUBSET PAIRED IN TIME
(SUBDIVIDED INTO STABILITY AND WIND SPEED CLASSES)

1-HOUR AVERAGES TRACER: SO2 SITE: WIDOWS CREEK

MODEL: RTDM (ONSITE) THRESHOLD: .00 ug/m**3

(Concentrations given in units of microseconds per cubic meter.)

HIGHEST 1-HOUR VALUES, UNPAIRED IN SPACE:

	STABILITY D			STABILITY E			STABILITY F		
WIND SPEED(M/S)	0-1	1-3	GT 3	0-1	1-3	GT 3	0-1	1-3	GT 3
# OF DATA PAIRS	31	341	2118	26	385	1422	50	369	323
MEAN FOR OBS	158.81	70.19	57.05	392.80	92.85	64.36	161.84	84.38	104.99
MEAN FOR PRE	.62	.41	5.09	344.30	112.15	36.20	639.39	209.26	53.20
BIAS (PRE/OBS)	.00	.01	.09	.88	1.21	.56	3.95	2.48	.51
RMS ERROR	516.28	186.66	93.23	803.85	261.53	134.00	1810.39	660.08	246.69
V/Co2	10.57	7.07	2.67	4.19	7.93	4.33	125.14	61.19	5.52
V/(CoCp)	2723.5	1220.3	29.94	4.78	6.57	7.71	31.67	24.68	10.90
% WITHIN FACTOR 2	16.	1.	9.	42.	31.	18.	22.	21.	21.

AVERAGE OF THE TOP 10 VALUES FROM EACH 1-HOUR PERIOD:

	STABILITY D			STABILITY E			STABILITY F		
WIND SPEED(M/S)	0-1	1-3	GT 3	0-1	1-3	GT 3	0-1	1-3	GT 3
# OF DATA PAIRS	31	341	2118	26	385	1422	50	369	323
MEAN FOR OBS	32.57	22.19	17.71	71.81	26.72	19.30	33.10	20.48	21.93
MEAN FOR PRE	.16	.07	.66	73.80	22.46	5.10	79.11	29.37	7.59
BIAS (PRE/OBS)	.00	.00	.04	1.03	.84	.26	2.39	1.43	.35
RMS ERROR	100.88	55.57	23.74	132.4	62.38	27.00	203.74	74.39	32.44
V/Co2	9.59	6.27	1.80	3.40	5.45	1.96	37.89	13.19	2.19
V/(CoCp)	1981.8	1971.2	48.16	3.31	6.48	7.40	15.85	9.20	6.32
% WITHIN FACTOR 2	16.	1.	5.	38.	30.	13.	24.	20.	17.

APPENDIX F
SCATTER PLOTS OF PEAK HOURLY MODEL PREDICTIONS AND OBSERVATIONS

APPENDIX F

SCATTER PLOTS OF PEAK HOURLY MODEL PREDICTIONS AND OBSERVATIONS

Scatter plots of modeled predictions versus observations were generated to augment the statistic tables of model evaluation results presented elsewhere in this report. For the FSPS, Westvaco, and Widows Creek sites, plots of the predicted-to-observed ratio of peak-concentrations versus plume travel distance are presented as residual plots. In these plots, each point represents the average of the top 10 concentrations at each monitor. A guide to the figures in this appendix is given below.

Figures	Description
F-1 through F-6	Predicted vs. observed peak 1-hour SF_6 concentrations at CCB
F-7 through F-12	Predicted vs. observed peak 1-hour CF_3Br concentrations at CCB
F-13 through F-18	Predicted vs. observed peak 1-hour SF_6 concentrations at HBR
F-19 through F-24	Predicted vs observed peak 1-hour CF_3Br concentrations at HBR
F-25 through F-32	Predicted vs. observed peak 1-hour SF_6 concentrations at FSPS
F-33 through F-38	Predicted vs. observed peak 1-hour CF_3Br concentrations at FSPS
F-39 through F-44	Predicted observed ratio vs. distance for SF_6 concentrations at FSPS
F-45 thorugh F-50	Predicted observed ratio vs. distance for CF_3Br concentrations at FSPS
F-51 through F-56	Predicted vs. observed peak 1-hour SO_2 concentrations at Westvaco
F-57 through F-62	Predicted vs. observed peak 3-hour SO_2 concentrations at Westvaco
F-63 thorugh F-68	Predicted/observed ratio vs. distance for 1-hour SO_2 concentrations at Westvaco
F-69 through F-74	Predicted vs. observed peak 1-hour SO_2 concentrations at Widows Creek

Figures	Description
F-75 through F-80	Predicted vs. observed peak 3-hour SO_2 concentrations at Widows Creek
F-81 through F-86	Predicted/observed ratio vs. distance for 1-hour SO_2 concentrations at Widows Creek

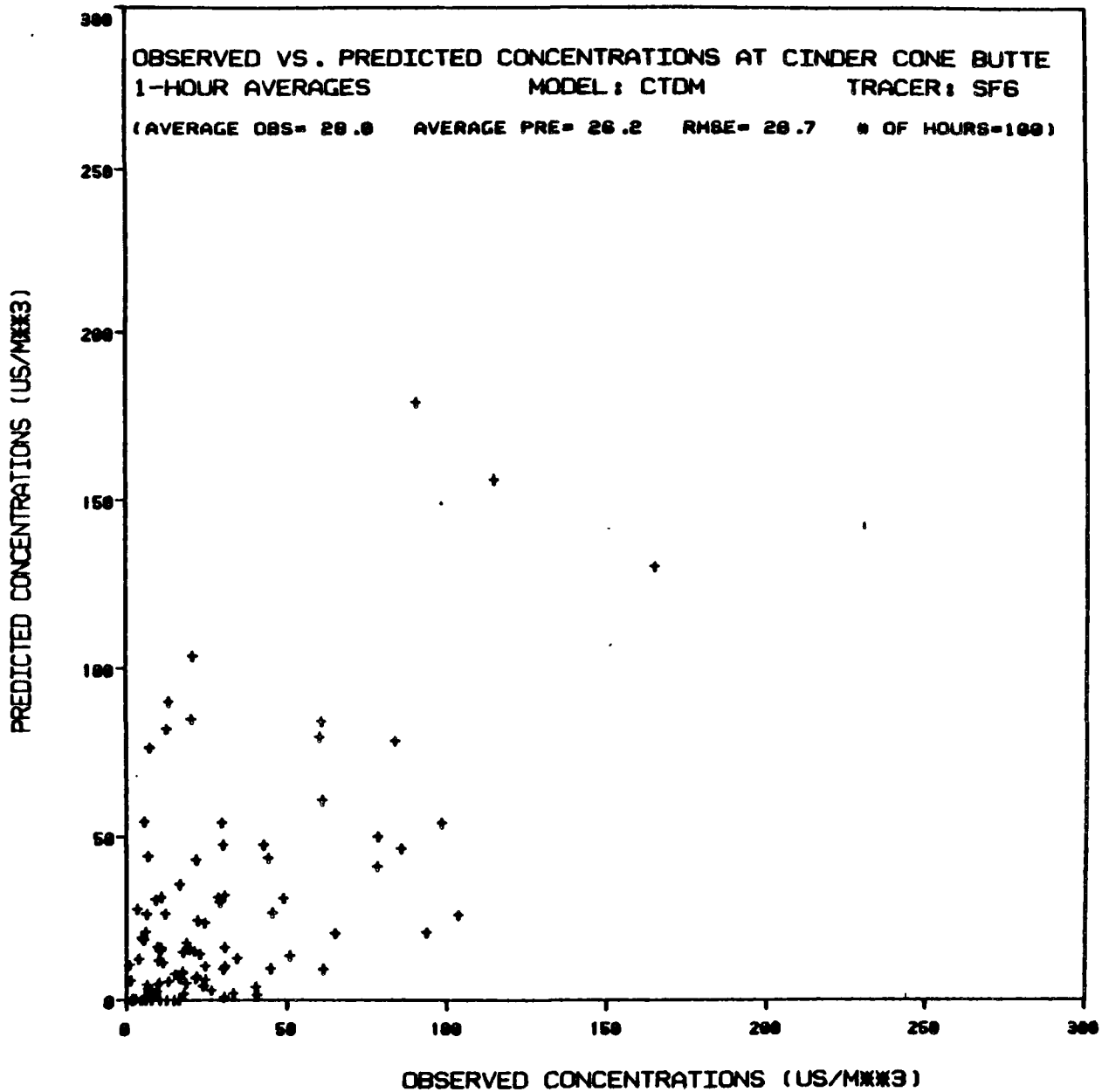
OBSERVED VS. PREDICTED CONCENTRATIONS AT CINDER CONE BUTTE
1-HOUR AVERAGES MODEL: CTDM TRACER: SF6
(AVERAGE OBS= 28.0 AVERAGE PRE= 26.2 RMSE= 28.7 # OF HOURS=100)
PREDICTED CONCENTRATIONS (US/MXX3)
OBSERVED CONCENTRATIONS (US/MXX3)
0
50
100
150
200
250
300

Figure F-1

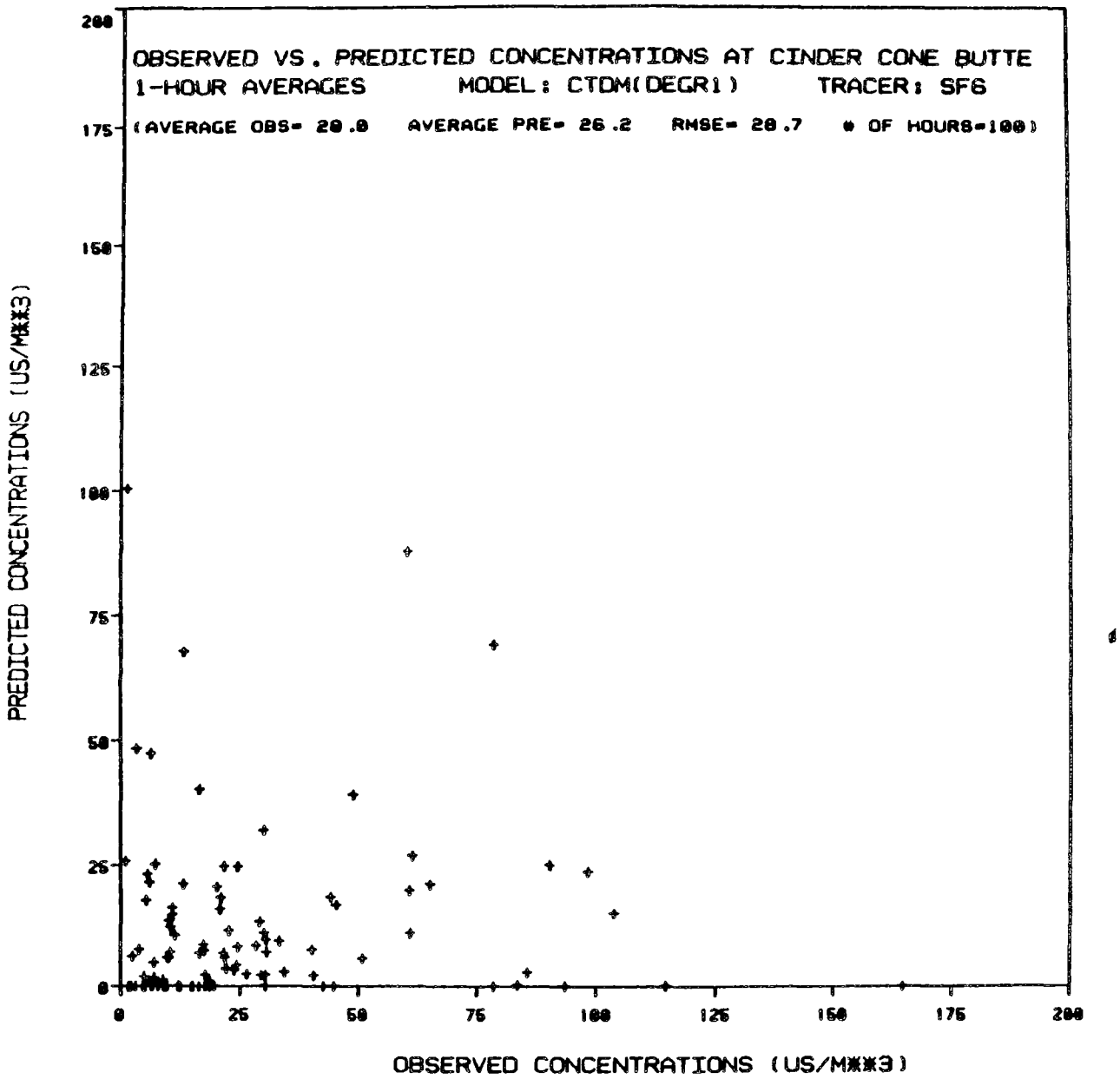
OBSERVED VS. PREDICTED CONCENTRATIONS AT CINDER CONE BUTTE
1-HOUR AVERAGES MODEL: CTDM(DEGR1) TRACER: SF6
(AVERAGE OBS= 20.0 AVERAGE PRE= 26.2 RMSE= 28.7 # OF HOURS=100)
PREDICTED CONCENTRATIONS (US/M**3)
OBSERVED CONCENTRATIONS (US/M**3)
0
25
50
75
100
125
150
175
200

Figure F-2

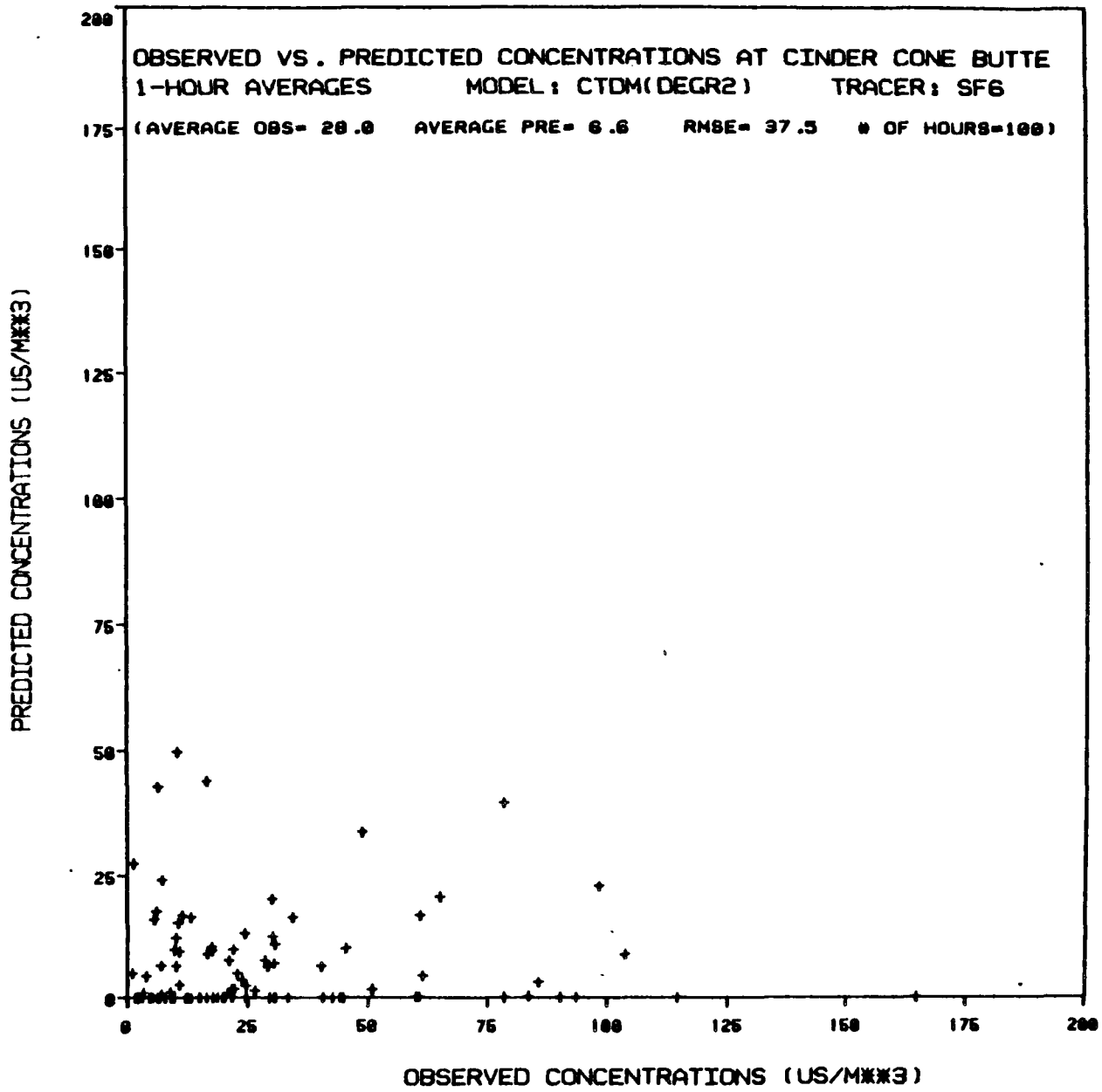
OBSERVED VS. PREDICTED CONCENTRATIONS AT CINDER CONE BUTTE
1-HOUR AVERAGES MODEL: CTDM(DEGR2) TRACER: SF6
(AVERAGE OBS= 28.0 AVERAGE PRE= 6.6 RMSE= 37.5 # OF HOURS=100)
PREDICTED CONCENTRATIONS (US/M**3)
OBSERVED CONCENTRATIONS (US/M**3)
0
25
50
75
100
125
150
175
200

Figure F-3

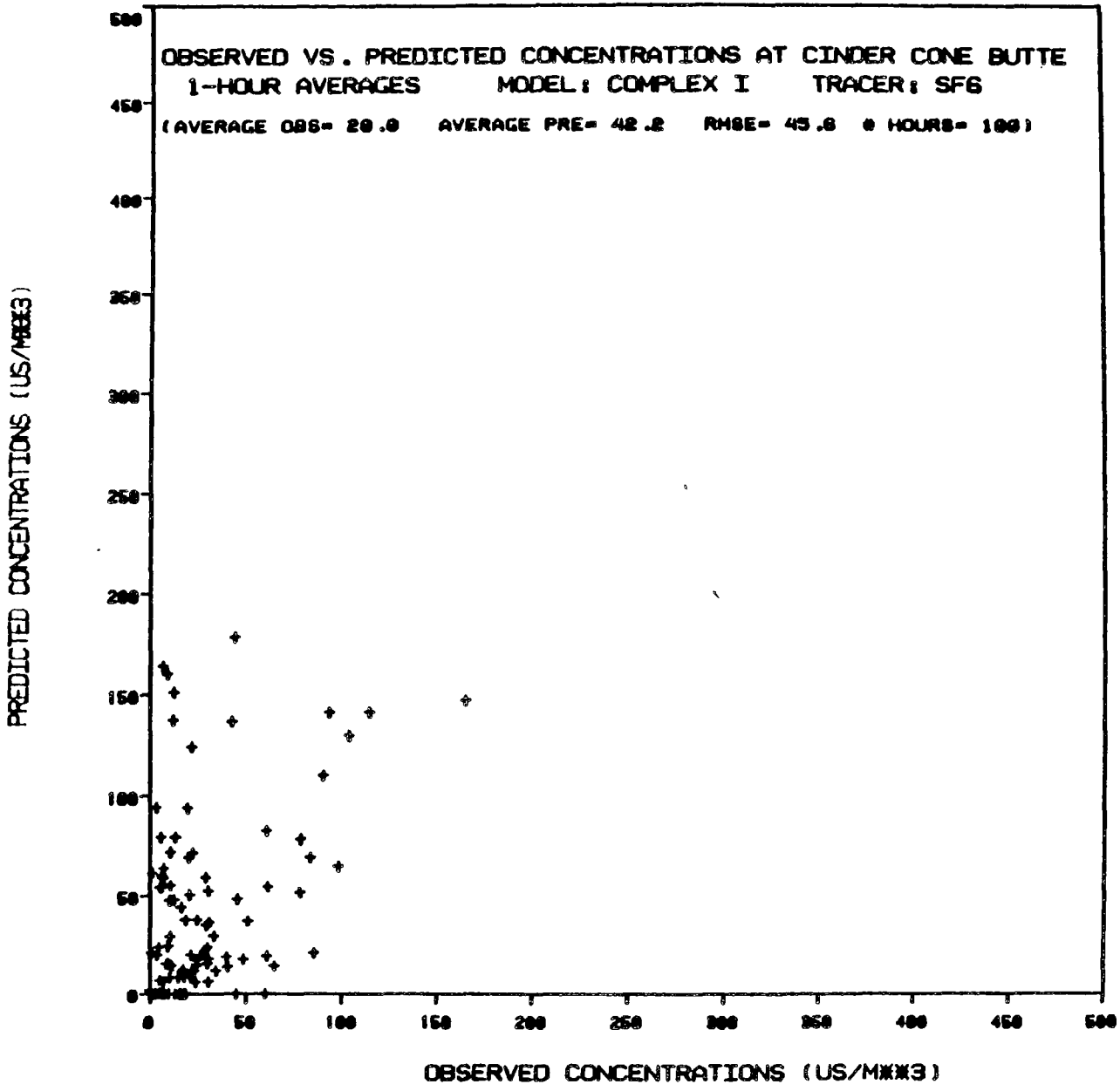
OBSERVED VS. PREDICTED CONCENTRATIONS AT CINDER CONE BUTTE
1-HOUR AVERAGES MODEL: COMPLEX I TRACER: SF6
(AVERAGE OBS= 20.0 AVERAGE PRE= 42.2 RMSE= 45.8 # HOURS= 100)
PREDICTED CONCENTRATIONS (US/MXX3)
OBSERVED CONCENTRATIONS (US/MXX3)
0
50
100
150
200
250
300
350
400
450
500

Figure F-4

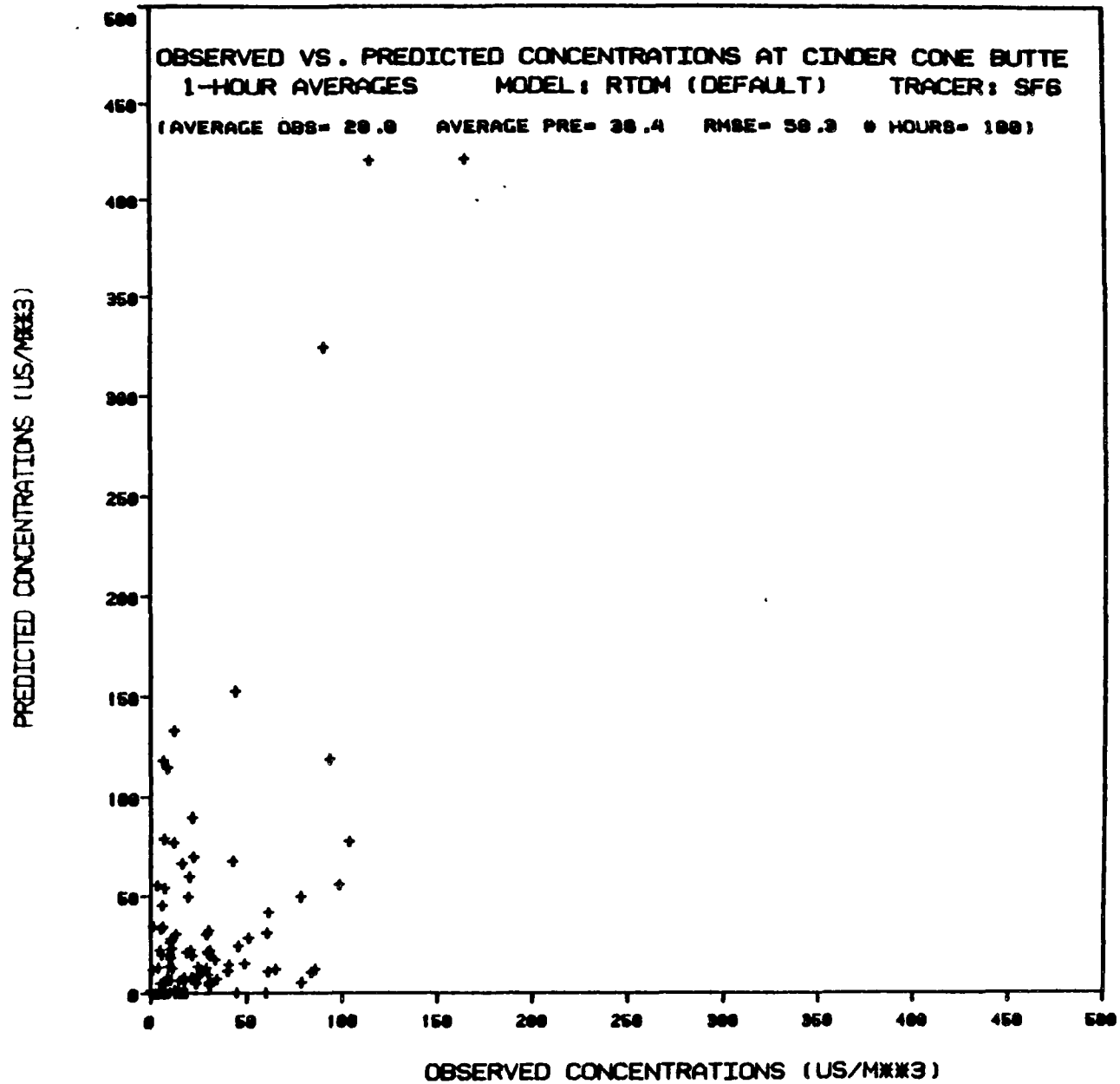
OBSERVED VS. PREDICTED CONCENTRATIONS AT CINDER CONE BUTTE
1-HOUR AVERAGES MODEL: RTDM (DEFAULT) TRACER: SF6
(AVERAGE OBS= 20.0 AVERAGE PRE= 38.4 RMSE= 58.3 # HOURS= 100)
PREDICTED CONCENTRATIONS (US/MXX3)
OBSERVED CONCENTRATIONS (US/MXX3)
0
50
100
150
200
250
300
350
400
450
500

Figure F-5 .

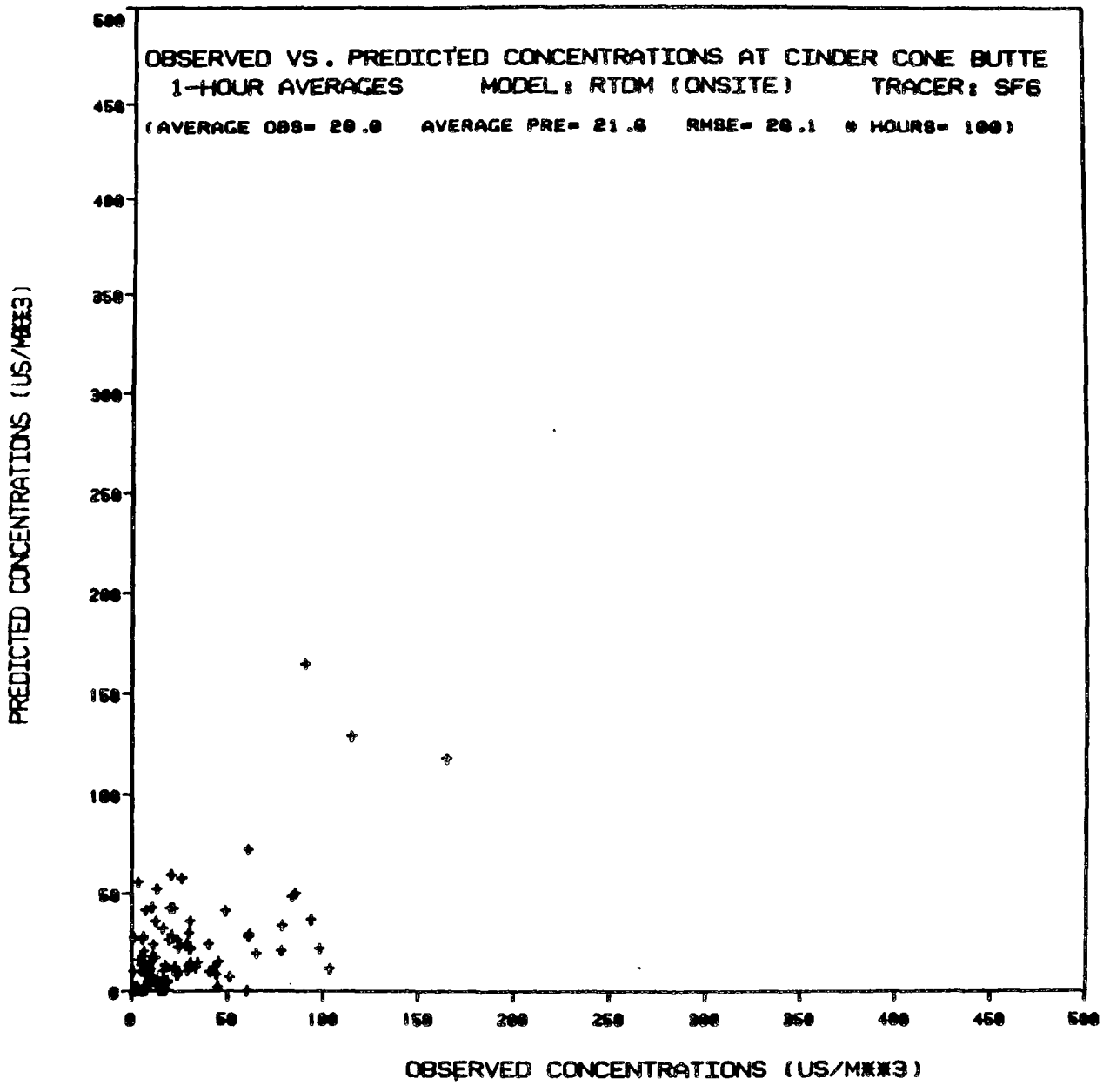
OBSERVED VS. PREDICTED CONCENTRATIONS AT CINDER CONE BUTTE
1-HOUR AVERAGES MODEL: RTDM (ONSITE) TRACER: SF6
(AVERAGE OBS= 20.0 AVERAGE PRE= 21.6 RMSE= 26.1 # HOURS= 100)
PREDICTED CONCENTRATIONS (US/MXX3)
OBSERVED CONCENTRATIONS (US/MXX3)
0
50
100
150
200
250
300
350
400
450
500

Figure F-6

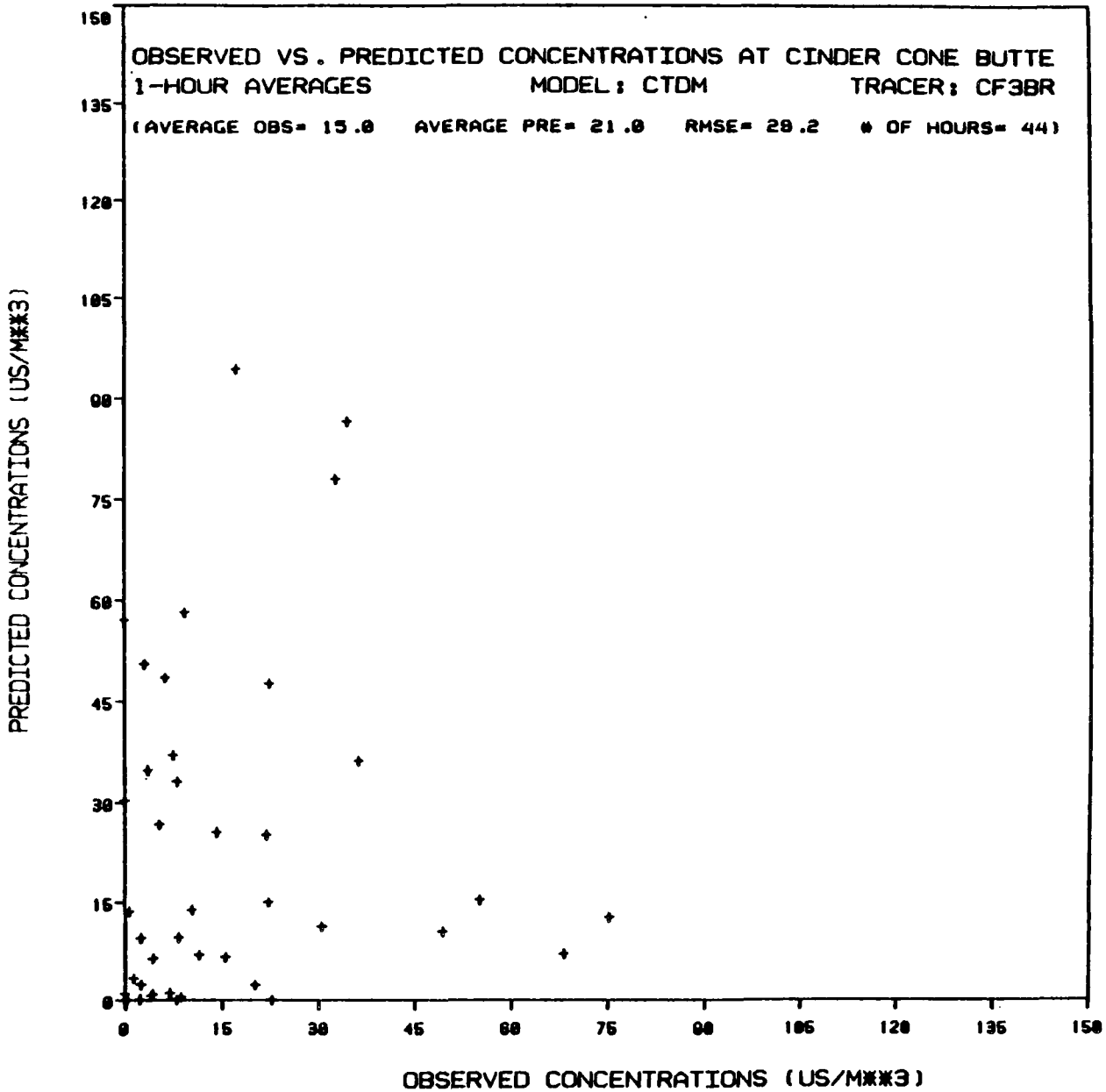
OBSERVED VS. PREDICTED CONCENTRATIONS AT CINDER CONE BUTTE
1-HOUR AVERAGES
MODEL: CTDM
TRACER: CF3BR
(AVERAGE OBS= 15.0 AVERAGE PRE= 21.0 RMSE= 28.2 # OF HOURS= 44)
PREDICTED CONCENTRATIONS (US/M**3)
OBSERVED CONCENTRATIONS (US/M**3)
0
15
30
45
60
75
90
105
120
135
150

Figure F-7

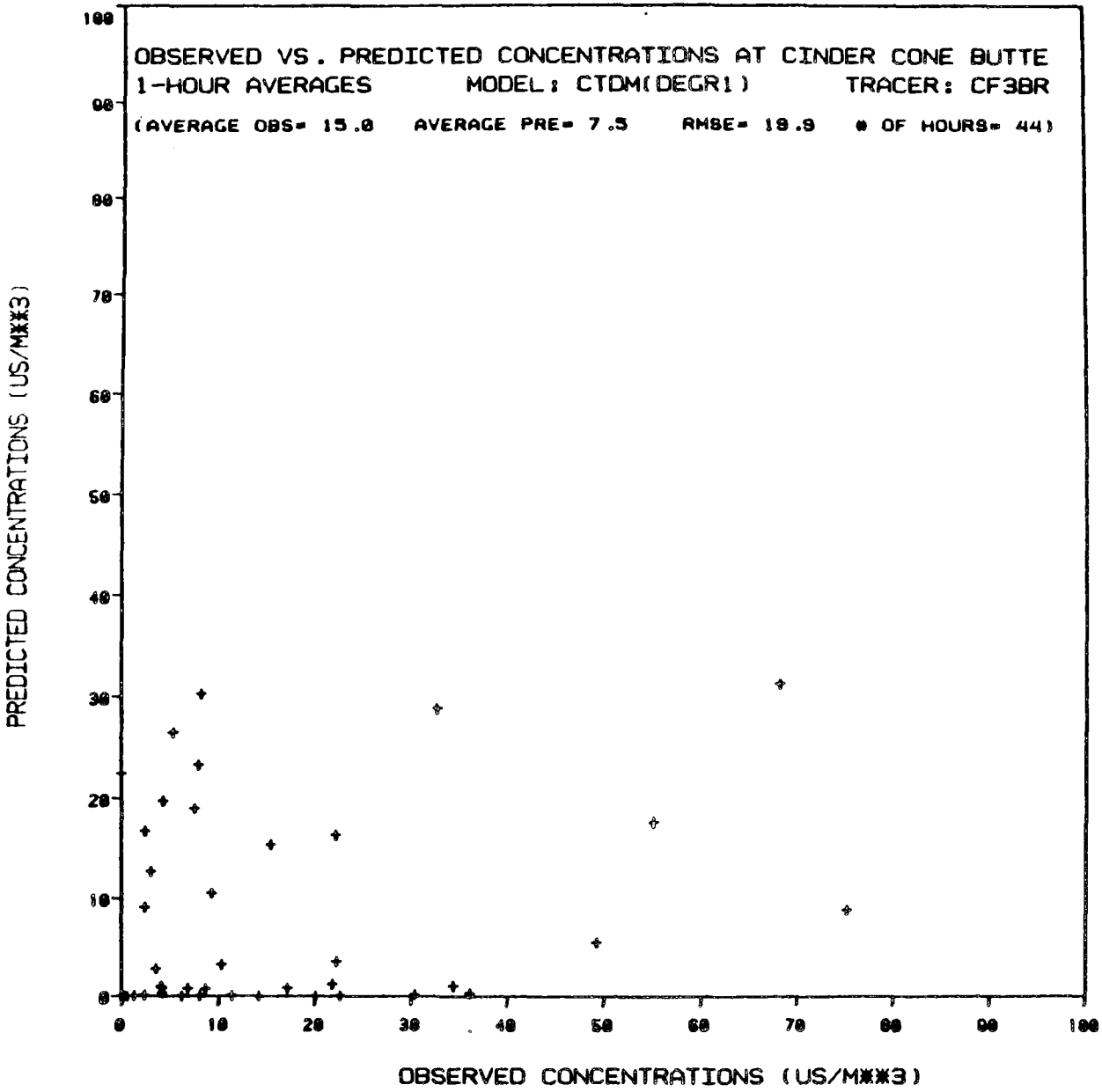
OBSERVED VS. PREDICTED CONCENTRATIONS AT CINDER CONE BUTTE
1-HOUR AVERAGES MODEL: CTDM(DEGR1) TRACER: CF3BR
(AVERAGE OBS= 15.0 AVERAGE PRE= 7.5 RMSE= 19.9 # OF HOURS= 44)
PREDICTED CONCENTRATIONS (US/M**3)
OBSERVED CONCENTRATIONS (US/M**3)
0
10
20
30
40
50
60
70
80
90
100

Figure F-8

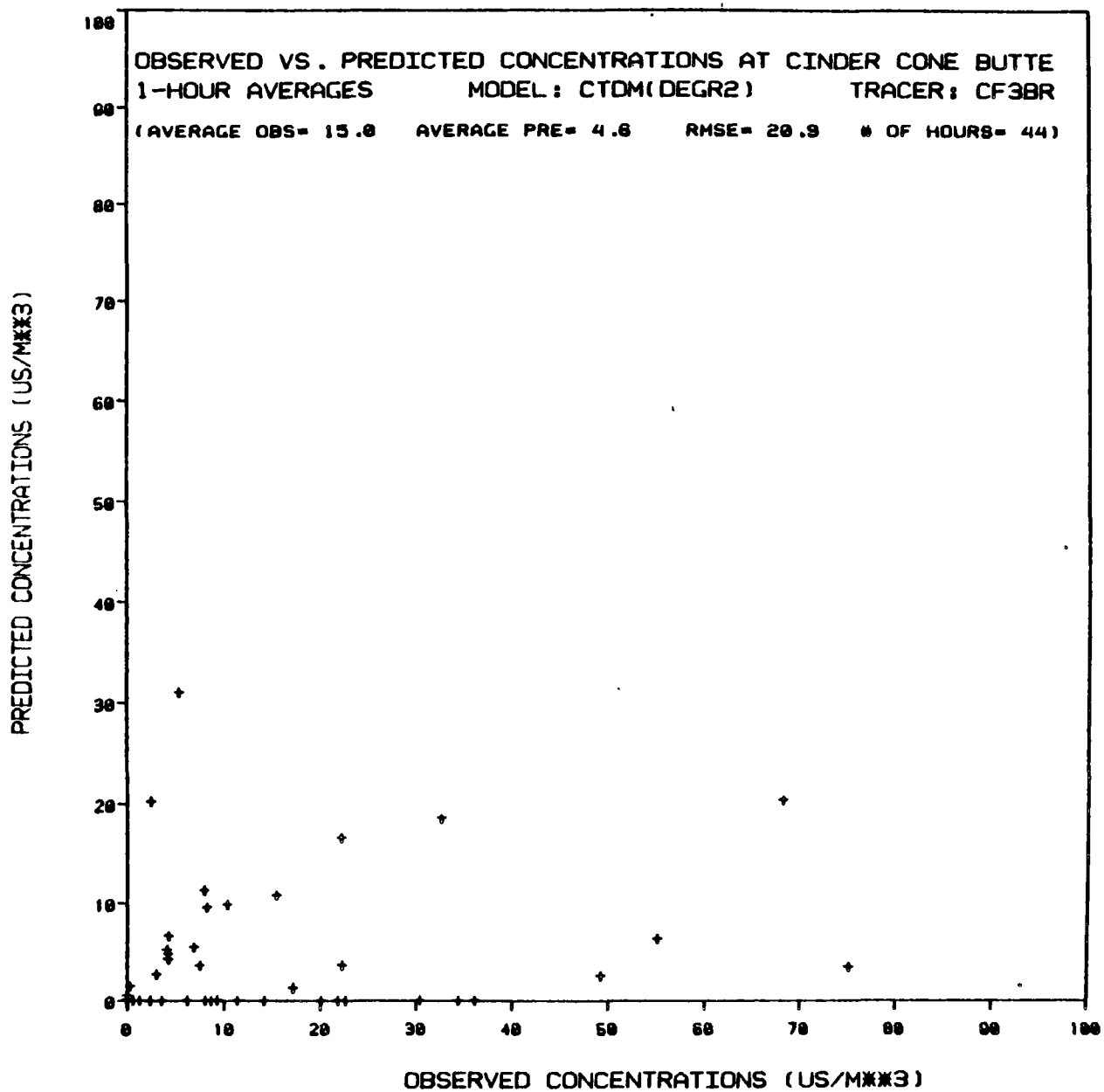
OBSERVED VS. PREDICTED CONCENTRATIONS AT CINDER CONE BUTTE
1-HOUR AVERAGES MODEL: CTDM(DEGR2) TRACER: CF3BR
(AVERAGE OBS= 15.0 AVERAGE PRE= 4.6 RMSE= 20.9 # OF HOURS= 44)
PREDICTED CONCENTRATIONS (US/M**3)
OBSERVED CONCENTRATIONS (US/M**3)
0
10
20
30
40
50
60
70
80
90
100

Figure F-9

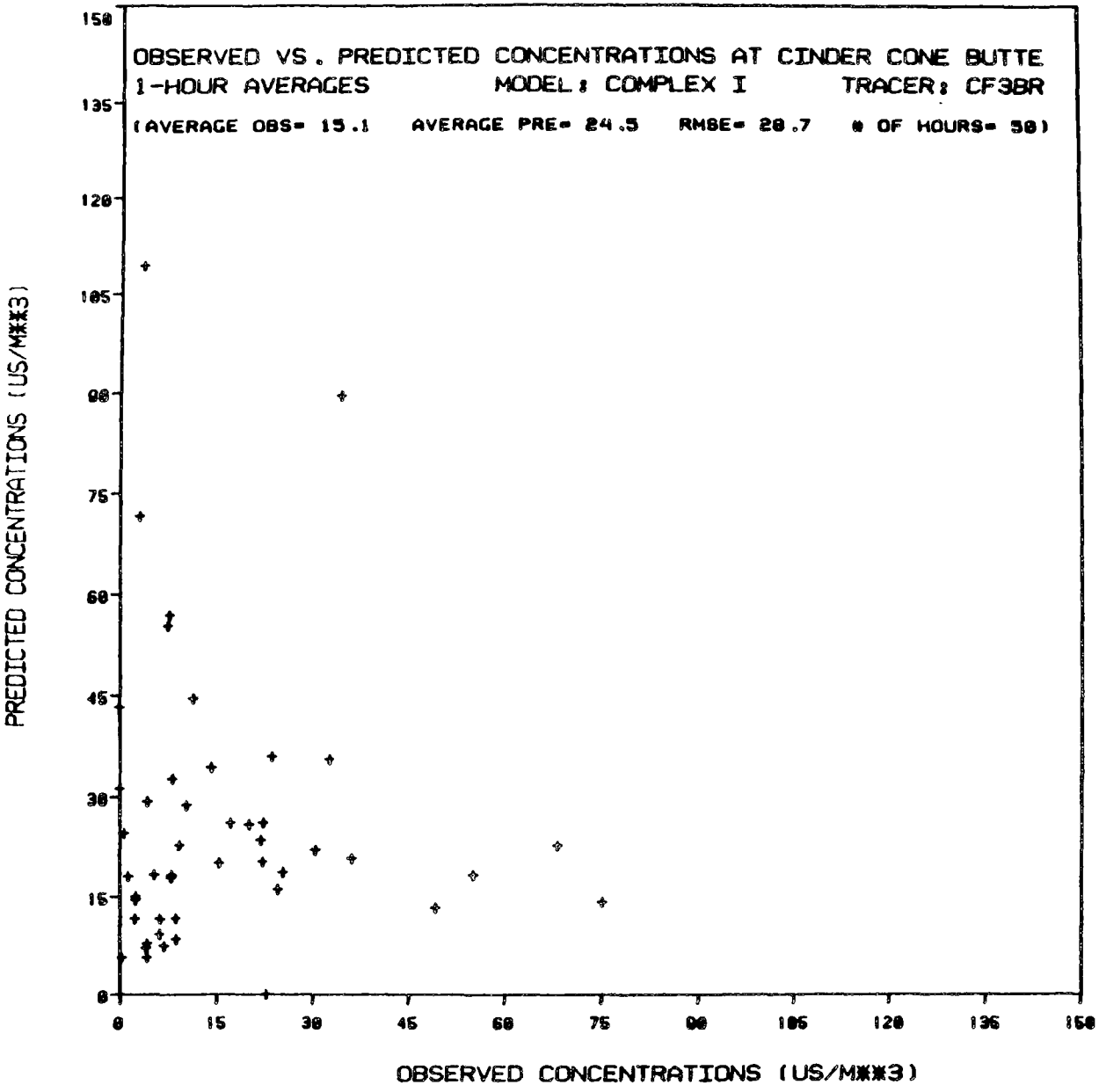
OBSERVED VS. PREDICTED CONCENTRATIONS AT CINDER CONE BUTTE
1-HOUR AVERAGES
MODEL: COMPLEX I
TRACER: CF3BR
(AVERAGE OBS= 15.1 AVERAGE PRE= 24.5 RMSE= 28.7 # OF HOURS= 50)
PREDICTED CONCENTRATIONS (US/M**3)
OBSERVED CONCENTRATIONS (US/M**3)
0
15
30
45
60
75
90
105
120
135
150

Figure F-10

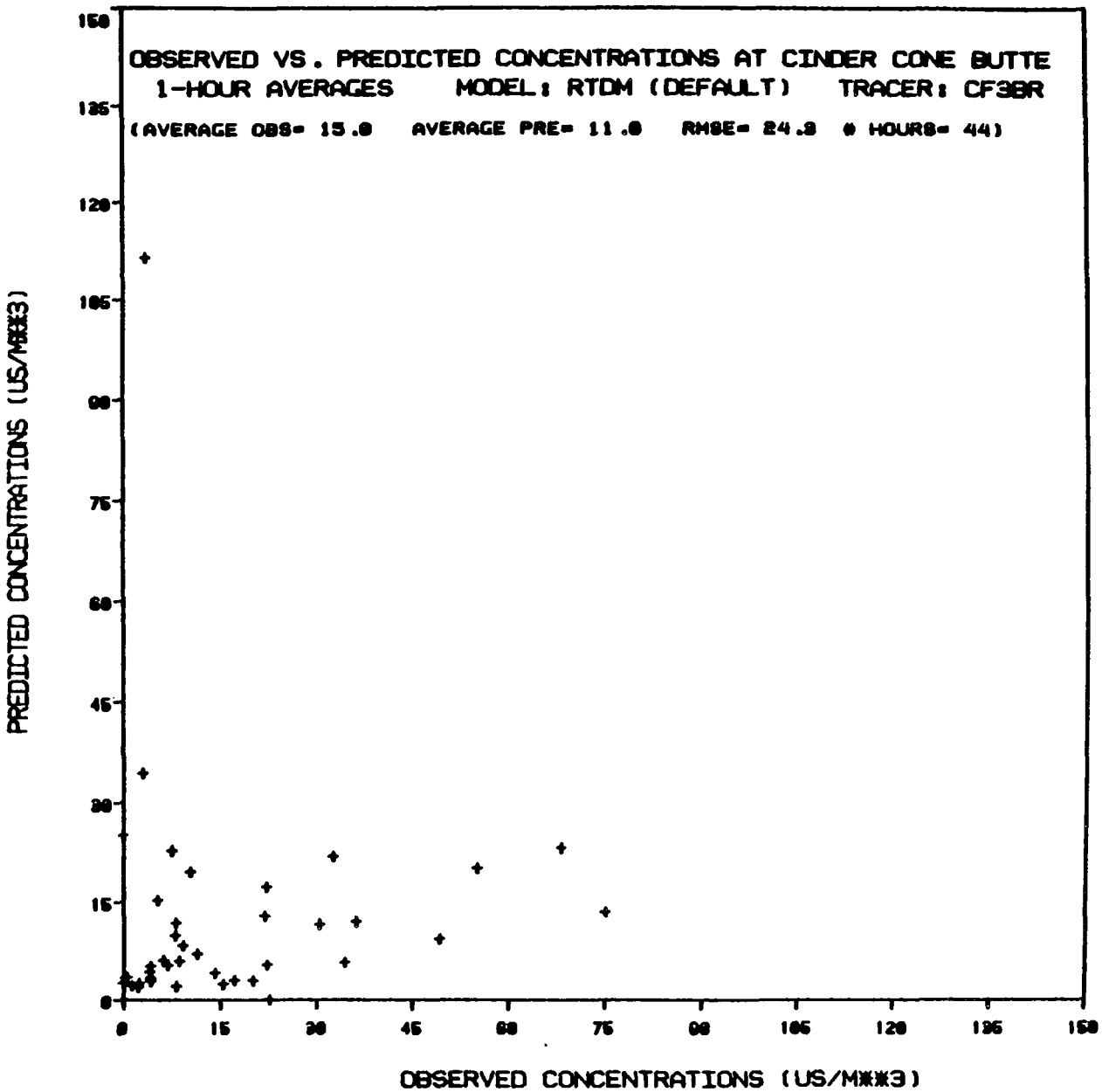
OBSERVED VS. PREDICTED CONCENTRATIONS AT CINDER CONE BUTTE
1-HOUR AVERAGES MODEL: RTDM (DEFAULT) TRACER: CF3BR
(AVERAGE OBS= 15.0 AVERAGE PRE= 11.0 RMSE= 24.3 # HOURS= 44)
PREDICTED CONCENTRATIONS (US/M**3)
OBSERVED CONCENTRATIONS (US/M**3)
0
15
30
45
60
75
90
105
120
135
150

Figure F-11

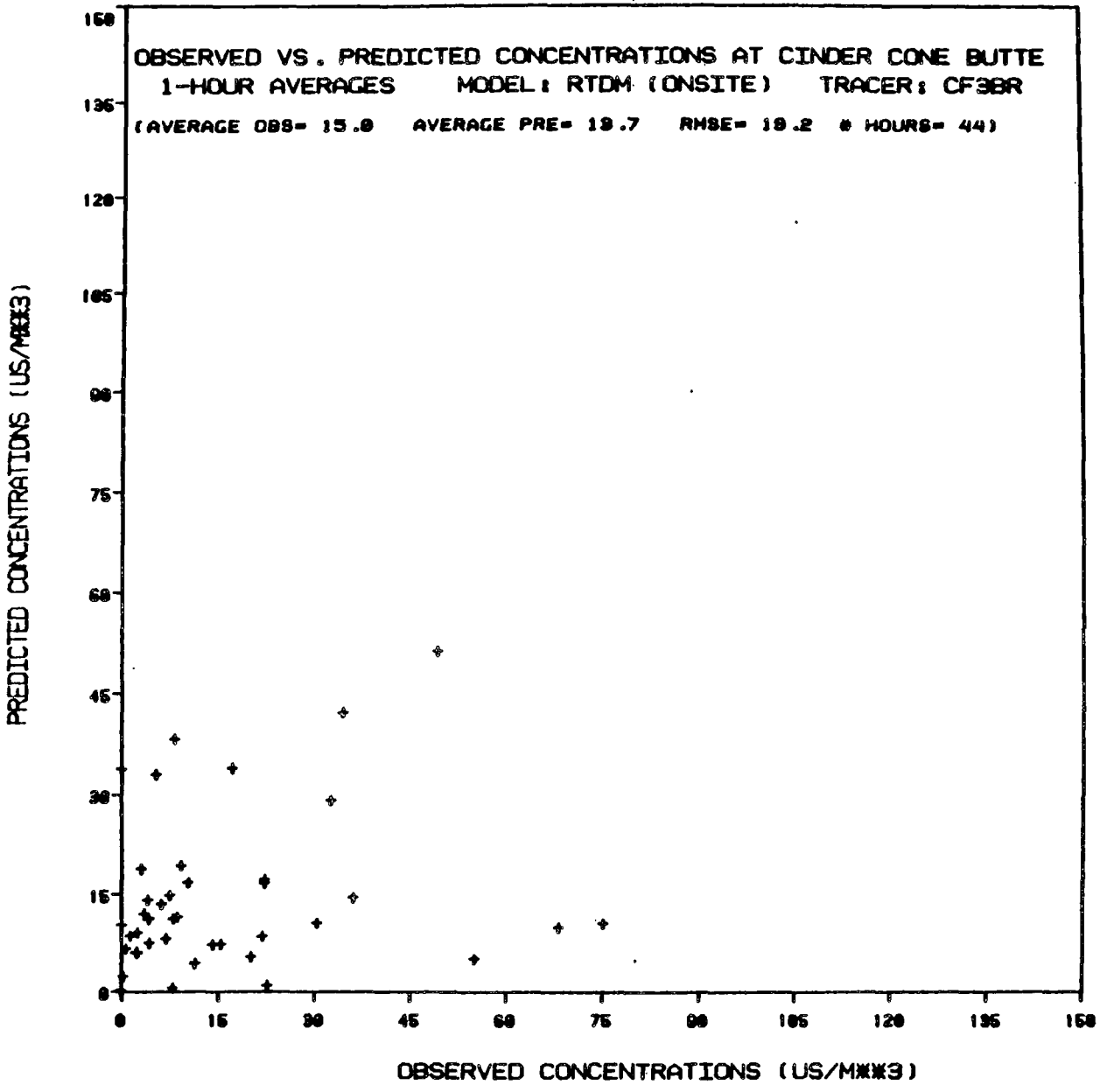
OBSERVED VS. PREDICTED CONCENTRATIONS AT CINDER CONE BUTTE
1-HOUR AVERAGES MODEL: RTDM (ONSITE) TRACER: CF3BR
(AVERAGE OBS= 15.0 AVERAGE PRE= 19.7 RMSE= 19.2 # HOURS= 44)
PREDICTED CONCENTRATIONS (US/M**3)
OBSERVED CONCENTRATIONS (US/M**3)
0
15
30
45
60
75
90
105
120
135
150

Figure F-12

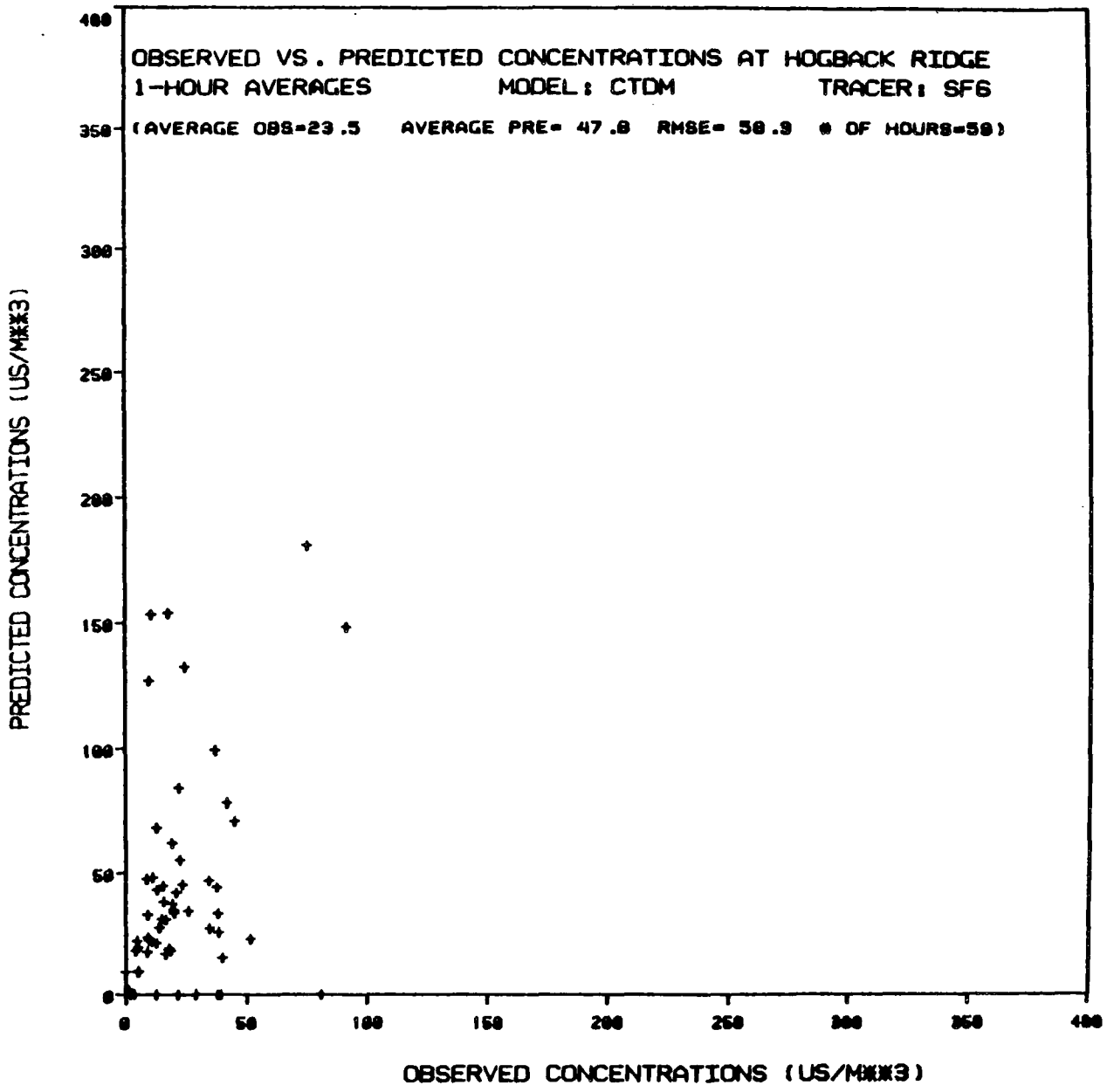
OBSERVED VS. PREDICTED CONCENTRATIONS AT HOGBACK RIDGE
1-HOUR AVERAGES MODEL: CTDM TRACER: SF6
(AVERAGE OBS=23.5 AVERAGE PRE= 47.8 RMSE= 58.9 # OF HOURS=59)
PREDICTED CONCENTRATIONS (US/M**3)
OBSERVED CONCENTRATIONS (US/M**3)
0
50
100
150
200
250
300
350
400

Figure F-13

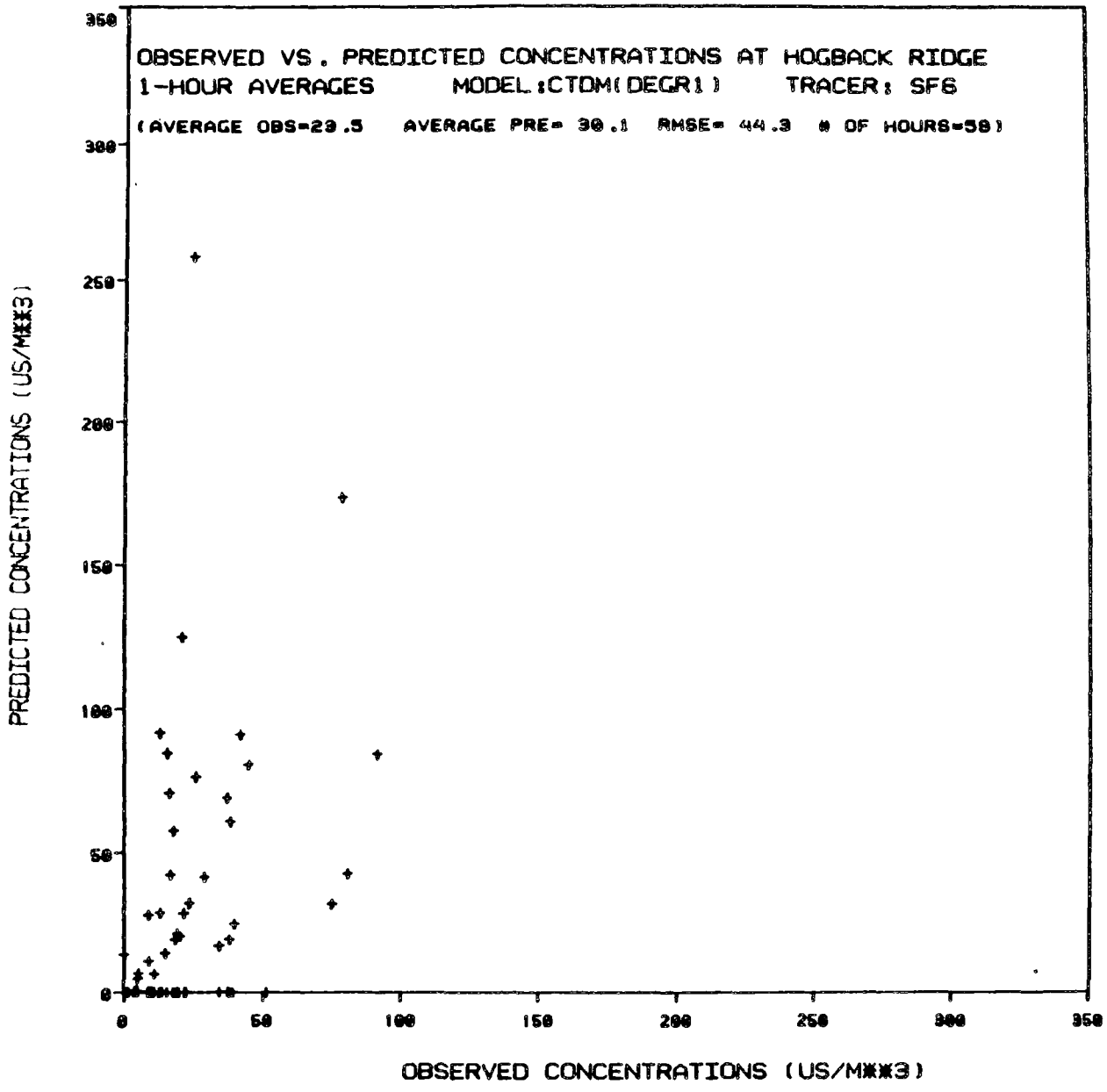
OBSERVED VS. PREDICTED CONCENTRATIONS AT HOGBACK RIDGE
1-HOUR AVERAGES MODEL:CTDM(DEGR1) TRACER: SF6
(AVERAGE OBS=23.5 AVERAGE PRE= 30.1 RMSE= 44.3 # OF HOURS=59)
PREDICTED CONCENTRATIONS (US/M**3)
OBSERVED CONCENTRATIONS (US/M**3)
0
50
100
150
200
250
300
350

Figure F-14

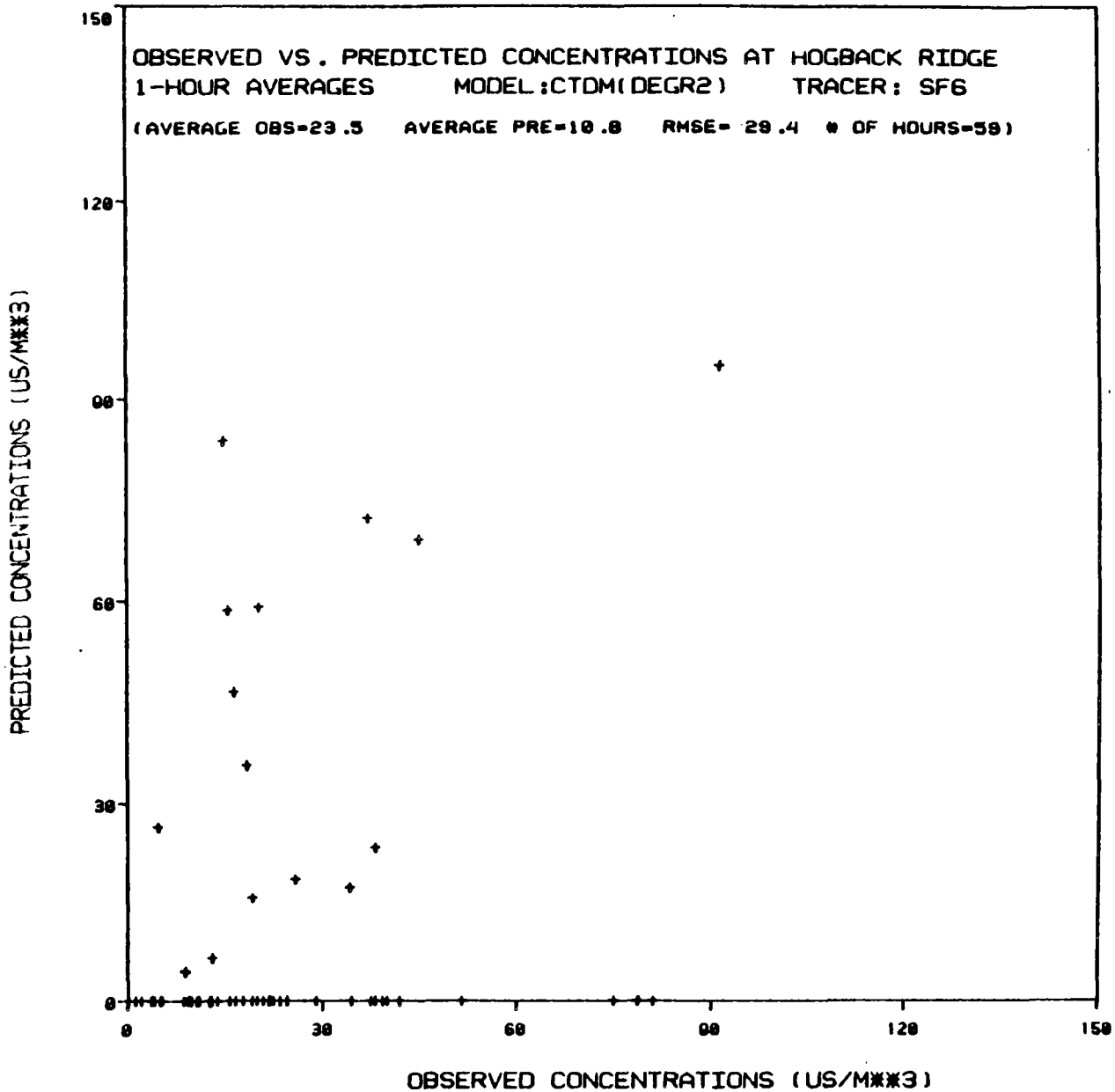
OBSERVED VS. PREDICTED CONCENTRATIONS AT HOGBACK RIDGE
1-HOUR AVERAGES MODEL:CTDM(DEGR2) TRACER: SF6
(AVERAGE OBS=23.5 AVERAGE PRE=10.8 RMSE= 29.4 # OF HOURS=59)
PREDICTED CONCENTRATIONS (US/M**3)
OBSERVED CONCENTRATIONS (US/M**3)
150
120
90
60
30
0
0
30
60
90
120
150

Figure F-15

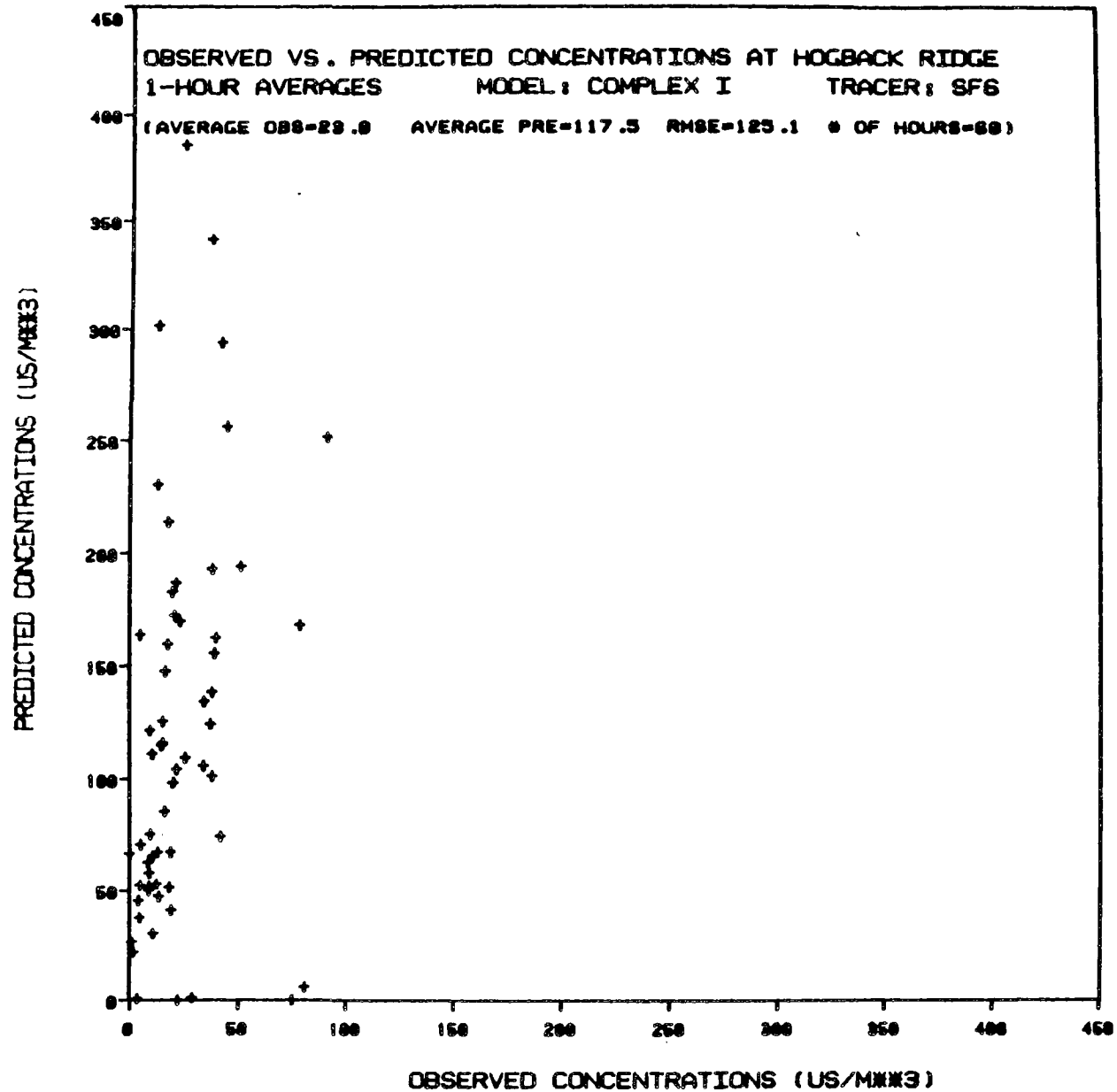
OBSERVED VS. PREDICTED CONCENTRATIONS AT HOGBACK RIDGE
1-HOUR AVERAGES MODEL: COMPLEX I TRACER: SF6
(AVERAGE OBS=23.0 AVERAGE PRE=117.5 RMSE=125.1 # OF HOURS=60)
PREDICTED CONCENTRATIONS (US/MXX3)
OBSERVED CONCENTRATIONS (US/MXX3)
0
50
100
150
200
250
300
350
400
450

Figure F-16

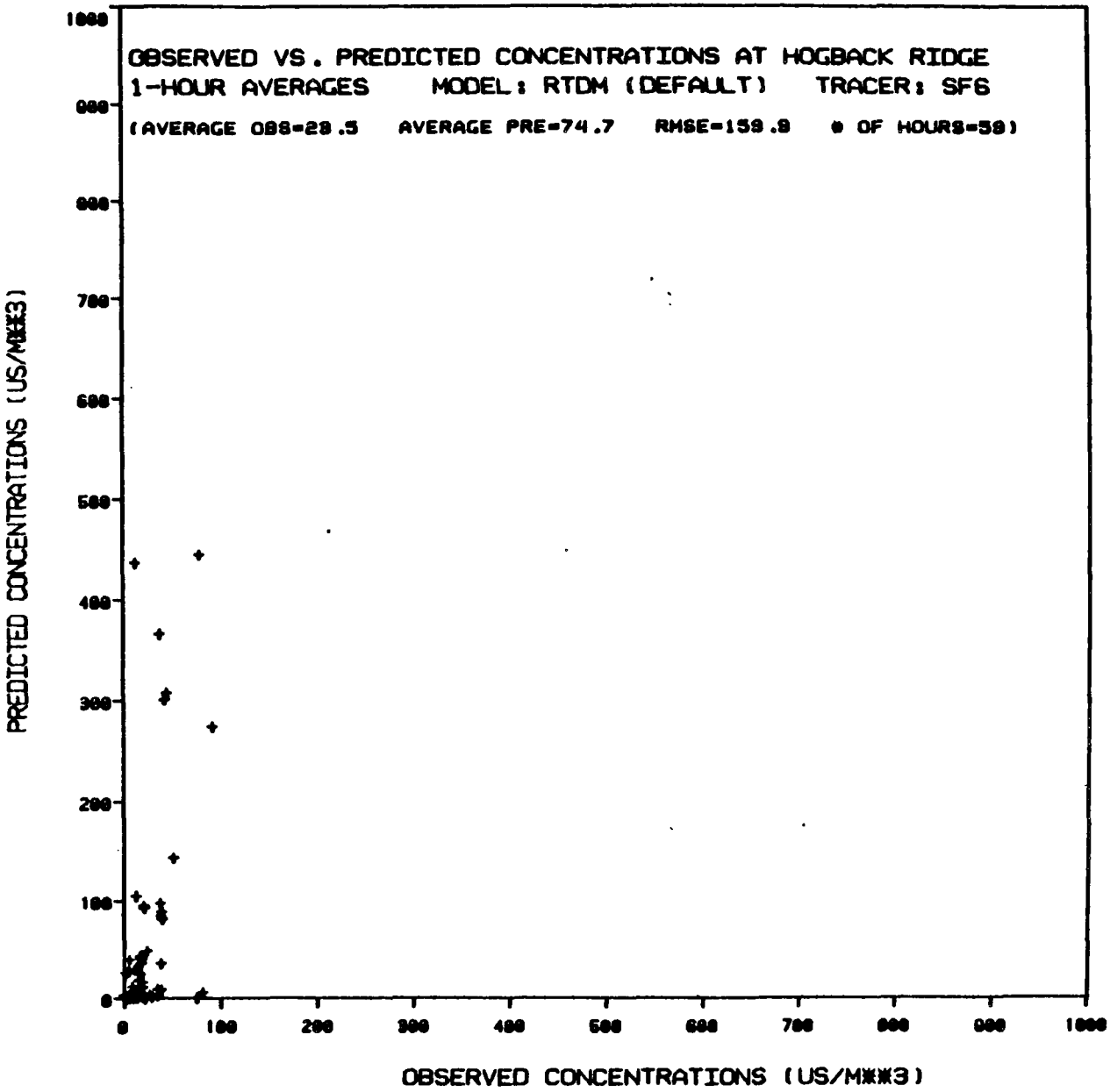
OBSERVED VS. PREDICTED CONCENTRATIONS AT HOGBACK RIDGE
1-HOUR AVERAGES MODEL: RTDM (DEFAULT) TRACER: SF6
(AVERAGE OBS=28.5 AVERAGE PRE=74.7 RMSE=159.8 # OF HOURS=58)
PREDICTED CONCENTRATIONS (US/M**3)
OBSERVED CONCENTRATIONS (US/M**3)
0
100
200
300
400
500
600
700
800
900
1000

Figure F-17

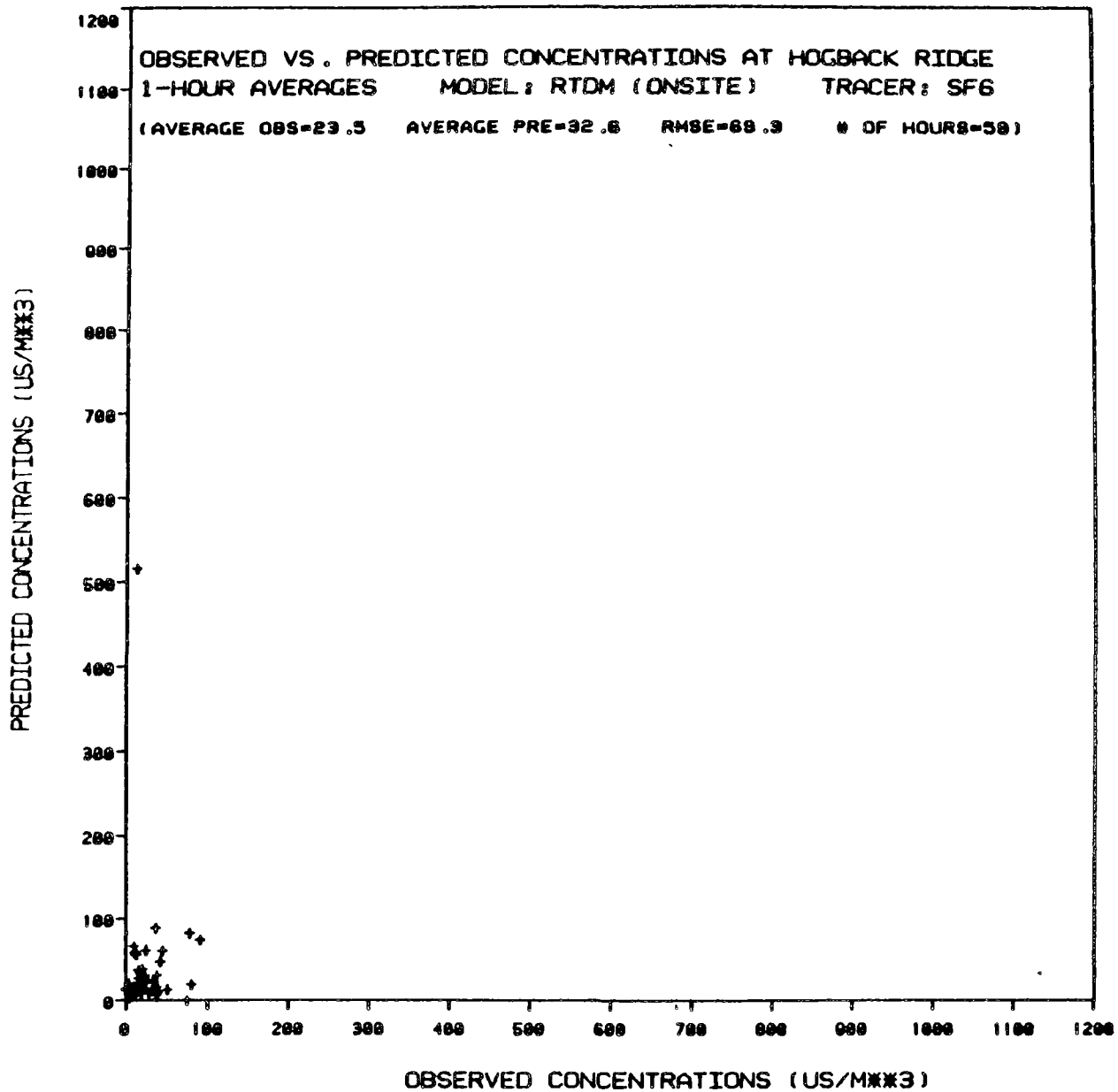
OBSERVED VS. PREDICTED CONCENTRATIONS AT HOGBACK RIDGE
1-HOUR AVERAGES MODEL: RTDM (ONSITE) TRACER: SF6
(AVERAGE OBS=23.5 AVERAGE PRE=32.6 RMSE=68.3 # OF HOURS=59)
PREDICTED CONCENTRATIONS (US/M**3)
OBSERVED CONCENTRATIONS (US/M**3)
0
100
200
300
400
500
600
700
800
900
1000
1100
1200

Figure F-18

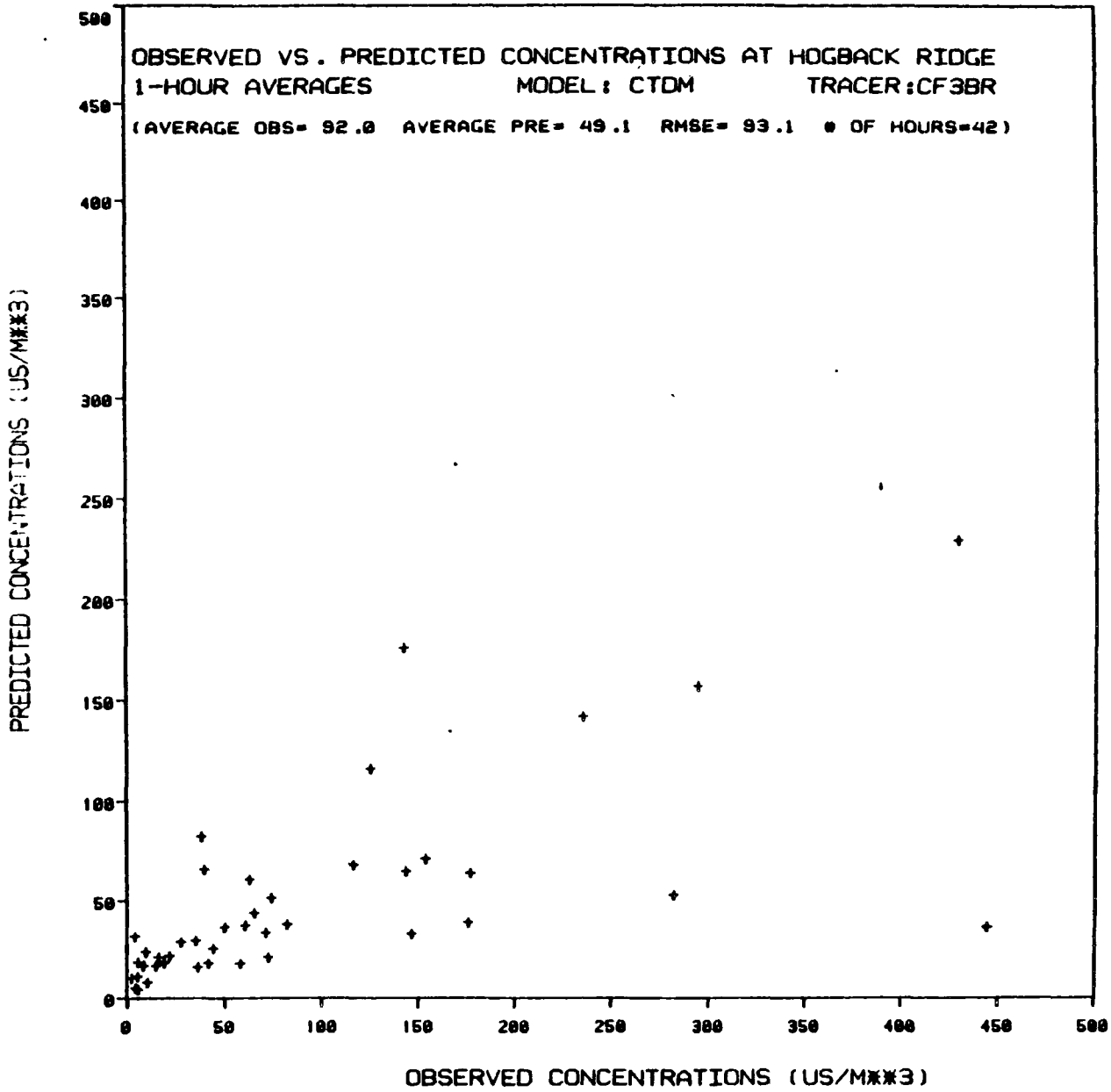
OBSERVED VS. PREDICTED CONCENTRATIONS AT HOGBACK RIDGE
1-HOUR AVERAGES MODEL: CTDM TRACER:CF3BR
(AVERAGE OBS= 92.0 AVERAGE PRE= 49.1 RMSE= 93.1 # OF HOURS=42)
PREDICTED CONCENTRATIONS (US/M**3)
OBSERVED CONCENTRATIONS (US/M**3)
0
50
100
150
200
250
300
350
400
450
500

Figure F-19

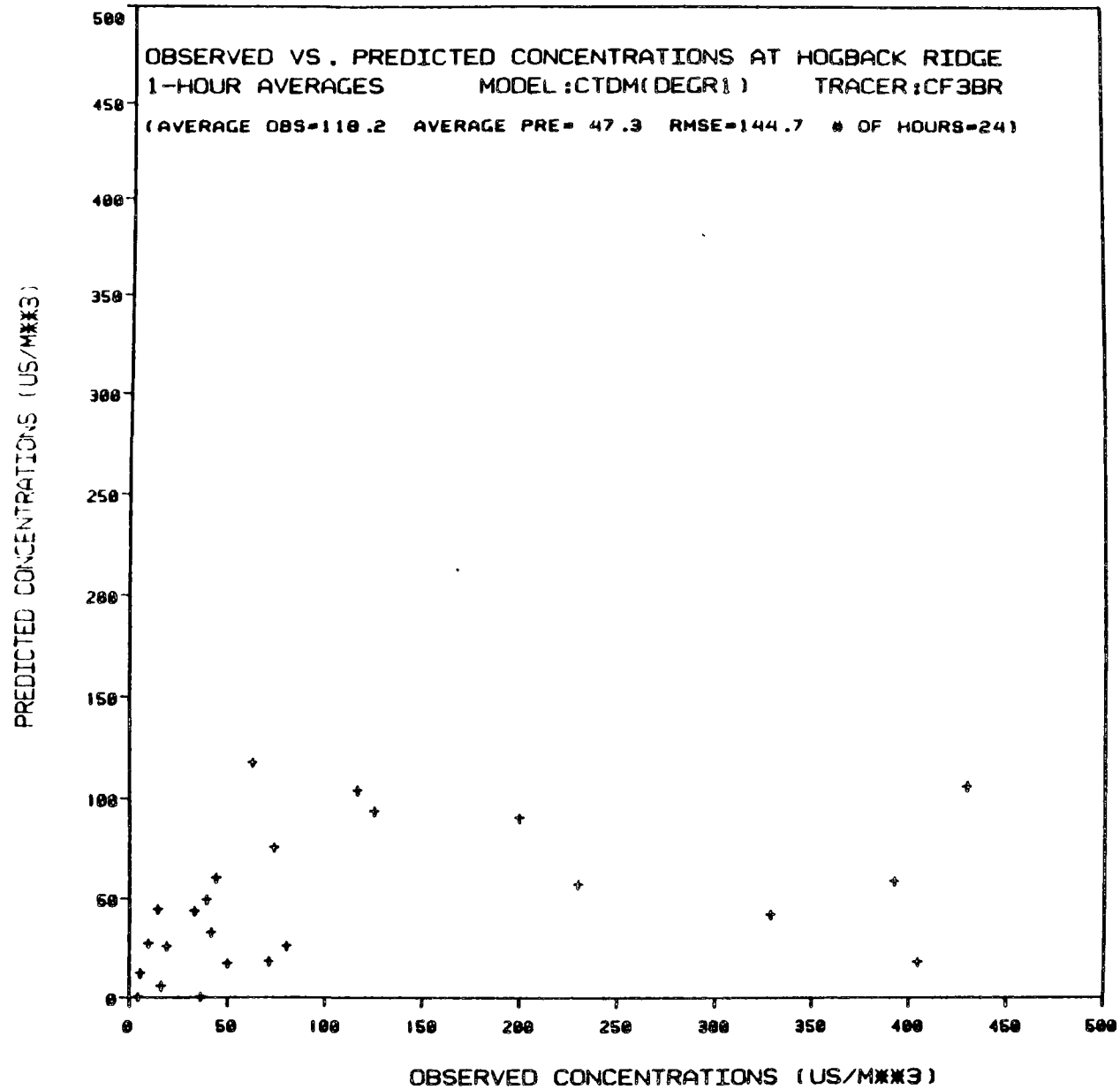
OBSERVED VS. PREDICTED CONCENTRATIONS AT HOGBACK RIDGE
1-HOUR AVERAGES MODEL:CTDM(DEGR1) TRACER:CF3BR
(AVERAGE OBS=118.2 AVERAGE PRE= 47.3 RMSE=144.7 # OF HOURS=24)
PREDICTED CONCENTRATIONS (US/M**3)
OBSERVED CONCENTRATIONS (US/M**3)
0
50
100
150
200
250
300
350
400
450
500

Figure F-20

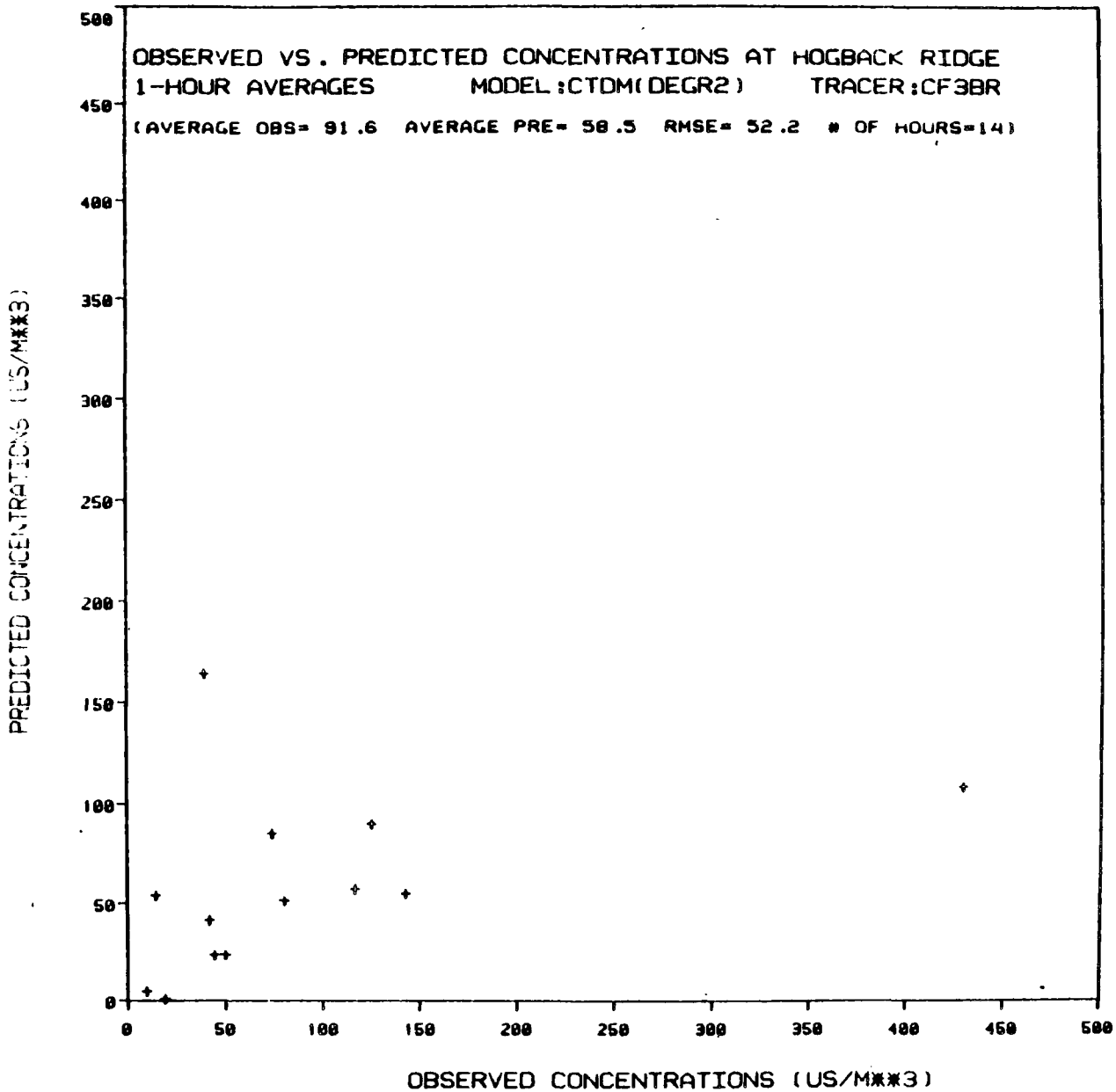
OBSERVED VS. PREDICTED CONCENTRATIONS AT HOGBACK RIDGE
1-HOUR AVERAGES MODEL:CTDM(DEGR2) TRACER:CF3BR
(AVERAGE OBS= 91.6 AVERAGE PRE= 58.5 RMSE= 52.2 # OF HOURS=14)
PREDICTED CONCENTRATIONS (US/M**3)
OBSERVED CONCENTRATIONS (US/M**3)
0
50
100
150
200
250
300
350
400
450
500

Figure F-21

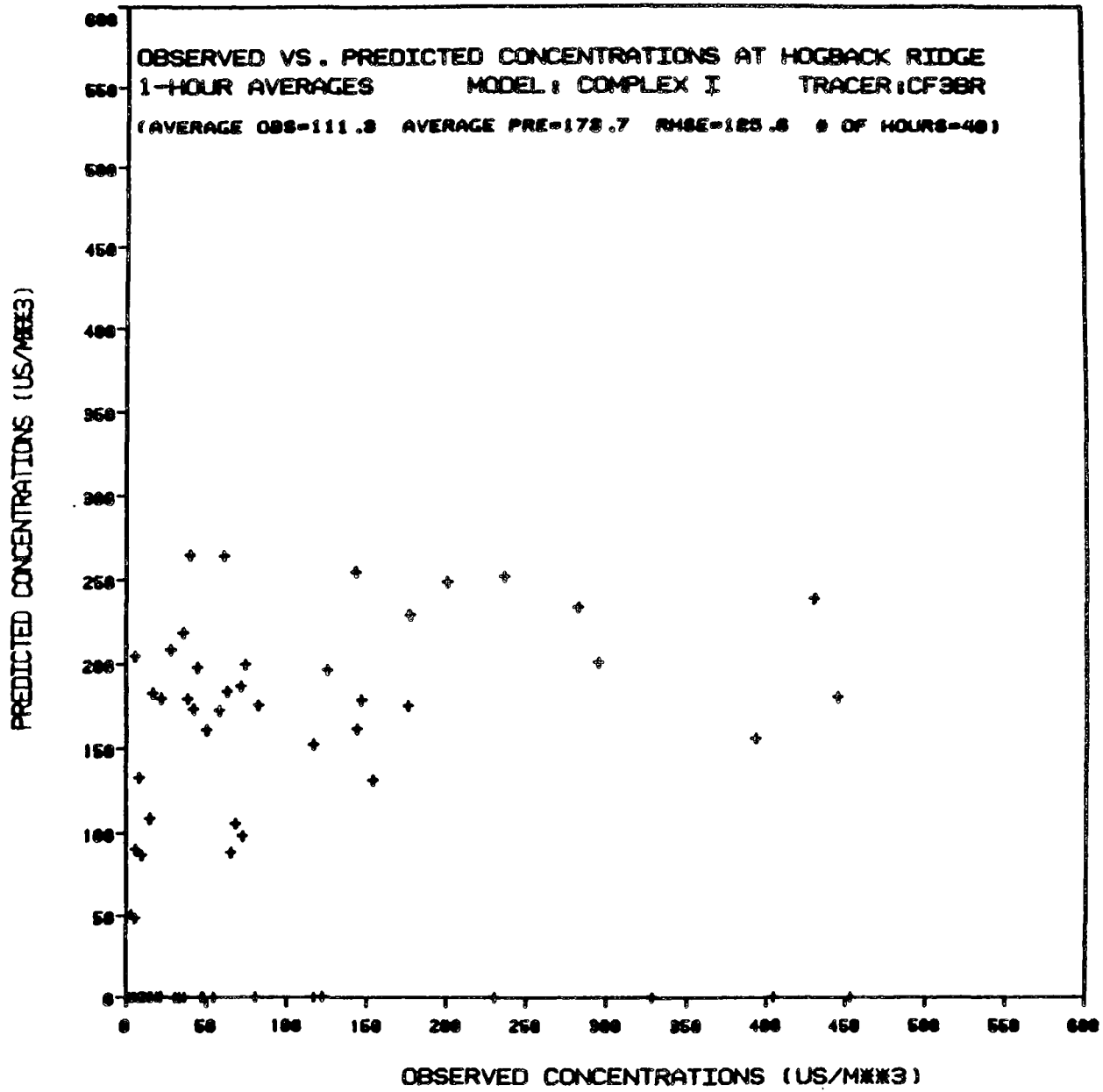
OBSERVED VS. PREDICTED CONCENTRATIONS AT HOGBACK RIDGE
1-HOUR AVERAGES MODEL: COMPLEX I TRACER:CF3BR
(AVERAGE OBS=111.8 AVERAGE PRE=178.7 RMSE=125.8 # OF HOURS=40)
PREDICTED CONCENTRATIONS (US/M**3)
OBSERVED CONCENTRATIONS (US/M**3)
0
50
100
150
200
250
300
350
400
450
500
550
600

Figure F-22

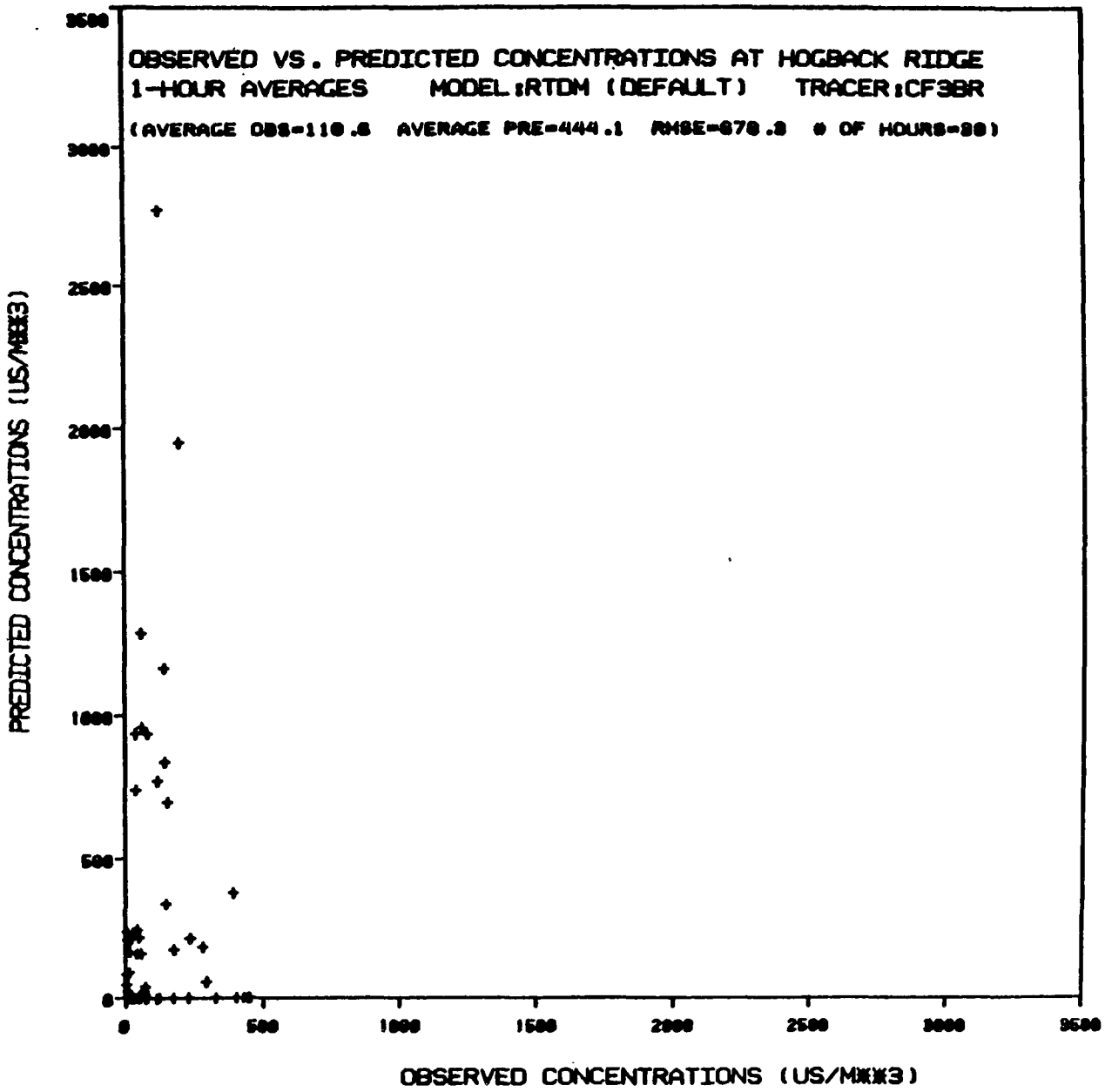
OBSERVED VS. PREDICTED CONCENTRATIONS AT HOGBACK RIDGE
1-HOUR AVERAGES MODEL:RTDM (DEFAULT) TRACER:CF3BR
(AVERAGE OBS=110.6 AVERAGE PRE=444.1 RMSE=670.8 # OF HOURS=98)
PREDICTED CONCENTRATIONS (US/M**3)
OBSERVED CONCENTRATIONS (US/M**3)
0
500
1000
1500
2000
2500
3000
3500

Figure F-23

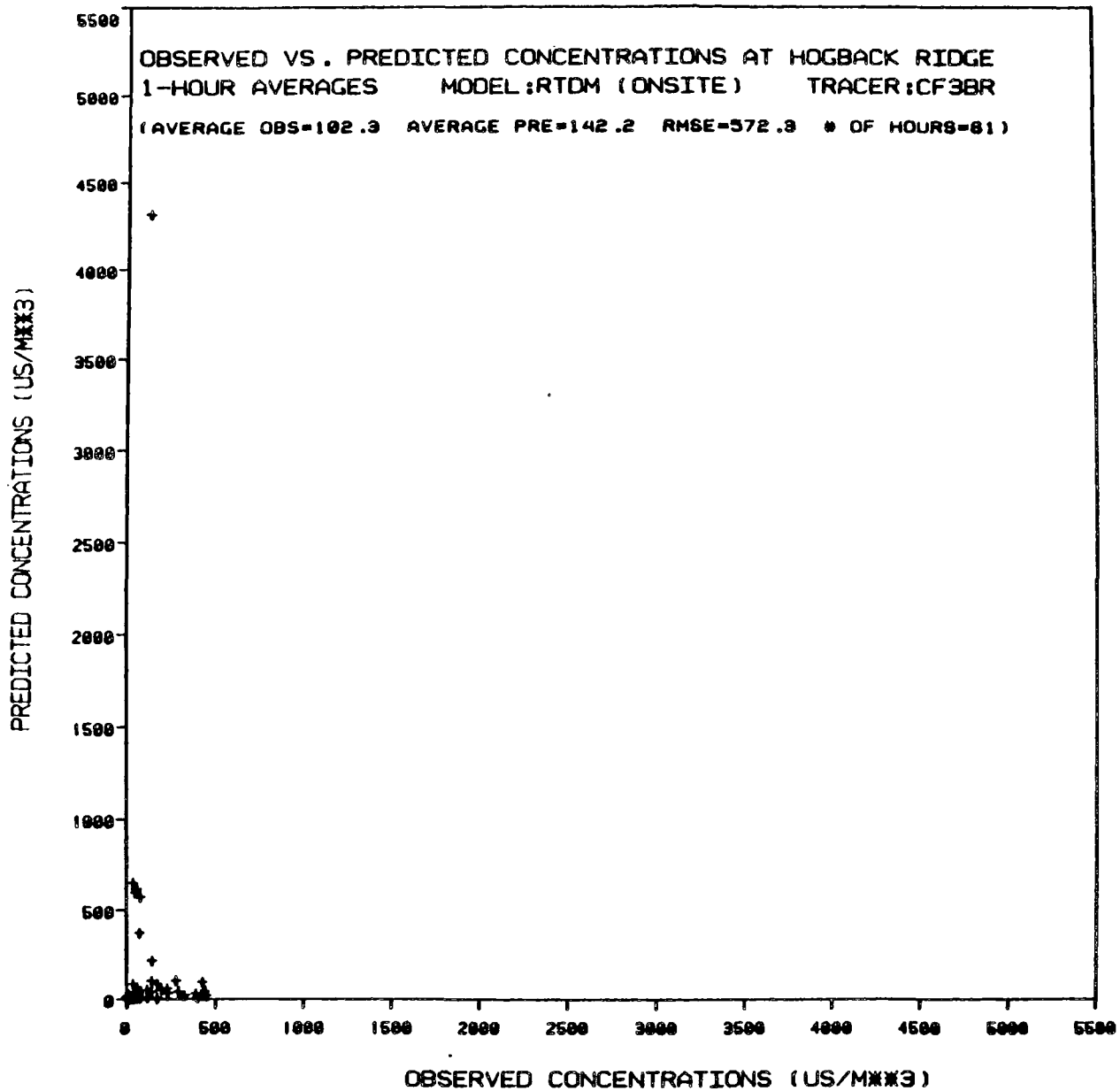
OBSERVED VS. PREDICTED CONCENTRATIONS AT HOGBACK RIDGE
1-HOUR AVERAGES MODEL:RTDM (ONSITE) TRACER:CF3BR
(AVERAGE OBS=102.3 AVERAGE PRE=142.2 RMSE=572.8 # OF HOURS=81)
PREDICTED CONCENTRATIONS (US/M**3)
OBSERVED CONCENTRATIONS (US/M**3)
0
500
1000
1500
2000
2500
3000
3500
4000
4500
5000
5500

Figure F-24

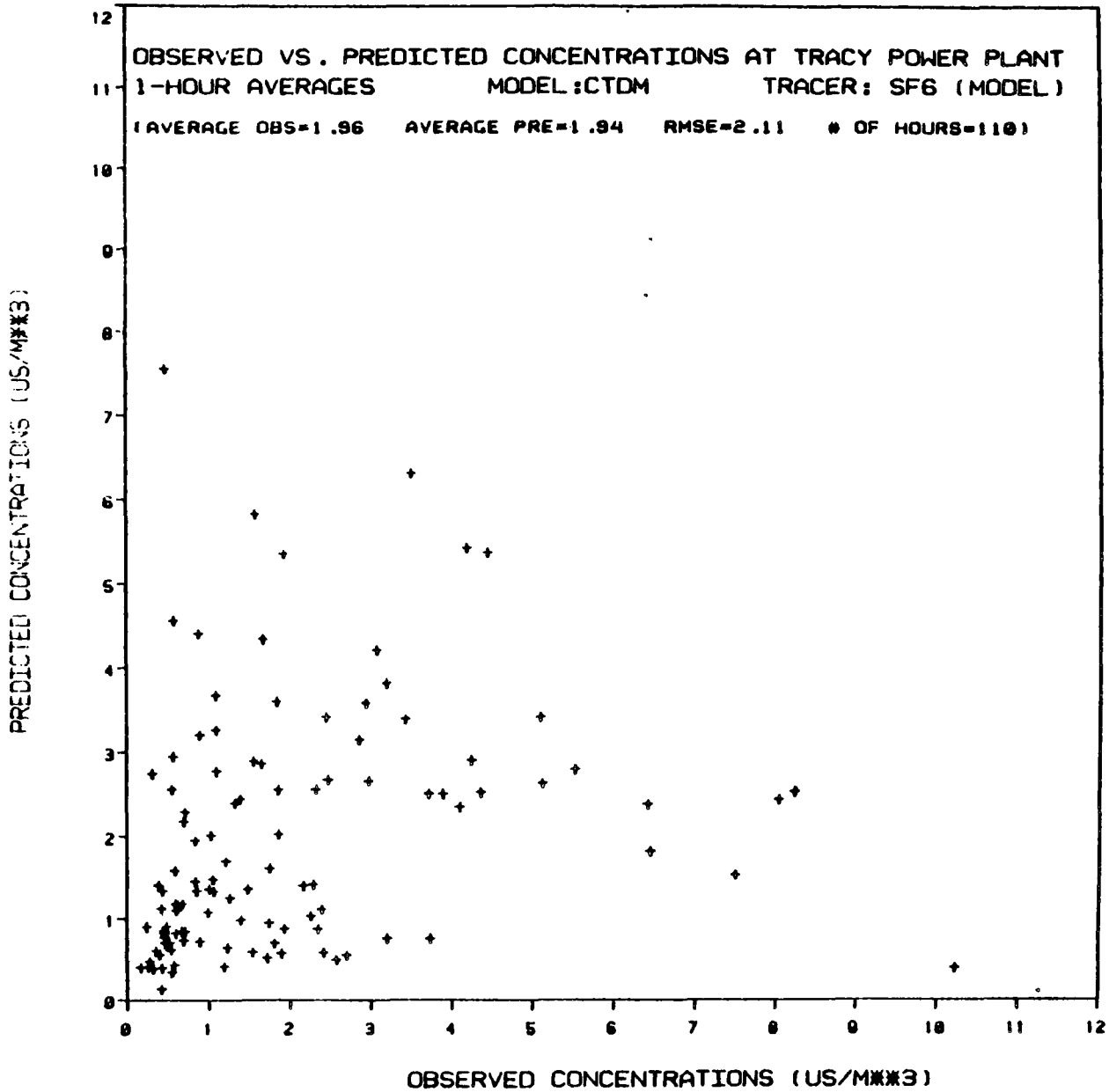
OBSERVED VS. PREDICTED CONCENTRATIONS AT TRACY POWER PLANT
1-HOUR AVERAGES MODEL:CTDM TRACER: SF6 (MODEL)
(AVERAGE OBS=1.96 AVERAGE PRE=1.94 RMSE=2.11 # OF HOURS=110)
PREDICTED CONCENTRATIONS (US/M**3)
OBSERVED CONCENTRATIONS (US/M**3)
0
1
2
3
4
5
6
7
8
9
10
11
12

Figure F-25

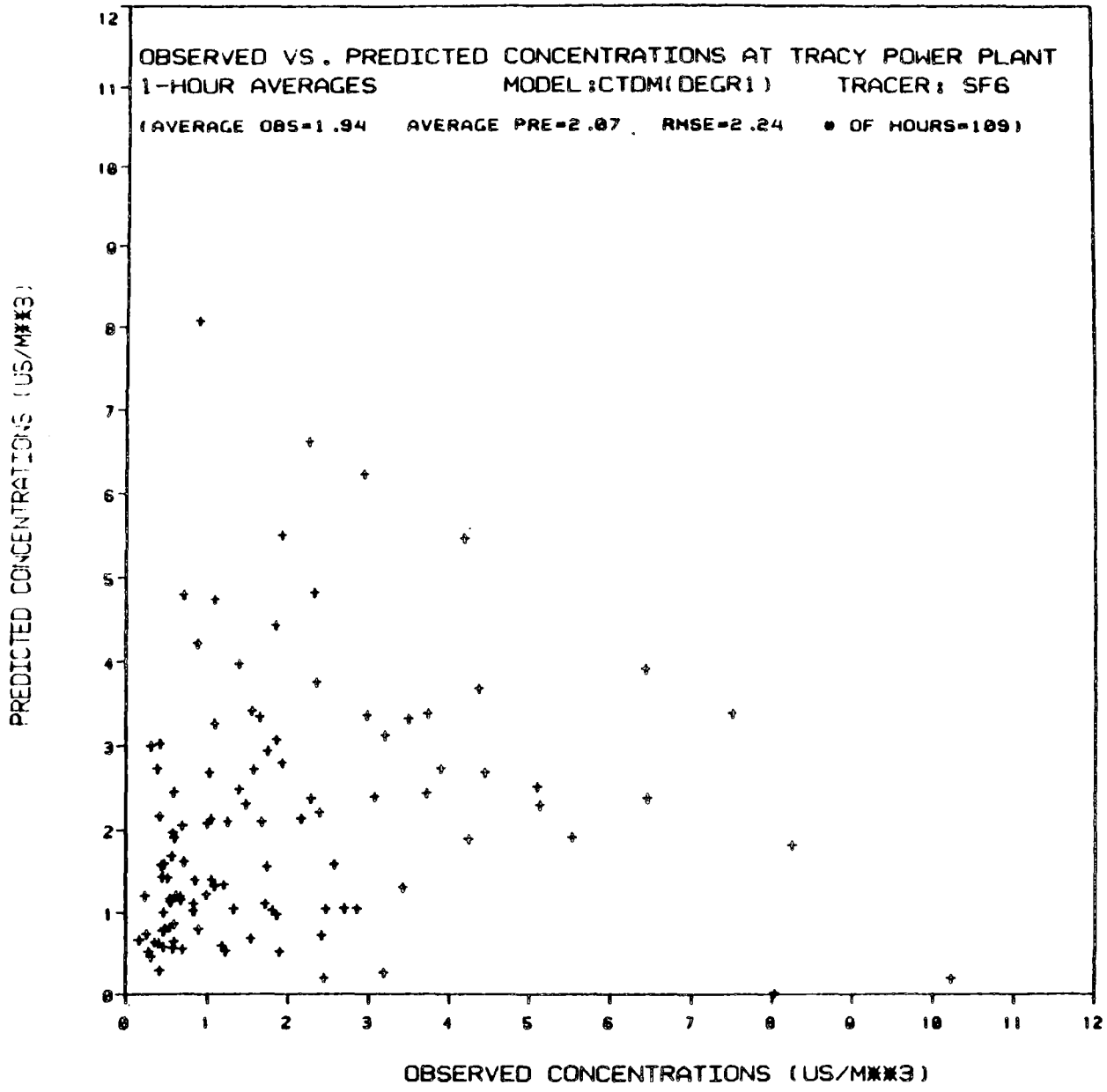
OBSERVED VS. PREDICTED CONCENTRATIONS AT TRACY POWER PLANT
1-HOUR AVERAGES
MODEL:CTDM(DEGR1)
TRACER: SF6
(AVERAGE OBS=1.94 AVERAGE PRE=2.07 RMSE=2.24 # OF HOURS=109)
PREDICTED CONCENTRATIONS (US/M**3)
OBSERVED CONCENTRATIONS (US/M**3)
0
1
2
3
4
5
6
7
8
9
10
11
12

Figure F-26

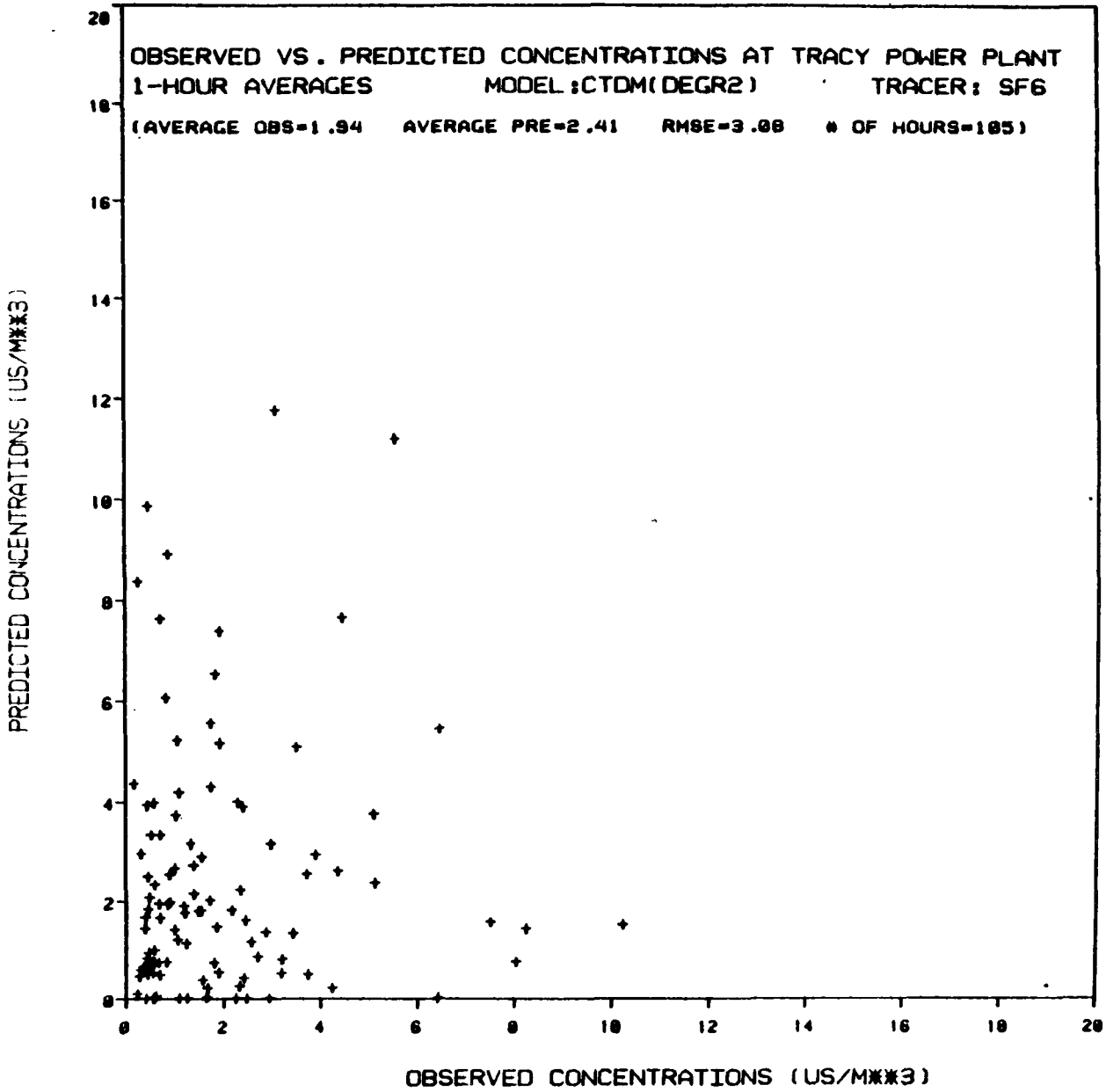
OBSERVED VS. PREDICTED CONCENTRATIONS AT TRACY POWER PLANT
1-HOUR AVERAGES MODEL:CTDM(DEGR2) TRACER: SF6
(AVERAGE OBS=1.94 AVERAGE PRE=2.41 RMSE=3.08 # OF HOURS=185)
PREDICTED CONCENTRATIONS (US/M**3)
OBSERVED CONCENTRATIONS (US/M**3)
0
2
4
6
8
10
12
14
16
18
20

Figure F-27.

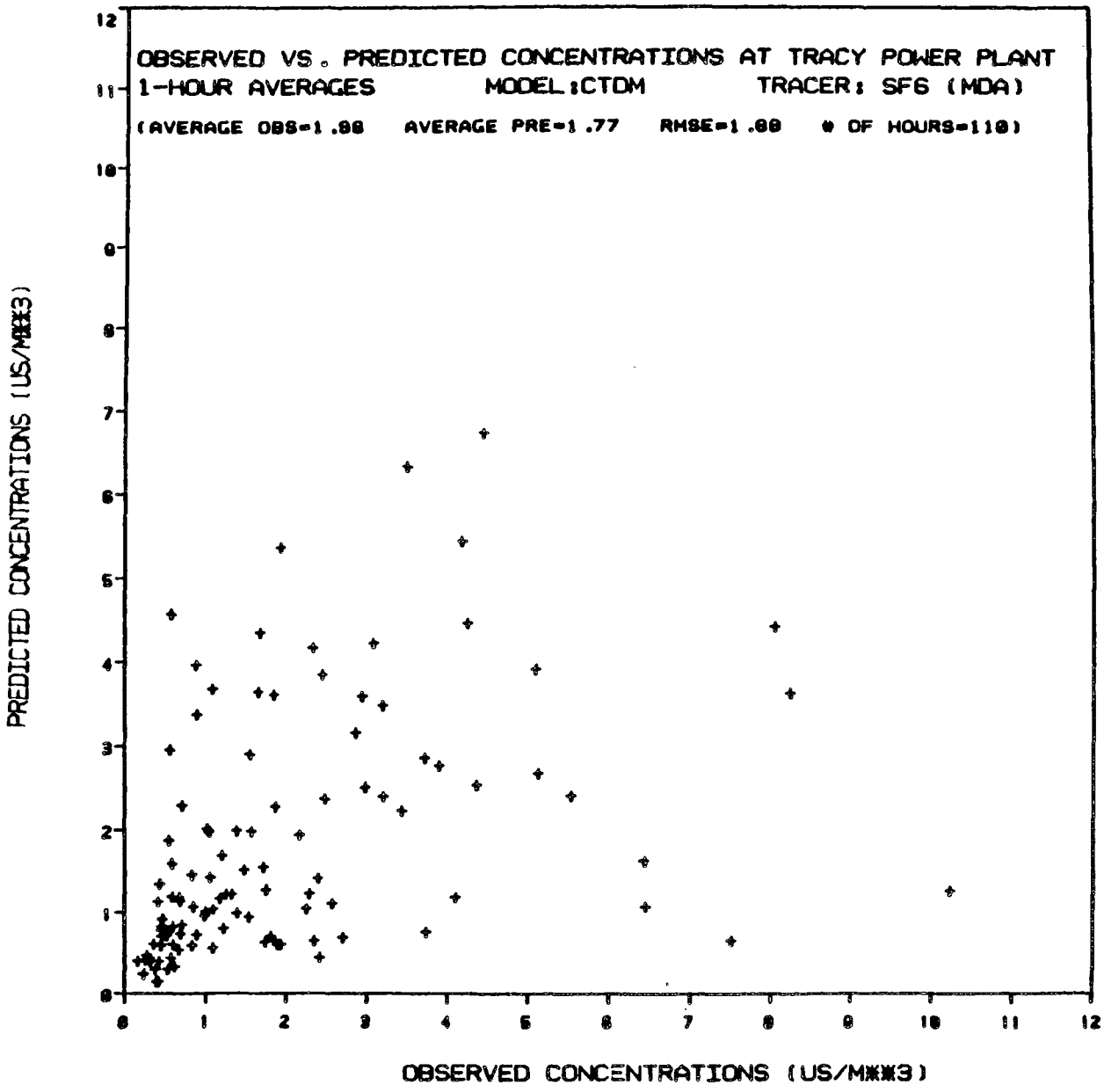
OBSERVED VS. PREDICTED CONCENTRATIONS AT TRACY POWER PLANT
1-HOUR AVERAGES MODEL:CTDM TRACER: SF6 (MDA)
(AVERAGE OBS=1.88 AVERAGE PRE=1.77 RMSE=1.88 # OF HOURS=110)
PREDICTED CONCENTRATIONS (US/M**3)
OBSERVED CONCENTRATIONS (US/M**3)
0
1
2
3
4
5
6
7
8
9
10
11
12

Figure F-28

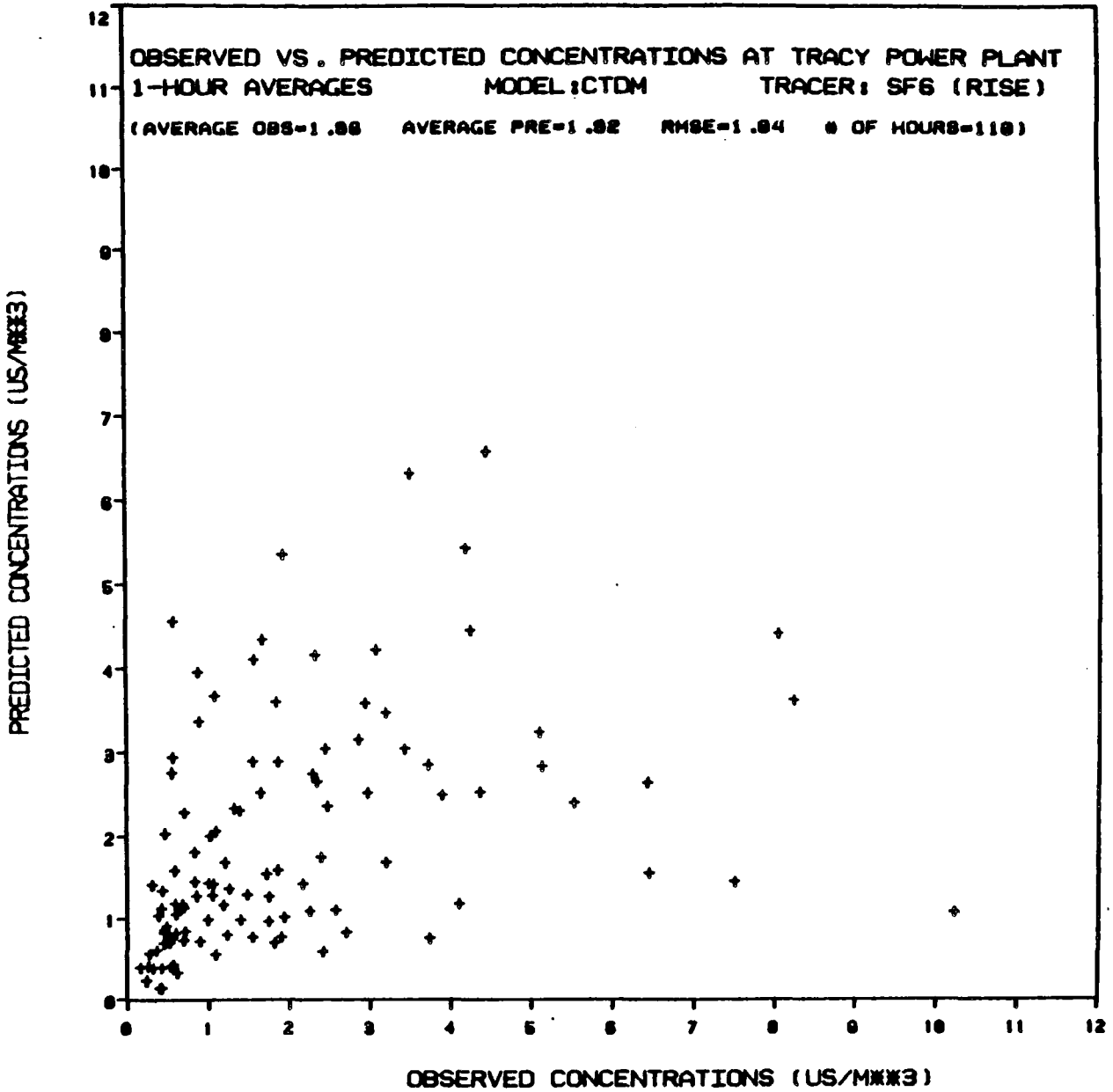
OBSERVED VS. PREDICTED CONCENTRATIONS AT TRACY POWER PLANT
1-HOUR AVERAGES MODEL:CTDM TRACER: SF6 (RISE)
(AVERAGE OBS=1.88 AVERAGE PRE=1.92 RMSE=1.84 # OF HOURS=118)
PREDICTED CONCENTRATIONS (US/M**3)
OBSERVED CONCENTRATIONS (US/M**3)
0
1
2
3
4
5
6
7
8
9
10
11
12

Figure F-29

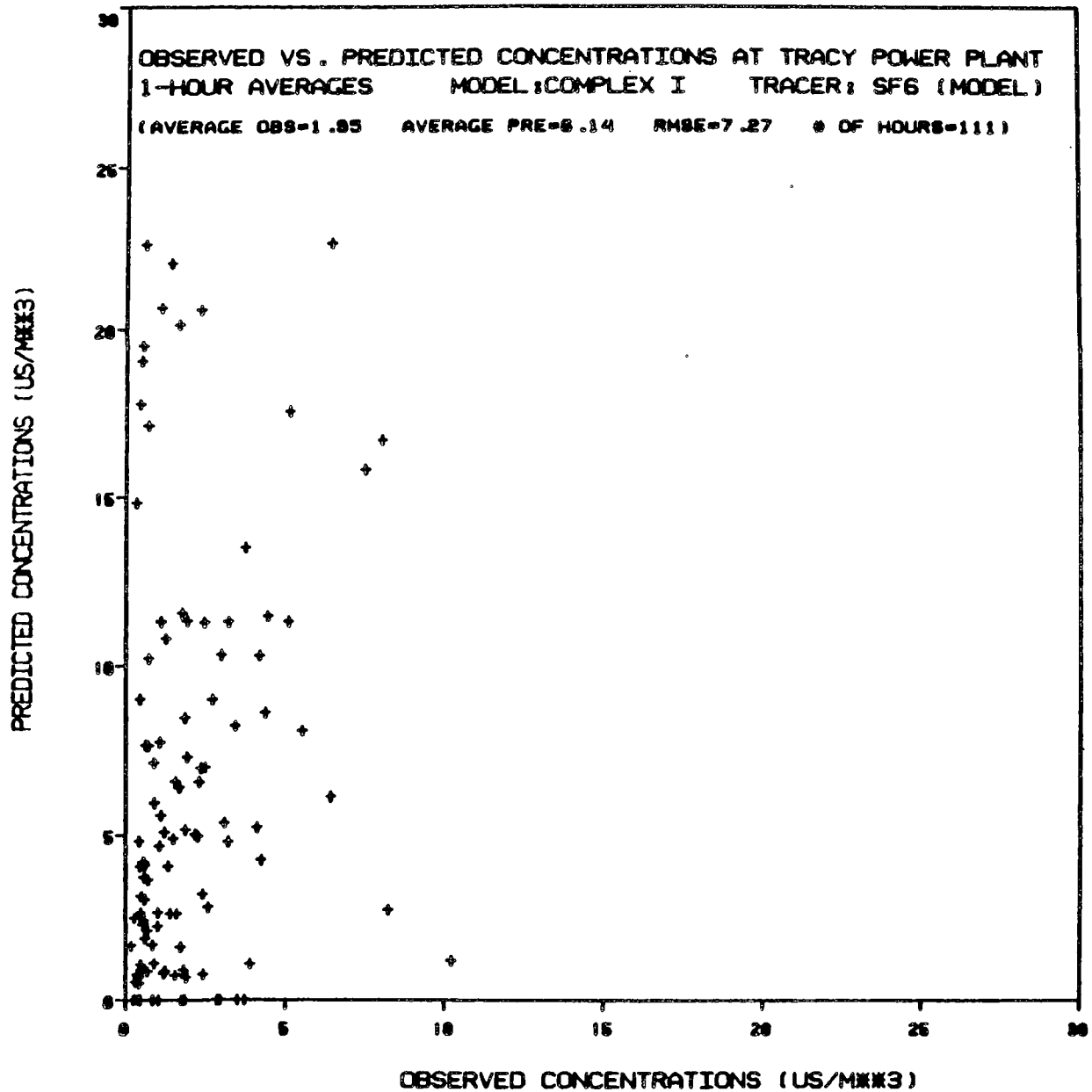
OBSERVED VS. PREDICTED CONCENTRATIONS AT TRACY POWER PLANT
1-HOUR AVERAGES MODEL:COMPLEX I TRACER: SF6 (MODEL)
(AVERAGE OBS=1.85 AVERAGE PRE=8.14 RMSE=7.27 # OF HOURS=111)
PREDICTED CONCENTRATIONS (US/MXX3)
OBSERVED CONCENTRATIONS (US/MXX3)
0
5
10
15
20
25
30

Figure F-30

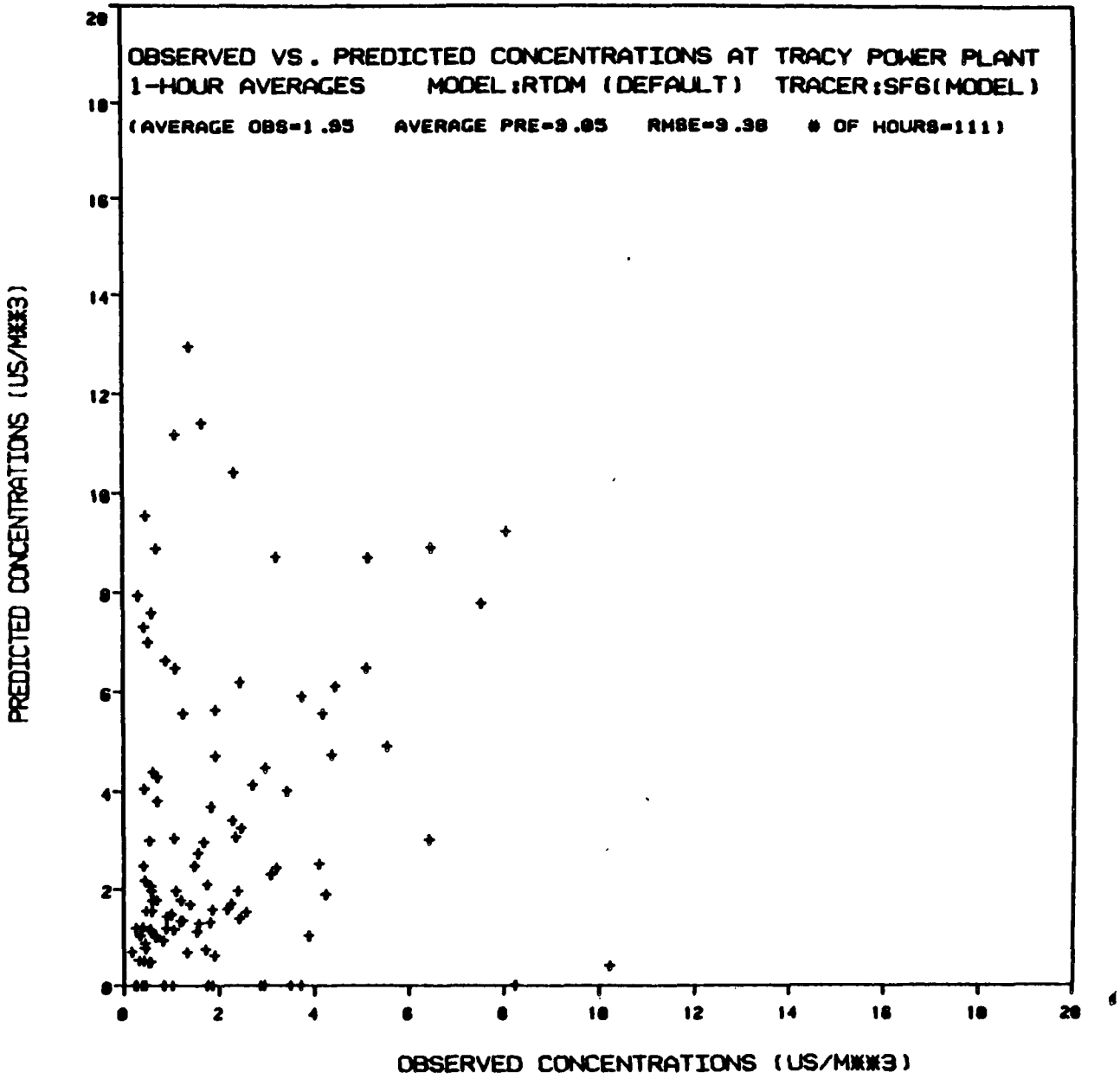
OBSERVED VS. PREDICTED CONCENTRATIONS AT TRACY POWER PLANT
1-HOUR AVERAGES MODEL:RTDM (DEFAULT) TRACER:SF6(MODEL)
(AVERAGE OBS=1.95 AVERAGE PRE=9.85 RMSE=9.38 # OF HOURS=111)
PREDICTED CONCENTRATIONS (US/M**3)
OBSERVED CONCENTRATIONS (US/M**3)
0
2
4
6
8
10
12
14
16
18
20

Figure F-31

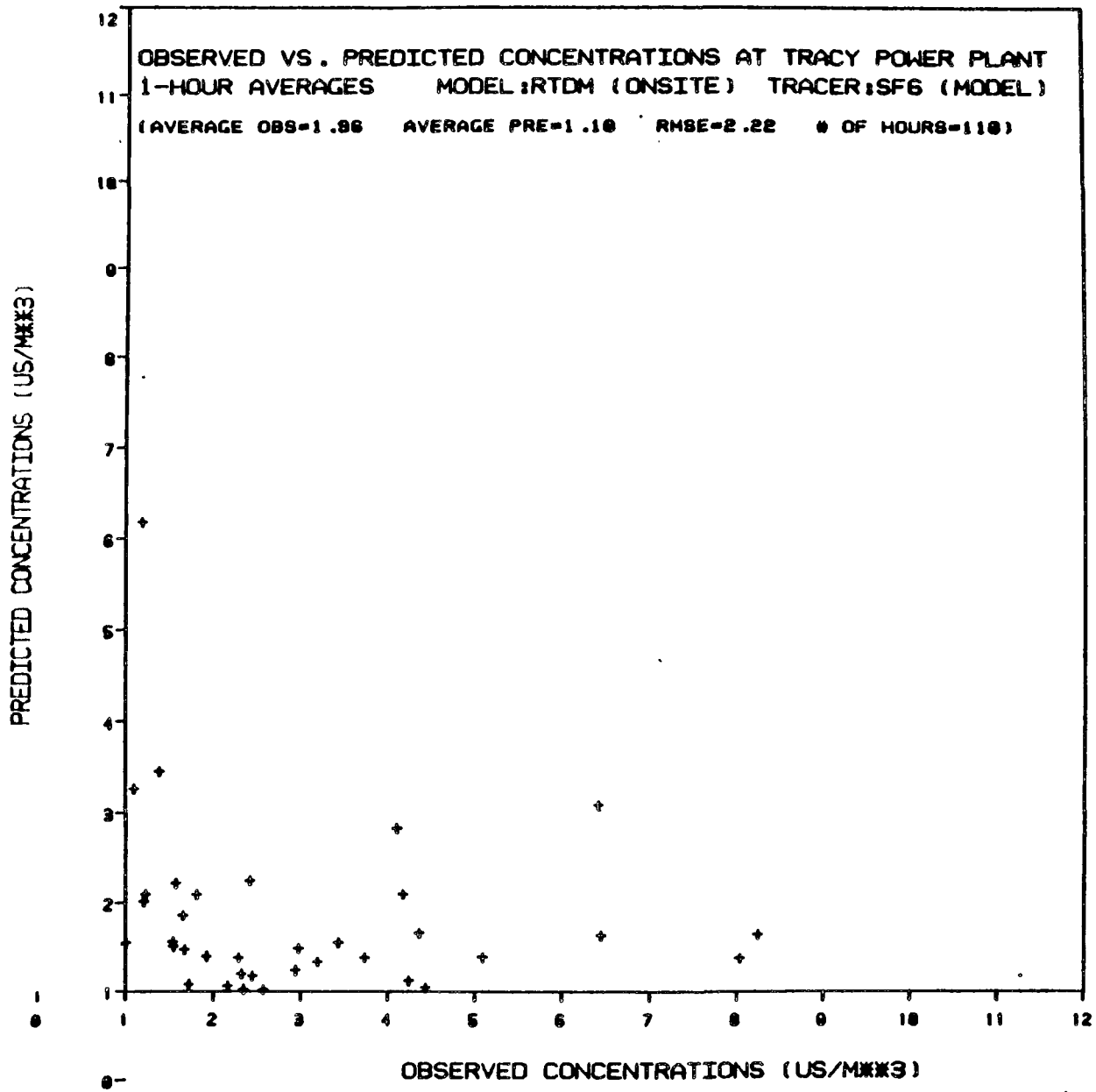
OBSERVED VS. PREDICTED CONCENTRATIONS AT TRACY POWER PLANT
1-HOUR AVERAGES MODEL:RTDM (ONSITE) TRACER:SF6 (MODEL)
(AVERAGE OBS=1.96 AVERAGE PRE=1.10 RMSE=2.22 # OF HOURS=110)
PREDICTED CONCENTRATIONS (US/M**3)
OBSERVED CONCENTRATIONS (US/M**3)
0
1
2
3
4
5
6
7
8
9
10
11
12

Figure F-32

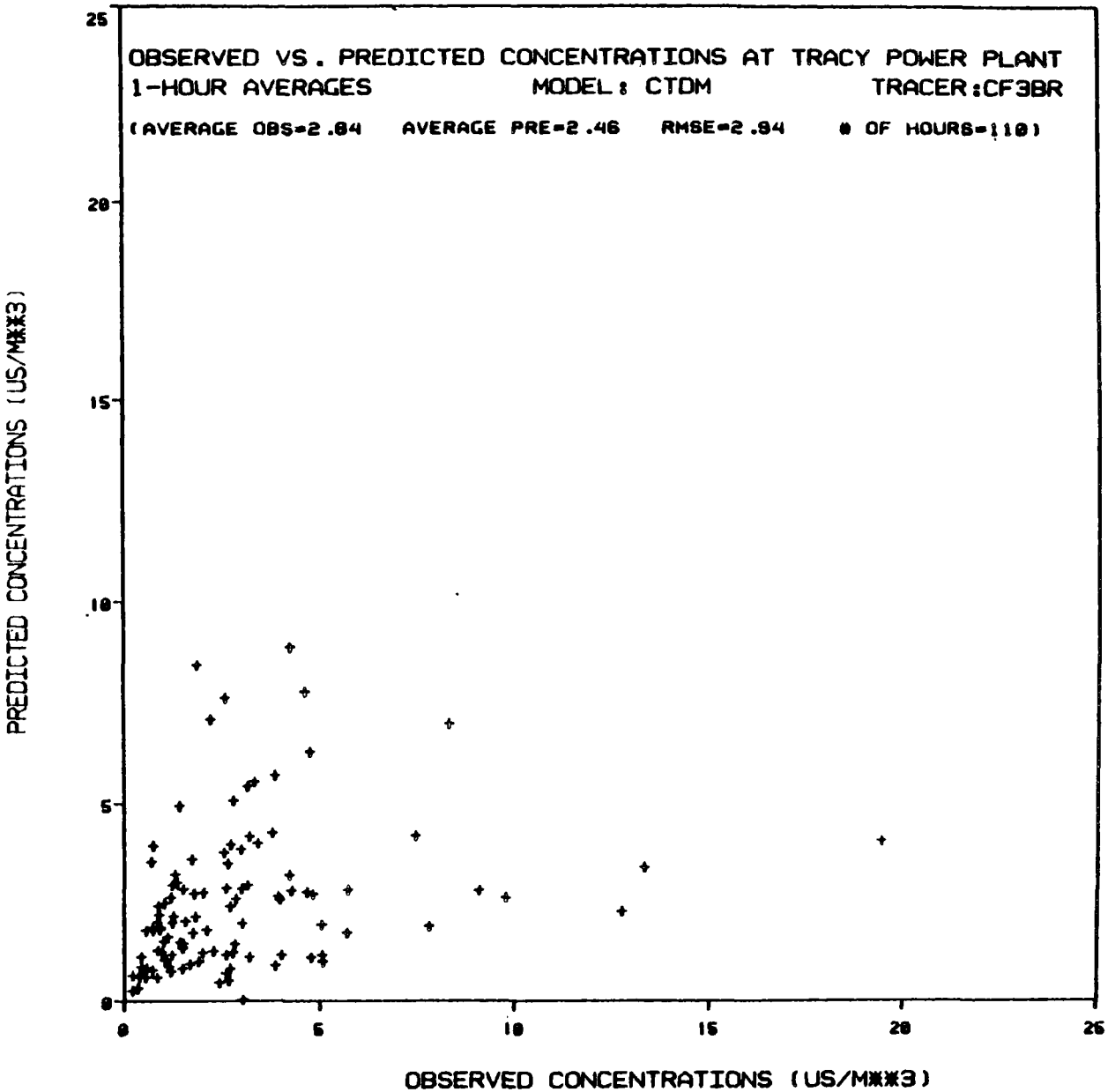
OBSERVED VS. PREDICTED CONCENTRATIONS AT TRACY POWER PLANT
1-HOUR AVERAGES
MODEL: CTDM
TRACER:CF3BR
(AVERAGE OBS=2.84 AVERAGE PRE=2.46 RMSE=2.94 # OF HOURS=110)
PREDICTED CONCENTRATIONS (US/M**3)
OBSERVED CONCENTRATIONS (US/M**3)
0
5
10
15
20
25

Figure F-33

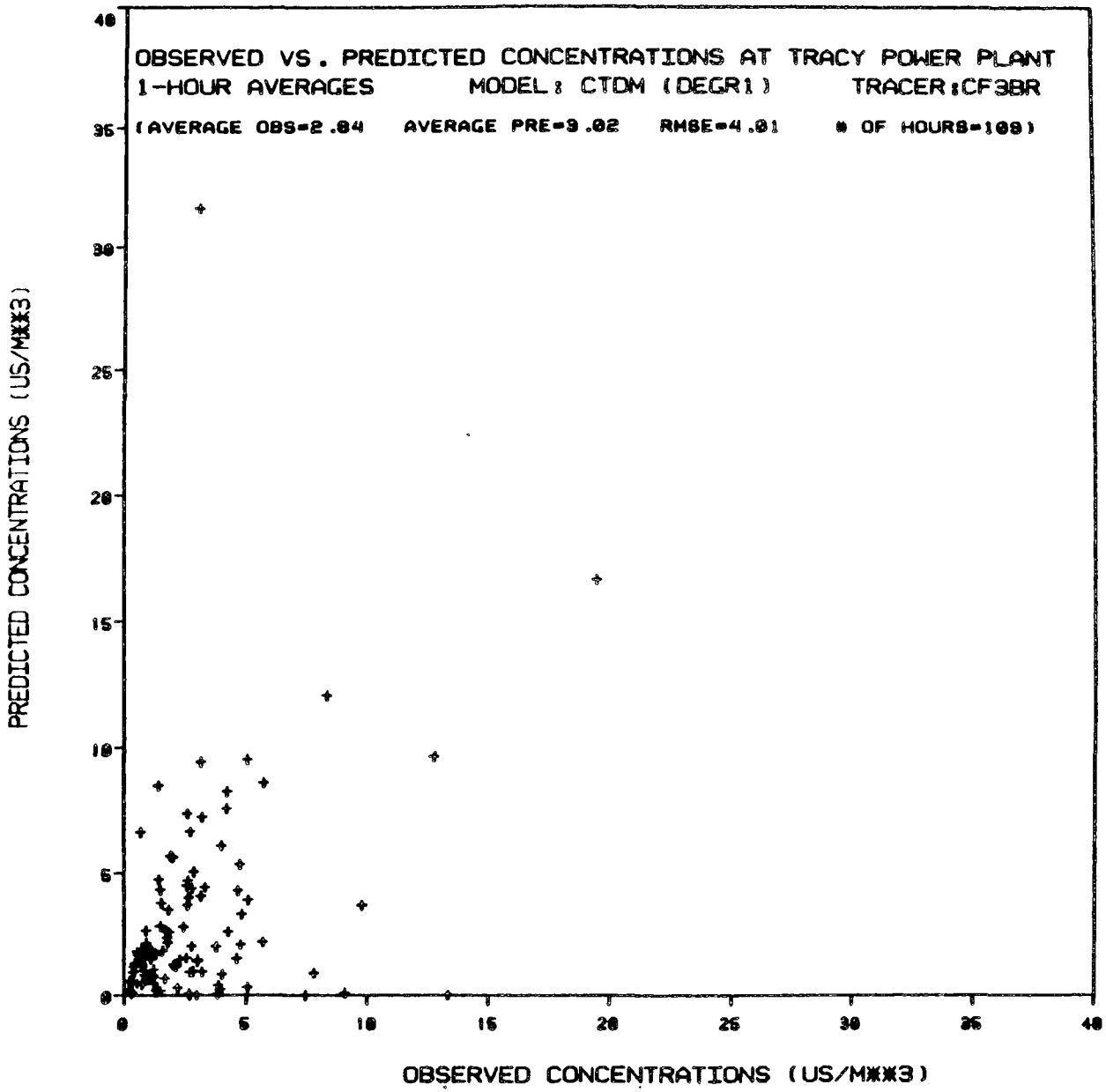
OBSERVED VS. PREDICTED CONCENTRATIONS AT TRACY POWER PLANT
1-HOUR AVERAGES MODEL: CTDM (DEGR1) TRACER:CF3BR
(AVERAGE OBS=2.84 AVERAGE PRE=3.02 RMSE=4.01 # OF HOURS=109)
PREDICTED CONCENTRATIONS (US/M**3)
OBSERVED CONCENTRATIONS (US/M**3)
0
5
10
15
20
25
30
35
40

Figure F-34

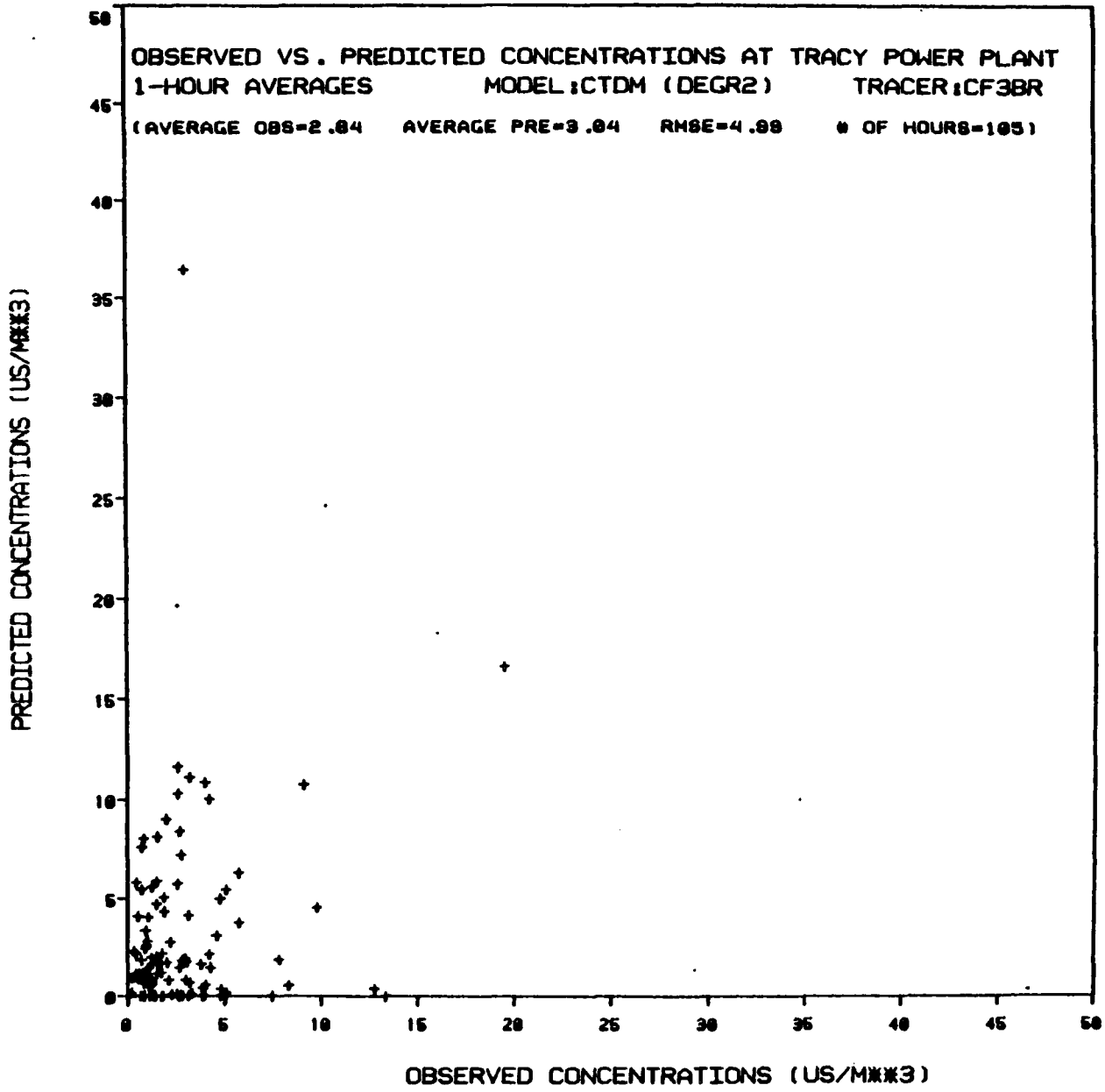
OBSERVED VS. PREDICTED CONCENTRATIONS AT TRACY POWER PLANT
1-HOUR AVERAGES MODEL:CTDM (DEGR2) TRACER:CF3BR
(AVERAGE OBS=2.04 AVERAGE PRE=3.04 RMSE=4.99 # OF HOURS=105)
PREDICTED CONCENTRATIONS (US/M**3)
OBSERVED CONCENTRATIONS (US/M**3)
0
5
10
15
20
25
30
35
40
45
50

Figure F-35

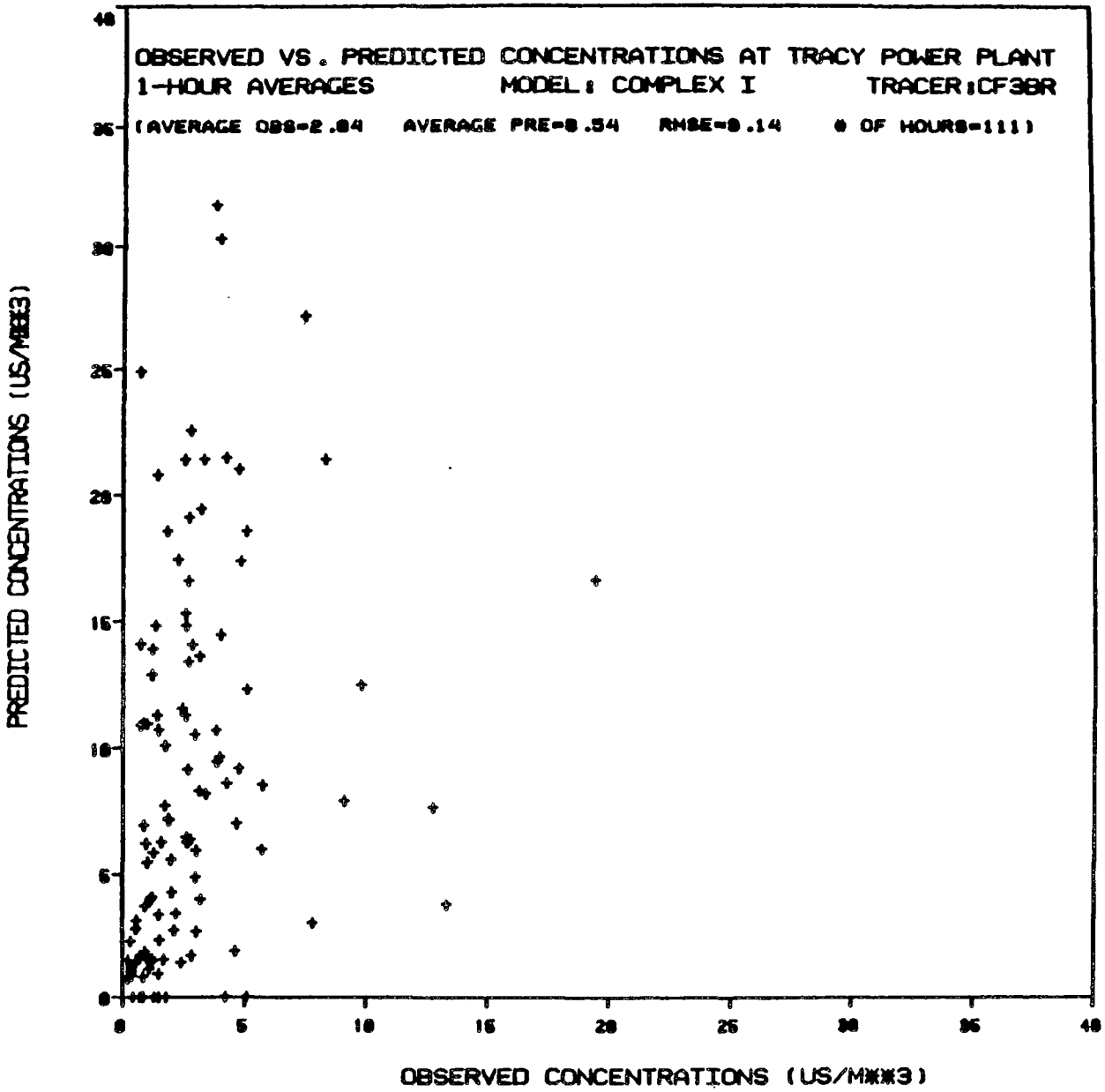
OBSERVED VS. PREDICTED CONCENTRATIONS AT TRACY POWER PLANT
1-HOUR AVERAGES MODEL: COMPLEX I TRACER:CF3BR
(AVERAGE OBS=2.84 AVERAGE PRE=0.54 RMSE=0.14 # OF HOURS=111)
PREDICTED CONCENTRATIONS (US/MXX3)
OBSERVED CONCENTRATIONS (US/MXX3)
0
5
10
15
20
25
30
35
40

Figure F-36

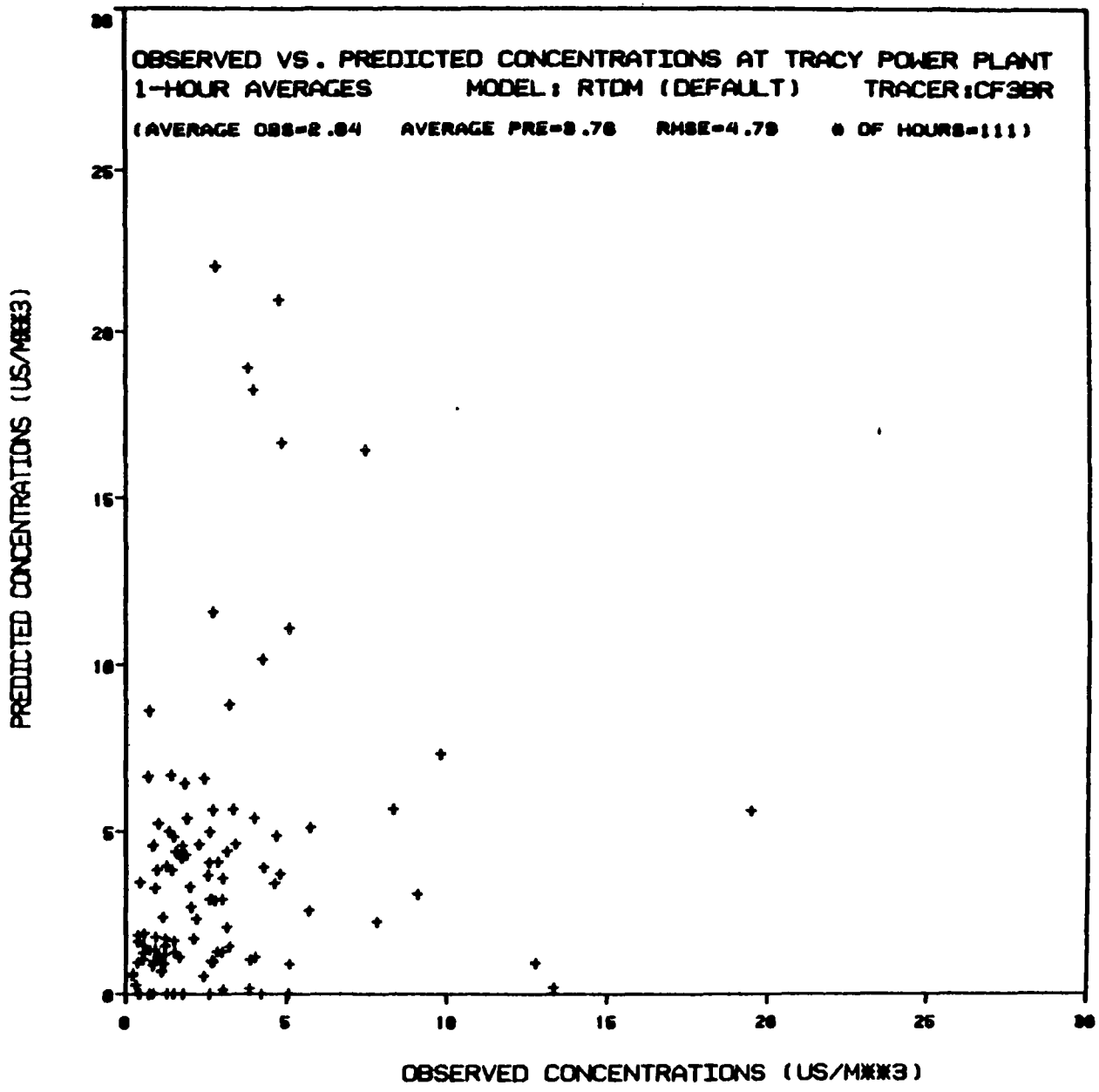
OBSERVED VS. PREDICTED CONCENTRATIONS AT TRACY POWER PLANT
1-HOUR AVERAGES MODEL: RTDM (DEFAULT) TRACER:CF3BR
(AVERAGE OBS=2.84 AVERAGE PRE=3.78 RMSE=4.79 # OF HOURS=111)
PREDICTED CONCENTRATIONS (US/M***3)
OBSERVED CONCENTRATIONS (US/M***3)
0
5
10
15
20
25
30

Figure F-37

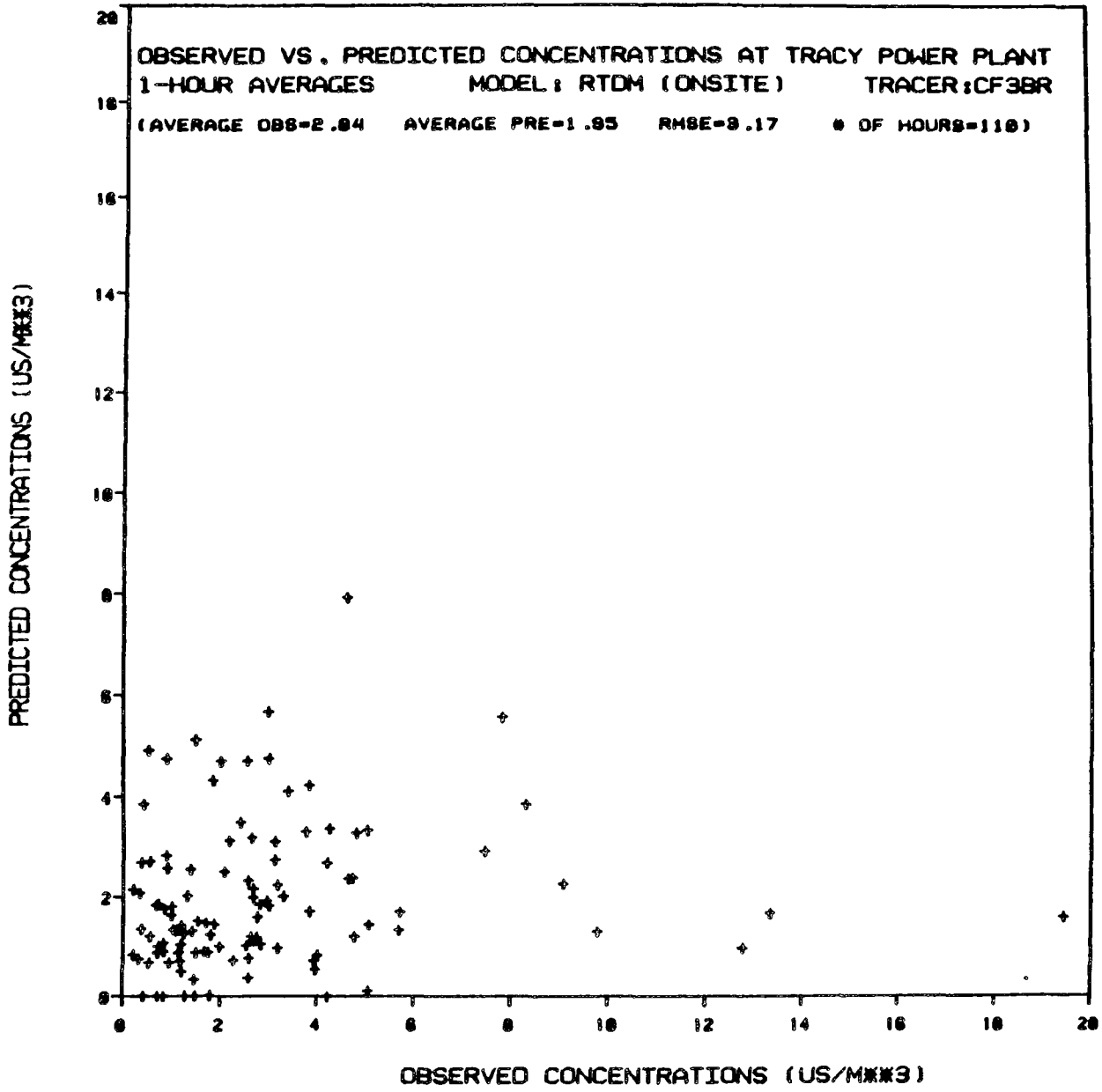
OBSERVED VS. PREDICTED CONCENTRATIONS AT TRACY POWER PLANT
1-HOUR AVERAGES MODEL: RTDM (ONSITE) TRACER:CF3BR
(AVERAGE OBS=2.84 AVERAGE PRE=1.85 RMSE=3.17 # OF HOURS=118)
PREDICTED CONCENTRATIONS (US/M**3)
OBSERVED CONCENTRATIONS (US/M**3)
0
2
4
6
8
10
12
14
16
18
20

Figure F-38

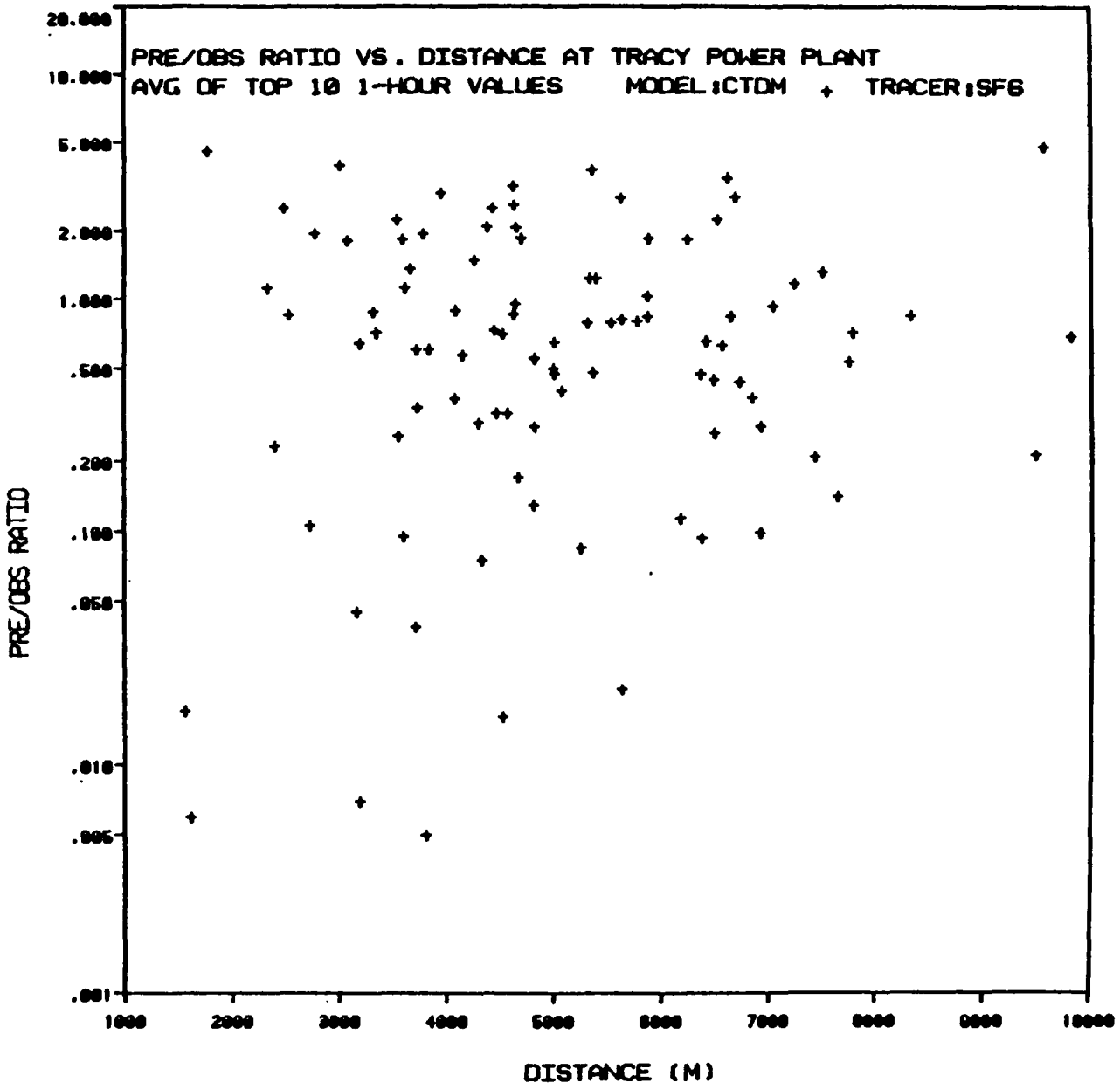
PRE/OBS RATIO VS. DISTANCE AT TRACY POWER PLANT
AVG OF TOP 10 1-HOUR VALUES MODEL:CTDM + TRACER:SF6
PRE/OBS RATIO
20.000
10.000
5.000
2.000
1.000
.500
.200
.100
.050
.010
.005
.001
1000
2000
3000
4000
5000
6000
7000
8000
9000
10000
DISTANCE (M)

Figure F-39

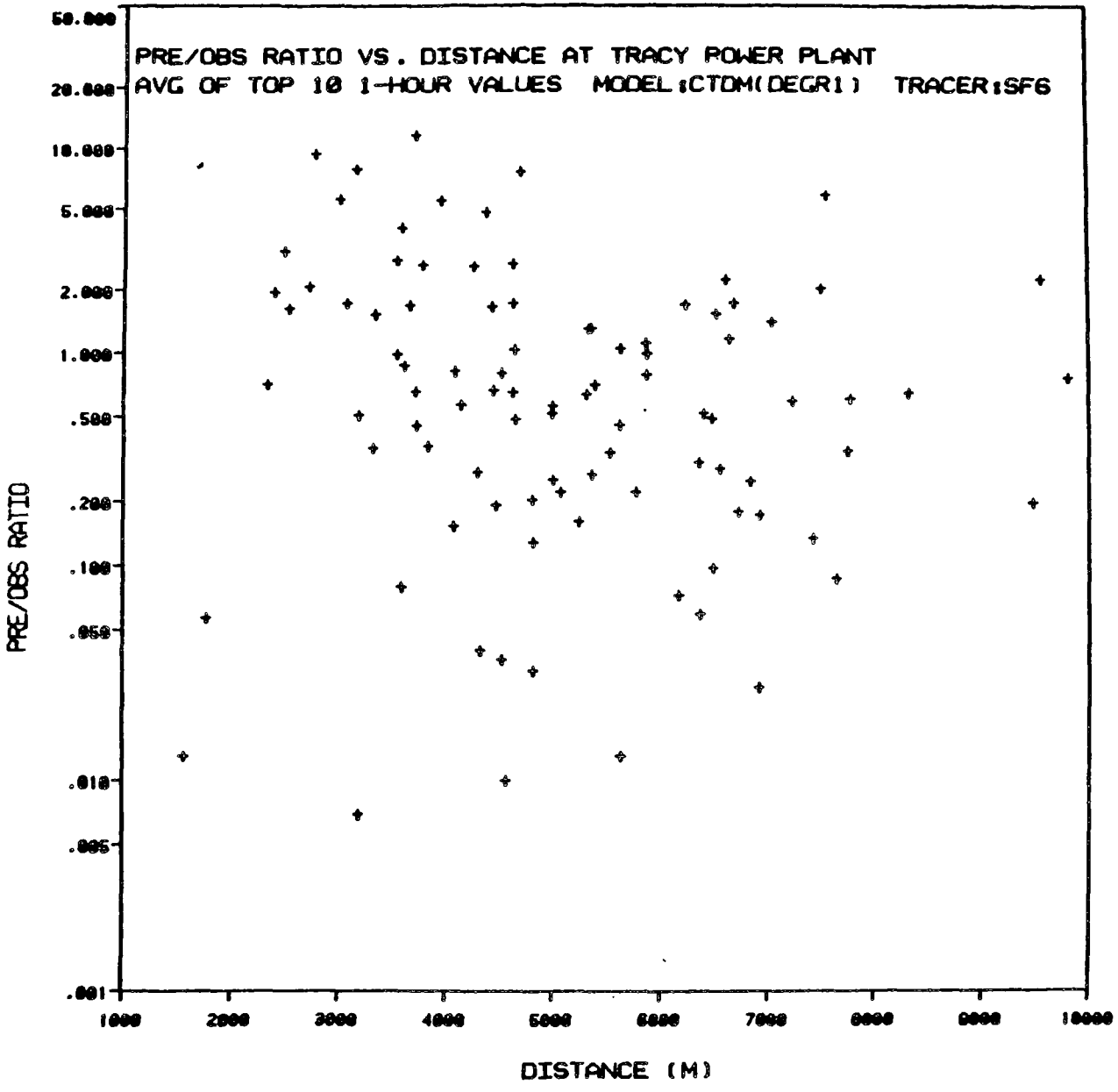
PRE/OBS RATIO VS. DISTANCE AT TRACY POWER PLANT
AVG OF TOP 10 1-HOUR VALUES MODEL:CTDM(DEGR1) TRACER:SF6
50.000
20.000
10.000
5.000
2.000
1.000
.500
.200
.100
.050
.010
.005
.001
PRE/OBS RATIO
1000
2000
3000
4000
5000
6000
7000
8000
9000
10000
DISTANCE (M)

Figure F-40

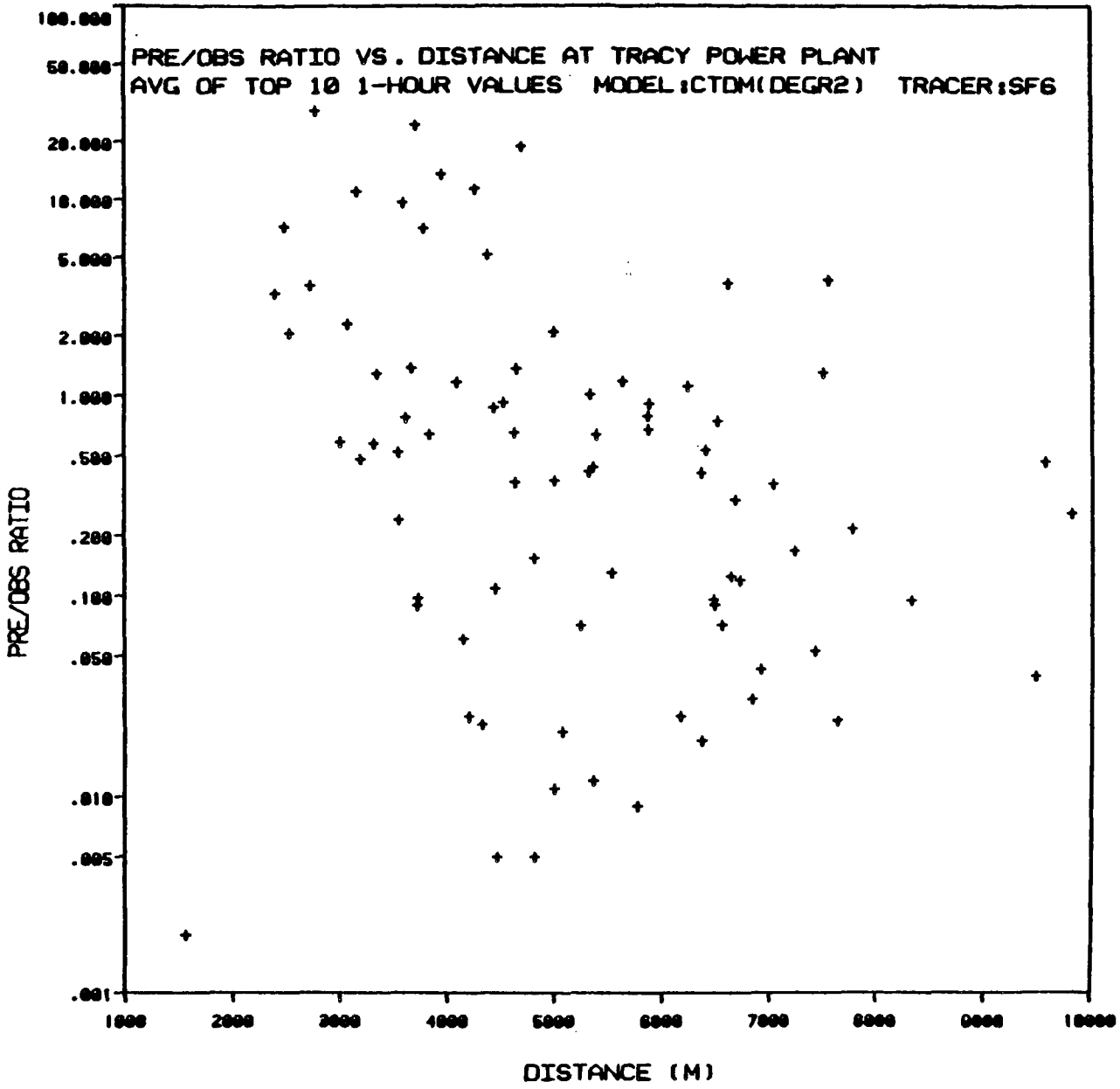
PRE/OBS RATIO VS. DISTANCE AT TRACY POWER PLANT
AVG OF TOP 10 1-HOUR VALUES MODEL:CTDM(DEGR2) TRACER:SF6
PRE/OBS RATIO
100.000
50.000
20.000
10.000
5.000
2.000
1.000
.500
.200
.100
.050
.010
.005
.001
1000
2000
3000
4000
5000
6000
7000
8000
9000
10000
DISTANCE (M)

Figure F-41

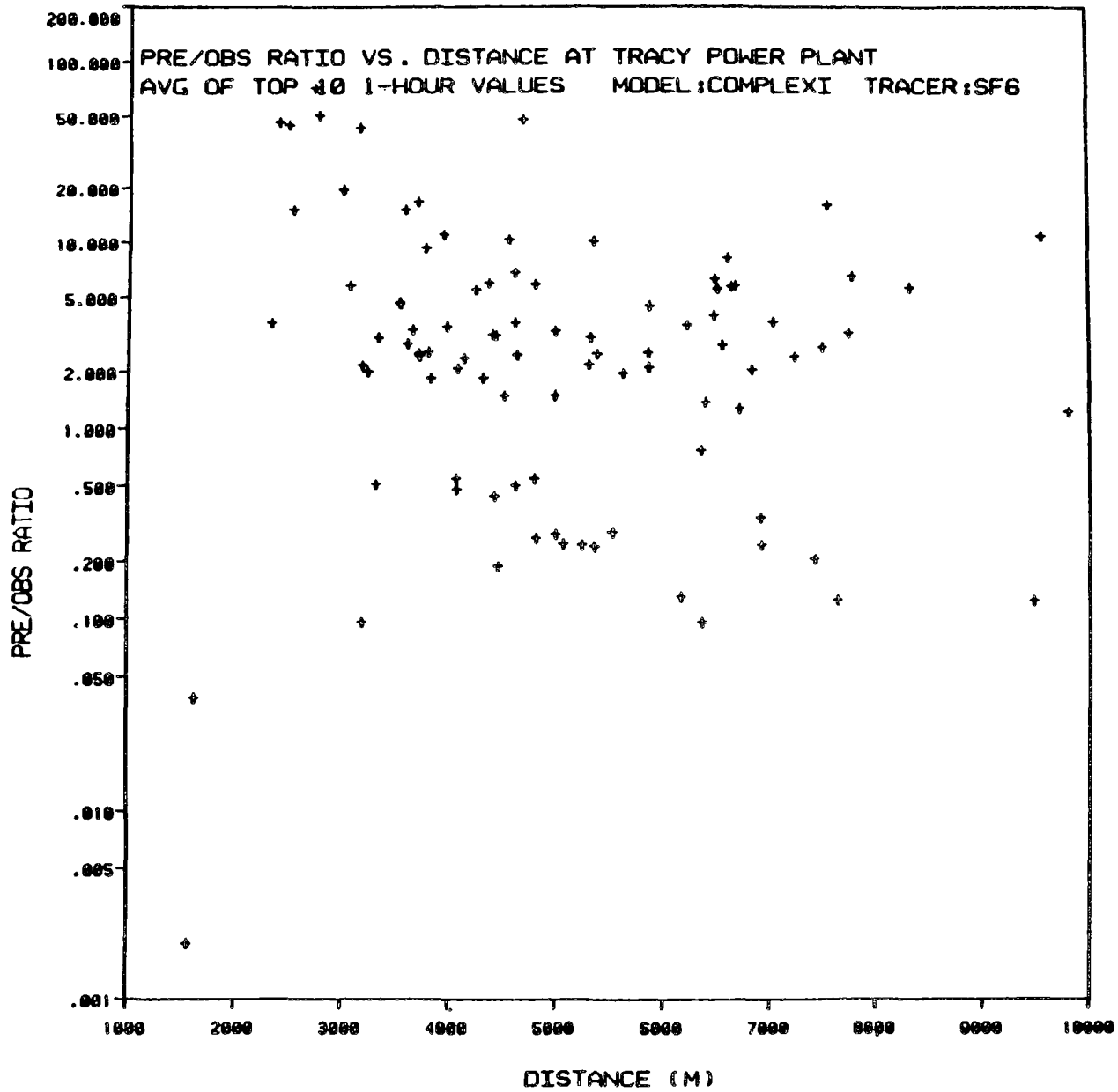
PRE/OBS RATIO VS. DISTANCE AT TRACY POWER PLANT
AVG OF TOP 10 1-HOUR VALUES MODEL:COMPLEXI TRACER:SF6
PRE/OBS RATIO
200.000
100.000
50.000
20.000
10.000
5.000
2.000
1.000
.500
.200
.100
.050
.010
.005
.001
1000
2000
3000
4000
5000
6000
7000
8000
9000
10000
DISTANCE (M)

Figure F-42

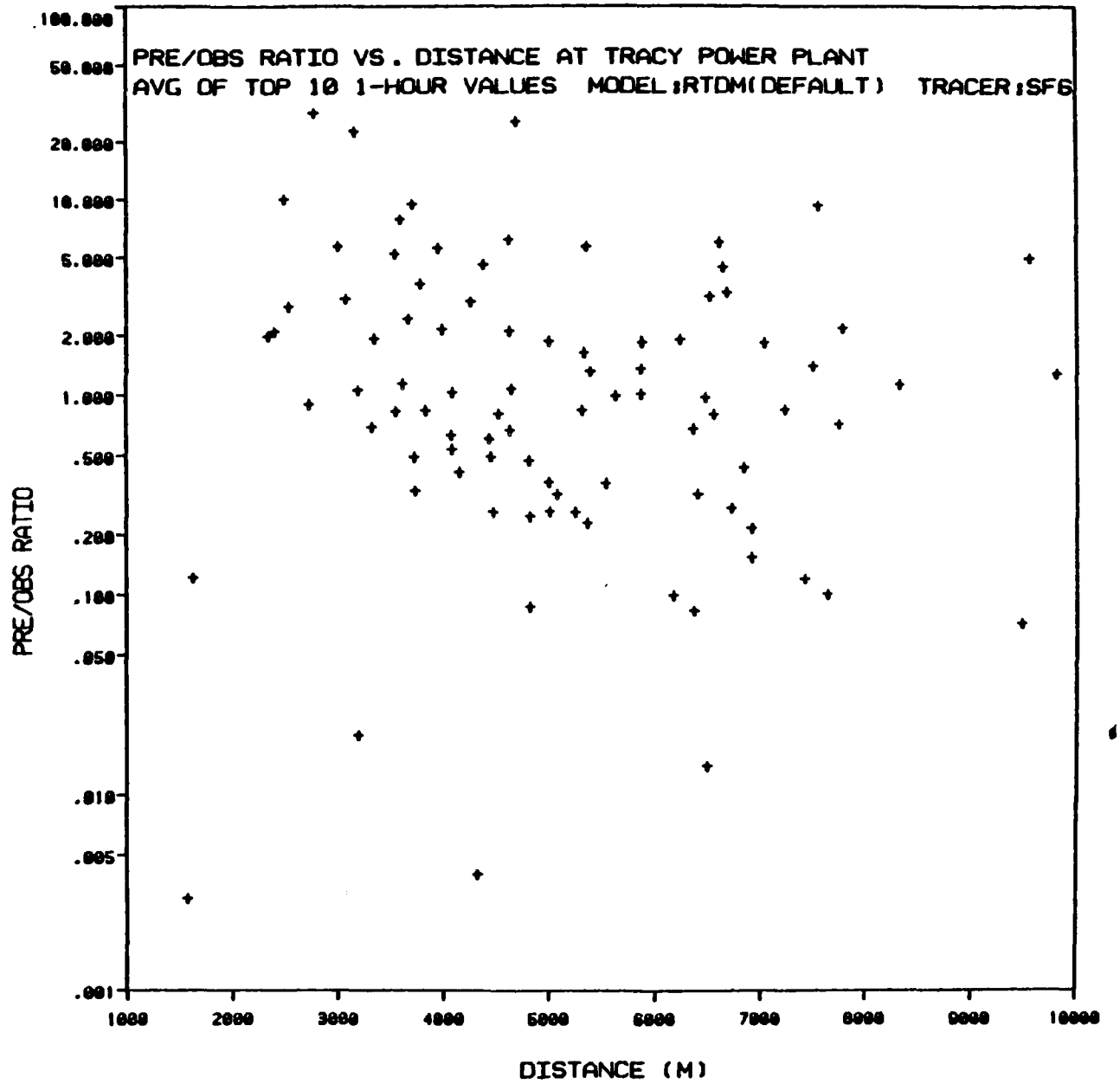
PRE/OBS RATIO VS. DISTANCE AT TRACY POWER PLANT
AVG OF TOP 10 1-HOUR VALUES MODEL:RTDM(DEFAULT) TRACER:SF6
PRE/OBS RATIO
100.000
50.000
20.000
10.000
5.000
2.000
1.000
.500
.200
.100
.050
.010
.005
.001
1000
2000
3000
4000
5000
6000
7000
8000
9000
10000
DISTANCE (M)

Figure F-43

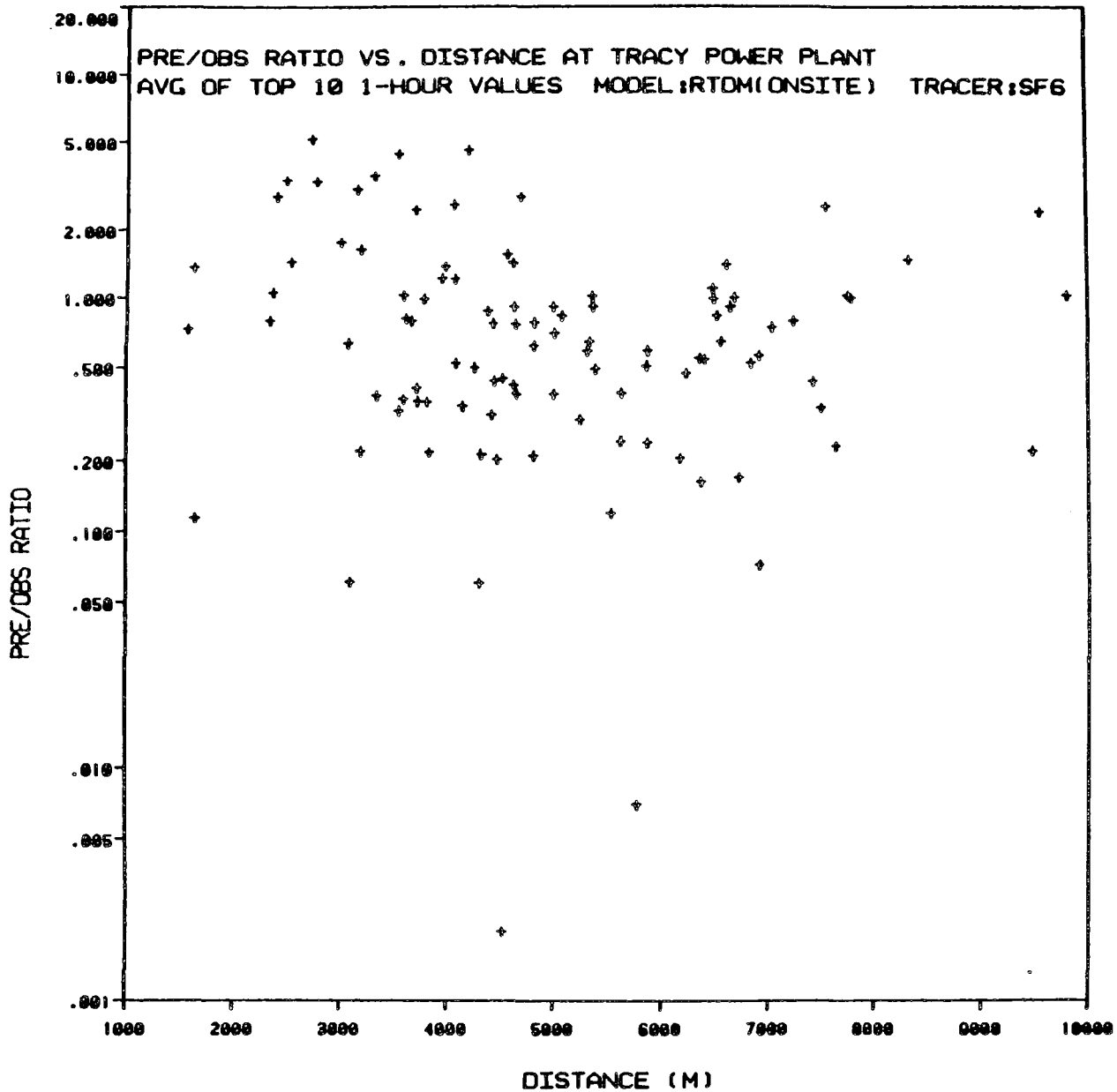
PRE/OBS RATIO VS. DISTANCE AT TRACY POWER PLANT
AVG OF TOP 10 1-HOUR VALUES MODEL:RTDM(ONSITE) TRACER:SF6
PRE/OBS RATIO
20.000
10.000
5.000
2.000
1.000
.500
.200
.100
.050
.010
.005
.001
1000
2000
3000
4000
5000
6000
7000
8000
9000
10000
DISTANCE (M)

Figure F-44

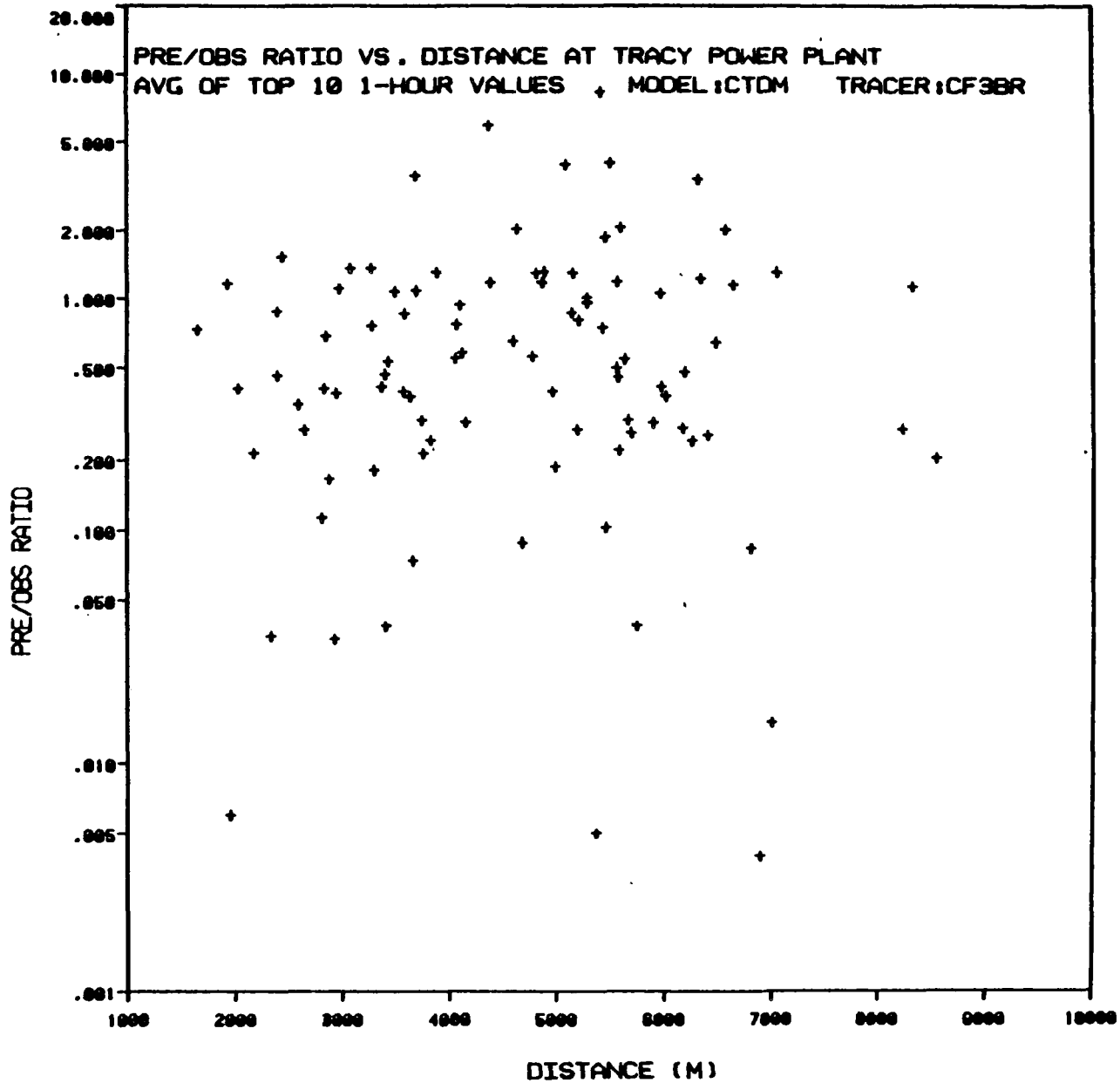
PRE/OBS RATIO VS. DISTANCE AT TRACY POWER PLANT
AVG OF TOP 10 1-HOUR VALUES + MODEL:CTDM TRACER:CF3BR
PRE/OBS RATIO
20.000
10.000
5.000
2.000
1.000
.500
.200
.100
.050
.010
.005
.001
1000
2000
3000
4000
5000
6000
7000
8000
9000
10000
DISTANCE (M)

Figure F-45

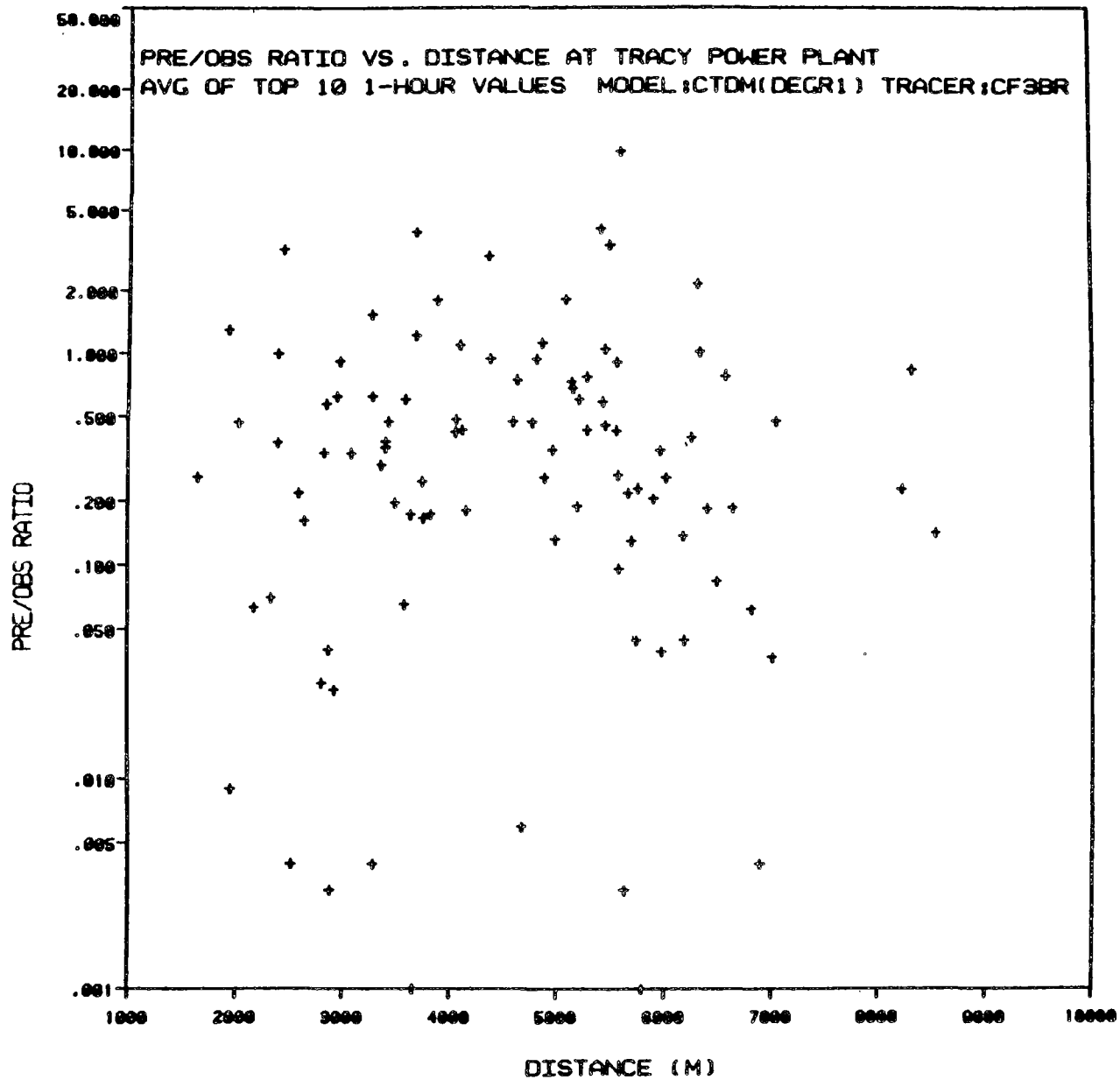
PRE/OBS RATIO VS. DISTANCE AT TRACY POWER PLANT
AVG OF TOP 10 1-HOUR VALUES MODEL:CTDM(DEGR1) TRACER:CF3BR
50.000
20.000
10.000
5.000
2.000
1.000
.500
.200
.100
.050
.010
.005
.001
PRE/OBS RATIO
1000
2000
3000
4000
5000
6000
7000
8000
9000
10000
DISTANCE (M)

Figure F-46

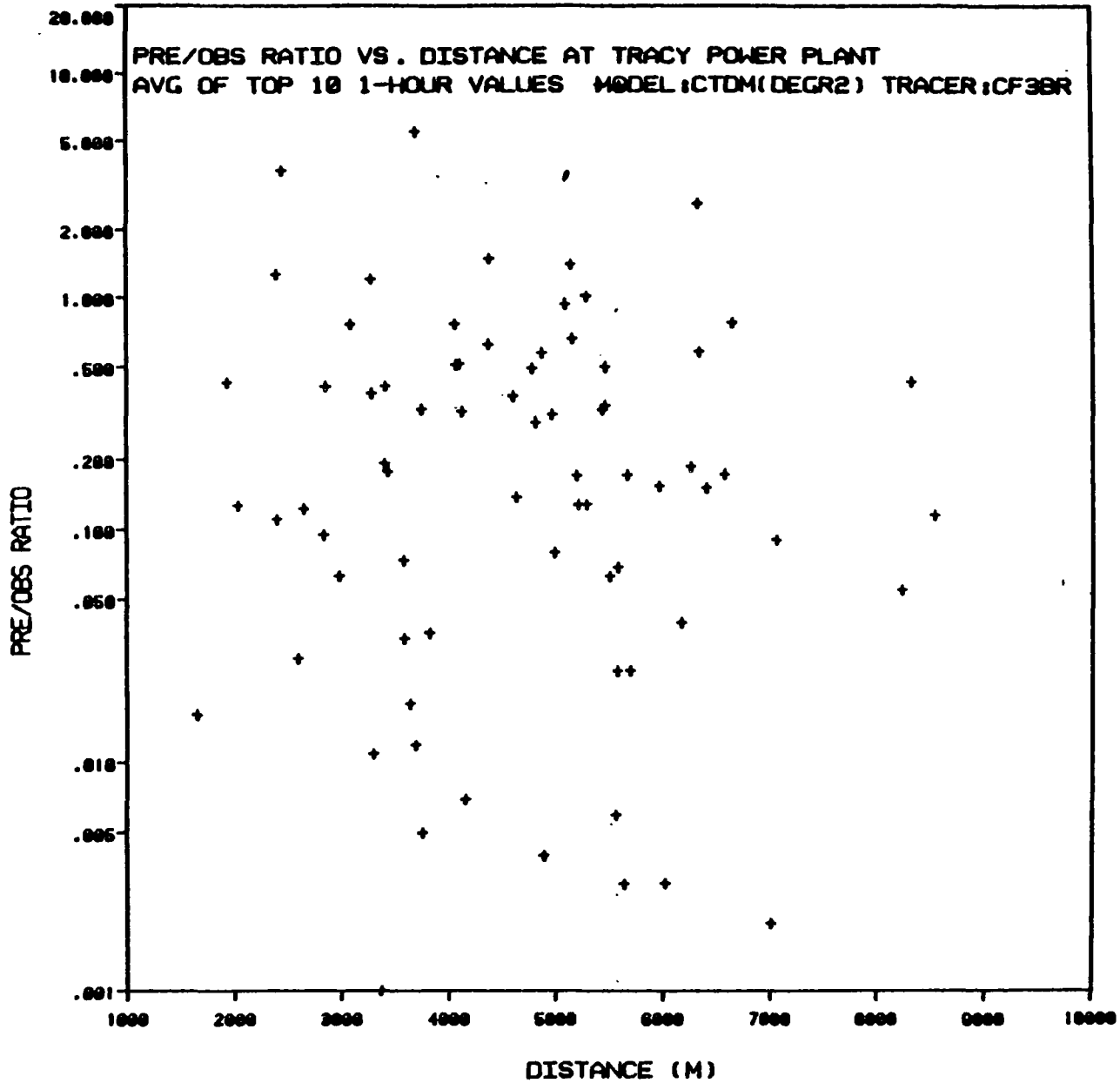
PRE/OBS RATIO VS. DISTANCE AT TRACY POWER PLANT
AVG OF TOP 10 1-HOUR VALUES MODEL:CTDM(DEGR2) TRACER:CF3BR
PRE/OBS RATIO
20.000
10.000
5.000
2.000
1.000
.500
.200
.100
.050
.010
.005
.001
1000
2000
3000
4000
5000
6000
7000
8000
9000
10000
DISTANCE (M)

Figure F-47

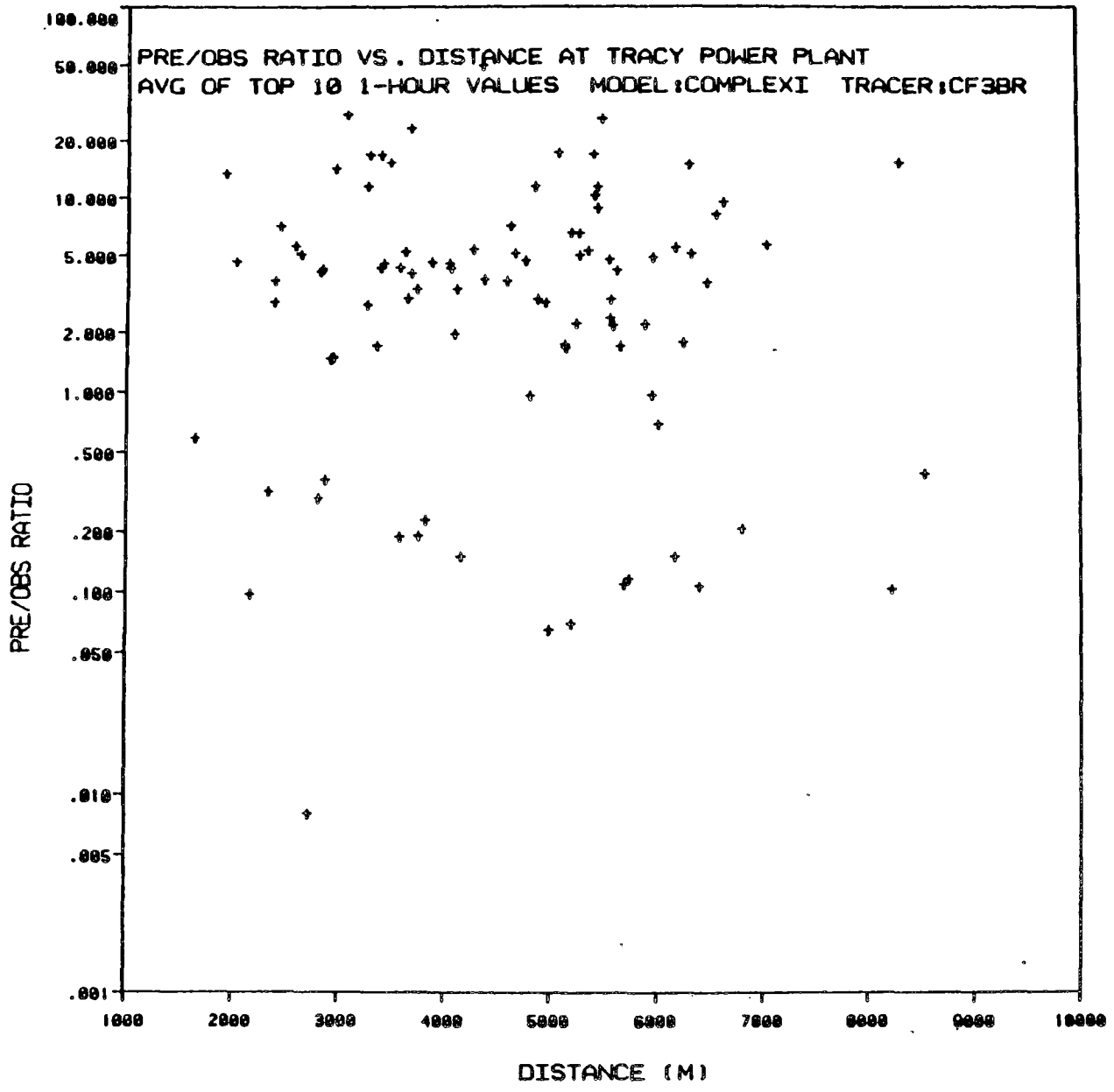
PRE/OBS RATIO VS. DISTANCE AT TRACY POWER PLANT
AVG OF TOP 10 1-HOUR VALUES MODEL:COMPLEXI TRACER:CF3BR
PRE/OBS RATIO
100.000
50.000
20.000
10.000
5.000
2.000
1.000
.500
.200
.100
.050
.010
.005
.001
1000
2000
3000
4000
5000
6000
7000
8000
9000
10000
DISTANCE (M)

Figure F-48

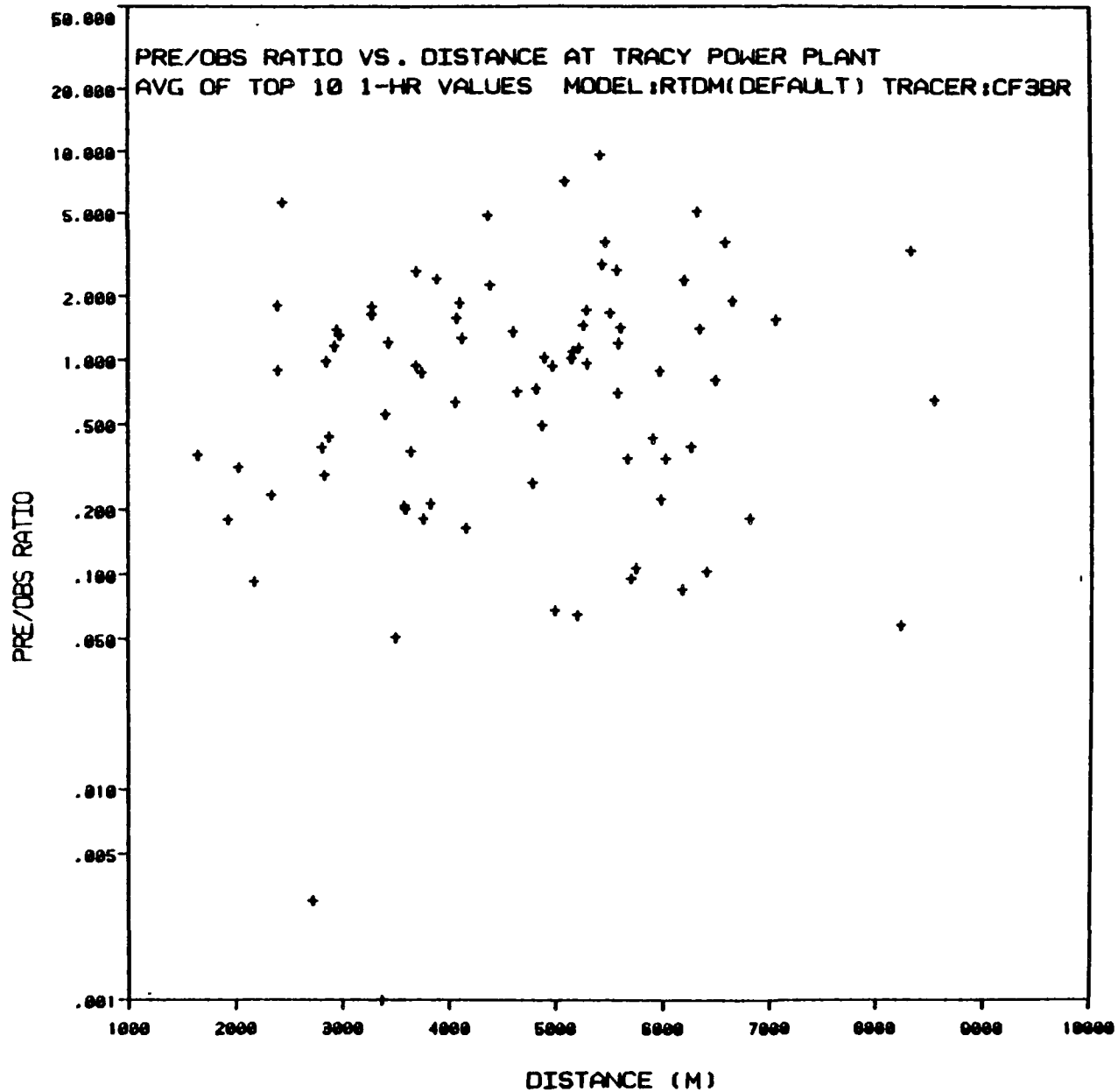
PRE/OBS RATIO VS. DISTANCE AT TRACY POWER PLANT
AVG OF TOP 10 1-HR VALUES MODEL:RTDM(DEFAULT) TRACER:CF3BR
50.000
20.000
10.000
5.000
2.000
1.000
.500
.200
.100
.050
.010
.005
.001
PRE/OBS RATIO
1000
2000
3000
4000
5000
6000
7000
8000
9000
10000
DISTANCE (M)

Figure F-49

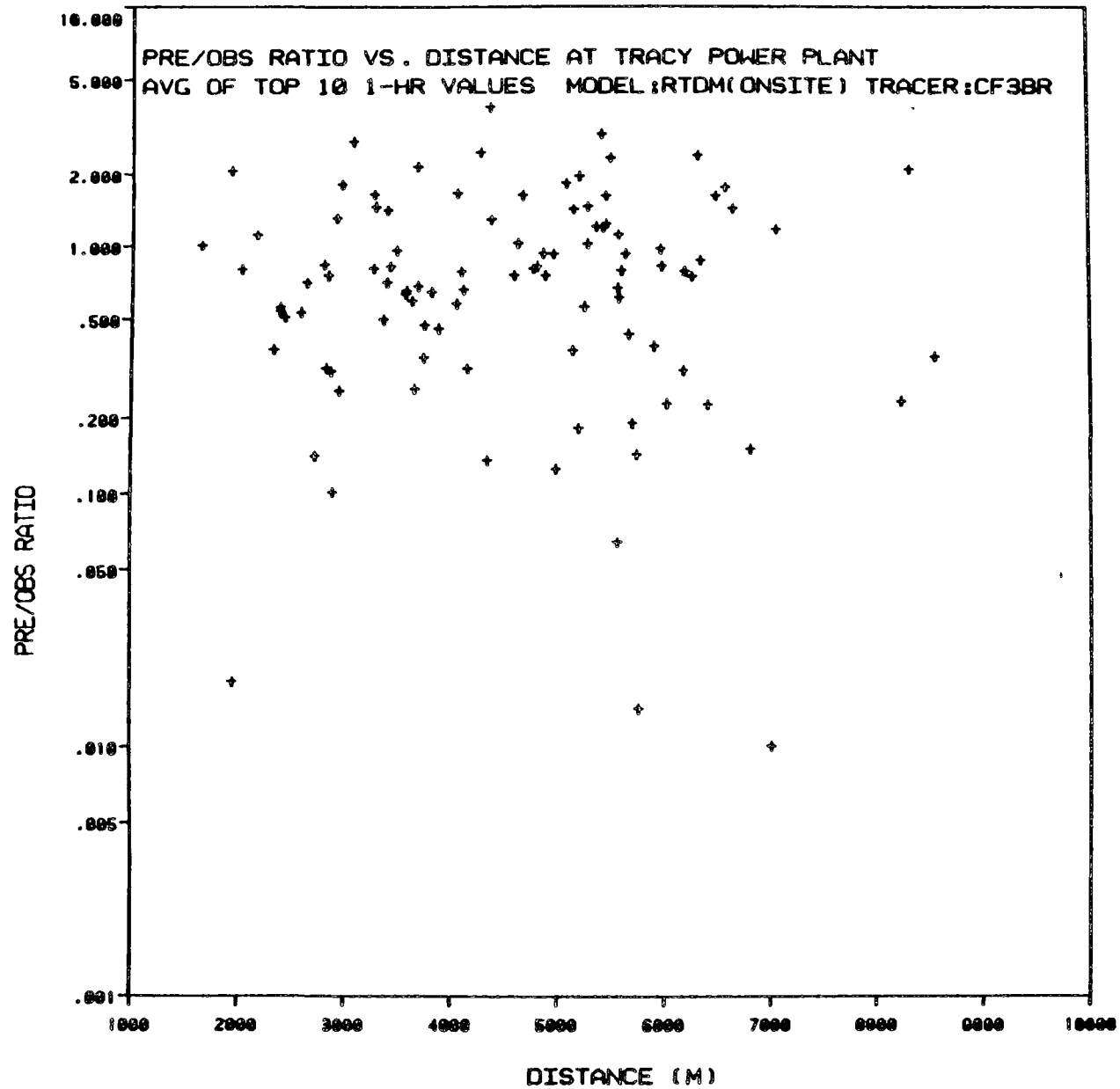
PRE/OBS RATIO VS. DISTANCE AT TRACY POWER PLANT
AVG OF TOP 10 1-HR VALUES MODEL:RTDM(ONSITE) TRACER:CF3BR
PRE/OBS RATIO
10.000
5.000
2.000
1.000
.500
.200
.100
.050
.010
.005
.001
1000
2000
3000
4000
5000
6000
7000
8000
9000
10000
DISTANCE (M)

Figure F-50

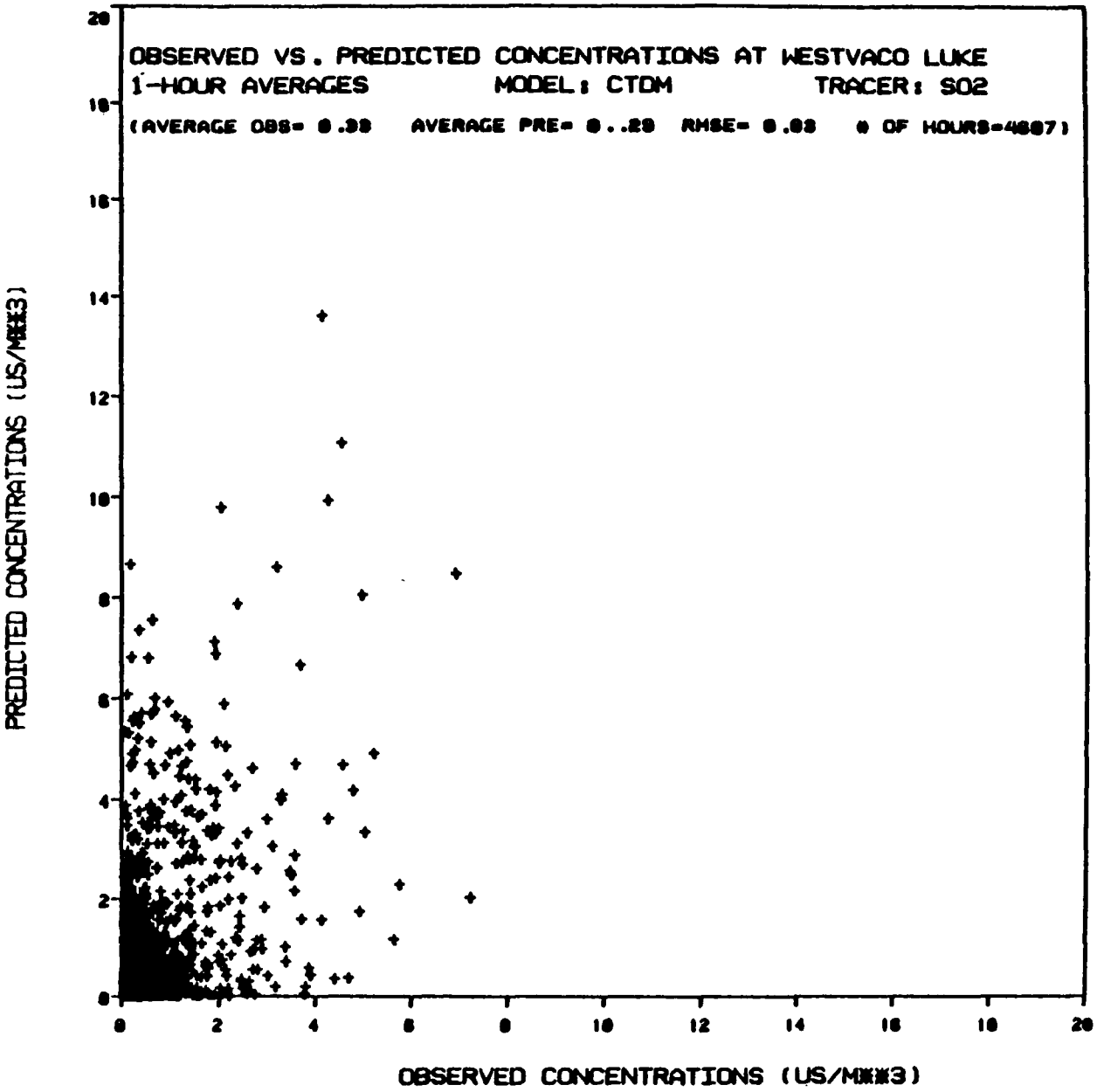
OBSERVED VS. PREDICTED CONCENTRATIONS AT WESTVACO LUKE
1-HOUR AVERAGES MODEL: CTDM TRACER: SO2
(AVERAGE OBS= 0.38 AVERAGE PRE= 0..28 RMSE= 0.83 # OF HOURS=4887)
PREDICTED CONCENTRATIONS (US/M**3)
OBSERVED CONCENTRATIONS (US/M**3)
0
2
4
6
8
10
12
14
16
18
20

Figure F-51

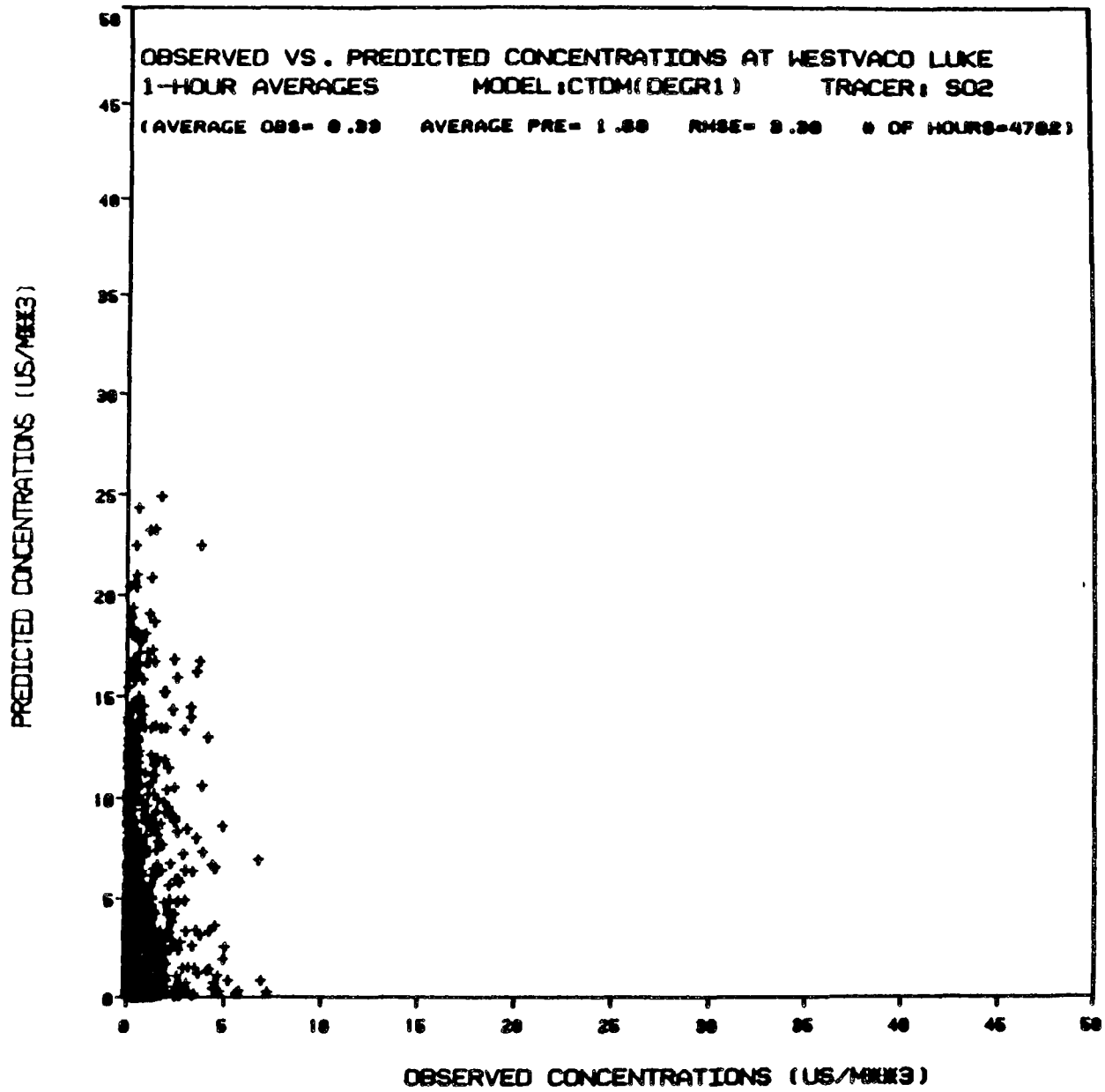
OBSERVED VS. PREDICTED CONCENTRATIONS AT WESTVACO LUKE
1-HOUR AVERAGES MODEL:CTDM(DEGR1) TRACER: SO2
(AVERAGE OBS= 0.39 AVERAGE PRE= 1.58 RMSE= 3.30 # OF HOURS=4782)
PREDICTED CONCENTRATIONS (US/M**3)
OBSERVED CONCENTRATIONS (US/M**3)
0
5
10
15
20
25
30
35
40
45
50

Figure F-52

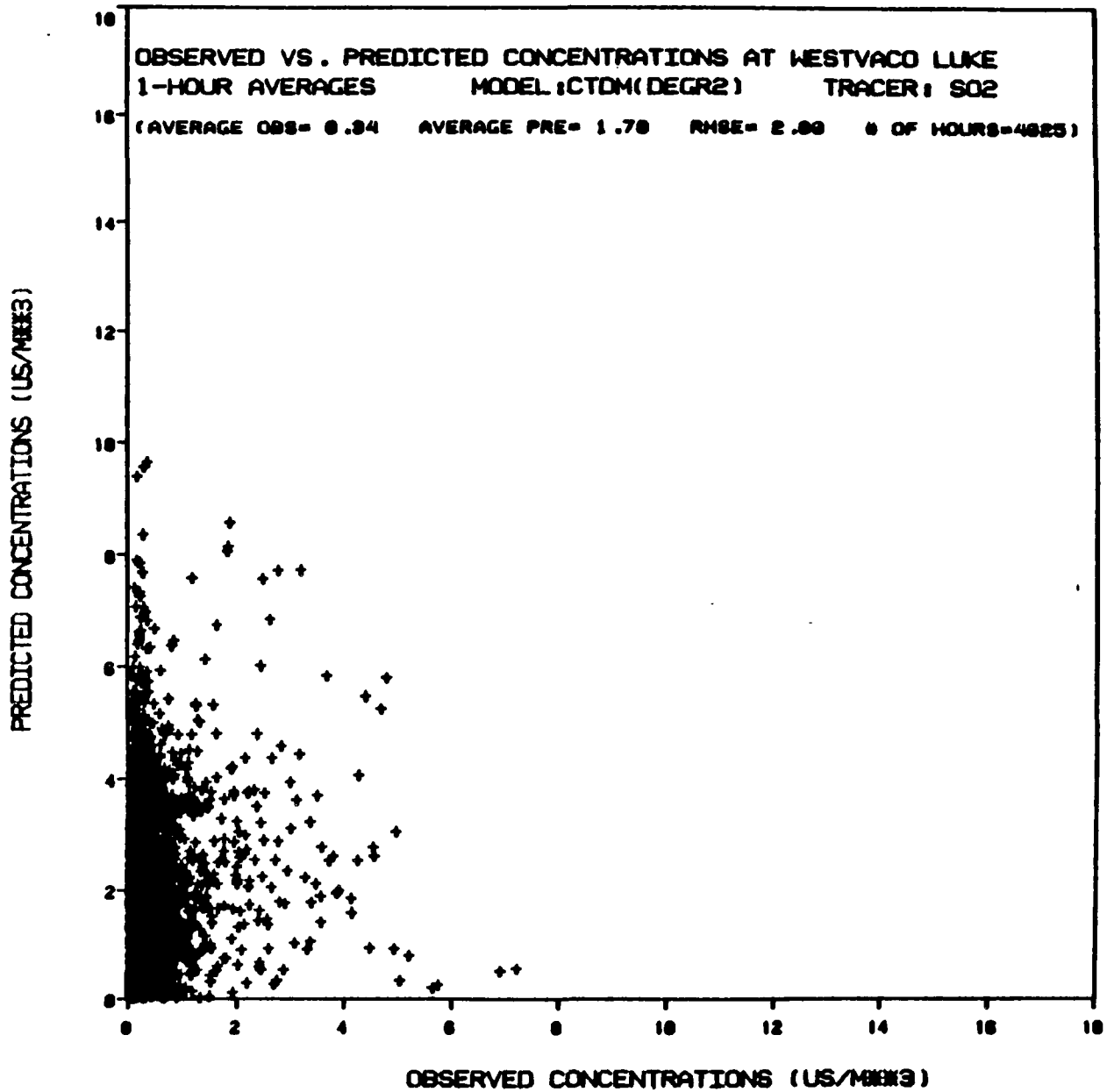
OBSERVED VS. PREDICTED CONCENTRATIONS AT WESTVACO LUKE
1-HOUR AVERAGES MODEL:CTDM(DEGR2) TRACER: SO2
(AVERAGE OBS= 0.84 AVERAGE PRE= 1.70 RMSE= 2.00 # OF HOURS=4825)
PREDICTED CONCENTRATIONS (US/M**3)
OBSERVED CONCENTRATIONS (US/M**3)
0
2
4
6
8
10
12
14
16
18

Figure F-53

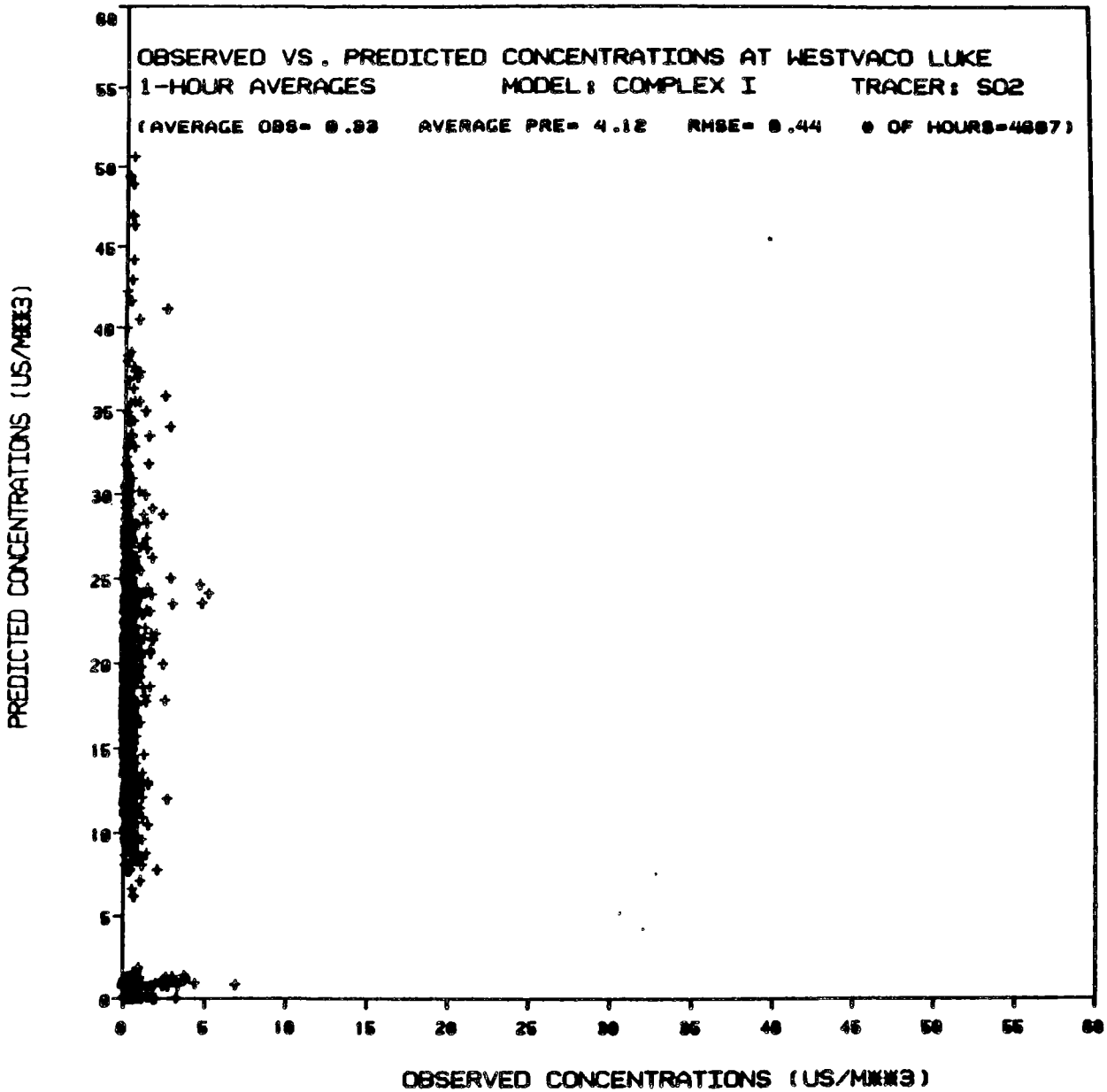
OBSERVED VS. PREDICTED CONCENTRATIONS AT WESTVACO LUKE
1-HOUR AVERAGES
MODEL: COMPLEX I
TRACER: SO2
(AVERAGE OBS= 0.93 AVERAGE PRE= 4.12 RMSE= 0.44 # OF HOURS=4887)
PREDICTED CONCENTRATIONS (US/MXX3)
OBSERVED CONCENTRATIONS (US/MXX3)
0
5
10
15
20
25
30
35
40
45
50
55
60

Figure F-54

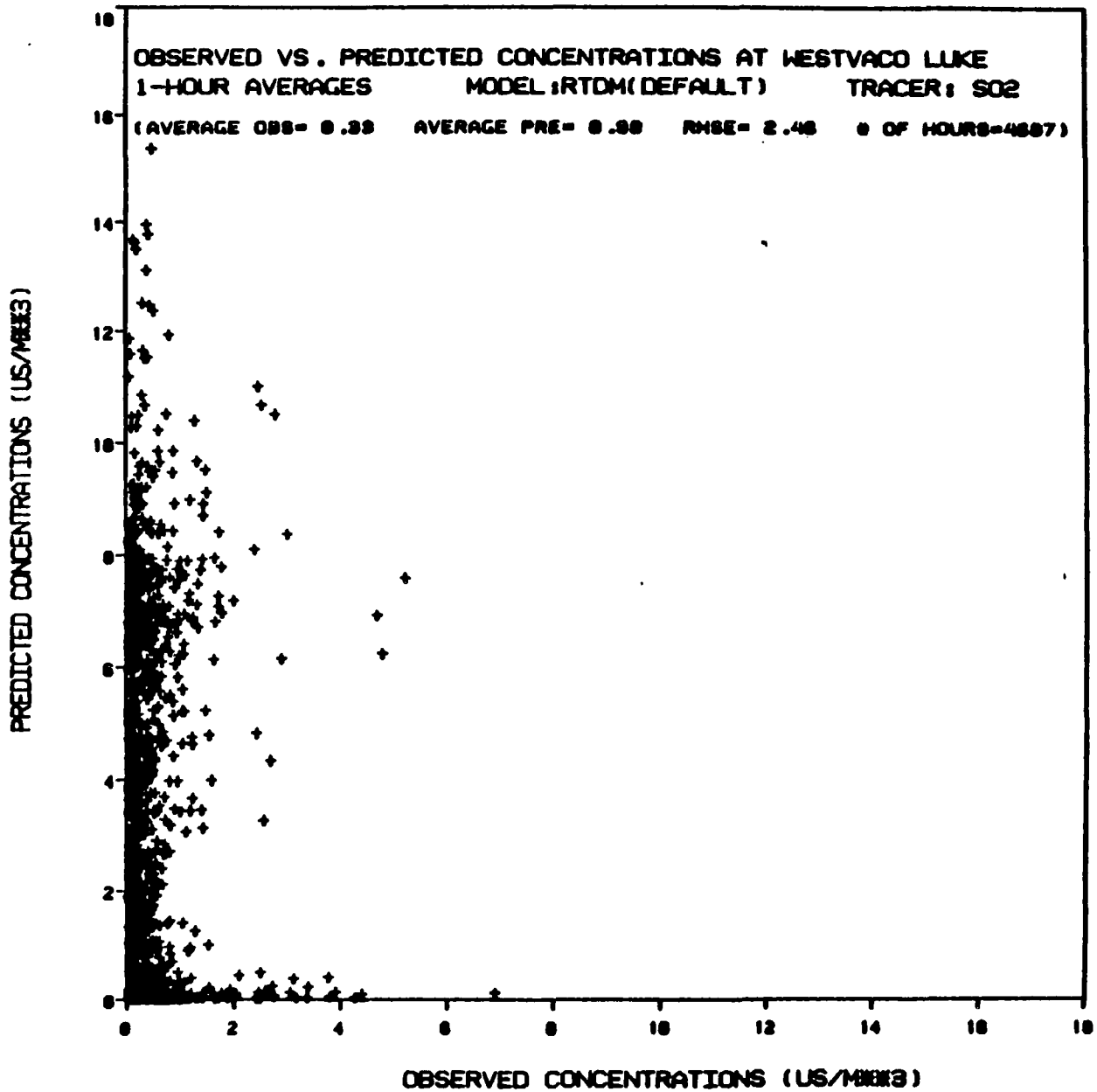
OBSERVED VS. PREDICTED CONCENTRATIONS AT WESTVACO LUKE
1-HOUR AVERAGES MODEL:RTDM(DEFAULT) TRACER: SO2
(AVERAGE OBS= 0.39 AVERAGE PRE= 0.38 RMSE= 2.46 # OF HOURS=4607)
PREDICTED CONCENTRATIONS (US/M**3)
OBSERVED CONCENTRATIONS (US/M**3)
0
2
4
6
8
10
12
14
16
18

Figure F-55

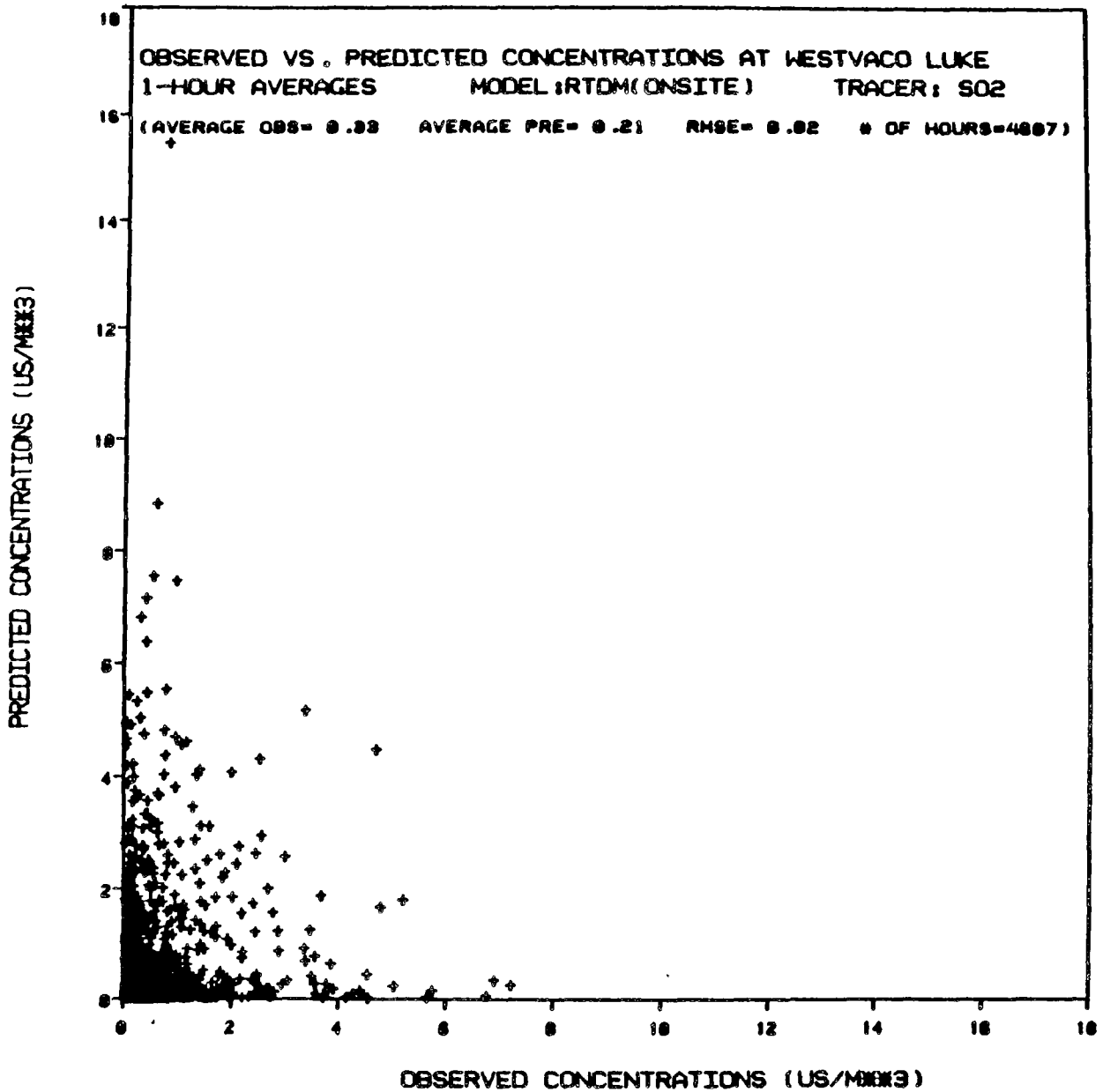
OBSERVED VS. PREDICTED CONCENTRATIONS AT WESTVACO LUKE
1-HOUR AVERAGES MODEL:RTDM(ONSITE) TRACER: SO2
(AVERAGE OBS= 0.33 AVERAGE PRE= 0.21 RMSE= 0.82 # OF HOURS=4887)
PREDICTED CONCENTRATIONS (US/M**3)
OBSERVED CONCENTRATIONS (US/M**3)
0
2
4
6
8
10
12
14
16
18

Figure F-56

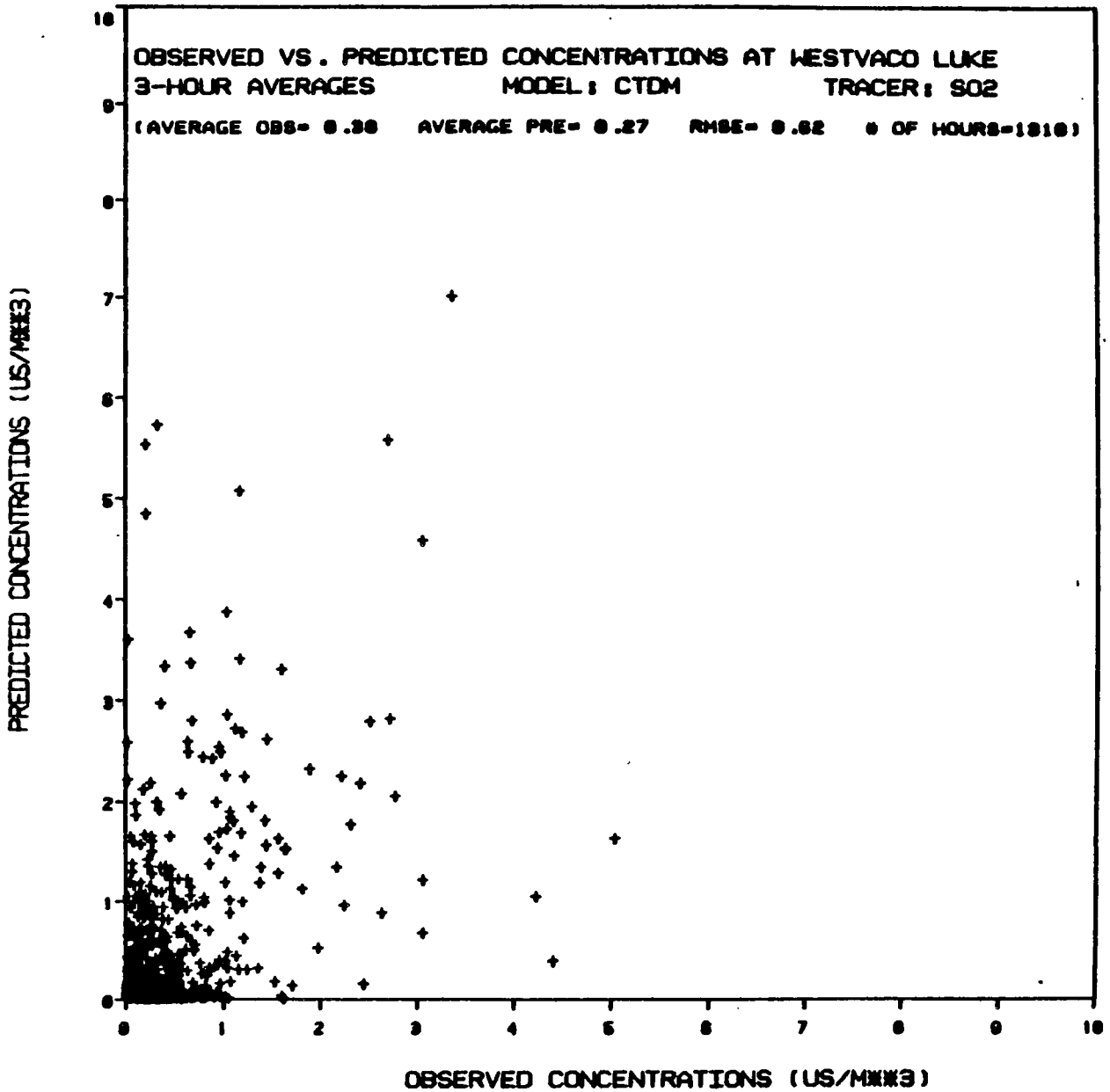
OBSERVED VS. PREDICTED CONCENTRATIONS AT WESTVACO LUKE
3-HOUR AVERAGES MODEL: CTDM TRACER: SO2
(AVERAGE OBS= 0.38 AVERAGE PRE= 0.27 RMSE= 0.82 # OF HOURS=1818)
PREDICTED CONCENTRATIONS (US/M**3)
OBSERVED CONCENTRATIONS (US/M**3)
0
1
2
3
4
5
6
7
8
9
10

Figure F-57

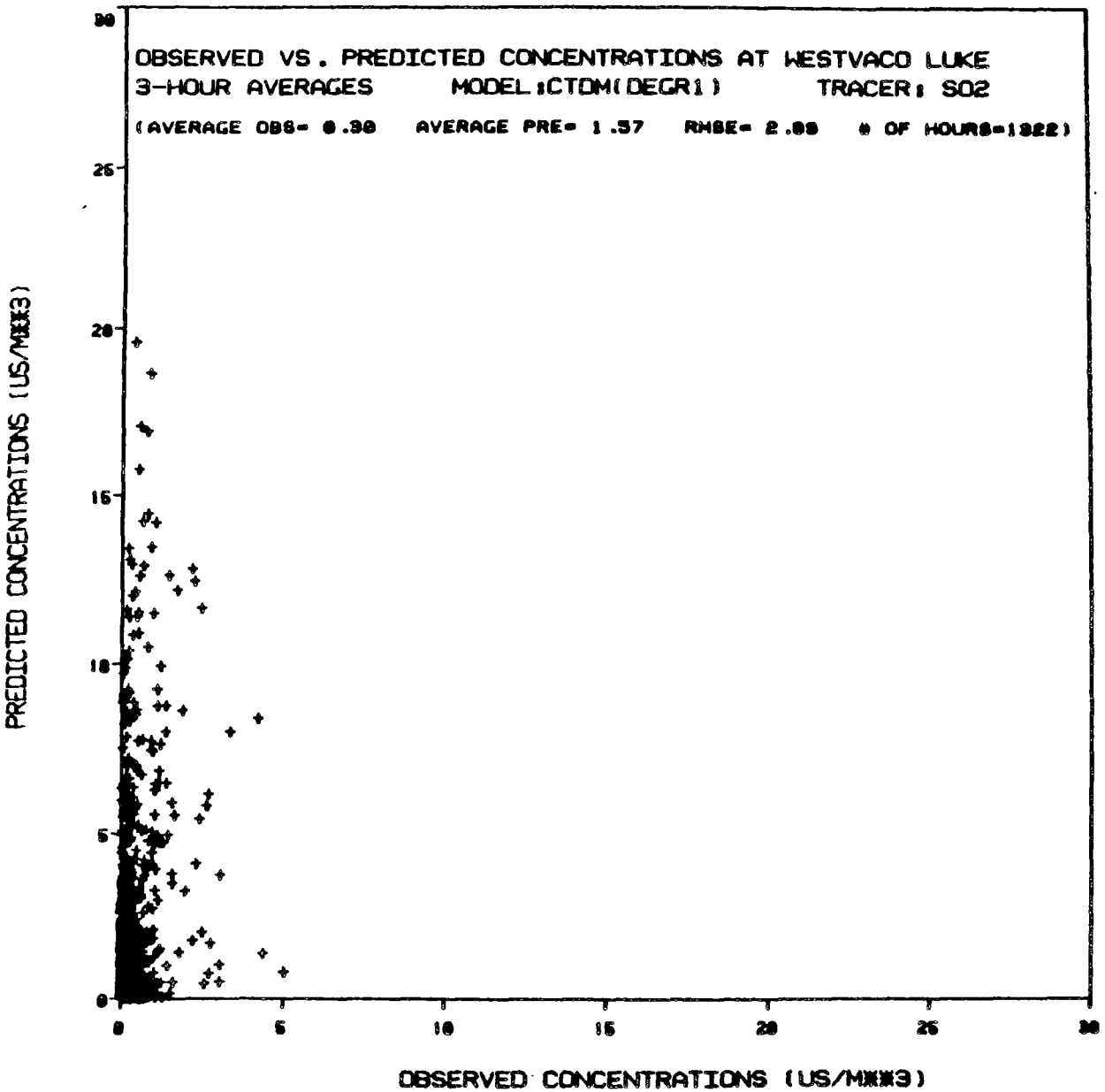
OBSERVED VS. PREDICTED CONCENTRATIONS AT WESTVACO LUKE
3-HOUR AVERAGES MODEL:CTDM(DEGR1) TRACER: SO2
(AVERAGE OBS= 0.30 AVERAGE PRE= 1.57 RMSE= 2.09 # OF HOURS=1822)
PREDICTED CONCENTRATIONS (US/M**3)
OBSERVED CONCENTRATIONS (US/M**3)
0
5
10
15
20
25
30

Figure F-58

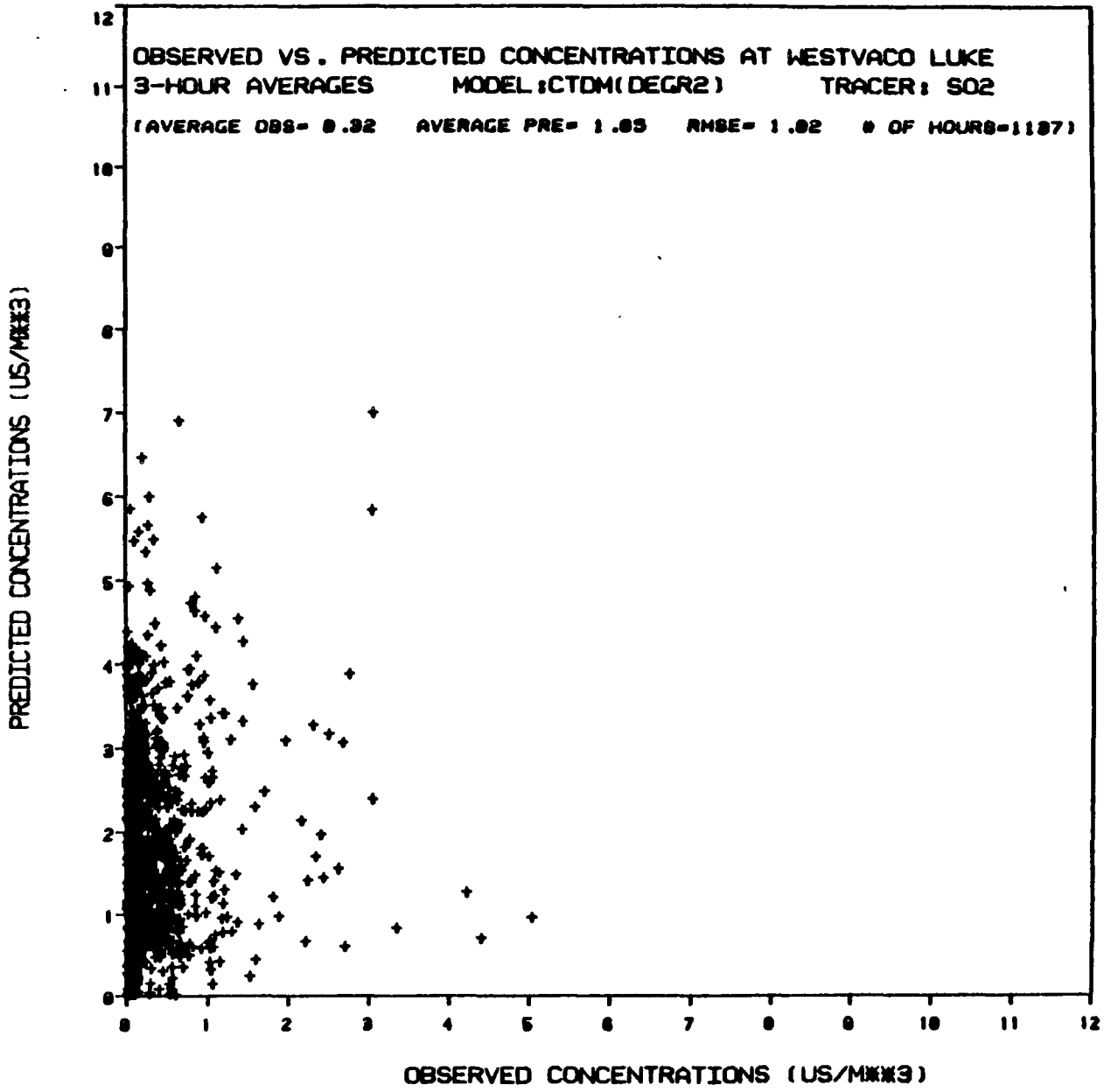
OBSERVED VS. PREDICTED CONCENTRATIONS AT WESTVACO LUKE
3-HOUR AVERAGES MODEL:CTDM(DEGR2) TRACER: SO2
(AVERAGE OBS= 0.32 AVERAGE PRE= 1.05 RMSE= 1.02 # OF HOURS=1187)
PREDICTED CONCENTRATIONS (US/M***3)
OBSERVED CONCENTRATIONS (US/M***3)
0
1
2
3
4
5
6
7
8
9
10
11
12

Figure F-59

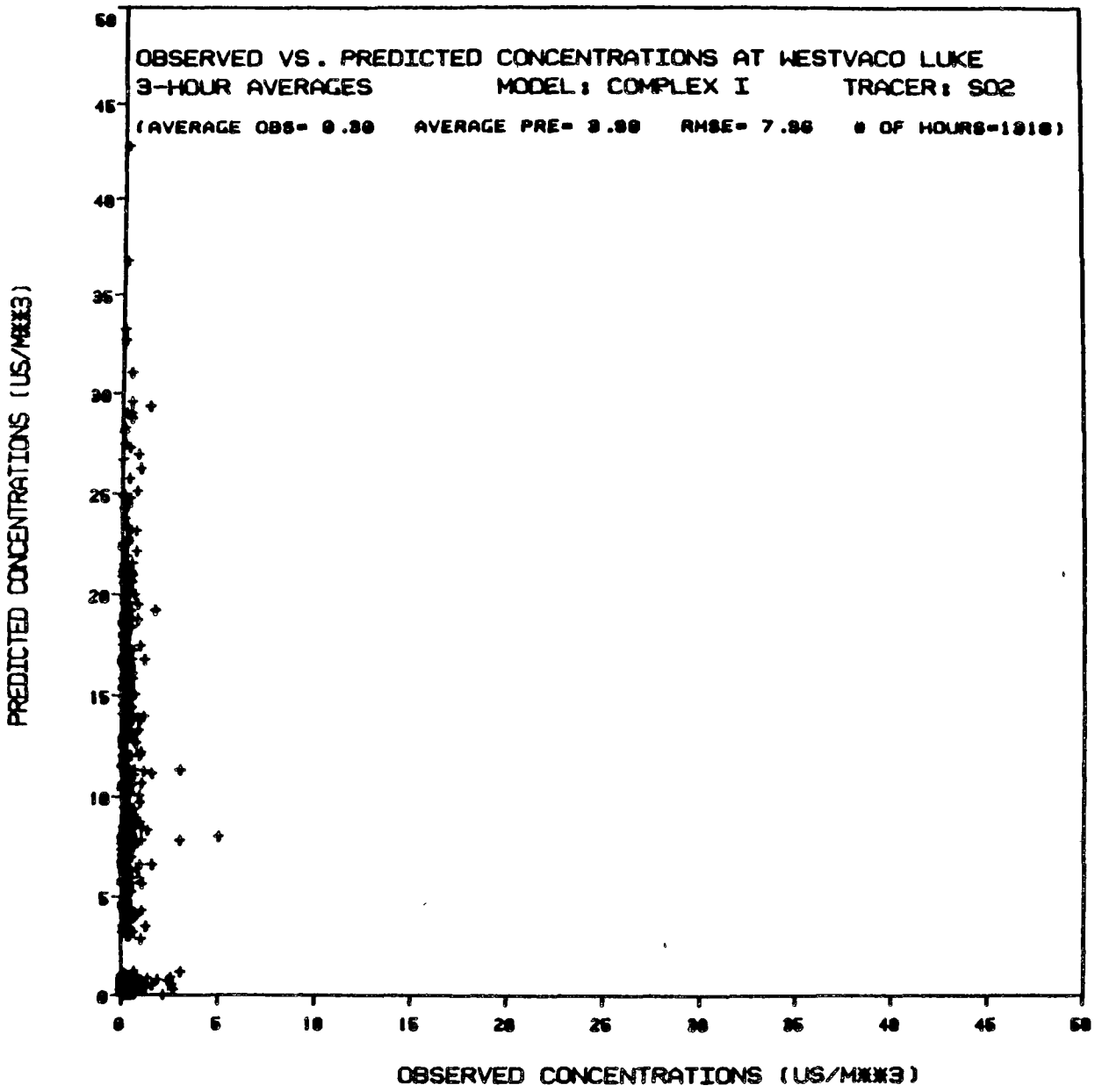
OBSERVED VS. PREDICTED CONCENTRATIONS AT WESTVACO LUKE
3-HOUR AVERAGES
MODEL: COMPLEX I
TRACER: SO2
(AVERAGE OBS= 0.00 AVERAGE PRE= 0.00 RMSE= 7.00 # OF HOURS=1010)
PREDICTED CONCENTRATIONS (US/M**3)
OBSERVED CONCENTRATIONS (US/M**3)
0
5
10
15
20
25
30
35
40
45
50

Figure F-60

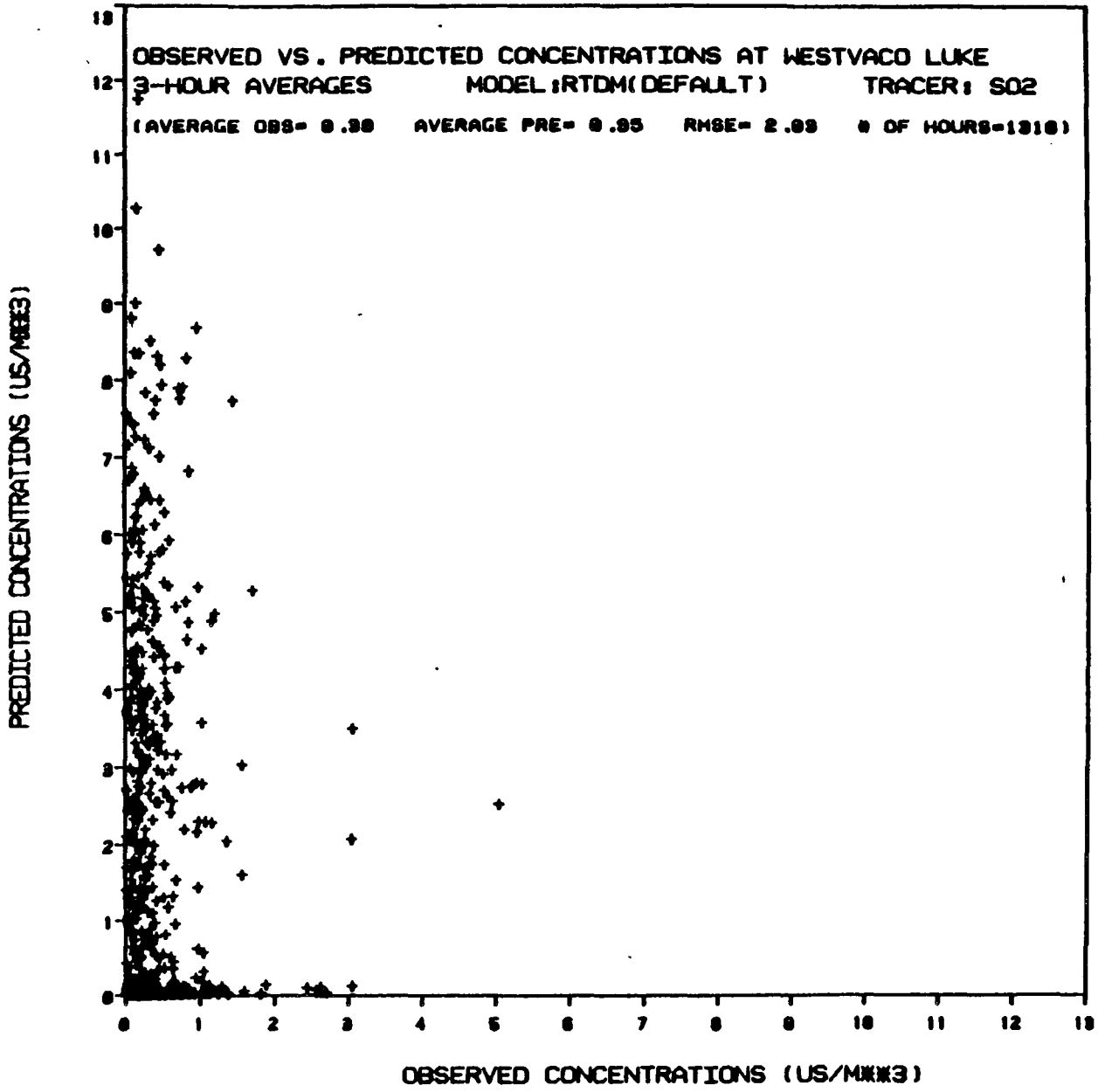
OBSERVED VS. PREDICTED CONCENTRATIONS AT WESTVACO LUKE
3-HOUR AVERAGES MODEL:RTDM(DEFAULT) TRACER: SO2
(AVERAGE OBS= 0.30 AVERAGE PRE= 0.95 RMSE= 2.09 # OF HOURS=1318)
PREDICTED CONCENTRATIONS (US/M***3)
OBSERVED CONCENTRATIONS (US/M***3)
0
1
2
3
4
5
6
7
8
9
10
11
12
13

Figure F-61

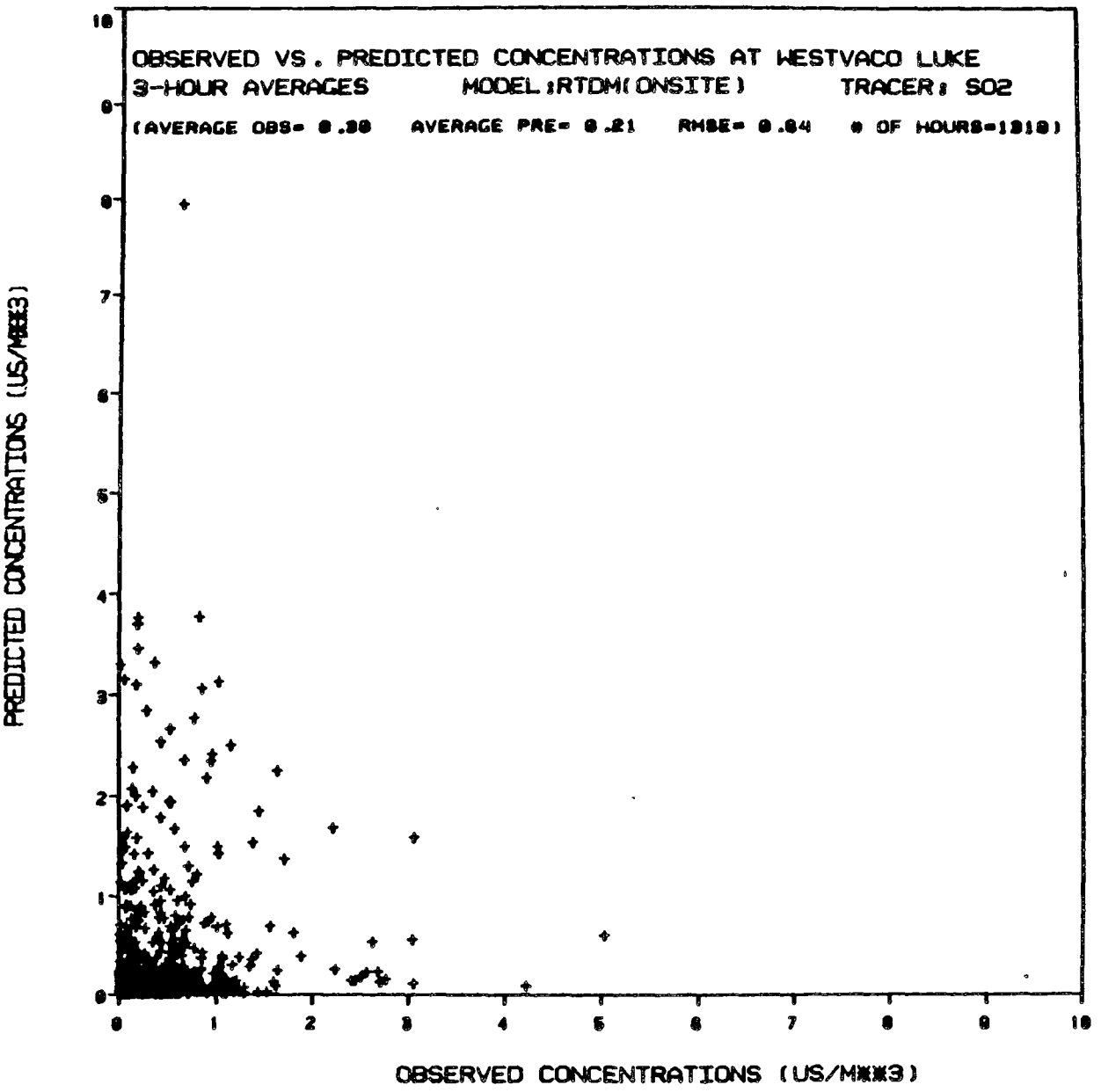
OBSERVED VS. PREDICTED CONCENTRATIONS AT WESTVACO LUKE
3-HOUR AVERAGES MODEL:RTDM(ONSITE) TRACER: SO2
(AVERAGE OBS= 0.30 AVERAGE PRE= 0.21 RMSE= 0.84 # OF HOURS=1910)
PREDICTED CONCENTRATIONS (US/M**3)
OBSERVED CONCENTRATIONS (US/M**3)
0
1
2
3
4
5
6
7
8
9
10

Figure F-62

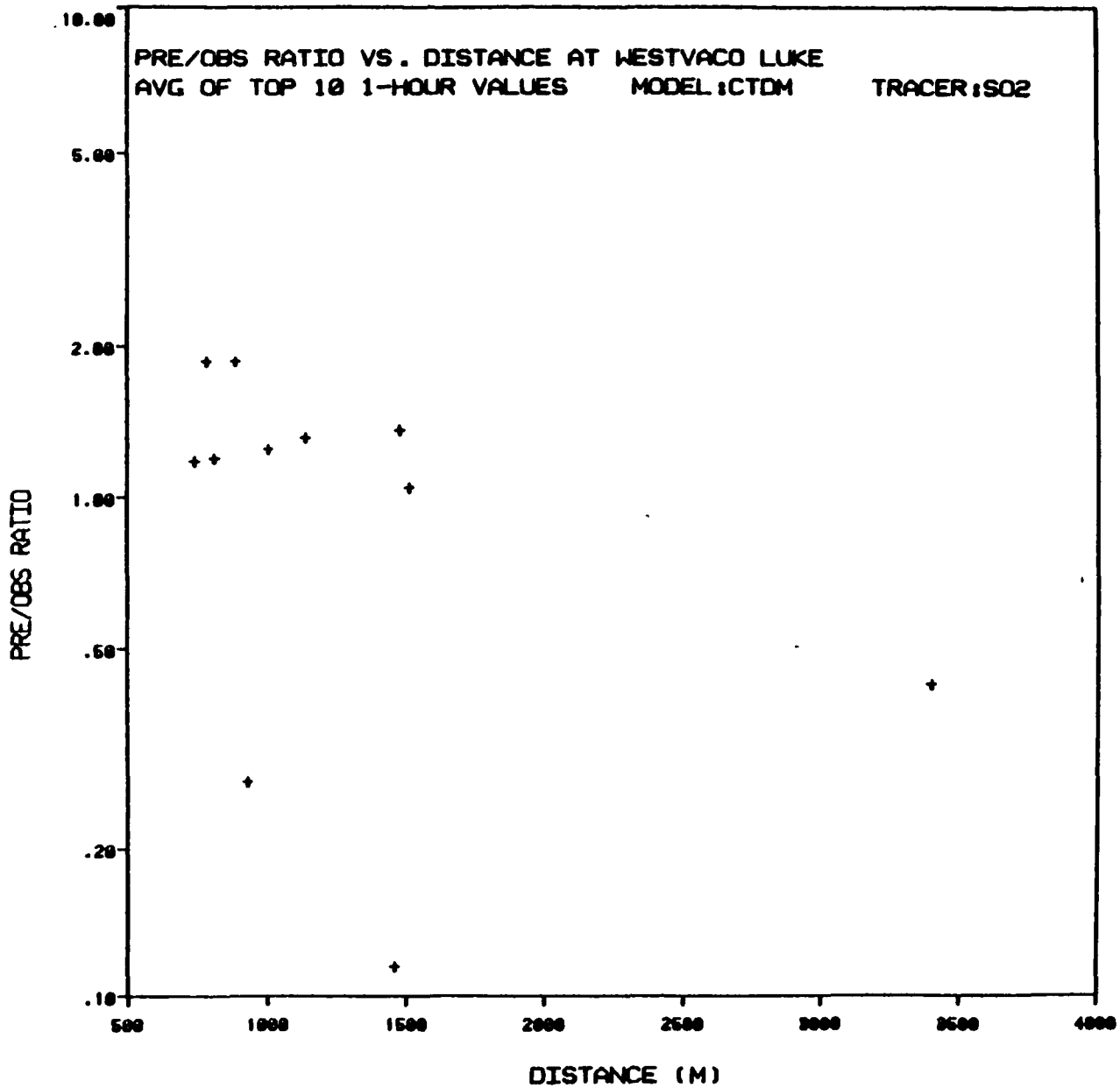
PRE/OBS RATIO VS. DISTANCE AT WESTVACO LUKE
AVG OF TOP 10 1-HOUR VALUES MODEL:CTDM TRACER:SO2
10.00
5.00
2.00
1.00
.60
.20
.10
PRE/OBS RATIO
500
1000
1500
2000
2500
3000
3500
4000
DISTANCE (M)

Figure F-63

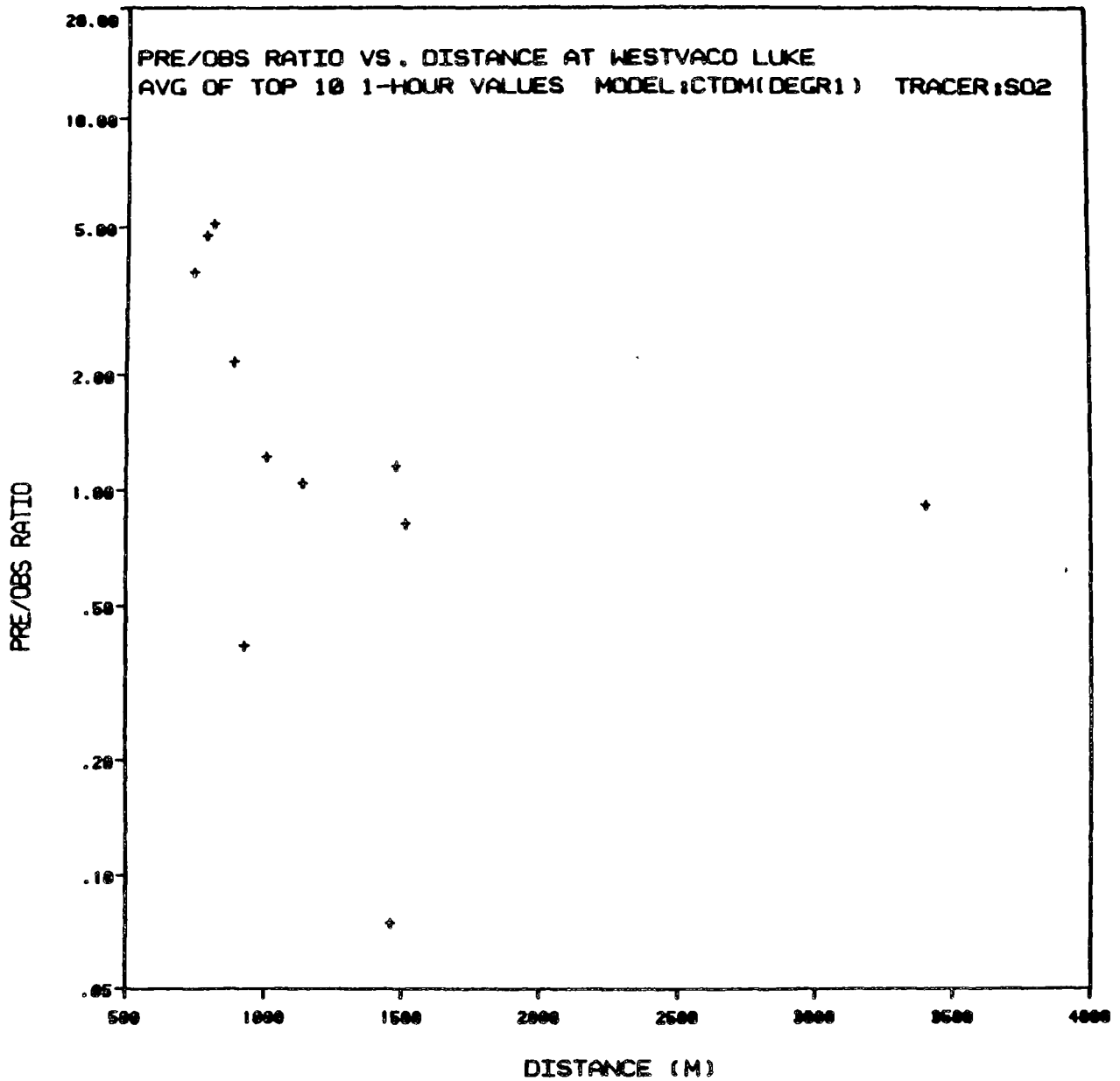
PRE/OBS RATIO VS. DISTANCE AT WESTVACO LUKE
AVG OF TOP 10 1-HOUR VALUES MODEL:CTDM(DEGR1) TRACER:SO2
PRE/OBS RATIO
20.00
10.00
5.00
2.00
1.00
.50
.20
.10
.05
500
1000
1500
2000
2500
3000
3500
4000
DISTANCE (M)

Figure F-64

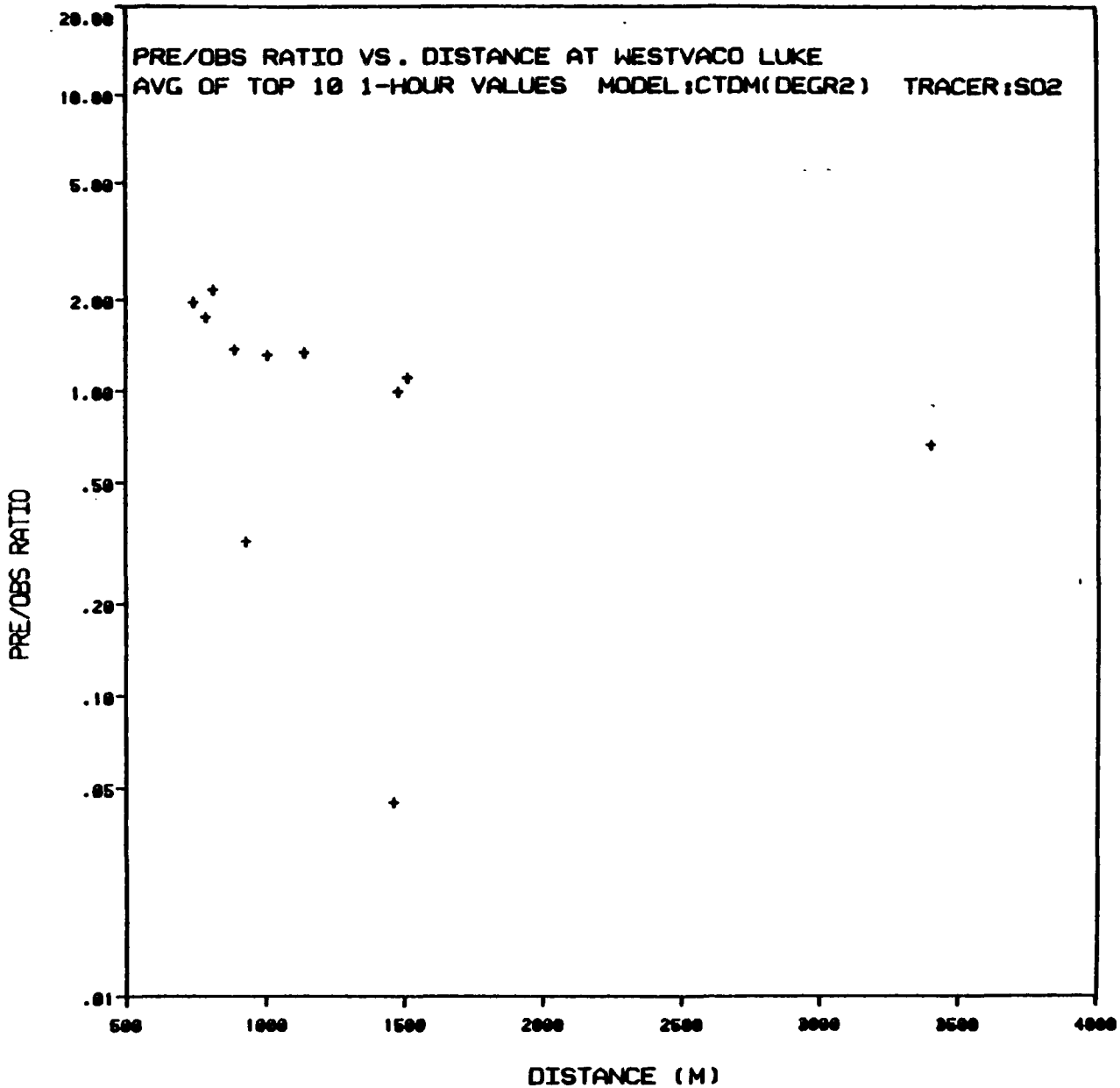
PRE/OBS RATIO VS. DISTANCE AT WESTVACO LUKE
AVG OF TOP 10 1-HOUR VALUES MODEL:CTDM(DEGR2) TRACER:SO2
PRE/OBS RATIO
20.00
10.00
5.00
2.00
1.00
.50
.20
.10
.05
.01
500
1000
1500
2000
2500
3000
3500
4000
DISTANCE (M)

Figure F-65

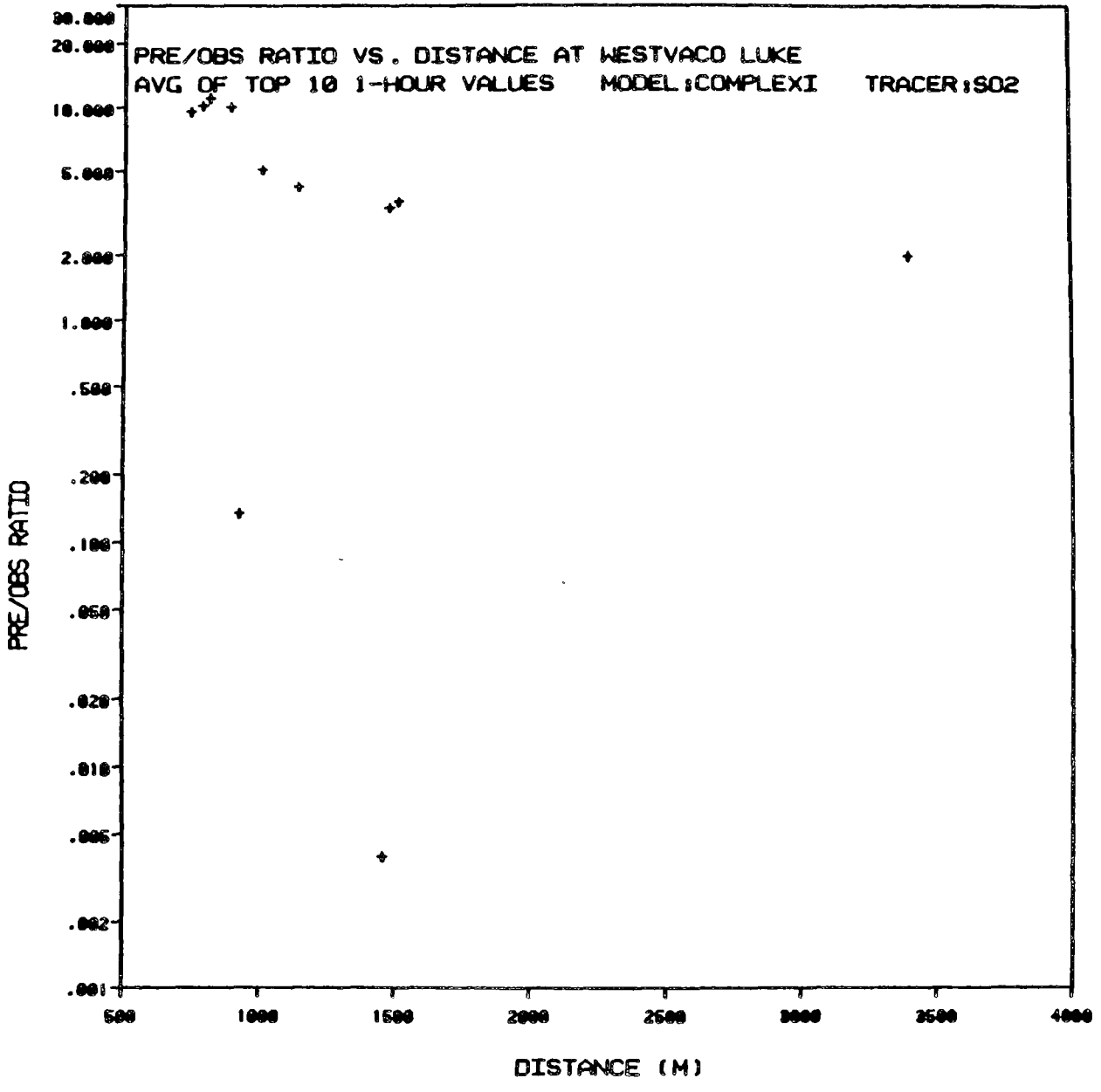
PRE/OBS RATIO VS. DISTANCE AT WESTVACO LUKE
AVG OF TOP 10 1-HOUR VALUES MODEL:COMPLEXI TRACER:SO2
PRE/OBS RATIO
20.000
10.000
5.000
2.000
1.000
.500
.200
.100
.050
.020
.010
.005
.002
.001
500
1000
1500
2000
2500
3000
3500
4000
DISTANCE (M)

Figure F-66

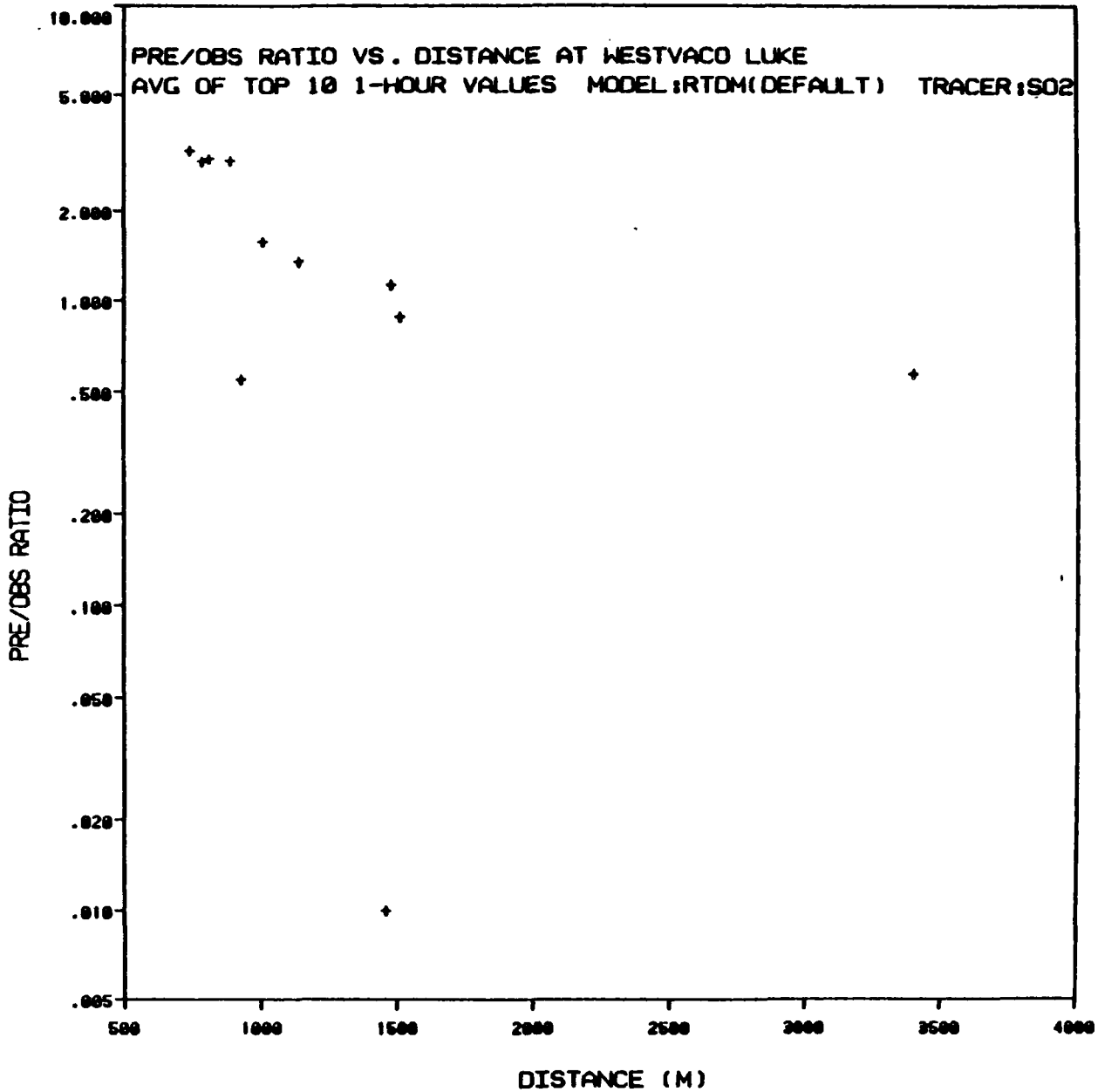
PRE/OBS RATIO VS. DISTANCE AT WESTVACO LUKE
AVG OF TOP 10 1-HOUR VALUES MODEL:RTDM(DEFAULT) TRACER:SO2
PRE/OBS RATIO
10.000
5.000
2.000
1.000
.500
.200
.100
.050
.020
.010
.005
500
1000
1500
2000
2500
3000
3500
4000
DISTANCE (M)

Figure F-67

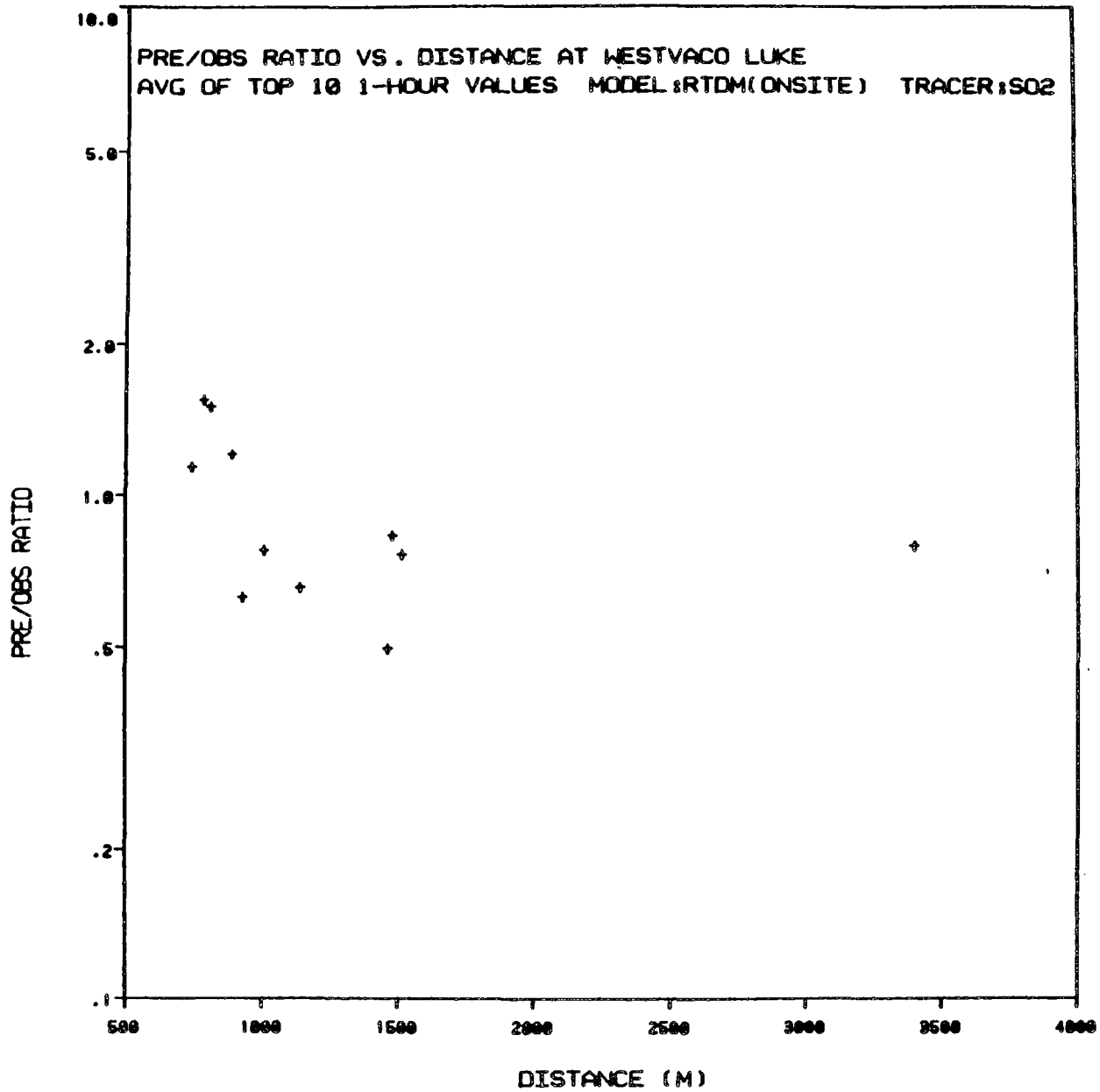
PRE/OBS RATIO VS. DISTANCE AT WESTVACO LUKE
AVG OF TOP 10 1-HOUR VALUES MODEL:RTDM(ONSITE) TRACER:SO2
10.0
5.0
2.0
1.0
.5
.2
.1
PRE/OBS RATIO
500
1000
1500
2000
2500
3000
3500
4000
DISTANCE (M)

Figure F-68

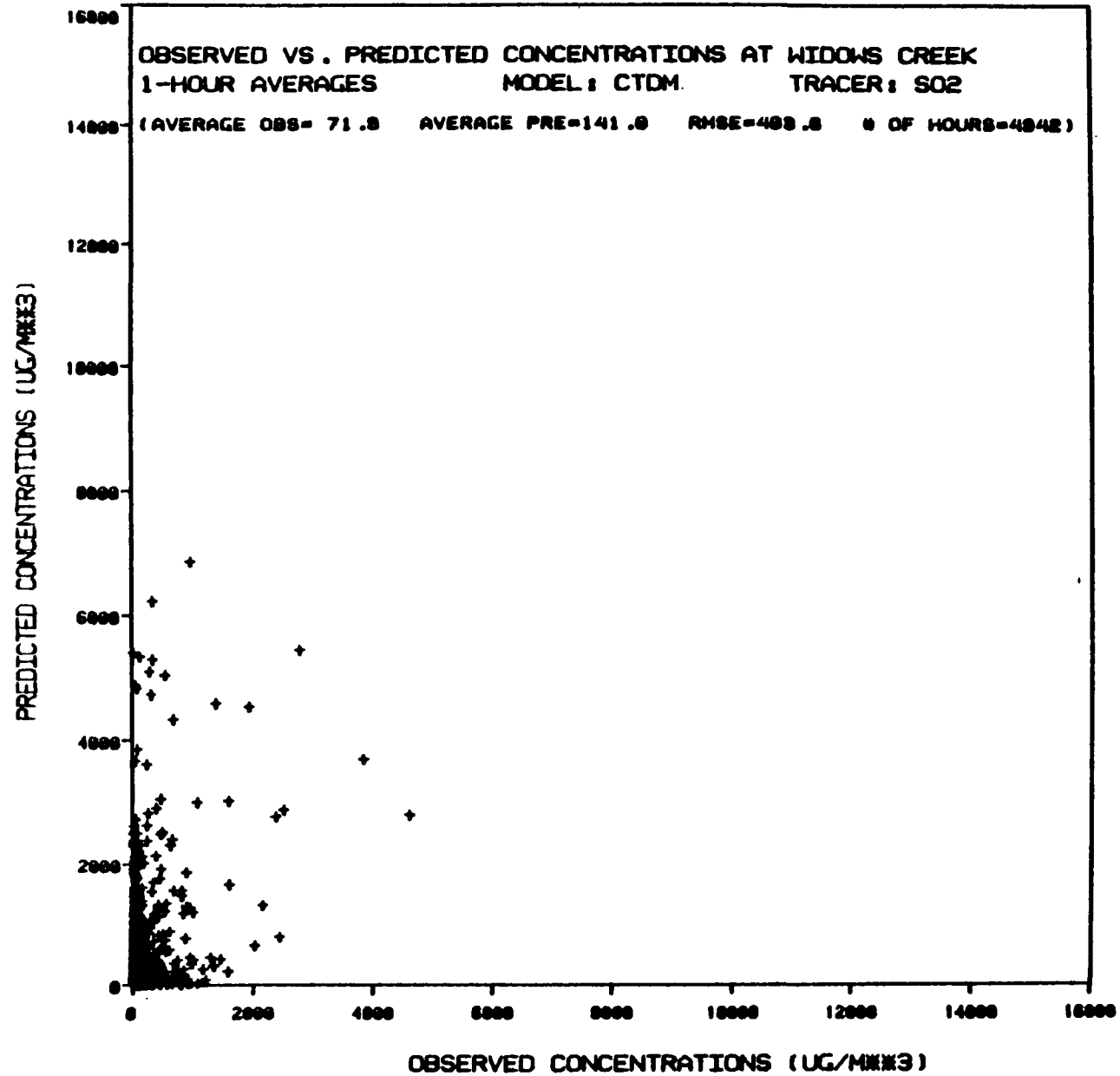
OBSERVED VS. PREDICTED CONCENTRATIONS AT WIDOWS CREEK
1-HOUR AVERAGES MODEL: CTDM TRACER: SO2
(AVERAGE OBS= 71.8 AVERAGE PRE=141.0 RMSE=488.8 # OF HOURS=4842)
PREDICTED CONCENTRATIONS (UG/M**3)
OBSERVED CONCENTRATIONS (UG/M**3)
0
2000
4000
6000
8000
10000
12000
14000
16000

Figure F-69

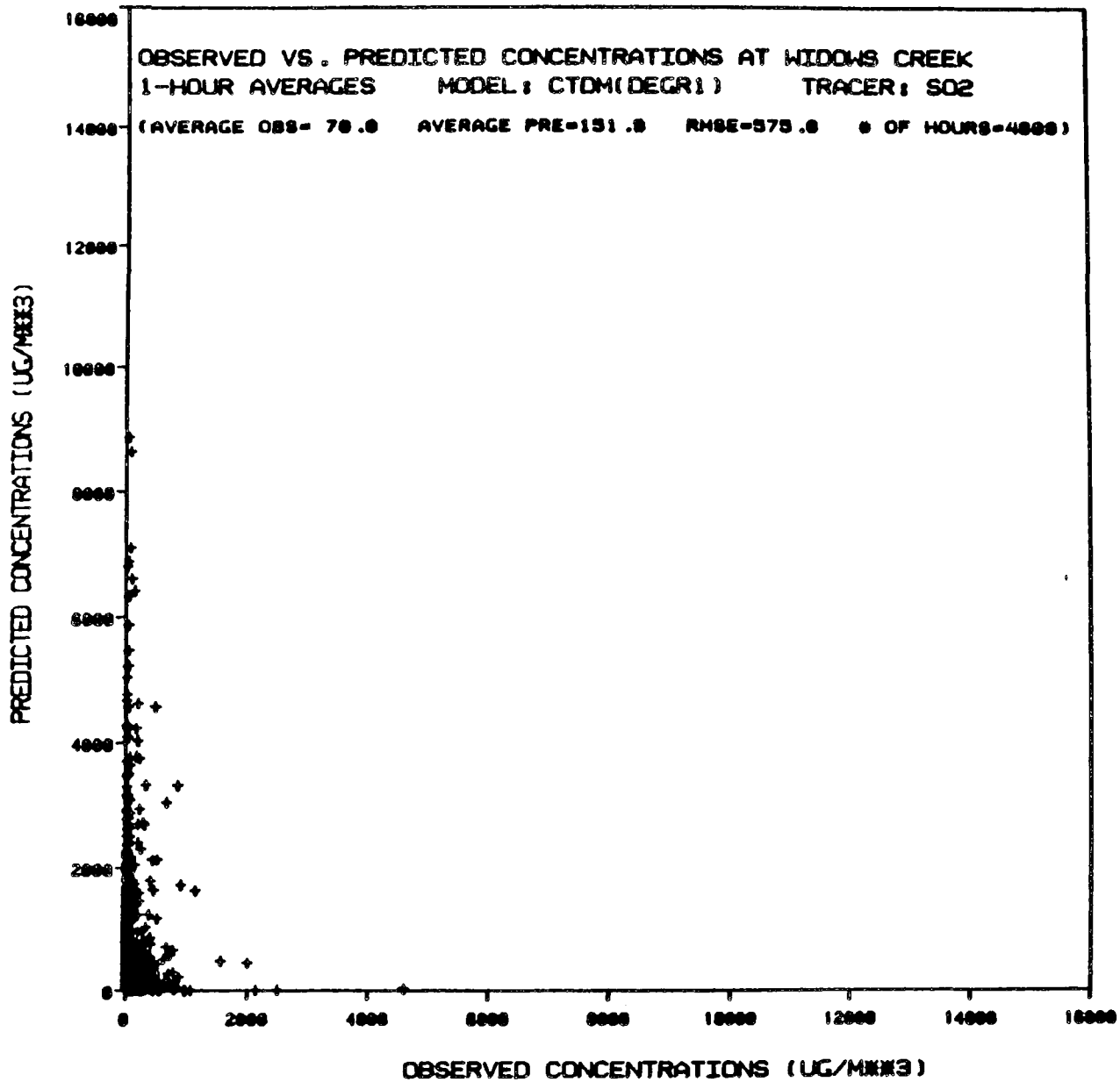
OBSERVED VS. PREDICTED CONCENTRATIONS AT WIDOWS CREEK
1-HOUR AVERAGES MODEL: CTDM(DEGR1) TRACER: SO2
(AVERAGE OBS= 70.0 AVERAGE PRE=151.0 RMSE=575.0 # OF HOURS=4000)
PREDICTED CONCENTRATIONS (UG/M**3)
OBSERVED CONCENTRATIONS (UG/M**3)
0
2000
4000
6000
8000
10000
12000
14000
16000

Figure F-70

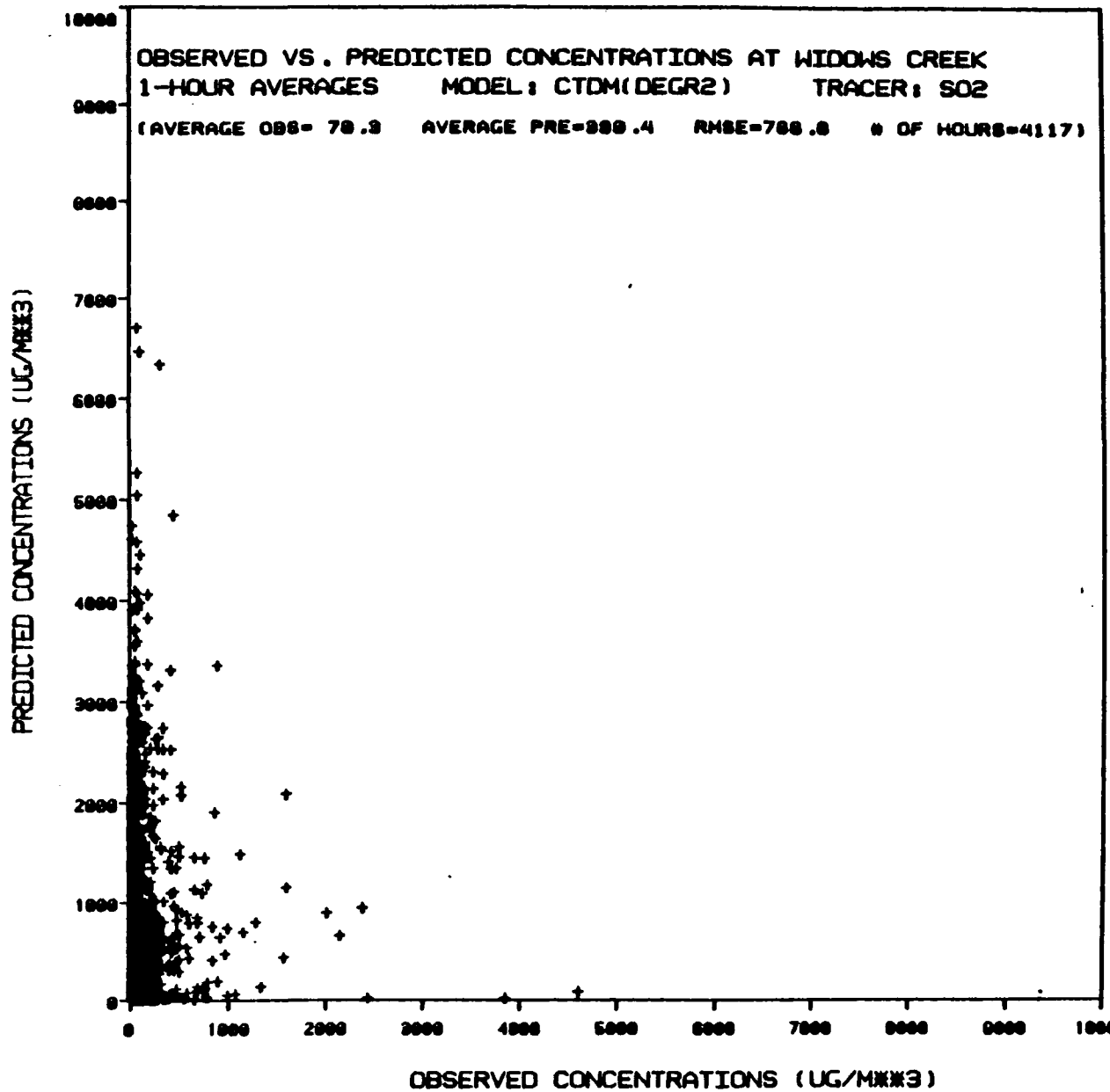
OBSERVED VS. PREDICTED CONCENTRATIONS AT WIDOWS CREEK
1-HOUR AVERAGES MODEL: CTDM(DEGR2) TRACER: SO2
(AVERAGE OBS= 78.3 AVERAGE PRE=888.4 RMSE=788.8 # OF HOURS=4117)
PREDICTED CONCENTRATIONS (UG/M**3)
OBSERVED CONCENTRATIONS (UG/M**3)
0
1000
2000
3000
4000
5000
6000
7000
8000
9000
10000

Figure F-71

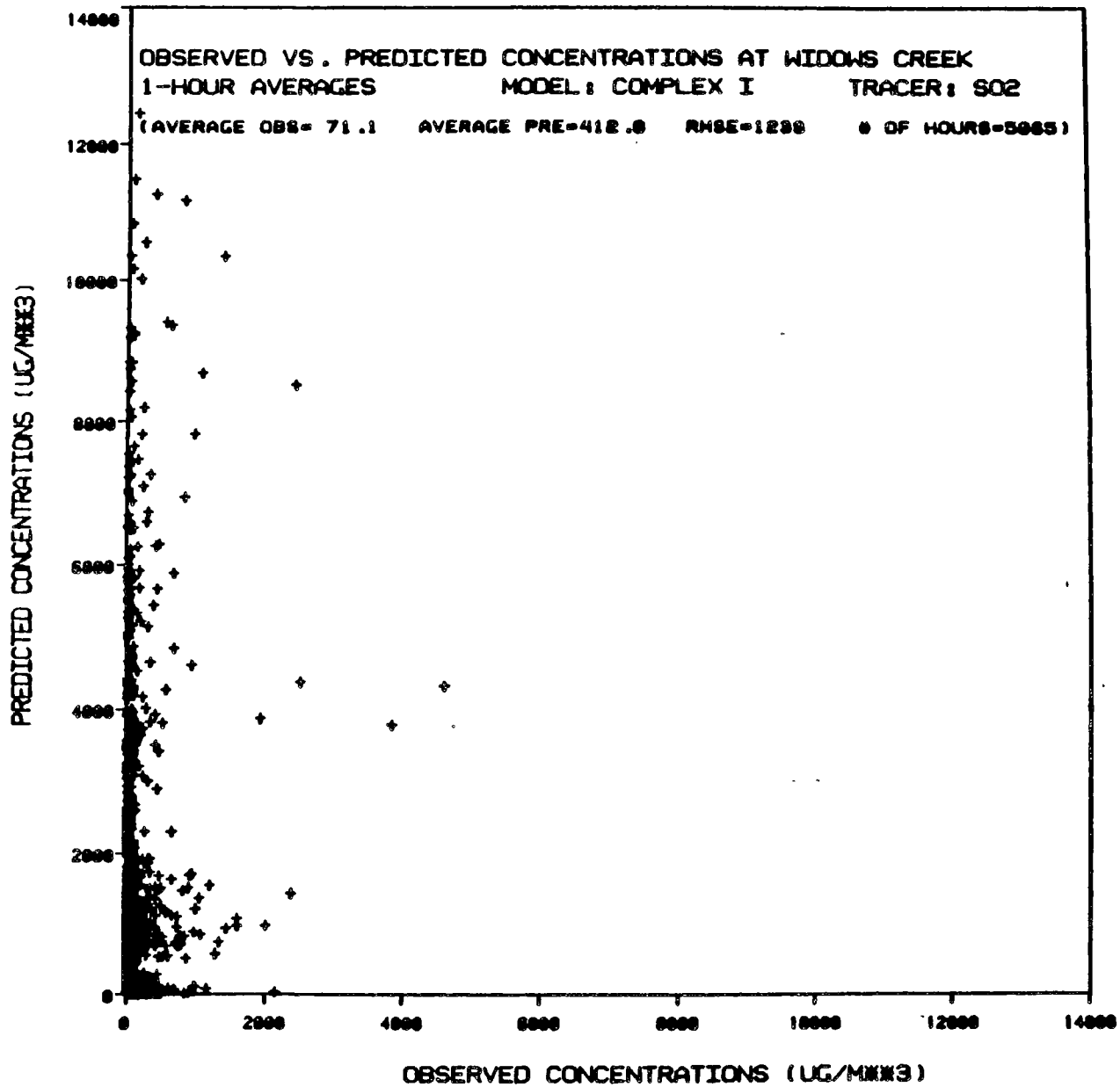
OBSERVED VS. PREDICTED CONCENTRATIONS AT WIDOWS CREEK
1-HOUR AVERAGES
MODEL: COMPLEX I
TRACER: SO2
(AVERAGE OBS= 71.1
AVERAGE PRE=412.8
RMSE=1238
# OF HOURS=5065)
PREDICTED CONCENTRATIONS (UG/M**3)
OBSERVED CONCENTRATIONS (UG/M**3)
0
2000
4000
6000
8000
10000
12000
14000

Figure F-72

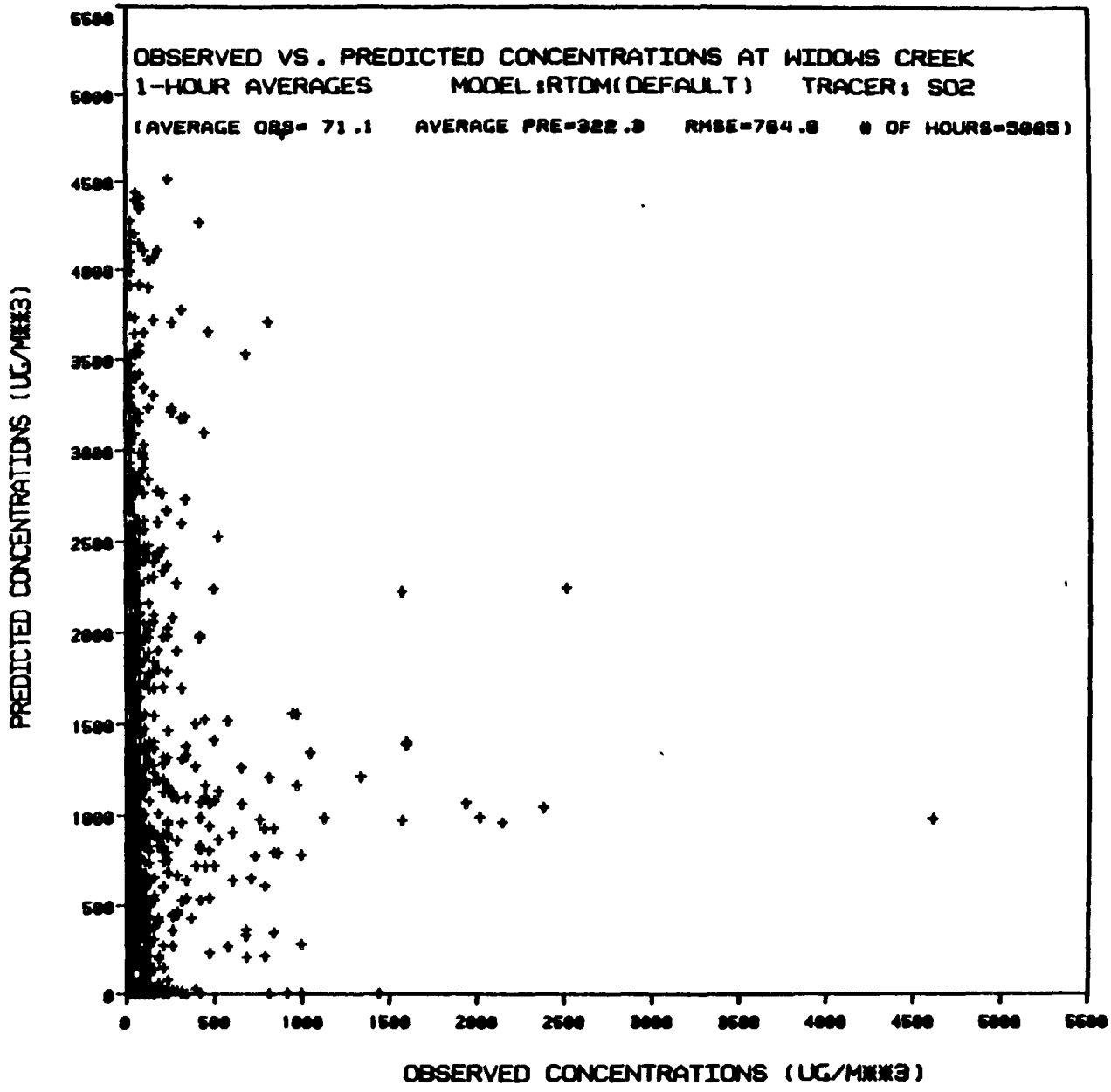
OBSERVED VS. PREDICTED CONCENTRATIONS AT WIDOWS CREEK
1-HOUR AVERAGES MODEL:RTDM(DEFAULT) TRACER: SO2
(AVERAGE OBS= 71.1 AVERAGE PRE=322.8 RMSE=784.8 # OF HOURS=3885)
PREDICTED CONCENTRATIONS (UG/M**3)
OBSERVED CONCENTRATIONS (UG/M**3)
0
500
1000
1500
2000
2500
3000
3500
4000
4500
5000
5500

Figure F-73

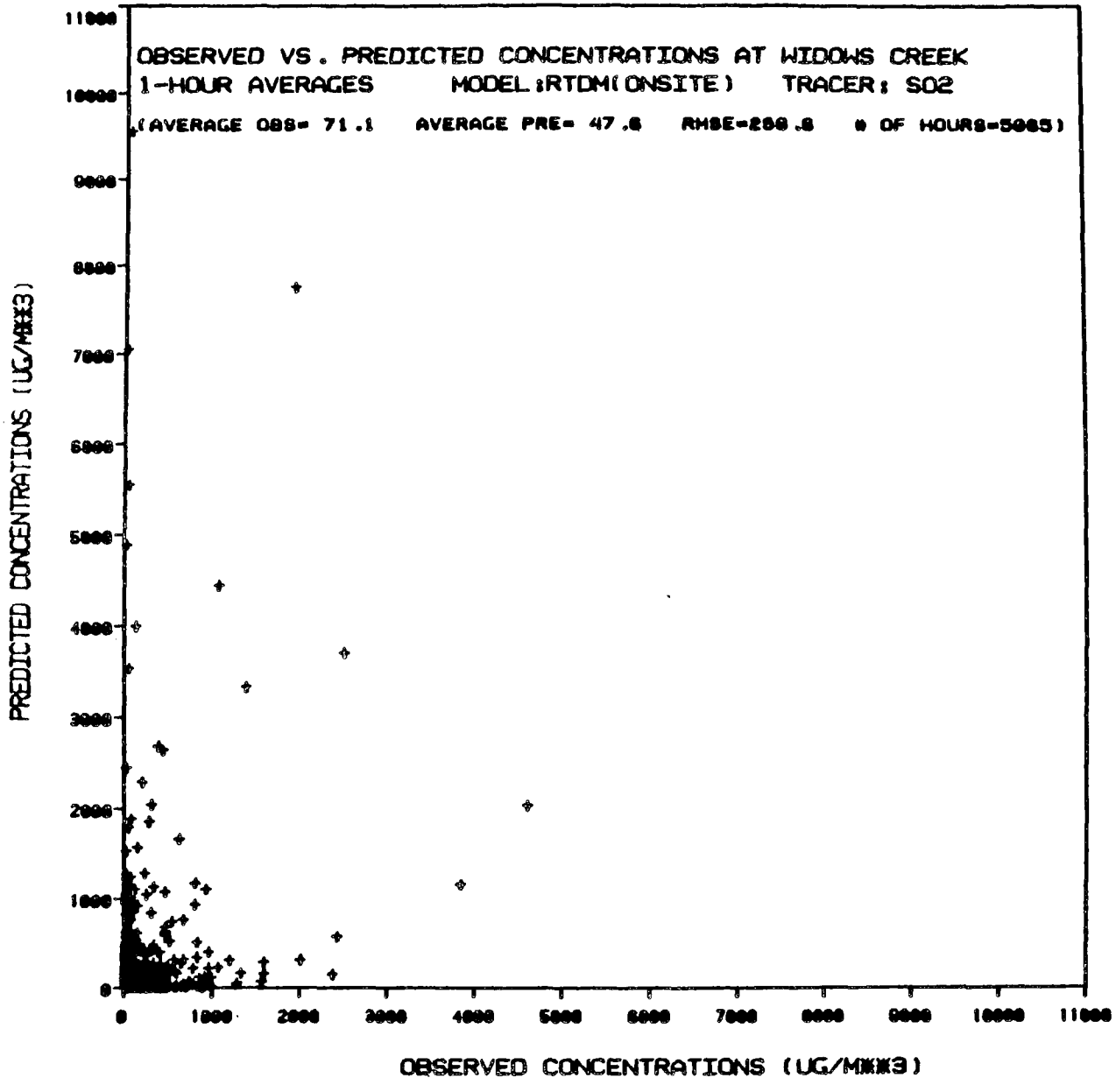
OBSERVED VS. PREDICTED CONCENTRATIONS AT WIDOWS CREEK
1-HOUR AVERAGES MODEL:RTDM(ONSITE) TRACER: SO2
(AVERAGE OBS= 71.1 AVERAGE PRE= 47.6 RMSE=200.8 # OF HOURS=5085)
PREDICTED CONCENTRATIONS (UG/M**3)
OBSERVED CONCENTRATIONS (UG/M**3)
0
1000
2000
3000
4000
5000
6000
7000
8000
9000
10000
11000

Figure F-74

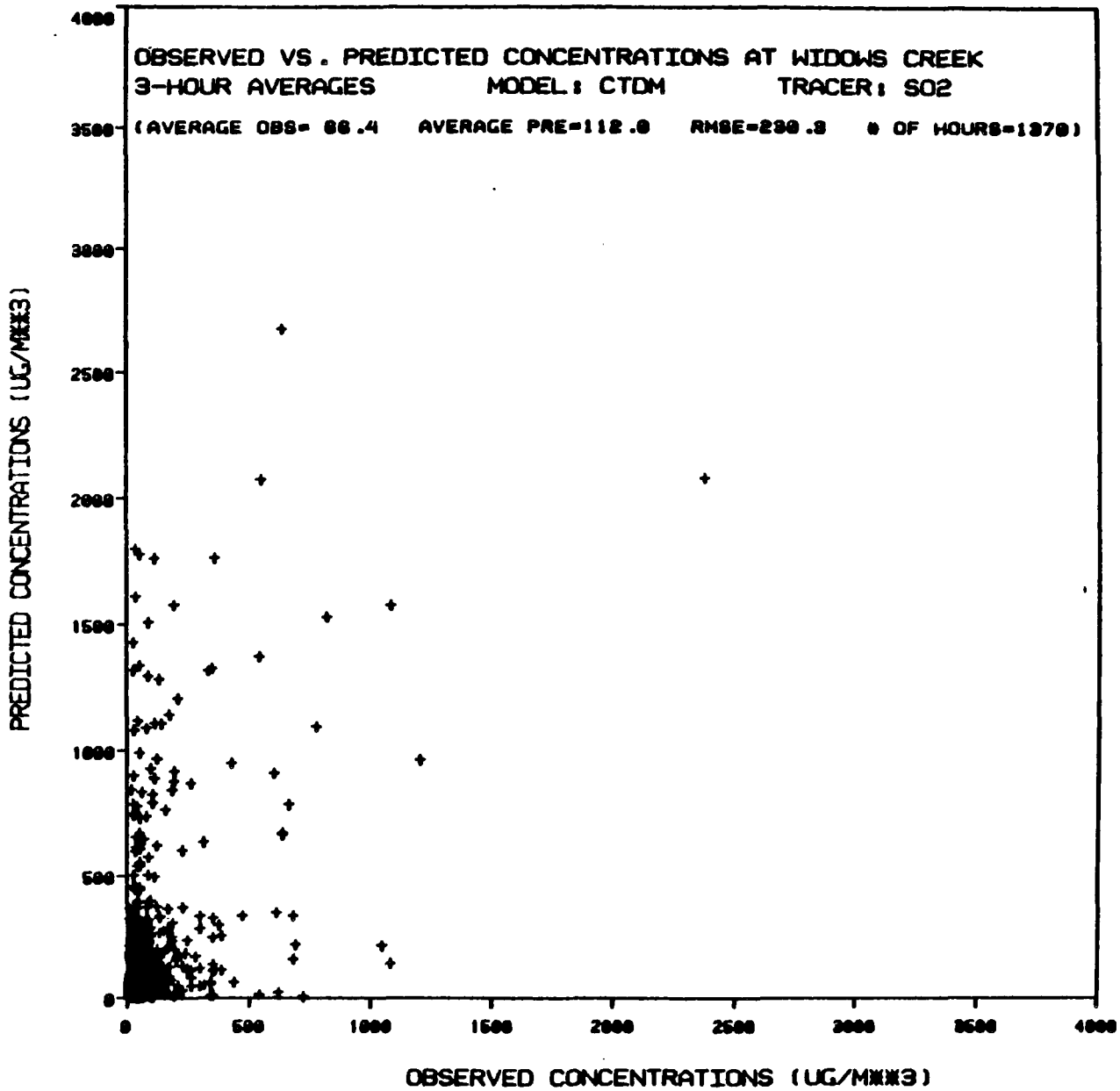
OBSERVED VS. PREDICTED CONCENTRATIONS AT WIDOWS CREEK
3-HOUR AVERAGES MODEL: CTDM TRACER: SO2
(AVERAGE OBS= 86.4 AVERAGE PRE=112.0 RMSE=230.3 # OF HOURS=1370)
PREDICTED CONCENTRATIONS (UG/M**3)
OBSERVED CONCENTRATIONS (UG/M**3)
0
500
1000
1500
2000
2500
3000
3500
4000

Figure F-75

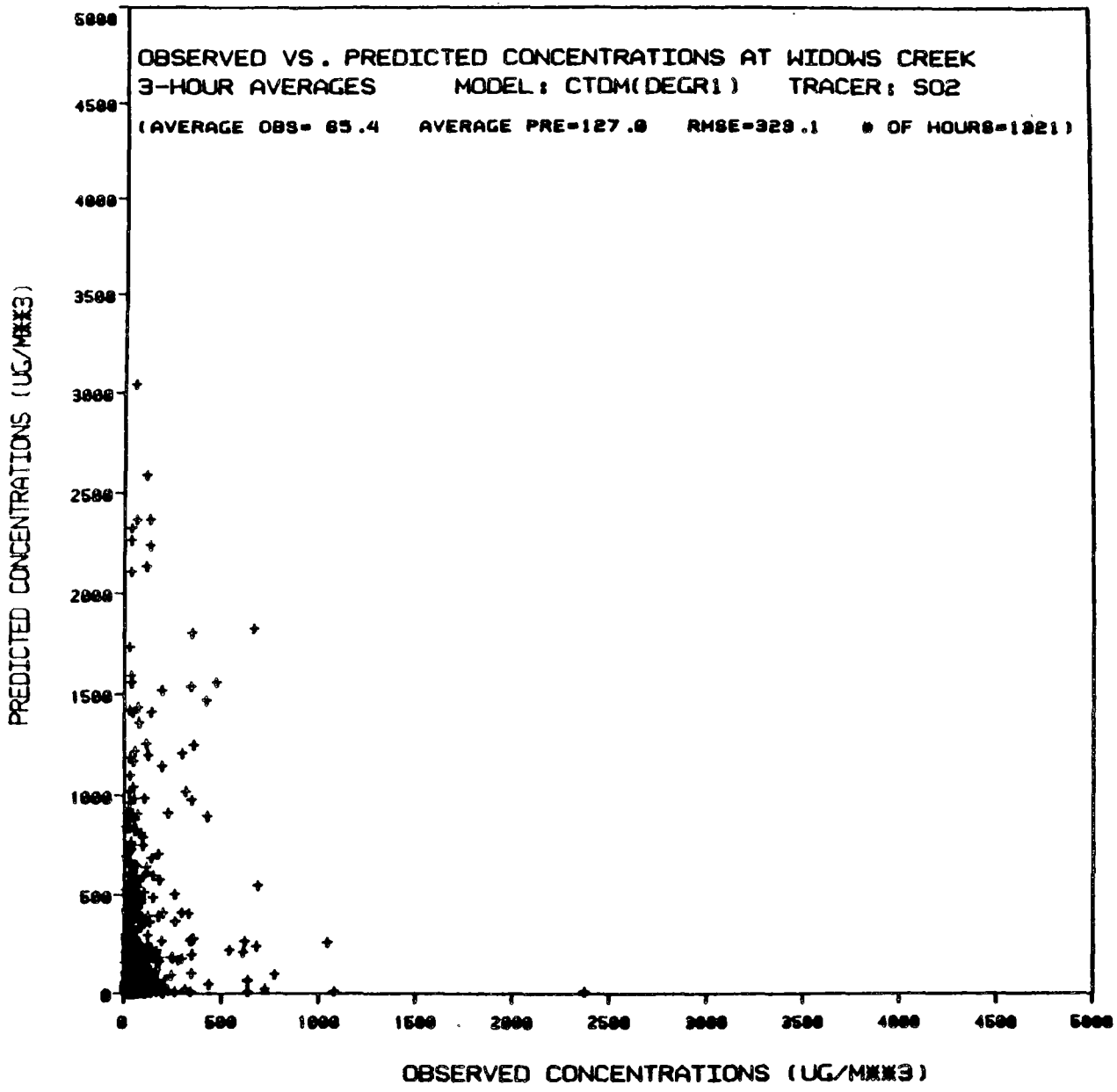
OBSERVED VS. PREDICTED CONCENTRATIONS AT WIDOWS CREEK
3-HOUR AVERAGES MODEL: CTDM(DEGRI) TRACER: SO2
(AVERAGE OBS= 65.4 AVERAGE PRE=127.0 RMSE=329.1 # OF HOURS=1921)
PREDICTED CONCENTRATIONS (UG/M**3)
OBSERVED CONCENTRATIONS (UG/M**3)
0
500
1000
1500
2000
2500
3000
3500
4000
4500
5000

Figure F-76

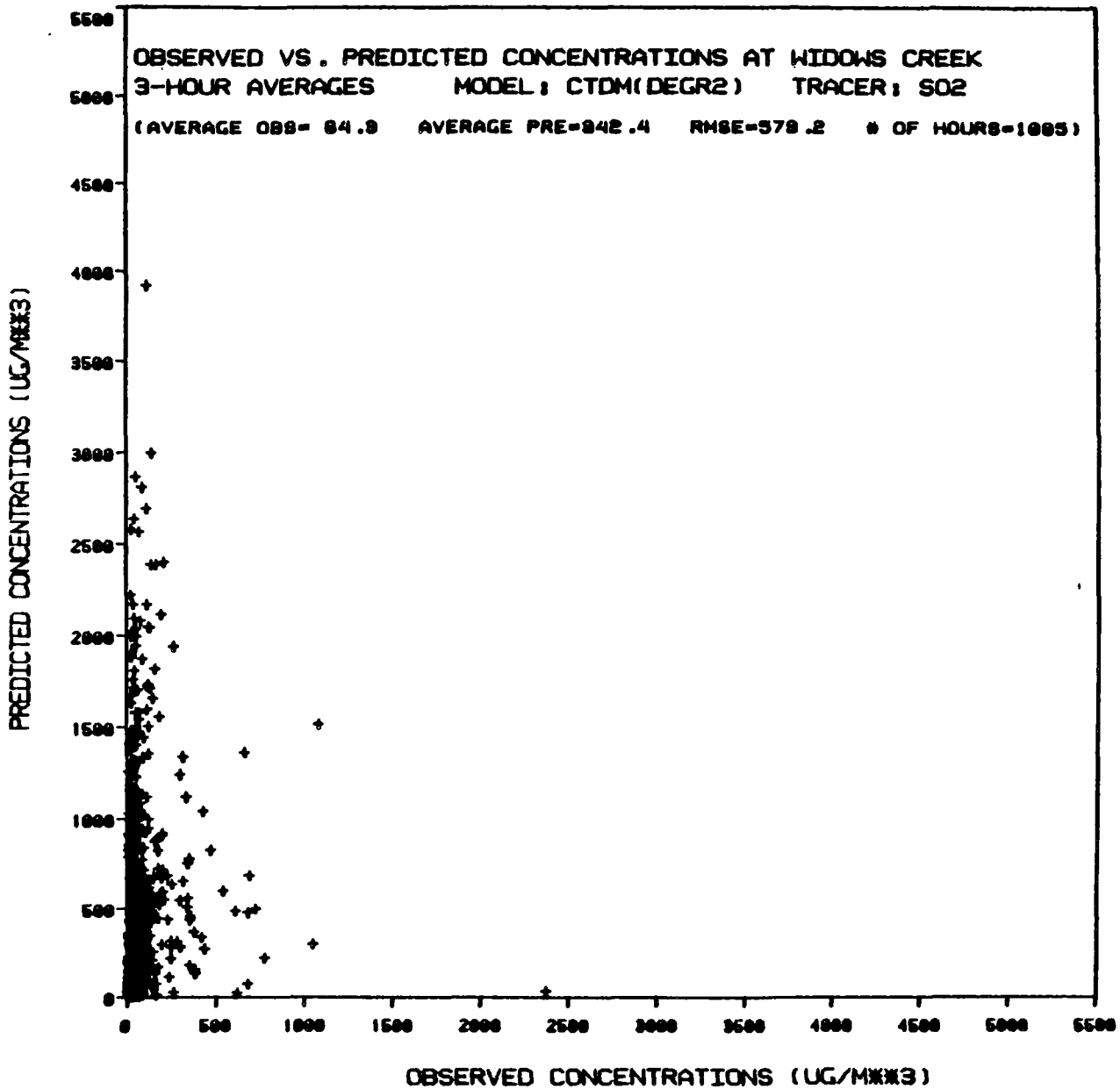
OBSERVED VS. PREDICTED CONCENTRATIONS AT WIDOWS CREEK
3-HOUR AVERAGES MODEL: CTDM(DEGR2) TRACER: SO2
(AVERAGE OBS= 84.9 AVERAGE PRE=942.4 RMSE=579.2 # OF HOURS=1085)
PREDICTED CONCENTRATIONS (UG/M**3)
OBSERVED CONCENTRATIONS (UG/M**3)
0
500
1000
1500
2000
2500
3000
3500
4000
4500
5000
5500

Figure F-77

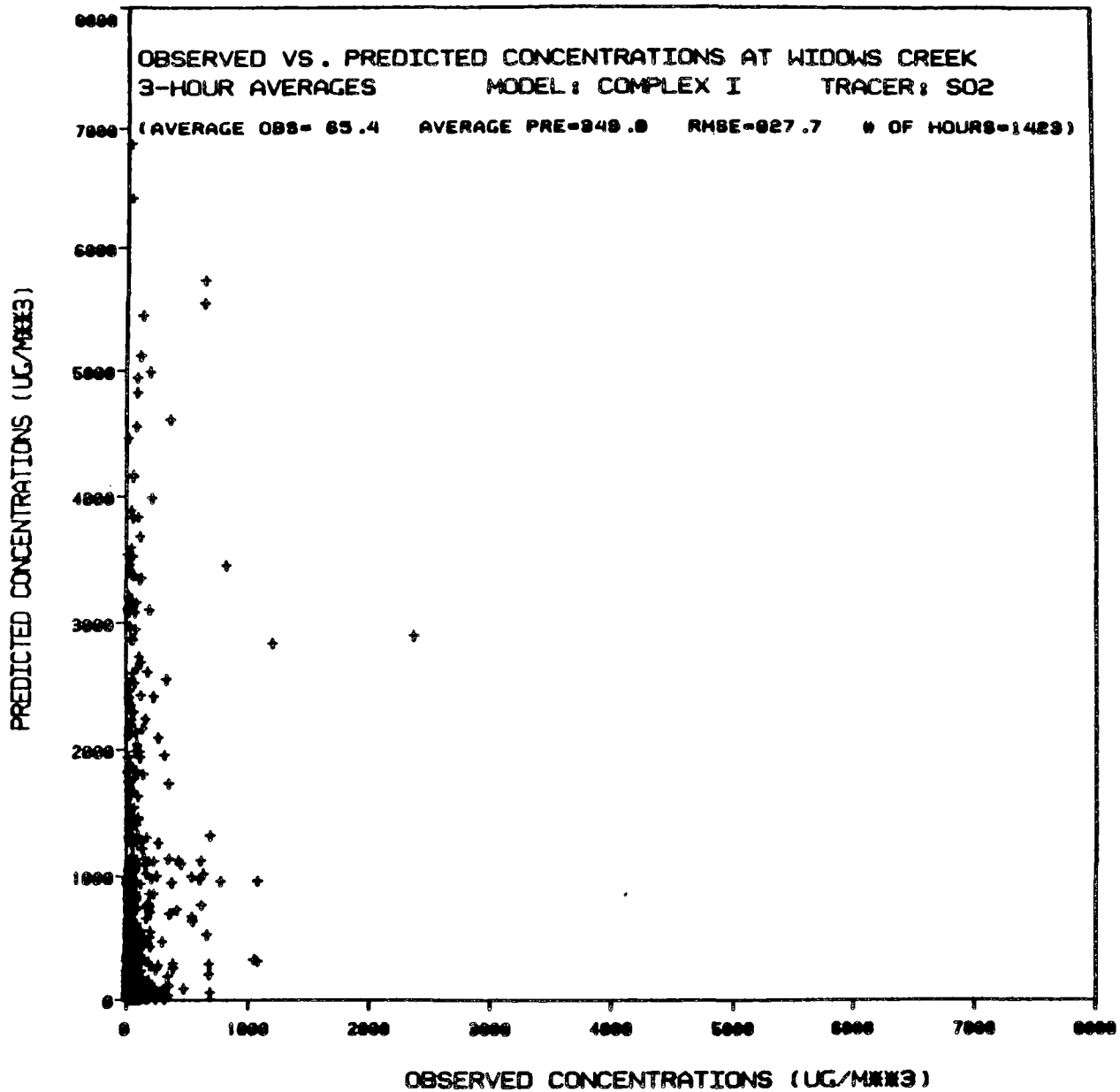
OBSERVED VS. PREDICTED CONCENTRATIONS AT WIDOWS CREEK
3-HOUR AVERAGES MODEL: COMPLEX I TRACER: SO2
(AVERAGE OBS= 85.4 AVERAGE PRE=348.8 RMSE=827.7 # OF HOURS=1423)
PREDICTED CONCENTRATIONS (UG/M**3)
OBSERVED CONCENTRATIONS (UG/M**3)
0
1000
2000
3000
4000
5000
6000
7000
8000

Figure F-78

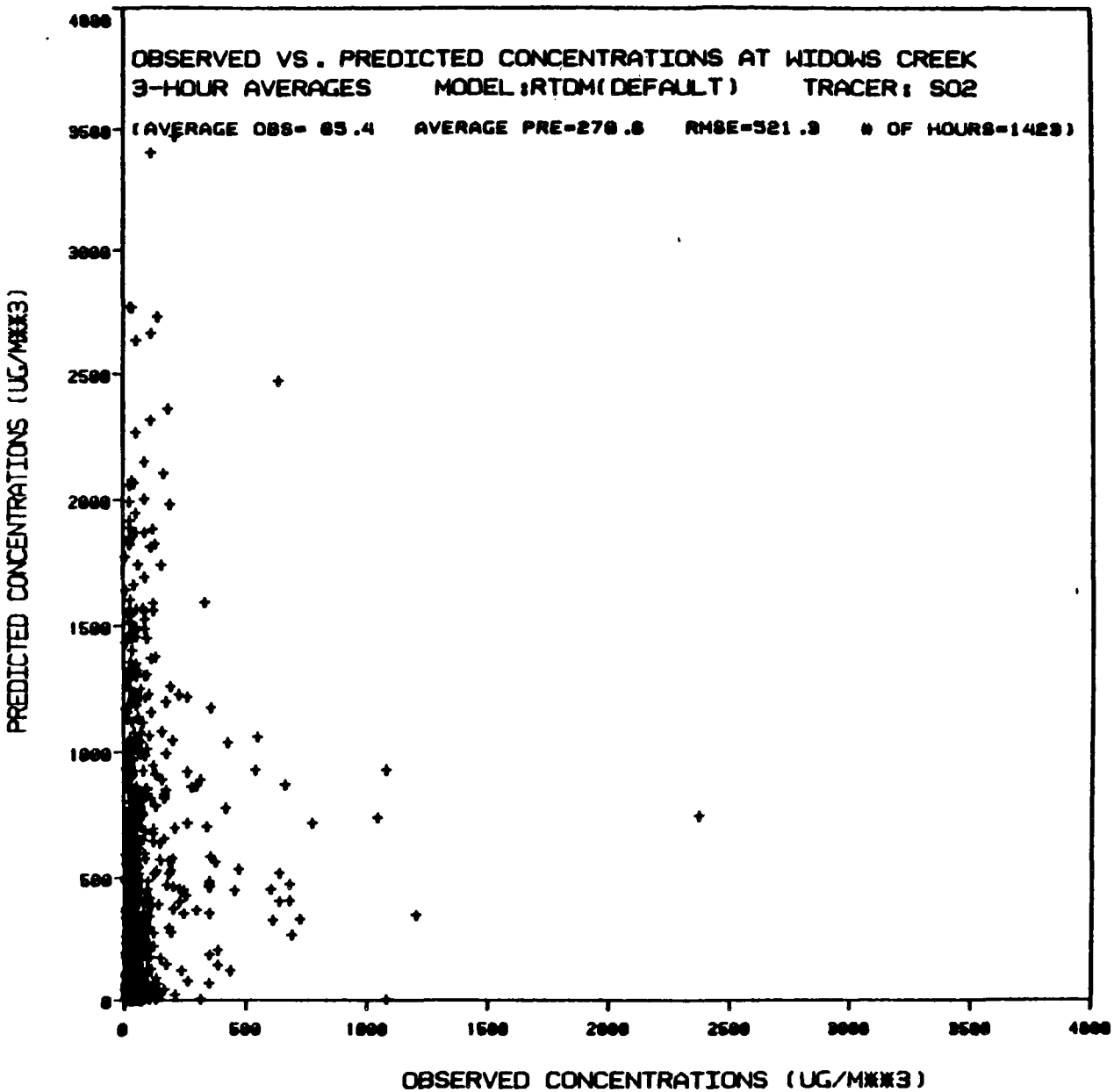
OBSERVED VS. PREDICTED CONCENTRATIONS AT WIDOWS CREEK
3-HOUR AVERAGES MODEL:RTDM(DEFAULT) TRACER: SO2
(AVERAGE OBS= 85.4 AVERAGE PRE=270.8 RMSE=521.9 # OF HOURS=1423)
PREDICTED CONCENTRATIONS (UG/M**3)
OBSERVED CONCENTRATIONS (UG/M**3)
0
500
1000
1500
2000
2500
3000
3500
4000

Figure F-79

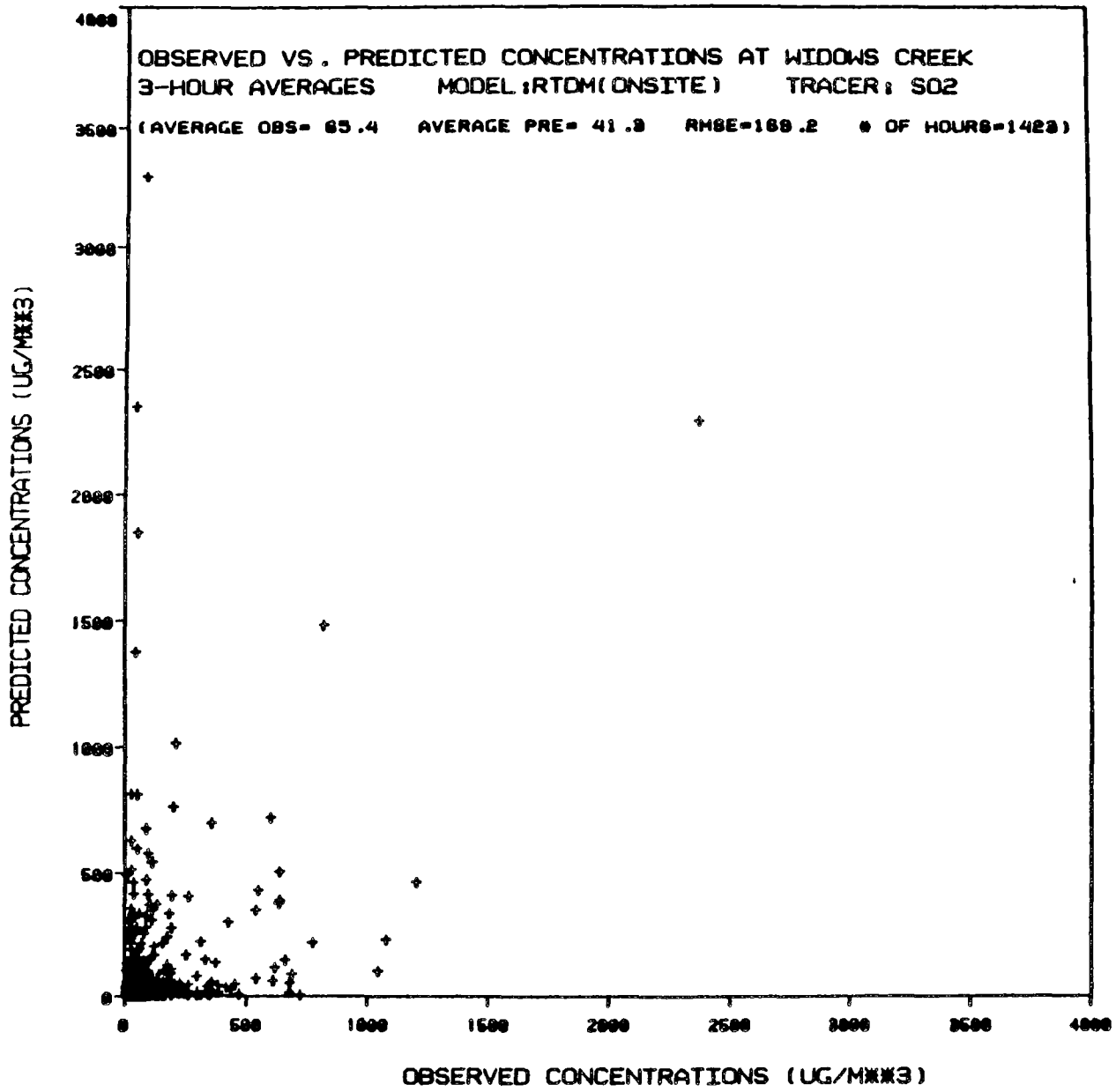
OBSERVED VS. PREDICTED CONCENTRATIONS AT WIDOWS CREEK
3-HOUR AVERAGES MODEL:RTDM(ONSITE) TRACER: SO2
(AVERAGE OBS= 65.4 AVERAGE PRE= 41.8 RMSE=169.2 # OF HOURS=1423)
PREDICTED CONCENTRATIONS (UG/M**3)
OBSERVED CONCENTRATIONS (UG/M**3)
0
500
1000
1500
2000
2500
3000
3500
4000

Figure F-80

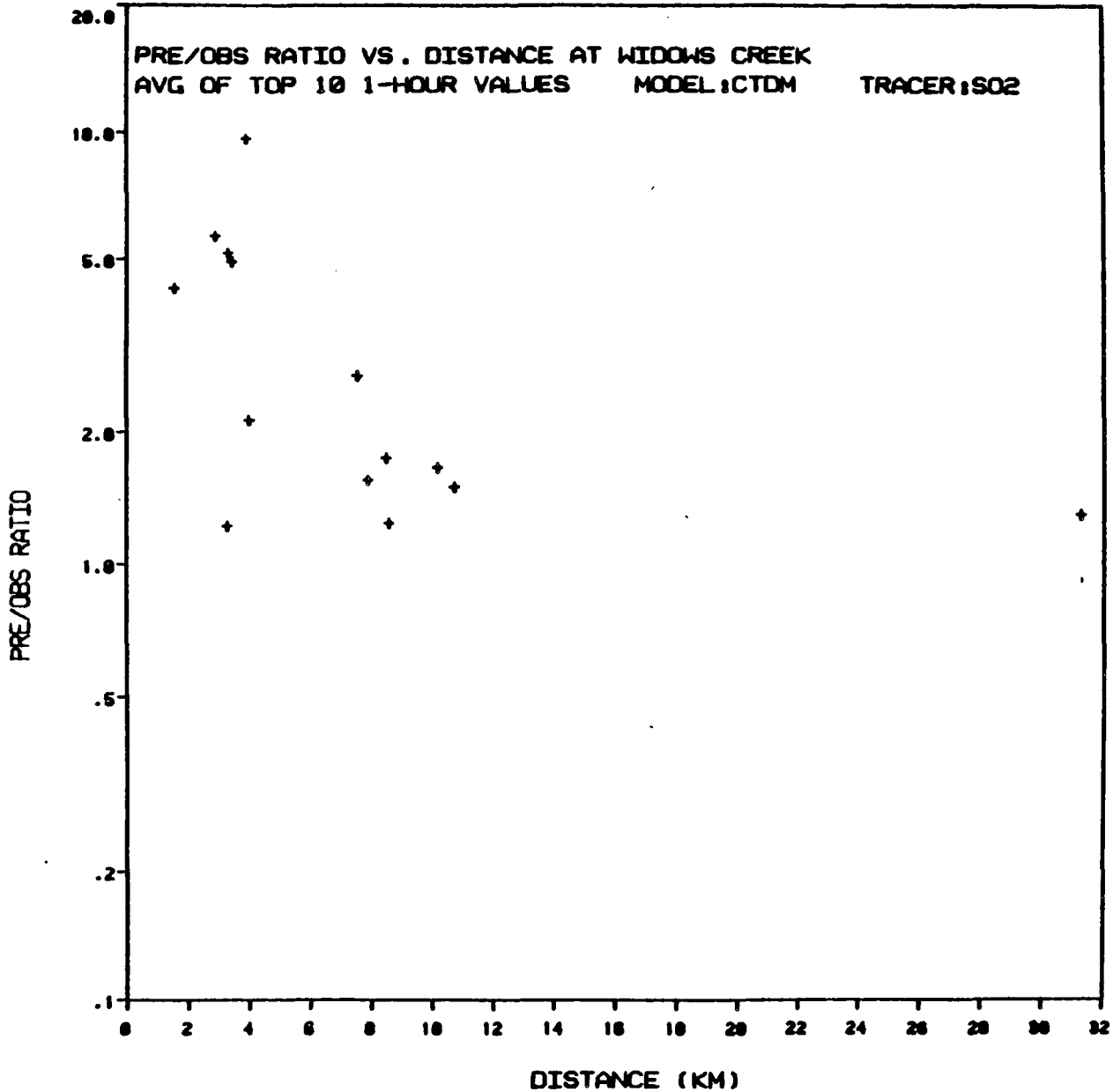
PRE/OBS RATIO VS. DISTANCE AT WIDOWS CREEK
AVG OF TOP 10 1-HOUR VALUES MODEL:CTDM TRACER:SO2
PRE/OBS RATIO
20.0
10.0
5.0
2.0
1.0
.5
.2
.1
0
2
4
6
8
10
12
14
16
18
20
22
24
26
28
30
32
DISTANCE (KM)

Figure F-81

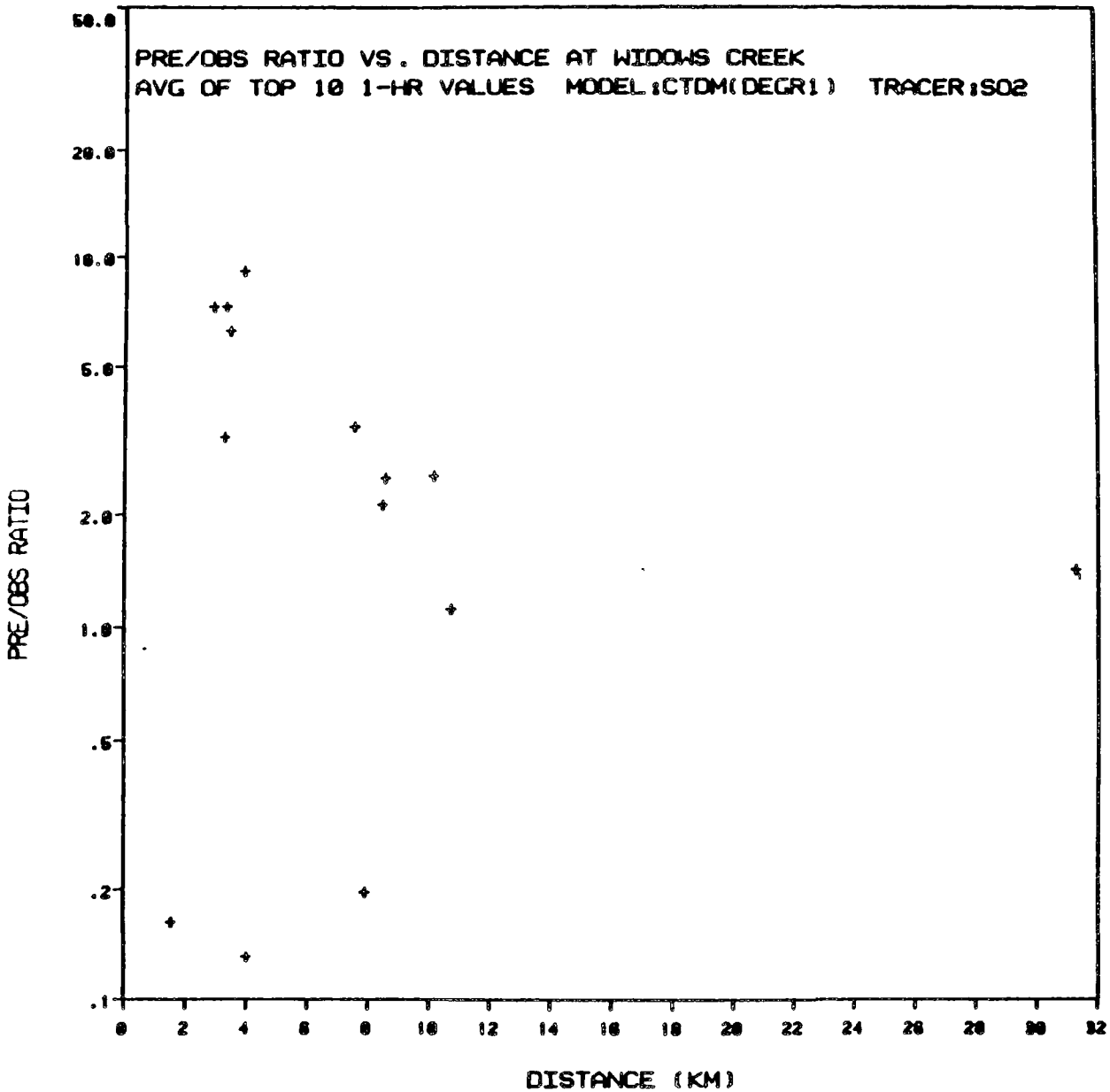
PRE/OBS RATIO VS. DISTANCE AT WIDOWS CREEK
AVG OF TOP 10 1-HR VALUES MODEL:CTDM(DEGR1) TRACER:SO2
50.0
20.0
10.0
5.0
2.0
1.0
.5
.2
.1
PRE/OBS RATIO
0
2
4
6
8
10
12
14
16
18
20
22
24
26
28
30
32
DISTANCE (KM)

Figure F-82

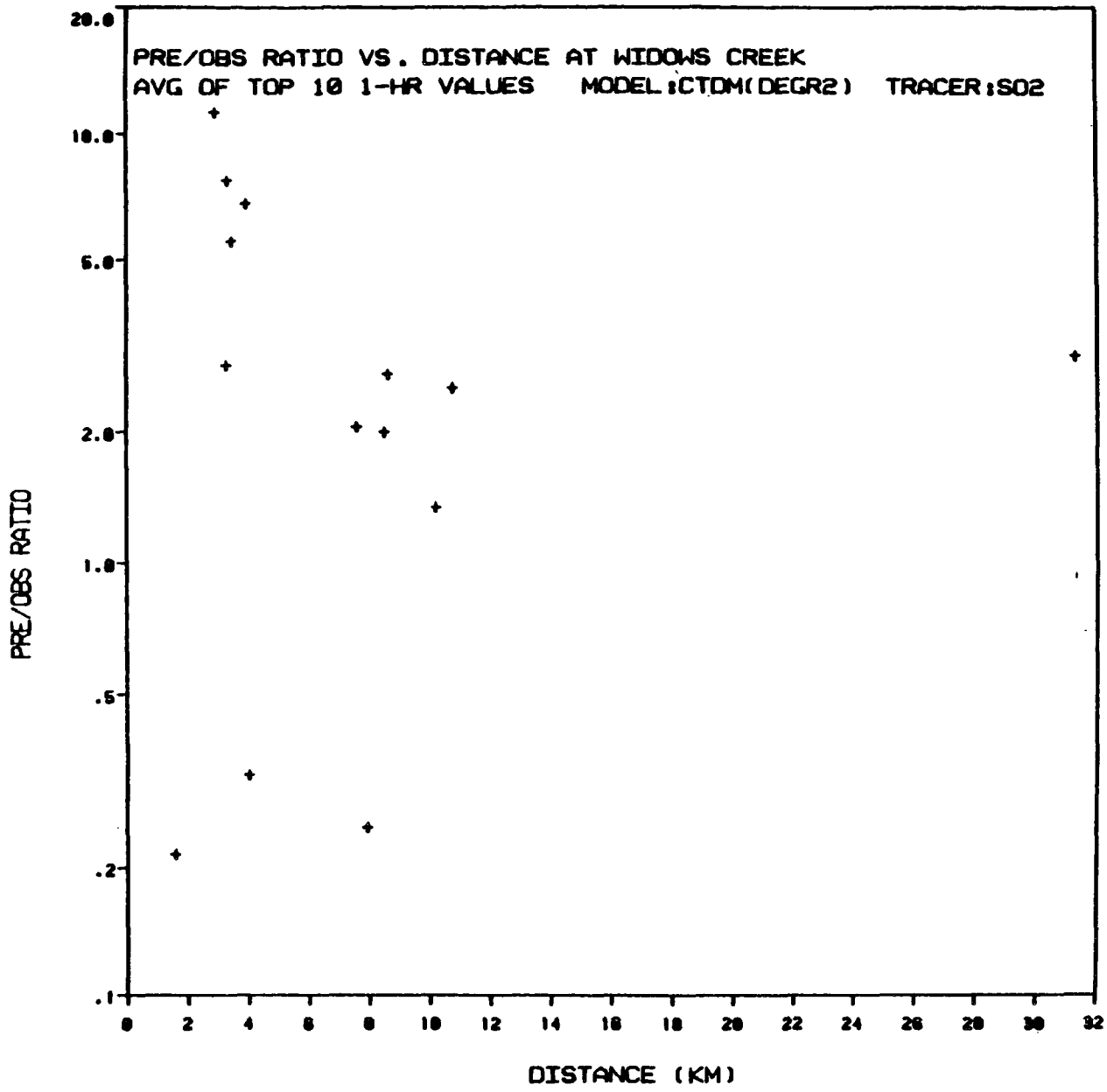
PRE/OBS RATIO VS. DISTANCE AT WIDOWS CREEK
AVG OF TOP 10 1-HR VALUES MODEL:CTDM(DEGR2) TRACER:SO2
PRE/OBS RATIO
20.0
10.0
5.0
2.0
1.0
.5
.2
.1
0
2
4
6
8
10
12
14
16
18
20
22
24
26
28
30
32
DISTANCE (KM)

Figure F-83

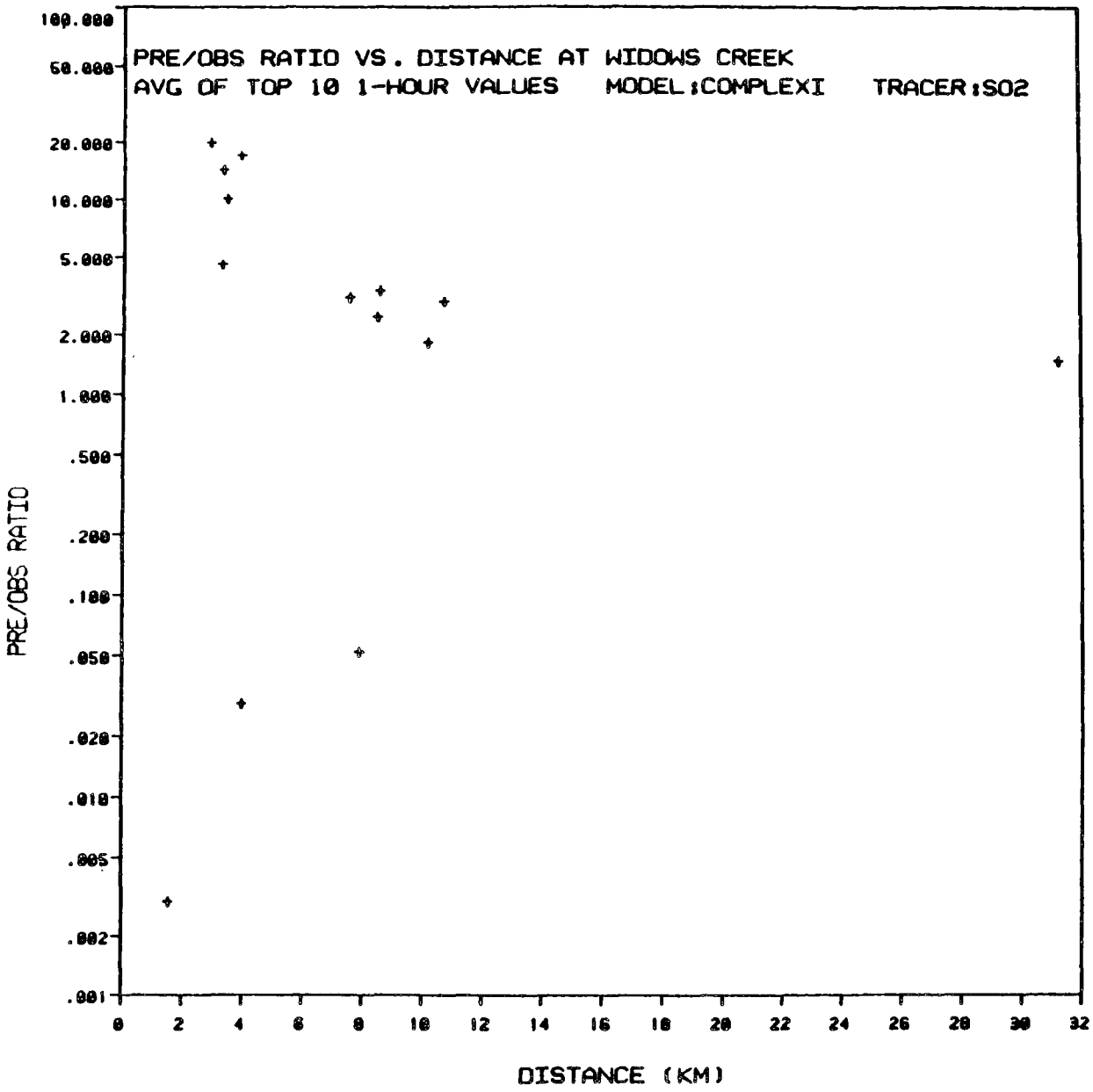
PRE/OBS RATIO VS. DISTANCE AT WIDOWS CREEK
AVG OF TOP 10 1-HOUR VALUES MODEL:COMPLEXI TRACER:SO2
PRE/OBS RATIO
100.000
50.000
20.000
10.000
5.000
2.000
1.000
.500
.200
.100
.050
.020
.010
.005
.002
.001
0
2
4
6
8
10
12
14
16
18
20
22
24
26
28
30
32
DISTANCE (KM)

Figure F-84

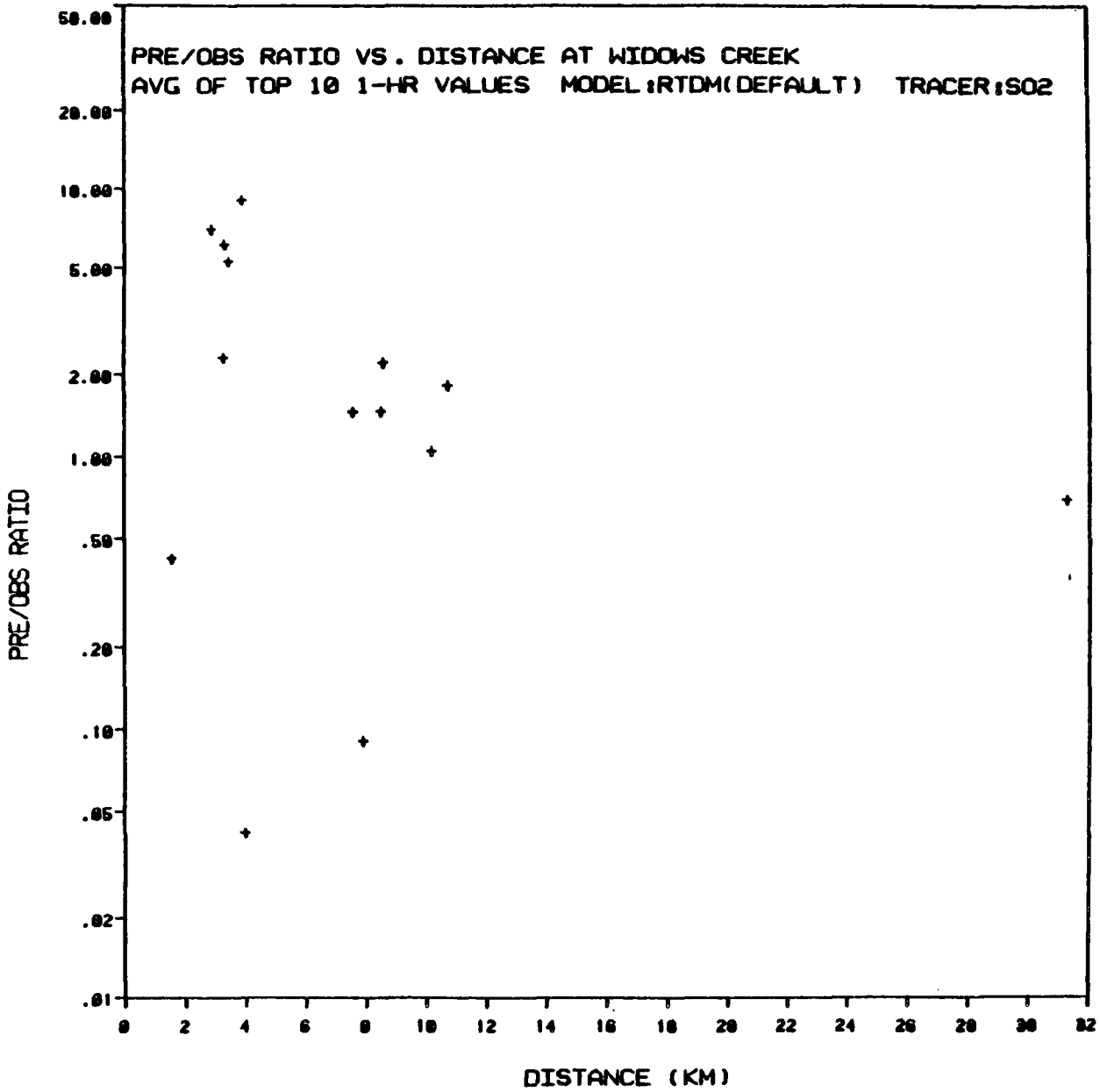
PRE/OBS RATIO VS. DISTANCE AT WIDOWS CREEK
AVG OF TOP 10 1-HR VALUES MODEL:RTDM(DEFAULT) TRACER:SO2
PRE/OBS RATIO
50.00
20.00
10.00
5.00
2.00
1.00
.50
.20
.10
.05
.02
.01
0
2
4
6
8
10
12
14
16
18
20
22
24
26
28
30
32
DISTANCE (KM)

Figure F-85

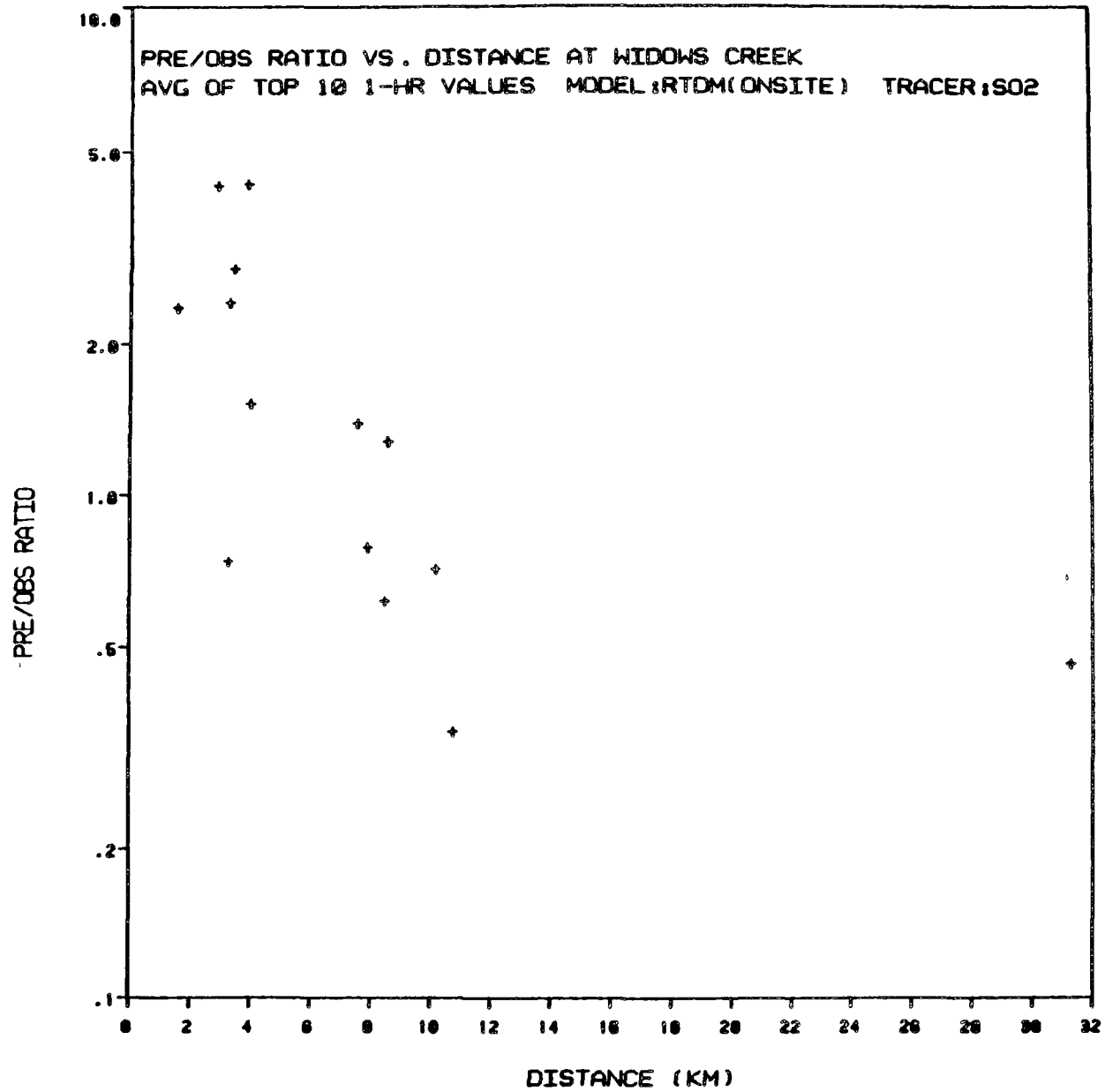
PRE/OBS RATIO VS. DISTANCE AT WIDOWS CREEK
AVG OF TOP 10 1-HR VALUES MODEL:RTDM(ONSITE) TRACER:SO2
PRE/OBS RATIO
10.0
5.0
2.0
1.0
.5
.2
.1
0
2
4
6
8
10
12
14
16
18
20
22
24
26
28
30
32
DISTANCE (KM)

Figure F-86

APPENDIX G
SUMMARY OF CASE-STUDY ANALYSES OF CTDM PREDICTIONS AT THE TRACER SITES

APPENDIX G

SUMMARY OF CASE-STUDY ANALYSES OF CTDM PREDICTIONS AT THE TRACER SITES

Patterns of CTDM predictions and observed concentrations at the SF_6 and CF_3Br sampler sites have been analyzed for the CCB, HBR, and FSPS experiments. The examination of results for each hour involved a comparison of the average of the top 5 predicted and observed concentrations. The height of the plume as well as peak predicted and observed concentrations relative to H_c were noted, as well as a plume-height wind speed category. Comments about the locations of the peak predicted and observed concentrations were also logged. Case-by-case results are given in Tables G-1 through G-6. Summary statistics by wind speed category and by the plume height relative to H_c are listed in Tables G-7 through G-12. An index to these tables is given below.

Table	Description
G-1	Individual case results for tracer SF_6 at CCB
G-2	Individual case results for tracer CF_3Br at CCB
G-3	Individual case results for tracer SF_6 at HBR
G-4	Individual case results for tracer CF_3Br at HBR
G-5	Individual case results for tracer SF_6 at FSPS
G-6	Individual case results for tracer CF_3Br at FSPS
G-7	Summary statistics for case-hour categories for SF at CCB 6
G-8	Summary statistics for case-hour categories for CF Br at CCB 3
G-9	Summary statistics for case-hour categories for SF at HBR 6
G-10	Summary statistics for case-hour categories for CF Br at HBR 3
G-11	Summary statistics for case-hour categories for SF at FSPS 6
G-12	Summary statistics for case-hour categories for CF Br at FSPS 3

TABLE G-1

SUMMARY OF PREDICTED AND OBSERVED DATA FOR SF6 TRACER AT CINDER CONE BUTTE SITE*

JUL. DAY	HR	PLUME HEIGHT VS Hc	WIND SPD CAT	TOP 5 AVE CONC DATA (uS/M**3) TOP 5 AVE PRE	TOP 5 AVE OBS	PRE/OBS RATIO	RATIO CAT	ELEV OF PRE MAX VS Hc/ ELEV OF OBS MAX VS Hc	COMMENTS
290	18	A	4	10.	24.	.431	<	A/A	C,F
290	19	A	3	6.6	21.	.311	<	A/A	C,F
290	21	A	3	90.	17.	5.167	>>	A/A	
290	22	N	3	63.	19.	3.311	>	N/A	
290	23	N	3	51.	22.	2.321	>	N/B	
291	18	A	4	4.2	18.	.229	<	A/A	C,F
291	19	A	4	1.8	20.	.089	<<	A/A	C,F
291	20	A	4	21.	42.	.503	<=	A/A	C,F
291	21	A	4	30.	27.	1.134	>=	A/A	C,F
291	22	A	4	9.9	23.	.428	<	A/A	C,F
291	23	A	4	.98E-07	11.	.000	<<	?/A	J
294	2	B	3	.46E-01	4.8	.010	<<	N/B	D,F
294	3	B	2	23.	2.1	10.914	>>	N/A	D,F
294	5	A	3	63.	2.7	23.231	>>	A/A	D,F
294	6	B	2	25.	19.	1.262	>=	B/B	
294	7	N	2	82.	16.	5.154	>>	N/B	D,F
294	8	A	3	87.	30.	2.873	>	A/B	
295	1	B	2	33.	8.2	4.061	>	B/B	D,E
295	2	B	2	5.4	9.9	.546	<=	B/B	C,F
295	6	B	2	19.	9.5	1.965	>=	B/N	C,F
295	7	B	2	32.	7.0	4.553	>	B/N	D,F
297	2	A	4	.35E-01	1.9	.019	<<	N/A	
297	3	A	4	1.8	5.7	.309	<	A/A	C,E
297	4	A	4	16.	19.	.847	<=	A/A	C,E
297	5	A	4	17.	18.	.911	<=	A/B	C,F
297	6	A	4	14.	17.	.804	<=	A/N	D,F
297	7	B	2	42.	9.2	4.563	>	B/B	D,E
297	8	N	2	.10E+03	12.	8.582	>>	A/N	D,F
298	2	A	4	1.3	21.	.065	<<	A/A	C,F
298	3	A	4	.97	14.	.072	<<	B/B	A,C,E
298	4	A	3	62.	46.	1.347	>=	A/A	B,C,E
298	5	A	3	85.	33.	2.586	>	A/A	D,E
298	6	N	2	.14E+03	86.	1.673	>=	N/B	D,F
298	7	N	2	.16E+03	67.	2.373	>	N/N	A,D,F
298	8	N	2	.11E+03	.11E+03	.972	<=	N/B	D,F
299	2	A	3	13.	8.2	1.623	>=	A/N	D,F
299	3	A	3	4.7	2.9	1.615	>=	N/A	D,F
299	4	A	3	16.	10.	1.519	>=	A/A	D,F
301	20	A	4	13.	7.9	1.636	>=	A/A	C,F
301	21	A	4	5.8	4.7	1.236	>=	A/A	B,C,E
301	23	A	3	11.	.26	43.446	>>	N/N	D,E
302	1	N	3	34.	4.3	7.824	>>	N/B	D,F
302	18	A	3	13.	1.6	8.006	>>	A/A	B,C,E
302	19	A	3	26.	4.7	5.609	>>	A/A	C,E

****

*SEE INTERPRETATION OF CODES AT END OF TABLE

TABLE G-1 (Page 2 of 4)

SUMMARY OF PREDICTED AND OBSERVED DATA FOR SF6 TRACER AT CINDER CONE BUTTE SITE*

JUL. DAY	HR	PLUME HEIGHT VS Hc	WIND SPD CAT	TOP 5 AVE CONC DATA (uS/M**3) TOP 5 AVE PRE	TOP 5 AVE OBS	PRE/OBS RATIO	RATIO CAT	ELEV OF PRE MAX VS Hc/ ELEV OF OBS MAX VS Hc	COMMENTS
302	20	N	2	44.	4.7	9.422	>>	N/B	D,E
302	24	B	2	68.	6.1	11.184	>>	B/B	
303	1	B	2	73.	15.	4.802	>	N/B	C,F
304	1	B	2	4.3	.91	4.700	>	N/B	C,F
304	2	A	3	5.4	14.	.399	<	N/B	C,F
304	3	A	4	.80E-02	8.1	.001	<<	?/B	J
304	4	A	4	.98E-03	5.4	.000	<<	?/B	J
304	6	A	4	.68E-03	3.2	.000	<<	?/A	J
304	7	A	4	2.5	3.5	.713	<=	A/A	C,E
305	1	B	2	24.	10.	2.338	>	B/B	D,F
305	2	N	3	19.	5.0	3.886	>	N/A	
305	3	N	2	19.	2.9	6.571	>>	N/N	
305	4	B	2	8.2	37.	.218	<	B/B	C,F
305	5	B	2	52.	74.	.698	<=	B/A	D,F
305	6	N	3	16.	35.	.456	<	N/A	B,C,E
305	7	N	2	3.9	6.6	.596	<=	A/N	C,E
309	4	B	2	29.	.83	35.328	>>	N/B	C,F
309	5	B	2	41.	29.	1.413	>=	B/B	
309	6	B	2	17.	14.	1.262	>=	N/B	D,F
309	7	B	2	14.	11.	1.271	>=	B/B	D,F
309	8	B	2	40.	4.2	9.474	>>	B/B	D,F
310	4	B	2	36.	22.	1.626	>=	B/B	A,D,F
310	5	B	2	19.	52.	.359	<	B/B	B,D,F
310	6	N	3	41.	63.	.650	<=	A/N	D,F
310	7	A	3	31.	9.7	3.170	>	A/N	D,F
311	1	B	2	25.	26.	.965	<=	N/B	A,D,F
311	2	N	3	1.1	3.5	.324	<	A/A	D,F
311	3	B	2	5.7	4.5	1.263	>=	B/N	C,F
311	4	B	2	21.	18.	1.185	>=	N/B	D,F
311	5	N	3	22.	35.	.642	<=	N/N	D,F
311	6	B	2	14.	7.6	1.887	>=	B/B	C,F
314	1	B	3	.97	20.	.047	<<	N/B	D,F
314	2	B	2	9.0	28.	.319	<	B/N	C,F
314	3	B	3	8.6	57.	.150	<<	B/N	C,F
314	4	B	3	4.1	18.	.234	<	A/A	D,F
314	5	B	3	8.1	8.6	.940	<=	A/B	B
314	6	B	2	.20	2.3	.085	<<	B/B	C,F
314	7	B	2	4.2	5.4	.772	<=	B/B	
314	8	B	2	1.2	.66	1.876	>=	B/B	C,F
315	3	N	3	25.	25.	.992	<=	A/N	D,F
315	4	N	3	43.	69.	.624	<=	A/A	D,F
315	5	N	3	50.	59.	.845	<=	A/A	D,F
315	7	A	4	21.	16.	1.270	>=	A/N	C,E
315	8	A	4	12.	29.	.404	<	A/A	A,C,E

****

*SEE INTERPRETATION OF CODES AT END OF TABLE

TABLE G-1 (Page 3 of 4)

SUMMARY OF PREDICTED AND OBSERVED DATA FOR SF6 TRACER AT CINDER CONE BUTTE SITE*

JUL. DAY	HR	PLUME HEIGHT VS Hc	WIND SPD CAT	TOP 5 AVE CONC DATA (uS/M**3) TOP 5 AVE PRE	TOP 5 AVE OBS	PRE/OBS RATIO	RATIO CAT	ELEV OF PRE MAX VS Hc/ ELEV OF OBS MAX VS Hc	COMMENTS
317	3	A	3	12.	7.1	1.662	>=	A/A	C,F
317	4	A	4	7.2	21.	.348	<	A/A	C,F
317	5	A	4	7.9	16.	.505	<=	A/A	
317	6	A	4	4.2	7.5	.560	<=	A/A	
317	7	A	4	6.3	13.	.505	<=	A/A	C,F
317	8	A	4	8.1	15.	.547	<=	A/A	C,F

****

*SEE INTERPRETATION OF CODES AT END OF TABLE

TABLE G-1 (Page 4 of 4)

INTERPRETATION OF CODES:

TABLE ITEM	CODE	MEANING
PLUME HEIGHT VS Hc	N	Plume height within 5 m of Hc
	A	Plume height > Hc + 5 m
	B	Plume height < Hc - 5 m
WIND SPEED CATEGORY	1	Wind speed less than 1 m/sec
	2	Wind speed between 1 and 3 m/sec
	3	Wind speed between 3 and 6 m/sec
	4	Wind speed greater than or equal to 6 m/sec
RATIO CATEGORY OF PREDICTED TO OBSERVED AVERAGES OF HIGHEST 5 CONCENTRATIONS	<<	Ratio < .2
	<	Ratio is between .2 and .5
	<=	Ratio is between .5 and 1.0
	>=	Ratio is between 1.0 and 2.0
	>	Ratio is between 2.0 and 5.0
	>>	Ratio is greater than or equal to 5.0
ELEVATION OF MAXIMUM PREDICTED OR OBSERVED CONCENTRATION VS Hc	N	Elevation of maximum is within 5 m of Hc
	A	Elevation of maximum > Hc + 5 m
	B	Elevation of maximum < Hc - 5 m
COMMENTS	A	The location of the predicted maximum coincides with or is at the closest adjacent receptor to the location of the observed maximum
	B	The location of the predicted maximum is at a receptor close to the location of the observed maximum (with no more than 1 or 2 receptors closer to the location of the predicted maximum)
	C	The predicted maximum concentration is on the far side of the hill/ridge
	D	The predicted maximum concentration is on the near side of the hill/ridge
	E	The observed maximum concentration is on the far side of the hill/ridge
	F	The observed maximum concentration is on the near side of the hill/ridge
	G	The observed maximum concentration occurs north of the predicted maximum concentration
	H	The predicted maximum concentration occurs south of the predicted maximum concentration
	I	The angle formed by the intersection of the stack-predicted maximum concentration receptor and the stack-observed maximum concentration receptor lines is more than 90 degrees
	J	Predicted map is all zeroes
	K	Observed map is all zeroes

TABLE G-2

SUMMARY OF PREDICTED AND OBSERVED DATA FOR CF3BR TRACER AT CINDER CONE BUTTE SITE*

JUL. DAY	HR	PLUME HEIGHT VS Hc	WIND SPD CAT	TOP 5 AVE CONC DATA (uS/M**3) TOP 5 AVE PRE	TOP 5 AVE OBS	PRE/OBS RATIO	RATIO CAT	ELEV OF PRE MAX VS Hc/ ELEV OF OBS MAX VS Hc	COMMENTS
301	20	A	4	26.	2.6	9.924	>>	A/A	B
301	21	A	4	14.	9.0	1.571	>=	A/A	B
301	23	N	3	17.	2.3	7.269	>>	N/N	D,E
302	1	N	3	37.	2.5	15.059	>>	N/B	D,F
304	1	N	3	.27E-01	1.6	.017	<<	B/B	B,D,F
304	3	N	3	63.	20.	3.178	>	N/A	B,C,E
304	4	A	3	53.	6.7	7.845	>>	N/A	B,C,E
304	6	A	3	8.9	35.	.256	<	A/A	D,E
304	7	A	3	14.	47.	.287	<	N/A	C,E
305	3	B	2	30.	2.5	11.880	>>	B/B	B,C,E
305	4	A	3	7.2	1.2	6.081	>>	N/A	C,F
305	5	A	3	3.0	.95	3.192	>	A/N	
305	6	A	4	.22	1.0	.211	<	A/A	D,F
305	7	A	4	.33	7.0	.047	<<	A/A	B,D,F
305	8	A	3	6.7	4.8	1.384	>=	N/A	D,F
309	5	A	3	.64	7.7	.083	<<	N/B	B,C,E
309	6	A	3	12.	24.	.497	<	N/A	C,E
309	7	A	2	21.	8.6	2.428	>	N/A	C,F
309	8	A	3	8.6	.27	32.416	>>	N/?	K
310	4	A	2	89.	11.	8.208	>>	A/A	D,F
310	5	N	2	40.	.79	51.224	>>	A/A	D,F
310	6	A	3	11.	6.7	1.660	>=	A/A	D,F
311	1	A	3	6.6	1.5	4.519	>	N/A	C,E
311	2	A	3	1.5	.26	5.657	>>	A/A	A,D,F
311	5	A	4	7.0	11.	.628	<=	A/A	
311	6	A	3	21.	12.	1.790	>=	N/N	A,C,E
314	1	N	3	45.	5.9	7.652	>>	N/A	D,E
314	2	N	3	44.	11.	3.918	>	N/B	D,E
314	3	N	3	52.	15.	3.557	>	N/N	D,E
314	4	A	3	61.	1.5	40.851	>>	N/A	D,F
314	5	A	3	.11E+03	6.9	15.455	>>	N/A	D,F
314	6	B	3	4.3	8.0	.529	<=	B/A	C,F
315	7	N	3	22.	35.	.641	<=	A/N	B,C,E
315	8	N	3	25.	29.	.864	<=	A/N	C,E
317	4	A	4	2.3	6.0	.384	<	A/A	D,E
317	5	A	4	2.2	2.3	.935	<=	A/A	D,E
317	6	A	4	.79	.63E-01	12.615	>>	A/A	D,E
317	7	A	4	1.8	2.8	.643	<=	A/A	D,E
317	8	A	4	2.1	2.5	.850	<=	A/A	D,E

****

*SEE INTERPRETATION OF CODES AT END OF TABLE

TABLE G-2 (Continued)

INTERPRETATION OF CODES:

TABLE ITEM	CODE	MEANING
PLUME HEIGHT VS Hc	N	Plume height within 5 m of Hc
	A	Plume height > Hc + 5 m
	B	Plume height < Hc - 5 m
WIND SPEED CATEGORY	1	Wind speed less than 1 m/sec
	2	Wind speed between 1 and 3 m/sec
	3	Wind speed between 3 and 6 m/sec
	4	Wind speed greater than or equal to 6 m/sec
RATIO CATEGORY OF PREDICTED TO OBSERVED AVERAGES OF HIGHEST 5 CONCENTRATIONS	<<	Ratio < .2
	<	Ratio is between .2 and .5
	<=	Ratio is between .5 and 1.0
	>=	Ratio is between 1.0 and 2.0
	>	Ratio is between 2.0 and 5.0
	>>	Ratio is greater than or equal to 5.0
ELEVATION OF MAXIMUM PREDICTED OR OBSERVED CONCENTRATION VS Hc	N	Elevation of maximum is within 5 m of Hc
	A	Elevation of maximum > Hc + 5 m
	B	Elevation of maximum < Hc - 5 m
COMMENTS	A	The location of the predicted maximum coincides with or is at the closest adjacent receptor to the location of the observed maximum
	B	The location of the predicted maximum is at a receptor close to the location of the observed maximum (with no more than 1 or 2 receptors closer to the location of the predicted maximum)
	C	The predicted maximum concentration is on the far side of the hill/ridge
	D	The predicted maximum concentration is on the near side of the hill/ridge
	E	The observed maximum concentration is on the far side of the hill/ridge
	F	The observed maximum concentration is on the near side of the hill/ridge
	G	The observed maximum concentration occurs north of the predicted maximum concentration
	H	The predicted maximum concentration occurs south of the predicted maximum concentration
	I	The angle formed by the intersection of the stack-predicted maximum concentration receptor and the stack-observed maximum concentration receptor lines is more than 90 degrees
	J	Predicted map is all zeroes
	K	Observed map is all zeroes

TABLE G-3

SUMMARY OF PREDICTED AND OBSERVED DATA FOR SF6 TRACER AT HOG BACK RIDGE SITE*

JUL. DAY	HR	PLUME HEIGHT VS Hc	WIND SPD CAT	TOP 5 AVE CONC DATA (uS/M**3) TOP 5 AVE PRE	TOP 5 AVE OBS	PRE/OBS RATIO	RATIO CAT	ELEV OF PRE MAX VS Hc/ ELEV OF OBS MAX VS Hc	COMMENTS
284	3	B	2	22.	44.	.500	<	B/A	D,F
284	5	A	2	14.	33.	.416	<	B/A	D,F,H
285	2	B	2	34.	16.	2.157	>	B/A	D,E
285	3	B	2	27.	29.	.932	<=	B/B	D,F
286	2	A	2	17.	3.4	5.010	>>	A/A	D,F
286	5	N	2	21.	9.0	2.378	>	N/N	D,F
286	7	N	2	38.	11.	3.316	>	N/A	D,E
286	8	B	2	32.	27.	1.163	>=	B/A	D,F
287	2	B	2	43.	7.5	5.776	>>	B/B	D,F
287	3	B	2	39.	18.	2.211	>	B/A	D,E
287	4	B	2	46.	33.	1.395	>=	B/A	D,E
287	5	B	2	.26E+03	62.	4.156	>	B/A	D,F
287	6	B	2	89.	29.	3.104	>	B/A	D,E
287	7	B	2	.13E+03	63.	2.115	>	B/A	D,E
288	4	B	2	31.	13.	2.490	>	B/B	D,F
288	5	B	2	47.	17.	2.694	>	B/N	D,E
288	6	B	2	33.	19.	1.748	>=	N/A	D,F
288	7	B	2	24.	28.	.843	<=	N/A	D,E
288	8	B	2	36.	15.	2.418	>	B/A	D,F
295	2	B	2	76.	35.	2.185	>	B/A	D,E
295	3	N	2	36.	9.4	3.815	>	N/B	B
295	4	B	2	16.	13.	1.238	>=	B/A	D,E
295	5	N	2	21.	7.4	2.873	>	A/A	D,E
295	6	A	2	16.	2.4	6.465	>>	A/A	C,F
295	7	A	3	21.	3.9	5.471	>>	A/A	
295	8	A	2	28.	12.	2.236	>	N/A	
296	1	N	2	.12E+03	12.	9.681	>>	B/N	B,D,F
296	2	B	2	19.	14.	1.381	>=	B/A	D,F
296	3	B	2	37.	9.4	3.899	>	B/N	D,E
296	5	A	2	17.	7.9	2.141	>	A/A	D,F
296	6	A	2	21.	11.	1.938	>=	N/A	D,F
296	7	A	3	35.	18.	1.934	>=	N/A	D,E
297	2	A	2	8.8	.12	73.928	>>	A/N	
297	3	A	2	8.9	1.5	5.859	>>	A/N	
297	4	A	2	23.	8.1	2.812	>	B/A	D,F
297	5	A	2	7.6	3.5	2.168	>	A/A	D,E
297	7	A	3	1.3	.41	3.077	>	A/A	C,F
297	9	A	3	18.	16.	1.125	>=	N/A	D,F
299	3	N	2	76.	17.	4.594	>	B/A	D,F
299	4	A	2	32.	19.	1.746	>=	N/A	D,F
299	6	A	2	40.	21.	1.877	>=	B/B	D,F
299	7	A	2	31.	13.	2.451	>	N/B	D,F,H
299	8	N	2	57.	17.	3.407	>	N/B	D,F
299	9	A	2	39.	35.	1.132	>=	N/A	D,F

****

*SEE INTERPRETATION OF CODES AT END OF TABLE

TABLE G-3 (Continued)

SUMMARY OF PREDICTED AND OBSERVED DATA FOR SF6 TRACER AT HOG BACK RIDGE SITE*

JUL. DAY	HR	PLUME HEIGHT VS Hc	WIND SPD CAT	TOP 5 AVE CONC DATA (uS/M**3) TOP 5 AVE PRE	TOP 5 AVE OBS	PRE/OBS RATIO	RATIO CAT	ELEV OF PRE MAX VS Hc/ ELEV OF OBS MAX VS Hc	COMMENTS
302	1	B	2	50.	19.	2.655	>	B/A	D,F
302	2	B	2	99.	22.	4.584	>	B/N	D,F
302	3	B	2	.13E+03	61.	2.216	>	B/B	D,F
302	4	N	2	76.	7.2	10.579	>>	N/N	D,E
302	5	B	2	.13E+03	5.0	25.754	>>	N/?	K
302	7	N	2	29.	7.8	3.714	>	N/B	H
302	8	N	2	39.	7.6	5.136	>>	B/A	

****

*SEE INTERPRETATION OF CODES AT END OF TABLE

TABLE G-3 (Continued)

INTERPRETATION OF CODES:

TABLE ITEM	CODE	MEANING
PLUME HEIGHT VS Hc	N	Plume height within 5 m of Hc
	A	Plume height > Hc + 5 m
	B	Plume height < Hc - 5 m
WIND SPEED CATEGORY	1	Wind speed less than 1 m/sec
	2	Wind speed between 1 and 3 m/sec
	3	Wind speed between 3 and 6 m/sec
	4	Wind speed greater than or equal to 6 m/sec
RATIO CATEGORY OF PREDICTED TO OBSERVED AVERAGES OF HIGHEST 5 CONCENTRATIONS	<<	Ratio < .2
	<	Ratio is between .2 and .5
	<=	Ratio is between .5 and 1.0
	>=	Ratio is between 1.0 and 2.0
	>	Ratio is between 2.0 and 5.0
	>>	Ratio is greater than or equal to 5.0
ELEVATION OF MAXIMUM PREDICTED OR OBSERVED CONCENTRATION VS Hc	N	Elevation of maximum is within 5 m of Hc
	A	Elevation of maximum > Hc + 5 m
	B	Elevation of maximum < Hc - 5 m
COMMENTS	A	The location of the predicted maximum coincides with or is at the closest adjacent receptor to the location of the observed maximum
	B	The location of the predicted maximum is at a receptor close to the location of the observed maximum (with no more than 1 or 2 receptors closer to the location of the predicted maximum)
	C	The predicted maximum concentration is on the far side of the hill/ridge
	D	The predicted maximum concentration is on the near side of the hill/ridge
	E	The observed maximum concentration is on the far side of the hill/ridge
	F	The observed maximum concentration is on the near side of the hill/ridge
	G	The observed maximum concentration occurs north of the predicted maximum concentration
	H	The predicted maximum concentration occurs south of the predicted maximum concentration
	I	The angle formed by the intersection of the stack-predicted maximum concentration receptor and the stack-observed maximum concentration receptor lines is more than 90 degrees
	J	Predicted map is all zeroes
	K	Observed map is all zeroes

TABLE G-4

SUMMARY OF PREDICTED AND OBSERVED DATA FOR CF3BR TRACER AT HOG BACK RIDGE SITE*

JUL. DAY	HR	PLUME HEIGHT VS Hc	WIND SPD CAT	TOP 5 AVE CONC DATA (uS/M**3) TOP 5 AVE PRE	TOP 5 AVE OBS	PRE/OBS RATIO	RATIO CAT	ELEV OF PRE MAX VS Hc/ ELEV OF OBS MAX VS Hc	COMMENTS
285	1	N	2	47.	58.	.807	<=	B/B	D,F,H
285	2	B	2	38.	98.	.388	<	B/B	B,D,F
285	3	B	2	33.	67.	.499	<	B/B	D,F
285	24	B	2	19.	65.	.295	<	B/B	A,D,F
286	5	B	2	20.	63.	.316	<	B/A	D,F
286	7	B	2	57.	.13E+03	.445	<	B/N	D,F
286	8	B	2	34.	.26E+03	.129	<<	B/B	D,F,H
287	2	B	2	59.	.13E+03	.473	<	B/B	D,F,H
287	3	B	2	52.	.12E+03	.438	<	B/A	D,F
287	4	B	2	.10E+03	.10E+03	.971	<=	B/N	D,F
287	5	B	2	.15E+03	.14E+03	1.084	>=	B/B	A,D,F
287	7	B	2	.18E+03	.21E+03	.836	<=	B/B	D,F,H
287	8	B	2	.17E+03	.16E+03	1.044	>=	B/B	D,F
287	24	B	2	63.	18.	3.498	>	B/B	D,F,H
288	5	B	2	35.	49.	.726	<=	B/B	D,F,H
288	6	B	2	32.	66.	.490	<	B/N	D,F,H
288	7	B	2	24.	40.	.592	<=	B/A	D,F
288	8	B	2	50.	50.	1.009	>=	B/B	D,F
295	3	B	2	15.	13.	1.115	>=	B/B	D,F,H
295	6	B	2	30.	33.	.909	<=	B/A	D,F
295	7	B	2	18.	38.	.469	<	B/B	B,D,F
295	24	B	2	.14E+03	78.	1.763	>=	B/B	D,F,H
296	6	B	2	16.	6.3	2.613	>	B/B	D,F,G
296	7	B	2	36.	43.	.842	<=	N/N	B,D,F
297	2	B	2	6.5	1.2	5.549	>>	B/A	D,E
297	3	B	2	18.	15.	1.228	>=	B/N	D,F,G
297	4	A	2	23.	8.3	2.739	>	B/B	D,F,G
297	6	B	2	8.9	1.1	7.968	>>	B/B	A,D,F
297	7	N	2	3.2	3.4	.927	<=	A/A	D,F,G
299	3	B	2	73.	29.	2.522	>	B/B	D,F
299	4	B	2	61.	96.	.634	<=	A/A	D,F,H
299	5	B	2	52.	.11E+03	.480	<	B/B	A,D,F
299	6	B	2	44.	56.	.779	<=	B/N	B,D,F
299	8	B	2	10.	5.6	1.826	>=	B/N	D,F
299	9	N	2	7.3	7.8	.936	<=	N/B	D,F,H
302	2	B	2	18.	3.2	5.503	>>	N/B	D,F
302	3	N	2	28.	1.5	18.549	>>	A/A	D,E
302	4	B	2	20.	15.	1.371	>=	B/N	D,F,G
302	5	B	2	15.	48.	.316	<	N/A	D,F,G
302	7	B	2	20.	19.	1.090	>=	A/A	D,F
302	8	N	2	24.	25.	.948	<=	A/A	D,E
302	9	B	2	14.	30.	.464	<	N/A	D,F,H

****

*SEE INTERPRETATION OF CODES AT END OF TABLE

TABLE G-4 (Continued)

INTERPRETATION OF CODES:

TABLE ITEM	CODE	MEANING
PLUME HEIGHT VS Hc	N	Plume height within 5 m of Hc
	A	Plume height > Hc + 5 m
	B	Plume height < Hc - 5 m
WIND SPEED CATEGORY	1	Wind speed less than 1 m/sec
	2	Wind speed between 1 and 3 m/sec
	3	Wind speed between 3 and 6 m/sec
	4	Wind speed greater than or equal to 6 m/sec
RATIO CATEGORY OF PREDICTED TO OBSERVED AVERAGES OF HIGHEST 5 CONCENTRATIONS	<<	Ratio < .2
	<	Ratio is between .2 and .5
	<=	Ratio is between .5 and 1.0
	>=	Ratio is between 1.0 and 2.0
	>	Ratio is between 2.0 and 5.0
	>>	Ratio is greater than or equal to 5.0
ELEVATION OF MAXIMUM PREDICTED OR OBSERVED CONCENTRATION VS Hc	N	Elevation of maximum is within 5 m of Hc
	A	Elevation of maximum > Hc + 5 m
	B	Elevation of maximum < Hc - 5 m
COMMENTS	A	The location of the predicted maximum coincides with or is at the closest adjacent receptor to the location of the observed maximum
	B	The location of the predicted maximum is at a receptor close to the location of the observed maximum (with no more than 1 or 2 receptors closer to the location of the predicted maximum)
	C	The predicted maximum concentration is on the far side of the hill/ridge
	D	The predicted maximum concentration is on the near side of the hill/ridge
	E	The observed maximum concentration is on the far side of the hill/ridge
	F	The observed maximum concentration is on the near side of the hill/ridge
	G	The observed maximum concentration occurs north of the predicted maximum concentration
	H	The predicted maximum concentration occurs south of the predicted maximum concentration
	I	The angle formed by the intersection of the stack-predicted maximum concentration receptor and the stack-observed maximum concentration receptor lines is more than 90 degrees
	J	Predicted map is all zeroes
	K	Observed map is all zeroes

TABLE G-5

SUMMARY OF PREDICTED AND OBSERVED DATA FOR SF6 TRACER AT TRACY POWER PLANT SITE*

JUL. DAY	HR	PLUME HEIGHT VS Hc	WIND SPD CAT	TOP 5 AVE CONC DATA (uS/M**3) TOP 5 AVE PRE	TOP 5 AVE OBS	PRE/OBS RATIO	RATIO CAT	ELEV OF PRE MAX VS Hc/ ELEV OF OBS MAX VS Hc	COMMENTS
219	4	N	3	.74	.64	1.170	>=	A/B	B
219	5	N	3	.78	1.3	.602	<=	A/A	
219	6	A	2	2.9	2.2	1.331	>=	A/A	A
219	7	N	2	2.6	1.8	1.445	>=	A/A	
220	4	N	3	2.9	2.5	1.175	>=	A/A	A
220	5	B	2	1.8	5.2	.348	<	A/A	
220	6	B	2	2.7	2.8	.962	<=	B/B	
220	7	B	2	2.8	3.7	.746	<=	A/A	
222	21	A	4	.29	.23	1.260	>=	A/A	
222	22	A	4	.52E-01	.19	.270	<	A/A	
222	23	A	4	.56	.19	2.938	>	A/A	
222	24	A	3	.78	.37	2.111	>	A/A	I
223	1	A	2	.59	.38	1.530	>=	A/A	
223	2	A	2	1.0	.57	1.773	>=	A/A	
223	3	A	3	2.3	.62	3.678	>	A/A	
223	4	A	3	3.3	.86	3.850	>	A/A	
223	5	B	2	1.2	.84	1.409	>=	A/A	
223	6	N	3	.63	1.8	.343	<	A/A	B
223	21	A	3	.53	.72	.739	<=	A/A	B
223	22	A	3	.60	.39	1.508	>=	A/A	
223	24	A	3	.92	.54	1.700	>=	A/A	I
224	1	A	3	1.3	.66	2.014	>	A/A	I
224	2	B	3	2.6	.54	4.895	>	A/A	A
224	3	B	2	.54	.82	.651	<=	A/A	I
224	4	B	2	2.8	.83	3.319	>	A/A	
224	5	B	2	2.5	.71	3.553	>	A/B	I
224	6	B	2	4.3	2.6	1.637	>=	A/A	
224	21	A	4	.23	.25	.918	<=	A/A	
224	22	A	3	.19	2.2	.087	<<	?/A	J
224	23	A	3	.47	.36	1.304	>=	A/B	
224	24	A	3	.66	.59	1.122	>=	B/A	
225	1	A	3	1.4	.70	2.040	>	A/A	I
225	2	N	2	3.0	.80	3.759	>	A/N	I
225	3	B	2	1.9	1.1	1.754	>=	A/A	
225	4	B	2	1.8	4.3	.416	<	A/A	
225	5	B	2	1.9	4.8	.403	<	A/A	A
225	6	B	2	1.4	3.3	.428	<	A/A	I
228	23	A	3	.51	1.6	.324	<	A/N	
228	24	A	4	.52	1.0	.513	<=	A/A	A
229	1	A	4	.44	1.2	.359	<	A/A	
229	2	A	3	.52	1.2	.437	<	A/B	
229	3	A	4	.29	.85	.337	<	A/A	
229	4	A	4	.37	1.0	.352	<	A/B	
229	5	B	3	1.8	2.2	.806	<=	A/A	

****

*SEE INTERPRETATION OF CODES AT END OF TABLE

TABLE G-5 (Page 2 of 4)

SUMMARY OF PREDICTED AND OBSERVED DATA FOR SF6 TRACER AT TRACY POWER PLANT SITE*

JUL. DAY	HR	PLUME HEIGHT VS Hc	WIND SPD CAT	TOP 5 AVE CONC DATA (uS/M**3) TOP 5 AVE PRE	TOP 5 AVE OBS	PRE/OBS RATIO	RATIO CAT	ELEV OF PRE MAX VS Hc/ ELEV OF OBS MAX VS Hc	COMMENTS
229	6	A	3	.34	1.8	.186	<<	A/A	
229	7	A	2	.53	2.3	.232	<	A/A	B
229	23	A	3	.46	.24	1.909	>=	A/A	B
229	24	A	3	.44	.48	.930	<=	A/N	
230	1	A	3	.63	.37	1.715	>=	A/B	B
230	2	A	3	.75	.36	2.057	>	A/A	
230	3	A	4	1.2	.30	3.887	>	A/A	
230	4	A	3	1.2	.94	1.242	>=	A/B	
230	5	B	3	1.4	1.7	.823	<=	A/A	A
230	6	B	2	2.3	2.7	.863	<=	B/A	
230	7	A	2	2.5	4.5	.564	<=	A/A	
230	23	A	4	.47	.35	1.346	>=	A/A	
230	24	A	4	.69	.38	1.800	>=	A/A	
231	1	A	4	.59	.57	1.039	>=	A/N	
231	2	A	4	1.1	.73	1.464	>=	A/B	
231	3	A	3	1.6	.74	2.091	>	A/A	
231	4	A	3	2.1	.42	4.998	>	A/A	
231	5	N	3	1.2	.72	1.723	>=	B/A	
231	6	N	3	1.3	2.0	.628	<=	A/A	
231	7	N	3	2.1	1.7	1.279	>=	A/A	
233	23	A	3	.76	.58	1.309	>=	N/A	
233	24	A	3	2.5	.55	4.481	>	B/N	
234	1	A	3	1.1	.44	2.489	>	A/A	B
234	2	A	4	.98	.73	1.340	>=	A/A	
234	3	A	4	1.3	1.3	.973	<=	A/B	A
234	4	A	4	1.9	1.1	1.703	>=	A/A	
234	5	A	4	1.2	.79	1.569	>=	B/A	
234	6	B	3	.77	1.7	.445	<	B/A	
234	7	N	3	2.0	1.1	1.762	>=	A/A	
234	24	A	3	.49	.43	1.140	>=	A/A	
235	1	A	2	1.7	.49	3.533	>	A/A	I
235	2	A	2	.51	.46	1.121	>=	A/A	I
235	3	B	2	2.9	.73	4.049	>	A/A	I
235	4	B	2	4.4	2.9	1.536	>=	A/A	
235	5	B	2	2.1	4.7	.444	<	N/A	I
235	6	B	2	2.5	2.6	.957	<=	B/B	I
235	7	B	2	4.8	1.6	2.937	>	A/A	I
235	24	A	3	.73	.54	1.340	>=	A/B	B
236	1	A	3	1.1	.85	1.331	>=	A/A	
236	2	A	2	.52	.45	1.176	>=	A/B	
236	3	B	2	.67	.34	1.962	>=	A/B	I
236	4	B	2	2.3	.26	8.805	>>	A/B	I
236	5	B	2	3.7	2.1	1.809	>=	A/A	
236	6	B	2	1.3	3.7	.347	<	A/A	I

****

*SEE INTERPRETATION OF CODES AT END OF TABLE

TABLE G-5 (Page 3 of 4)

SUMMARY OF PREDICTED AND OBSERVED DATA FOR SF6
TRACER AT TRACY POWER PLANT SITE*

JUL. DAY	HR	PLUME HEIGHT VS Hc	WIND SPD CAT	TOP 5 AVE CONC DATA (uS/M**3) TOP 5 AVE PRE	TOP 5 AVE OBS	PRE/OBS RATIO	RATIO CAT	ELEV OF PRE MAX VS Hc/ ELEV OF OBS MAX VS Hc	COMMENTS
236	7	B	2	.72	.98	.730	<=	A/A	I
238	1	B	3	.12	.11	1.118	>=	A/A	A
238	2	B	3	.24	.20	1.175	>=	A/A	
238	3	A	2	.15	.30	.488	<	A/A	
238	4	B	2	4.5	.27	16.536	>>	B/A	B
238	5	N	2	.56	1.4	.400	<	A/A	
238	6	B	2	1.8	2.1	.856	<=	A/A	
238	7	B	2	.91	1.2	.737	<=	A/A	
239	1	B	2	1.2	.25	4.753	>	A/A	
239	2	B	2	2.1	.52	4.119	>	A/A	
239	3	B	2	3.3	1.8	1.846	>=	A/A	
239	4	B	2	1.9	1.5	1.294	>=	B/B	
239	5	B	2	3.1	.81	3.889	>	A/A	
239	6	B	2	2.1	1.9	1.117	>=	A/A	
239	7	B	2	2.0	2.8	.732	<=	A/A	
240	1	B	3	.79	.19	4.201	>	A/A	
240	2	A	3	1.3	.31	4.227	>	A/B	
240	3	A	2	.67	1.4	.465	<	A/A	
240	4	B	2	.64	1.6	.391	<	B/B	
240	5	A	2	1.9	3.2	.608	<=	A/A	
240	6	B	2	2.0	2.1	.945	<=	A/A	
240	7	B	2	3.1	1.4	2.156	>	A/B	

****

*SEE INTERPRETATION OF CODES AT END OF TABLE

TABLE G-5 (Page 4 of 4)

INTERPRETATION OF CODES:

TABLE ITEM	CODE	MEANING
PLUME HEIGHT VS Hc	N	Plume height within 10 m of Hc
	A	Plume height > Hc + 10 m
	B	Plume height < Hc - 10 m
WIND SPEED CATEGORY	1	Wind speed less than 1 m/sec
	2	Wind speed between 1 and 3 m/sec
	3	Wind speed between 3 and 6 m/sec
	4	Wind speed greater than or equal to 6 m/sec
RATIO CATEGORY OF PREDICTED TO OBSERVED AVERAGES OF HIGHEST 5 CONCENTRATIONS	<<	Ratio < .2
	<	Ratio is between .2 and .5
	<=	Ratio is between .5 and 1.0
	>=	Ratio is between 1.0 and 2.0
	>	Ratio is between 2.0 and 5.0
	>>	Ratio is greater than or equal to 5.0
ELEVATION OF MAXIMUM PREDICTED OR OBSERVED CONCENTRATION VS Hc	N	Elevation of maximum is within 10 m of Hc
	A	Elevation of maximum > Hc + 10 m
	B	Elevation of maximum < Hc - 10 m
COMMENTS	A	The location of the predicted maximum coincides with or is at the closest adjacent receptor to the location of the observed maximum
	B	The location of the predicted maximum is at a receptor close to the location of the observed maximum (with no more than 1 or 2 receptors closer to the location of the predicted maximum)
	C	The predicted maximum concentration is on the far side of the hill/ridge
	D	The predicted maximum concentration is on the near side of the hill/ridge
	E	The observed maximum concentration is on the far side of the hill/ridge
	F	The observed maximum concentration is on the near side of the hill/ridge
	G	The observed maximum concentration occurs north of the predicted maximum concentration
	H	The predicted maximum concentration occurs south of the predicted maximum concentration
	I	The angle formed by the intersection of the stack-predicted maximum concentration receptor and the stack-observed maximum concentration receptor lines is more than 90 degrees
	J	Predicted map is all zeroes
	K	Observed map is all zeroes

TABLE G-6

SUMMARY OF PREDICTED AND OBSERVED DATA FOR CF3BR TRACER AT TRACY POWER PLANT SITE*

JUL. DAY	HR	PLUME HEIGHT VS Hc	WIND SPD CAT	TOP 5 AVE CONC DATA (uS/M**3) TOP 5 AVE PRE	TOP 5 AVE OBS	PRE/OBS RATIO	RATIO CAT	ELEV OF PRE MAX VS Hc/ ELEV OF OBS MAX VS Hc	COMMENTS
219	4	B	2	1.6	.52	3.083	>	B/B	A
219	5	B	2	2.1	1.6	1.351	>=	B/A	
219	6	B	2	4.3	2.2	1.954	>=	B/B	A
219	7	B	2	2.2	1.8	1.206	>=	B/B	
220	4	B	2	4.6	1.5	2.948	>	B/A	B
220	5	B	2	2.7	3.7	.722	<=	B/B	
220	6	B	2	2.1	2.9	.735	<=	A/B	
220	7	B	2	1.9	7.8	.248	<	B/B	
222	21	A	4	.17	.31	.550	<=	A/A	
222	22	B	4	.61E-01	.15	.393	<	A/A	A
222	23	A	4	.79	.55	1.453	>=	A/N	
222	24	A	3	1.5	.49	2.968	>	A/B	
223	1	N	2	2.5	.60	4.208	>	B/A	
223	2	B	2	1.4	.66	2.076	>	A/B	
223	3	B	3	1.1	1.3	.874	<=	A/A	B
223	4	N	3	3.0	1.5	2.007	>	A/A	
223	5	B	2	1.7	1.5	1.125	>=	B/B	
223	6	B	2	1.0	4.0	.247	<	A/B	
223	21	A	3	.52	.51	1.013	>=	A/B	
223	22	A	3	.60	1.1	.572	<=	A/B	
223	24	A	3	.93	.57	1.630	>=	A/B	
224	1	A	3	1.2	.78	1.594	>=	A/B	A
224	2	A	3	2.1	3.9	.537	<=	A/A	B
224	3	B	2	.99	1.1	.903	<=	B/B	
224	4	B	2	2.2	1.0	2.193	>	B/B	A
224	5	B	2	.76	4.0	.188	<<	B/A	
224	6	B	2	4.8	4.5	1.051	>=	B/A	
224	21	A	4	.20	.15	1.340	>=	A/N	I
224	22	A	3	.11	.20	.556	<=	A/A	I
224	23	A	3	.45	.68	.659	<=	A/A	
224	24	A	2	.78	.75	1.038	>=	B/A	
225	1	A	3	1.5	.79	1.876	>=	B/A	
225	2	N	2	2.9	1.1	2.614	>	A/A	A
225	3	B	2	3.6	1.3	2.642	>	A/A	
225	4	B	2	2.3	3.8	.612	<=	A/A	A
225	5	B	2	1.8	2.9	.634	<=	B/B	A
225	6	B	2	1.8	.79	2.263	>	A/A	I
228	23	A	4	.94	1.5	.611	<=	A/B	
228	24	A	4	.77	1.1	.679	<=	A/A	
229	1	A	4	.59	1.0	.582	<=	A/A	B
229	2	A	4	.93	.87	1.068	>=	A/A	
229	3	A	4	.56	.41	1.353	>=	A/B	
229	4	A	4	1.2	1.2	.967	<=	A/B	
229	5	A	3	2.8	2.3	1.256	>=	B/A	

****

*SEE INTERPRETATION OF CODES AT END OF TABLE

SUMMARY OF PREDICTED AND OBSERVED DATA FOR CF3BR TRACER AT TRACY POWER PLANT SITE*

JUL. DAY	HR	PLUME HEIGHT VS Hc	WIND SPD CAT	TOP 5 AVE CONC DATA (uS/M**3) TOP 5 AVE PRE	TOP 5 AVE OBS	PRE/OBS RATIO	RATIO CAT	ELEV OF PRE MAX VS Hc/ ELEV OF OBS MAX VS Hc	COMMENTS
229	6	A	3	1.5	2.1	.732	<=	B/A	
229	7	B	2	1.1	1.7	.640	<=	B/A	
229	23	A	3	1.2	.38	3.062	>	B/B	A
229	24	A	3	.78	.46	1.693	>=	A/A	A
230	1	A	4	.93	.36	2.607	>	N/A	B
230	2	A	4	1.3	.87	1.517	>=	A/B	
230	3	A	4	2.0	.83	2.362	>	A/A	
230	4	B	3	1.1	1.4	.783	<=	A/B	
230	5	B	2	1.7	3.1	.553	<=	A/A	
230	6	B	3	.96	6.1	.157	<<	B/A	
230	7	B	2	2.7	3.1	.869	<=	B/B	
230	23	A	4	.45	.31	1.453	>=	A/A	B
230	24	A	3	.58	.39	1.482	>=	A/A	A
231	1	A	3	.54	.32	1.679	>=	A/N	
231	2	A	3	.65	.43	1.506	>=	A/A	B
231	3	A	3	.94	.60	1.565	>=	A/N	
231	4	A	3	1.2	.40	2.941	>	A/B	
231	5	N	3	1.3	1.0	1.282	>=	A/B	B
231	6	N	3	1.3	3.2	.397	<	A/B	
231	7	N	3	1.5	3.0	.507	<=	A/B	B
233	23	A	3	1.2	.68	1.822	>=	B/B	A
233	24	A	3	3.7	1.3	2.948	>	B/A	
234	1	A	3	1.9	.84	2.309	>	A/A	
234	2	A	4	1.5	2.4	.617	<=	A/A	
234	3	A	4	1.3	1.4	.956	<=	A/A	A
234	4	A	4	2.0	1.8	1.141	>=	A/A	
234	5	A	4	1.8	2.6	.685	<=	B/N	A
234	6	B	3	.76	2.3	.327	<	B/A	
234	7	B	3	3.0	2.4	1.246	>=	B/A	
234	24	A	2	1.1	.81	1.391	>=	A/A	
235	1	B	2	1.1	.95	1.154	>=	B/B	I
235	2	B	2	1.1	.85	1.347	>=	A/A	I
235	3	B	2	.24	1.3	.177	<<	A/B	
235	4	B	2	1.2	1.9	.610	<=	B/B	
235	5	B	2	1.4	2.3	.630	<=	A/B	I
235	6	B	2	1.0	4.9	.210	<	A/A	
235	7	B	2	2.0	3.0	.665	<=	B/B	
235	24	A	3	1.1	1.1	1.011	>=	A/B	B
236	1	B	2	1.2	1.3	.912	<=	B/A	
236	2	N	2	1.2	1.2	1.004	>=	A/A	
236	3	B	2	.69	2.6	.263	<	A/A	
236	4	B	2	2.9	2.0	1.454	>=	B/A	I
236	5	B	2	1.7	2.7	.649	<=	B/B	A
236	6	B	2	.68	2.8	.246	<	A/A	I

****

*SEE INTERPRETATION OF CODES AT END OF TABLE

TABLE G-6 (Page 3 of 4)

SUMMARY OF PREDICTED AND OBSERVED DATA FOR CF3BR TRACER AT TRACY POWER PLANT SITE*

JUL. DAY	HR	PLUME HEIGHT VS Hc	WIND SPD CAT	TOP 5 AVE CONC DATA (uS/M**3) TOP 5 AVE PRE	TOP 5 AVE OBS	PRE/OBS RATIO	RATIO CAT	ELEV OF PRE MAX VS Hc/ ELEV OF OBS MAX VS Hc	COMMENTS
236	7	B	2	1.1	1.7	.620	<=	B/A	
238	1	A	3	.67	.88	.765	<=	A/A	A
238	2	B	2	.66	.60	1.096	>=	A/A	A
238	3	B	2	1.3	.61	2.189	>	B/B	
238	4	B	2	.78	1.1	.704	<=	A/A	
238	5	B	2	.41	1.2	.340	<	A/A	I
238	6	B	2	1.3	1.1	1.171	>=	A/A	
238	7	B	2	.79	3.1	.257	<	B/A	
239	1	B	2	3.3	.26	12.458	>>	B/A	I
239	2	B	2	2.7	.80	3.381	>	B/A	
239	3	B	2	1.1	6.0	.188	<<	B/B	
239	4	B	2	.87	3.4	.252	<	A/B	I
239	5	B	2	2.0	2.6	.760	<=	B/B	
239	6	B	2	1.9	2.3	.843	<=	B/B	
239	7	B	2	3.0	3.1	.946	<=	B/B	
240	1	A	3	1.5	.66	2.262	>	B/B	
240	2	B	3	.74	1.3	.573	<=	N/B	
240	3	B	2	1.5	2.3	.652	<=	B/B	A
240	4	B	2	1.0	2.8	.369	<	N/N	B
240	5	B	2	1.5	2.6	.561	<=	A/A	
240	6	B	2	1.7	1.9	.906	<=	A/A	
240	7	B	2	1.3	4.2	.305	<	A/B	B

****

*SEE INTERPRETATION OF CODES AT END OF TABLE

TABLE G-6 (Page 4 of 4)

INTERPRETATION OF CODES:

TABLE ITEM	CODE	MEANING
PLUME HEIGHT VS Hc	N	Plume height within 10 m of Hc
	A	Plume height > Hc + 10 m
	B	Plume height < Hc - 10 m
WIND SPEED CATEGORY	1	Wind speed less than 1 m/sec
	2	Wind speed between 1 and 3 m/sec
	3	Wind speed between 3 and 6 m/sec
	4	Wind speed greater than or equal to 6 m/sec
RATIO CATEGORY OF PREDICTED TO OBSERVED AVERAGES OF HIGHEST 5 CONCENTRATIONS	<<	Ratio < .2
	<	Ratio is between .2 and .5
	<=	Ratio is between .5 and 1.0
	>=	Ratio is between 1.0 and 2.0
	>	Ratio is between 2.0 and 5.0
	>>	Ratio is greater than or equal to 5.0
ELEVATION OF MAXIMUM PREDICTED OR OBSERVED CONCENTRATION VS Hc	N	Elevation of maximum is within 10 m of Hc
	A	Elevation of maximum > Hc + 10 m
	B	Elevation of maximum < Hc - 10 m
COMMENTS	A	The location of the predicted maximum coincides with or is at the closest adjacent receptor to the location of the observed maximum
	B	The location of the predicted maximum is at a receptor close to the location of the observed maximum (with no more than 1 or 2 receptors closer to the location of the predicted maximum)
	C	The predicted maximum concentration is on the far side of the hill/ridge
	D	The predicted maximum concentration is on the near side of the hill/ridge
	E	The observed maximum concentration is on the far side of the hill/ridge
	F	The observed maximum concentration is on the near side of the hill/ridge
	G	The observed maximum concentration occurs north of the predicted maximum concentration
	H	The predicted maximum concentration occurs south of the predicted maximum concentration
	I	The angle formed by the intersection of the stack-predicted maximum concentration receptor and the stack-observed maximum concentration receptor lines is more than 90 degrees
	J	Predicted map is all zeroes
	K	Observed map is all zeroes

TABLE G-7

SUMMARY STATISTICS OF CTDM MODEL EVALUATION
SITE = CINDER CONE BUTTE TRACER = SF6

CASE 1: WIND SPEED CATEGORY = 1, PLUME HEIGHT BELOW Hc: NO CASES

CASE 2: WIND SPEED CATEGORY = 1, PLUME HEIGHT NEAR Hc: NO CASES

CASE 3: WIND SPEED CATEGORY = 1, PLUME HEIGHT ABOVE Hc: NO CASES

CASE 4: WIND SPEED CATEGORY = 2, PLUME HEIGHT BELOW Hc*

ELEV OF PRE MAX VS Hc/ ELEV OF OBS MAX VS Hc	DISTRIBUTION OF HOURS BY RATIO CATEGORY OF TOP 5 AVE. PREDICTED TO TOP 5 AVE. OBSERVED CONCENTRATIONS ********** <<	<	<=	>=	>	>>	TOTAL HOURS
B/B	1	2	2	6	3	2	16
B/N	0	1	0	2	1	0	4
B/A	0	0	1	0	0	0	1
N/B	0	0	1	2	2	1	6
N/N	0	0	0	0	0	0	0
N/A	0	0	0	0	0	1	1
A/B	0	0	0	0	0	0	0
A/N	0	0	0	0	0	0	0
A/A	0	0	0	0	0	0	0
TOTALS	1	3	4	10	6	4	28

****
*SEE INTERPRETATION OF CODES AT END OF TABLE

CASE 5: WIND SPEED CATEGORY = 2, PLUME HEIGHT NEAR Hc*

ELEV OF PRE MAX VS Hc/ ELEV OF OBS MAX VS Hc	DISTRIBUTION OF HOURS BY RATIO CATEGORY OF TOP 5 AVE. PREDICTED TO TOP 5 AVE. OBSERVED CONCENTRATIONS ********** <<	<	<=	>=	>	>>	TOTAL HOURS
B/B	0	0	0	0	0	0	0
B/N	0	0	0	0	0	0	0
B/A	0	0	0	0	0	0	0
N/B	0	0	1	1	0	2	4
N/N	0	0	0	0	1	1	2
N/A	0	0	0	0	0	0	0
A/B	0	0	0	0	0	0	0
A/N	0	0	1	0	0	1	2
A/A	0	0	0	0	0	0	0
TOTALS	0	0	2	1	1	4	8

****
*SEE INTERPRETATION OF CODES AT END OF TABLE

TABLE G-7 (Page 2 of 4)

SUMMARY STATISTICS OF CTDM MODEL EVALUATION
SITE = CINDER CONE BUTTE TRACER = SF6

CASE 6: WIND SPEED CATEGORY = 2, PLUME HEIGHT ABOVE Hc: NO CASES

CASE 7: WIND SPEED CATEGORY = 3, PLUME HEIGHT BELOW Hc*

ELEV OF PRE MAX VS Hc/ ELEV OF OBS MAX VS Hc	DISTRIBUTION OF HOURS BY RATIO CATEGORY OF TOP 5 AVE. PREDICTED TO TOP 5 AVE. OBSERVED CONCENTRATIONS ********** <<	<	<=	>=	>	>>	TOTAL HOURS
B/B	0	0	0	0	0	0	0
B/N	1	0	0	0	0	0	1
B/A	0	0	0	0	0	0	0
N/B	2	0	0	0	0	0	2
N/N	0	0	0	0	0	0	0
N/A	0	0	0	0	0	0	0
A/B	0	0	1	0	0	0	1
A/N	0	0	0	0	0	0	0
A/A	0	1	0	0	0	0	1
TOTALS	3	1	1	0	0	0	5

****
*SEE INTERPRETATION OF CODES AT END OF TABLE

CASE 8: WIND SPEED CATEGORY = 3, PLUME HEIGHT NEAR Hc*

ELEV OF PRE MAX VS Hc/ ELEV OF OBS MAX VS Hc	DISTRIBUTION OF HOURS BY RATIO CATEGORY OF TOP 5 AVE. PREDICTED TO TOP 5 AVE. OBSERVED CONCENTRATIONS ********** <<	<	<=	>=	>	>>	TOTAL HOURS
B/B	0	0	0	0	0	0	0
B/N	0	0	0	0	0	0	0
B/A	0	0	0	0	0	0	0
N/B	0	0	0	0	1	1	2
N/N	0	0	1	0	0	0	1
N/A	0	1	0	0	2	0	3
A/B	0	0	0	0	0	0	0
A/N	0	0	2	0	0	0	2
A/A	0	1	2	0	0	0	3
TOTALS	0	2	5	0	3	1	11

****
*SEE INTERPRETATION OF CODES AT END OF TABLE

TABLE G-7 (Page 3 of 4)

SUMMARY STATISTICS OF CTDM MODEL EVALUATION
SITE = CINDER CONE BUTTE TRACER = SF6

CASE 9: WIND SPEED CATEGORY = 3, PLUME HEIGHT ABOVE Hc*

ELEV OF PRE MAX VS Hc/ ELEV OF OBS MAX VS Hc	DISTRIBUTION OF HOURS BY RATIO CATEGORY OF TOP 5 AVE. PREDICTED TO TOP 5 AVE. OBSERVED CONCENTRATIONS ********** <<	<	<=	>=	>	>>	TOTAL HOURS
B/B	0	0	0	0	0	0	0
B/N	0	0	0	0	0	0	0
B/A	0	0	0	0	0	0	0
N/B	0	1	0	0	0	0	1
N/N	0	0	0	0	0	1	1
N/A	0	0	0	1	0	0	1
A/B	0	0	0	0	1	0	1
A/N	0	0	0	1	1	0	2
A/A	0	1	0	3	1	4	9
TOTALS	0	2	0	5	3	5	15

****
*SEE INTERPRETATION OF CODES AT END OF TABLE

CASE 10: WIND SPEED CATEGORY = 4, PLUME HEIGHT BELOW Hc: NO CASES

CASE 11: WIND SPEED CATEGORY = 4, PLUME HEIGHT NEAR Hc: NO CASES

CASE 12: WIND SPEED CATEGORY = 4, PLUME HEIGHT ABOVE Hc*

ELEV OF PRE MAX VS Hc/ ELEV OF OBS MAX VS Hc	DISTRIBUTION OF HOURS BY RATIO CATEGORY OF TOP 5 AVE. PREDICTED TO TOP 5 AVE. OBSERVED CONCENTRATIONS ********** <<	<	<=	>=	>	>>	TOTAL HOURS
B/B	1	0	0	0	0	0	1
B/N	0	0	0	0	0	0	0
B/A	0	0	0	0	0	0	0
N/B	3	0	0	0	0	0	3
N/N	0	0	0	0	0	0	0
N/A	1	0	0	0	0	0	1
A/B	0	0	1	0	0	0	1
A/N	0	0	1	1	0	0	2
A/A	3	6	7	3	0	0	19
TOTALS	8	6	9	4	0	0	27

****
*SEE INTERPRETATION OF CODES AT END OF TABLE

INTERPRETATION OF CODES:

TABLE ITEM	CODE	MEANING
WIND SPEED CATEGORY	1	Wind speed less than 1 m/sec
	2	Wind speed between 1 and 3 m/sec
	3	Wind speed between 3 and 6 m/sec
	4	Wind speed greater than or equal to 6 m/sec
RATIO CATEGORY OF PREDICTED TO OBSERVED AVERAGES OF HIGHEST 5 CONCENTRATIONS	<<	Ratio < .2
	<	Ratio is between .2 and .5
	<=	Ratio is between .5 and 1.0
	>=	Ratio is between 1.0 and 2.0
	>	Ratio is between 2.0 and 5.0
	>>	Ratio is greater than or equal to 5.0
ELEVATION OF MAXIMUM PREDICTED OR OBSERVED CONCENTRATION VS Hc	N	Elevation of maximum is within 5 m of Hc
	A	Elevation of maximum > Hc + 5 m
	B	Elevation of maximum < Hc - 5 m

TABLE G-8

SUMMARY STATISTICS OF CTDM MODEL EVALUATION
SITE = CINDER CONE BUTTE TRACER = CF3BR

CASE 1: WIND SPEED CATEGORY = 1, PLUME HEIGHT BELOW Hc: NO CASES

CASE 2: WIND SPEED CATEGORY = 1, PLUME HEIGHT NEAR Hc: NO CASES

CASE 3: WIND SPEED CATEGORY = 1, PLUME HEIGHT ABOVE Hc: NO CASES

CASE 4: WIND SPEED CATEGORY = 2, PLUME HEIGHT BELOW Hc*

ELEV OF PRE MAX VS Hc/ ELEV OF OBS MAX VS Hc	DISTRIBUTION OF HOURS BY RATIO CATEGORY OF TOP 5 AVE. PREDICTED TO TOP 5 AVE. OBSERVED CONCENTRATIONS ********** <<	<	<=	>=	>	>>	TOTAL HOURS
B/B	0	0	0	0	0	1	1
B/N	0	0	0	0	0	0	0
B/A	0	0	0	0	0	0	0
N/B	0	0	0	0	0	0	0
N/N	0	0	0	0	0	0	0
N/A	0	0	0	0	0	0	0
A/B	0	0	0	0	0	0	0
A/N	0	0	0	0	0	0	0
A/A	0	0	0	0	0	0	0
TOTALS	0	0	0	0	0	1	1

****
*SEE INTERPRETATION OF CODES AT END OF TABLE

CASE 5: WIND SPEED CATEGORY = 2, PLUME HEIGHT NEAR Hc*

ELEV OF PRE MAX VS Hc/ ELEV OF OBS MAX VS Hc	DISTRIBUTION OF HOURS BY RATIO CATEGORY OF TOP 5 AVE. PREDICTED TO TOP 5 AVE. OBSERVED CONCENTRATIONS ********** <<	<	<=	>=	>	>>	TOTAL HOURS
B/B	0	0	0	0	0	0	0
B/N	0	0	0	0	0	0	0
B/A	0	0	0	0	0	0	0
N/B	0	0	0	0	0	0	0
N/N	0	0	0	0	0	0	0
N/A	0	0	0	0	0	0	0
A/B	0	0	0	0	0	0	0
A/N	0	0	0	0	0	0	0
A/A	0	0	0	0	0	1	1
TOTALS	0	0	0	0	0	1	1

****
*SEE INTERPRETATION OF CODES AT END OF TABLE

SUMMARY STATISTICS OF CTDM MODEL EVALUATION
SITE = CINDER CONE BUTTE TRACER = CF3BR

CASE 6: WIND SPEED CATEGORY = 2, PLUME HEIGHT ABOVE Hc*

ELEV OF PRE MAX VS Hc/ ELEV OF OBS MAX VS Hc	DISTRIBUTION OF HOURS BY RATIO CATEGORY OF TOP 5 AVE. PREDICTED TO TOP 5 AVE. OBSERVED CONCENTRATIONS ********** <<	<	<=	>=	>	>>	TOTAL HOURS
B/B	0	0	0	0	0	0	0
B/N	0	0	0	0	0	0	0
B/A	0	0	0	0	0	0	0
N/B	0	0	0	0	0	0	0
N/N	0	0	0	0	0	0	0
N/A	0	0	0	0	1	0	1
A/B	0	0	0	0	0	0	0
A/N	0	0	0	0	0	0	0
A/A	0	0	0	0	0	1	1
TOTALS	0	0	0	0	1	1	2

****
*SEE INTERPRETATION OF CODES AT END OF TABLE

CASE 7: WIND SPEED CATEGORY = 3, PLUME HEIGHT BELOW Hc*

ELEV OF PRE MAX VS Hc/ ELEV OF OBS MAX VS Hc	DISTRIBUTION OF HOURS BY RATIO CATEGORY OF TOP 5 AVE. PREDICTED TO TOP 5 AVE. OBSERVED CONCENTRATIONS ********** <<	<	<=	>=	>	>>	TOTAL HOURS
B/B	0	0	0	0	0	0	0
B/N	0	0	0	0	0	0	0
B/A	0	0	1	0	0	0	1
N/B	0	0	0	0	0	0	0
N/N	0	0	0	0	0	0	0
N/A	0	0	0	0	0	0	0
A/B	0	0	0	0	0	0	0
A/N	0	0	0	0	0	0	0
A/A	0	0	0	0	0	0	0
TOTALS	0	0	1	0	0	0	1

****
*SEE INTERPRETATION OF CODES AT END OF TABLE

TABLE G-8 (Page 3 of 5)

SUMMARY STATISTICS OF CTDM MODEL EVALUATION
SITE = CINDER CONE BUTTE TRACER = CF3BR

CASE 8: WIND SPEED CATEGORY = 3, PLUME HEIGHT NEAR Hc*

ELEV OF PRE MAX VS Hc/ ELEV OF OBS MAX VS Hc	DISTRIBUTION OF HOURS BY RATIO CATEGORY OF TOP 5 AVE. PREDICTED TO TOP 5 AVE. OBSERVED CONCENTRATIONS ********** <<	<	<=	>=	>	>>	TOTAL HOURS
B/B	1	0	0	0	0	0	1
B/N	0	0	0	0	0	0	0
B/A	0	0	0	0	0	0	0
N/B	0	0	0	0	1	1	2
N/N	0	0	0	0	1	1	2
N/A	0	0	0	0	1	1	2
A/B	0	0	0	0	0	0	0
A/N	0	0	2	0	0	0	2
A/A	0	0	0	0	0	0	0
TOTALS	1	0	2	0	3	3	9

****
*SEE INTERPRETATION OF CODES AT END OF TABLE

CASE 9: WIND SPEED CATEGORY = 3, PLUME HEIGHT ABOVE Hc*

ELEV OF PRE MAX VS Hc/ ELEV OF OBS MAX VS Hc	DISTRIBUTION OF HOURS BY RATIO CATEGORY OF TOP 5 AVE. PREDICTED TO TOP 5 AVE. OBSERVED CONCENTRATIONS ********** <<	<	<=	>=	>	>>	TOTAL HOURS
B/B	0	0	0	0	0	0	0
B/N	0	0	0	0	0	0	0
B/A	0	0	0	0	0	0	0
N/B	1	0	0	0	0	0	1
N/N	0	0	0	1	0	0	1
N/A	0	2	0	1	1	5	9
A/B	0	0	0	0	0	0	0
A/N	0	0	0	0	1	0	1
A/A	0	1	0	1	0	1	3
TOTALS	1	3	0	3	2	6	15

****
*SEE INTERPRETATION OF CODES AT END OF TABLE

TABLE G-8 (Page 4 of 5)

SUMMARY STATISTICS OF CTDM MODEL EVALUATION
SITE = CINDER CONE BUTTE TRACER = CF3BR

CASE 10: WIND SPEED CATEGORY = 4, PLUME HEIGHT BELOW Hc: NO CASES

CASE 11: WIND SPEED CATEGORY = 4, PLUME HEIGHT NEAR Hc: NO CASES

CASE 12: WIND SPEED CATEGORY = 4, PLUME HEIGHT ABOVE Hc*

ELEV OF PRE MAX VS Hc/ ELEV OF OBS MAX VS Hc	DISTRIBUTION OF HOURS BY RATIO CATEGORY OF TOP 5 AVE. PREDICTED TO TOP 5 AVE. OBSERVED CONCENTRATIONS ********** <<	<	<=	>=	>	>>	TOTAL HOURS
B/B	0	0	0	0	0	0	0
B/N	0	0	0	0	0	0	0
B/A	0	0	0	0	0	0	0
N/B	0	0	0	0	0	0	0
N/N	0	0	0	0	0	0	0
N/A	0	0	0	0	0	0	0
A/B	0	0	0	0	0	0	0
A/N	0	0	0	0	0	0	0
A/A	1	2	4	1	0	2	10
TOTALS	1	2	4	1	0	2	10

****
*SEE INTERPRETATION OF CODES AT END OF TABLE

TABLE G-8 (Page 5 of 5)

INTERPRETATION OF CODES:

TABLE ITEM	CODE	MEANING
WIND SPEED CATEGORY	1	Wind speed less than 1 m/sec
	2	Wind speed between 1 and 3 m/sec
	3	Wind speed between 3 and 6 m/sec
	4	Wind speed greater than or equal to 6 m/sec
RATIO CATEGORY OF PREDICTED TO OBSERVED AVERAGES OF HIGHEST 5 CONCENTRATIONS	<<	Ratio < .2
	<	Ratio is between .2 and .5
	<=	Ratio is between .5 and 1.0
	>=	Ratio is between 1.0 and 2.0
	>	Ratio is between 2.0 and 5.0
	>>	Ratio is greater than or equal to 5.0
ELEVATION OF MAXIMUM PREDICTED OR OBSERVED CONCENTRATION VS Hc	N	Elevation of maximum is within 5 m of Hc
	A	Elevation of maximum > Hc + 5 m
	B	Elevation of maximum < Hc - 5 m

TABLE G-9

SUMMARY STATISTICS OF CTDM MODEL EVALUATION
SITE = HOG BACK RIDGE TRACER = SF6

CASE 1: WIND SPEED CATEGORY = 1, PLUME HEIGHT BELOW Hc: NO CASES

CASE 2: WIND SPEED CATEGORY = 1, PLUME HEIGHT NEAR Hc: NO CASES

CASE 3: WIND SPEED CATEGORY = 1, PLUME HEIGHT ABOVE Hc: NO CASES

CASE 4: WIND SPEED CATEGORY = 2, PLUME HEIGHT BELOW Hc*

ELEV OF PRE MAX VS Hc/ ELEV OF OBS MAX VS Hc	DISTRIBUTION OF HOURS BY RATIO CATEGORY OF TOP 5 AVE. PREDICTED TO TOP 5 AVE. OBSERVED CONCENTRATIONS ********** <<	<	<=	>=	>	>>	TOTAL HOURS
B/B	0	0	1	0	2	1	4
B/N	0	0	0	0	3	0	3
B/A	0	1	0	4	8	0	13
N/B	0	0	0	0	0	0	0
N/N	0	0	0	0	0	1	1
N/A	0	0	1	1	0	0	2
A/B	0	0	0	0	0	0	0
A/N	0	0	0	0	0	0	0
A/A	0	0	0	0	0	0	0
TOTALS	0	1	2	5	13	2	23

****
*SEE INTERPRETATION OF CODES AT END OF TABLE

CASE 5: WIND SPEED CATEGORY = 2, PLUME HEIGHT NEAR Hc*

ELEV OF PRE MAX VS Hc/ ELEV OF OBS MAX VS Hc	DISTRIBUTION OF HOURS BY RATIO CATEGORY OF TOP 5 AVE. PREDICTED TO TOP 5 AVE. OBSERVED CONCENTRATIONS ********** <<	<	<=	>=	>	>>	TOTAL HOURS
B/B	0	0	0	0	0	0	0
B/N	0	0	0	0	0	1	1
B/A	0	0	0	0	1	1	2
N/B	0	0	0	0	3	0	3
N/N	0	0	0	0	1	1	2
N/A	0	0	0	0	1	0	1
A/B	0	0	0	0	0	0	0
A/N	0	0	0	0	0	0	0
A/A	0	0	0	0	1	0	1
TOTALS	0	0	0	0	7	3	10

****
*SEE INTERPRETATION OF CODES AT END OF TABLE

TABLE G-9 (Page 2 of 4)

SUMMARY STATISTICS OF CTDM MODEL EVALUATION
SITE = HOG BACK RIDGE TRACER = SF6

CASE 6: WIND SPEED CATEGORY = 2, PLUME HEIGHT ABOVE Hc*

ELEV OF PRE MAX VS Hc/ ELEV OF OBS MAX VS Hc	DISTRIBUTION OF HOURS BY RATIO CATEGORY OF TOP 5 AVE. PREDICTED TO TOP 5 AVE. OBSERVED CONCENTRATIONS ********** <<	<	<=	>=	>	>>	TOTAL HOURS
B/B	0	0	0	1	0	0	1
B/N	0	0	0	0	0	0	0
B/A	0	1	0	0	1	0	2
N/B	0	0	0	0	1	0	1
N/N	0	0	0	0	0	0	0
N/A	0	0	0	3	1	0	4
A/B	0	0	0	0	0	0	0
A/N	0	0	0	0	0	2	2
A/A	0	0	0	0	2	2	4
TOTALS	0	1	0	4	5	4	14

****
*SEE INTERPRETATION OF CODES AT END OF TABLE

CASE 7: WIND SPEED CATEGORY = 3, PLUME HEIGHT BELOW Hc: NO CASES

CASE 8: WIND SPEED CATEGORY = 3, PLUME HEIGHT NEAR Hc: NO CASES

CASE 9: WIND SPEED CATEGORY = 3, PLUME HEIGHT ABOVE Hc*

ELEV OF PRE MAX VS Hc/ ELEV OF OBS MAX VS Hc	DISTRIBUTION OF HOURS BY RATIO CATEGORY OF TOP 5 AVE. PREDICTED TO TOP 5 AVE. OBSERVED CONCENTRATIONS ********** <<	<	<=	>=	>	>>	TOTAL HOURS
B/B	0	0	0	0	0	0	0
B/N	0	0	0	0	0	0	0
B/A	0	0	0	0	0	0	0
N/B	0	0	0	0	0	0	0
N/N	0	0	0	0	0	0	0
N/A	0	0	0	2	0	0	2
A/B	0	0	0	0	0	0	0
A/N	0	0	0	0	0	0	0
A/A	0	0	0	0	1	1	2
TOTALS	0	0	0	2	1	1	4

****
*SEE INTERPRETATION OF CODES AT END OF TABLE

TABLE G-9 (Page 3 of 4)

SUMMARY STATISTICS OF CTDM MODEL EVALUATION
SITE = HOG BACK RIDGE TRACER = SF6

CASE 10: WIND SPEED CATEGORY = 4, PLUME HEIGHT BELOW Hc: NO CASES

CASE 11: WIND SPEED CATEGORY = 4, PLUME HEIGHT NEAR Hc: NO CASES

CASE 12: WIND SPEED CATEGORY = 4, PLUME HEIGHT ABOVE Hc: NO CASES

TABLE G-9 (Page 4 of 4)

INTERPRETATION OF CODES:

TABLE ITEM	CODE	MEANING
WIND SPEED CATEGORY	1	Wind speed less than 1 m/sec
	2	Wind speed between 1 and 3 m/sec
	3	Wind speed between 3 and 6 m/sec
	4	Wind speed greater than or equal to 6 m/sec
RATIO CATEGORY OF PREDICTED TO OBSERVED AVERAGES OF HIGHEST 5 CONCENTRATIONS	<<	Ratio < .2
	<	Ratio is between .2 and .5
	<=	Ratio is between .5 and 1.0
	>=	Ratio is between 1.0 and 2.0
	>	Ratio is between 2.0 and 5.0
	>>	Ratio is greater than or equal to 5.0
ELEVATION OF MAXIMUM PREDICTED OR OBSERVED CONCENTRATION VS Hc	N	Elevation of maximum is within 5 m of Hc
	A	Elevation of maximum > Hc + 5 m
	B	Elevation of maximum < Hc - 5 m

TABLE G-10

SUMMARY STATISTICS OF CTDM MODEL EVALUATION
SITE = HOG BACK RIDGE TRACER = CF3BR

CASE 1: WIND SPEED CATEGORY = 1, PLUME HEIGHT BELOW Hc: NO CASES

CASE 2: WIND SPEED CATEGORY = 1, PLUME HEIGHT NEAR Hc: NO CASES

CASE 3: WIND SPEED CATEGORY = 1, PLUME HEIGHT ABOVE Hc: NO CASES

CASE 4: WIND SPEED CATEGORY = 2, PLUME HEIGHT BELOW Hc*

ELEV OF PRE MAX VS Hc/ ELEV OF OBS MAX VS Hc	DISTRIBUTION OF HOURS BY RATIO CATEGORY OF TOP 5 AVE. PREDICTED TO TOP 5 AVE. OBSERVED CONCENTRATIONS ********** <<	<	<=	>=	>	>>	TOTAL HOURS
B/B	1	6	2	5	3	1	18
B/N	0	2	2	3	0	0	7
B/A	0	2	2	0	0	1	5
N/B	0	0	0	0	0	1	1
N/N	0	0	1	0	0	0	1
N/A	0	2	0	0	0	0	2
A/B	0	0	0	0	0	0	0
A/N	0	0	0	0	0	0	0
A/A	0	0	1	1	0	0	2
TOTALS	1	12	8	9	3	3	36

****
*SEE INTERPRETATION OF CODES AT END OF TABLE

CASE 5: WIND SPEED CATEGORY = 2, PLUME HEIGHT NEAR Hc*

ELEV OF PRE MAX VS Hc/ ELEV OF OBS MAX VS Hc	DISTRIBUTION OF HOURS BY RATIO CATEGORY OF TOP 5 AVE. PREDICTED TO TOP 5 AVE. OBSERVED CONCENTRATIONS ********** <<	<	<=	>=	>	>>	TOTAL HOURS
B/B	0	0	1	0	0	0	1
B/N	0	0	0	0	0	0	0
B/A	0	0	0	0	0	0	0
N/B	0	0	1	0	0	0	1
N/N	0	0	0	0	0	0	0
N/A	0	0	0	0	0	0	0
A/B	0	0	0	0	0	0	0
A/N	0	0	0	0	0	0	0
A/A	0	0	2	0	0	1	3
TOTALS	0	0	4	0	0	1	5

****
*SEE INTERPRETATION OF CODES AT END OF TABLE

TABLE G-10 (Continued)

SUMMARY STATISTICS OF CTDM MODEL EVALUATION
SITE = HOG BACK RIDGE TRACER = CF3BR

CASE 6: WIND SPEED CATEGORY = 2, PLUME HEIGHT ABOVE Hc*

ELEV OF PRE MAX VS Hc/ ELEV OF OBS MAX VS Hc	DISTRIBUTION OF HOURS BY RATIO CATEGORY OF TOP 5 AVE. PREDICTED TO TOP 5 AVE. OBSERVED CONCENTRATIONS ********** <<	<	<=	>=	>	>>	TOTAL HOURS
B/B	0	0	0	0	1	0	1
B/N	0	0	0	0	0	0	0
B/A	0	0	0	0	0	0	0
N/B	0	0	0	0	0	0	0
N/N	0	0	0	0	0	0	0
N/A	0	0	0	0	0	0	0
A/B	0	0	0	0	0	0	0
A/N	0	0	0	0	0	0	0
A/A	0	0	0	0	0	0	0
TOTALS	0	0	0	0	1	0	1

****
*SEE INTERPRETATION OF CODES AT END OF TABLE

CASE 7: WIND SPEED CATEGORY = 3, PLUME HEIGHT BELOW Hc: NO CASES

CASE 8: WIND SPEED CATEGORY = 3, PLUME HEIGHT NEAR Hc: NO CASES

CASE 9: WIND SPEED CATEGORY = 3, PLUME HEIGHT ABOVE Hc: NO CASES

CASE 10: WIND SPEED CATEGORY = 4, PLUME HEIGHT BELOW Hc: NO CASES

CASE 11: WIND SPEED CATEGORY = 4, PLUME HEIGHT NEAR Hc: NO CASES

CASE 12: WIND SPEED CATEGORY = 4, PLUME HEIGHT ABOVE Hc: NO CASES

TABLE G-10 (Continued)

INTERPRETATION OF CODES:

TABLE ITEM	CODE	MEANING
WIND SPEED CATEGORY	1	Wind speed less than 1 m/sec
	2	Wind speed between 1 and 3 m/sec
	3	Wind speed between 3 and 6 m/sec
	4	Wind speed greater than or equal to 6 m/sec
RATIO CATEGORY OF PREDICTED TO OBSERVED AVERAGES OF HIGHEST 5 CONCENTRATIONS	<<	Ratio < .2
	<	Ratio is between .2 and .5
	<=	Ratio is between .5 and 1.0
	>=	Ratio is between 1.0 and 2.0
	>	Ratio is between 2.0 and 5.0
	>>	Ratio is greater than or equal to 5.0
ELEVATION OF MAXIMUM PREDICTED OR OBSERVED CONCENTRATION VS Hc	N	Elevation of maximum is within 5 m of Hc
	A	Elevation of maximum > Hc + 5 m
	B	Elevation of maximum < Hc - 5 m

TABLE G-11

SUMMARY STATISTICS OF CTDM MODEL EVALUATION
SITE = TRACY POWER PLANT TRACER = SF6

CASE 1: WIND SPEED CATEGORY = 1, PLUME HEIGHT BELOW Hc: NO CASES

CASE 2: WIND SPEED CATEGORY = 1, PLUME HEIGHT NEAR Hc: NO CASES

CASE 3: WIND SPEED CATEGORY = 1, PLUME HEIGHT ABOVE Hc: NO CASES

CASE 4: WIND SPEED CATEGORY = 2, PLUME HEIGHT BELOW Hc*

ELEV OF PRE MAX VS Hc/ ELEV OF OBS MAX VS Hc	DISTRIBUTION OF HOURS BY RATIO CATEGORY OF TOP 5 AVE. PREDICTED TO TOP 5 AVE. OBSERVED CONCENTRATIONS ********** <<	<	<=	>=	>	>>	TOTAL HOURS
B/B	0	1	2	1	0	0	4
B/N	0	0	0	0	0	0	0
B/A	0	0	1	0	0	1	2
N/B	0	0	0	0	0	0	0
N/N	0	0	0	0	0	0	0
N/A	0	1	0	0	0	0	1
A/B	0	0	0	1	2	1	4
A/N	0	0	0	0	0	0	0
A/A	0	5	7	7	6	0	25
TOTALS	0	7	10	9	8	2	36

****
*SEE INTERPRETATION OF CODES AT END OF TABLE

CASE 5: WIND SPEED CATEGORY = 2, PLUME HEIGHT NEAR Hc*

ELEV OF PRE MAX VS Hc/ ELEV OF OBS MAX VS Hc	DISTRIBUTION OF HOURS BY RATIO CATEGORY OF TOP 5 AVE. PREDICTED TO TOP 5 AVE. OBSERVED CONCENTRATIONS ********** <<	<	<=	>=	>	>>	TOTAL HOURS
B/B	0	0	0	0	0	0	0
B/N	0	0	0	0	0	0	0
B/A	0	0	0	0	0	0	0
N/B	0	0	0	0	0	0	0
N/N	0	0	0	0	0	0	0
N/A	0	0	0	0	0	0	0
A/B	0	0	0	0	0	0	0
A/N	0	0	0	0	1	0	1
A/A	0	1	0	1	0	0	2
TOTALS	0	1	0	1	1	0	3

****
*SEE INTERPRETATION OF CODES AT END OF TABLE

TABLE G-11 (Page 2 of 5)

SUMMARY STATISTICS OF CTDM MODEL EVALUATION
SITE = TRACY POWER PLANT TRACER = SF6

CASE 6: WIND SPEED CATEGORY = 2, PLUME HEIGHT ABOVE Hc*

ELEV OF PRE MAX VS Hc/ ELEV OF OBS MAX VS Hc	DISTRIBUTION OF HOURS BY RATIO CATEGORY OF TOP 5 AVE. PREDICTED TO TOP 5 AVE. OBSERVED CONCENTRATIONS ********** <<	<	<=	>=	>	>>	TOTAL HOURS
B/B	0	0	0	0	0	0	0
B/N	0	0	0	0	0	0	0
B/A	0	0	0	0	0	0	0
N/B	0	0	0	0	0	0	0
N/N	0	0	0	0	0	0	0
N/A	0	0	0	0	0	0	0
A/B	0	0	0	1	0	0	1
A/N	0	0	0	0	0	0	0
A/A	0	3	2	4	1	0	10
TOTALS	0	3	2	5	1	0	11

****
*SEE INTERPRETATION OF CODES AT END OF TABLE

CASE 7: WIND SPEED CATEGORY = 3, PLUME HEIGHT BELOW Hc*

ELEV OF PRE MAX VS Hc/ ELEV OF OBS MAX VS Hc	DISTRIBUTION OF HOURS BY RATIO CATEGORY OF TOP 5 AVE. PREDICTED TO TOP 5 AVE. OBSERVED CONCENTRATIONS ********** <<	<	<=	>=	>	>>	TOTAL HOURS
B/B	0	0	0	0	0	0	0
B/N	0	0	0	0	0	0	0
B/A	0	1	0	0	0	0	1
N/B	0	0	0	0	0	0	0
N/N	0	0	0	0	0	0	0
N/A	0	0	0	0	0	0	0
A/B	0	0	0	0	0	0	0
A/N	0	0	0	0	0	0	0
A/A	0	0	2	2	2	0	6
TOTALS	0	1	2	2	2	0	7

****
*SEE INTERPRETATION OF CODES AT END OF TABLE

TABLE G-11 (Page 3 of 5)

SUMMARY STATISTICS OF CTDM MODEL EVALUATION
SITE = TRACY POWER PLANT TRACER = SF6

CASE 8: WIND SPEED CATEGORY = 3, PLUME HEIGHT NEAR Hc*

ELEV OF PRE MAX VS Hc/ ELEV OF OBS MAX VS Hc	DISTRIBUTION OF HOURS BY RATIO CATEGORY OF TOP 5 AVE. PREDICTED TO TOP 5 AVE. OBSERVED CONCENTRATIONS ********** <<	<	<=	>=	>	>>	TOTAL HOURS
B/B	0	0	0	0	0	0	0
B/N	0	0	0	0	0	0	0
B/A	0	0	0	1	0	0	1
N/B	0	0	0	0	0	0	0
N/N	0	0	0	0	0	0	0
N/A	0	0	0	0	0	0	0
A/B	0	0	0	1	0	0	1
A/N	0	0	0	0	0	0	0
A/A	0	1	2	3	0	0	6
TOTALS	0	1	2	5	0	0	8

****
*SEE INTERPRETATION OF CODES AT END OF TABLE

CASE 9: WIND SPEED CATEGORY = 3, PLUME HEIGHT ABOVE Hc*

ELEV OF PRE MAX VS Hc/ ELEV OF OBS MAX VS Hc	DISTRIBUTION OF HOURS BY RATIO CATEGORY OF TOP 5 AVE. PREDICTED TO TOP 5 AVE. OBSERVED CONCENTRATIONS ********** <<	<	<=	>=	>	>>	TOTAL HOURS
B/B	0	0	0	0	0	0	0
B/N	0	0	0	0	1	0	1
B/A	0	0	0	1	0	0	1
N/B	0	0	0	0	0	0	0
N/N	0	0	0	0	0	0	0
N/A	0	0	0	1	0	0	1
A/B	0	1	0	4	1	0	6
A/N	0	1	1	0	0	0	2
A/A	2	0	1	5	9	0	17
TOTALS	2	2	2	11	11	0	28

****
*SEE INTERPRETATION OF CODES AT END OF TABLE

CASE 10: WIND SPEED CATEGORY = 4, PLUME HEIGHT BELOW Hc: NO CASES

CASE 11: WIND SPEED CATEGORY = 4, PLUME HEIGHT NEAR Hc: NO CASES

TABLE G-11 (Page 4 of 5)

SUMMARY STATISTICS OF CTDM MODEL EVALUATION
SITE = TRACY POWER PLANT TRACER = SF6

CASE 12: WIND SPEED CATEGORY = 4, PLUME HEIGHT ABOVE Hc*

ELEV OF PRE MAX VS Hc/ ELEV OF OBS MAX VS Hc	DISTRIBUTION OF HOURS BY RATIO CATEGORY OF TOP 5 AVE. PREDICTED TO TOP 5 AVE. OBSERVED CONCENTRATIONS ********** <<	<	<=	>=	>	>>	TOTAL HOURS
B/B	0	0	0	0	0	0	0
B/N	0	0	0	0	0	0	0
B/A	0	0	0	1	0	0	1
N/B	0	0	0	0	0	0	0
N/N	0	0	0	0	0	0	0
N/A	0	0	0	0	0	0	0
A/B	0	1	1	1	0	0	3
A/N	0	0	0	1	0	0	1
A/A	0	3	2	5	2	0	12
TOTALS	0	4	3	8	2	0	17

****
*SEE INTERPRETATION OF CODES AT END OF TABLE

TABLE G-11 (Page 5 of 5)

INTERPRETATION OF CODES:

TABLE ITEM	CODE	MEANING
WIND SPEED CATEGORY	1	Wind speed less than 1 m/sec
	2	Wind speed between 1 and 3 m/sec
	3	Wind speed between 3 and 6 m/sec
	4	Wind speed greater than or equal to 6 m/sec
RATIO CATEGORY OF PREDICTED TO OBSERVED AVERAGES OF HIGHEST 5 CONCENTRATIONS	<<	Ratio < .2
	<	Ratio is between .2 and .5
	<=	Ratio is between .5 and 1.0
	>=	Ratio is between 1.0 and 2.0
	>	Ratio is between 2.0 and 5.0
	>>	Ratio is greater than or equal to 5.0
ELEVATION OF MAXIMUM PREDICTED OR OBSERVED CONCENTRATION VS Hc	N	Elevation of maximum is within 10 m of Hc
	A	Elevation of maximum > Hc + 10 m
	B	Elevation of maximum < Hc - 10 m

TABLE G-12

SUMMARY STATISTICS OF CTDM MODEL EVALUATION
SITE = TRACY POWER PLANT TRACER = CF3BR

CASE 1: WIND SPEED CATEGORY = 1, PLUME HEIGHT BELOW Hc: NO CASES

CASE 2: WIND SPEED CATEGORY = 1, PLUME HEIGHT NEAR Hc: NO CASES

CASE 3: WIND SPEED CATEGORY = 1, PLUME HEIGHT ABOVE Hc: NO CASES

CASE 4: WIND SPEED CATEGORY = 2, PLUME HEIGHT BELOW Hc*

ELEV OF PRE MAX VS Hc/ ELEV OF OBS MAX VS Hc	DISTRIBUTION OF HOURS BY RATIO CATEGORY OF TOP 5 AVE. PREDICTED TO TOP 5 AVE. OBSERVED CONCENTRATIONS ********** <<	<	<=	>=	>	>>	TOTAL HOURS
B/B	1	1	11	4	3	0	20
B/N	0	0	0	0	0	0	0
B/A	1	1	3	3	2	1	11
N/B	0	0	0	0	0	0	0
N/N	0	1	0	0	0	0	1
N/A	0	0	0	0	0	0	0
A/B	1	3	2	0	1	0	7
A/N	0	0	0	0	0	0	0
A/A	0	4	5	3	2	0	14
TOTALS	3	10	21	10	8	1	53

****
*SEE INTERPRETATION OF CODES AT END OF TABLE

CASE 5: WIND SPEED CATEGORY = 2, PLUME HEIGHT NEAR Hc*

ELEV OF PRE MAX VS Hc/ ELEV OF OBS MAX VS Hc	DISTRIBUTION OF HOURS BY RATIO CATEGORY OF TOP 5 AVE. PREDICTED TO TOP 5 AVE. OBSERVED CONCENTRATIONS ********** <<	<	<=	>=	>	>>	TOTAL HOURS
B/B	0	0	0	0	0	0	0
B/N	0	0	0	0	0	0	0
B/A	0	0	0	0	1	0	1
N/B	0	0	0	0	0	0	0
N/N	0	0	0	0	0	0	0
N/A	0	0	0	0	0	0	0
A/B	0	0	0	0	0	0	0
A/N	0	0	0	0	0	0	0
A/A	0	0	0	1	1	0	2
TOTALS	0	0	0	1	2	0	3

****
*SEE INTERPRETATION OF CODES AT END OF TABLE

SUMMARY STATISTICS OF CTDM MODEL EVALUATION
SITE = TRACY POWER PLANT TRACER = CF3BR

CASE 6: WIND SPEED CATEGORY = 2, PLUME HEIGHT ABOVE Hc*

ELEV OF PRE MAX VS Hc/ ELEV OF OBS MAX VS Hc	DISTRIBUTION OF HOURS BY RATIO CATEGORY OF TOP 5 AVE. PREDICTED TO TOP 5 AVE. OBSERVED CONCENTRATIONS ********** <<	<	<=	>=	>	>>	TOTAL HOURS
B/B	0	0	0	0	0	0	0
B/N	0	0	0	0	0	0	0
B/A	0	0	0	1	0	0	1
N/B	0	0	0	0	0	0	0
N/N	0	0	0	0	0	0	0
N/A	0	0	0	0	0	0	0
A/B	0	0	0	0	0	0	0
A/N	0	0	0	0	0	0	0
A/A	0	0	0	1	0	0	1
TOTALS	0	0	0	2	0	0	2

****
*SEE INTERPRETATION OF CODES AT END OF TABLE

CASE 7: WIND SPEED CATEGORY = 3, PLUME HEIGHT BELOW Hc*

ELEV OF PRE MAX VS Hc/ ELEV OF OBS MAX VS Hc	DISTRIBUTION OF HOURS BY RATIO CATEGORY OF TOP 5 AVE. PREDICTED TO TOP 5 AVE. OBSERVED CONCENTRATIONS ********** <<	<	<=	>=	>	>>	TOTAL HOURS
B/B	0	0	0	0	0	0	0
B/N	0	0	0	0	0	0	0
B/A	1	1	0	1	0	0	3
N/B	0	0	1	0	0	0	1
N/N	0	0	0	0	0	0	0
N/A	0	0	0	0	0	0	0
A/B	0	0	1	0	0	0	1
A/N	0	0	0	0	0	0	0
A/A	0	0	1	0	0	0	1
TOTALS	1	1	3	1	0	0	6

****
*SEE INTERPRETATION OF CODES AT END OF TABLE

TABLE G-12 (Page 3 of 5)

SUMMARY STATISTICS OF CTDM MODEL EVALUATION
SITE = TRACY POWER PLANT TRACER = CF3BR

CASE 8: WIND SPEED CATEGORY = 3, PLUME HEIGHT NEAR Hc*

ELEV OF PRE MAX VS Hc/ ELEV OF OBS MAX VS Hc	DISTRIBUTION OF HOURS BY RATIO CATEGORY OF TOP 5 AVE. PREDICTED TO TOP 5 AVE. OBSERVED CONCENTRATIONS ********** <<	<	<=	>=	>	>>	TOTAL HOURS
B/B	0	0	0	0	0	0	0
B/N	0	0	0	0	0	0	0
B/A	0	0	0	0	0	0	0
N/B	0	0	0	0	0	0	0
N/N	0	0	0	0	0	0	0
N/A	0	0	0	0	0	0	0
A/B	0	1	1	1	0	0	3
A/N	0	0	0	0	0	0	0
A/A	0	0	0	0	1	0	1
TOTALS	0	1	1	1	1	0	4

****
*SEE INTERPRETATION OF CODES AT END OF TABLE

CASE 9: WIND SPEED CATEGORY = 3, PLUME HEIGHT ABOVE Hc*

ELEV OF PRE MAX VS Hc/ ELEV OF OBS MAX VS Hc	DISTRIBUTION OF HOURS BY RATIO CATEGORY OF TOP 5 AVE. PREDICTED TO TOP 5 AVE. OBSERVED CONCENTRATIONS ********** <<	<	<=	>=	>	>>	TOTAL HOURS
B/B	0	0	0	1	2	0	3
B/N	0	0	0	0	0	0	0
B/A	0	0	1	2	1	0	4
N/B	0	0	0	0	0	0	0
N/N	0	0	0	0	0	0	0
N/A	0	0	0	0	0	0	0
A/B	0	0	1	4	2	0	7
A/N	0	0	0	2	0	0	2
A/A	0	0	4	3	1	0	8
TOTALS	0	0	6	12	6	0	24

****
*SEE INTERPRETATION OF CODES AT END OF TABLE

TABLE G-12 (Page 4 of 5)

SUMMARY STATISTICS OF CTDM MODEL EVALUATION
SITE = TRACY POWER PLANT TRACER = CF3BR

CASE 10: WIND SPEED CATEGORY = 4, PLUME HEIGHT BELOW Hc*

ELEV OF PRE MAX VS Hc/ ELEV OF OBS MAX VS Hc	DISTRIBUTION OF HOURS BY RATIO CATEGORY OF TOP 5 AVE. PREDICTED TO TOP 5 AVE. OBSERVED CONCENTRATIONS ********** <<	<	<=	>=	>	>>	TOTAL HOURS
B/B	0	0	0	0	0	0	0
B/N	0	0	0	0	0	0	0
B/A	0	0	0	0	0	0	0
N/B	0	0	0	0	0	0	0
N/N	0	0	0	0	0	0	0
N/A	0	0	0	0	0	0	0
A/B	0	0	0	0	0	0	0
A/N	0	0	0	0	0	0	0
A/A	0	1	0	0	0	0	1
TOTALS	0	1	0	0	0	0	1

****
*SEE INTERPRETATION OF CODES AT END OF TABLE

CASE 11: WIND SPEED CATEGORY = 4, PLUME HEIGHT NEAR Hc: NO CASES

CASE 12: WIND SPEED CATEGORY = 4, PLUME HEIGHT ABOVE Hc*

ELEV OF PRE MAX VS Hc/ ELEV OF OBS MAX VS Hc	DISTRIBUTION OF HOURS BY RATIO CATEGORY OF TOP 5 AVE. PREDICTED TO TOP 5 AVE. OBSERVED CONCENTRATIONS ********** <<	<	<=	>=	>	>>	TOTAL HOURS
B/B	0	0	0	0	0	0	0
B/N	0	0	1	0	0	0	1
B/A	0	0	0	0	0	0	0
N/B	0	0	0	0	0	0	0
N/N	0	0	0	0	0	0	0
N/A	0	0	0	0	1	0	1
A/B	0	0	2	2	0	0	4
A/N	0	0	0	2	0	0	2
A/A	0	0	5	3	1	0	9
TOTALS	0	0	8	7	2	0	17

****
*SEE INTERPRETATION OF CODES AT END OF TABLE

INTERPRETATION OF CODES:

TABLE ITEM	CODE	MEANING
WIND SPEED CATEGORY	1	Wind speed less than 1 m/sec
	2	Wind speed between 1 and 3 m/sec
	3	Wind speed between 3 and 6 m/sec
	4	Wind speed greater than or equal to 6 m/sec
RATIO CATEGORY OF PREDICTED TO OBSERVED AVERAGES OF HIGHEST 5 CONCENTRATIONS	<<	Ratio < .2
	<	Ratio is between .2 and .5
	<=	Ratio is between .5 and 1.0
	>=	Ratio is between 1.0 and 2.0
	>	Ratio is between 2.0 and 5.0
	>>	Ratio is greater than or equal to 5.0
ELEVATION OF MAXIMUM PREDICTED OR OBSERVED CONCENTRATION VS Hc	N	Elevation of maximum is within 10 m of Hc
	A	Elevation of maximum > Hc + 10 m
	B	Elevation of maximum < Hc - 10 m

APPENDIX H
CONTRIBUTIONS OF THE FLUID MODELING FACILITY TO EPA'S COMPLEX TERRAIN MODEL DEVELOPMENT PROGRAM

EPA Report Number
May 1987

CONTRIBUTIONS OF THE FLUID MODELING FACILITY TO EPA's COMPLEX TERRAIN MODEL DEVELOPMENT PROGRAM

by

WILLIAM H. SNYDER

Meteorology and Assessment Division
Atmospheric Sciences Research Laboratory
U.S. Environmental Protection Agency
Research Triangle Park, NC 27711

May 1987

Atmospheric Sciences Research Laboratory
Office of Research and Development
U.S. Environmental Protection Agency
Research Triangle Park, NC 27711

NOTICE

This information in this document has been funded by the United States Environmental Protection Agency. It has been subject to the Agency's peer and administrative review, and it has been approved for publication as an EPA document. Mention of trade names or commercial products does not constitute endorsement or recommendation for use.

The author, William H. Snyder, is a physical scientist in the Meteorology and Assessment Division, Atmospheric Sciences Research Laboratory, U.S. Environmental Protection Agency, Research Triangle Park, NC. He is on assignment from the National Oceanic and Atmospheric Administration, U.S. Department of Commerce.

FORWARD

The Atmospheric Sciences Research Laboratory (ASRL) conducts intramural and extramural research programs in the physical sciences to detect, define, and quantify air pollution and its effects on urban, regional, and global atmospheres and the subsequent impact on water quality and land use. The Laboratory is responsible for planning, implementing, and managing research and development programs designed to quantify the relationships between emissions of pollutants for all types of sources with air quality and atmospheric effects, and to uncover and characterize hitherto unidentified air pollution problems. Information from ASRL programs and from the programs of other government agencies, private industry, and the academic community are integrated by the Laboratory to develop the technical basis for air pollution control strategies for various pollutants.

The Complex Terrain Model Development Program (CTMDP) is designed to develop reliable atmospheric dispersion models that are applicable to large pollutant sources located in complex terrain. The major field studies of this six-year program were conducted during 1980 at Cinder Cone Butte near Boise, Idaho, during 1982 at Hogback Ridge near Farmington, New Mexico, and during 1983–84 at the Tracy Power Plant near Reno, Nevada. Data from these field studies along with measurements of fluid modeling simulations performed in the EPA Fluid Modeling Facility are being used to quantify the effects of terrain obstacles on stable plume dispersion. A series of annual milestone reports has been issued to describe the development of the Complex Terrain Dispersion Model (CTDM) and to contrast the performance evaluation of the CTDM against existing complex terrain dispersion models. This report describes the contributions of the Fluid Modeling Facility to the Complex Terrain Model Development Program.

A.H. Ellison
Director
Atmospheric Sciences Research Laboratory

ABSTRACT

The contributions of the EPA Fluid Modeling Facility (FMF) to the Complex Terrain Model Development Program (CTMDP) are described. These contributions included a wide range of laboratory studies and a limited amount of numerical modeling of flow and diffusion in neutral and stably stratified conditions in complex terrain. The goal of the CTMDP is the development of a dispersion model valid in complex terrain, with emphasis on plume impaction on nearby hills during nighttime stable conditions. Work at the FMF prior to the inception of the program provided the basic framework for the model – the dividing–streamline concept – and the focal point around which the field program was designed. Throughout the course of the CTMDP, the FMF interacted vigorously with the model developers by providing support in various ways. Early work provided direct support as an aid to planning the details and strategies of the field experiments and testing the limits of applicability of the dividing–streamline concept. Later work included exercises of "filling in the gaps" in the field data, furthering the understanding of the physical mechanisms important to plume impaction in complex terrain and in stably stratified flows in general, testing various modeling assumptions, providing data for "calibration" of various modeling parameters, and testing the ability of the laboratory models to simulate full–scale conditions. Simultaneously, the FMF responded to the needs of the regulatory arm of EPA, the Office of Air Quality Planning and Standards (OAQPS), by providing guidance concerning expected terrain effects and by conducting demonstration studies. Finally, several supplemental studies were conducted, broadening and expanding upon the specific requests of the model developers and the OAQPS.

CONTENTS

LIST OF FIGURES

LIST OF FIGURES

Number **Title** **Page**

LIST OF SYMBOLS AND ABBREVIATIONS

Symbols

A Terrain amplification factor, χ_{mx}/χ^{o}_{mx}

F Froude number, U_∞/Nh

g Acceleration due to gravity

h Hill height

h_o Height of density interface from surface

H_D Dividing–streamline height

H_s Source height

L Length of ridge

N Brunt–Väisälä frequency, $[-(g/\rho)d\rho/dz]$

U_∞ Towing speed or free–stream velocity

x_s Source position in along–wind direction (origin at hill center)

y_s Source position in crosswind direction (origin at hill center)

$\Delta\rho$ Density difference across interface

ρ Fluid density

ρ_1 Density of fluid between interface and surface

σ_y Standard deviation of crosswind plume width

σ_z Standard deviation of vertical plume width

χ_{mx} Maximum surface concentration

χ^{o}_{mx} Maximum surface concentration in absence of hill

Abbreviations

ACCB	Axisymmetric (idealized) Cinder Cone Butte
CCB	Cinder Cone Butte
CTDM	Complex Terrain Dispersion Model
CTMDP	Complex Terrain Model Development Program
EPA	Environmental Protection Agency
ERT	Environmental Research and Technology, Inc.
FFT	Fast Fourier Transform
FMF	Fluid Modeling Facility
HBR	Hogback Ridge
OAQPS	Office of Air Quality Planning and Standards
TAF	Terrain Amplification Factor

ACKNOWLEDGEMENTS

Many people have contributed to the work described in this report. I am particularly grateful to R.E. Lawson for his untiring efforts in the day–to–day operations of the laboratory, to R.S. Thompson for his unfailing support and many enlightening discussions, to J.C.R. Hunt for his continual encouragement, unending infusion of new ideas, and enduring patience in teaching me so much about stratified flow over obstacles, to R.E. Britter and I.P. Castro for their many contributions, to G.L. Marsh for his dogged persistence in operating the towing–tank experiments, to M.S. Shipman for his quiet but solid computer support, to J.C. Smith for his many hours at the filling station, to G.C. Holzworth for his insistence upon FMF involvement in the CTMD Program and his acceptance of different viewpoints, and to F.A. Schiermeier for letting us "do our thing". Finally, I wish to express thanks to the entire FMF staff, past and present, who do the real work day in and day out, and whose efforts too often go unrecognized and unrewarded.

1. INTRODUCTION

In the late 1970's the Office of Air Quality Planning and Standards (OAQPS) of the Environmental Protection Agency (EPA) identified a crucial need to develop a mathematical model that dealt with plume impaction from large sources located in mountainous terrain under stable flow conditions, with demonstrated reliability. A workshop was convened (Hovind *et al.*, 1979) to focus on complex terrain modeling problems and to develop recommendations to EPA with respect to the design of a program of experiments and model development efforts. Subsequently, Holzworth (1980) outlined the EPA plan to achieve the objective through an integrated program of model development, fluid modeling experiments and field studies of plume–terrain interactions on hills of progressively increasing size and complexity. This multi–year, multi–faceted program is known as the Complex Terrain Model Development Program (CTMDP). The prime contractor for this effort is Environmental Research and Technology (ERT), which has produced a comprehensive series of annual reports, called Milestone Reports, that describe all phases of the research program. The specific references are: (1) Lavery *et al* (1982), (2) Strimaitis *et al* (1983), (3) Lavery *et al* (1983), (4) Strimaitis *et al* (1985), and (5) DiCristofaro *et al* (1986); a final report is to be completed in 1987.

The Fluid Modeling Facility (FMF) interacted vigorously with various subgroups participating in the CTMDP, and provided direct support and guidance in many different ways. Whereas the field work and model development effort up to the present time has been specifically focused on plume impaction under stable conditions, the work at the FMF has taken a much broader view. The FMF research program has ranged from the development of broad guidelines (*e.g.*, terrain amplification factors) and physical concepts (*e.g.*, dividing–streamline height) to specific site studies (*e.g.*, Cinder Cone Butte) and regulatory applications (*e.g.*, good–engineering–practice stack height). The FMF has provided laboratory data to "fill in the gaps" in the field data (*e.g.*, measurements of plume deformations over hills) and tested the validity of convenient modeling assumptions (*e.g.*, cut–off hill approach).

This report summarizes the contributions, both direct and indirect, of the FMF to the CTMDP. The discussion provides a historical perspective and a comprehensive list of FMF's accomplishments with respect to furthering the physical understanding of flow and diffusion in complex terrain. In many cases the early research results were first published as internal documents or project reports or presented at workshops or conferences in order to speed the flow of information to the model developers. In most cases, these results have been published in peer-reviewed journals (which took, in one extreme case, 8 years to appear in print). For completeness and to provide the proper perspective, both references are cited at first mention in the text that follows; thereafter, only the journal publication is cited.

2. BACKGROUND

Research work conducted at the FMF prior to the inception of the CTMDP had a strong influence on the directions to be taken in the field work and on the type of model (*i.e.*, physical concepts) to be developed. The stratified towing tank was commissioned in 1976 (Thompson and Snyder, 1976) and rather fundamental studies were begun immediately on the structure of stably stratified flow over idealized three-dimensional hills and on diffusion from a point source within a stably stratified field of turbulence.

The first published reports on this work (Hunt *et al*, 1978; Hunt and Snyder, 1980) described the flow structure observed over a bell-shaped hill under neutral and stably stratified conditions. Earlier theoretical work by Drazin (1961), model experiments by Brighton (1978) and Riley *et al* (1976), and observations (*e.g.*, Queney *et al*, 1960) all indicated that, when the stratification is strong enough, the air flows in approximately horizontal planes around the topography. And this observation had been used by EPA in estimating the surface concentrations on hills caused by upwind sources of pollution (Burt and Slater, 1977). Up to that time, however, there had been little firm laboratory or field data as to how *strong* the stratification must be for any given streamline starting below the hill top to pass *round the side* rather than *over the top* of the hill. The Hunt and Snyder (1980) paper suggested a criterion for this change-over to occur on the basis of the low-Froude-number theory of Drazin (1961), and confirmed that criterion with experimental data.

The Drazin (1961) theory is applicable to strongly stratified flows around three-dimensional hills; indeed, it is asympotically valid at zero-Froude-number. In simplistic terms, the theory suggests that the stratification inhibits vertical motions, so that fluid parcels are constrained to move in horizontal planes. Hence, the flow may be described in terms of two-dimensional flow around a cylinder which is not necessarily circular but, in fact, has the cross-sectional shape of the intersection of a horizontal plane with the three-dimensional hill. Hunt and Snyder (1980)

verified that, for a bell-shaped hill, a linearly stratified environment, and an effectively uniform approach-flow velocity profile, Drazin's theory was applicable in the range $F < 0.4$, where F is the Froude number ($= U_\infty/Nh$, U_∞ being the towing speed, N the Brunt-Väisälä frequency, and h the hill height).

More importantly, Hunt and Snyder (1980) showed evidence for a dividing streamline (on the centerplane determined by the flow and the axis of the axisymmetric hill) of height H_s such that streamlines below H_s would impinge on the hill surface and follow the surface around the sides, whereas streamlines above H_s would go over the top. They suggested the simple formula

$$H_s = h\,(1 - F) \tag{1}$$

as the criterion to determine whether a plume embedded in the flow approaching the hill would impact on the surface or surmount the top, for $0 < F < 1$.

Snyder *et al* (1980) presented further evidence from towing-tank experiments in support of the simple formula; they showed it was applicable to other shapes of axisymmetric hills, namely a cone and a hemisphere. Furthermore, they presented another simple formula and supporting experimental data for determining whether an elevated (step) inversion would surmount a hill. This second formula, which predicts the point at which the interface just reaches the hilltop, is

$$\frac{U_\infty^2}{(gh_o\Delta\rho/\rho_1)} = 2\left[\frac{h}{h_o} - 1\right], \tag{2}$$

where g is the acceleration due to gravity, h_o is the height of the interface (far upwind), $\Delta\rho$ is the density difference across the interface, and ρ_1 is the density of the fluid between the interface and the surface.

The Hunt and Snyder (1980) work also classified the types and causes of lee-wave patterns and separated flow regions on the lee side of this bell-shaped hill. Many measurements were made of surface flow patterns, separated regions, velocity profiles, impinging plumes, and streamline displacements over the hill. Hill-surface concentrations resulting from impinging plumes were measured simultaneously with the flow-structure measurements. Whereas the data were distributed to and used by numerous model developers and the information obtained therefrom was utilized for planning and model-development purposes, except for limited presentation at a 1979 symposium (Snyder *et al*, 1980), the bulk of the results did not actually appear in print until much later (Snyder and Hunt, 1984).

The implications of this flow structure with regard to plume impingement

and resulting surface concentrations were amplified by Hunt *et al* (1979). This primarily theoretical work described two conceptual models for dealing with the problem of plume impingement. The first model was applicable to *strongly* stratified flow around three–dimensional hills, where vertical motion and vertical diffusion is negligible. The advective–diffusive equation around a three–dimensional hill which is axisymmetric about a vertical axis was solved (using an eddy diffusivity) to show how source positions on and off the centerline affect the trajectories and splitting of impinging plumes and the value and position of the maximum surface concentration on the hill. The results showed that the plume behavior is very sensitive to quite small changes in wind direction away from the direction that transports the plume onto a stagnation point, and the model provided a simple way to estimate the effect of these changes. This model also allowed the computation of concentrations within the separated, horizontally recirculating wake of the hill (source upwind of hill).

In the second model, a plume in a neutrally stable potential flow around a hemisphere was analyzed, also using the diffusion equation. The solutions showed how, because streamlines approach the surface of a three–dimensional hill much more closely than that of a two–dimensional hill, the maximum surface concentration on the hill *can* become very much greater than in the absence of the hill (but only for a limited range of source heights).

Prior to the inception of the CTMDP, another complex terrain model was developed by ERT under contract to EPA. The algorithm developed at that stage was generally applicable to plume behavior in stability conditions ranging from neutral to slightly stable. The general approach followed the theory of turbulent plumes embedded in potential flow fields as developed by Hunt and Mulhearn (1973), Snyder and Hunt (1984 – original manuscript made available to ERT in 1978), and Hunt *et al* (1979). This theory was applied to the calculation of ground–level concentrations using a Gaussian form of solution to the diffusion equation. Stream functions appropriate to the potential flow over a cylinder (aspect ratio, $h/L = \infty$) and to the potential flow over a sphere ($h/L = 1$) form the cornerstones of the model. These solutions were extended to describe flows over terrain features of intermediate crosswind aspect ratio by a weighting of the two limiting stream functions. The derivation of this weighing scheme relied heavily on wind–tunnel experiments of flows over hills of various aspect ratios (Snyder and Britter, 1987; data reports made

available to ERT in 1979). Strictly speaking, this algorithm was applicable to neutral flows, but an empirical approximation was included to define streamline lowering caused by an imposed stable stratification. This empirical scheme was derived on the basis of the stratified towing-tank experiments of Hunt and Snyder (1980). Extensive comparisons of model predictions with FMF laboratory data were made for both neutral and weakly stable conditions. A full account of these model-development efforts and the essential physics of the model are provided by Bass *et al* (1981). These algorithms were subsequently incorporated into a routine operational model called COMPLEX/PFM (Potential Flow Model; Strimaitis *et al*, 1982). In COMPLEX/PFM, potential flow calculations are performed whenever the plume lies above the dividing-streamline height and the stability is between neutral and slightly stable; when the plume is below the dividing-streamline height, the model reverts to the standard COMPLEX I computation (see Wackter and Londergan, 1984). The COMPLEX I computation makes the level-plume assumption, with an effective doubling of surface concentration above the plume centerline concentration (Burt and Slater, 1977). This particular aspect of the complex terrain diffusion problem was one of the hotly contested issues that provided the impetus for the CTMDP.

A "strawman" was proposed by Holzworth and Snyder (1979) for discussion at the 1979 workshop convened by EPA to make recommendations with regard to the directions to be taken under the CTMDP. This strawman was hotly debated at the workshop and, in the end, was largely accepted by the workshop participants (Hovind *et al*, 1979). The plan that emerged (Holzworth, 1980) called for an enlargement of some of the major concepts arising from the previous work at the FMF, and for a verification of these concepts through the conduct of a series of field studies on hills of progressively increasing size and complexity.

Prior to the request for bids on the CTMD contract, a preliminary one-week field study of the nighttime flow patterns at Cinder Cone Butte was organized and conducted primarily by FMF personnel (Snyder *et al*, 1980); the primary purpose was to assess the suitability of Cinder Cone Butte as the site for the first small hill study (identified in the ERT Milestone reports as Small Hill Impaction Study # 1). Numerous observations were made of the flow structure and plume behavior around the hill, including (1) plumes spread broadly in the lateral direction but very thinly in the vertical direction

over the hill in neutral conditions, (2) lee-side separation under high-wind-speed, neutral conditions, (3) plume impingement under light wind, strongly stable approach flows, and (4) katabatic winds under light-wind, neutral approach flow conditions with clear night sky. Cinder Cone Butte was judged as ideally suited for the first small hill study in several respects. Finally, numerous suggestions were offered as an aid to the design and conduct of future field studies at this site (most of which were adopted in the later studies).

To recap the "state of the science" immediately prior to the contract award, the dividing-streamline concept had been shown to be a useful conceptual framework to use in describing the structure of strongly stratified flow around three-dimensional hills. It had only been shown to be valid, however, for quite a limited number of hill shapes, all of which were axisymmetric. It had only been verified under uniform stratification (linear density gradient) or under a step inversion (sharp density interface), under a uniform approach-flow velocity profile, and, of course, only under steady-state, small-scale laboratory conditions (although the preliminary field study provided reassurances of the validity of the concept).

3. DESCRIPTIONS OF EXPERIMENTS AND RESULTS

3.1 Direct Interactions with the Model Developers

The period 1980 through 1981

The major CTMDP contract was awarded in June, 1980, and the work plan called for the small hill impaction study to begin at Cinder Cone Butte (CCB) in September. Almost immediately, the FMF was called upon to conduct towing-tank experiments to aid in the detailed planning and design of the field experiments. The first request was to provide quidance with regard to the location of the main meteorological tower. The second request was to provide guidance for smoke- and tracer-release strategies, for preselecting locations for samplers and cameras, and for choosing in advance several different sampler strategies to account for variations in flow regimes and wind fields. The third request was to test the validity of an integral formula for predicting the dividing-streamline height.

At an early July meeting at ERT headquarters in Boston, MA, the question arose as to how to predict the dividing-streamline height when the wind profile was not uniform and the density gradient was not linear. This was of paramount importance in planning the release scenarios, as the release locations and heights were to be chosen in real time during the field study based upon the incoming real-time meteorological data. J.C.R. Hunt immediately sketched the now well-known integral formula (on the back of an envelope!) as

$$\frac{1}{2}\rho U_\infty^2 (H_s) = g \int_{H_s}^{h} (h-z) \left[-\frac{\partial \rho}{\partial z}\right] dz \, . \qquad (3)$$

This formula had, in fact, been published 24 years earlier by Sheppard (1956) as a small note, actually in answer to his own question which arose at a meeting of the Royal Meteorological Society, although Sheppard's note was virtually unknown to the modeling community at that time. This integral formula is based upon simple energy arguments. Sheppard asked the question: in a strongly stratified flow approaching a hill, does a particular fluid parcel at some height upstream possess sufficient kinetic energy to overcome

the potential energy required to lift itself through the potential density gradient from its upstream elevation to the hill top? The left-hand side may be interpreted as the kinetic energy of the parcel far upstream at elevation H_s, and the right-hand side as the potential energy gained by the parcel in being lifted from the dividing-streamline height H_s to the hill top h through the density gradient $d\rho/dz$. This integral formula was presumably applicable to a fluid with any shape of stable density profile and, presumably, with any shape of approach-flow velocity profile. In practice, it must be solved iteratively, because the unknown H_s is the lower limit of integration; the formula can easily be reduced to the simpler formulae (1) and (2) by using the boundary conditions applicable to those special cases. The third request to the FMF was thus to verify this integral formula.

Three studies were conducted in the summer of 1980, and three reports were prepared in response to these requests. In the first study (Snyder, 1980a), twenty six separate tows of a model of CCB were made through the tank in a two-week period. The objective was to assess the suitability of the particular site chosen for the main (150m) meteorological tower, *i.e*, was it close enough to CCB to be representative of the flow approaching the hill, yet far enough away that the measurements were unaffected by the hill itself? It was impossible, of course, to meet both these criteria for all wind directions; the question addressed in the towing-tank studies, then, was whether the flow field at the proposed tower site would be perturbed by the hill, given the climatological ranges of prevailing wind directions for light, nighttime winds. Measurements were made of surface flow patterns, deformation of material lines, velocity profiles and streamline patterns over a model of CCB, and these measurements were compared favorably with predictions of potential flow theory. The findings from the study suggested that no significant perturbations to the approach wind field were to be expected due to the presence of the hill when the wind direction was outside the range of the prevailing wind directions. Nevertheless, a shorter (20m) tower was recommended, to be erected at the trailer site (3km ESE of the hill). This recommendation was indeed implemented in the field study.

This was, in fact, the first real-terrain model (*i.e.*, non-idealized shape) to be studied in the stratified towing tank. As a side benefit, therefore, the study provided reassurances that the basic flow features and, of course, the same physical principles applied to more realistically shaped

hills. Some examples are provided here to illustrate the point. Figure 1 shows an oblique view of the hill, where neutrally buoyant dye streamers were released from a horizontal rake upstream of the hill under strongly stratified conditions. The horizontal nature of the flow field is immediately obvious. Figure 2 shows a top or plan view of the CCB model under roughly similar conditions. One of the dye streamers obviously impinged on the upwind shoulder of CCB. Flow separation in the lee of the hill is dramatically illustrated in Figure 3, where vortex roll-up and eddy-shedding in the lee are quite vivid. The Kármán vortex street was a common occurrence at low Froude number; a street appeared to form at all elevations below the dividing-streamline height (at least for small Froude numbers), but the shedding frequency seemed to vary with elevation and motions at different elevations were seemingly uncorrelated with one another.

In the second phase of this summer series, eleven tows of the CCB model were made during which two of the model developers from ERT participated as observers. In this case, vertical rakes of tubes emitted neutrally buoyant dye at up to 6 elevations, with different colors of dye being emitted at the different levels. Each tow was filmed from the side using a camera that moved with the hill, and from directly below using a fixed camera pointed upward at the (inverted) model hill. The films were viewed with an analyst's projector, and the plume paths and envelopes were sketched. These results corroborated the previous results of Hunt and Snyder (1980) on idealized hills, *i.e.*, that plumes below the dividing-streamline height H_s and on a stagnation streamline would impinge on the upwind side of the butte and flow around the sides, and that plumes released just above H_s may produce maximum ground-level concentrations on the upwind side as they pass over the top. The results further emphasized that plumes travelling in a direction only slightly away from that of the stagnation streamline would tend to pass around CCB without significant impact, and that plumes released somewhat higher above H_s may be caught in strong downslope flows and produce maximum ground-level concentrations on the *lee* side of the hill. The results were also used, of course, for the originally intended purpose as a guide for planning of release and sampler strategies and selection of sampler and camera locations. The results are described by Bass (1980).

In the third phase of this summer series, the goal was to test the validity of the integral formula for the height of the dividing streamline

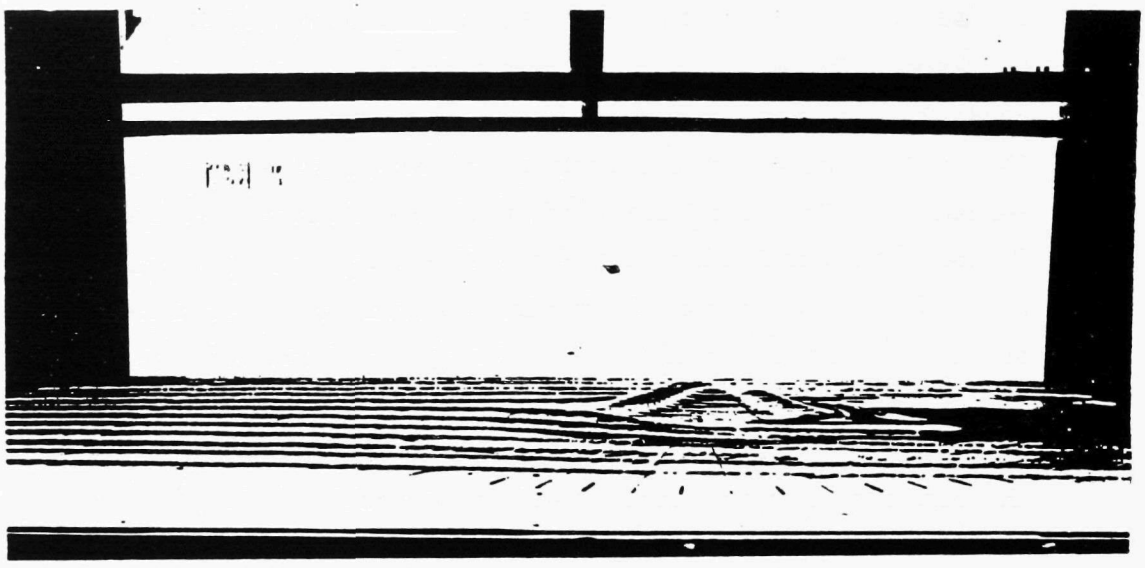

Figure 1. Oblique view of dye streamers released from a horizontal rake upwind of the CCB model at $z/h = 0.3$ under strongly stratified conditions ($F = 0.2$). Flow is from the left.

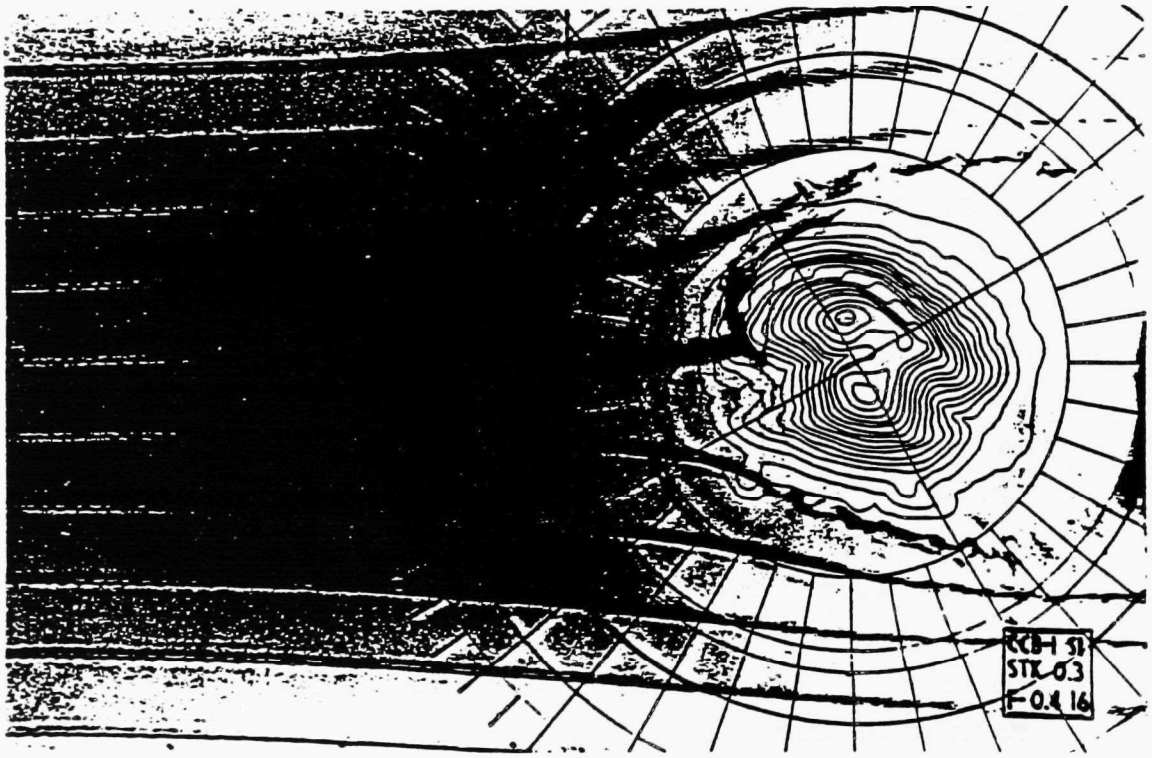

Figure 2. Top view of dye streamers impinging on CCB under strongly stratified conditions ($z/h = 0.3$, $F = 0.4$).

Figure 3. Vortex rollup and eddy-shedding in the lee of CCB under strongly stratified conditions ($z/h = 0.6$, $F = 0.2$).

under density profiles more typical of those expected at CCB. A typical nighttime temperature profile in the Snake River Basin (site of CCB) was found to consist of a strong, surface–based immersion of depth 50 to 100m and a weaker inversion above extending to several hill heights. Hence, the stratified towing tank was filled with a strong density gradient near the surface and a weaker gradient above. (In actuality, the weaker gradient was *below* the stronger gradient, but, as the model is towed upside down, we will, for clarity, describe the behavior as if the model were right–side–up.) The break–point between the two gradients was initially slightly above the crest of CCB (at 1.25*h*). A vertical rake of 3 tubes was positioned well upwind of the hill, with vertical spacing between the tubes of 1cm, which is equivalent to 6.4m full scale or 0.064*h*. Neutrally buoyant dye was emitted from each tube. For each tow, a particular stack height (center tube) was chosen and the general formula was integrated numerically using the measured density profile to predict the towing speed required such that the center streamer would rise to the elevation of the saddle point of CCB, *i.e.*, the minimum height of the draw between the two peaks. If the formula were correct, then, the lower streamer should go around the side of the hill, the upper streamer should go over the top, and the center one should split. The height of the break–point between the two gradients was then reduced and the process repeated. In all, twelve tows were made, varying the height of the break–point or the dividing–streamline height (release height) each time.

Figure 4 shows a side view of the impinging streamers during a typical tow, *i.e.*, the upper streamer going through the draw, the lower streamer going round the side, and the middle one splitting. Figure 5 shows the results in quantitative fashion. The density profiles were integrated in accordance with Equation (3) to find the dividing–streamline heights (based on the height of the saddle point) as functions of the towing speed. These predictions are shown in Figure 5 as the continuous lines. The observations of the dividing–streamline heights made during the twelve tows are also plotted in the figure; the agreement between the predictions and observations is regarded as excellent. The error bars result because of some fluctuating behavior of the streamers, especially at the higher speeds; occasionally, an intermittent vortex at the top windward side of the hill would engulf all three streamers and they would all go round the sides temporarily; on other occasions, parts of the lower streamer could be observed passing through the draw. The results

Figure 4. Oblique view of impinging streamers on CCB. Middle dye streamer is released at the dividing–streamline height; others at ±1cm (±6m full scale).

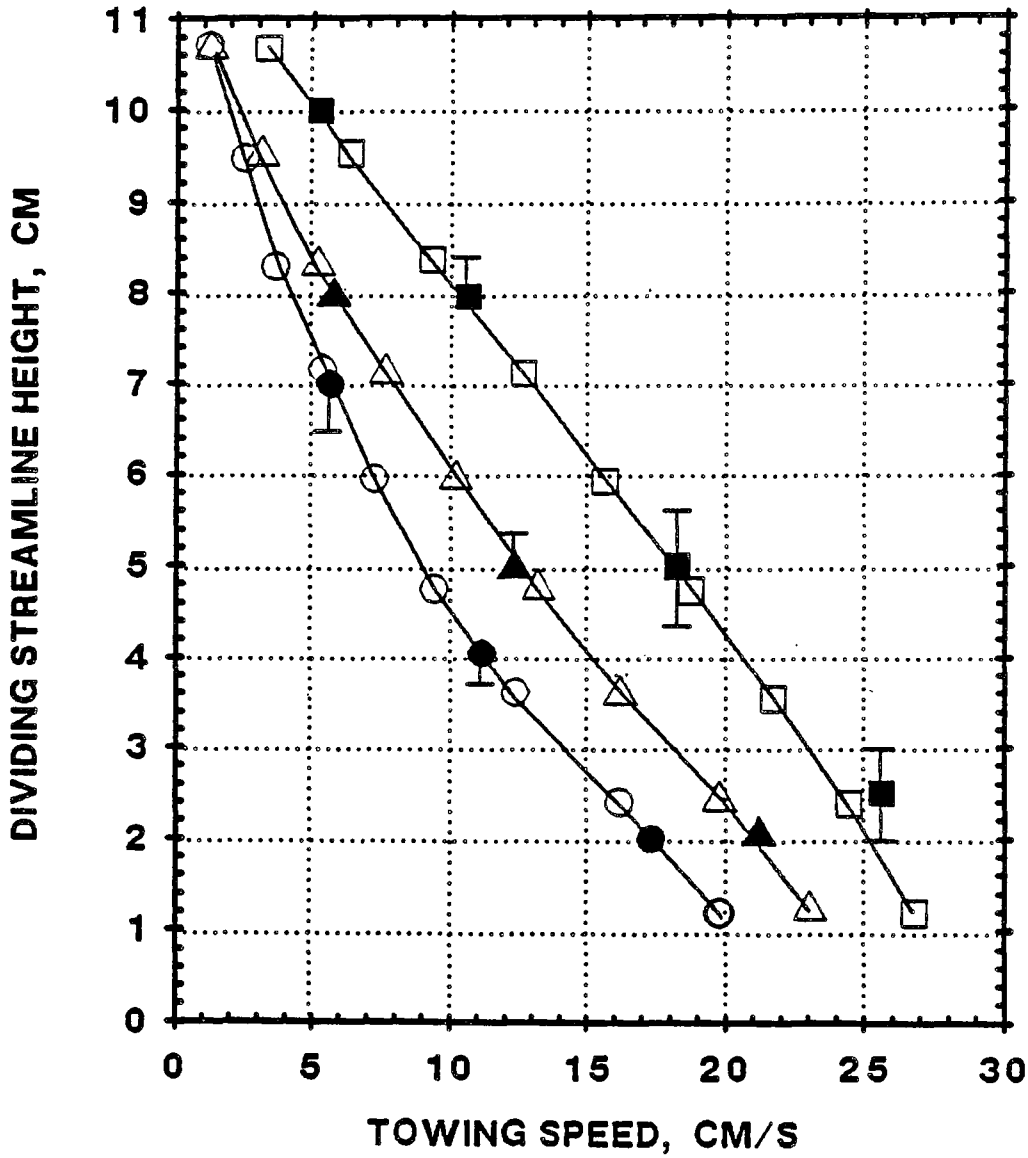

Figure 5. Comparison of predicted dividing-streamline heights with observations as functions of towing speed. Open symbols: predictions using integral formula; closed symbols: observations.

of this set of experiments (Snyder, 1980b) provided confidence in the validity of the general integral formula for predicting the height of the dividing streamline for a wide range of shapes of stable density profiles.

During the six-week field study at CCB, detailed measurements were made of wind, turbulence, and temperature profiles in the approach flow and at other positions on the hill. Sulfur hexafluoride (as a tracer) and smoke (for flow visualization) were released from a platform suspended from a mobile crane that allowed flexibility in positioning the source (height and location). One hundred samplers on the hill collected data on surface concentrations, and lidar was used to obtain plume trajectories and dimensions.

One particular hour from the field study was selected for simulation in the towing tank (Snyder and Lawson, 1981). That hour was 0500 to 0600, 24 October 1980 (Case 206), which may be characterized as very stable, *i.e.*, light winds and strong stable temperature gradients. Measurements made during the towing-tank experiments included ground-level concentrations under various stabilities and wind directions, vertical distributions of concentration at selected points, plume distributions in the absence of the hill, and visual observations of plume characteristics and trajectories.

This series of tows showed that the surface-concentration distributions were extremely sensitive to changes in wind direction. For example, Figure 6 shows that the distribution shifted from the north side of the hill to the south side with a shift of only 5° in wind direction. Comparisons of individual distributions with field results showed very much larger maximum surface concentrations and much narrower distributions in the model results. To account for the large variability in the winds measured during the hour, a matrix of 18 tows (three wind directions × six wind speeds) was conducted, and the concentration patterns were superimposed. A scatter plot of superimposed model concentrations versus field concentrations (Figure 7) shows a marked improvement over the single-tow comparisons. The largest model concentrations were within a factor of two of the highest field values, and 70% of the model concentrations were within a factor of two of the observed field values.

It was interesting to learn that, whereas the *location* of the maximum shifted dramatically with small shifts in wind direction, the *value* of the maximum changed very little with changes in wind direction or wind speed. Maximum surface concentrations approached those at the plume centerline in the

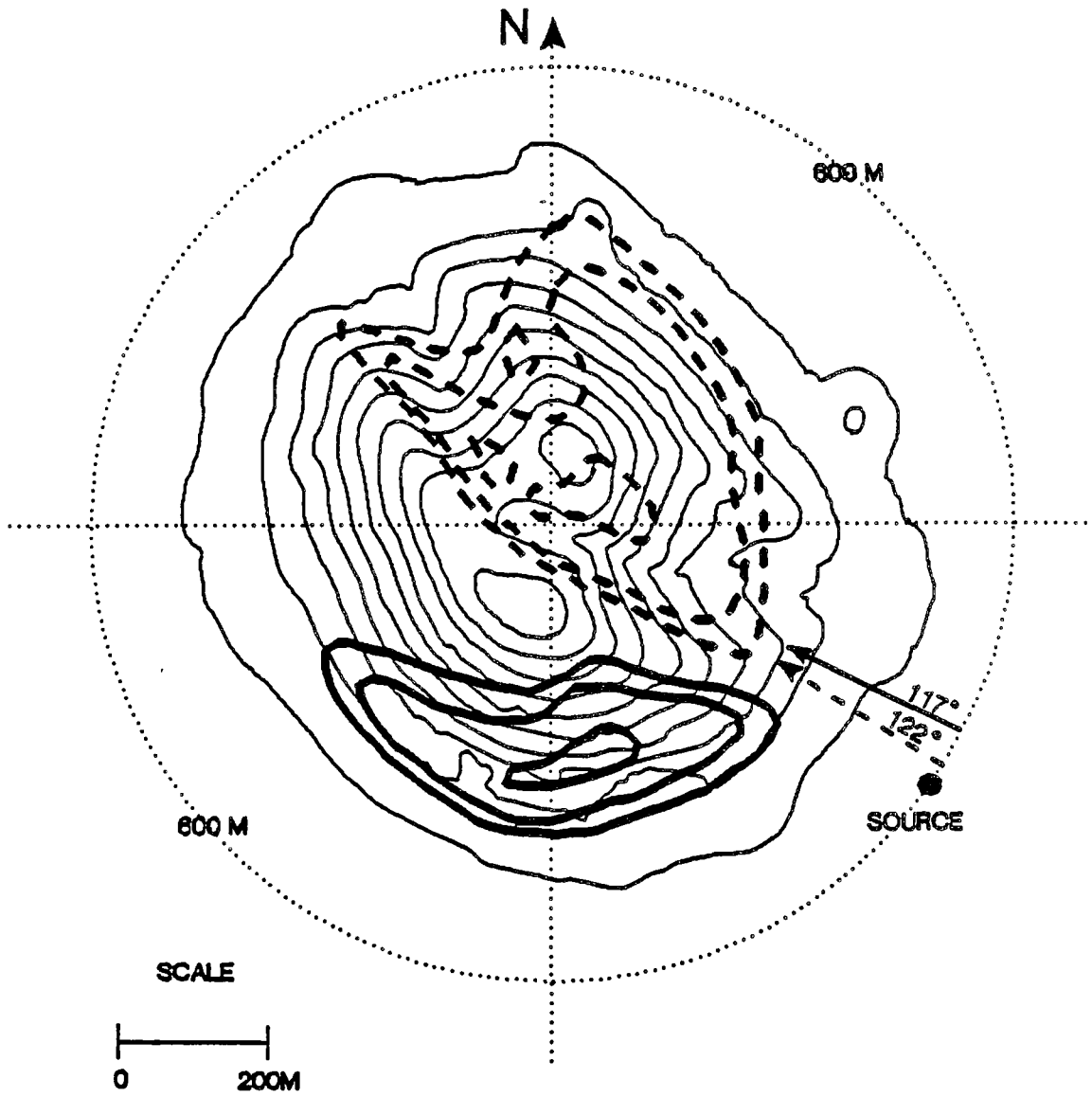

Figure 6. Concentration distributions measured during individual tows of CCB with $H_s/h = 0.31$ and $H_D/h = 0.38$; wind direction : ——— 117°, – – – 122°.

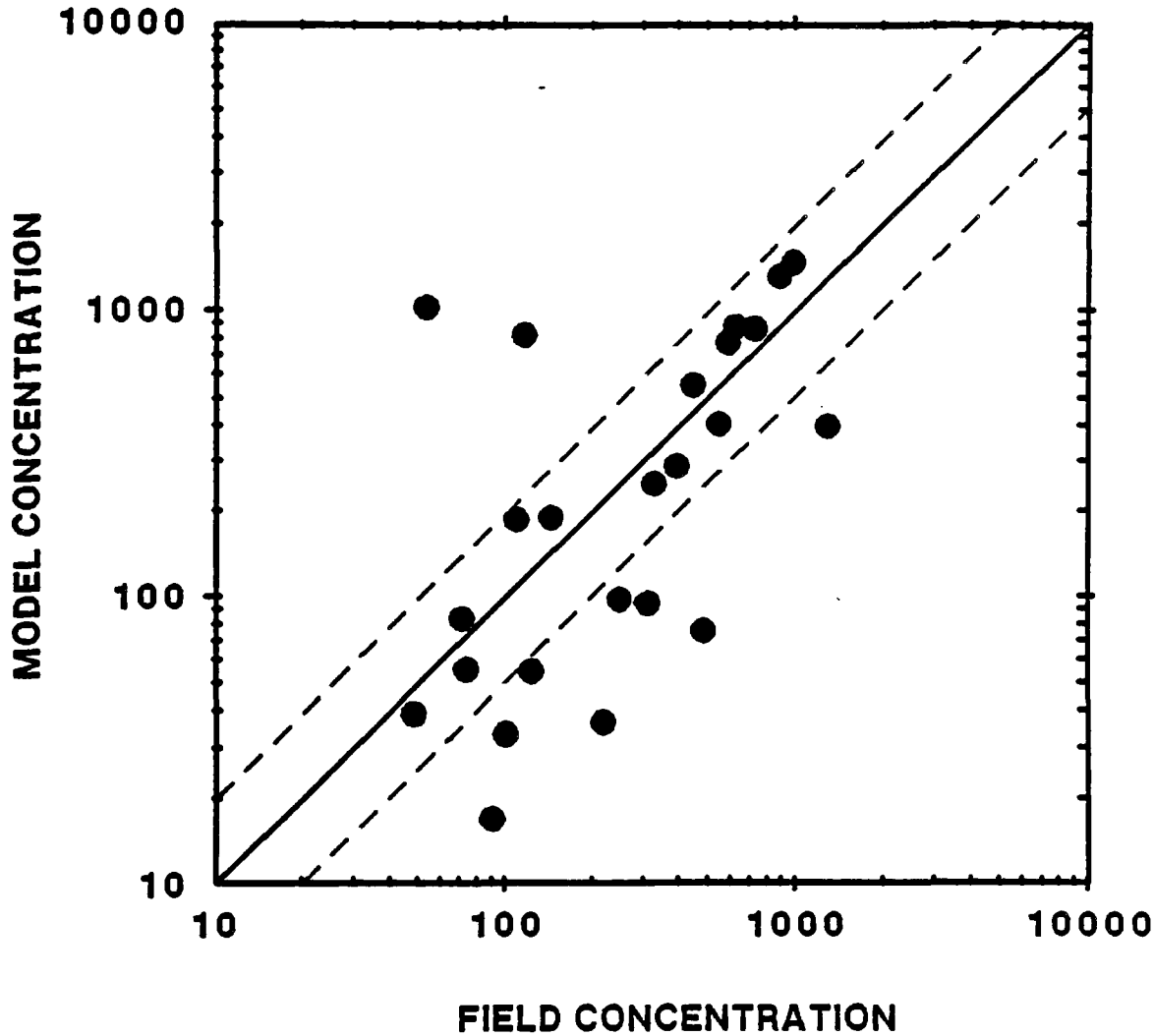

Figure 7. Scatter diagram comparing superposition of concentration distributions measured over Cinder Cone Butte with field distributions. Dotted lines denote factor of two on either side of perfect fit.

absence of the hill during individual tows, but because of the extreme sensitivity of the location to wind direction, the plume was "smeared" broadly across the hill surface as the wind direction changed through only a few degrees. Therefore, short-term averages (≈5min) in the field may be expected to approach plume-centerline concentrations; longer-term averages (≈1h) may be expected to be reduced by factors of five to ten (or more depending upon the magnitudes of the fluctuations in wind speed and direction).

The period 1982 through 1983

Although considerable work had been done concerning the validity and limits of applicability of the dividing-streamline concept, several questions still remained. One question concerned the effects of shear in the approach-flow velocity profile. Another concerned the effects of the aspect ratio (ratio of crosswind length of the hill to its height) and, in particular, its applicability in strongly stable flows to a truly two-dimensional ridge. A third questioned the effects of the *slope* of the hill, and a fourth, the effect of wind angle on a long ridge.

A few other studies had shed light on some of these problems. Baines (1979), for example, had conducted towing-tank studies of low-Froude-number flows around a barrier with a gap. His results suggested

$$H_s/h = 1-2F \tag{4}$$

for barriers with very small gaps, tending toward $H_s/h = 1-F$ (Equation 1) for those with wider gaps. Weil *et al* (1981) conducted similar towing-tank studies, extending the work of Baines, and found quite similar results. However, data from a field study by Rowe *et al* (1982) of stable air flow over a "long" ridge showed much better agreement with the data for axisymmetric hills (Equation 1) than for ridges with gaps (Equation 4).

In the early 1980's, a series of experiments was done by numerous investigators at the FMF and for a variety of different purposes. The overall objective was to gain fundamental understanding of flow and diffusion under stably stratified conditions in complex terrain, but the individual projects were designed with very specific and limited objectives in mind. Nevertheless, one aspect of each of the projects was to examine the concept of the dividing-streamline height, as it obviously had very important consequences with respect to the CTMDP. The results of most of these projects were published separately and independently, as will be referenced below, but

the results concerning the validity and applicability of the dividing-streamline concept were extracted and published as an appendix (Snyder *et al*, 1983) to the Second Milestone Report (Strimaitis *et al*, 1983) in order to provide timely support and guidance to (1) the mathematical modelers attempting to expand their models to include a wide variety of terrain shapes and approach flows and (2) planners of the Second Small Hill Impaction Study, which was to take place at the Hogback Ridge in northwestern New Mexico. This paper was subsequently published in a journal (Snyder *et al*, 1985). The individual laboratory experiments included:

1. Towing-tank studies on truncated, steep-sided ridges of various crosswind aspect ratios. These included examination of upstream "blockage" regions, surface flow patterns and lee-wave structure and were reported by Castro *et al* (1983); those aspects dealing specifically with the dividing-streamline concept were reported by Snyder *et al* (1983) and Snyder *et al* (1985).

2. Stratified wind-tunnel studies (in Japan) on *shear* flow over vertical fences of various crosswind aspect ratios and over a model of Cinder Cone Butte. (Snyder and Ogawa, 1982; Snyder *et al*, 1985).

3. Towing-tank studies on a truncated sinusoidal ridge with a maximum slope of 40° positioned perpendicular and at other angles to the approach wind direction (Lee *et al*, 1984a, 1984b).

4. Towing-tank studies on an "infinite" triangular ridge and a long sinusoidal ridge to test the validity of the "steady-state" assumption of flow upwind of an obstacle under strongly stratified conditions.

The conclusion from the studies with truncated triangular and sinusoidal ridges perpendicular to the wind was that the aspect ratio *per se*, does not have a significant influence on the dividing-streamline height H_s. Deviations from the $H_s/h = 1-F$ rule were attributed to the combination of shear in the approach flow and the very steep slope of the triangular ridges, which resulted in the formation of an upwind vortex with downward flow on the front faces of the ridges. The "1-*F*" rule was validated for the sinusoidal ridge with a length-to-height ratio greater from 16:1; in this case, the shear in the approach flow was much less pronounced, and the upwind slope was substantially smaller. Note that these deviations to the "1-*F*" rule did not invalidate Sheppard's concept, but required a reinterpretation of the rule as a necessary but not sufficient condition, *i.e.*, a fluid parcel may possess

sufficient kinetic energy to surmount a hill, but it does not necessarily do so.

In the stratified wind-tunnel studies, reasonably strong shear layers with depths more than twice the hill heights were developed in conjunction with strong stable temperature gradients. These approach flows provided dividing-streamline heights as large as 0.75*h*. In the vertical fence studies with a stratified approach flow, the shear was found to have an overwhelming influence. The conclusions were: (a) as in the triangular ridge studies, the aspect ratio was relatively unimportant; the basic flow structure was independent of aspect ratio; (b) the shear, in conjunction with the steep slope, created an upwind vortex such that plumes were downwashed on the front faces; and (c) under strong enough stratification, there was a limit to the downward penetration of elevated streamlines; the extent of this penetration appeared to be predictable as a balance between kinetic and potential energies. However, when these same shear flows approached the much lower sloped CCB model, there was *no* evidence of upwind vortex formation. Limited concentration measurements on the CCB model suggested that Sheppard's integral formula correctly predicted the height of the dividing streamline.

From the sinusoidal ridge studies with wind angles at other than 90°, it was concluded that the effect of deviations in wind direction (from 90°) are relatively insignificant until the wind direction is in the vicinity of 45° to the ridge axis. At 30°, significant departures from the "1–*F*" rule were observed; the fluid had sufficient kinetic energy to surmount the ridge, but found a path requiring less potential energy round the end of the ridge. When the dye streamers were moved closer to the upstream stagnation streamline (upwind of the upstream end of the ridge), they behaved according to the "1–*F*" rule.

The two-dimensional ridge studies showed that steady-state conditions are not established in strongly stratified flows (say $F < 1$). Two different physical mechanisms give rise to this unsteadiness; one is called "squashing", the other, upstream wave propagation. Brief explanations will be given here; the interested reader should consult the cited references.

The squashing phenomenon is most easily described in terms of the simple energy arguments as used in deriving Sheppard's formula (Equation 3). As discussed there, a fluid parcel with insufficient kinetic energy to overcome the potential energy requirement to surmount the hill must pass round the

sides of the hill. But a two–dimensional hill has no sides around which to pass (in a towing–tank, a "two–dimensional" hill is one that spans the entire width of the tank). Hence, the fluid parcel must be brought to rest. In the towing tank, since the fluid is generally at rest and the hill is towed, this means that the fluid ahead (upstream) of the hill must be pushed ahead of the hill, instead of being allowed to surmount the hill top. However, the upstream endwall of the towing tank, of course, prohibits this fluid from being pushed. Hence, the fluid between the hill and the upstream endwall is "squashed" as the hill approaches the endwall; because the fluid is incompressible, it must rise and spill over the top of the hill, just as the water in a bucket will rise and spill over the top when the sides are "squashed".

This squashing phenomenon seems to have no counterpart in the atmosphere. If true blocking occurred upwind of an "infinite" ridge in the atmosphere, it seems that the flow would be blocked to infinity upwind (*i.e.*, there is no "endwall" forcing the flow toward the ridge). In more practical terms, "blocking" upstream of a very long ridge would imply "upstream influence" to very large distances, possibly through an upstream–propagating front, which would imply non–steady–state behavior. From another viewpoint, there are no infinite ridges in the real world, so that fluid parcels can always be diverted around the obstacles without changing their elevation.

The results leading to the "1–2F^2" formula (Equation 4) by Baines (1979) and Weil *et al* (1981) for two–dimensional ridges and ridges with gaps were surprising because they suggested that fluid parcels could surmount the hills even though they had insufficient kinetic energy to do so. Snyder *et al* (1983, 1985) suggested that these earlier results were erroneous; that they were largely due to the squashing phenomenon, *i.e.*, the gaps in their ridges were insufficiently large to allow a "relief valve" to avoid the squashing.

Upstream *wave* propagation is also possible in stratified flows. The introduction of an obstacle in a stratified flow on which lee waves can form will result in "columnar" disturbances extending upstream (see Turner, 1973); if such motions are present, they will modify the approaching flow. These columnar disturbances take a sinusoidal form in the vertical, with the "mode" (number of oscillations) being dependent upon the Froude number based on the depth of the tank. An example of an upstream columnar disturbance is shown in Figure 8. Dye crystals were dropped into the stratified tank at a position

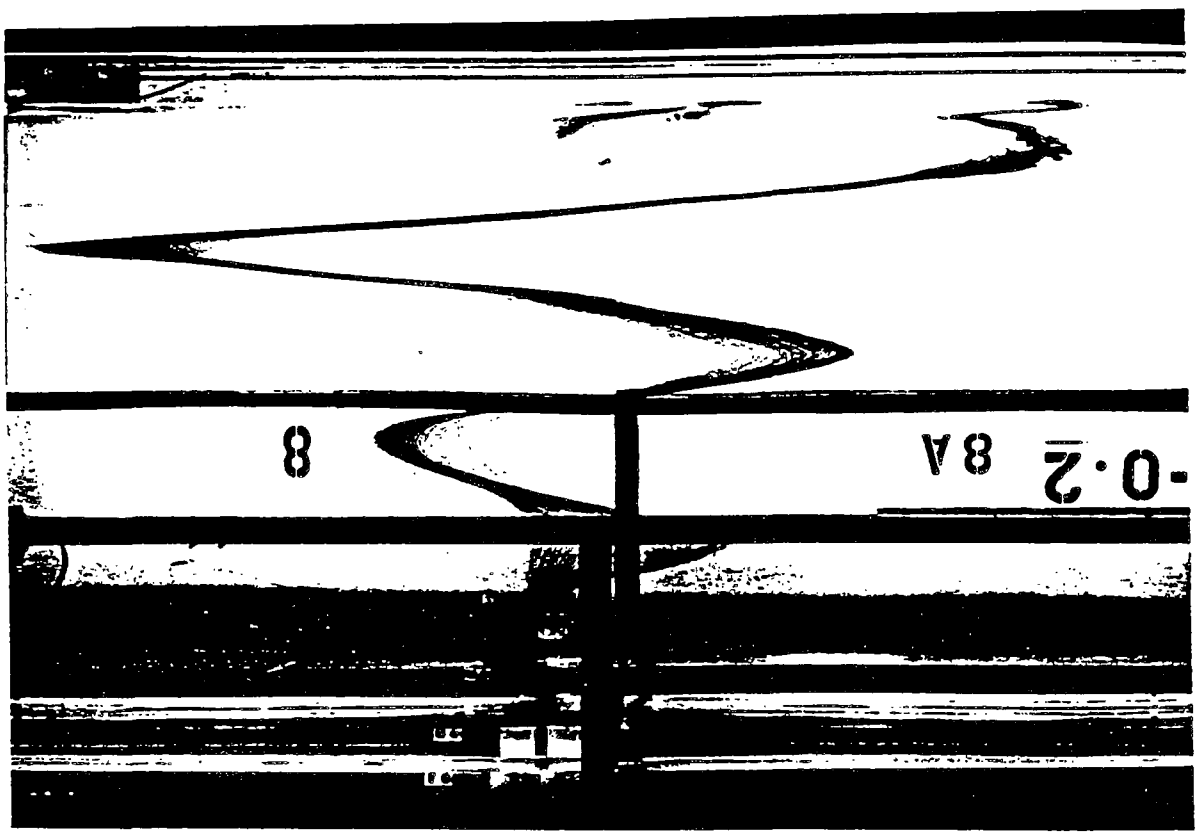

Figure 8. Deformation of vertical dye line by upstream columnar disturbances. Dye line was formed at a location 16m upstream of starting position of fence, at time when fence was at $x = 12.5$m (18.6h upstream of fence). Photograph was taken when fence was at $x = 13.8$m (11.6h upstream of fence). Fence is out of photograph, approaching from top left.

16m upstream of the starting position of an obstacle (in this case, a vertical fence) which was to be towed along the water surface. These crystals dissolved as they sank to the bottom, leaving behind a vertical dye line. The dye line was formed after the commencement of the tow, and the photograph was taken well before the obstacle reached the dye–line position, *i.e.*, the dye line was deformed by the upstream columnar disturbance into the sinuous curve shown in Figure 8.

These columnar disturbances, unlike the squashing phenomenon, do have counterparts in the real atmosphere. They result in "blocking" and "upstream influence". However, in the laboratory tank, these upstream waves are reflected from the upstream endwall of the tank and return to modify the flow locally around the model hill; this reflection from the upstream endwall does *not* have a counterpart in the real atmosphere. Baines (1979) argued that valid observations could be made of the flow over and around the obstacle in isolation (in the absence of end effects) by making the observations after steady state was reached (estimated by direct observation), but before reflected upstream motions arrived. Evidently, he believed that a *local* steady state was achieved in that, at some not–too–distant point upstream of the obstacle, steady–state velocity and density profiles were established before the reflected motions returned to modify them.

Snyder *et al* (1983; 1985) showed that steady–state conditions are not established in strongly stratified flows (say $F<1$) over two–dimensional ridges. The squashing phenomenon and reflections of upstream columnar disturbances continuously changed the shapes of the "approach flow" velocity and density profiles. Thus, these experiments have no analogue in the real atmosphere. Further, because long ridges cut by periodic small gaps require very long tow distances in order for steady state to be established, Snyder *et al* concluded that the previous laboratory studies were not valid models of atmospheric flows; specifically, the $H_s/h = 1-2F$ formula proposed for flow about ridges with small gaps is not expected to apply to the real atmosphere.

Further work was done to better understand the nature and causes of these upstream motions and lee waves by Thompson and Snyder (1984), Castro (1987) and Castro and Snyder (1987b, 1987c), but the interpretation of these results is somewhat controversial. More work is required to establish the precise relationships between model size and shape, stability, and tank size, shape and configuration in order to determine the limits of applicability of fluid

modeling and ranges of transferability to the atmosphere.

The second Small Hill Impaction Study was conducted during October 1982 at Hogback Ridge (HBR) near Farmington, NM. In providing input to the experimental design, the FMF conducted a series of wind-tunnel and towing-tank flow-visualization experiments prior to the field study. The laboratory studies were designed to investigate

- plume height above the surface over the hill crest and at the upwind edge of the hill,
- apparent size of any plume deformation upwind of the hill,
- lee wave importance and structure, and
- sensitivity of the plume trajectory to "wind angle".

This information was subsequently used by the field designers to guide the design of the smoke and tracer-gas release protocols at HBR, and to help select sampler and camera locations.

Two tests were made in the wind tunnel. One test was done with the ridge perpendicular to the flow, the other with the ridge rotated by 30°. These tests suggested that in neutral conditions the streamline patterns were similar to those expected from potential flow theory; a plume released at a given height upwind of the ridge should traverse the crest at an elevation of one-half its initial height. The test with the ridge at an angle to the flow showed only a very small ($<4^{\circ}$) deflection of the plume path as the plume traversed the ridge.

Eight individual tows of the HBR model were done in the stratified towing tank, varying the Froude number and wind direction, and each time releasing dye at eleven different elevations upstream. Heights of these dye streamers were measured at the upstream base and at the crest of the ridge. These experiments showed that, during weakly stratified conditions, plumes rose near the upwind base and fell over the crest to near or slightly lower than their upstream heights. Low-level releases experienced extensive mixing. More detailed results are contained in the Third Milestone Report (Lavery *et al*, 1983, p. 117-123).

Around this same time period, the FMF undertook two separate laboratory experiments that attempted to simulate two specific one-hour periods as observed in the field at Cinder Cone Butte. The first simulated a neutral stability period in the Meteorological Wind Tunnel (Thompson *et al*, 1983).

The second simulated a moderately stable period in the stratified towing tank (Eskridge *et al*, 1983). [Recall that the simulation of a strongly stable period was described earlier (Snyder and Lawson, 1981).]

In the summer of 1983, Ben Greene and colleagues from ERT, in cooperation with the FMF staff, conducted experiments in the Meteorological Wind Tunnel to characterize the response of the Climatronics UVW propeller anemometers. The primary objectives of the experiments were to determine the calibration curves and the non-cosine response corrections, especially at low wind speeds. The results of these tests are contained in the Fourth Milestone Report (Strimaitis *et al*, 1985, p. 85-93). The calibration factors and non-cosine response correction factors were applied to the HBR data base in forming the Modeler's Data Archive.

In late summer of 1983, discussions were held with ERT concerning possible contributions of FMF to the Full-Scale Plume Study planned for the following year at the Tracy Power Plant near Reno, NV. Considerations of scaling the site for towing-tank studies revealed that, at any reasonable scale, the model would appear as a two-dimensional ridge with a small gap (river valley) running through it. Recent work at the FMF as discussed above had shown that this situation could not be modeled under strongly stable conditions. Hence, specific site modeling at the Tracy Power Plant was not undertaken at the FMF. Instead, other studies in direct support of the model-development effort were undertaken as described below.

The period 1984 through 1985

In September 1983, A. Venkatram, D. Strimaitis and R. Britter from ERT requested that the FMF conduct two studies in support of their model-development efforts. The first study attempted to shed light on the question of the validity of the assumption of a *flat* dividing-streamline surface, a key assumption in the model under development. The second study was to provide a complete set of data on neutral flow and diffusion around a three-dimensional hill with a shape and slope approximating that of Cinder Cone Butte. These data were to help ERT to evaluate the separate effects of plume deformation kinematics and those of increased turbulence around the hill.

The first study, testing the validity of the flat dividing-streamline assumption, consisted of a series of 26 tows of a model hill in the stratified

towing tank. The model hill was the fourth–order polynomial (45° maximum slope) used by Hunt *et al* (1978), except that it was in this case instrumented with 100 sampling ports located along 8 radial lines. The density gradient was linear and the dividing–streamline height was fixed at half the hill height. Effluent was released at three elevations above the dividing–streamline height. *Pairs* of tows were made such that, in one tow, the hill (upside down) was fully immersed in the water and the towing speed was adjusted to provide a "natural" dividing–streamline surface. In the second tow of the pair, the model (baseplate, hill, and source, as a unit) was raised out of the water to the point where only the top half of the hill was immersed, thus, forcing a *flat* dividing–streamline surface, while all other conditions remained identical. Concentration distributions were measured on the hill surface (and in the absence of the hill). Concentration distributions from each pair of tows were compared to ascertain any differences between the "natural" dividing–streamline surface and the (forced) flat dividing–streamline surface. A comparison of surface–concentration patterns from a typical pair of tows is shown in Figure 9, and a scatter plot comparing concentrations on a port by port basis is shown in Figure 10. These results showed that the assumption of a flat dividing–streamline surface is a reasonable assumption to make, at least with regard to predicting the locations and values of the maximum surface concentrations and areas of coverage on the windward side of the hill. The results are contained in an appendix to the Fourth Milestone Report (Snyder and Lawson, 1985a) and were presented at the Third International Symposium on Stratified Flows (Snyder and Lawson, 1987).

The second study, providing a relatively complete set of data on flow and diffusion around a three–dimensional hill, was conducted in the Meteorological Wind Tunnel. The primary objective was to determine the influence of the hill on the maximum ground–level concentration (glc) and to locate the source positions where this influence was greatest. All measurements were made with an approach flow that simulated the neutral atmospheric boundary layer measured at Cinder Cone Butte. However, the nearly axisymmetric CCB shape was replaced by a truly axisymmetric hill represented by a simple mathematical formula, and having a maximum slope of 24° (the same as CCB).

The measure of the hill's influence on the maximum glc was the "terrain amplification factor" *A*. This factor is defined as the ratio of the maximum

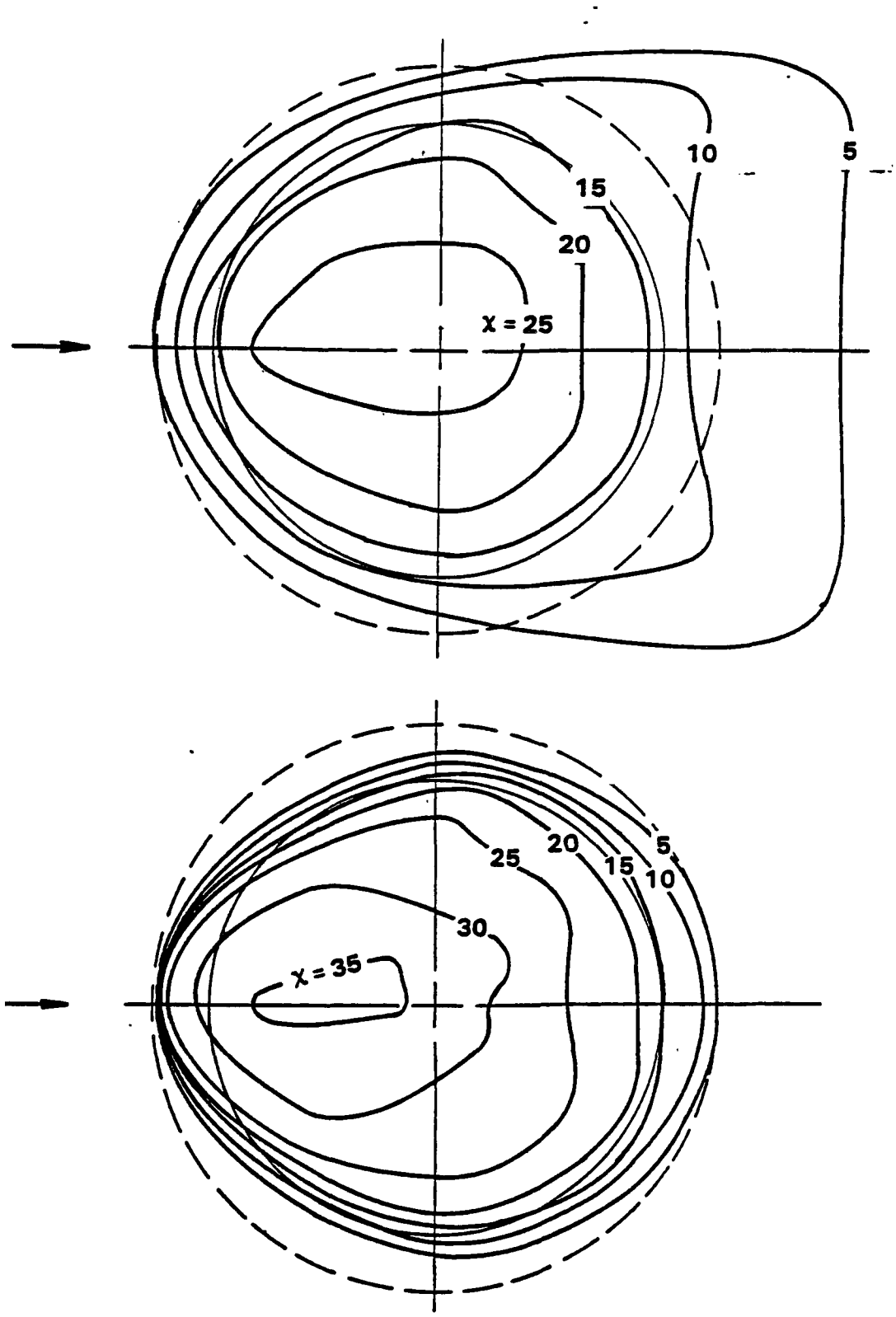

Figure 9. Concentration distributions measured on the hill surface with $H_D/h = 0.5$ and $H_s/h = 0.6$. Top: fully submerged; bottom: half submerged. Dotted circle indicates half the hill height.

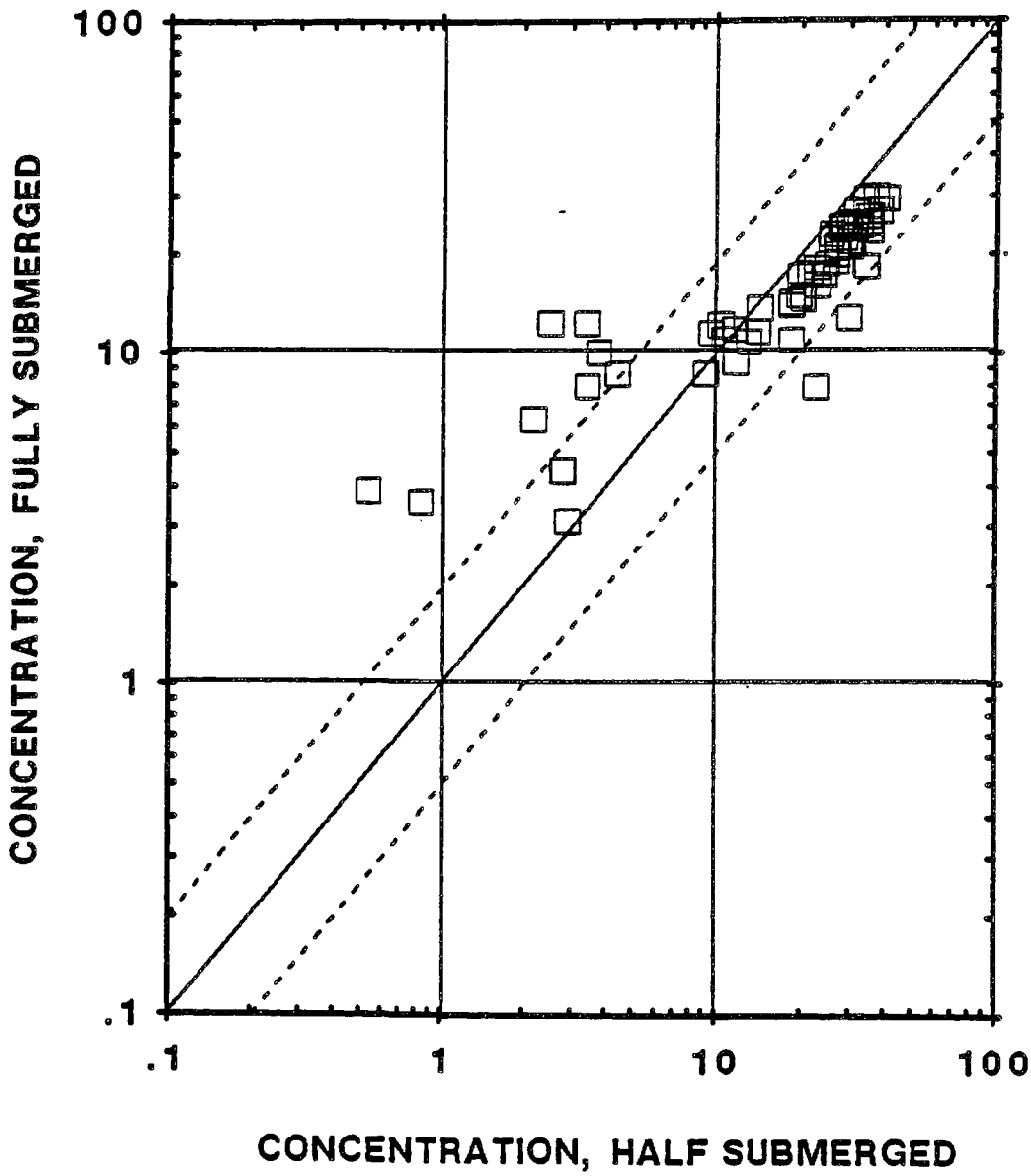

Figure 10. Scatter plot comparing concentrations on fully immersed hill with those on half-immersed hill on a port by port basis. $H_s/h = 0.6$, $H_D/h = 0.5$.

glc observed in the presence of the hill to the maximum observed in the absence of the hill. The locations of the maxima are not considered in this evaluation; the maxima may be found at entirely different places in the presence and in the absence of the hill.

A matrix of source locations was used covering the range from 4 to 16 hill heights (h) upstream of the hill center and to 1.25h in the vertical. A map of terrain amplification factors is shown in Figure 11. The presence of the hill was found to influence the transport and dispersion of the plume and to increase the maximum glc in three ways. For low sources at moderate distances from the hill, the reduction in mean wind speed and increase in turbulence allow the plume to reach the ground surface closer to the source, thus producing higher concentrations than in the absence of the hill. Plumes from higher sources may be thought of as being intercepted by the hill, that is, the hill penetrates the plume to where the concentrations are greater than those that would occur at ground-level farther downstream over flat terrain. For yet higher sources, the streamline convergence over the hill top and the corresponding downward flow and much enhanced turbulence in the lee of the hill again bring the plume to the ground more rapidly than over flat terrain. Terrain amplification factors ranged from near 1.0 to 3.63, and the range of source locations that produced an amplification factor greater than 1.4 extended to an upwind distance of 14 hill heights. These results were reported in an appendix to the Fourth Milestone Report (Thompson and Snyder, 1985b).

In the fall of 1984, ERT requested a list of data sets available from previous complex terrain studies that had been conducted at the FMF. A report was prepared by Thompson *et al* (1985) listing 24 separate complex terrain studies. Each project was synopsized with a brief description of the project, the name of the principal investigator(s), the facilities used, types of data collected, names of data reports available, major conclusions reached, listing of published results from the project, and a listing and description of the data files available.

An earlier request (prior to summer 1983) from the modelers at ERT had been to provide data on streamline trajectories in neutral and stratified flow over a three-dimensional hill, *i.e.*, to provide data to use in developing algorithms for predicting lateral and vertical streamline displacements over a hill as functions of source location and stratification. Earlier work on this

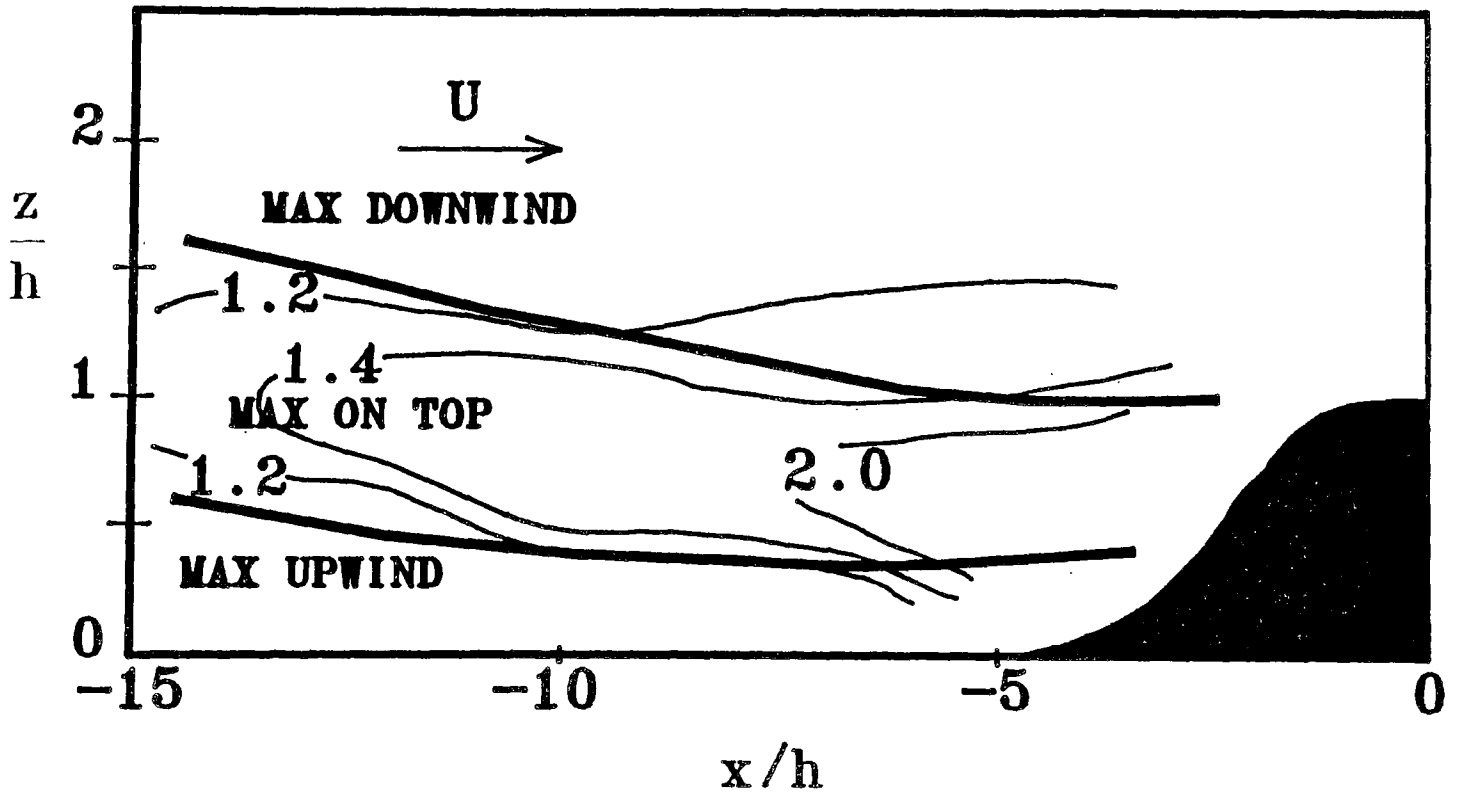

Figure 11. Terrain amplification factors measured upwind of axisymmetric CCB model. Heavy lines divide the region into areas where the source produced the maximum glc upwind of the hill top, between the hill top and the separation point, and downwind of the hill. Note that the vertical scale is exaggerated by a factor of 3.

project had been set aside because of experimental difficulties and because of the more urgent requests described immediately above. Having completed those studies, work commenced again on the streamline trajectories.

In attempting to predict the maximum glc from a source upwind of a hill, the most important feature of the flow is the displacement of the mean streamline through the source, because that displacement determines how near to the surface the "centerline" of the plume will reach. The exact path taken by the plume in circumventing the hill and the plume's closeness of approach to the hill surface are critical in determining the location and magnitude of the glc's. These displacements are known to be strongly affected by the hill shape and especially by the stratification in the approach flow. The purpose of this study was thus to characterize the effects of stability on the horizontal and vertical deflections around an isolated hill. A large set of streamline trajectories over the axisymmetric CCB model was measured using the stratified towing tank. Three-dimensional coordinates of the streamlines (86 independent trajectories) were determined through stereographic analysis of photographs of dye streak lines released at a matrix of source positions (heights and lateral offsets from the hill/flow centerline), and at stabilities ranging from strongly stable to neutral (Froude numbers of 0.6, 1.0, 2.0, and ∞). These measurements provided a relatively complete data set for testing mathematical models and algorithms of the detailed structure of stratified flow over hills. The results were presented in an appendix to the Fifth Milestone Report (Snyder *et al*, 1986).

As an example use of the data set, a particular mathematical model using linear theory and a Fast Fourier Transform (FFT) technique to predict these streamline trajectories was evaluated and described in the above appendix by Snyder *et al* (1986) and, with some additional work and computations, by Thompson and Shipman (1986). The calculated results agreed well with the experimental results for neutral flow. In the stable flow ($Fr = 2.0$), however, lateral deflections were underpredicted and vertical deflections were overpredicted using the FFT model.

The period 1986 through present

In February 1986, ERT conducted a Complex Terrain Workshop at Research Triangle Park, NC (Lavery *et al*, 1986). Each participant was beforehand provided a diskette containing the Complex Terrain Dispersion Model (CTDM)

code and a draft User's Guide and was asked to exercise the model to assess its overall effectiveness and validity in whatever way he chose. The purpose of the workshop, then, was to exchange information on the results of these exercises and to make recommendations to the model developers concerning further refinements of the CTDM model.

The present author exercised the CTDM by comparing is predictions with previous laboratory measurements of flow and diffusion over hills made in the FMF. This was accomplished in four phases. In phase 1, CTDM calculations were compared with wind-tunnel simulations of plumes released upwind of two- and three-dimensional hills in a neutral atmospheric boundary layer. Terrain amplification factors were compared for a matrix of source locations upwind of the hills. This phase was intended to test the LIFT module of CTDM, where the stratification was neutral and the potential flow calculations of LIFT should be most applicable. In phase 2, CTDM calculations were compared with stably stratified towing-tank observations, where plumes were released above the dividing-streamline height upwind of a three-dimensional hill. This phase was intended to again test the LIFT module, but this time under strongly stratified conditions. In phase 3, CTDM calculations were compared with strongly stratified towing-tank observations wherein plumes were released below the dividing-streamline height upwind of the Cinder Cone Butte model. This phase was intended to test the WRAP module exclusively. In phase 4, CTDM calculations were made for one selected hour of field conditions, and were compared with results of towing-tank observations. This phase was intended to exercise both the LIFT and WRAP modules of CTDM.

The results, made available in a detailed report that was distributed to the workshop participants (Snyder, 1986), may be summarized as follows:

1. From the neutral flow simulations (phase 1), the hill effects (as exemplified through computations of terrain amplification factors) appeared to be much too small. Reasons speculated for this discrepancy included: (a) plume trajectories were too far from the hill surface, (b) potential flow calculations did not properly handle the deep boundary-layer flow approaching the hill, or, more likely (c) the plume centerline did approach the hill surface closely enough, but the plume did not mix to the the surface through the hill-surface boundary layer.

2. From the stable flow simulations with releases above the dividing-streamline height (phase 2), it appeared that the plume trajectories were again too far from the hill surface. Vertical deflections of streamlines appeared to be strongly overestimated and lateral deflections appeared to be strongly underestimated. In the

towing tank, plumes released slightly above the dividing-streamline height spread broadly but thinly to cover the entire hill surface above the dividing-streamline height, whereas the CTDM plume was apparently deformed only slightly – it "hung together" in going over the top of the hill. An apparent shortcoming of LIFT at that time was its lack of appropriate treatment of the stratification effects in the flow that surmounted the hill, *i.e.*, streamline (hence, plume) deformations under quite strongly stratified flows (Fr≈1) were treated the same as those for neutral flow (Fr=∞).

3. From the stable flow simulations with releases below the dividing-streamline height (phase 3), the WRAP module yielded rather poor results except when the input parameters (primarily σ_v) were within a fairly closely restricted range. WRAP could not handle narrow plumes.

4. From the Case 206 simulations (phase 4), CTDM appeared to do a reasonable job of predicting the values of the highest concentrations. Improvements in predictions from the 12/5-minute mode over the 1-hour mode appeared to be small, at least in terms of calculating the highest concentrations, and did not appear to be justified on the basis of the additional computation costs.

Also at the CTDM Workshop, the participants were divided into three workgroups to discuss and make recommendations concerning (a) algorithms, (b) evaluations and (c) applications. One outcome of the Algorithm Workgroup was the postulate of a hill-surface boundary layer that would result in rapid mixing of plume material to the hill surface [a possible mechanism, lacking from CTDM, that could have resulted in the rather poor agreement between the neutral wind-tunnel results (discussed above) and the predictions of CTDM]. Further discussions of the workgroup indicated the need for a "definitive" data set on plume deformations over a realistic hill shape, for appropriate adjustment or "calibration" of the T-factors (terrain correction factors) in CTDM. Hence, the FMF agreed to conduct further studies with the following goals:

1. Investigate the existence and/or effects of a "hill-surface boundary layer" that might result in rapid mixing of material from an elevated plume onto a hill surface.

2. Provide detailed plume-structure data over a realistic hill shape, *i.e.*, horizontal and vertical plume deflections and deformations over a hill.

To satisfy the first goal, two interchangeable axisymmetric (idealized) Cinder Cone Butte (ACCB) models were constructed. One of the models had a smooth surface; the other was covered with gravel. Effluent was released from

an upstream source with height such as to obtain a plume that just "grazed" the hill top. The postulate here was that the roughness on the surface would maximize the effects of a rapid-mixing layer near the hill surface, thus mixing material from this elevated plume to the surface, whereas the smooth surface would minimize the effects of this mixing layer. The results showed that the postulate of an "inner hill-surface boundary layer" was untenable; extremely steep concentration gradients remained near the hill surface, even when the hill was roughened, so that rapid mixing was not induced by the hill-surface boundary layer.

To satisfy the second goal, a series of measurements was made of plume characteristics in flat terrain and over a three-dimensional hill. Effluent was released at a number of elevations, upwind distances, and positions laterally offset from the centerplane determined by the wind direction and the center of the hill. Sufficient concentration measurements were made to enable the construction of plume cross sections at the downwind position of the hill center and, in a few cases, at the upwind base of the hill. These data were analyzed to provide the desired information on horizontal and vertical plume deflections and deformations effected by the hill. One of the more dramatic examples is shown in Figure 12. In this case, the source was on the centerplane at ground level, 6 hill heights upwind of the hill center (the skirt of the hill extended to 5h). Plume cross sections measured at the position of the center of the hill, both in the presence and in the absence of the hill, are shown. The hill effected a 91% increase in the lateral plume width. In this case, the maximum surface concentration (at the same downwind distance) was decreased by a factor of 2 but, of course, the area of coverage by large concentrations was greatly increased. Detailed data reports were provided to ERT in March 1986, and the results were published by Snyder and Lawson (1986).

Subsequent to the CTMD Workshop (and as a result of the rather poor comparisons of the CTDM predictions of terrain amplification factors with wind-tunnel data), refinements were made to CTDM. Specifically, the strain inferred or measured over the crests of two- and three-dimensional hills in the wind tunnel were used in the calculations, *i.e.*, the T-factors in the model were adjusted in accordance with wind-tunnel data. Substantial improvements in the CTDM predictions of terrain amplification factors were obtained, as described by Strimaitis and Snyder (1986).

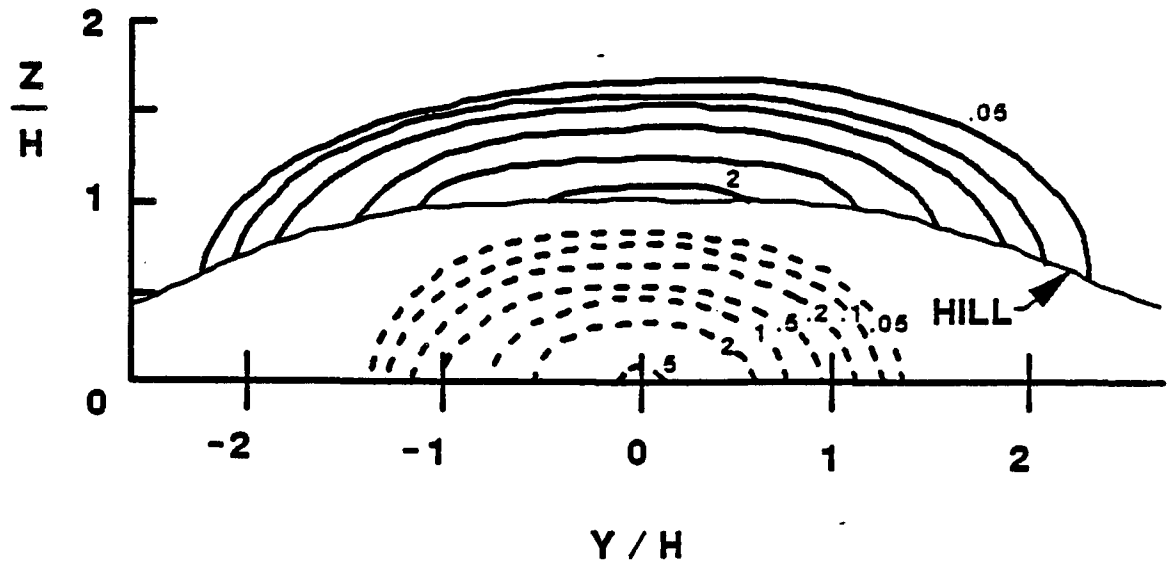

Figure 12. Plume cross sections measured in presence (———) and in absence (— — —) of axisymmetric CCB model at $x=0$ (hill center). $H_s/h=0$, $x_s/h=-6$, $y_s/h=0$.

3.2 Supplemental Modeling of Complex Terrain

In addition to the modeling done in direct support of the CTMDP, numerous other complex terrain studies were conducted at the FMF, primarily in response to envisioned needs of and direct requests from the OAQPS, the regulatory arm of EPA. These ranged from generic studies attempting to understand the fundamental physics of flow and diffusion in neutral and stable environments to a practical demonstration to determine the good-engineering-practice stack height for a specific power plant located in complex terrain. Whereas the studies done in direct support of the CTDMP were primarily concerned with plume impingement from upwind sources and focussed primarily on strongly stable conditions, the supplemental studies were broader ranging, for example, including sources on the tops and lee sides of hills, perhaps a broader range in stability from strongly stable to neutral, and investigation of similarity criteria – rules to ensure that the behavior of the flow in the laboratory simulates that in the real world. An example of the latter is the *Guideline for Fluid Modeling of Atmospheric Diffusion,* prepared by Snyder (1981) in response to a request from the OAQPS. In several cases, studies that were initiated through the CTDM developers were subsequently enlarged upon and expanded so as to be useful to the modeling community at large. Hence, in many cases, studies could have been described as supplemental (this section) or in direct support of the CTMDP (Section 3.1). The choices have been somewhat arbitrary.

One of the important overall goals in this effort was to ascertain what circumstances lead to the largest ground-level concentrations, *i.e.*, are larger glc's expected when the plume from an upwind source impinges on a hill or when the source is downwind of that hill such that the plume is caught in a recirculation region and downwashed to the surface? Which are likely to lead to larger glc's, two-dimensional or three-dimensional hills? Stable conditions or neutral conditions? In each of these circumstances, what order of magnitude of surface concentrations may be expected?

Neutral-Flow Wind-Tunnel Studies

A simple method used to intercompare effects of terrain on the maximum glc and to determine worst-case conditions is through the terrain amplification factor, as mentioned in Section 3.1. Again, the terrain

amplification factor, A, is defined as the ratio of the maximum ground-level concentration occurring in the presence of the terrain feature, χ_{mx}, to the maximum that would occur from the same source located in flat terrain, χ^{o}_{mx}, *i.e.*, $A = \chi_{mx}/\chi^{o}_{mx}$. This definition is useful only for elevated sources, of course, because for ground-level sources, the maximum surface concentration occurs at the source itself.

Numerous neutral-flow wind-tunnel studies have been conducted at the FMF on diffusion over two-dimensional terrain features: (a) a ramp with a slope of 14° followed by a plateau (Snyder and Pendergrass, 1980; Pendergrass and Arya, 1983; Pendergrass and Snyder, 1987), (b) a bell-shaped hill with a maximum slope of 12° (Courtney, 1979; Courtney and Arya, 1980), (c) a steep triangular ridge with a slope of 63° (Arya and Shipman, 1981; Arya *et al*, 1981), (d) a series of smooth shaped hills of various slopes (Khurshudyan *et al*, 1981; Capuano, 1983; and Lawson and Snyder, 1985, 1987) and (e) a valley formed between two ridges of sinusoidal cross section (Lee et al, 1981). Three studies have been performed to determine the effects of the crosswind aspect ratio of a triangular ridge on dispersion from nearby sources. As mentioned in Section 2, Snyder and Britter (1987) investigated surface concentrations on the ridges from upwind sources. (Note that the work was done in 1979, much earlier than the publication date, so that the results were available, indeed, *used* in the development of a forerunner to CTDM.) Castro and Snyder (1982) extended the study by measuring the sizes and shapes of the recirculation regions downwind of these hills of various crosswind aspect ratio, and by measuring the concentration fields resulting from sources placed at various downwind locations. Recently, Castro and Snyder (1987a) have further extended this work to include the case when the approaching wind is not perpendicular to the long axis of the hill. This allows one to use the wind-tunnel data to estimate the effects of long-time-scale wind meander. Other generic three-dimensional hill studies included: (a) conical hills with slopes of 26.5° and 17.5° with sources located at the hill top or at the downwind base (Gadiyaram, 1984; Arya and Gadiyaram, 1986) and (b) the axisymmetric CCB model with downwind sources (Lawson and Snyder, 1985, 1987). These various studies were summarized through publications at various stages by Thompson and Snyder (1981, proceedings published 1985a) and Snyder (1983a, 1983b, 1984). Only a broad overview and a few typical results will be presented here.

Table 1 shows the terrain amplification factors for the cases listed above, in order of decreasing A. From the standpoint of a fixed stack height, the worst location for a source appears to be just downwind of a two–dimensional ridge. Downwind sources generally result in larger glc's because of the excess turbulence generated by the hills and because the effluent is generally emitted into a low speed region where the streamlines are descending toward the surface. Maximum A's are considerably larger than those downwind of three–dimensional hills. A probable cause of this effect is that, in three–dimensional flows, lateral and vertical turbulence intensities are enhanced by roughly equal factors, whereas in two–dimensional flows, the lateral turbulence intensities are not enhanced as much as are the vertical turbulence intensities (because of the two–dimensionality). Since the maximum glc depends upon the ration σ_z/σ_y (Pasquill, 1974), we may expect the A's downwind of two–dimensional hills to be larger than those downwind of three–dimensional hills. Also, the sizes of the recirculating cavity regions downwind of three–dimensional hills are generally much smaller than those downwind of two–dimensional ridges.

TABLE 1. SUMMARY OF TERRAIN AMPLIFICATION FACTORS FOR SOURCES IN THE VICINITY OF HILLS IN NEUTRAL FLOW

Source Location	Hill Type	A
Downwind	Two-Dimensional	10-15
Downwind	Three-Dimensional	5-6
Upwind	Three-Dimensional	2-4
Upwind	Two-Dimensional	1-3
Top	Two-Dimensional	0.5-1

With regard to upwind sources, terrain amplification factors are larger for three–dimensional hills because, in such flows, streamlines can impinge on the surface and/or approach the surface more closely than in two–dimensional flows.

Table 1 listed approximate values of maximum terrain amplification factors that were found in the various situations. They are useful only for scoping a particular problem or for finding the worst possible situation.

They do not provide practical estimates for use by, say, an air pollution meteorologist in determining the maximum glc resulting from a particular power plant or for determining the best location for that plant. For that purpose, the concept of a "window" of excess concentrations, as introduced by Hunt *et al* (1979) is more useful. For any given plant location (say, upwind of the hill), there is a *limited* range of stack heights H_s for which a *significant* amplification of the glc will occur. (For sake of argument, we will here define significant as a factor of 2.) This amplification can occur only if the position of the maximum glc lies on or near the hill surface. For small H_s, χ_{mx} will occur upwind of the hill and thus be little influenced by the hill, so that A ($\equiv\chi_{mx}/\chi^{\circ}_{mx}$) will approach unity. If H_s is too large (for example, $H_s \gg h$, the hill height), χ_{mx} will lie well beyond the hill and A will again approach unity. In either case, there is little amplification. These "windows" of critical H_s values have been measured by Lawson and Snyder (1985, 1987) for two typical hill shapes that might be found in the real world, one axisymmetric, the other two-dimensional. The results are shown in Figure 13. The 1.4-window, for example, extends to about $14h$ upstream, $10h$ downstream, and as high as $1.8h$ in the vertical for the axisymmetric hill. For the two-dimensional hill, this 1.4-window extends about $8h$ upstream, $15h$ downstream, and as high as $2.2h$ in the vertical.

Such contour maps as provided in Figure 13 can be very useful for the practitioner. Once an acceptable terrain amplification factor (or "excess concentration") is decided upon, it is a simple matter to trace the window on the contour map to determine the area (plant location and/or stack height) to be avoided. Conversely, from such maps, the likely maximum glc for a potential site and stack height can be estimated. The use of terrain amplification factors simplifies the application of these data to full-scale situations. The expected maximum glc in flat terrain is calculated (from mathematical models or standard curves), then the concentration in the presence of the hill is simply the product of this quantity and the TAF. This study was initiated through a request from the EPA Office of Air Quality Planning and Standards (OAQPS) to aid in the decision-making process with regard to the promulgation of the Stack Height Regulations under the Clean Air Act, and the data were provided to OAQPS much earlier than the publication dates shown.

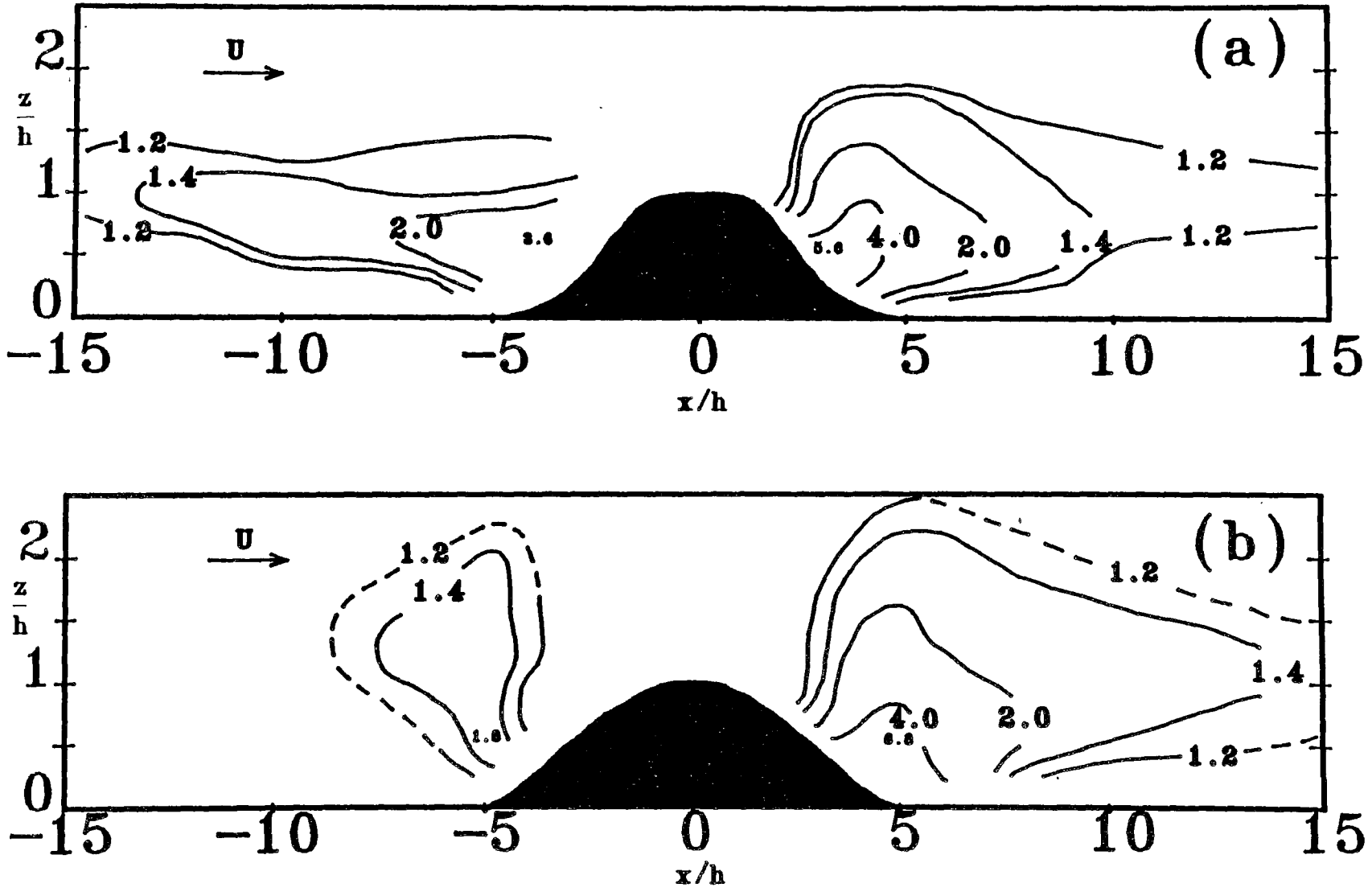

Figure 13. Contours of constant terrain amplification factors over (a) axisymmetric hill and (b) two-dimensional ridge. Note that vertical scale is exaggerated by a factor of 3.

Subsequent to the idealized study described above, the OAQPS requested the FMF to conduct a study demonstrating the application of the fluid modeling approach to the determination of good-engineering-practice (GEP) stack height for a power plant in complex terrain, *i.e.*, to provide an example study/report for industry to follow in the conduct of a GEP determination. The site chosen for this demonstration was the Clinch River Power Plant in southwestern Virginia, and a 1:1920 scale model of the surrounding terrain was constructed. Measurements were presented (Snyder and Lawson, 1985b) that described the simulated atmospheric boundary layer structure, plume-dispersion characteristics in that boundary layer, and the maximum glc of effluent downstream from the plant, both in the presence of all significant terrain surrounding the plant and in the absence of "nearby" upwind terrain. Analysis of the maximum glc showed that, in this case, a stack height of 326m met the GEP criteria under 50% load conditions, *i.e.*, the nearby upwind terrain effected an increase of 40% in the maximum ground-level concentration. This study followed the general guidance set forth in the *Guideline for Fluid Modeling of Atmospheric Diffusion* (Snyder, 1981) and the specific recommendations set forth in the *Guideline for Use of Fluid Modeling to Determine Good Engineering Practice Stack Height* (EPA, 1981) and the *Guideline for Determination of Good Engineering Practice Stack Height (Technical Support Document for the Stack Height Regulations,* Revised Draft) (EPA, 1985).

Stably Stratified Towing-Tank Studies

Lamb and Britter (1984) conducted a combined numerical and laboratory study of so-named shallow water flow over an isolated hill. They showed how certain geometrical and flow parameters affect the tendency of a fluid to flow around rather than over an obstacle in the case of a homogeneous single layer fluid, *i.e.*, simulating the atmospheric condition of an elevated step inversion. A series of numerical experiments was conducted using a finite-difference model. Measures were suggested for quantitative assessment of the tendency of the fluid to flow around the obstacle as a function of the relative hill height and the Froude number. The laboratory experiments examined the motions of two superposed homogeneous layers of fluid past a conical hill in the towing tank. The resulting motions were found to agree with the results of the numerical experiments and extended the understanding gained from them. Flow visualization techniques were used to demonstrate the

impingement of the interface on the obstacle, and its dependence on flow speed and hill height.

Another numerical model was acquired and implemented at the FMF for comparison with laboratory results. The numerical model was originally developed by Mason and Sykes (1979); it integrates the Navier–Stokes equations for incompressible stratified flow using a finite–difference scheme. Direct comparisons were made between the results of this model and laboratory experiments for density–stratified flow around the idealized axisymmetric CCB model by Rottman *et al* (1987) for three specific experimental arrangements. First, a small towing tank was used in which both the Reynolds number and Froude number were matched exactly with the numerical model. This provided an overall assessment of the accuracy of the approximations made in the numerical model. Second, the large towing tank was used in which mean plume trajectories were measured and compared with particle paths computed through the numerical model. Third, some comparisons were made with wind–tunnel measurements of the flow structure over the hill. In general, the numerical model qualitatively reproduced the experimental results on the flow structure, but there were some substantial differences, particularly near the hill surface and in the wake and at the larger values of the Reynolds number.

Whereas the following area of investigation is not directly related to complex terrain, it is included here because it played an important (and somewhat controversial) role in the CTDM formulation. This is the area of describing the effects of stable stratification on turbulent diffusion or, put another way, estimating vertical plume growth in the nighttime stable boundary layer. Experiments were conducted (Britter *et al*, 1983) in which a grid was towed horizontally along the stratified towing tank. The vertical velocity fluctuations produced near the grid were reduced under strong stratification by up to 30%, but the decay rates of the turbulent velocity fluctuations were found to be unaffected by the stratification over a considerable distance downstream. Turbulent diffusion from a point source located downstream of the grid was also measured. The lateral plume widths were found to be largely unaffected by the stratification and grew with the 1/2-power of time. The vertical plume growth, however, was found to reach an asymptotic limit. These results were largely in agreement with the theoretical models of Csanady (1964) and Pearson *et al* (1983), but in contradiction to the theory and limited data of Venkatram *et al* (1984). The latter data suggest a continuous

vertical plume growth (for large times), but the measurements did not, in fact, extend very far downwind (maximum downwind distance of about 1 km).

Further grid–turbulence studies were done in the towing tank with the aim of investigating internal wave effects and providing guidance on the partitioning of wave and turbulence energies in stably stratified flows (Rottman and Britter, 1986). The results suggested that the mixing efficiency increases monotonically with increasing stability, with some indication that it approaches a constant as the flow becomes strongly stable.

A cooperative project was completed with the Los Alamos National Laboratory to examine the conditions under which flushing of a valley between two ridges will occur, *i.e.*, to answer the question of when a stable crosswind will sweep the valley clean and when the flow will separate from the top lee side of the first ridge, reattach at the top windward side of the second ridge, and thus form a nearly stagnant region in the valley beneath. In this series of towing–tank studies, three experimental parameters were varied: the steepness of the ridge/valley slopes (40°, 27° and 13°), the separation distance between the ridges, and the Froude number that characterizes the stability of the crosswind. In broad terms, the characteristics of the flow between the ridges may be explained using criteria for boundary–layer separation from the lee side of a single ridge. The downstream ridge appears to induce separation from the lee side of the upstream ridge only when it is steep–sided (Lee *et al*, 1984a,b, 1986, 1987). As an offshoot of this work, the conditions conducive to the onset of severe downslope winds on the lee sides of mountains was investigated (Rottman and Smith, 1987). The results showed that an intrusion (breaking wave – associated with severe downslope winds) existed when the Froude number based on the ridge height was in the range $0.2 \leq F \leq 0.6$ for a steep–sloped ridge (maximum slope 40°) and $0.2 \leq F \leq 1.1$ for a low–sloped ridge (13°).

An overview of fluid modeling of pollutant transport and diffusion in stably stratified flows over complex terrain was provided for *Annual Review of Fluid Mechanics* by Snyder (1985).

4. SUMMARY

The EPA Fluid Modeling Facility has conducted a wide range of laboratory studies and a limited amount of numerical modeling of flow and diffusion in association with the Complex Terrain Model Development Program. The goal of the CTMDP is the development of a dispersion model valid in complex terrain, with emphasis on plume impaction on nearby hills during nighttime stable conditions. Work at the FMF prior to the inception of the program provided the basic framework for the model – the dividing–streamline concept – and the focal point around which to design the field program.

Throughout the course of the CTMDP, the FMF interacted vigorously with the model developers by providing support in various ways. Early work provided direct support in planning the details and strategies of the field experiments and solidifying and testing the limits of applicability of the dividing–streamline concept. Later work included exercises of "filling in the gaps" in the field data, furthering the understanding of the physical mechanisms important to plume impaction in complex terrain and in stably stratified flows in general, and testing the ability of the laboratory models to simulate full–scale field conditions. And, as the needs arose, the FMF tested various modeling assumptions, concepts, and hypotheses and provided data for "calibration" of various parameters within the CTDM model.

Simultaneously, the FMF responded to the needs of the regulatory arm of EPA, the Office of Air Quality Planning and Standards, by providing guidance concerning expected terrain effects and by providing a demonstration study – an example for industries to follow in conducting good–engineering–practice stack height determinations in complex terrain. Also, a broad range of supplemental studies was conducted, expanding and enlarging upon the specific requests of the OAQPS and the CTDM model developers to provide information of general use to the scientific and air pollution modeling communities. Many of the data sets generated in the course of this program have been provided to and used by various groups (nationally and internationally) in the development, testing and evaluation of complex terrain dispersion models.

REFERENCES

* Arya, S.P.S. & Gadiyaram, P.S. 1986 An Experimental Study of Flow and Dispersion in the Wakes of Three-Dimensional Low Hills. *Atmos. Envir.*, **20**, 729–40.

* Arya, S.P.S. & Shipman, M.S. 1981 An Experimental Investigation of Flow and Diffusion in the Disturbed Boundary Layer over a Ridge, Part I: Mean Flow and Turbulence Structure. *Atmos. Envir.*, **15**, 1173–84.

* Arya, S.P.S., Shipman, M.S. & Courtney, L.Y. 1981 An Experimental Investigation of Flow and Diffusion in the Disturbed Boundary Layer over a Ridge, Part II: Diffusion from a Continuous Point Source. *Atmos. Envir.*, **15**, 1185–94.

Baines, P.G. 1979 Observations of Stratified Flow Past Three-Dimensional Barriers. *J. Geophys. Res.*, **84**, no. C12, 7834–8.

* Bass, A. 1980 Towing Tank Studies in Support of Field Experiments at Cinder Cone Butte, Idaho, Part II: Plume Behavior with Froude Number and Incident Wind Direction. Rpt. by Envir. Res. & Tech. on cooperative work with Fluid Mod. Facility, Envir. Prot. Agcy., Res. Tri. Pk., NC.

Bass, A., Strimaitis, D.G. & Egan, B.A. 1981 Potential Flow Model for Gaussian Plume Interaction with Simple Terrain Features. Rpt. under Contract No. 68-02-2759, Envir. Prot. Agcy., Res. Tri. Pk., NC, 201p.

Brighton, P.W.M. 1978 Strongly Stratified Flow Past Three-Dimensional Obstacles. *Quart. J. Roy. Meteorol. Soc.*, **104**, 289–307.

* Britter, R.E., Hunt, J.C.R., Marsh, G.L. & Snyder, W.H. 1983 The Effects of Stable Stratification on Turbulent Diffusion and the Decay of Grid Turbulence. *J. Fluid Mech.*, **127**, 27–44.

Burt, E.W. & Slater, H.H. 1977 Evaluation of the Valley Model. AMS-APCA Joint Conf. on Appl. of Air Poll. Meteorol., Salt Lake City, UT, Amer. Meteorol. Soc., Boston, MA.

* Capuano, M.E. 1983 The Effects of Hill Slope on Flow and Dispersion over Two-dimensional Hills – A Wind Tunnel Study. M.S. Thesis, Dept. Marine, Earth, Atmos. Sci., NC State Univ., Raleigh, NC, 153p.

* Castro, I.P . 1987 A Note on Lee Wave Structures in Stratified Flow over Three-Dimensional Obstacles. *Tellus*, **39A**, 72–81.

* Castro, I.P. & Snyder, W.H. 1982 A Wind Tunnel Study of Dispersion from Sources Downwind of Three-Dimensional Hills. *Atmos. Envir.*, **16**, 1869–87.

* Castro, I.P. & Snyder, W.H. 1987a Wind Direction Effects on Dispersion from Sources Downwind of Steep Hills. *Atmos. Envir.* (to be submitted).

---

* Publications generated from research conducted within the Fluid Modeling Facility.

* Castro, I.P. & Snyder, W.H. 1987b Obstacle Drag and Upstream Motions in Stratified Flow. *Proc. Third Int. Symp. Stratified Flows*, Cal. Inst. Tech., Pasadena, CA, Feb. 3–5 (general session).

* Castro, I.P. & Snyder, W.H. 1987c Upstream Motions in Stratified Flow. *J. Fluid Mech.* (submitted).

* Castro, I.P., Snyder, W.H. & Marsh, G.L. 1983 Stratified Flow over Three–Dimensional Ridges. *J. Fluid Mech.*, **135**, 261–82.

* Courtney, L.Y. 1979 A Wind Tunnel Study of Flow and Diffusion over a Two–Dimensional Low Hill. M.S. Thesis, Dept. of Meteorol., NC State Univ., Raleigh, NC, 134p.

* Courtney, L.Y. & Arya, S.P.S. 1980 Boundary Layer Flow and Diffusion over a Two–dimensional Low Hill. Preprints Vol., 2nd Jt. Conf. Appl. Air Poll. Meteorol., Mar. 24–28, New Orleans, LA, 551–8. Amer. Meteorol. Soc., Boston, MA.

Csanady, G.T. 1964 Turbulent Diffusion in a Stratified Fluid. *Atmos. Sci.*, **21**, 439–47.

DiCristofaro, D.C., Strimaitis, D.G., Greene, B.R., Yamartino, R.J., Venkatram A., Godden, D.A., Lavery, T.F. & Egan, B.A. 1986 EPA Complex Terrain Model Development Fifth Milestone Report – 1985. Rpt. No. EPA/600/3–85/069, Envir. Prot. Agcy., Res. Tri. Pk., NC, 277p.

Drazin, P.G. 1961 On the Steady Flow of a Fluid of Variable Density Past an Obstacle. *Tellus*, **13**, 239–51.

EPA 1981 Guideline for Use of Fluid Modeling to Determine Good Engineering Practice Stack Height. Rpt. No. EPA–450/4–81–003, Envir. Prot. Agcy., Res. Tri. Pk., NC, 47p.

EPA 1985 Guideline for Determination of Good Engineering Practice Stack Height (Technical Support Document for the Stack Height Regulations). Rpt. No. EPA–450/4–80–023R (Revised June 1985), Envir. Prot. Agcy., Res. Tri. Pk., NC, 102p.

* Eskridge, R.E., Lawson, R.E. Jr. & Marsh, G.L. 1983 Simulation of an Atmospheric Tracer Experiment in Complex Terrain Using a Stratified Towing Tank: A Case Study. 6th Symp. Turb. & Diffusion, Boston, MA, Mar. 22–25, Amer. Meteorol. Soc., Boston, MA.

* Gadiyaram, P.S. 1984 Flow and Dispersion over Three–Dimensional Axisymmetric Hills: A Wind Tunnel Study. M.S. Thesis, Dept. Marine, Earth, Atmos. Sci., NC State Univ., Raleigh, NC, 126p.

Holzworth, G.C. 1980 The EPA Program for Dispersion Model Development for Sources in Complex Terrain. 2nd Jt. Conf. Appl. Air Poll. Meteorol., March 24–27, New Orleans, LA, Amer. Meteorol. Soc., Boston, MA.

* Holzworth, G.C. & Snyder, W.H. 1979 Program Plan for Development of a Mathematical Air Quality Assessment System for Use in Complex Terrain. Rpt. No. EPA–600/9–79–041, *Workshop on Atmos. Disp. Models in Complex Terrain*, 137–50. Envir. Prot. Agcy., Res. Tri. Pk., NC.

Hovind, E.L., Edelstein, M.W. & Sutherland, V.C. 1979 Workshop on Atmospheric Dispersion Models in Complex Terrain. Rpt. No. EPA–600/9–79–041, Envir. Prot. Agcy., Res. Tri. Pk., NC, 213p.

Hunt, J.C.R. & Mulhearn, P.J. 1973 Turbulent Dispersion from Sources Near Two-Dimensional Obstacles. *J. Fluid Mech.*, 61, 245–74.

* Hunt, J.C.R., Puttock, J.S. & Snyder, W.H. 1979 Turbulent Diffusion from a Point Source in Stratified and Neutral Flows around a Three-Dimensional Hill: Part I: Diffusion Equation Analysis. *Atmos. Envir.*, 13, 1227–39.

* Hunt, J.C.R. & Snyder, W.H. 1980 Experiments on Stably and Neutrally Stratified Flow over a Model Three-Dimensional Hill. *J. Fluid Mech.*, 96, 671– 704.

* Hunt, J.C.R., Snyder, W.H. & Lawson, R.E. Jr. 1978 Flow Structure and Turbulent Diffusion around a Three-Dimensional Hill: Fluid Modeling Study on Effects of Stratification; Part I: Flow Structure. Rpt. No. EPA-600/4-78-041, Envir. Prot. Agcy., Res. Tri. Pk., NC..

* Khurshudyan, L.H., Snyder, W.H. & Nekrasov, I.V. 1981 Flow and Dispersion of Pollutants over Two-Dimensional Hills: Summary Report on Joint Soviet-American Study. Rpt. No. EPA-600/4-81-067, Envir. Prot. Agcy., Res. Tri. Pk., NC, 143p.

* Lamb, V.R. & Britter, R.E. 1984 Shallow Water Flow over an Isolated Obstacle. *J. Fluid Mech.*, 147, 291–313.

Lavery, T.F., Bass, A., Strimaitis, D.G., Venkatram, A., Greene, B.R., Drivas, P.J. & Egan, B.A. 1982 EPA Complex Terrain Modeling Program: First Milestone Report – 1981. Rpt. No. EPA-600/3-82-036, Envir. Prot. Agcy., Res. Tri. Pk., NC, 304p.

Lavery, T.F., Strimaitis, D.G. & Egan, B.A. 1986 A Workshop Report on the Complex Terrain Model Development Project (February 4–6, 1986). Rpt. under Contract 68-02-3421, Envir. Prot. Agcy., Res. Tri. Pk., NC, 75p.

Lavery, T.F., Strimaitis, D.G., Venkatram, A., Greene, B.R., DiCristofaro, D.C. and Egan, B.A. 1983 EPA Complex Terrain Model Development: Third Milestone Report – 1983. Rpt. No. EPA-600/3-83-101, Envir. Prot. Agcy., Res. Tri. Pk., NC, 271p.

* Lawson, R.E. Jr. & Snyder, W.H. 1985 Stack Heights and Locations in Complex Terrain. Preprints Vol: 7th Symp. Turb. Diff., Nov. 12–15, Boulder, CO, 223–6. Amer. Meteorol. Soc., Boston, MA.

* Lawson, R.E. Jr. & Snyder, W.H. 1987 Estimation of Pollutant Concentration from Sources Near Complex Terrain in Neutral Flow. *Atmos. Envir.* (to be submitted).

* Lee, J.T., Barr, S., Lawson, R.E., Jr., Snyder, W.H. & Marsh, G.L. 1984a Towing Tank Studies of Stratified Flow over Ridges and Valleys. Rpt. No. LA-UR-84-1314, Los Alamos National Laboratory, Los Alamos, NM, 29p.

* Lee, J.T., Barr, S., Lawson, R.E., Jr., Snyder, W.H. & Marsh, G.L. 1984b Towing Tank Studies of Stratified Flow over Ridges and Valleys. Preprints Vol. 3rd Conf. Mtn. Meteorol., Portland, OR, 37–41. Amer. Meteorol. Soc., Boston, MA.

* Lee, J.T., Barr, S., Snyder, W.H. & Lawson, R.E. Jr. 1981 Wind Tunnel Studies of Flow Channeling in Valleys. Preprint Vol. 2nd Conf. Mtn. Meteorol., Nov. 9–12, Steamboat Springs, CO, Amer. Meteorol. Soc., Boston, MA.

* Lee, J.T., Lawson, R.E. Jr. & Marsh, G.L. 1986 Flow Visualization Experiments on Stably Stratified Flow over Ridges and Valleys. Proc. 3rd Int. Workshop on Wind and Water Tunnel Modeling of Atmos. Flow and Dispersion, Sept., Lausanne, Switzerland.

* Lee, J.T., Lawson, R.E. Jr. & Marsh, G.L. 1987 Flow Visualization Experiments on Stably Stratified Flow Over Ridges and Valleys: Final Report. Rpt. No. LA-UR-87-127, Los Alamos National Laboratory, Los Alamos, NM.

Mason, P.J. & Sykes, R.I. 1979 Three-Dimensional Numerical Integrations of the Navier-Stokes Equations for Flow Over Surface-Mounted Obstacles. *J. Fluid Mech.*, 91, 433-50.

Pasquill, F. 1974 *Atmospheric Diffusion.* 2nd Ed., Chichester, Ellis Horwood Ltd., John Wiley & Sons, NY, NY, 429p.

Pearson, H.J., Puttock, J.S. & Hunt, J.C.R. 1983 A Statistical Model of Fluid-Element Motions and Vertical Diffusion in a Homogeneous Stratified Turbulent Flow. *J. Fluid Mech.*, 129, 219-49.

* Pendergrass, W.R. & Arya, S.P.S. 1983 Vortex Development in Boundary Layer Flows over Two-Dimensional Ramps. Preprint Vol. 6th Symp. Turb. & Diff., Mar. 22-25, Boston, MA, Amer. Meteorol. Soc., Boston, MA.

* Pendergrass, W.R. & Snyder, W.H. 1987 Wind Tunnel Measurements of Terrain Amplification Factors for Sources Upwind of Two-Dimensional Ramps of Various Slopes. *Atmos. Envir.* (to be submitted).

Queney, P., Corby, G.A., Gerbier, N., Koschmieder, H. & Zierep, J. 1960 The Airflow over Mountains. *World Meteorol. Org.*, Tech. Note No. 34. Geneva, Switz.

Riley, J.J., Liu, H.T. & Geller, E.W. 1976 A Numerical and Experimental Study of Stably Stratified Flow Around Complex Terrain. Rpt. No. EPA-600/4-76-021, Envir. Prot. Agcy., Res. Tri. Pk., NC, 41p.

* Rottman, J.W. & Britter, R.E. 1986 The Mixing Efficiency and Decay of Grid-Generated Turbulence in Stably Stratified Fluids. Proc. 9th Australasian Fluid Mech. Conf., Dec. 8-12, Univ. Auckland, Auckland, New Zealand.

* Rottman, J.W., Lawson, R.E. Jr. & Snyder, W.H. 1987 A Comparison of Numerical and Laboratory Experiments on Density-Stratified Flows around a Three-Dimensional Hill. *Proc. Third Int. Symp. Stratified Flows*, Cal. Inst. Tech., Pasadena, CA, Feb. 3-5.

* Rottman, J.W. & Smith, R.B. 1987 Tow-Tank Simulations of the Severe Downslope Wind. *Proc. Third Int. Symp. on Stratified Flows*, Cal. Inst. Tech., Pasadena, CA, Feb. 3-5.

Rowe, R.D., Benjamin, S.F., Chung, K.P., Havlena, J.J. & Lee, C.Z. 1982 Field Studies of Stable Air Flow over and around a Ridge. *Atmos. Envir.*, 16, 643- 53.

Sheppard, P.A. 1956 Airflow over Mountains. *Quart. J. Roy. Meteorol. Soc.*, 82, 528-9.

* Snyder, W.H. 1980a Towing Tank Studies in Support of Field Experiments at Cinder Cone Butte, Idaho, Phase I: Influence of Hill on Wind Field at the Meteorological Tower Site. Fluid Modeling Facility Internal Rpt., July 30, 20p. Envir. Prot. Agcy., Res. Tri. Pk., NC.

* Snyder, W.H. 1980b Towing Tank Studies in Support of Field Experiments at Cinder Cone Butte, Idaho, Phase III: Verification of Formula for Prediction of Dividing Streamline Height. Fluid Modeling Facility Internal Rpt., Aug. 29, Envir. Prot. Agcy., Res. Tri. Pk., NC, 12p.

* Snyder, W.H. 1981 Guideline for Fluid Modeling of Atmospheric Diffusion. Rpt. No. EPA-600/8-81-009, Envir. Prot. Agcy., Res. Tri. Pk., NC, 200p.

* Snyder, W.H. 1983a Fluid Modeling of Terrain Aerodynamics and Plume Dispersion - A Perspective View. Invited Presentation, AMS Workshop on Dispersion in Complex Terrain, Keystone, CO, May 17-20.

* Snyder, W.H. 1983b Fluid Modeling of Terrain Aerodynamics and Plume Dispersion - A Perspective View. Preprint Vol. 6th Symp. Turb. & Diff., March 22-25, Boston, MA, 317-20. Amer. Meteorol. Soc., Boston, MA.

* Snyder, W.H. 1984 Terrain Aerodynamics and Plume Dispersion: A Perspective View Gained from Fluid Modeling Studies. Proc. Symp. Tibetan Plateau & Mtn. Meteorol., Beijing, P.R.C., March.

* Snyder, W.H. 1985 Fluid Modeling of Pollutant Transport and Diffusion in Stably Stratified Flows over Complex Terrain. *Ann. Rev. Fluid Mech.*, 17, 239-66.

* Snyder, W.H. 1986 Comparisons of CTDM Calculations with Fluid Modeling Observations. *Complex Terrain Workshop*, Research Triangle Park, NC, Feb. 4-6, 45p.

* Snyder, W.H. & Britter, R.E. 1987 A Wind Tunnel Study of the Flow Structure and Dispersion from Sources Upwind of Three-Dimensional Hills. *Atmos. Envir.*, 21, 735.

* Snyder, W.H., Britter, R.E. & Hunt, J.C.R. 1980 A Fluid Modeling Study of the Flow Structure and Plume Impingement on a Three-Dimensional Hill in Stably Stratified Flow. Proc. Fifth Int. Conf. on Wind Engr. (J.E. Cermak, ed.), 1, 319-29. Pergamon Press, NY, NY.

* Snyder, W.H. & Hunt, J.C.R. 1984 Turbulent Diffusion from a Point Source in Stratified and Neutral Flows around a Three-Dimensional Hill, Part II: Laboratory Measurements of Surface Concentrations. *Atmos. Envir.*, 18, 1969-2002.

* Snyder, W.H. & Lawson, R.E. Jr. 1981 Laboratory Simulation of Stable Plume Dispersion over Cinder Cone Butte: Comparison with Field Data. Appendix: EPA Complex Terrain Model Development First Milestone Report - 1982, Rpt. No. EPA-600/3-82-036, p. 250-304. Envir. Prot. Agcy., Res. Tri. Pk., NC.

* Snyder, W.H. & Lawson, R.E. Jr. 1985a Stable Plume Dispersion over an Isolated Hill: Releases above the Dividing-Streamline Height. Appendix A: EPA Complex Terrain Model Development Fourth Milestone Report - 1984, Rpt. No. EPA/600/3-84/110, 233-68. Envir. Prot. Agcy., Res. Tri. Pk, NC.

* Snyder, W.H. & Lawson, R.E. Jr. 1985b Fluid Modeling Demonstration of Good–Engineering–Practice Stack Height in Complex Terrain. Rpt. No. EPA–600/3–85/022, Envir. Prot. Agcy., Res. Tri. Pk., NC, 89p.

* Snyder, W.H. & Lawson, R.E. Jr. 1986 Laboratory Observations of Plume Deformations in Neutral Flow over a Three–Dimensional Hill. Preprint Vol. AMS 5th Jt. Conf. Appl. Air Poll. Meteorol. with APCA, Nov., Chapel Hill, NC, Amer. Meteorol. Soc., Boston, MA.

* Snyder, W.H. & Lawson, R.E. Jr. 1987 Stable Plume Dispersion over an Isolated Hill: Releases above the Dividing–Streamline Height. *Proc. Third Int. Symp. Stratified Flows*, Cal. Inst. Tech., Pasadena, CA, Feb. 3–5.

* Snyder, W.H., Lawson, R.E. Jr., Thompson, R.S. & Holzworth, G.C. 1980 Observations of Flow around Cinder Cone Butte, Idaho. Rpt. No. EPA–600/7–80–150, Envir. Prot. Agcy., Res. Tri. Pk., NC, 30p.

* Snyder, W.H. & Ogawa, Y. 1982 Simulation of Flow and Diffusion over Cinder Cone Butte in a Stratified Wind Tunnel. Data Report, National Inst. for Envir. Studies, Tsukuba, Japan.

* Snyder, W.H. & Pendergrass, W.R. III 1980 Ramp Study: Idealized Widows Creek. Unpublished Data Rpt., Fluid Modeling Facility, Envir. Prot. Agcy., Res. Tri. Pk., NC.

* Snyder, W.H., Thompson, R.S., Eskridge, R.E., Lawson, R.E., Jr., Castro, I.P., Lee, J.T., Hunt, J.C.R. & Ogawa, Y. 1983 The Structure of Strongly Stratified Flow over Hills: Dividing–Streamline Concept. Appendix: EPA Complex Terrain Model Development Second Milestone Report – 1982, Rpt. No. EPA–600/3–83–015, p. 319–75. Envir. Prot. Agcy., Res. Tri. Pk., NC.

* Snyder, W.H., Thompson, R.S., Eskridge, R.E., Lawson, R.E., Jr., Castro, I.P., Lee, J.T., Hunt, J.C.R. & Ogawa, Y. 1985 The Structure of Strongly Stratified Flow over Hills: Dividing–Streamline Concept. *J. Fluid Mech.*, **152**, 249–88.

* Snyder, W.H., Thompson, R.S. & Shipman, M.S. 1986 Streamline Trajectories in Neutral and Stratified Flow over a Three–Dimensional Hill. Appendix: Rpt. No. EPA/600/3–85/069, EPA Complex Terrain Model Development Fifth Milestone Report – 1985, 240–277. Envir. Prot. Agcy., Res. Tri. Pk., NC.

Strimaitis, D.G., Lavery, T.F., Venkatram, A., DiCristofaro, D.C., Greene, B.R. & Egan, B.A. 1985 EPA Complex Terrain Model Development: Fourth Milestone Report – 1984. Rpt. No. EPA–600/3–84–110, Envir. Prot. Agcy., Res. Tri. Pk., NC.

Strimaitis, D.G., Scire, J.S. & Bass, A. 1982 COMPLEX/PFM Air Quality Model User's Guide. Rpt. (awaiting printing), Envir. Prot. Agcy., Res. Tri. Pk., NC, 114p.

* Strimaitis, D.G. & Snyder, W.H. 1986 An Evaluation of the Complex Terrain Dispersion Model Against Laboratory Observations: Neutral Flow over 2–D and 3–D Hills. Preprint Vol. AMS 5th Jt. Conf. Appl. Air Poll. Meteorol. with APCA, Nov., Chapel Hill, NC, Amer. Meteorol. Soc., Boston, MA.

Strimaitis, D.G., Venkatram, A., Greene, B.R., Hanna, S., Heisler, S., Lavery, T.F., Bass, A., & Egan, B.A. 1983 EPA Complex Terrain Model Development: Second Milestone Report - 1982. Rpt. No. EPA-600/3-83-015, Envir. Prot. Agcy., Res. Tri. Pk., NC. ,

* Thompson, R.S. & Shipman, M.S. 1986 Streamlines in Stratified Flow over a Three-Dimensional Hill. Preprint Vol. AMS 5th Jt. Conf. Appl. Air Poll. Meteorol. with APCA, Nov., Chapel Hill, NC, Amer. Meteorol. Soc., Boston, MA.

* Thompson, R.S., Shipman, M.S. & Snyder, W.H. 1985 Synopses of FMF Projects in Complex Terrain. Rpt. to ERT on CTMD Program, Envir. Prot. Agcy., Res. Tri. Pk., NC, 24p.

* Thompson, R.S. & Snyder, W.H. 1976 EPA Fluid Modeling Facility. Proc. Conf. on Modeling & Simulation, Rpt. No. EPA-600/9-76-016, Envir. Prot. Agcy., Wash. D.C., July.

* Thompson, R.S. & Snyder, W.H. 1981 Air Pollution and Terrain Aerodynamics: A Review of Fluid Modeling Studies at the EPA Fluid Modeling Facility. ASCE Fall Conv., St. Louis, MO, Oct.

* Thompson, R.S. & Snyder, W.H. 1984 Fluid Modeling of Blocking and Upstream Influences of Stable Flow over Two-Dimensional Hills. Proc. 2nd Workshop Wind/Water Tunnel Dispersion Modeling, Oxford, England, Sept. 26-28, C3.1-3.7.

* Thompson, R.S. & Snyder, W.H. 1985a Air Pollution and Terrain Aerodynamics: A Review of Fluid Modeling Studies at the EPA Fluid Modeling Facility. *J. Wind Engr. & Indus. Aerodyn.*, 21, 1-19.

* Thompson, R.S. & Snyder, W.H. 1985b Dispersion from a Source Upwind of a Three-Dimensional Hill of Moderate Slope. Appendix B: EPA Complex Terrain Model Development Fourth Milestone Report - 1984, Rpt. No. EPA/600/3-84/110, 269-86. Envir. Prot. Agcy., Res. Tri. Pk., NC.

* Thompson, R.S., Snyder, W.H. & Lawson, R.E. Jr. 1983 Laboratory Simulation of Neutral Plume Dispersion over Cinder Cone Butte: Comparison with Field Data. Appendix: EPA Complex Terrain Model Development Third Milestone Report - 1983, Rpt. No. EPA-600/3-83-101, p. 212-51. Envir. Prot. Agcy., Res. Tri. Pk., NC.

Turner, J.S. 1973 *Buoyancy Effects in Fluids.* Cambridge Univ. Press, Cambridge, England, 368p.

Venkatram, A., Strimaitis, D. & DiCristofaro, D. 1984 A Semiempirical Model to Estimate Vertical Dispersion of Elevated Releases in the Stable Boundary Layer. *Atmos. Envir.*, 18, 923-8.

Wackter, D.J. & Londergan, R.J. 1984 Evaluation of Complex Terrain Air Quality Models. Rpt. under Contract No. 68-02-3514, Envir. Prot. Agcy., Res. Tri. Pk., NC, 233p.

Weil, J.C., Traugott, S.C. & Wong, D.K. 1981 Stack Plume Interaction and Flow Characteristics for a Notched Ridge. Rpt. No. PPRP-61, Martin Marietta Corp., Baltimore, MD, 92p.